QC
879.4
.T57
1964
v.1

TIROS VII RADIATION DATA CATALOG AND USERS' MANUAL

Volume 1

(June 19, 1963 - September 30, 1963)

GODDARD SPACE FLIGHT CENTER
GREENBELT, MARYLAND

144 659

TIROS VII
RADIATION DATA CATALOG
AND
USERS' MANUAL

VOLUME I
JUNE 19, 1963 – SEPTEMBER 30, 1963

ATMOSPHERIC SCIENCES
LIBRARY
APR 26 1968
E. S. S. A.
U. S. Dept. of Commerce

By
Staff Members
of the
Aeronomy and Meteorology Division
U. S. Goddard Space Flight Center. Lab for Atmospheric and Biological Sciences.
National Aeronautics and Space Administration

QC
879.4
.T57
1964
V.1

September 30, 1964

144 659

National Oceanic and Atmospheric Administration
TIROS Satellites and Satellite Meteorology

ERRATA NOTICE

One or more conditions of the original document may affect the quality of the image, such as:

Discolored pages
Faded or light ink
Binding intrudes into the text

This has been a co-operative project between the NOAA Central Library and the Climate Database Modernization Program, National Climate Data Center (NCDC). To view the original document contact the NOAA Central Library in Silver Spring, MD at (301) 713-2607 x124 or Library.Reference@noaa.gov.

HOV Services
Imaging Contractor
12200 Kiln Court
Beltsville, MD 20704-1387
January 26, 2009

Blank page retained for pagination

FOREWORD

This combination Catalog and Users' Manual follows the same documentation format for the TIROS VII five-channel medium resolution scanning radiometer experiment that was used for the TIROS IV experiment. It replaces the two separate companion volumes which were published previously for TIROS II and TIROS III. The quantity of radiation data already acquired from TIROS VII exceeds several times over the total quantity acquired from any of the previous TIROS radiation experiments, and as of this writing data are still being acquired from TIROS VII. As a result, the TIROS VII Catalog-Manual will be published in several separate volumes. This, the first volume, contains general discussions about the nature of the experiment, the calibration, and the processing of data, in addition to specific information concerning the data acquired during the period from launch on June 19, 1963 to September 30, 1963. The corresponding specific information concerning data acquired after September 30, 1963, will be found in succeeding volumes.

In this Volume of the TIROS VII Catalog-Manual, the radiometer and its calibration, the data processing, the "Final Meteorological Radiation Tape", the observed radiometer response behavior patterns, and possible corrections are discussed. This Volume also includes, in two forms, documentation of each orbit of successfully reduced radiation data acquired from launch, June 19, 1963, to September 30, 1963. One method of presentation is the Index of Final Meteorological Radiation Tapes and the other is a Subpoint Track Summary of Available Radiation Data in diagrammatic form.

Many members of the staff of the Aeronomy and Meteorology Division contributed to the success of the TIROS VII medium resolution radiometer experiment. Valuable contributions in the area of computer programming for data processing came from the National Weather Satellite Center, U. S. Weather Bureau, whose efforts are gratefully acknowledged.

The task of assembling the information contained in this manual into written form suitable for publication was largely accomplished by the following members of the Aeronomy and Meteorology Division:

Mr. George Nicholas, Editor
Miss Musa Halev, Co-editor
Mr. W. R. Bandeen
Mr. Robert Hite
Mr. Andrew McCullough
Mr. Harold Thompson
Mr. Frederick Woolfall

The efforts of these individuals are hereby acknowledged.

The preparation of the material presented in Appendix B was accomplished mainly through the effort of Mr. Eldon Bowman.

ABSTRACT

The TIROS VII Meteorological Satellite contains a medium resolution scanning radiometer. Two of the channels of this instrument are sensitive to reflected solar radiation and the other three respond to emitted thermal radiation from the earth and its atmosphere. Channel 1 of TIROS VII is sensitive within the 15μ carbon dioxide region and replaces the 6.0-6.5μ, water vapor channel of TIROS II, III, and IV. The three thermal channels are calibrated in terms of equivalent blackbody temperatures, and the reflected solar radiation channels in terms of effective radiant emittances. The calibration data, along with orbital and attitude data, and the radiation data from the satellite were incorporated in a computer program for an IBM 7094 which was used to produce, in binary form, the "Final Meteorological Radiation Tape" which is the basic repository of all radiation data.

Before work with the TIROS VII radiation data is attempted, an understanding of the radiometer, its calibration, and the problems encountered in the experiment, especially from the radiometer response behavior, is essential. The instrumental design, development work, and the calibrations herein described were performed by the Goddard Space Flight Center staff, whereas the computer and programming efforts were carried out jointly by the staffs of the National Weather Satellite Center, U. S. Weather Bureau, and the Goddard Space Flight Center.

TABLE OF CONTENTS

	Page
Foreword	iii
Abstract	iv
List of Figures	vi
List of Tables	viii
List of Common Symbols	viii
I. INTRODUCTION	1
II. DESCRIPTION OF THE MEDIUM RESOLUTION RADIOMETER EXPERIMENT	3
2.1 Principle of the Radiometer	3
2.2 Description of the Sensors	4
2.3 Geographic Limitations of Data Utilization	4
III. CALIBRATION	4
3.1 Effective Spectral Response	5
3.2 Effective Radiant Emittance	6
3.3 Radiation Data Flow Sequence	7
3.4 Relation between Electronics, Radiometer Housing, and TV Clock No. 2 Temperatures	7
3.5 Space-Viewed Level	8
3.6 Target Blackbody Temperature, T_{bb}, and Target Effective Radiant Emittance, $\overline{W}$, vs. Digital Number, D	9
3.7 Field of View Measurements	10
3.8 Summary of the Calibration	10
IV. RADIATION DATA PROCESSING	11
4.1 Information Flow in the Satellite	11
4.2 Information Flow at the Command and Data Acquisition Station	12
4.3 Information Flow at the Data Processing Center	12
4.4 Information Flow at the Data Reduction Center	13
4.5 Format of the "Final Meteorological Radiation Tape"	13
4.6 IBM 7094 Computer Flow Diagram	17
V. RADIATION DATA COVERAGE AND DOCUMENTATION	18
5.1 Radiation Data Coverage	18
5.2 Documentation of Radiation Data	20
VI. PRE-LAUNCH AND POST-LAUNCH PERFORMANCE OF THE RADIATION EXPERIMENT	20
6.1 Pre-Launch Behavior of the Experiment	20
6.2 Post-Launch Behavior of the Experiment	20
6.3 Estimate of the Accuracy of the Data	27
6.4 Comments on Significant Engineering Aspects of the Experiment	27
VII. CONCLUSIONS	28

VIII. REFERENCES 29

APPENDIX A Index of Final Meteorological Radiation Tapes 119

APPENDIX B Subpoint Track Summary of Available Radiation Data for the Period June 19, 1963-September 30, 1963 147

LIST OF FIGURES

		Page
1.	Block Diagram of the Scanning Radiometer	34
2.	ϕ_λ vs. λ, Channel 1	35
3.	ϕ_λ vs. λ, Channel 2	36
4.	ϕ_λ vs. λ, Channel 3	37
5.	ϕ_λ vs. λ, Channel 4	38
6.	ϕ_λ vs. λ, Channel 5	39
7.	T_{BB} vs. $\overline{W}$, Channel 1	40
8.	T_{BB} vs. $\overline{W}$, Channel 2	41
9.	T_{BB} vs. $\overline{W}$, Channel 4	42
10.	Radiation Data Flow Diagram	43
11.	F_{SC} vs. V_{RAD}, Channel 1	44
12.	F_{SC} vs. V_{RAD}, Channel 2	45
13.	F_{SC} vs. V_{RAD}, Channel 3	46
14.	F_{SC} vs. V_{RAD}, Channel 4	47
15.	F_{SC} vs. V_{RAD}, Channel 5	48
16.(a)	Percent of Time the Satellite Spends in Sunlight	49
(b)	T_E, T_V, and T_C vs. Orbit Number	49
17.	Variation of T_C as a Function of the Time the Satellite is in Sunlight or in the Earth's Shadow	50
18.	Portions of the Orbital Period when the Satellite is in Sunlight or the Earth's Shadow vs. Orbit Number	51
19.	F_{SC} and D vs. T_{BB} @ $T_C = 0°C$, Channel 1	52
20.	F_{SC} and D vs. T_{BB} @ $T_C = 7°C$, Channel 1	53
21.	F_{SC} and D vs. T_{BB} @ $T_C = 12°C$, Channel 1	54
22.	F_{SC} and D vs. T_{BB} @ $T_C = 18°C$, Channel 1	55
23.	F_{SC} and D vs. T_{BB} @ $T_C = 25°C$, Channel 1	56
24.	F_{SC} and D vs. T_{BB} @ $T_C = 35°C$, Channel 1	57
25.	F_{SC} and D vs. T_{BB} @ $T_C = 40°C$, Channel 1	58
26.	F_{SC} and D vs. T_{BB} @ $T_C = 0°C$, Channel 2	59
27.	F_{SC} and D vs. T_{BB} @ $T_C = 7°C$, Channel 2	60
28.	F_{SC} and D vs. T_{BB} @ $T_C = 12°C$, Channel 2	61
29.	F_{SC} and D vs. T_{BB} @ $T_C = 18°C$, Channel 2	62
30.	F_{SC} and D vs. T_{BB} @ $T_C = 25°C$, Channel 2	63
31.	F_{SC} and D vs. T_{BB} @ $T_C = 32°C$, Channel 2	64
32.	F_{SC} and D vs. T_{BB} @ $T_C = 40°C$, Channel 2	65
33.	F_{SC} and D vs. $\overline{W}$ @ $T_C = 0°C$, Channel 3	66
34.	F_{SC} and D vs. $\overline{W}$ @ $T_C = 7°C$, Channel 3	67

35. F_{SC} and D vs. $\overline{W}$ @ T_C = 12°C, Channel 3 ---------- 68
36. F_{SC} and D vs. $\overline{W}$ @ T_C = 18°C, Channel 3 ---------- 69
37. F_{SC} and D vs. $\overline{W}$ @ T_C = 25°C, Channel 3 ---------- 70
38. F_{SC} and D vs. $\overline{W}$ @ T_C = 35°C, Channel 3 ---------- 71
39. F_{SC} and D vs. $\overline{W}$ @ T_C = 40°C, Channel 3 ---------- 72
40. F_{SC} and D vs. T_{BB} @ T_C = 0°C, Channel 4 ---------- 73
41. F_{SC} and D vs. T_{BB} @ T_C = 7°C, Channel 4 ---------- 74
42. F_{SC} and D vs. T_{BB} @ T_C = 12°C, Channel 4 ---------- 75
43. F_{SC} and D vs. T_{BB} @ T_C = 18°C, Channel 4 ---------- 76
44. F_{SC} and D vs. T_{BB} @ T_C = 25°C, Channel 4 ---------- 77
45. F_{SC} and D vs. T_{BB} @ T_C = 32°C, Channel 4 ---------- 78
46. F_{SC} and D vs. T_{BB} @ T_C = 40°C, Channel 4 ---------- 79
47. F_{SC} and D vs. $\overline{W}$ @ T_C = 0°C, Channel 5 ---------- 80
48. F_{SC} and D vs. $\overline{W}$ @ T_C = 7°C, Channel 5 ---------- 81
49. F_{SC} and D vs. $\overline{W}$ @ T_C = 12°C, Channel 5 ---------- 82
50. F_{SC} and D vs. $\overline{W}$ @ T_C = 18°C, Channel 5 ---------- 83
51. F_{SC} and D vs. $\overline{W}$ @ T_C = 25°C, Channel 5 ---------- 84
52. F_{SC} and D vs. $\overline{W}$ @ T_C = 35°C, Channel 5 ---------- 85
53. F_{SC} and D vs. $\overline{W}$ @ T_C = 40°C, Channel 5 ---------- 86
54. Calibration Flow Diagram ---------- 87
55. Field of View Measurements, Channel 1 ---------- 88
56. Field of View Measurements, Channel 2 ---------- 89
57. Field of View Measurements, Channel 3 ---------- 90
58. Field of View Measurements, Channel 4 ---------- 91
59. Field of View Measurements, Channel 5 ---------- 92
60. Block Diagram of the Radiation Experiment in the Satellite 93
61. Block Diagram of Information Flow at a Command and Data Acquisition Station ---------- 94
62. Block Diagram of Information Flow at the Data Processing Center ---------- 95
63. Interpretation of FMR Tape Format ---------- 96
64. Flow Diagram of the IBM 7094 Computer Program ------ 97
65. World-Wide Radiation Data Coverage ---------- 101
66. Heliocentric Views of the Earth ---------- 102
67. Solar Illuminated Latitudes for TIROS VII ---------- 103
68. Frequency Difference Between Flight and Calibrated Space-Viewed Levels vs. Orbit Number: (a) Channels 1, 2, and 4; (b) Channels 3 and 5 ---------- 104
69. Schematic Representation of the Compound Degradation Model ---------- 106
70. $\overline{W}^{i}_{ave}$ for Channel 1 vs. Days After Launch ---------- 107
71. $\overline{W}^{i}_{ave}$ for Channel 2 vs. Days After Launch ---------- 108
72. $\overline{W}^{i}_{ave}$ for Channel 4 vs. Days After Launch ---------- 109
73. A^{i} for Channel 3 vs. Days After Launch ---------- 110
74. A^{i} for Channel 5 vs. Days After Launch ---------- 111
75. $\overline{W}$ vs. Time from Map Averages and Pacific Ocean Averages over One Year, Indicating Instrumental Degradation and a Variation with the Orbit-Sun Phase Geometry ---------- 112
76. Conversion from $\overline{W}$ to W for Channel 2 and Channel 4 ---- 113

77. δT_{BB} vs. Orbit Number, Channel 1 ---------- 114
78. δT_{BB} vs. Orbit Number, Channel 2 ---------- 115
79. δT_{BB} vs. Orbit Number, Channel 4 ---------- 116
80. κ^i and ρ^i vs. Orbit Number, Channel 3 ---------- 117
81. κ^i and ρ^i vs. Orbit Number, Channel 5 ---------- 118
A-1 Observed Motion of the TIROS VII Spin Vector on the Celestial Sphere ---------- 122
A-2 Time History of the TIROS VII Spin Rate ---------- 123
B-1 Scanning Modes of the TIROS Radiometer ---------- 149
B-2 Nominal Boundary Satellite Nadir Angles for the Various Scanning Modes ---------- 150

LIST OF TABLES

Page
I. Mean Orbital Characteristics of TIROS VII ---------- 1
II. Channel Bandwidths of the TIROS VII Medium ---------- 4
III. Filter and Lens Materials ---------- 31
IV. Effective Spectral Response, Channel 1 ---------- 31
V. Effective Spectral Response, Channel 2 ---------- 31
VI. Effective Spectral Response, Channel 3 ---------- 31
VII. Effective Spectral Response, Channel 4 ---------- 31
VIII. Effective Spectral Response, Channel 4 ---------- 32
IX. T_{BB} vs. $\overline{W}$, Channel 1 ---------- 32
X. T_{BB} vs. $\overline{W}$, Channel 2 ---------- 32
XI. T_{BB} vs. $\overline{W}$, Channel 4 ---------- 32
XII. Changes in T_{BB} and $\overline{W}$ vs. Differences of T_E and T_C ---------- 32
XIII. Vertical Alignment of the 5 Channels of the TIROS VII Radiometer ---------- 33

LIST OF COMMON SYMBOLS

A Albedo, assumed to be equal to $\overline{W}/\overline{W}^* \cos \Theta_O$

A^i Quasi-global albedo at orbit i, taken from a smoothed curve through a large number of measurements. It is assumed that the downward trend of the smoothed curve is due solely to instrumental degradation

A_λ Spectral Absorptivity of the thermistor detector

D Digital Number: scale 0 to 127

F Number of cycles-per-second above the base frequency of a given 50 cps subcarrier band

ΔF The flight measured space-viewed level (both directions viewing outer space) minus the ground-calibrated "space-viewed" level (both directions viewing blackbodies of liquid nitrogen temperatures (−196°C)) in terms of cycles-per-second of a given 50 cps subcarrier band

F_{HC} Output frequency of the voltage controlled oscillator

J_λ Spectral radiant intensity of visible light source, i.e., a standard tungsten lamp or the sun (watts/steradian/micron)

R_λ^B Spectral reflectivity of the black half of the chopper disk
R_λ^M Spectral reflectivity of the aluminized half of the chopper disk
R_λ^P Spectral reflectivity of the radiometer prism
R Distance from the visible light source to the center of the diffuse reflector
T_{BB} Equivalent blackbody temperature (degrees Kelvin)
T_C Radiometer housing temperature
T_E Satellite electronics temperature
T_V Television system clock number 2 temperature
V_{RAD} Output voltage of the radiometer
W Total outgoing longwave flux (watts/meter ^{2})
$W_\lambda(T)$ Spectral radiant emittance (the Planck function) for a blackbody of temperature T (watts/meter ^{2}/micron)
$\overline{W}$ Effective radiant emittance (watts/meter ^{2})—defined by equation (2) for channels 1, 2, and 4, and defined by equation (5) for channels 3 and 5
$\overline{W}_{ave}^i$ Average quasi-global effective radiant emittance at orbit i, taken from a smoothed curve through a large number of measurements. It is assumed that the downward trend of the smoothed curve is due solely to instrumental degradation
$\overline{W}^*$ The effective solar constant, defined by equation (6)
f_λ Spectral transmission of the fiter-lens combination
k Slope of F_{SC} vs. $\overline{W}$ transfer function
r_λ Spectral reflectivity of the diffuse reflector employed in the calibration of the reflected solar radiation channels
$\Delta\phi$ Right ascension of the sun minus the right ascension of the orbital ascending node
Ω Solid angle of the sun as viewed from the earth
γ Incidence angle of radiation from visible light source impinging upon diffuse reflector employed in the calibration of the visible channels
δT_{BB} Thermal channel temperature correction resulting from instrumental degradation
θ Zenith angle
κ^i Degradation parameter at orbit i in equations (7) and (8)
λ Wavelength in microns
ρ^i Degradation parameter at orbit i in equation (7)
ϕ_λ Effective spectral response of the radiometer defined by equation (1)

Subscript:
ave Average
$\odot$ Sun

Superscripts:
$'$ Indicates a measurement or other value which may be affected by instrumental degradation
i Orbit number

I. INTRODUCTION

The TIROS VII Meteorological Satellite was injected into orbit on June 19, 1963. Its mean orbital characteristics are listed in Table I.

TABLE I

Perigee Altitude	622 km
Apogee Altitude	648 km
Anomalistic Period	97.42 minutes
Inclination	58.2°

The experiments flown in the satellite include two television cameras, two radiometers, and an electron temperature probe experiment. The radiometers measure emitted thermal and reflected solar radiation from the earth and its atmosphere. One radiometer is the University of Wisconsin's heat balance experiment.

This manual is concerned only with the second radiation measuring device, a five-channel medium resolution scanning radiometer, which responds to radiation in five different spectral regions. Three of these channels respond to emitted thermal radiation from the earth and its atmosphere, and the other two channels respond to reflected solar radiation. One of the thermal radiation channels responds to the 15μ carbon dioxide band and replaces the 6.0μ-6.5μ "water vapor absorption" channel of the radiometers flown on TIROS II, TIROS III, and TIROS IV. The three thermal radiation channels are calibrated in terms of equivalent blackbody temperatures and the reflected solar radiation channels in terms of effective radiant emittances.

The radiation data from the medium resolution radiometer experiment are processed together with attitude information and calibration data on an IBM 7094 computer to produce a binary "Final Meteorological Radiation (FMR) Tape," which is the basic repository of the radiation data in terms of equivalent blackbody temperature or effective radiant emittance.

Before attempting to interpret the radiation data from TIROS VII which are contained on the FMR tapes, careful consideration should be given to all points discussed in this manual. An understanding of the significance of the equivalent blackbody temperatures or effective radiant emittance values and a familiarity with the principles of the radiometer, its peculiarities, and the method of calibration are essential. Before attempting to utilize the radiation data, the effects of calibration degradation on the data must also be considered.

This combination Catalog and Users' Manual follows the same documentation format as that used for the TIROS IV Radiation Data Catalog and Users' Manual,[1] replacing the two separate volumes which were published for the TIROS II and TIROS III five-channel radiometer experiments.[2,3,4,5] At this writing TIROS VII has successfully returned radiation data for over one year, being almost three times as long as the useful lifetimes of any of the previous scanning radiometer experiments. This large quantity of information has, thus, necessitated publishing the TIROS VII Catalog-Manual in several volumes. This, the first volume, discusses the radiometer and its calibration, the data processing, the "Final Meteorological Radiation Tape," the observed behavior of the radiometer responses, and possible corrections to the data due to the degradation of the instrumental response. This volume also includes, in two forms, documentation of each orbit of successfully reduced radiation data acquired from launch, June 19, 1963, to September 30, 1963. One form is an Index of all FMR tapes; the other is a diagrammatic Subpoint Track Summary of the available radiation data for each orbit. Future volumes will include information concerning the radiometer response behavior and general developments of the experiment along with an Index and a Subpoint Track Summary covering subsequent time periods.

The radiation data are available in various "hard copy" formats suitable for presenting limited portions of the data, as well as, the "binary" FMR tape format, suitable for computer processing and containing the originally reduced data in their entirety. The data are reduced to the FMR Tape format by the experimenters at the following address:

TIROS Radiation Data, Code ~~651~~ 620
Aeronomy and Meteorology Division
NASA, Goddard Space Flight Center
Greenbelt, Maryland 20771

Duplicates of the FMR Tapes are archived at the following data center:

National Weather Records Center
U. S. Weather Bureau
Federal Building
Asheville, North Carolina 28801

Copies of the data in the various standard formats listed below can be obtained for production costs by writing to the National Weather Records Center (NWRC). Unless otherwise requested, the NWRC will routinely provide cost estimates prior to filling orders. *In addition, limited quantities of the data in the standard formats may be obtained by investigators without charge by writing to the Goddard Space Flight Center (GSFC) experimenters.* Detailed descriptions of most of these formats are contained in the TIROS II and TIROS III Radiation Data Catalogs [2,4] and in the various Radiation Data Users' manuals.[1,3,5] These publications should be consulted before orders are placed. Some flexibility in the machine programs is possible, and users having requirements which cannot be satisfied by the available standard formats should write to either of the above addresses for further information.

The data are presently available in the following standard formats:

A. *Copies of Final Meteorological Radiation (FMR) Tapes (binary)*

The FMR Tape is the product of a computer program whose input is the attitude/orbital data, digitized radiation data, and the TIROS radiometer calibration package. These tapes are usable only on IBM compatible electronic data processing equipment having a core storage capacity of the equivalent of at least 4096 36-bit words.

NWRC Price (including tape) $60 per reel
or, if user provides tape $30 per reel

B. *Data Listings (Program MS 500)*

Machine programs are available which will produce a printed list of the calibrated information for a specified time period from all five sensors together with appropriate locator information (see Section IX of the TIROS III Catalog [4]). The NWRC cost for the listings is dependent upon the size of the sample and its position within the tape data files. For example, a listing of 10 minutes of satellite data (about 100 swaths with 50 samples per swath which would cover an area the size of U.S.) would cost about $20 to $30.

C. *Grid Print Maps*

A series of programs produce printed and contoured data referenced to a square mesh grid on polar stereographic or Mercator map bases. Grid print maps may be produced for either a single orbit (see Section IV of the TIROS II Catalog [2] and Sections V, VI, VII, and VIII of the TIROS III Catalog [4]) or a composite of several orbits (see Section IX of the TIROS III Catalog [4]). The following standard options are available and should be specified when requesting grid print maps:

1. Map and Approximate Scale
   a. Polar Stereographic, 1/30 million (approx.) (AW950)
   b. Polar Stereographic, 1/10 million (approx.) (MS501)
   c. Multi-Resolution Mercator (MSC 2)
      (1) 5.0 degrees Long. per mesh interval—1/40 million (approx.)
      (2) 2.5 degrees Long. per mesh interval—1/20 million (approx.)
      (3) 1.25 degrees Long. per mesh interval—1/10 million (approx.)
2. Maximum Sensor Nadir Angle (unless otherwise specified, 58° will be used)
3. Field Values and Contouring (unless otherwise specified, all maps will include field values and contouring except Mercator Maps of scales larger than 1/20 million which will contain no field values or contouring (see Section IV of the TIROS III Catalog [4]).

A data population map, indicating the number of individual measurements con-

tained in each grid point average, as well as a sample latitude-longitude overlay for geographically locating the data, will ordinarily be provided along with each grid print map.

The NWRC cost for grid print maps will vary, of course, according to the option selected. To illustrate, for a Mercator (60°N-60°S) grid print map, involving one sensor and one orbit, the cost would be about $25 to $35.

When ordering "hard copy" data, the following identifying information should be given:

1. Satellite (e.g. TIROS VII)
2. Read-Out Orbit No. (cf. Index of FMR Tapes in Appendix A)
3. Channel No. (e.g. Channel 2, 8.0-12.0 microns; Channel 3, 0.2-6.0 microns; etc.)
4. Calendar Date of Equator Crossing (cf. Index of FMR Tapes in Appendix A)
5. Beginning and Ending Times of Data in GMT (cf. Index of FMR Tapes and Subpoint Track Summary in Appendix A and Appendix B)
6. Format Desired

When ordering FMR Tapes, only items 1 and 2 above need be given, plus:

7. FMR Tape Reel No.(s) (cf. Index of FMR Tapes, Appendix A)

Television pictures taken concurrently with the radiation data may also be obtained from the National Weather Records Center. The availability of such pictures is documented in the Key to Meteorological Records Documentation No. 5.37, "Catalog to Meteorological Satellite Data-TIROS VII Television Cloud Photography", copies of which may be obtained from the Superintendent of Documents, U. S. Government Printing Office, Washington 25, D. C.

II. DESCRIPTION OF THE MEDIUM RESOLUTION RADIOMETER EXPERIMENT

2.1 *Principle of the Radiometer*[6, 7]

The principle of the radiometer is illustrated in Figure 1 which shows the components of a single channel. The fields of view of the channels are approximately coincident, each being about five degrees wide at the half-power point of the response. The optical axis of each channel is bi-directional, 180° apart. As the half-aluminized, half-black chopper disk rotates, radiation from first one direction and then the other reaches the thermistor bolometer detector. This results in a chopped output which is amplified and rectified, giving a DC signal which (neglecting electronic noise and possible optical imbalance) is theoretically proportional to the difference in energy flux viewed in the two directions. Variations in the amplitude of the radiometer signal are converted into subcarrier frequency deviations and stored by means of a miniature magnetic tape recorder. When the satellite is interrogated, while within range of a Command and Data Acquisition Station, the information is telemetered to the earth where it is recorded on magnetic tape. The further processing of these magnetic tapes is discussed in Section IV of this manual.

The radiometer is mounted in the satellite such that the optical axes are inclined 45° to the satellite spin axis. (The viewing directions are designated "wall" and "floor" according to their orientation in the satellite.) When one optic views the earth, the other views outer space. The outer space radiation level (assumed to be zero) is used as a reference. When both optics are viewing outer space, the resultant signal is designated as the "space-viewed level." Theoretically, this signal should be zero, but in reality is not, due to electronic noise and any initial optical imbalance, plus subsequent changes in balance caused by the degradation of certain channels after the laboratory calibration.

As the satellite rotates on its axis, the radiometer scan pattern on the surface of the earth is defined by the intersection of a 45° half-angle cone and a sphere. This pattern ranges from a circle when the spin vector is parallel to the orbital radius vector, to two hyperbola-like branches when the spin vector is perpendicular to the radius vector. The orbital motion of the satellite provides

the scan advance. When viewing vertically downward from a height of about 635 km, the spatial resolution of the radiometer is about 55 km; i.e., the "spot" on earth viewed by the radiometer has a diameter of 55 km.

2.2 *Description of the Sensors*

The nominal channel bandwidths for the TIROS VII medium resolution radiometer are given in Table II.

TABLE II

Channel	Nominal Bandwidth (Microns)	Nature of Band
1	14.8 -15.5	carbon dioxide absorption
2	8.0 -12.0	atmospheric window
3	0.2 - 6.0	reflected solar radiation
4	8.0 -30.0	thermal radiation from the earth and atmosphere
5	0.55- 0.75	response of the TV system

In the 14.8 to 15.5 micron channel a maximum absorption due to carbon dioxide is encountered. Energy in this channel is received mainly from the vicinity of 15 to 35 kilometers. Regions below 10 and above 40 kilometers contribute only very little to the radiance at normal incidence; however, when regions near the horizon are within the field of view of the sensor, the center of mass of the emission function shifts upward to higher altitudes and warmer temperatures; hence, limb-brightening occurs. The radiance for this channel can be interpreted in terms of mean stratospheric temperatures, weighted over varying altitudes, depending upon atmospheric structure and sensor viewing angle; however, the radiance is virtually independent of the state of cloudiness of the atmosphere; and is, therefore, not correlated to the other channels.[8, 9, 10] The energy received in the 8.0 to 12.0 micron channel originates mainly from either the earth's surface and/or clouds since absorption due to any of the atmospheric constituents—except ozone which covers only a minor portion of this channel—is every small. The total solar energy reflected from the earth and its atmosphere is contained in the 0.2 to 6.0 micron channel. The 8.0 to 30.0 micron channel radiation includes a substantial contribution by the 8-12 micron region. The emission over the remainder of the 8-30 micron region is primarily from the carbon dioxide and rotational water vapor absorption bands, and the radiance at the top of the atmosphere in these bands originates mostly in the atmosphere and thus represents lower temperatures than those detected by the 8-12 micron channel. The 0.55 to 0.75 micron channel covers the maximum of the solar energy distribution and is similar in its spectral response to the TV cameras on the satellite.

The interpretation of the radiation data in terms of physically significant qualities has been given in the literature.[10-38]

2.3 *Geographic Limitations of Data Utilization*

Care should be exercised in the use of the correlation of the radiation data with geographic locations, such as attempted comparison with synoptic situations. Uncertainties in attitude lead to an estimated error of 1° to 2° in great circle arc. At a nadir angle of zero, a 2° error would result in a position error on the earth's surface of less than 20 miles, while a 2° error for a nadir angle of 60° corresponds to an error of over 200 miles. It should be emphasized that such errors result in distortions as well as translations, and a simple linear shift of the data is in general not sufficient for correction.[39-44]

In addition to attitude errors, time errors also contribute to difficulties in geographic correlation.[39] The principal sources of time errors are: mistakes at the ground station in transmission of the end-of-tape pulse, erroneous sensing by the analog-to-digital converter of the end-of-tape pulse, and the necessity of counting through noise on the relative satellite clock frequency. These errors are generally estimated to be less than ten seconds in TIROS VII. However, users are cautioned to be watchful for those rare cases where there still might be larger errors of the order of one minute or more. Time errors also result in distortions as well as translations.

III. CALIBRATION

Before considering the calibration flow

sequence, it is necessary to discuss two quantities which are fundamental to the calibration. These are the effective spectral response and the effective radiant emittance.

3.1 *Effective Spectral Response*

The radiation received by the radiometer is modified by the various elements in the optical train before being absorbed by the bolometer detector. These include the reflecting properties of the prism and chopper, and the transmission characteristics of the filters and lenses. By assuming equal optical properties and temperatures for both sides of the prism, an effective spectral response, ϕ_λ, can be defined as

$$\phi_\lambda = R_\lambda^P \, (R_\lambda^M - R_\lambda^B) \, f_\lambda \, A_\lambda \qquad (1)$$

The various optical elements in each channel were evaluated as to reflectance or transmittance using combinations of three commercial spectrophotometers. Combined, these instruments cover the wavelength range of 0.25—35 microns. All three units can be used for either transmittance or reflectance measurements. The Beckman DK-2 using an SiO_2 prism operates through the region of 0.25—2.5 microns. A MgO coated integrating sphere reflectance attachment yielding either total or diffuse reflectance of a sample for energy incident at an angle of approximately 5° may be employed with this device. The two infrared instruments, the Beckman IR-5 and IR-5A, use rock salt and cesium bromide respectively as prism materials to cover the region of 2.0—35 microns with an overlap at 11-15 microns. Reflectance measurements here are performed using attachments that are inserted in the reference and sample beam.

These give specular reflectance only, and the beam is at an angle of incidence of 30° to the sample.

The materials used in the lenses and filters of each channel are given in Table III.

All of the terms in Equation 1 for each channel of the TIROS VII radiometer were taken from Barnes Engineering Company measurements. A discussion of the terms from which ϕ_λ is derived follows.

Spectral Reflectivity of the Radiometer Prism, R_λ^P

Total reflectance measurements of the prism relative to a standard (freshly burned magnesium oxide) for a 5° angle of incidence are made. The measurements in the visible portion of the spectrum up to 2.5 microns are performed on both surfaces of the prism and over different areas of each side to check the uniformity of reflectance. The measurements in the infrared consists of comparing the spectral reflectance for a 30° angle of incidence of the sample to a reference beam of infrared transmittance through air. The reference level is normalized to 100% with a standard silicon monoxide coated aluminized mirror.

Spectral Reflectivity of the Radiometer Chopper, $(R_\lambda^M - R_\lambda^B)$

Spectral reflectance of both the black (absorptive) and aluminized (reflective) surfaces of the chopper are measured independently. In the visible portion of the spectrum the aluminized surface measurements are performed in the same manner as the reflectance measurements of the prism. The 100% line is adjusted using magnesium oxide in the reference and sample holders. Then the aluminized surface is placed in the sample part and the reflectance of the sample is compared to the reflectance of the magnesium oxide. Because of the great difference in the reflectances of the two halves of the chopper face and the fact that the reflectance of the black absorbing surface is low, a technique was established to determine the amount of energy that is reflected from the black surface only. A second measurement is performed with the same equipment setup, but with the absorptive sample removed from the holder. This is a measure of the relative amount of energy which is collected by the detector but not contributed by the sample surface. The actual reflectance is obtained by subtracting the relative transmittance due to the instrument construction from the black surface measurement.

In the infrared region the measurement is identical to the prism reflectance measurement for the reflective and absorptive surfaces.

Spectral Transmission of the Filter-Lens Combination in the Radiometer, f_λ

Spectral transmittance measurements are performed on all lens materials using the same Beckman spectrophotometers. In the visible and near-infrared portions of the spectrum, the Beckman DK-2 spectrophotometer is used with air as the reference. The 100% line is set with air versus air. Then the measurement is performed to provide the relative transmittance of the lens material to that of air. Plane parallel samples, equivalent in thickness to that of the lenses, are measured with the instrument. Measuring this equivalent sample (having the same mean thickness as the lens used in the system) is an accepted measurement technique. This method is used because measurements of the lenses themselves would produce errors due to lens curvature.

Spectral transmittance of the filters is performed in the same manner used to measure the lenses. Measurements are performed using air as the reference for comparative energy transmission measurements. The 100% line is adjusted using air vesus air to detect any difference between the two paths before a test is run using the sample versus air.

Spectral Absorptivity of the Thermistor Detector, A_λ

The spectral absorptivity of the thermistor detector is measured by irradiating the detector with a fixed amount of monochromatic energy at each successive wavelength increment over the spectrum from the ultraviolet to the far infrared. The test setup contains a source radiating energy in the portion of the spectrum being investigated.

Two detectors are used—one is the reference and the second is the detector under test. Monochromatic energy is directed to the reference cell first and the energy onto the detector is adjusted until the same amount of energy is obtained at each wavelength increment. Because the reference cell response is assumed to be spectrally flat, the energy is adjusted until the same voltmeter reading is obtained. Then the voltmeter readings are plotted as a relative spectral response normalized to 100% at the highest level.

Tables IV through VIII and Figures 2 through 6 give the effective spectral response for each of the channels of the TIROS VII radiometer.

3.2 *Effective Radiant Emittance*

The preflight calibration of the three emitted thermal radiation channels (channels 1, 2, and 4) was carried out by simulating the space-referenced earth signal in the laboratory. The TIROS VII radiometer and its associated electronics were calibrated as a system. The radiometer's field of view was filled in one direction by a blackbody target at liquid nitrogen temperature (80°K)—which is essentially equivalent to the space reference—while the field of view in the other direction was filled with a blackbody target whose temperature varied over the range expected when viewing the earth and its atmosphere. Thus, the infrared measurements are in terms of an "equivalent temperature, T_{BB}," of a blackbody filling the field of view which would cause the same response from the radiometer. Since the spectral response of the radiometer is assumed to be known from the spectral characteristics of the individual reflecting, refracting, and transmitting components of the optics, that portion of the radiant emittance of any source that falls within the spectral response curve of the instrument can be calculated. This quantity is defined as the effective radiant emittance, $\overline{W}$ $\left(\frac{\text{watts}}{\text{meter}^2}\right)$ and can be written as

$$\overline{W} = \int_0^\infty W_\lambda \ (T_{BB}) \ \phi_\lambda \, d\lambda. \qquad (2)$$

The data from the three channels, which detect emitted thermal radiation, can, therefore, be expressed either as T_{BB}, in degrees Kelvin, or as $\overline{W}$, in watts per square meter, of radiant emittance within the spectral response curve of the channel. The $\overline{W}$ vs. T_{BB} function for channels 1, 2, and 4 are given in Tables IX, X, and XI and in Figures 7, 8, and 9.

In calibrating the two channels which de-

tect reflected solar radiation (channels 3 and 5) one direction of the channels was merely masked with black tape to simulate space. To simulate reflected solar radiation from the earth and its atmosphere, a white diffuse reflector of known spectral reflectivity was illuminated at normal incidence from a standard lamp of known spectral intensity at a measured distance away. From these parameters the spectral radiant emittance from the reflecting surface was determined. With the illuminated reflector filling the field of view, the output signal from each channel is measured. The spectral radiant emittance from the reflector is integrated over the spectral response curves of the solar channels to yield that portion of the radiation viewed to which each channel responds. The result of such integration is the "effective radiant emittance, $\overline{W}$". Thus, the reflected solar radiation measurements are in terms of that portion of diffuse radiation, $\overline{W}$, from a target filling the field of view, to which each channel responds. In order to interpret these measurements in terms of reflectance (loosely, "albedo") one must know the effective radiant emittance, $\overline{W}^*$, which would be measured by each channel if the field of view were filled by a perfectly diffuse surface of unit reflectivity when illuminated by one solar constant at normal incidence. The expressions for $\overline{W}$ and $\overline{W}^*$ for channels 3 and 5 are defined in Section 3.6.2.

3.3 *Radiation Data Flow Sequence*

The radiation data flow sequence is shown in Figure 10. The sequence from satellite through ground station is illustrated in Figure 10(a). When an effective radiant emittance $\overline{W}$ is viewed by one side of the radiometer while the other side views outer space, and with a radiometer housing temperature, T_C, a radiometer output voltage, V_{RAD} is obtained. This relationship $V_{RAD} = f(\overline{W}, \text{SIDE}, T_C)$ is shown schematically in Figure 10(b). The signal, V_{RAD}, is fed into a voltage controlled oscillator which produces an output frequency, F_{SC}, when the oscillator electronics temperature is T_E. This relationship, $F_{SC} = f(V_{RAD}, T_E)$, is shown schematically in Figure 10(c), and is given in Figures 11-15 for channels 1, 2, 3, 4, and 5.

At the ground station, the frequency, F_{SC}, now increased by a factor of 30, is fed into a demodulator, the output of which enters an analog-to-digital converter which converts F_{SC} to a digital number, D. The conversion formula is

$$D = \frac{127}{50} F_{SC} \qquad (3)$$

and is shown schematically in Figure 10(d). The resulting digital number, D, and the temperatures, T_E and T_C, which are also telemetered from the satellite, are used to obtain the valve $\overline{W}$ (or T_{BB}) for channels 1, 2, and 4 and the value $\overline{W}$ for channels 3 and 5 from the calibration data as indicated below.

In practice, for the purpose of simplifying the data reduction, each channel is calibrated for different values of T_C while maintaining a fixed relationship between T_E and T_C rather than calibrating the radiometer and each oscillator as separate units to obtain the transfer functions shown in Figures 10(b) and 10(c). In addition, each oscillator is calibrated as a function of T_E to obtain the transfer function as shown in Figure 10(c).

3.4 *Relation Between Electronics, Radiometer Housing, and TV Clock No. 2 Temperatures*

The calibration of the TIROS VII radiometer-oscillator system was corrected according to the equation

$$T_E = T_C + 10°\text{C} \qquad (4)$$

This was necessary because during flight a 10°C difference between electronics and radiometer housing temperatures was present. The TIROS VII calibration curves, which are presented in this manual, therefore, include this correction.

The validity of the TIROS VII calibration with regard to equation (4) was checked using the flight data for T_E and T_C through orbit 1276. After orbit 1276 the channel which provides for the telemetry of T_E and T_C did not function. The comparison of T_E and T_C to orbit 1276 is shown in Figure 16(b); it can be seen that there is some variation of T_E and T_C from equation (4)

and the maximum is 7°C. The effect on T_{BB} or $\overline{W}$ for each channel of a 7°C temperature difference from the calibrated T_E and T_C relationship is given in Table XII. The maximum T_{BB} difference in the thermal radiation channels occurs for channel 1 and is 1°C while the maximum difference in $\overline{W}$ for the reflected solar radiation channels, in percent of one solar constant radiated from a diffuse source, is 0.4%.

After orbit 1276, T_C was derived from one of the television systems carried on the satellite, namely from the TV clock No. 2 temperature, T_V. The TV clock No. 2 is located almost diametrically opposite from the radiometer housing and 11.5 inches from the center of the satellite. A very good relationship can be established between T_V and T_C before orbit 1276, and from this relationship T_C can be derived from T_V after orbit 1276. The difference between T_V and T_C is not constant but is a function of both the total amount of time during one orbital period and the time prior to readout that the satellite is exposed to the sun or in the earth's shadow. T_C varies by as much as 5.7°C throughout an orbital period (Figure 17) depending upon the fractional part of the orbital period that the satellite is exposed to the sun. T_V is known for only one time during an orbital period, at the time the satellite is being interrogated by a Command and Data Acquisition Station, but should be expected to vary as T_C varies. The variation of T_C and T_V during an orbital period is related to the time when the satellite is in the sunlight or the earth's shadow. Figure 17 shows that the maximum T_C occurs after the satellite enters the earth's shadow and the time of occurrence is a function of the time the satellite is in the sunlight. It also shows that the minimum T_C occurs after the satellite enters sunlight and the time of occurrence is, likewise, a function of the time the satellite is exposed to the sun during one orbital period.

Figure 16(a) shows the percent of an orbital period that the satellite was in sunlight vs. orbit number for orbits from launch to 1525. Also shown is $\Delta\phi$, the difference between the right ascension of the sun and the orbital ascending node (described in detail in Section 5.1). Figure 18, shows similar information in a different format. This figure gives the fractional part of the 97.4 minute orbital period that the satellite spent in sunlight and the earth's shadow, expressed in minutes after ascending node vs. orbit number. Figure 16(b) shows T_V and the measured T_C from launch to orbit 1276, and T_V and the derived T_C from orbit 1276 to 1525.

Actually an average T_C for each orbit is used to reduce all of the data for that orbit on the FMR tape and, thus, as much as a ±2.85°C error in T_C can be introduced during a portion of the orbit. One can by the use of Figures 17 and 18 establish expressions relating the time of the occurrence of sunlight and shadow and the average T_C, to give a good approximation of the actual T_C throughout an orbit. By letting T_C vary instead of being an average T_C, a slightly more accurate T_{BB} or $\overline{W}$ can be obtained.

3.5 *Space-Viewed Level*

Although there is no specified on-board calibration mechanism on the TIROS VII radiometer, the "space-viewed level" can be considered as a single-point check-of-calibration while in orbit. Any observed shift in the space-viewed level after the original calibration is sufficient but not necessary to indicate a change in the calibration of the instrument (i.e., knowledge of the shift of a given point on a curve is sufficient to indicate a change in position of the curve; whereas, knowledge of the lack of a shift of the point is not sufficient to preclude a rotation of the curve about the point). It is important, therefore, to include a measurement of space-viewed levels in the calibration of the instrument. Within the spectral regions of sensitivity of the emitted thermal radiation channels, radiation from a blackbody target at liquid nitrogen temperatures is practically the equivalent of the radiation levels of outer space. To simulate space radiation for the reflected solar radiation channels, it is necessary only to turn off the lights in the laboratory. The space-viewed levels are calibrated as a function of radiometer housing temperature.

3.6 *Target Blackbody Temperature, T_{BB}, and Target Effective Radiant Emittance, $\overline{W}$, versus Digital Number, D*

The calibration curves and the following discussion are concerned with the original calibration carried out at the Goddard Space Flight Center.

3.6.1 *Emitted Thermal Radiation, Channels 1, 2, and 4.* Two laboratory blackbody targets, placed in a container so that liquid or gaseous nitrogen could flow around them, were used in the calibration procedure. At a certain radiometer housing temperature, T_C, regulated by the temperature of alcohol flowing through tubes in thermal contact with the radiometer housing in a vacuum chamber, liquid nitrogen, at −196°C, was pumped through the tubes in one target while the temperature of the nitrogen flowing through tubes in the other target was varied from −196°C to about +40°C. This procedure was carried out at seven different radiometer housing temperatures (0°, 7°, 12°, 18°, 25°, 32° or 35°, and 40°) while viewing the warm target respectively through the wall and floor sides of the radiometer. The temperatures of each target were recorded by means of thermocouples. Using the frequency, F_{SC}, to digital number, D, conversion, shown schematically in Figure 10(d), a curve of T_{BB} vs. D and F_{SC} was constructed for each channel on both wall and floor sides for each of the seven values of T_C (Figures 19-32 and 40-46). If the quantity $\overline{W}$ is desired, it may be determined from the $\overline{W}$ vs. T_{BB} graphs for each channel (Figures 7-9). The complete calibration procedure is shown schematically in Figure 54(a).

3.6.2 *Reflected Solar Radiation Channels 3 and 5.* A tungsten filament lamp calibrated by the National Bureau of Standards was used in the calibration procedure as a standard source. Radiation from the lamp was diffusely reflected from a sheet of white Kodak paper of known spectral reflectivity. The output signal of each channel was read with the illuminated paper normal to rays from the lamp and completely filling one field of view of the radiometer. The other field of view was covered with black tape. In order to obtain more than one point per calibration, the white paper was placed at different distances from the tungsten lamp. The effective radiant emittance was computed using

$$\overline{W} = \frac{\cos\gamma}{R^2}\int_0^\infty J_\lambda\, r_\lambda\, \varnothing_\lambda\, d\lambda. \qquad (5)$$

A curve of $\overline{W}$ vs. $V_{R,1D}$ was then constructed, with T_C being the ambient temperature of the room in which the calibration was made. In order to construct $\overline{W}$ vs. F_{SC} curves at various values of T_C, it was necessary to make additional measurements in vacuum where T_C could be controlled. Two targets consisting of diffusers illuminated by light bulbs, one target for each of the wall and floor sides, were used for both channels in this calibration. Since the voltages could be regulated, a certain range of voltages was selected and measurements at the various values of T_C were made of each voltage, recording corresponding radiometer voltage and output frequency at each level. Measurements were made by illuminating alternately both wall and floor sides, keeping the lights off on the side that was to simulate space viewing. In order to correlate the vacuum measurements with the tungsten-filament lamp source measurements, it was necessary to make one set of vacuum measurements at the same T_C as for the air measurements. By relating bulb voltage levels to $\overline{W}$ at the air measurements, $\overline{W}$ vs. F_{SC} and D curves were constructed for T_C of 0°, 7°, 12°, 18°, 25°, 35° and 40° (Figures 33-39 and 47-53).

In order to calculate the reflectance (loosely, "albedo") from the incident solar radiation of a spot on earth viewed by the radiometer, one must know the effective solar constant, $\overline{W}^*$, the particular value of $\overline{W}$ which would be measured if the spot viewed were a perfectly diffuse reflector, having unit reflectivity, and illuminated by solar radiation at normal incidence. Using equation (5) for this calculation, and setting $\gamma = 0°$, $R = 1$ astronomical unit, $r_\lambda = 1$, and $J_\lambda = W_\lambda(T) \times$ (cross-sectional area of sun)$/\pi$, we have

$$\overline{W}^* = \frac{\Omega}{\pi}\int_0^\infty W_\lambda(T)\, \varnothing_\lambda\, d\lambda. \qquad (6)$$

Calculations of W^* were made taking the sun as a 5800°K blackbody for channel 3 and a 6000°K blackbody for channel 5, yielding values of 484.36 watts/meter^2 and 117.13 watts/meter^2, respectively. The complete calibration procedure is shown schematically in Figure 54(b).

3.6.3 *History of the Radiometer Subsystem from Initial Calibration Until Launch.* In the original calibration the radiometer was placed in a high vacuum chamber while the electronics canister was placed in a thermally-controlled environmental chamber. Between the original calibration carried out at the Goddard Space Flight Center during the period April 1-27, 1963 and the launch of the satellite on June 19, 1963, several check-of-calibration measurements of all channels were made under varying conditions of pressure (ambient as well as high vacuum) and of housing and infrared target temperatures. These checks indicated that the original calibration of channels 1, 2, 3, and 5 remained essentially unchanged. This behavior contrasted with the behavior of channels 3 and 5 of TIROS IV which showed a marked decrease in response after the original calibration and before launch (see Section 3.6 of *TIROS IV Catalog-Manual.*[1]) The check-of-calibration of channel 4 of TIROS VII, on the other hand, showed a shift to higher frequencies by two and one-half cps. This shift was not due to an increase in the radiometer voltage output, but was due to an increase in the frequency output of the oscillator. Each check-of-calibration was for a relatively short period of time, the longest being about two hours, and it was, therefore, not possible to determine whether the shift was a function of temperature change or a function of the short running time of the radiometer. An in-flight check of the space-viewed level showed that within three days after launch, the frequency had returned to the calibrated space-viewed level. This return was also accompanied by a decrease of T_c from 20°C to 2°C; however, an increase of T_c to 27°C on TIROS VII Day 31 was not accompanied by a shift of the frequency and the observed space-viewed level remained essentially consistent with the calibration through September 30, 1963. The behavior of channel 4 is discussed further in Section VI.

3.7 *Field of View Measurements*

The Barnes Engineering Company made field of view measurements of the various channels of the TIROS VII radiometer. A line source consisting of a filament wire, 0.040 inches in diameter, was used. The line source remained in a plane perpendicular to the geometric axes, about 54 inches from the thermistor bolometers in the wall direction (where 1 inch normal displacement ~1°). The line source was moved from right to left looking out from the radiometer in the wall direction (horizontal field of view measurements) and from top (up) to bottom (down) in the wall direction (vertical field of view measurements). The line source was kept normal to its direction of motion across the field of view during both horizontal and vertical measurements. These measurements are shown in Figures 55-59. Laboratory measurements for the floor side are not available.

Alignment measurements were made by RCA after the radiometer was mounted on the base plate of the satellite. A line source was moved from top to bottom to determine the vertical field of view from the wall side. These measurements and resulting computations to determine the optical angle with respect to the base plate and the error angle from the design-value of 45° to the spin axis are given in Table XIII. These measurements show that the optical axes for channels 1, 3, and 5 are very nearly coincident with the 45° line, whereas, for channels 2 and 4 the optical axes are misaligned by approximately 1¾° and 1¼°, respectively; and are misaligned relative to each other by 3°.

3.8 *Summary of the Calibration*

When a certain value of effective radiant emittance $\overline{W}$ or equivalent blackbody temperature T_{bb} is viewed by the radiometer through a given side with a given radiometer housing temperature an output signal F_{sc}

results. If T_E and T_C are within $\pm 7°C$ of the relationship,

$$T_E = T_C + 10°C$$

and if the T_C's, deduced from the component temperature, T_V, are correct, only a negligible error in T_{BB} or $\overline{W}$ is introduced. From F_{SC} and T_C, which are measured independently, the measured value of T_{BB} or $\overline{W}$ can be determined from the calibration curves.

The calibration for each side of each channel is carried out for seven parametric values of T_C; hence, it is necessary to interpolate between two transfer functions bracketing an actual value of T_C to arrive at the calibration for a given orbital period.

IV. RADIATION DATA PROCESSING

4.1 *Information Flow in the Satellite* [6,45]

The radiation experiment instrumentation is independent of the television camera system except for power, command, certain timing signals, and antennas (Figure 60). The output of the five medium resolution radiometer channels is fed into five subcarrier oscillators. These voltage controlled oscillators are of the phase shift type with symmetric amplifiers in the feedback loops, the gains of which are controlled by the balanced input signal. A sixth channel is provided for telemetry of the University of Wisconsin's heat balance data; data from an electron temperature measuring probe; the environmental temperatures; and the instrumentation canister pressure. In channel 6, a mechanical commutator switches resistive sensors in one branch of a phase shift oscillator. These sensors stopped switching after orbit 1276 in TIROS VII and remained set on the electron temperature probe sensor. Thereafter, the radiometer housing temperature (one of the environmental temperatures) was derived from the TV clock No. 2 temperature of the satellite, available upon interrogation. The seventh channel, a tuning fork oscillator, serves as a reference frequency and timing signal. The outputs from each of the seven channels are summed and the resultant composite signal equalized in a record amplifier which drives the head of a miniature tape recorder. An oscillator provides an alternating current bias to the record head and the signal required for the erase head. For convenience, erase of the magnetic tape occurs immediately before recording. The record spectrum extends from 100 cps to 550 cps. The tape recorder is an endless-loop, two speed design running at 0.4 ips record and 12 ips playback speed. The endless loop records continuously, day and night, except during a playback sequence. A hysteresis synchronous motor generates torque in the record mode through a mylar belt speed reduction. The fourth subharmonic of the tuning fork oscillator, generated by flip flops, drives a cam shaft which activates a bank of microswitches connected to the five commutated subchannels of the time-sharing sixth channel. Each is sampled for six seconds and the fifth includes a group of seven to be subcommutated.

Playback is initiated upon command by applying power to a direct current motor. A magnetized flywheel generates a frequency proportional to the motor speed. A frequency discriminator feeds the error signal to the stabilized power supply of the motor and closes the servo loop. Playback speed is essentially constant from 0° to 50°C. A low flutter and wow of 2.5% peak-to-peak, measured without frequency limitations, is achieved by using precision bearings and ground-in-place shafts having tolerances of better than 50 parts per million. A command pulse activates the playback motor, the playback amplifier, and the 238 mc FM telemetry transmitter feeding the duplexer and antenna.

The playback time, approximately 200 seconds, is controlled by a switch which operates only during the playback mode. This switch rotates one revolution in 200 seconds, activating a microswitch which returns the system to the record mode and, thus, terminates the playback mode with one complete revolution of the magnetic tape. However, the playback mode experienced a malfucntion at low temperatures in TIROS

VII from Orbit 573. Due to an apparent frictional drag on the shaft by the clutch in the mechanical linkage from the record motor to the reduction gears, the switch was rotated during the record mode. Consequently, at the start of the playback mode, the switch was in such a position that less than one complete revolution of the tape was required before the switch activated the return to record mode. This necessitated another command signal to be sent to initiate a second and complete playback of the tape. Some data were lost, since at the termination of the first playback, the record mode erased the data on the tape; thus, only data from the end-of-tape to the beginning of the second playback were recovered. Fortunately, the first playback, although variable in length, was short, resulting in the loss of only a small amount of data from each orbit.

In order to permit comparison of the radiation data with TV pictures, each TV shutter action generates a 1.5 second pulse which is recorded as an amplitude modulation of the channel 7 timing signal.

There are nine solar cells mounted behind narrow slits for north angle determination. These slits have an opening angle of close to 180° in planes through the spin axis. The sun illumination generates pulses as long as illumination parallel to the spin axis is avoided. One of these sensors generates a 0.5 second pulse in addition to the north indicator code so that spin rate information and a measurement of relative sun position is available. Again, this pulse is recorded as an amplitude modulation of channel 7.

Reconstruction of the radiation information vitally depends on its correlation with absolute time. An accurate, but relative, timing signal is provided for by the tuning fork oscillator and a crude one by the sun pulses, except when the satellite is in the earth's umbra. Absolute time is transmitted to the satellite and recorded on the tape as a one-second dropout of channel 7. This pulse is designated as the End-of-Tape (E.O.T.), and its occurrence is known within milliseconds of absolute time.

4.2 *Information Flow at the Command and Data Acquisition Station* [6,45]

Upon interrogation, the 238 mc carrier is received by an antenna; the composite signal is recorded on magnetic tape and simultaneously fed to a "Quick Look" demodulator (Figure 61a). At the same time, the envelope of channel 7 and the clipped signal of channel 2 are graphically recorded. The 8–12μ "events" on the graphic record show alternately the earth and sky scan intervals as the satellite spins and progresses along the orbit. The channel 7 envelope shows the three distinctive types of AM pulses impressed on the clock frequency during recording; namely ,the sun sensor pulses, the TV camera pulses, and the "end-of-tape" pulse. Auxiliary uses of the radiation data (Figures 61b and 61c) include determination of the spin axis attitude in space and the times when the TV pictures were taken and recorded in the satellite to be read out later over a ground station.

The magnetic tapes are, then, routinely mailed every day to the Aeronomy and Meteorology Division, GSFC, Greenbelt, Maryland.

4.3 *Information Flow at the Data Processing Center* [6,45]

At the Data Processing Center of the Aeronomy and Meteorology Division, the master tapes containing the composite radiation signal are demultiplexed, demodulated, and fed into an analog-to-digital converter (Figure 62). The pressure is read separately. The analog-to-digital converter produces a magnetic "Radiation Data Tape" made up of 36 bit words suitable for an IBM 7094 computer. The sampling rate for data acquired between launch and orbit 1072 was the same as it had been on all previous TIROS five-channel radiometer experiments, i.e., one data sample for every 72nd cycle of the 550 c.p.s. channel 7 clock (or one sample every 0.1309 seconds). *To increase the resolution of the reduced data, the sampling rate was increased by a factor of two beginning with orbit 1080.* For orbit 1080 and all later orbits, therefore, a data sample was digitized

for every 36th clock cycle (or one sample every 0.06545 seconds). The result of this action was merely to double the number of data samples on the FMR tape. An auxiliary form for the repository of the radiation data is the oscillogram, or analog record, produced at this stage of the information flow. The analog record can be used for special "hand" analyses of the data.

4.4 *Information Flow at the Data Reduction Center* [6]

The IBM 7094 computer program requires input from three sources to produce, in binary form, the "Final Meteorological Radiation (FMR) Tapes". One source is the "Radiation Data Tape" containing radiation data and satellite environmental parameters in digital form. Another source is the calibration data for converting digital information to meaningful physical units. The third source is the "Orbital Tape" from the NASA Space Computing Center containing satellite position and attitude data as a function of time. The FMR tape then is the basic repository of data from the medium resolution scanning radiometer. In order to study and utilize the scanning radiometer data, appropriate computer programs must be written to read the FMR tape and provide for printing out data, punching cards, or producing maps. The format of the FMR tape and the make-up of the IBM 7094 computer program which produces it are discussed in detail in sections 4.5 and 4.6.

4.5 *Format of the "Final Meteorological Radiation Tape"*

TIROS VII radiation data are available on high density, binary tapes prepared on an IBM 7094 computer. The FMR tape is the product of a computer program whose input is the orbital data, digitized radiation data, and TIROS VII radiometer calibration data. The make-up of this program is discussed in section 4.6. The FMR tape contains calibrated radiation measurements, geographical locations associated with the radiation measurements, orbital data, solar ephemeris, and satellite environmental temperatures. The exact format of these data is described below. The purpose of this section is to emphasize certain features that will aid programmers in utilizing these data.

Each orbit of radiation data is treated as a file which contains a documentation record plus data records that represent approximately one minute intervals of time. The documentation record is the first record of each file and contains 14 data words whose format is described below. Dref is defined as the number of days between zero hour of September 1, 1957, and zero hour of launch date. TIROS VII time counts zero time as zero hour at Greenwich on the day of launch, thus launch time is given in GMT and launch day is zero day, with succeeding days numbered sequentially. However, the satellite life extends beyond 100 days, and for each succeeding period of approximately 100 days the value of dref is redefined by adding approximately 100, while the TIROS VII day is decreased by the same amount.

Each record of data covers approximately one minute of time, and the data are found in the decrement (D) and address (A) of each data word. The record terminates with the end of swath in progress at 60.0 seconds past the minute specified in words 1D, 1A, and 2D. In the case of satellite-earth orientation such that the radiometer continuously scans the earth for more than one rotation of the satellite, the record will terminate with the end of the revolution in progress at 60.0 seconds past the minute specified in words 1D, 1A, and 2D. The End of File gap will be duplicated at the end of the last file on each FMR tape.

For each earth-viewing swath, the radiation measured from channel 1 (14.8–15.5μ), channel 2 (8.0–12.0μ), and channel 4 (8.0–30.0μ) is reported as an equivalent blackbody temperature in °K, while the radiation measured from channel 3 (0.2–6.0μ) and channel 5 (0.55–0.75μ) is reported as an effective radiant emittance in watts/meter^2. For each fifth measurement in a swath, the point on earth being "viewed" by the radiometer is defined in terms of latitude and longitude. These computations are based on

the best available estimate of satellite attitude.

In order that the user may distinguish between data from the wall and floor sides of the satellite, the data words containing the measured energy are labeled with a 1 in position 19 when the wall side of the satellite is viewing the earth. The user should realize that if the signal from the satellite becomes noisy, swath sizes, as interpreted by the computer, may become abnormal and the data can be labeled and located incorrectly. In order to flag abnormal data, minus signs are inserted for the following three reasons:

1. A measurement within a swath whose digital response falls below the arbitrarily defined threshold between earth and space. (The end of a swath is arbitrarily defined by three consecutive measurements falling below the threshold.)

2. An entire swath is labeled with minus signs when the observed swath size falls outside of the theoretical swath size ±25%. The theoretically computed swath size is based on the best available estimate of satellite attitude, height, and spin rate.

3. The entire swath is labeled with minus signs when it is either the first or last swath in the closed mode. (In the closed scanning mode the radiometer continuously scans over the earth for more than one spin revolution without viewing the horizon or space.)

Channel 3 and channel 5 on TIROS VII can reach a saturation limit at lower radiation intensities than has been the case with any previous satellite. In order to detect this condition, the data word containing energy measured by channel 3 and channel 5 is labeled with a "one" in position 18 whenever the observed energy intensity exceeds the saturation limit. Saturation limits for the wall and floor sides separately are indicated at the upper right-hand extremities of the calibration curves for channel 3 (Figures 33–39) and channel 5 (Figures 47–53). For example in Figure 33 the effective radiant emittance "saturates" at 344.0 watts/meter^2 for the floor side and 333.0 watts/meter^2 for the wall side. *If any higher values of radiant emittance should actually be viewed by the radiometer, they would still be reported as the "saturation values" on the FMR tape.* However, in practice measurements exceeding the "saturation limits" have only rarely been observed in TIROS VII (except in periods when direct solar interference occurs; see Section VI below).

FORMAT OF FINAL METEOROLOGICAL RADIATION TAPE

Documentation Record

Word No.	Quantity	Units	Scaling	Remarks
1	Dref		$B = 35$	Number of days between zero hour of Sept. 1, 1957, and zero hour of launch day.
2	Date			Date of Interrogation expressed as a packed word, i.e., February 8, 1964 would be $(020864)_{10}$ or $(021004)_{8}$. These numbers are shifted to the extreme right side of the data word. Only the last digit of the year is retained for 1964.
3	Day	TIROS VII Day	$B = 35$	Start time of this file of radiation data.
4	Hour	Z Hour	$B = 35$	
5	Minute	Z Minute	$B = 35$	
6	Seconds	Z Seconds	$B = 26$	
7	Day	TIROS VII Day	$B = 35$	*Time of Interrogation*, i.e., end time of this file of radiation data.
8	Hour	Z Hour	$B = 35$	
9	Minute	Z Minute	$B = 35$	
10	Seconds	Z Seconds	$B = 26$	

Word No.	Quantity	Units	Scaling	Remarks
11	Satellite Spin Rate	Deg/Sec	$B = 26$	Satellite spin rate.
12	Frequency	36,72,144	$B = 35$	Data sampling frequency (cycles of a 550 cps tuning fork).
13	Orbit No.		$B = 35$	Orbit No. at time of Interrogation.
14	Station Code		$B = 35$	Code defining ground station ("1" for Wallops Is., Va., "2" for San Nicolas Is., Calif., "3" for Fairbanks, Alaska).
	Format of FMR Tape—Nth Record			
1D	Day		$B = 17$	TIROS VII Day
1A	Hour		$B = 35$	Z time in day specified in word 1D
2D	Minute		$B = 17$	
2A	GHA	Degrees	$B = 29$	Greenwich hour angle and declination of sun at time specified in words 1D, 1A, and 2D. 90° are added to declination to yield positive numbers.
3D	Decl.	Degrees	$B = 11$	
3A	T_c	Degrees K	$B = 35$	Reference temperature of the medium resolution radiometer.
4D	T_E	Degrees K	$B = 17$	Reference temperature of main deck electronics.
4A	Height	Kilometers	$B = 35$	Height of satellite at time specified in words 1D, 1A, and 2D.
5D	Latitude	Degrees	$B = 11$	Latitude of subsatellite point at time specified in words 1D, 1A, 2D. 90° are added to all latitudes to yield positive numbers.
5A	Longitude	Degrees	$B = 29$	Longitude of subsatellite point at time specified in words 1D, 1A, 2D. Longitudes are reported as 0 to 360°, with west being positive.
6D	Seconds		$B = 8$	Seconds past time specified in words 1D, 1A, 2D when first earth-viewing response is detected, and every fifth response thereafter.
6A	Latitude	Degrees	$B = 29$	Latitude of subsatellite point at time specified in words 1D, 1A, 2D, 6D. 90° are added to all latitudes to yield positive numbers.
7D	Longitude	Degrees	$B = 11$	Longitude of subsatellite point at time specified in words 1D, 1A, 2D, 6D. Longitudes are reported as 0 to 360°, with west being positive.
7A	Latitude	Degrees	$B = 29$	Latitude of point on earth being "viewed" by radiometer at time specified in words 1D, 1A, 2D, 6D. 90° are added to all latitudes to yield positive numbers.

Word No.	Quantity	Units	Scaling	Remarks
8D	Longitude	Degrees	$B = 11$	Longitude of point on earth being "viewed" by radiometer at time specified in words 1D, 1A, 2D, 6D. Longitudes are reported as 0 to 360°, with west being positive.
8A	Nadir Angle	Degrees	$B = 29$	Nadir angle of optic axis from radiometer to point specified in words 7A, 8D.
9D	Azimuth Angle	Degrees	$B = 11$	Azimuth angle of optic axis from radiometer to point specified in word 7A, 8D. This angle is measured clockwise from north and expressed as a positive number.
9A	Zero			
10D	T_{BB} (ch. 1)	Degrees K	$B = 14$	Measurement by each of the five medium resolution channels at time specified in 1D, 1A, 2D, 6D when radiometer is "viewing" point on earth specified in words 7A, 8D.
10A	T_{BB} (ch. 2)	Degrees K	$B = 32$	
11D	$\overline{W}$ (ch. 3)	Watts/m²	$B = 14$	
11A	T_{BB} (ch. 4)	Degrees K	$B = 32$	
12D	$\overline{W}$ (ch. 5)	Watts/m²	$B = 14$	
12A	Zero			
13D	T_{BB} (ch. 1)	Degrees K	$B = 14$	The data sample immediately following the measurement recorded in words 10D-12A.
13A	T_{BB} (ch. 2)	Degrees K	$B = 32$	
14D	$\overline{W}$ (ch. 3)	Watts/m²	$B = 14$	
14A	T_{BB} (ch. 4)	Degrees K	$B = 32$	
15D	$\overline{W}$ (ch. 5)	Watts/m²	$B = 14$	
15A	Zero			
16D	T_{BB} (ch. 1)	Degrees K	$B = 14$	The data sample immediately following the measurement recorded in words 13D-15A.
16A	T_{BB} (ch. 2)	Degrees K	$B = 32$	
17D	$\overline{W}$ (ch. 3)	Watts/m²	$B = 14$	
17A	T_{BB} (ch. 4)	Degrees K	$B = 32$	
18D	$\overline{W}$ (ch. 5)	Watts/m²	$B = 14$	
18A	Zero			
19D	T_{BB} (ch. 1)	Degrees K	$B = 14$	The data sample immediately following the measurement recorded in words 16D-18A.
19A	T_{BB} (ch. 2)	Degrees K	$B = 32$	
20D	$\overline{W}$ (ch. 3)	Watts/m²	$B = 14$	
20A	T_{BB} (ch. 4)	Degrees K	$B = 32$	
21D	$\overline{W}$ (ch. 5)	Watts/m²	$B = 14$	
21A	Zero			
22D	T_{BB} (ch. 1)	Degrees K	$B = 14$	The data sample immediately following the measurement recorded in words 19D-21A.
22A	T_{BB} (ch. 2)	Degrees K	$B = 32$	
23D	$\overline{W}$ (ch. 3)	Watts/m²	$B = 14$	
23A	T_{BB} (ch. 4)	Degrees K	$B = 32$	
24D	$\overline{W}$ (ch. 5)	Watts/m²	$B = 14$	
24A	Zero			

The block of data from words 6D to 24A will be repeated, thus defining every fifth measurement in a swath. The address of the third word in the last response of a swath will contain 010101010101010 to signal end of record. A "look ahead" feature is incorporated into TIROS VII data reduction; if the End of Tape signal occurs within an earth-viewing swath, that entire swath is discarded. Each time the swath terminates, two words (N and N+1) will follow the last "earth-viewing" response with the following format:

Word No.	Quantity	Units	Scaling	Remarks
ND	Code	111111111111111		Code indicating end of swath
NA	Nadir Angle	Degrees	$B = 29$	The minimum nadir angle that occurred in the previously defined swath
(N+1)D	Latitude	Degrees	$B = 11$	Latitude of point on earth being "viewed" by radiometer when the minimum nadir angle occurred. 90° are added to all latitudes to yield positive numbers
(N+1)A	Longitude	Degrees	$B = 29$	Longitude of point on earth being "viewed" by radiometer when minimum nadir angle occurred. Longitudes are reported as 0 to 360°, with west being positive.

Occasionally dropouts are encountered and the corresponding data records contain no radiation data. This event is relatively rare in TIROS VII data, but in such cases the radiation data record contains only five words (1D to 5A) which document the record with respect to time. In such records, the datum in the address of the third word (T_c) is destroyed by the End of Record code.

A flow diagram to aid in interpreting this format is shown in Figure 63. It is seen that the format is analogous to four "nested loops" (in programming language), i.e., groups of five responses, entire swaths, one-minute records, and files. It is pointed out that a particular swath (and, hence, a particular record and a particular file) can end either on the "anchor data response" or on any of the four following non-geographically located data responses and that Figure 63 merely illustrates one possible combination of ending responses.

4.6 *IBM 7094 Computer Flow Diagram*

The FMR tape as described in the previous section is prepared with an IBM 7094 computer program whose input consists of orbital data, digital radiation data, and TIROS VII radiometer calibration data. The flow chart shown in Figure 64 outlines the logical steps in this program and thus gives some insight into the mechanics of preparing these tapes. The flow chart has been greatly condensed since it is impossible to present a detailed flow chart within the space limitations of this publication.

The first phase of this program sets up the documentation data and then reads the entire file of radiation data to compute the start time from the end-of-tape time and the data sampling frequency. Given the starting and ending times, the program then searches the orbital tape to find orbital data (subsatellite point, height, nadir angle, right ascension, and declination) covering the same time interval. These data are then arranged in tables as a function of time so that interpolation subroutines can be used in the second phase to obtain values of the orbital characteristics for any specified time.

At this point, an optional feature allows the program to accept the attitude data from the orbital tape, or an alternate estimate of the attitude from a second documentation card. If the alternate attitude is accepted, the nadir angles are recomputed.

The second phase of the program reduces the digitized radiation data into useful meteorological data. This begins with a detailed examination of the radiation data to distinguish between earth and space-viewed data. This distinction is based on an arbitrarily defined threshold value applied to channel 2. Both sides are assumed to be viewing space when the measured radiation falls below the

threshold value, and one side is viewing the earth when the measured radiation exceeds the threshold value. The end of swath is arbitrarily defined as three consecutive space-viewed measurements.

For each earth-viewing swath, the program proceeds to determine which side is viewing the earth, computes the latitude and longitude of the point on earth being "viewed" by the radiometer for each fifth measurement in the swath, and converts the digitized data into radiation units for each measurement in the swath. The data words containing radiation measurements contain a "1" in position 19 when the wall side is viewing the earth, and a "1" in position 18 when the response from channel 3 or channel 5 exceeds saturation.

Each record on the FMR tape covers approximately one minute of time and terminates with the end of swath in progress at 60.0 seconds past the minute. When the end of tape is encountered, the program writes the last data record and reinitializes in preparation for the next orbit of radiation data.

V. RADIATION DATA COVERAGE AND DOCUMENTATION

5.1 *Radiation Data Coverage*

The discussion in this section concerning the radiation data coverage parallels the discussion by Widger and Wood [16] on the photographic coverage by the TIROS satellite.

The geographical area from which significant meteorological radiation data are obtained by TIROS VII is limited mainly to the area between 58.2°N and 58.2°S. The latitudinal limitation is due to the 58.2° inclination of the orbital plane to the equatorial plane.

The longitudinal limitation is imposed on obtaining radiation data due to the location of the Command and Data Acquisition stations since the range at which each station can contact the satellite and acquire data is limited to the line of sight from the ground to the satellite. To obtain as noise-free data as possible the antenna elevation angles are generally limited to a minimum of 10° above the horizon. Figure 65 shows the data acquisition circles for a 10° antenna elevation angle at Wallops Island, Virginia; San Nicolas Island, California; and Fairbanks, Alaska. Mountain ranges south of the Fairbanks station prevent the acquisition of data for elevation angles less than 17.8° which causes a perturbation of the 10° elevation circle between azimuth angles of 158° and 202° (measured clockwise from true north).

Figure 65 also shows the trace of the subpoint tracks for 10 successive orbits. This series of tracks shows that only a maximum of 9 orbits can be interrogated in one interrogation day. If orbit N can just be acquired by the Wallops Island station, then orbit N+9 is the first orbit which cannot be acquired by the Fairbanks station. The dashed line shows the last orbit which may be acquired by Fairbanks. Orbits with ascending nodes from longitude 70°E westward to longitude 75°W cannot be acquired by any of the stations. Also orbit N+4 is only rarely acquired since either its subpoint track falls between the San Nicolas and Fairbanks acquisition circles or if the track does cross the Fairbanks circle, there is insufficient time to playback the data.

The interrogation day includes all orbits interrogated in the series of 9 consecutive orbits which come within range of the acquisition stations during each 24-hour period as shown in Figure 65. The interrogation day can and often does occur on two separate calendar days. The shaded area of Figure 65 shows the geographical area where nearly all radiation data are acquired. The unshaded areas between 58.2°N and 58.2°S latitude show the longitudinal limitation on the acquisition of data due to the location of the acquisition stations. Because of the inclination of the sensors to the spin vector and/or the precession of the spin vector, some data are acquired to about 69°N and 69°S latitude. However, the number of data samples acquired in this area is small compared to the number in the shaded area of Figure 65.

Further latitudinal limitations are imposed on obtaining reflected solar radiation meas-

urements because of the need for solar illumination. Because of the slight bulge of the earth at the equator, the satellite orbital plane precesses in right ascension at the rate of −3.76 deg/day. This is illustrated in Figure 66, where the spin vector and orbital plane orientation for selected orbits of TIROS VII, as viewed from the sun, are shown. The quantity $\Delta\varnothing$ is defined as the right ascension of the sun minus the right ascension of the orbital ascending node. Due to the precession of the orbital plane and the movement of the earth in its orbit, a complete cycle of the precession of the plane of the satellite's orbit relative to the sun (synodic period) is completed in about 75.9 days.

For any single day the plane of the satellite orbit remains nearly fixed in absolute space while the earth rotates within the orbit. Thus, at a given latitude and considering only solar illumination, reflected solar radiation could be obtained for all longitudes during any single day. The precession of the orbital plane causes the illuminated latitudes, as seen by the satellite, to change during one synodic period as described below. In the following discussion, the solar illuminated area (where solar radiation data are available) is defined by requiring the solar zenith angle to be less than 70° and the "scan nadir angle" (i.e., the nadir angle of the radiometer optical axis) to be less than 58°. The following discussion is concerned only with the availability of reflected solar radiation measurements.

The time of the TIROS VII launch was chosen so that the heliocentric orbital geometry shown in Figure 66a resulted, and reflected solar radiation data were obtained from about 26°S to 69°N latitude. After about 10 days, the orbital plane and the sun have moved to a $\Delta\varnothing$ of 180° (Figure 66b) which means that the descending node occurs on the meridian of the subsolar point. At this time, reflected solar radiation data can be obtained from about 46°S to 69°N latitude. By TIROS VII Day 29, or 29 sequential days after launch day, $\Delta\varnothing$ is 270° (Figure 66c) and the southern part of the orbit is over the sunlit side of the earth, while the northern portion of the orbit is on the dark side. However, since the subsolar point is in the Northern Hemisphere at a declination of 21.1°, and since useful solar radiation data are defined for a solar zenith angle of less than 70°, only latitudes north of about 49°S are thus illuminated. Therefore, solar radiation data are not available because the data are obtained south of 49°S on the sunlit side of the earth, while the satellite is in the Northern Hemisphere only at night. On TIROS VII Day 48, $\Delta\varnothing$ is 0° and the ascending node of the orbit is on the sunlit side of the earth (Figure 66d). Reflected solar radiation data are available from 53°S to 69°N latitude. Continued precession until TIROS VII Day 67 moves the orbit to a $\Delta\varnothing$ of 90° (Figure 66e) where the solar data coverage is from 8°N to 69°N latitude. At this time the satellite is in the Southern Hemisphere only at night. On approximately TIROS VII Day 75.9, the orbital plane has the same orientation with respect to the sun as at launch. The whole precession cycle then repeats with a synodic period of about 75.9 days throughout the satellite's lifetime. The northern and southern latitudinal limits of reflected solar radiation coverage vary from one synodic period to the next due to the changing subsolar latitude.

The reflected solar radiation coverage for TIROS VII from June 19, 1963 to September 30, 1963 is summarized in Figure 67. The shaded area indicates the illuminated latitudes for each TIROS VII Day. Disregarding the solar illumination requirement, the medium resolution radiometer latitude coverage extends from 69°N to 69°S. However, reflected solar data could not be acquired for all latitudes between 69°S and 69°N due to inadequate illumination and the position of the orbital plane in relation to the sun. Reflected solar data for one period (centered at TIROS VII DAY 29) were essentially nonexistent since the satellite was in the northern hemisphere at night and crossed the high poorly-illuminated latitudes in the sunlit southern hemisphere in the daytime.

5.2 *Documentation of Radiation Data*

The radiation data available on the FMR tapes have been documented in an Index of Final Meteorological Tapes. This Index, which is found in Appendix A, lists information for the orbital ascending node, the spin vector attitude, and the spin rate for every TIROS VII orbit for which radiation data are available. The time interval for which radiation data are available in each processed orbit is also listed in Appendix A.

For each interrogation day, the time interval for the radiation data on the FMR tapes is summarized diagrammatically on the subpoint tracks for that day. Information concerning the minimum nadir angle is also included. The presentations are located in Appendix B and are identified by calendar date. This presentation allows the user to find applicable orbits quickly and approximate the geographical area of radiation data coverage. The user of reflected solar radiation data should also refer to Figure 67 to determine the latitudinal extent of the reflected solar radiation data coverage.

VI. PRE-LAUNCH AND POST-LAUNCH PERFORMANCE OF THE RADIATION EXPERIMENT

6.1 *Pre-Launch Behavior of the Experiment*

As indicated in Section 3.6 pre-launch checks of calibration made between 27 April and 19 June 1963 did not indicate any change in the response of channels 1, 2, 3, and 5. But due to an apparently unstable transistor, the channel 4 oscillator frequency-vs.-voltage curve was observed to have shifted upward about 2½ c.p.s. several days before shipment of the radiometer from the RCA factory to Cape Kennedy. This effect persisted for a few days after launch, after which it was observed to diminish (cf. Figure 68a).

Although pre-launch calibration tests did not show any degradation for channels 3 and 5, their initial "quasi-global" albedos are considerably lower than expected and required for internal consistency with measurements from the long-wave channels. Therefore, the possibility of a degradation of channels 3 and 5 occurring sometime before acquiring data from the first orbit can not be discounted; on the other hand, the explanation may lie in other areas, as yet undetermined.

6.2 *Post-Launch Behavior of the Experiment*

There is strong evidence that all channels of the TIROS VII medium resolution radiometer changed in response after going into orbit, as did all channels of previous instruments flown on TIROS II, III, and IV.[47,1] The post-launch degradation has been observed in two ways. First, as pointed out in Section 3.5 the space-viewed level can be considered to be a single-point check of calibration, and any shift observed in this level after the original calibration indicates that a change has occurred in the system. A shift could be caused by an imbalance which develops between the floor and wall optical paths in one of the emitted thermal radiation channels, or by a drift of the transfer functions of the satellite-borne electronics associated with either the reflected solar or thermal radiation channels (a detailed discussion of possible mechanism's for explaining instrumental degradation is found in the "TIROS III Radiation Data Users' Manual Supplement"[47] and will not be repeated here). Because the ground demodulation equipment is readily accessible and constantly checked and aligned, the possibility of its contributing to a persistent shift in the space-viewed level can be discounted.

The weight of evidence to date indicates that the primary cause of shifts of the space-viewed levels of the thermal radiation channels of previous TIROS radiometers has been an imbalance which developed between the floor and wall paths of the optics. This type of degradation is accompanied by characteristic "negative-going pulses" and is called "asymmetrical optical degradation.[47]" Because a shift in the space-viewed level due to asymmetrical optical degradation results from chopped thermal radiation emitted

from components of the radiometer within the passband of the filter, it follows that this type of degradation cannot be a cause of a shift in the space-viewed levels of the reflected solar radiation channels which are not sensitive in the infrared. In the period between launch and 30 September 1963 no appreciable asymmetrical optical degradation was detected in any of the channels of the TIROS VII radiometer.

However, for the first time, strong evidence exists that "electronic degradation" occurred in TIROS VII. Electronic degradation is uniquely characterized by a shift in the space-viewed level (without accompanying negative-going pulses in the case of a thermal radiation channel).[47] As previously indicated, this type of degradation was observed before and immediately after launch in channel 4. The shifts of the space-viewed levels, ΔF, of all channels of TIROS VII are shown in Figures 68a and 68b. Evidence of electronic degradation occurring in the channel 4 oscillator is seen in the initial ΔF value of 2.5 c.p.s. This value decreases rapidly within the first several days and remains at a value of about -0.75 c.p.s. for the remainder of the first 1525 orbits. Because of certain inaccuracies in determining the space-viewed levels, values of ΔF whose absolute magnitudes are less than 1 are not considered to be significant. Using this criterion there is evidence of some electronic degradation in channel 3 after orbit 500 when its ΔF dips slightly below -1.0 and stays there for the remainder of the first 1525 orbits. The ΔF values of all other channels generally stay within ± 1 c.p.s. throughout the first 1525 orbits.

As pointed out in the "TIROS III Supplement,[47]" it is very difficult to distinguish between the effects of a rotation in the oscillator transfer function and symmetrical optical degradation; hence, we shall adopt a *"compound degradation model" which considers electronic degradation and which may or may not include symmetrical optical degradation.* A schematic representation of this model is shown in Figure 69. The single transfer function shown applies to the combination of a voltage controlled oscillator and its associated radiometer channel (cf. Figure 10). From Figures 33-39 and 47-53 it is seen that the idealized linear transfer function of Figure 69 is a fairly good approximation. From Figure 69 it follows that the correction for a degraded measurement, $\overline{W'}$, is given by

$$\overline{W} = \kappa^i \, [\overline{W'} + \rho^i] \qquad (7)$$

where κ^i and ρ^i are parameters which are a function of the orbit number, i. When there is no shift in the space-viewed level (i.e., when $\Delta F = 0$ and, therefore, $\rho^i = 0$), Equation (7) reduces to the form

$$\overline{W} = \kappa^i \, \overline{W'} \qquad (8)$$

which is equivalent to that employed in the symmetrical optical degradation model.[47]

Symmetrical optical degradation may exist for all channels without any shift occurring in the space-viewed levels. In the absence of an adequate on-board calibration, this type of degradation has been indicated by the behavior of large quantities of data analyzed statistically by a computer program originally designed to study the "quasi-global" heat balance. This program (designed for the earlier TIROS experiments where the orbital inclinations were 48°) analyzes data acquired within the broad zone between 55°N latitude and 55°S latitude. In applying this program to TIROS VII, some high-latitude data are rejected because, with a 10°-larger orbital inclination, additional radiation measurements were made poleward of the 55° latitudes. Also (as in the previous TIROS experiments) there are areas equatorward of the 55° latitudes where data cannot be acquired due to the locations of the Command and Data acquisition stations. Nevertheless it was felt justified to use the existing computer program, with some modifications, to investigate possible degradation of the TIROS VII radiometer sensors. Throughout this volume, then, the term "quasi-globe" shall refer to that portion of the broad zone between 55°N latitude and 55°S latitude where data were acquired by the TIROS VII radiometer.

The "heat balance" program was designed to convert individual measurements from

channels 2 and 4 to total outgoing long-wave flux, W, by the methods given by Wark, Yamamoto, and Lienesch [33] and to average the calculations accumulated throughout a sustained period over time and area to yield the "cumulative quasi-global emitted radiant power." The program was also designed to calculate reflectances from individual measurements from channels 3 and 5 according to the Lambert cosine law and to average the calculations accumulated throughout a sustained period over time and area to yield the "cumulative quasi-global albedo."

Two specific modifications to the program (as it was used in the TIROS II, III, and IV analyses) were made for the TIROS VII degradation analysis (cf. References 1 and 47):

1. In the TIROS VII analyses the computer calculated daily averages from day 0 to day 38 and two-daily averages thereafter, instead of "cumulative" averages over sustained periods, which mask the true magnitude of the day by day changes in the instrument [1, 47], and

2. In the TIROS VII analyses of channels 2 and 4 the computer averaged measurements of effective radiant emittance, $\overline{W}$, directly, instead of converting the measurements to total outgoing long-wave flux, W, which serves to mask the true magnitude of the instrumental degradation.[1, 47]

Except for these two modifications the program operated with minor modifications in the same way that it had for the previous TIROS satellites. A full discussion of this program and of the models which attempt to correct the degraded measurements is found in the "TIROS III Supplement [47]" and will not be repeated here.

Although this volume is concerned only with the first 1525 orbits (days 0-103), results from computer runs using data acquired within the first 380 days are shown in Figures 70-74. Data after day 103 become progressively more sparse in these Figures because much of the data is not yet reduced to the FMR tape format. However, the results available at this time are shown to indicate possible long-term fluctuations which may be due to such factors as seasonal changes and the cyclic variations in the orbit—sun phase geometry (due to the regression of the orbital nodes and the opposing motion of the sun), rather than simply to instrumental degradation. Smoothed curves of the average quasi-global effective radiant emittance, $\overline{W^i}_{ave}$, and of the quasi-global albedo, A^i, are shown for the thermal channels (1, 2, and 4) and the reflected solar radiation channels (3 and 5) respectively vs. days after launch in Figures 70-74. Each of these Figures shows a more-or-less rapid decrease in the magnitude of its measurements with time. There remains the question of the absolute accuracies of the initial measurements in Figures 70-74, and this question must be answered before attempting to determine corrections to be applied to the measurements on the FMR tapes to account for degradation in the instrumental response (or for any other systematic factors contributing to the observed behavior of the experiment).

Of the five channels only channels 1 and 2 yield measurements in the first few days after launch in whose absolute values we have high confidence. Both of these channels showed stability in pre-launch checks-of-calibration and other tests and the validity of their calibrations have been confirmed by several post-launch studies. The validity of the initial measurements in the 14.8-15.5 micron region has been shown in papers by Bandeen et al.[9] and Nordberg et al.[10] The validity of the initial measurements in the 8-12 micron window has been confirmed by comparing the differences between climatological oceanic temperatures and channel 2 T_{BB} measurements over clear skies with the estimated differences given by Wark et al.[33] In general the two differences compared within 5°K.

On the other hand the initial T_{BB} measurements by channel 4 appear to be definitely too high (i.e. approximately equal to the channel 2 measurements), and this offset is attributed to a shift in the oscillator connected with the unstable transistor and observed rise in the space-viewed level previ-

ously discussed (this characteristic is evident in the beginning of Figure 72). From Figures 73 and 74 the initial quasi-global albedos calculated from channels 3 and 5 are about 20%. This value is similar to those of the initial albedos measured by previous TIROS satellites[1, 47] and, for as yet unexplained reasons, is apparently much too low.

A recent study of the planetary heat balance, using selected portions of data from TIROS VII over a period of one year, compares the planetary albedo as inferred directly from channel 5 measurements with the albedo required by the total outgoing long-wave flux inferred from channel 2 measurements in combination with the assumption that planetary radiative equilibrium exists over the year.[48] Channels 2 and 5 were chosen over channels 4 and 3 for this study because the long term stability aspects of each of the former were superior to those of the latter. The conversion of the essentially beam measurements of channel 2 to total outgoing flux was accomplished by the method of Wark et al,[33] and the data were extrapolated beyond latitudes 63.5° to each pole by paralleling the data given in the Northern hemispheric study of London.[49] Even after correcting the albedo values for the *apparent degradation* of channel 5 a planetary albedo of only 20.1% resulted. However, the albedo required by the long-wave measurements with the assumption of annual radiative equilibrium was 32.2%. The resulting ratio

$$\frac{32.2}{20.1} = 1.60 \qquad (9)$$

then represents the *adjustment factor* by which channel 5 measurements must further be multiplied even after correcting for all *apparent degradation* (assuming that the long-wave measurements are correct). Albedo measurements from all previous TIROS satellites have seemingly been too low by approximately the same factor, 1.60, and it is interestingly close to 1.7, an "adjustment" factor suggested by Fritz et al.[15] for channel 3 of TIROS III in a study concerning atmospheric absorption of solar radiation.

A further characteristic pointed up by the planetary heat balance study is the marked cyclic variation occurring over each 76-day orbital synodic cycle (cf. Figure 66). In Figure 75, taken from the study,[48] the over-all averages of channel 2 effective radiant emittances over the globe between latitudes 63.5° N and S are shown for each of 19 weekly periods during the first year of TIROS VII (dots with bars). The 19 periods are numbered along the upper abscissa. The Roman numerals indicate the calendar months represented by groupings of four consecutive periods used in seasonal analyses. The orbit-sun phase geometry is shown by the sinusoid. For example, the solar meridian is over, respectively, the descending node, the southern-most point, the ascending node, and the northern-most point of the orbit at mid-week of periods 2, 3, 4, and 5, which also correspond to 29 June, 18 July, 6 August, and 25 August respectively (cf. Figure 66). All periods are similarly spaced every quarter synodic period (i.e. 19 days) except 1 which occurs immediately after launch, 19 which duplicates the geometry of 1 a year later, and 14 which was delayed 9 days because of solar interference in the short-wave channels when the sun was over the descending node. A least-squares quadratic curve is shown for these over-all "map averages." However, there are unavoidable gaps in the data coverage, caused by such factors as noise and engineering considerations preventing the successful acquisition and reduction of every possible orbit, which might bias the map averages. Upon close examination of the data, such biases were ascertained in the map averages of Figure 75. Therefore, averages of the $\overline{W}$ values over an equatorial region of the Pacific Ocean which was uniformly covered by all 19 weekly maps were calculated and plotted (squares). The approximate boundaries of this area were 30°N, 150°W — 30°N, 120°W — 30°S, 150°W — 30°S, 180°. A least-squares quadratic fit for the Pacific Ocean averages is shown in Figure 75. This curve indicates virtually the same rate of degradation as the curve in Figure 71 and is interpreted as representing the

true instrumental degradation. An unmistakable cyclic pattern stands out in both types of data but especially in the Pacific Ocean averages. The highest values occur when the sun is over (or near) the descending node (i.e., periods 2, 6, 10, 14, and 17), with successive decreases over the following three periods. Only period 16 deviates from this pattern. The reason for this pattern is not clear at this time but is under investigation. From Figures 65, 66, and 75, it is seen that the highest values over the Pacific Ocean region occur near local midnight when viewing through the wall side only whereas the lowest values occur near local sunrise when viewing through both the floor and wall sides. If the lowest values over the Pacific Ocean had occurred one period earlier (i.e. near local noon when viewing through the floor side only) one would be tempted to conclude that there is a difference in the wall and floor calibrations. On the other hand one must be cautious in concluding that the variations are due *only* to diurnal meteorological effects (e.g. clouds) in view of the possibility of a difference between the floor and wall which does not manifest itself in an observed shift in the space-viewed level (cf. 6.2.1 below). The second-order corrections mentioned in Section 3.4 for the variations of T_C over an orbit were applied with the aid of Figures 17 and 18 and Figures 26-32 in producing the map averages and Pacific Ocean averages shown in Figure 75. These corrections amounted to about one-fifth of the observed periodic amplitudes in Figure 75 and actually served to *decrease* them slightly compared to the values calculated directly from the FMR tapes (where a mean value of T_C was assumed throughout each orbit in originally reducing the data). Thus the fluctuations of T_C over an orbital period cannot explain the 76-day periodicity of Figure 75. It is also evident from Figure 75 that such cyclic variations might be misinterpreted as being due to instrumental degradation in a shorter-lived satellite.

In comparing data from channels 2 and 4, the method developed by Wark et al.[33] for converting T_{BB} (or $\overline{W}$) measurements from these channels to total outgoing long-wave flux, W, was utilized. Plots of W vs. T_{BB} (and $\overline{W}$) calculated for three zenith angles are shown in Figure 76 (specifically, the equations for TIROS III and TIROS IV given in the Supplement to MSL Report 10[33] were used). The following linear fits were adopted for comparing data from channels 2 and 4 of TIROS VII:

$$\text{Chan. 2} \ldots W = 98.35 + 6.32\,\overline{W} \quad (10)$$

$$\text{Chan. 4} \ldots W = 20.79 + 4.92\,\overline{W} \quad (11)$$

Because of the angular motion of the spin vector of TIROS over the celestial sphere[44] (Figure A-1), occasionally the 45° half-angle conical figure, generated by the radiometer axis in the wall direction as the satellite spins, intersects the direct rays of the sun. Under these conditions, direct solar radiation impinges upon the sensors from the wall direction momentarily once during each satellite rotation. Such an unfavorable satellite-sun geometry will exist until it is eliminated by a change in the attitude of the spacecraft. There were three periods in the history of TIROS VII between launch and September 30, 1963, when such an unfavorable geometry occurred, viz., the periods including the orbits numbered 0321-0343 (TIROS VII days 22 and 23), 0452-0562 (days 30-38), and 1401-1466 (days 95-99). When the direct solar radiation interference affects the long-wavelength channels the data are not reduced. However, in several orbits where there was no interference with the long-wavelength channels but interference with the short-wavelength channels only, the data were reduced. Data users should note that these "sun spikes" in the short-wavelength channels will produce erroneous values. Mapping of these data is especially misleading; however, one can recognize and eliminate these "sun spikes" from computer listings of the data.

6.2.1 *Channel 1* The history of ΔF is shown in Figure 68a. The absolute magnitude of all values is less than 1 except for a few initial measurements which are only slightly greater than 1. Therefore the symmetrical optical degradation model[47] was used, assuming

that the smoothed curve in Figure 70 represents the true degradation of the instrumental response. The resulting correction nomogram is shown in Figure 77. These corrections are to be added to the wall and floor T_{BB}' measurements contained on the FMR tape. *In addition to the nomogram corrections there is evidence of another deviation from the original preflight calibration.* In a study of channel 1 data [10] it was found that measurements made over the same area a few minutes apart through the floor and the wall sides differed by varying amounts, generally from 4° to 6°K up to orbit 1525, with the measurements made through the floor being the higher. No consistent pattern has been detected, and we have as yet no satisfactory explanation for this effect. Such a difference between floor and wall measurements could readily be explained by the asymmetrical optical degradation model given in the "TIROS III Supplement [47]" *if negative-going pulses were observed. But no negative-going pulses are observed* in the channel 1 data, and additional investigations are now under way attempting to explain this phenomenon. Hence, for the lack of a better procedure at this time, we suggest increasing the wall measurements by an additional 2° to 3°K and decreasing the floor measurements by the same amount. For example, from Figure 77, it is seen that an equivalent blackbody temperature of 220°K measured by channel 1 during orbit 450 should be increased by 6°K, and further modified by 2.5°K, yielding a corrected wall measurement of 220° + 6° + 2.5° = 228.5°K or a corrected floor measurement of 220° + 6° −2.5° = 223.5°K.

6.2.2 Channel 2 The history of ΔF is shown in Figure 68a. The absolute magnitude of all values is less than 1. Therefore, the symmetrical optical degradation model [47] was used, assuming that the smoothed curve in Figure 71 represents the true degradation of the instrumental response. The resulting correction nomogram is shown in Figure 78. These corrections are to be added to the wall and floor T_{BB}' measurements contained on the FMR tape. For example from Figure 78 it is seen that an equivalent blackbody temperature of 260°K measured by channel 2 during orbit 1050 should be increased by 2°K, yielding a corrected measurement of 262°K.

6.2.3 Channel 4 The history of ΔF is shown in Figure 68a showing an initial value of +2.5 c.p.s. The lack of any "negative-going pulses" indicated that the degradation was at least partially electronic in nature, and the previous knowledge of an unstable oscillator transistor pointed to a shift in the frequency-voltage transfer function of that component. The compound degradation model was used in the initial degradation analysis in the manner described below.

From Figure 69 and equation (7) we can write

$$\overline{W}(T_{BB}) = \kappa^i \left[\overline{W}'(T_{BB}') + \rho^i\right] \quad (12)$$

where $\rho^i = (-\Delta F/k)$. From Figures 40-46 and Figure 9 a mean linearized curve of F_{SC} vs. $\overline{W}$ was drawn, determining the value of k. The parameter, ρ^i, was determined using values of ΔF from Figure 68a. The only remaining step was to determine κ^i, after which the equivalent blackbody temperature corrections $\delta T_{BB} = T_{BB} - T_{BB}'$, as a function of orbit number, were determined from equation (12) with the aid of Figure 9. It was assumed that the values of average quasi-global effective radiant emittance, $\overline{W}^i_{ave}$, from Figure 72 could be applied to equation (12), yielding

$$\overline{W}^i_{ave}{}^{(undegraded)} = \kappa^i\left[\overline{W}^i_{ave} + \rho^i\right]. \quad (13)$$

where $\overline{W}^{i\,(undegraded)}_{ave}$ refers to the value from Figure 72 which would be measured by an undegraded channel 4. It was decided to "normalize" $\overline{W}^{i\,(undegraded)}_{ave}$ for channel 4 to its channel 2 counterpart (which was assumed to be undegraded on launch day) by means of equations (10) and (11). From Figure 71 we have on launch day $\overline{W}^0_{ave} = 24.26$ watts/m^2. Substituting this value in equation (10) and combining equations (10) and (11) we have

$$98.35 + 6.32\,(24.26) = 20.79 + 4.92\,\overline{W}^i_{ave}{}^{(undegraded)}$$

$$\overline{W}^{i}_{ave}{}^{(undegraded)} = \overline{W}^{310}_{ave} = 46.9 \text{ watts/m}^2 \tag{14}$$

where "310" refers to the orbit (on TIROS VII day 21) at which the curve of $\overline{W}^{i}_{ave}$ in Figure 72 coincides with the "undegraded" value. This value agrees well with 47.1 watts/m^2, the value at which the quadratic least-squares portion of the fit in Figure 72 (beyond day 30) intersects the ordinate if extrapolated backward. Substituting equation (14) in equation (13) we have

$$\kappa^i = 46.9 \Big/ \left[\overline{W}^{i}_{ave} + \rho^i \right] \tag{15}$$

Values of κ^i then were calculated by equation (15).

From Figure 68a the initially large value of ΔF decreases and stabilizes at -0.7 c.p.s. after only 70 orbits or 5 days (at which time the parameter ρ^i was set equal to zero and the degradation model became equivalent to the symmetrical optical degradation model [47]), but the time duration of rapidly changing slope in Figure 72 extends over the first 30 days before apparently becoming stabilized. This behavior is interpreted as indicating that a marked "rotation" as well as "translation" of the oscillator frequency-voltage prevailed at launch and that the translation of the space-viewed level diminished after only 5 days, whereas the rotation did not disappear for some 30 days, after which symmetrical optical degradation apparently predominated until about day 249. Beginning on day 249 an erratic "stepped" characteristic was observed in the space-viewed portions of analog presentations of channel 4 data. This peculiar behavior quite probably is still another manifestation of the known oscillator instability and interjects added doubt as to the validity of attempting to correct the channel 4 data after day 249.

The correction nomogram for channel 4 is shown in Figure 79. These corrections are to be added algebraically to the wall and floor T_{BB}' measurements contained on the FMR tape. For example, from Figure 79 it is seen that an equivalent blackbody temperature of 240°K measured by channel 4 during orbit 100 should be *decreased* by 3.4°K, yielding a corrected measurement of 236.6°K.

6.2.4 Channel 3 The history of ΔF is shown in Figure 68b showing a continuing decrease to approximately orbit 550 after which ΔF stabilizes at about -1.25 c.p.s., indicating that a small amount of electronic degradation persists over most of the first 1525 orbits. Values of the quasi-global albedo were calculated assuming that all solar radiation was diffusely reflected according to the Lambert cosine law, and a least-squares quadratic curve was drawn through the data in Figure 73. The equation used was

$$A = \overline{W}/\overline{W}^* \cos \Theta_\odot \tag{16}$$

where $\Theta_\odot$, the solar zenith angle, was constrained within the limits $0° \leq \Theta_\odot \leq 60°$. The compound degradation model was used, and it was decided to "normalize" the data to the annual planetary albedo of 32.2% deduced from channel 2 and 5 data in Reference 48.

From Equations (7) and (16) and Figure 69 we have

$$A = \frac{\overline{W}}{\overline{W}^* \cos \Theta_\odot} = \kappa^i \left[\frac{\overline{W'} + \rho^i}{\overline{W}^* \cos \Theta_\odot} \right] = \kappa^i \left[A' - \frac{\Delta F}{k\overline{W}^* \cos \Theta_\odot} \right] \tag{17}$$

Taking the mean value of $\cos \Theta_\odot$ over many measurements as

$$\overline{\cos \Theta_\odot} = \frac{\int_{0°}^{60°} \cos \Theta_\odot \, d\Theta_\odot}{(60/57.296) \text{ radians}} = 0.827 \tag{18}$$

and taking the values

$A_{ave} = 0.322$ (from Reference 48)
$A'_{ave} = A^i$ (from Figure 73)
$k = 0.147$ c.p.s./watts m^{-2} (from Figures 33-39)
$\overline{W}^* = 484.36$ watts/m^2

we have, after substitution in equation (17),

$$\kappa^i = \left[\frac{0.322}{A^i - \left(\frac{\Delta F}{58.88} \right)} \right] \tag{19}$$

Values of κ^i were calculated using Equation (19) and Figures 73 and 68b, values of $\rho^i = (-\Delta F/k)$ were calculated, and both were plotted in the nomogram of Figure 80. From Figure 80 it is seen that the normalizing parameters for orbit 725 are $\kappa^i = 1.89$ and $\rho^i = +8.5$ *watts/m²*, and that the normalized value of a measurement $\overline{W'} = 50$ watts/m² becomes

$$\overline{W} = 1.89\ [50 + 8.5] = 110.6 \text{ watts/m}^2 \qquad (20)$$

6.2.5 Channel 5 The history of ΔF is shown in Figure 68b. The absolute magnitude of all values is less than 1. For generality the compound degradation model was used, although the small initial value of ρ^i rapidly diminished, and after orbit 70 it was set to zero (at which time the compound degradation model became equivalent to the symmetrical optical degradation model [47]).

With equation (18) and taking the values

$A_{ave} = 0.322$ (from Reference 48)
$A'_{ave} = A^i$ (from Figure 74)
$k = 0.675$ c.p.s./watt m^{-2} (from Figures 47-53)
$\overline{W}^* = 117.13$ watts/m²

we have, after substitution in Equation (17),

$$\kappa^i = \left[\frac{0.322}{A^i - \left(\frac{\Delta F}{65.38}\right)}\right] \qquad (21)$$

Values of κ^i were calculated using Equation (21) and Figures 74 and 68b, and values of $\rho^i = (-\Delta F/k)$ were calculated and plotted in the nomogram of Figure 81. In Figure 81 it is seen that the normalizing parameters for orbit 700 are $\kappa^i = 1.65$ and $\rho^i = 0$ watts/m², and that the normalized value of a measurement $\overline{W'} = 10$ watts/m² becomes

$$\overline{W} = 1.65\ [10] = 16.5 \text{ watts/m}^2 \qquad (22)$$

6.3 *Estimate of the Accuracy of the Data*

Inaccuracies in the data are caused not only by the degradation of the various channels after the original calibration, but also by such effects as wow and flutter in the magnetic tape, noise, drifts of T_E and T_C (and, after orbit 1276, T_V) from their assumed relationships, and uncertainties in the original calibration.

The estimates of accuracy given below apply to the mid-range of target intensities. It is evident from the figures of F_{SC} vs. T_{BB} that the accuracy of the thermal channels suffers at very low target temperatures.

6.3.1 Channel 1. The estimated short-term relative accuracy of T_{BB} measurements from a given side (floor or wall) is $\pm 2°K$, and the estimated absolute accuracy is $\pm 7°K$ after applying corrections from Figure 77.

6.3.2 Channel 2. The estimated short-term relative accuracy of T_{BB} measurements from a given side is $\pm 2°K$, and the estimated absolute accuracy is $\pm 5°K$ after applying corrections from Figure 78.

6.3.3 Channel 4. The estimated short-term relative accuracy of T_{BB} measurements from a given side is $\pm 2°K$, and the estimated absolute accuracy is $\pm 8°K$ after applying corrections from Figure 79.

6.3.4 Channel 3 and Channel 5. The estimated short-term relative accuracy of $\overline{W}$ measurements is ± 10 watts/m² and ± 2 watts/m² respectively for channels 3 and 5. Because of the lack of a satisfactory explanation for the adjustment factor (of the order of 1.60) by which channel 3 and 5 measurements of all TIROS satellites have seemingly been too low, no estimates of absolute accuracy are given.

6.4 *Comments on Significant Engineering Aspects of the Experiment*

In the preceding paragraphs, the behavior of the radiometer has been described in detail. In the following paragraphs a summary will be given of other types of behavior which affected the radiation data or their coverage.

Tiros VII had been in orbit only 39 days (orbit 573) when a malfunction developed in the playback mode (described in Section 4.1), requiring two playbacks to recover the data. The nature of the two-playback operation resulted in the loss of some data at the beginning of each orbit. The amount of data lost was variable but generally quite small.

As pointed out in Section 4.3, the sampling

rate used in digitizing the data at the Data Processing Center was doubled on TIROS VII day 73 (orbit 1080), providing twice as many measurements per unit time on the FMR tapes.

The Fairbanks, Alaska, Command and Data Acquisition station started to operate on Day 83, acquiring data from orbit 1230 as its first interrogation. The addition of the Fairbanks station did not, in general, provide for the acquisition of additional data than was previously provided by the Wallops and San Nicolas stations. However, on rare occasions the Fairbanks station acquired the fifth orbit of the nine orbit series which comprises an interrogation day. The fifth orbit could never be acquired by either Wallops or San Nicolas.

Beginning with the interrogation day for Tiros VII Day 87, the channel 6 commutator (described in Section 4.1) failed to switch and remained set on the electron temperature probe sensor. Thus, the radiometer housing temperature, among other elements, was not received from the satellite. As a consequence the housing temperature was derived from the TV clock number 2 temperature (described in Section 3.4).

VII. CONCLUSIONS

The major limitation of the TIROS VII medium resolution radiometer experiment is the uncertainty in the absolute values of the measurements, resulting from the degradation of the radiometer response and, also, from electronic degradation which, for the first time, was conclusively detected in TIROS VII. The degradation corrections given in Section VI can serve as a guide for interpreting the data in terms of absolute values. However, it must be emphasized that these corrections are only our best estimates, based upon certain simplifying assumptions, of the effects of a complicated degradation mechanism which we do not yet fully understand, and that the measurements thus corrected may still contain appreciable uncertainties.

Because of the extended lifetime of the radiometer, which as of this writing exceeds fifteen months, the potential of the TIROS VII radiometric data for climatological studies is significantly greater than it was for previous TIROS satellites. In utilizing the measurements over extended periods, however, channel 2 and 5 data should be used in lieu of channel 4 and 3 data respectively wherever possible because of the superior stability characteristics of the former two channels.

The data from all channels are of value throughout the period covered by this Volume for studies involving relative measurements over a short period of time, for example the contrast mapping of cloud systems.

VIII. REFERENCES

1. *"TIROS IV Radiation Data Catalog and Users' Manual."* Goddard Space Flight Center, Greenbelt, Maryland, 15 December 1963, 250 pp.
2. *"TIROS II Radiation Data Catalog"*, Goddard Space Flight Center, Greenbelt, Maryland, 15 August 1961, 356 pp.
3. *"TIROS II Radiation Data Users' Manual."* Goddard Space Flight Center, Greenbelt, Md., 15 August 1961, 57 pp.
4. *"TIROS III Radiation Data Catalog."* Goddard Space Flight Center, Greenbelt, Md., 15 December 1962, 388 pp.
5. *"TIROS III Radiation Data Users' Manual."* Goddard Space Flight Center, August 1962, 71 pp.
6. Bandeen, W. R., R. A. Hanel, John Licht, R. A. Stampfl, and W. G. Stroud. "Infrared and Reflected Solar Radiation Measurements from the TIROS II Meteorological Satellite". *J. of Geophys. Res., 66*, 3169-3185, October 1961.
7. Hanel, R. A. and W. G. Stroud. "Infrared Imaging from Satellites." *J. of the SMPTE, 69*, 25-26 January 1960.
8. Hanel, R. A., W. R. Bandeen, and B. J. Conrath. "The Infrared Horizon of the Planet Earth." *J. of the Atmos. Sciences, 20*, 73-86, March 1963.
9. Bandeen, W. R., B. J. Conrath and R. A. Hanel. "Experimental Confirmation from TIROS VII Meteorological Satellite of the Theoretically Calculated Radiance of the Earth Within the 15 Micron Band of Carbon Dioxide". *J. of the Atmos. Sciences, 20*, 609-614, November 1963.
10. Nordberg, W., W. R. Bandeen, G. Warnecke, and V. Kunde. "Stratospheric Temperature Patterns Based on Radiometric Measurements from the TIROS VII Satellite." (To be published in *Space Research V*, North-Holland Publishing Co., 1964.)
11. Astling, Elford G. and Lyle H. Horn. "Some Geographical Variations of Terrestrial Radiation Measured by TIROS II." *J. of Atmos. Sciences, 21*, 30-34, January 1964.
12. Bandeen, W. R., V. Kunde, W. Nordberg, and H. P. Thompson. "TIROS III Meteorological Satellite Radiation Observations of a Tropical Hurricane." *TELLUS* (to be published).
13. Deacon, E. L., "Water Vapor over the Sahara and TIROS III Observation". *J. of Atmos. Sciences, 20*, 614-615, November 1963.
14. Fritz, Sigmund, and Jay S. Winston. "Synoptic Use of Radiation Measurements from Satellite TIROS II." *Monthly Weather Review, 90*, 1-9, January 1962.
15. Fritz, S., P. Krishna Rao, and M. Weinstein. "Satellite Measurements of Reflected Solar Energy and the Energy Received at the Ground." *J. of Atmos. Sciences, 21*, 141-151, March 1964.
16. Furukawa, P. M., P. A. Davis, and W. Viezee. "An Examination of some TIROS II Radiation Data and Related Studies." *Final Report, Contract No. AF 19(628)-322*, Stanford Research Institute, Menlo Park, California, July 1962.
17. Greenfield, S. M. and W. W. Kellogg. "Calculations of Atmospheric Infrared Radiation as seen from a Meteorological Satellite." *J. of Meteor., 17*, 283-289, June 1960.
18. Hanel, R. A. and D. Q. Wark. "TIROS II Radiation Experiment and Its Physical Significance." *J. Opt. Soc. Am., 51*, 1394-1399, December 1961.
19. King, Jean I. F., "Meteorological Inferences from Satellite Radiometry." *J. of Atmos. Sciences, 20*, 245-250, July 1963.
20. Larsen, S. H. H., T. Fujita, and W. L. Fletcher. "Evaluation of Limb Darkening from TIROS III Radiation Data." *Research Paper No. 18*, Mesometeorology Project, Department of Geophysical Sciences, The University of Chicago, August 1963.
21. Pedersen, Finn and Tetsuya Fujita, "Synoptic Interpretation of TIROS III Measurements of Infrared Radiation." *Research Paper No. 19*, Mesometeorology Project, Department of Geophysical Science, The University of Chicago, October, 1963.
22. Larsen, S. H. H., T. Fujita, and W. L. Fletcher. "TIROS III Measurements of Terrestrial Radiation and Reflected and Scattered Solar Radiation." *Research Paper No. 20*, Mesometeorology Project, Department of the Geophysical Sciences, The University of Chicago, October 1963.
23. Fujita, T. and J. Arnold, "The Decaying Stage of Hurricane Anna of July 1961 as Portrayed by TIROS Cloud Photographs and Infrared Radiation from the Top of the Storm". *Research Paper No. 28*, Mesometeorology Project, Department of Geophysical Sciences, The University of Chicago, November 1963.
24. London, Julius, "Satellite Observations of Infrared Radiation." *Scientific Report No. 1, Contract No. AF 19(604)-5955*, College of Engineering, New York University, New York 53, N.Y., December 1959.
25. London, Julius, "Katsuyuki Ooyama, and Herbert Viebrock. "Satellite Observations of Infrared Radiation". *Report No. 2, Contract No. AF 19(604)-5955*, College of Engineering, New York University, New York 53, N.Y., July 1960.
26. London, Julius, Katsuyuki Ooyama, and Herbert Viebrock. "Satellite Observations of Infrared Radiation". *Final Report, Contract No. AF (604)-5955*, College of Engineering, New York University, New York 53, N.Y., October 1961.
27. Möller, Fritz. "Einige vorläufige Auswertungsen der Strahlungsmessungen von TIROS II." *Arch. f. Met., Geophys. u. Biokl., 12*, Ser. B. 78-94, July 1962. (Also "Some Preliminary Evaluations of TIROS II Radiation Measurements." Univ. München, Meteorologisches Inst., München 13, Amalienstr. 52/III, Germany, January 1962.)
28. Möller, Fritz and Ehrhard Raschke. "Evaluation of TIROS III Radiation Data." *Interim Report No. 1 (July 1963) and Final Report (March 1964) NASA Research Grant Ns G-305*, Ludwig-Maximilians-Universität, Meteorologisches Institut, München, Germany.

29. Nordberg, W., W. R. Bandeen, B. J. Conrath, V. Kunde, and I. Persano. "Preliminary Results of Radiation Measurements from the TIROS III Meteorological Satellite." *J. of the Atmos. Sciences, 19*, 20-30, January 1962.

30. Prabhakara, C., and S. I. Rasool. "Evaluation of TIROS Infrared Data." pp. 234-246 in *Proceedings of the First International Symposium on Rocket and Satellite Meteorology*, Washington, D. C., April 1962, edited by H. Wexler and J. E. Caskey, Jr., North-Holland Publishing Co., Amsterdam, 1963.

31. Rasool, S. I., "Cloud Heights and Nighttime Cloud Cover from TIROS Radiation Data." *J. of the Atmos. Sciences, 21*, 152-156, March 1964.

32. Wark, D. Q., "On Indirect Temperature Soundings of the Stratosphere from Satellites." *J. of Geophys. Research, 66*, 77-82, January 1961.

33. Wark, D. Q., G. Yamamoto, and J. H. Lienesch. "Methods of Estimating Infrared Flux and Surface Temperatures from Meteorological Satellites." *J. of the Atmos. Sciences, 19*, 369-384, September 1962. (Also "Infrared Flux and Surface Temperature Determinations from TIROS Radiometer Measurements." Meteorological Satellite Laboratory Report No. 10 (1962) and Supplement thereto (1963), U.S. Weather Bureau, Washington, D. C.)

34. Wexler, R., "Satellite Observations of Infrared Radiation." *First Semi-annual Technical Summary Report, Contract No. AF 19(604)-5968*, Allied Research Assoc., Inc., Boston, Mass., December 24, 1959.

35. Wexler, R., "Satellite Observations of Infrared Radiation." *Second Semi-annual Technical Summary Report, Contract No. AF 19(604)-5968*, Allied Research Assoc., Inc., Boston, Mass., June 30, 1960.

36. Wexler, R., "Interpretation of Satellite Observations of Infrared Radiation." *Scientific Report No. 1, Contract No. AF 19(604)-5968*, Allied Research Assoc., Inc., Boston, Mass., April 20, 1961.

37. Wexler, R., "Interpretation of TIROS II Radiation Measurements." *Final Report, Contract No. AF 19(604)-5968*, Allied Research Assoc., Inc., Boston, Mass., May 31, 1962.

38. Wexler, Raymond and Paul Sherr. "Synoptic Analysis of TIROS III Radiation Measurements." *Final Report, Contract No. AF 19 (628)-429*, Aracon Geophysics Co., Concord, Mass., January 31, 1964.

39. Bandeen, W. R. *"TIROS II Radiation Data Users' Manual Supplement."* Goddard Space Flight Center, Greenbelt, Md., 15 May 1962, 13 pp.

40. Doolittle, R. C., L. Miller, and I. Ruff. "Geographic Locations of Cloud Features." Appendix A of "Final Report on the TIROS I Meteorological Satellite System", Part II by Staff, Meteorological Satellite Laboratory, U.S. Weather Bureau, *NASA Technical Report R-131*, 1962.

41. Bristor, C. L., E. G. Albert, and J. B. Jones. "Problems in Mapping Data from Meteorological Satellites", *Space Research II, Proceedings of the Second International Space Science Symposium*, Florence, Italy, April 10-14, 1961, North-Holland Publishing Company, Holland.

42. Hubert, L. F. "TIROS I: Camera Attitude Data, Analysis of Location Errors, and Deviation of Correction for Calibration." *Meteorological Satellite Laboratory Report No. 14*, U.S. Weather Bureau.

43. Dean, C. "Attitude Determination from Picture Data. TIROS I: An Operational Evaluation of a New Meteorological Tool." *Second Semi-annual Technical Summary Report, Contract No. AF 19(604)-5581*, Allied Research Assoc., Inc., Boston, Mass., June 30, 1960.

44. Bandeen, William R. and Warren P. Manger. "Angular Motion of the TIROS I Meteorological Satellite due to Magnetic and Gravitational Torques". *J. of Geophys. Res., 65*, 2992-2995, September 1960.

45. Davis, J., R. Hanel, R. Stampfl, M. Strange, and M. Townsend, "Telemetering IR Data from the TIROS II Meteorological Satellite", *NASA TN D-1293*, Goddard Space Flight Center, Greenbelt, Md.

46. Widger, Jr., W. K. and C. P. Wood, "An Explanation of the Limitation to the Coverage Provided by TIROS". *Weatherwise, 14*, No. 6, December 1961.

47. Bandeen, W. R., R. E. Samuelson, I. P. Strange, *"TIROS III Radiation Data Users' Manual Supplement. Correction Models for Instrumental Response Degradation."* Goddard Space Flight Center, Greenbelt, Md., 1 December 1963, 56 pp.

48. Bandeen, W. R., M. Halev, and I. Strange, "A Radiation Climatology in the Visible and Infrared from the TIROS Meteorological Satellites." Paper presented at the International Radiation Symposium, I.U.G.G., Leningrad, August, 1964 (available in *document X-651-64-218*, Goddard Space Flight Center, Greenbelt, Md.; also to be published as *NASA* TN D-2534.)

49. London, Julius, "A Study of the Atmospheric Heat Balance." *Final Report, Contract No. AF 19(122)-165*, College of Engineering, New York University, New York 53, N. Y., July 1957.

TABLE III—*Filter and Lens Materials*

	Channel 1	Channel 2	Channel 3	Channel 4	Channel 5
Lens 1	KRS-5 (Thallium-bromo-iodide) with no coatings.	Germanium with both surfaces coated with pure ZnS of $\lambda/4$ optical thickness at 10μ.	Synthetic Barium Flouride (BaF_2) with no coatings.	KRS-5 (Thallium-Bromo-iodide) with no coatings.	Pure quartz (SiO_2) with no coatings.
Lens 2	None ----------	Germanium with both surfaces coated with ZnS of $\lambda/4$ optical thickness at 10μ.	Synthetic Sapphire (Al_2O_3) with no coatings.	None ----------	Synthetic Sapphire (Al_2O_3) with no coatings.
Filter 1	OCLI Band Pass Filter centered at 15.2μ with half amplitude at 14.8μ and 15.6μ.	Indium Antimonide (InSb) with both surfaces coated with pure ZnS of $\lambda/4$ optical thickness at 10μ.	None ----------	Indium Antimonide (InSb) coated with pure ZnS, one surface with $\lambda/4$ optical thickness at 13μ and the other at 20μ.	OCLI Band Pass Filter centered at 0.6μ with half amplitude at 0.56μ and 0.72μ.
Filter 2	None ----------	Arsenic Trisulfide (As_2S_3) glass, uncoated 0.5 mm plane piece.	None ----------	None ----------	None ----------

TABLE IV—*Effective Spectral Response, Channel 1*

$\lambda(\mu)$	ϕ_λ	$\lambda(\mu)$	ϕ_λ
14.00	0	15.25	.1798
14.10	.0040	15.30	.1730
14.20	.0040	15.37	.1400
14.30	.0081	15.40	.1232
14.40	.0200	15.50	.0820
14.50	.0286	15.60	.0658
14.60	.0410	15.70	.0409
14.70	.0575	15.80	.0326
14.80	.0822	15.90	.0164
14.90	.1152	16.00	.0122
15.00	.1575	16.10	.0082
15.10	.1823	16.20	.0082
15.13	.1863	16.30	0
15.20	.1904		

TABLE V—*Effective Spectral Response, Channel 2*

$\lambda(\mu)$	ϕ_λ	$\lambda(\mu)$	ϕ_λ
7.5	0	14.5	.0080
8.0	.1094	15.0	.0081
8.5	.1960	15.5	.0164
9.0	.2535	16.0	.0410
9.5	.2662	16.5	.0660
10.0	.2627	17.0	.0695
10.5	.2512	17.5	.0572
11.0	.2534	18.0	.0411
11.5	.2266	18.5	.0370
12.0	.1908	19.0	.0246
12.5	.1749	19.5	.0164
13.0	.1193	20.0	.0082
13.5	.0402	20.5	.0082
14.0	.0080	21.0	0.0

TABLE VI—*Effective Spectral Response, Channel 3*

$\lambda(\mu)$	ϕ_λ	$\lambda(\mu)$	ϕ_λ
.24	.0119	.65	.3074
.25	.0302	.70	.2969
.26	.0681	.75	.3031
.27	.1123	.80	.2904
.28	.1587	.85	.2984
.29	.1784	.90	.3145
.30	.2296	.95	.3318
.31	.2548	1.00	.3802
.32	.2785	1.50	.4460
.33	.2949	2.00	.4777
.34	.3075	2.50	.5182
.35	.3260	3.00	.5001
.36	.3331	3.50	.5319
.37	.3588	4.00	.5304
.38	.3643	4.50	.4957
.39	.3689	5.00	.4564
.40	.3686	5.50	.2869
.45	.3570	6.00	.1716
.50	.3505	6.50	.0188
.55	.3272	7.00	0
.60	.3285		

TABLE VII—*Effective Spectral Response, Channel 4*

$\lambda(\mu)$	ϕ_λ	$\lambda(\mu)$	ϕ_λ	$\lambda(\mu)$	ϕ_λ
7.0	.0000	16.5	.2873	26.0	.1535
7.5	.0141	17.0	.2853	26.5	.1389
8.0	.1392	17.5	.2766	27.0	.1295
8.5	.1627	18.0	.2794	27.5	.1068
9.0	.1887	18.5	.2732	28.0	.0886
9.5	.2021	19.0	.2691	28.5	.0828
10.0	.1994	19.5	.2508	29.0	.0768
10.5	.2058	20.0	.2425	29.5	.0678
11.0	.2119	20.5	.2356	30.0	.0586
11.5	.2236	21.0	.2285	30.5	.0606
12.0	.2406	21.5	.2214	31.0	.0411
12.5	.2389	22.0	.2118	31.5	.0310
13.0	.2556	22.5	.2041	32.0	.0274
13.5	.2689	23.0	.1914	32.5	.0210
14.0	.2742	23.5	.1758	33.0	.0335
14.5	.2821	24.0	.1667	33.5	.0210
15.0	.2850	24.5	.1657	34.0	.0133
15.5	.2877	25.0	.1623	34.5	.0190
16.0	.2848	25.5	.1602	35.0	.0138

TABLE VIII—*Effective Spectral Response, Channel 5*

$\lambda(\mu)$	$\phi\lambda$	$\lambda(\mu)$	$\phi\lambda$
.50	.0041	.90	.0132
.52	.0234	.92	.0088
.54	.1077	.94	.0054
.56	.2922	.96	.0035
.58	.3419	.98	.0025
.60	.3496	1.00	.0015
.62	.3398	1.02	.0012
.64	.3084	1.50	0.0
.66	.2692	1.60	.0045
.68	.2377	1.70	.0092
.70	.2105	1.80	.0093
.72	.1757	1.90	.0094
.74	.1488	2.00	.0057
.76	.1304	2.10	.0039
.78	.1000	2.20	.0039
.80	.0761	2.30	.0050
.82	.0541	2.40	.0105
.84	.0379	2.50	.0123
.86	.0266	2.60	.0144
.88	.0183	2.70	0.0

TABLE IX—T_{BB} *vs.* $\overline{W}$, *Channel 1*

T_{BB} (°K)	$\overline{W}$ (watts/m²)
160	.1821
180	.3528
200	.6000
220	.9283
240	1.338
260	1.827
280	2.391
300	3.024

TABLE X—T_{BB} *vs.* $\overline{W}$, *Channel 2*

T_{BB} (°K)	$\overline{W}$ (watts/m²)
77.0	.0011
97.0	.0126
117.0	.0721
137.0	.2752
157.0	.7960
177.0	1.884
197.0	3.837
217.0	6.966
237.0	11.56
257.0	17.88
277.0	26.12
297.0	36.42
317.0	48.86

TABLE XI—T_{BB} *vs.* $\overline{W}$, *Channel 4*

T_{BB} (°K)	$\overline{W}$ (watts/m²)
160	4.916
180	8.927
200	14.748
220	22.665
240	32.901
260	45.617
280	60.911
300	78.829
320	99.368

TABLE XII—*Changes in Blackbody Temperature* (T_{BB}) *and Effective Radiant Emittance* ($\overline{W}$) *Due to Differences of* T_C *from* T_E

Channel	Side	T_E (°C)	T_C (°C)	F_{sc} (cps)	T_{BB} (°K)	ΔT_{BB}	$\overline{W}$ (w/m²)	$\overline{W}/\overline{W}^*$	$\Delta(\overline{W}/\overline{W}^*)$
1	Floor	0	0	370.0	203.7				
		7	0	370.25	204.7	1.0			
		7	7	370.0	201.7				
		0	7	369.75	200.7	1.0			
	Wall	0	0	370.0	207.2				
		7	0	370.25	208.2	1.0			
		7	7	370.0	205.7				
		0	7	369.75	204.7	1.0			
2	Floor	0	0	185.0	263.2				
		7	0	185.2	263.4	0.2			
		7	7	185.0	258.7				
		0	7	184.8	258.5	0.2			
	Wall	0	0	185.0	261.7				
		7	0	185.2	261.9	0.2			
		7	7	185.0	254.2				
		0	7	184.8	254.0	0.2			
3	Floor	0	0	258.0			166	0.3356	
		7	0	258.5			167	0.3397	.0041
		7	7	258.0			152	0.3138	
		0	7	257.5			150	0.3097	.0041
	Wall	0	0	258.0			164	0.3386	
		7	0	258.5			167	0.3448	0.0060
		7	7	258.0			150	0.3097	
		0	7	257.5			148	0.3056	0.0041
4	Floor	0	0	325.0	271.7				
		7	0	325.2	272.0	0.3			
		7	7	325.0	264.5				
		0	7	324.8	264.2	0.3			
	Wall	0	0	325.0	269.2				
		7	0	325.2	269.5	0.3			
		7	7	325.0	262.4				
		0	7	324.8	262.0	0.4			
5	Floor	0	0	130.0			40	0.3415	
		7	0	130.25			40.5	0.3458	0.0043
		7	7	130.0			37.5	0.3202	
		0	7	129.75			37.0	0.3159	0.0043
	Wall	0	0	130.0			40	0.3415	
		7	0	130.25			40.5	0.3458	0.0043
		7	7	130.0			37.5	0.3202	
		0	7	129.75			37.0	0.3159	0.0043

TABLE XIII—*Vertical Alignment Check of the Various Channels of TIROS VII Radiometer*

	CHANNEL—1			CHANNEL—2			CHANNEL—3			CHANNEL—4			CHANNEL—5		
	DEG	MIN	SEC	DEG	MIN	SEC	DEG	MIN	SEC	DEG	MIN	SEC	DEG	MIN	SEC
Right Edge (top) Field of View	231	51	36.5	228	23	53.5	230	22	12.5	231	35	41.5	230	0	28
Left Edge (Bottom) Field of View	220	33	17	220	50	26	221	46	6	228	35	47	224	29	29.5
Total Field of View	11	18	19.5	7	33	27.5	8	36	6.5	7	59	54.5	5	30	58.5
Base Angle	181	22	35.5	181	22	35.5	181	22	35.5	181	22	35.5	181	22	35.5
(Computation)															
Left Edge Field of View	220	33	17	220	50	26	221	46	6	228	35	47	224	29	29.5
Minus Base Angle	—181	22	35.5	—181	22	35.5	—181	22	35.5	—181	22	35.5	—181	22	35.5
	39	10	41.5	39	27	50.5	40	23	30.5	42	13	11.5	43	6	54
Plus ½ field of View	+5	39	10	+3	46	44	+4	48	3	+3	59	57	+2	45	29
= Optical axis with respect to Base Plate	44	49	51.5	43	14	34.5	45	11	33.5	46	13	8.5	45	52	23
Error Angle from Optimum 45°	—0	10	8.5	—1	45	25.5	+0	11	33.5	+1	13	8.5	+0	52	23
Noise Voltage	1.35 VDC			.40 VDC			.41 VDC			.70 VDC			.36 VDC		

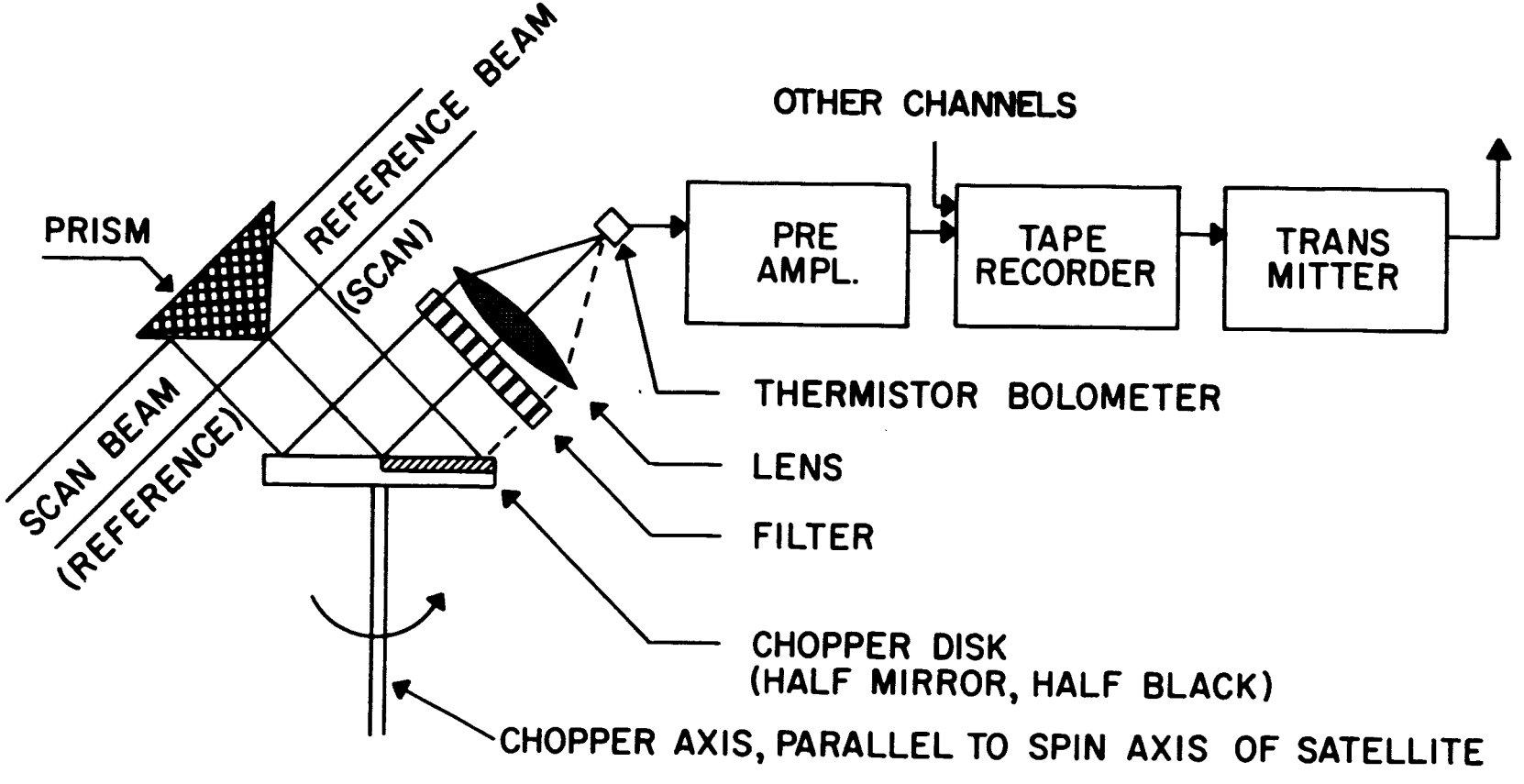

Figure 1—Block diagram of one channel of the medium resolution radiometer.

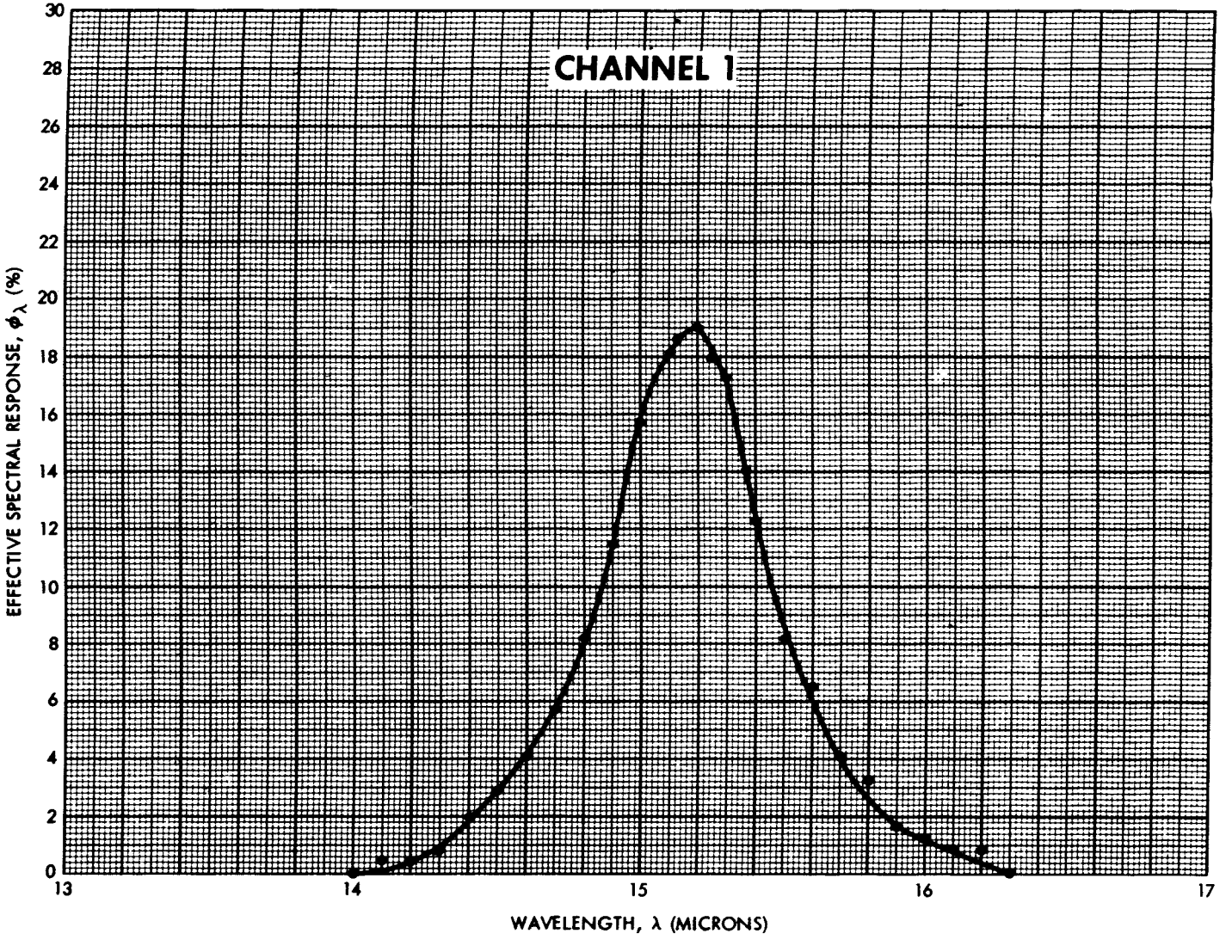

Figure 2—The effective spectral response of channel 1 versus wavelength.

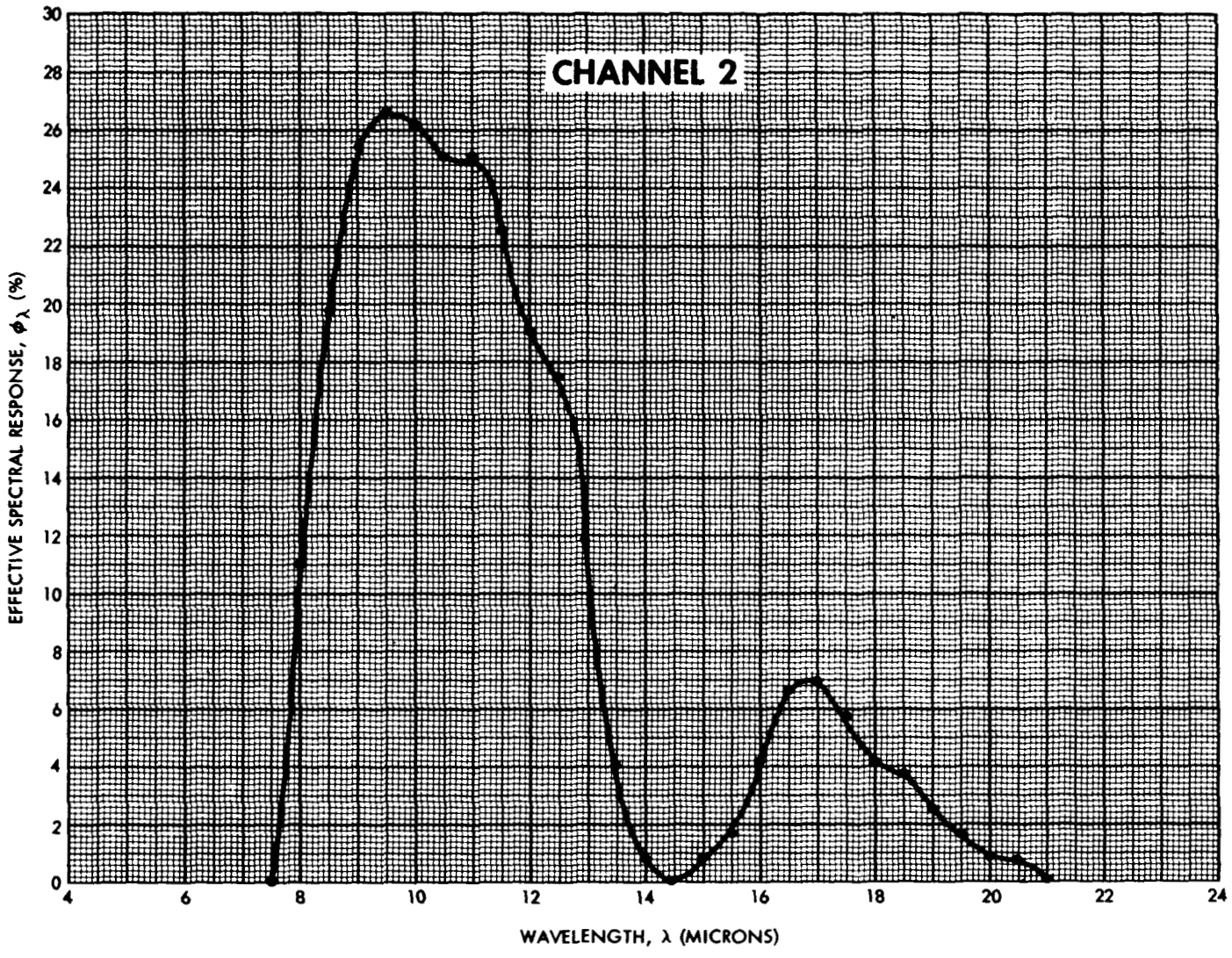

Figure 3—The effective spectral response of channel 2 versus wavelength.

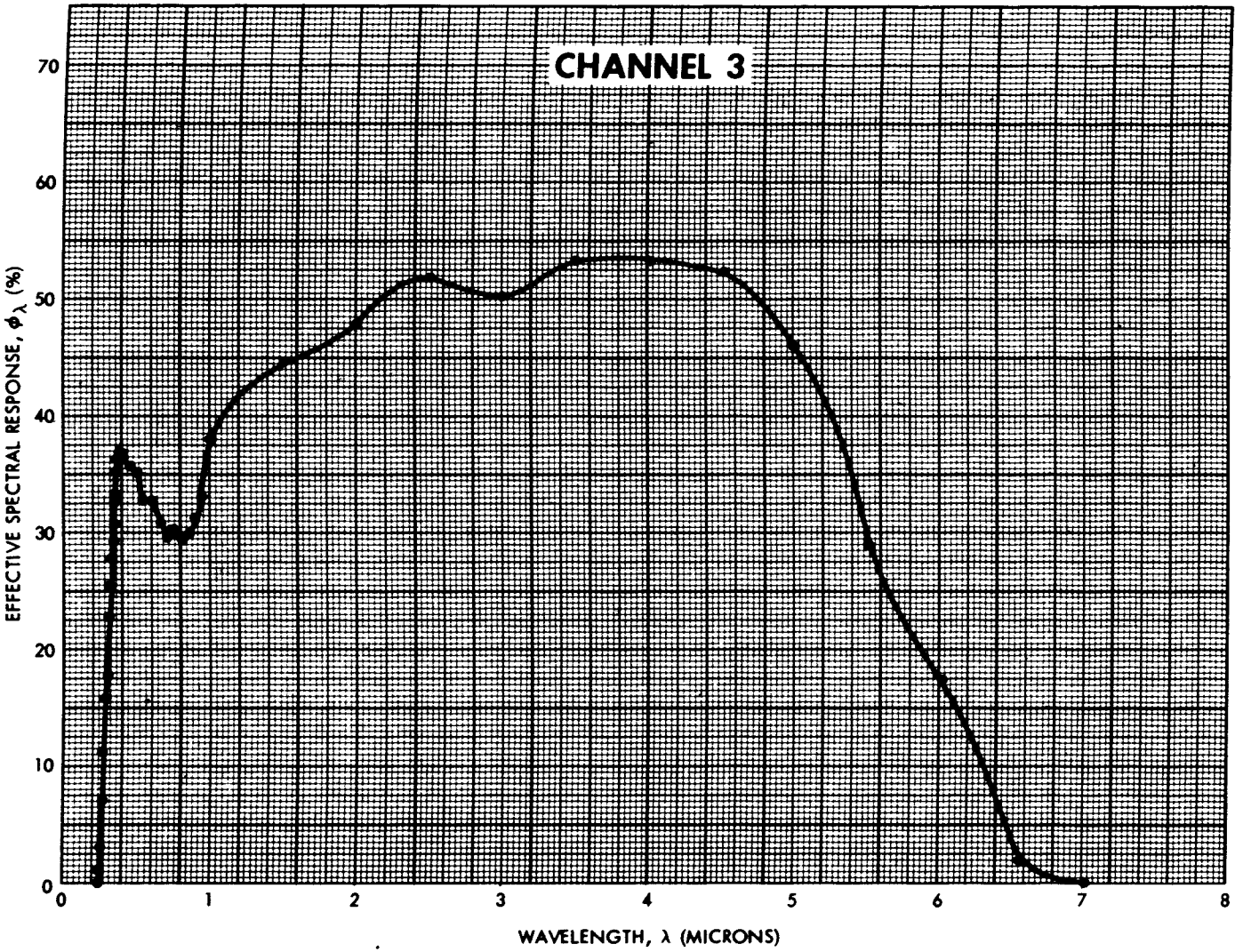

Figure 4—The effective spectral response of channel 3 versus wavelength.

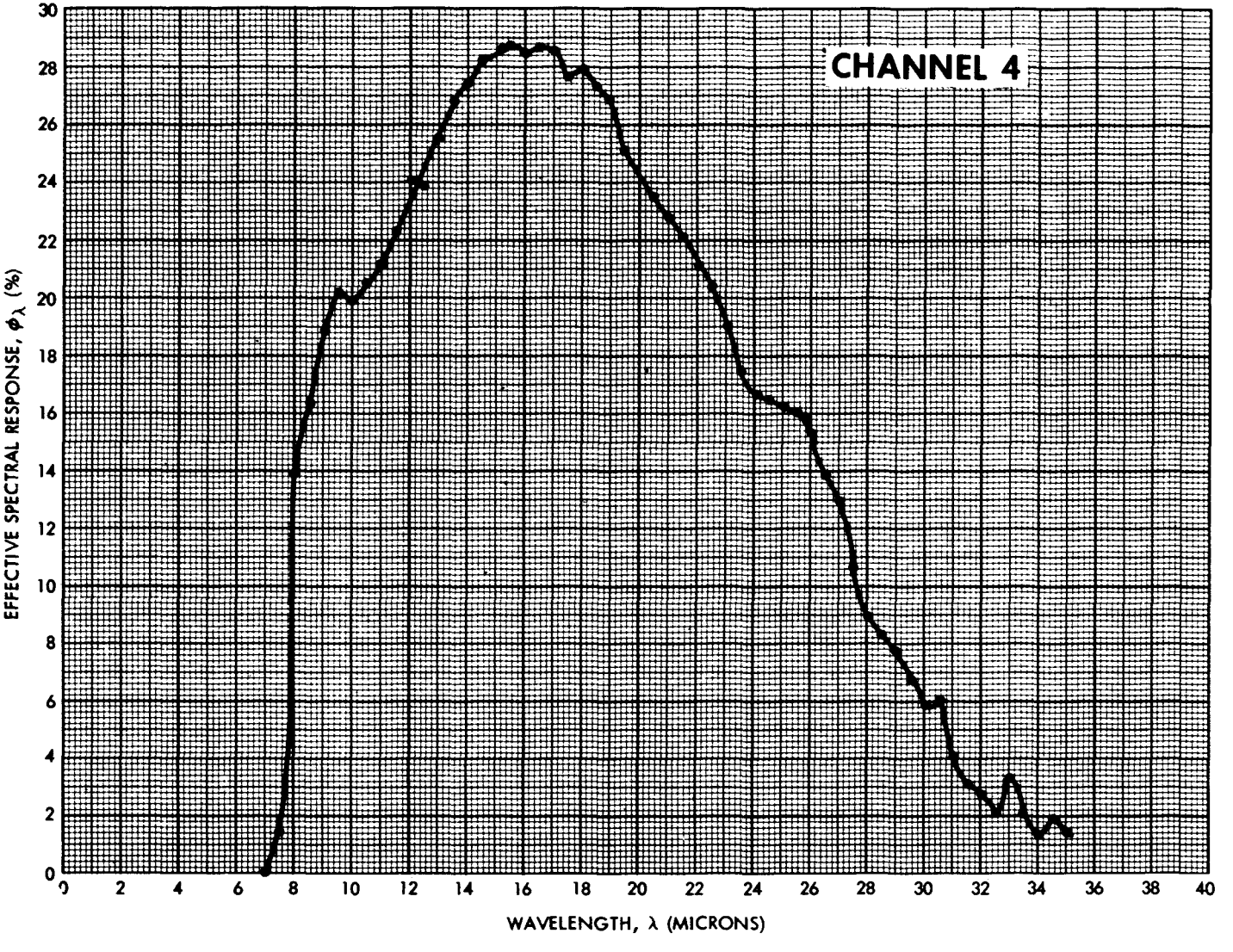

Figure 5—The effective spectral response of channel 4 versus wavelength.

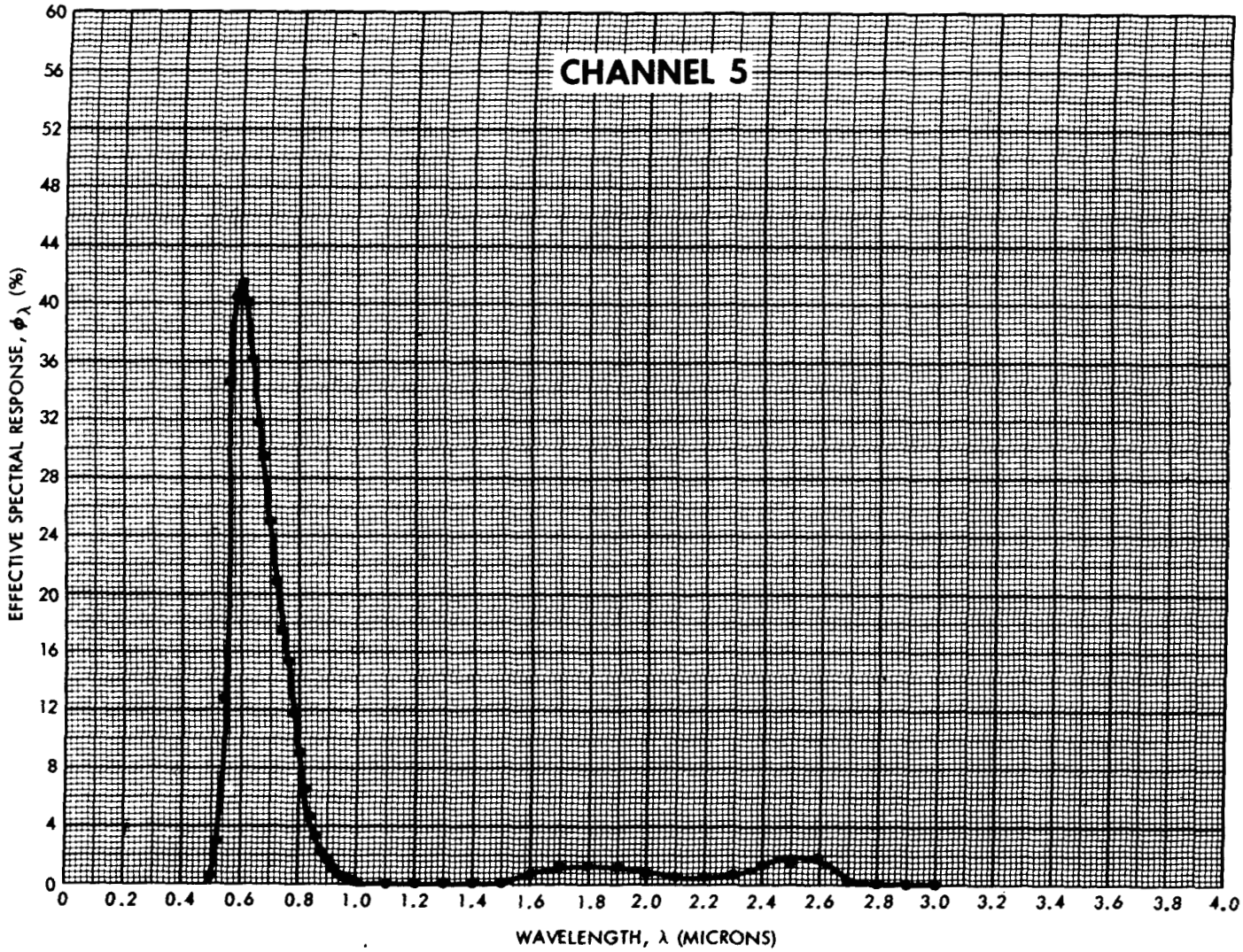

Figure 6—The effective spectral response of channel 5 versus wavelength.

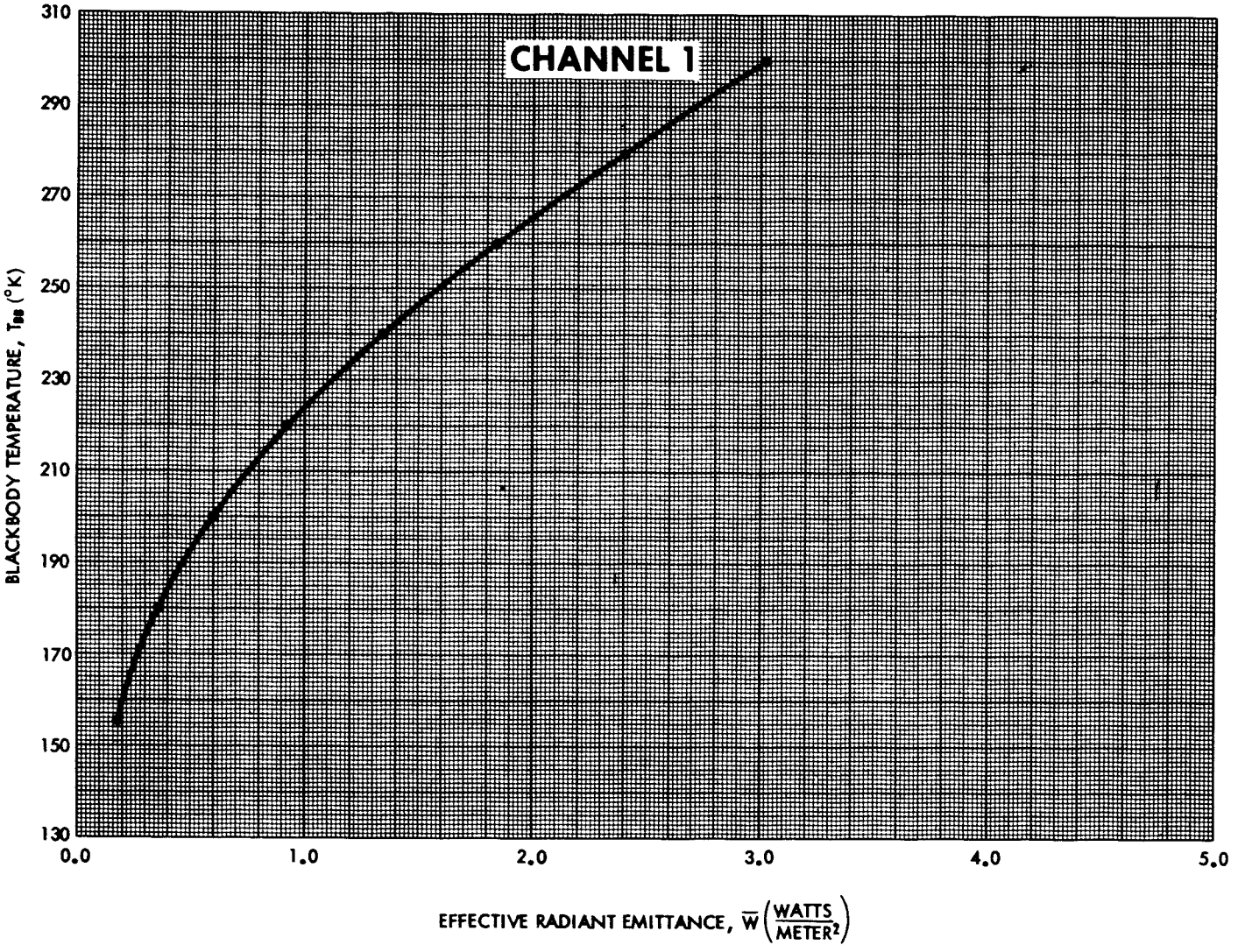

Figure 7—The equivalent blackbody temperature versus effective radiant emittance for channel 1.

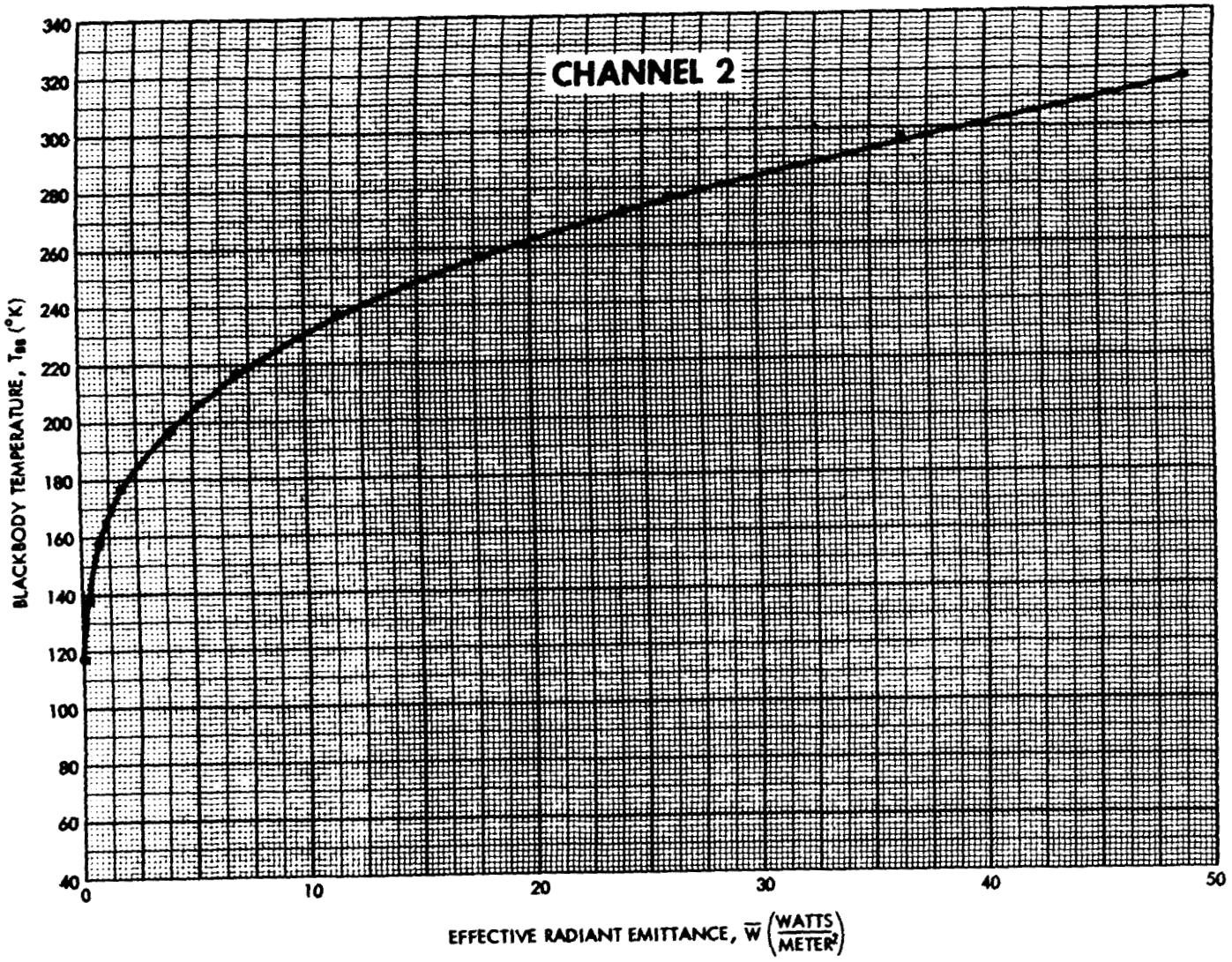

Figure 8—The equivalent blackbody temperature versus effective radiant emittance for channel 2.

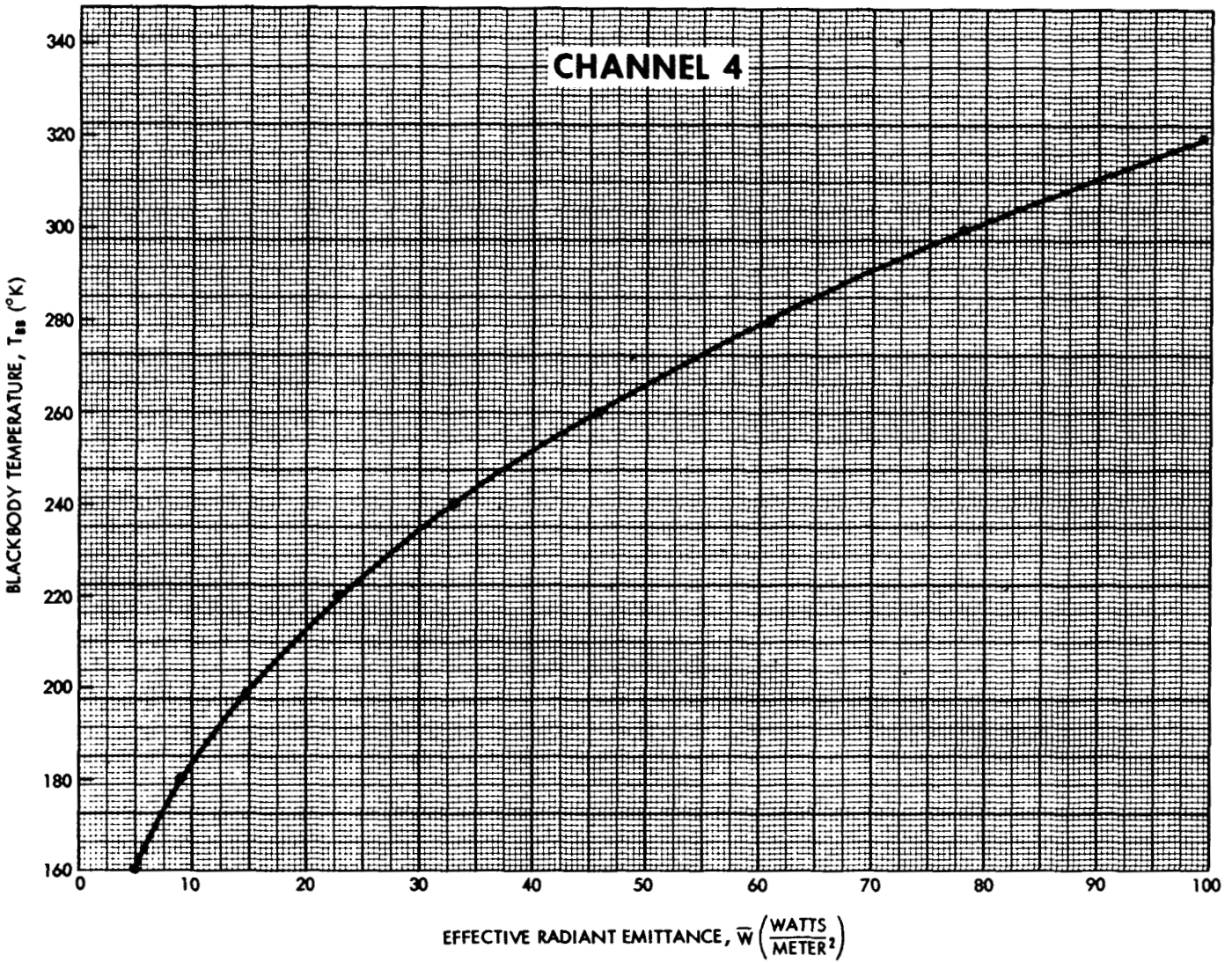

Figure 9—The equivalent blackbody temperature versus effective radiant emittance for channel 4.

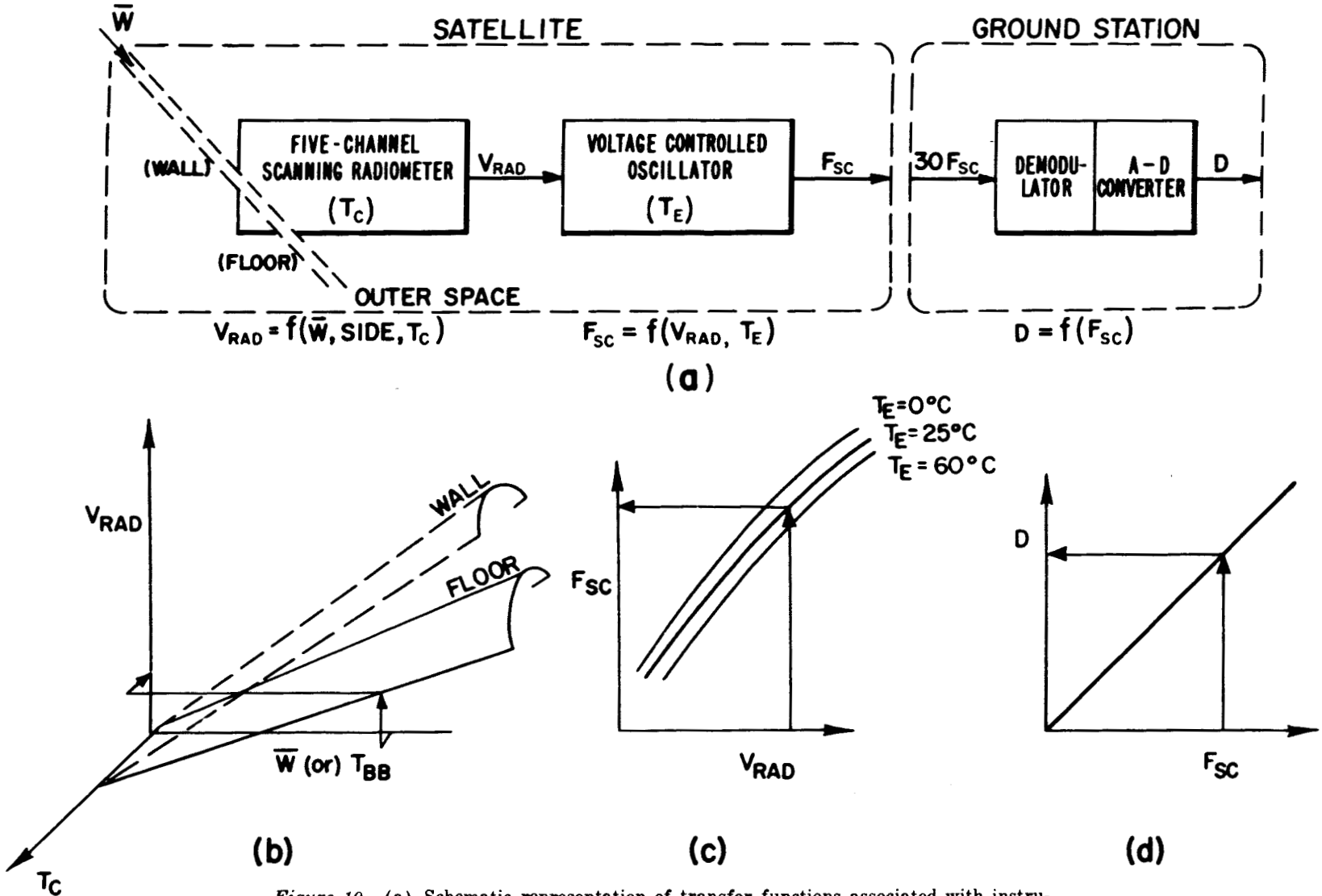

Figure 10—(a) Schematic representation of transfer functions associated with instrumentation in the satellite and at the ground station. (b) Three-dimensional representation of the response of the five-channel scanning radiometer. (c) The response of the voltage controlled oscillator shown as a parametric function of the electronics temperature, T_E. (d) Conversion from subcarrier frequency to digital number.

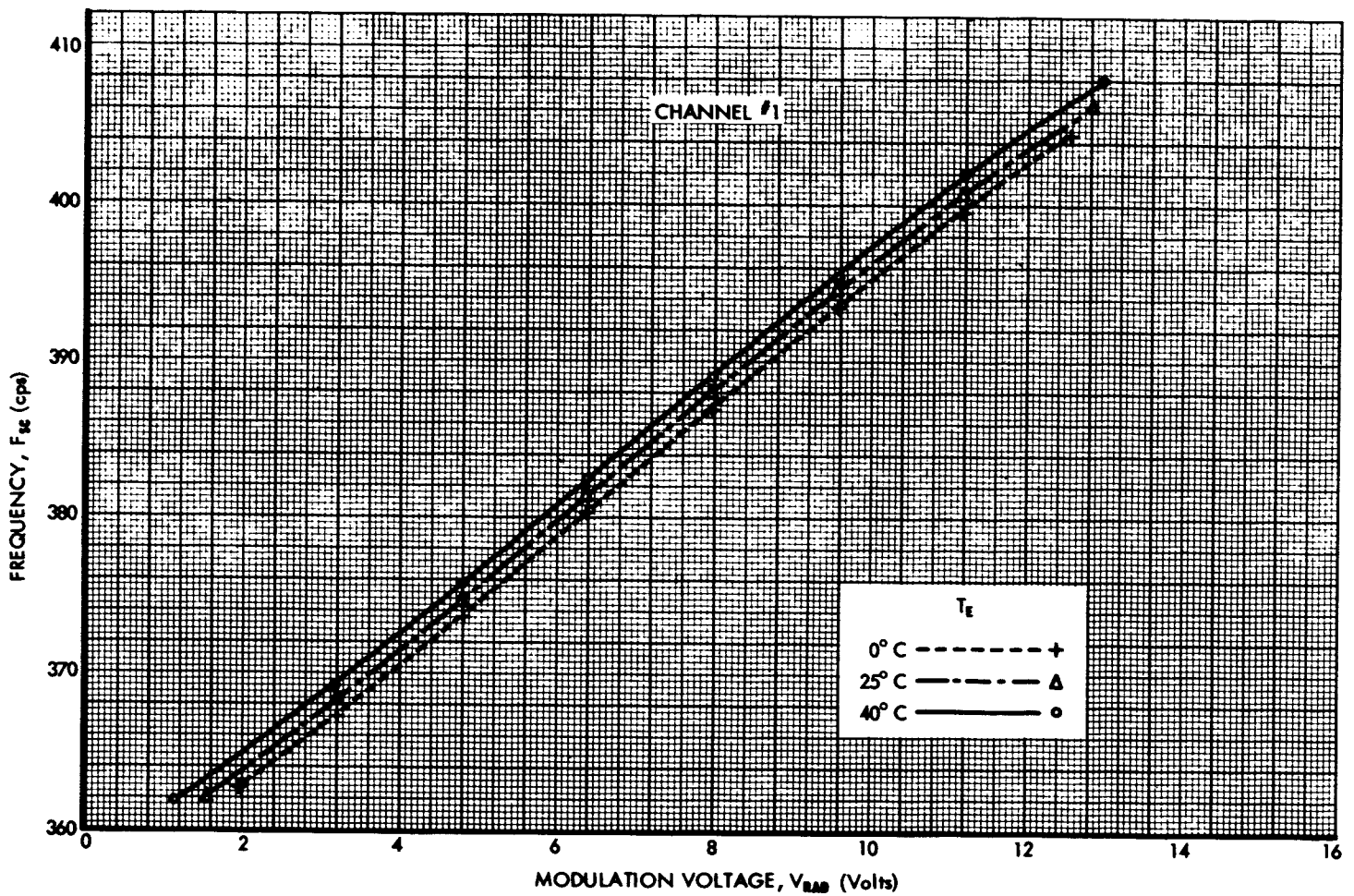

Figure 11—The response of the voltage controlled oscillator for channel 1 shown as a parametric function of the electronics temperature, T_E.

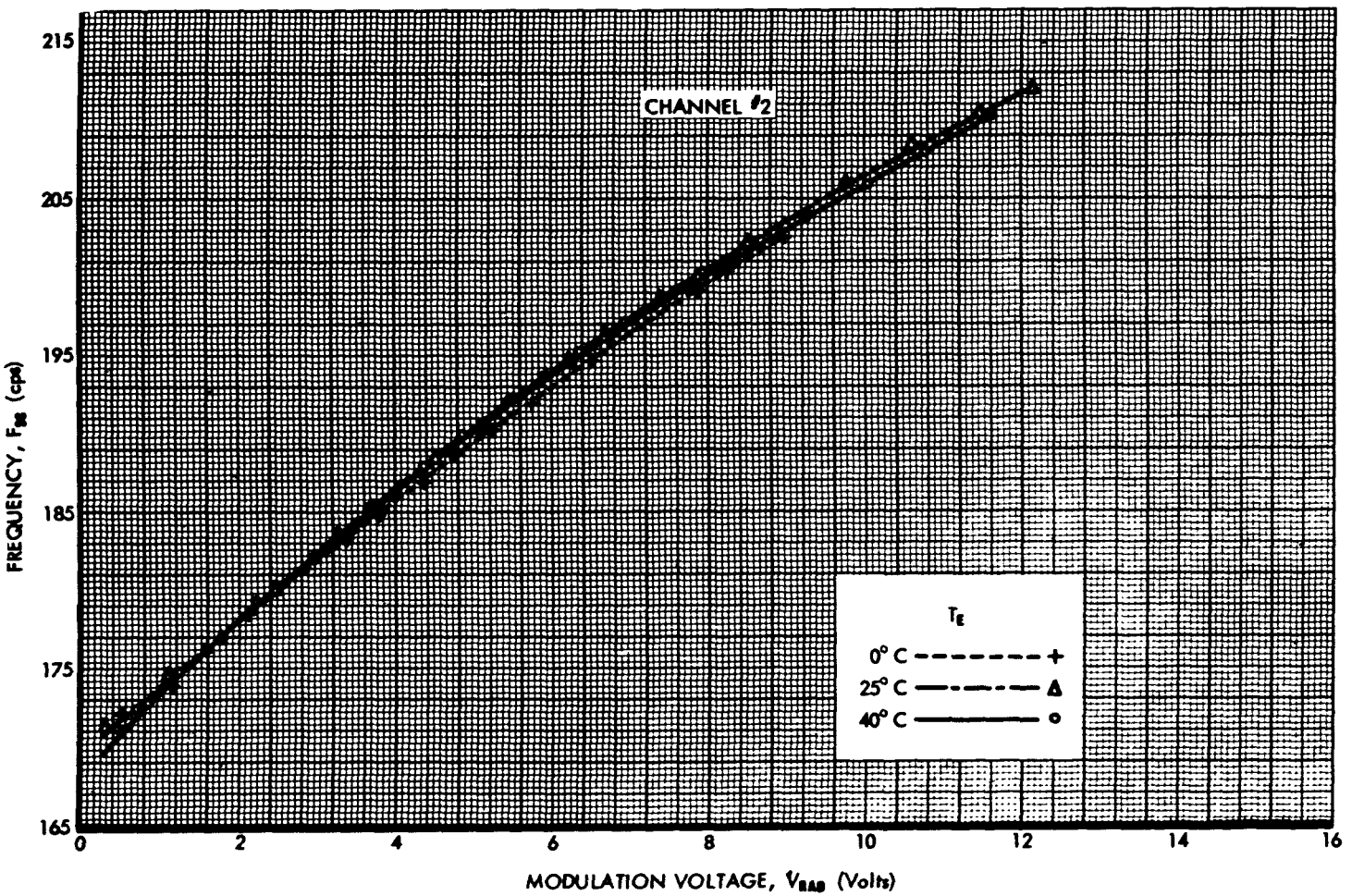

Figure 12—The response of the voltage controlled oscillator for channel 2 shown as a parametric function of the electronics temperature, T_E.

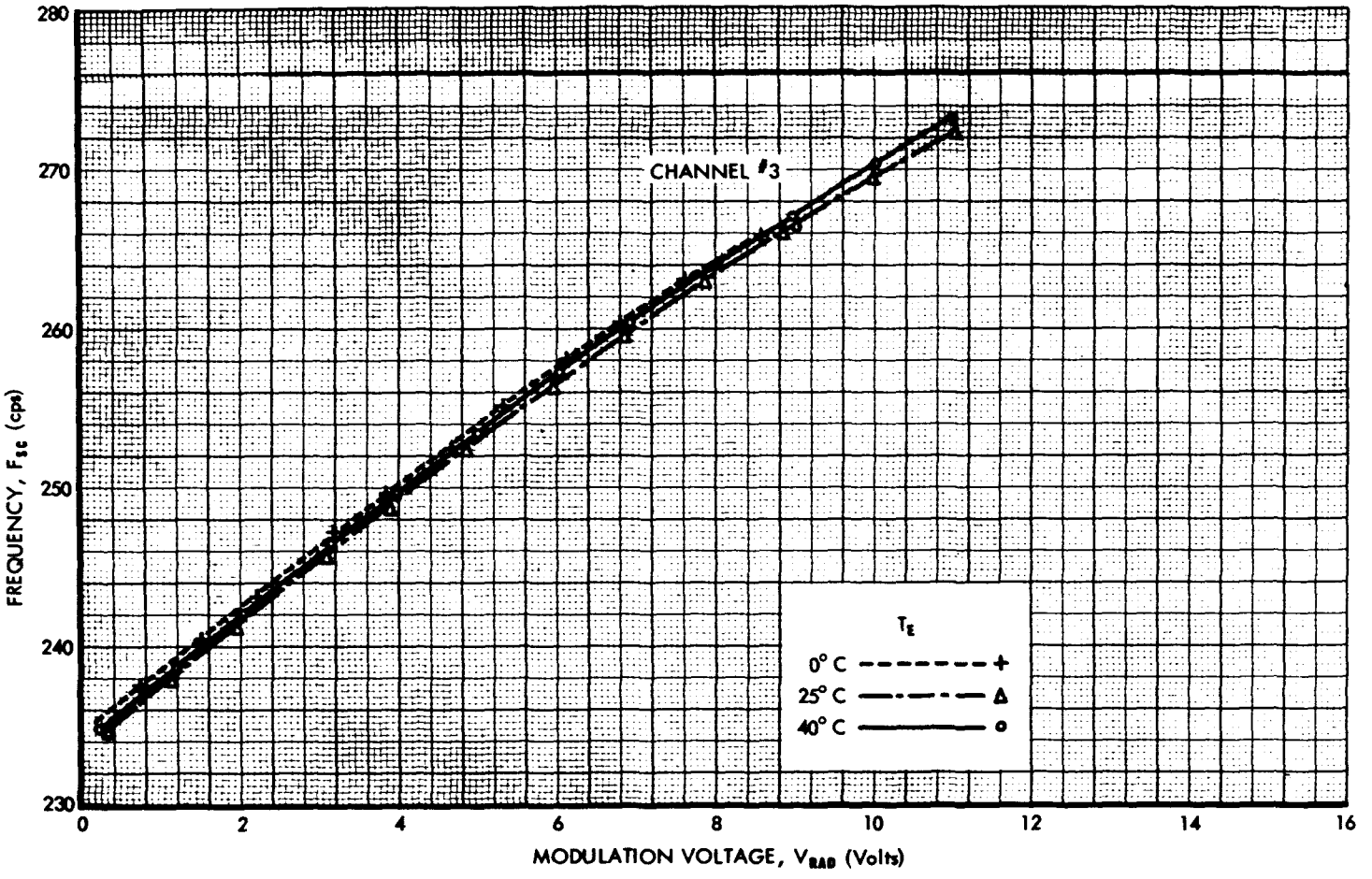

Figure 13—The response of the voltage controlled oscillator for channel 3 shown as a parametric function of the electronics temperature, T_E.

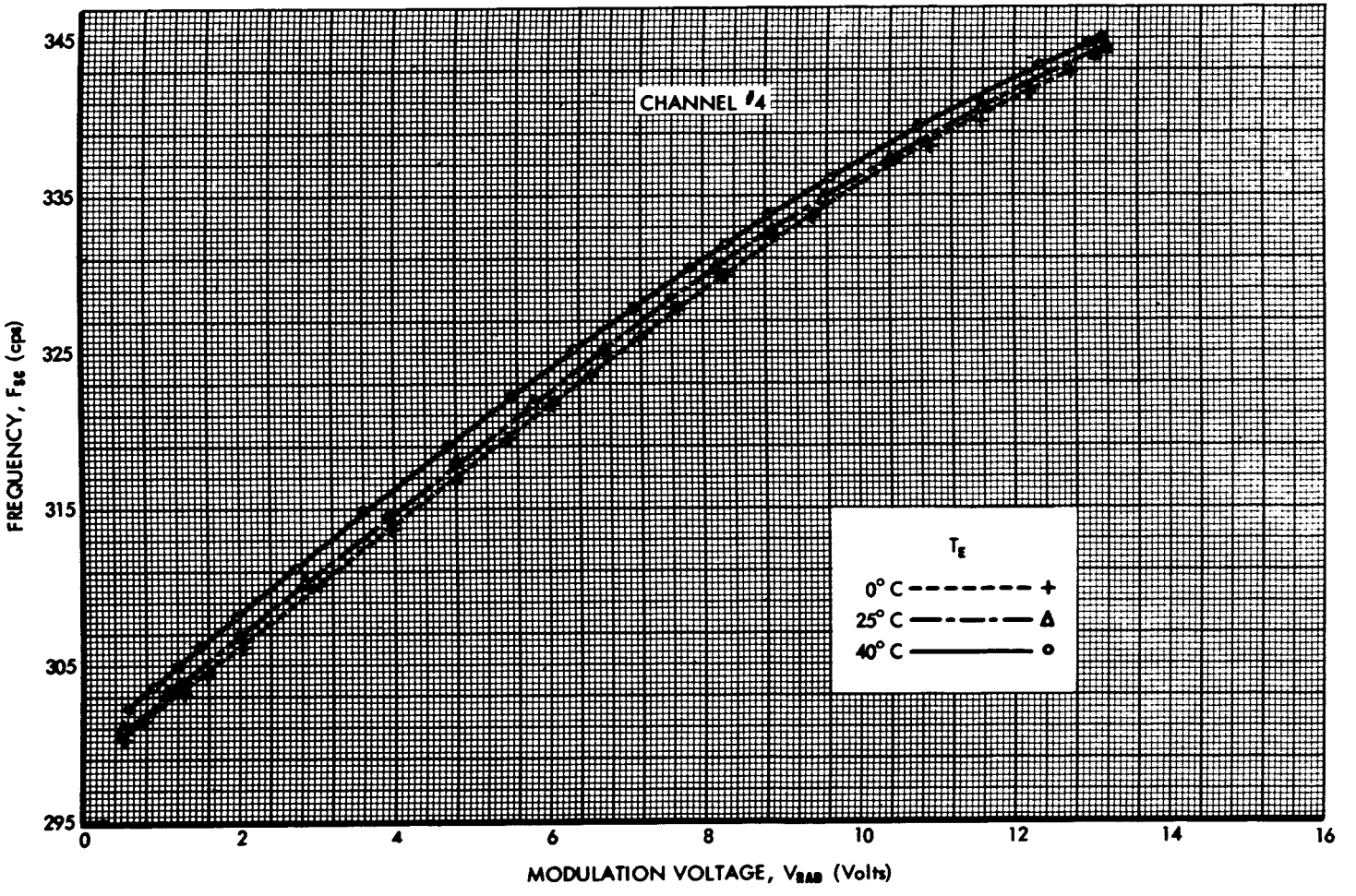

Figure 14—The response of the voltage controlled oscillator for channel 4 shown as a parametric function of the electronics temperature, T_E.

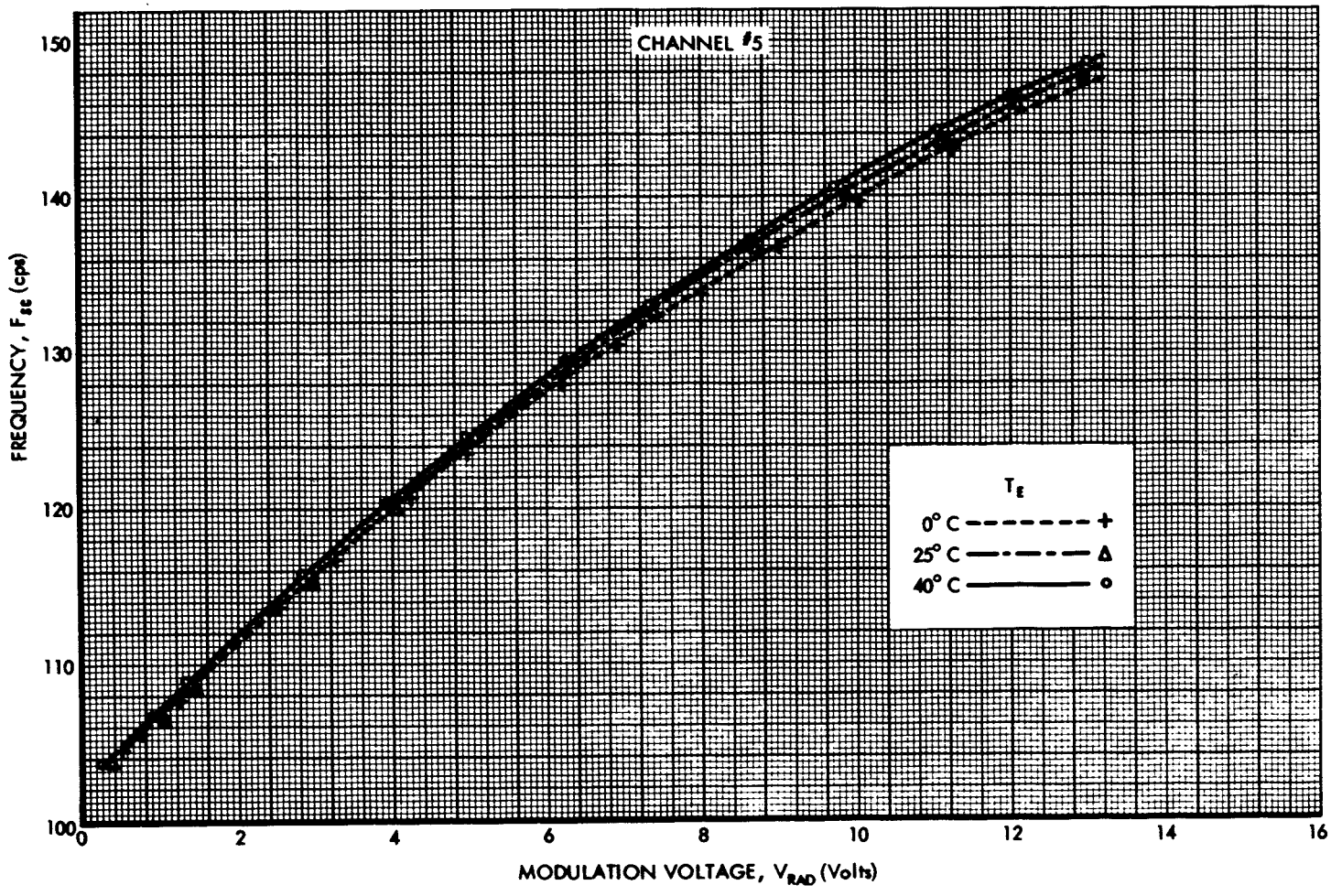

Figure 15—The response of the voltage controlled oscillator for channel 5 shown as a parametric function of the electronics temperature, T_E.

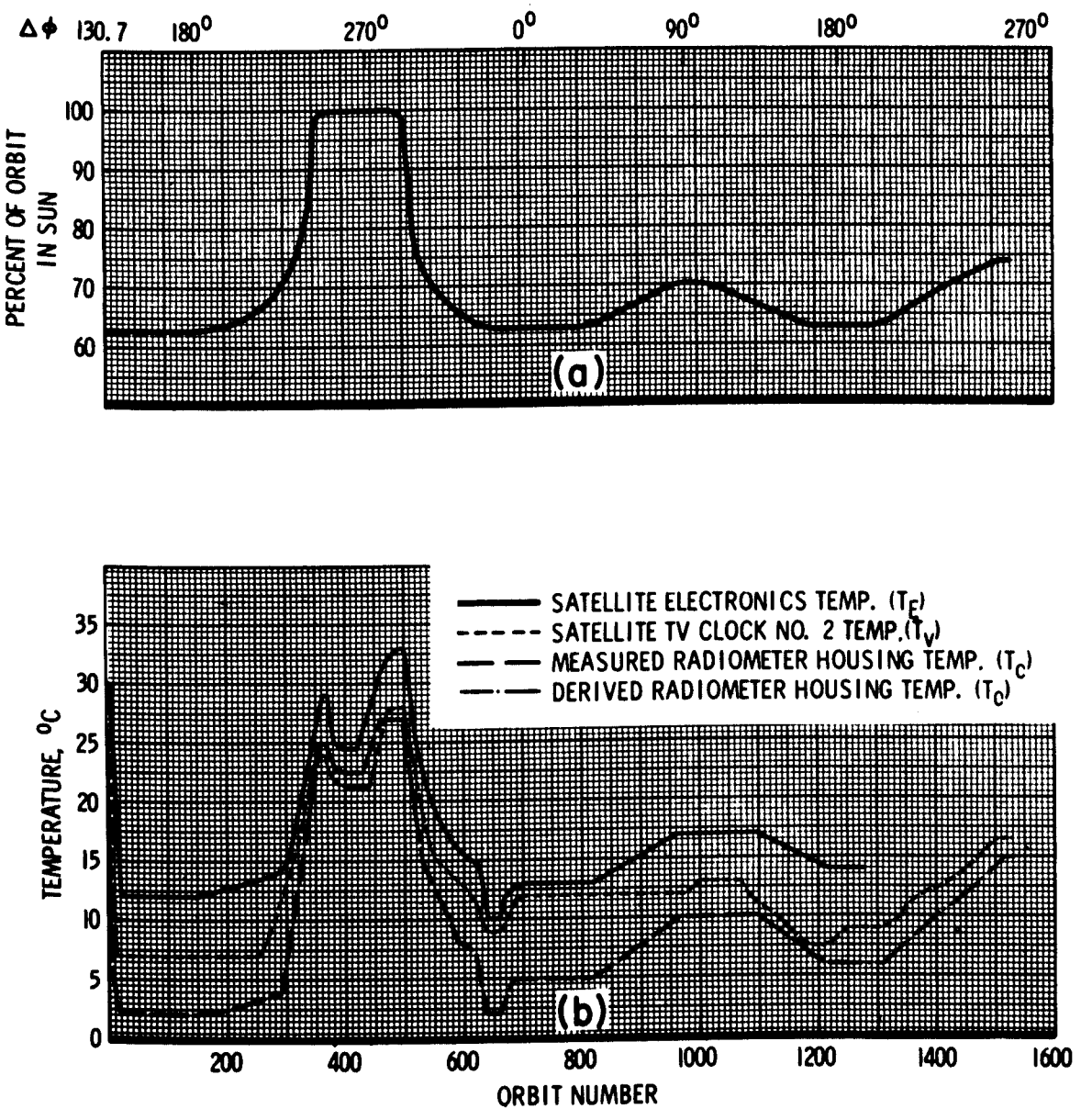

Figure 16—(a) Percent of the orbital period which the satellite spends in sunlight versus orbit number. Also shown on the upper abscissa is $\Delta\phi$, the right ascension of the sun minus the right ascension of the orbital ascending node. (b) Radiometer electronics temperature (T_E), television clock number 2 temperature (T_V), and measured and derived radiometer housing temperatures (T_C) versus orbit number. Telemetry of the "housekeeping information" for the radiometer ceased at orbit 1276, after which T_C was derived from T_V.

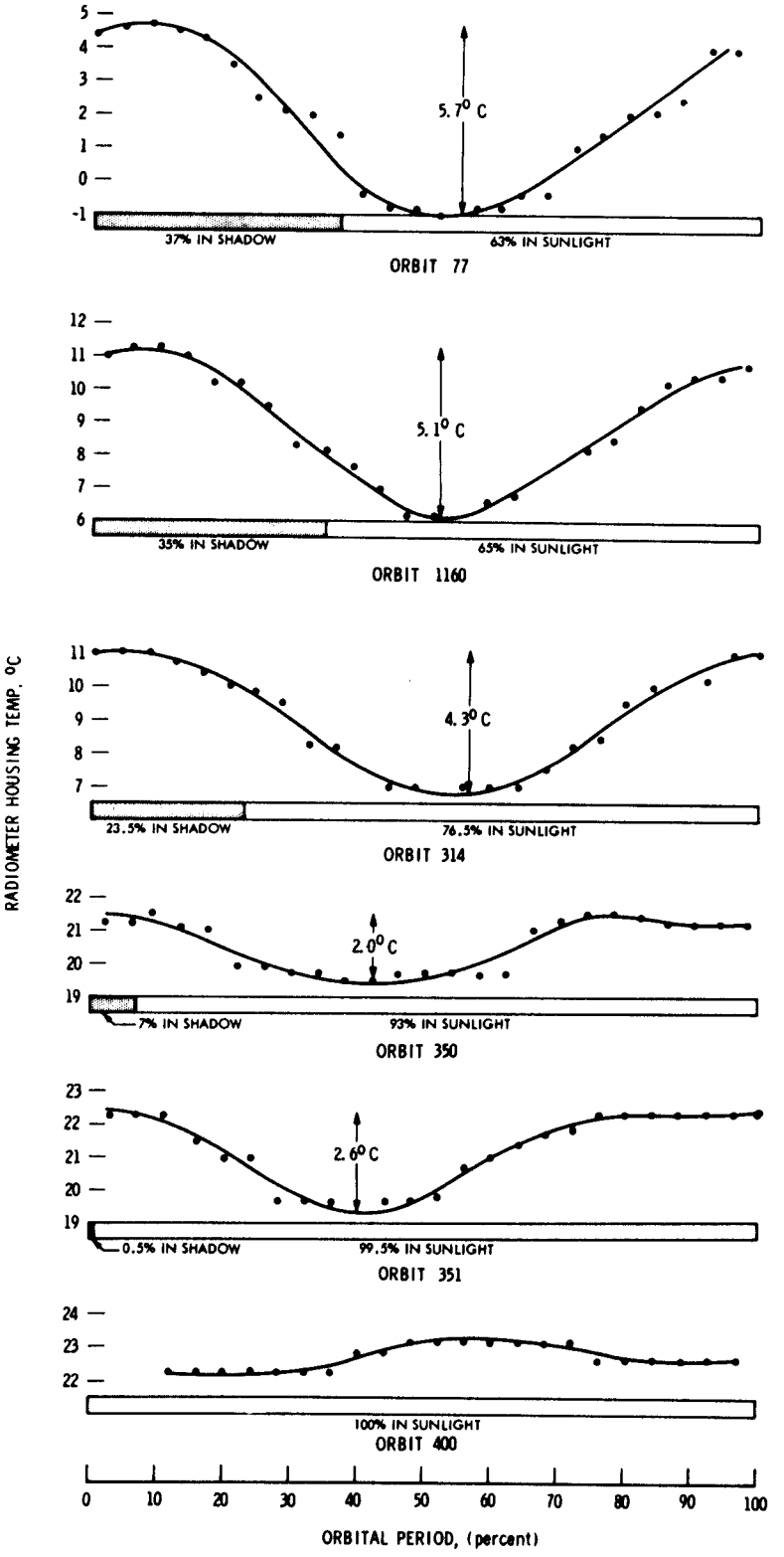

Figure 17—Selected TIROS VII orbits showing the variation of the satellite housing temperature, T_c, during an orbital period as a function of the time the satellite is in the earth's shadow or in sunlight.

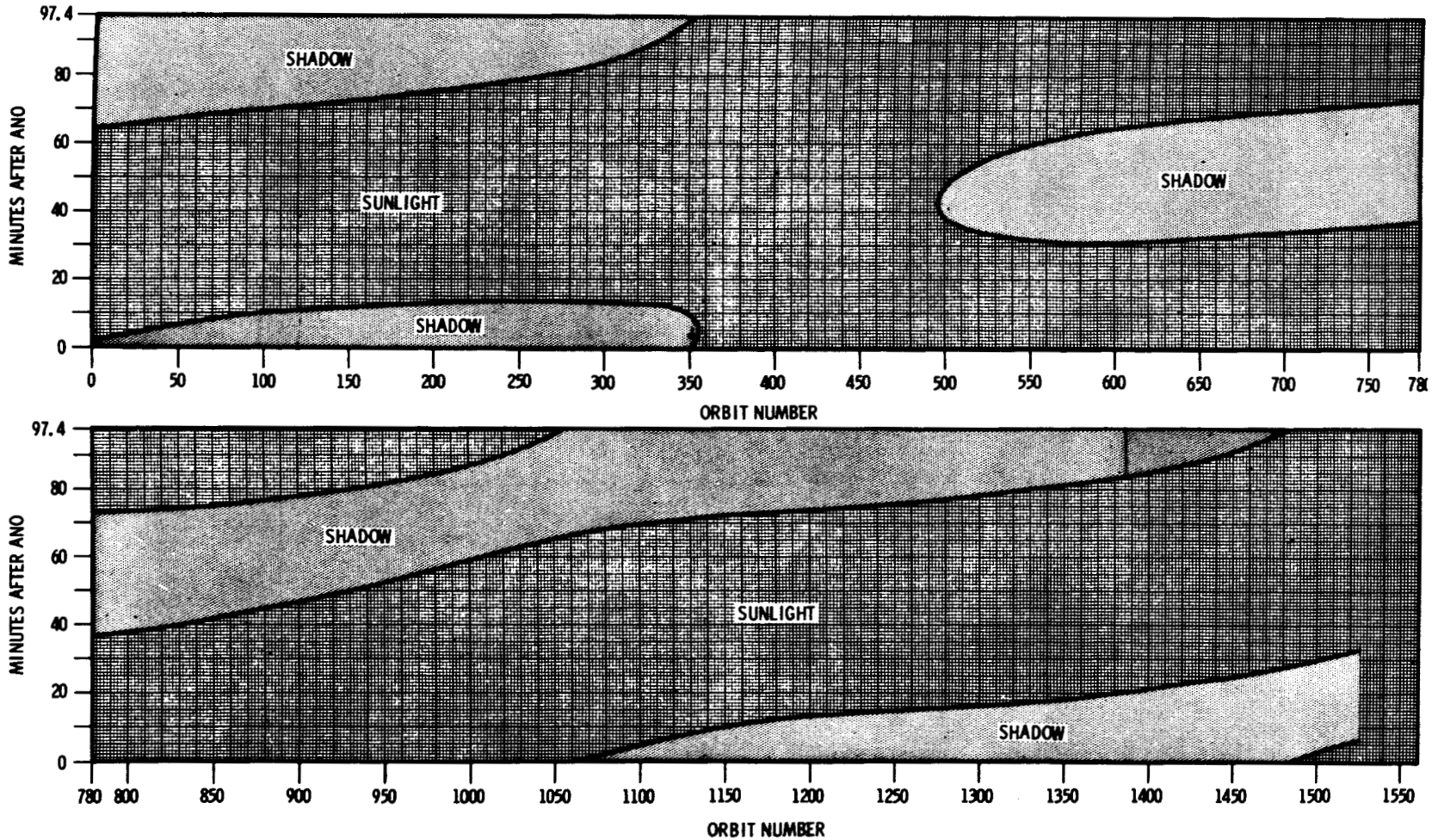

Figure 18—Portions of the 97.4-minute orbital period when the satellite is in sunlight and in the earth's shadow, expressed in minutes after the ascending node, versus orbit number.

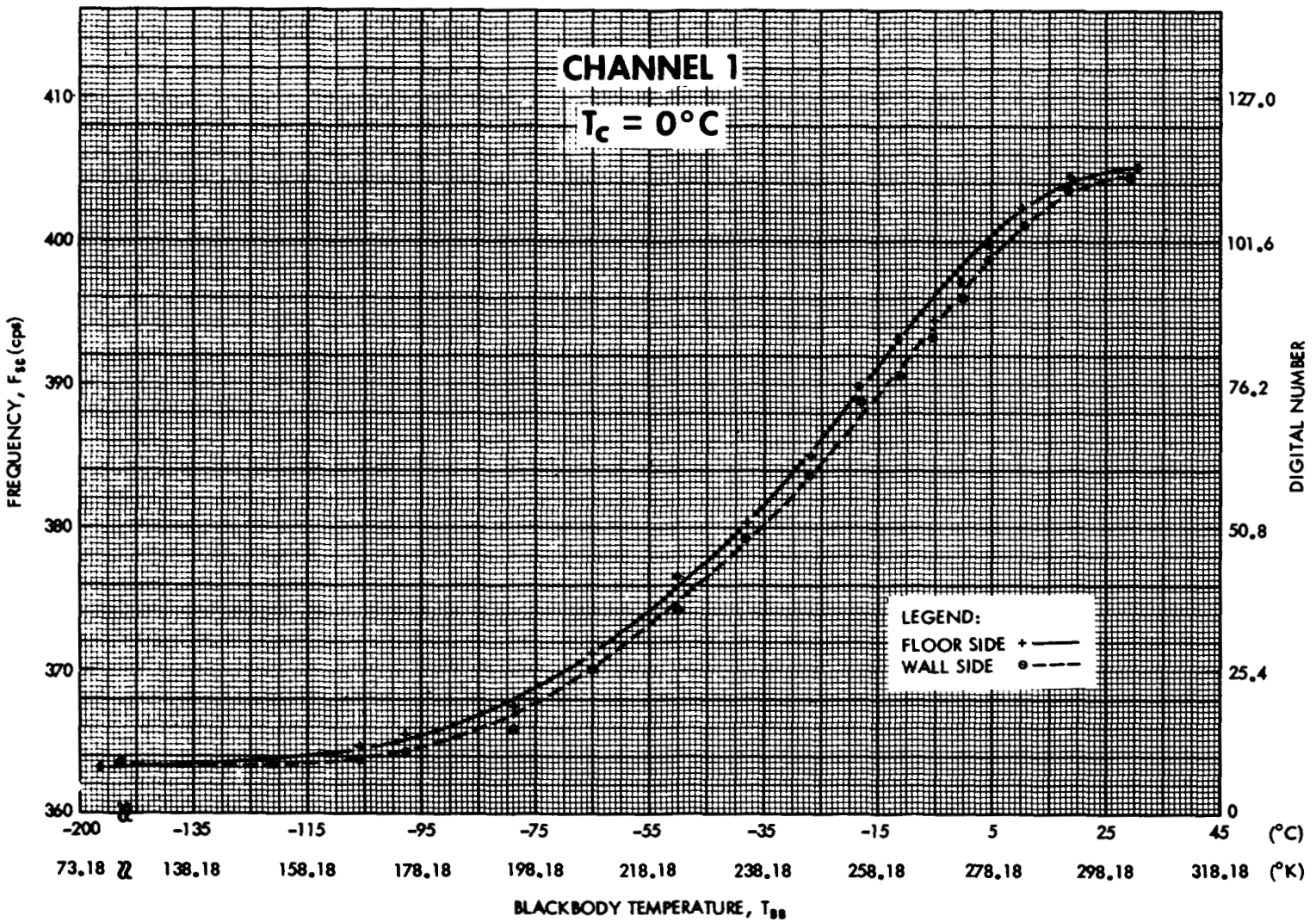

Figure 19—Subcarrier frequency and digital number versus equivalent blackbody temperature for floor and wall sides of channel 1. (T_c = 0°C)

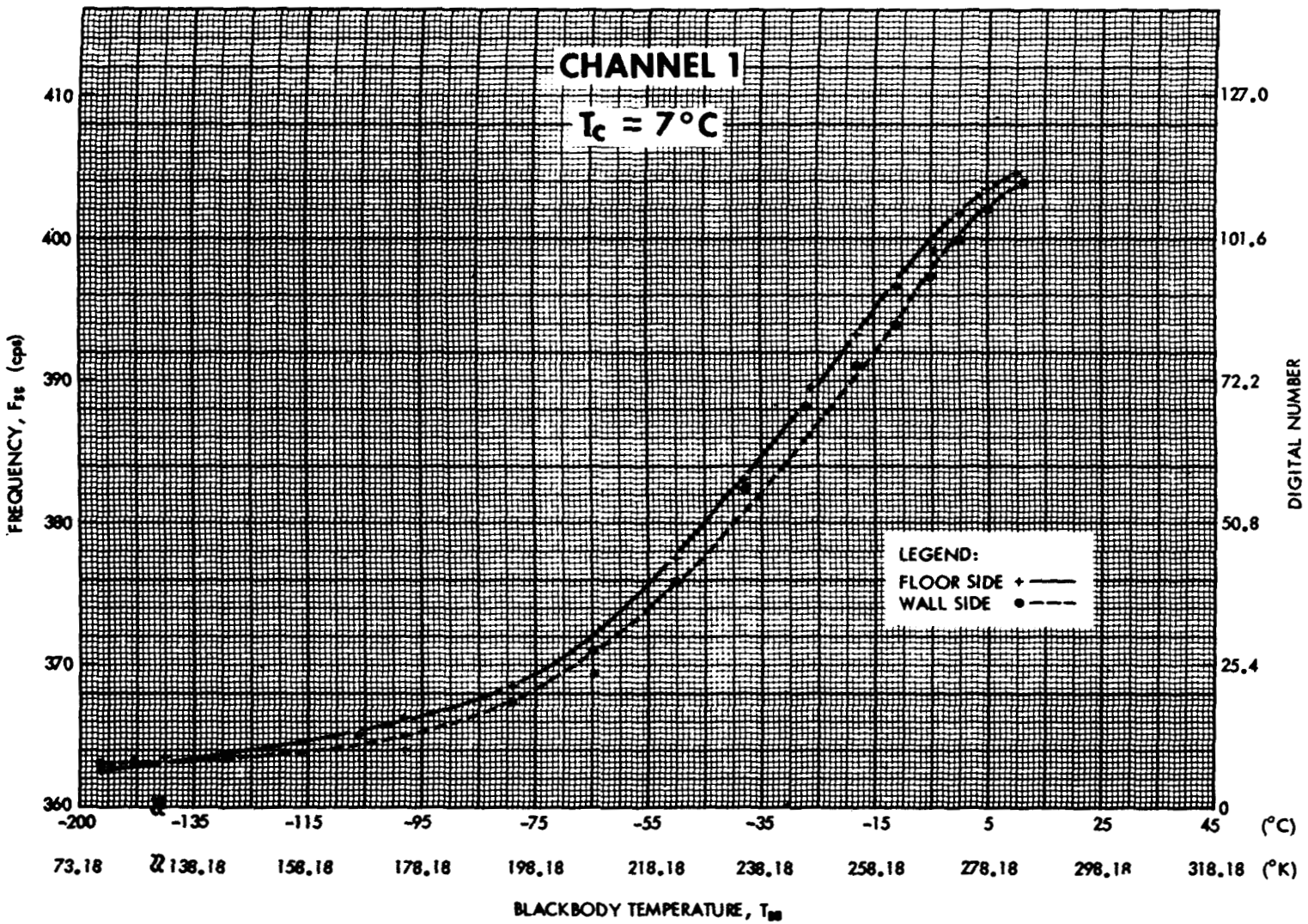

Figure 20—Subcarrier frequency and digital number versus equivalent blackbody temperature for floor and wall sides of channel 1. (T_c = 7°C)

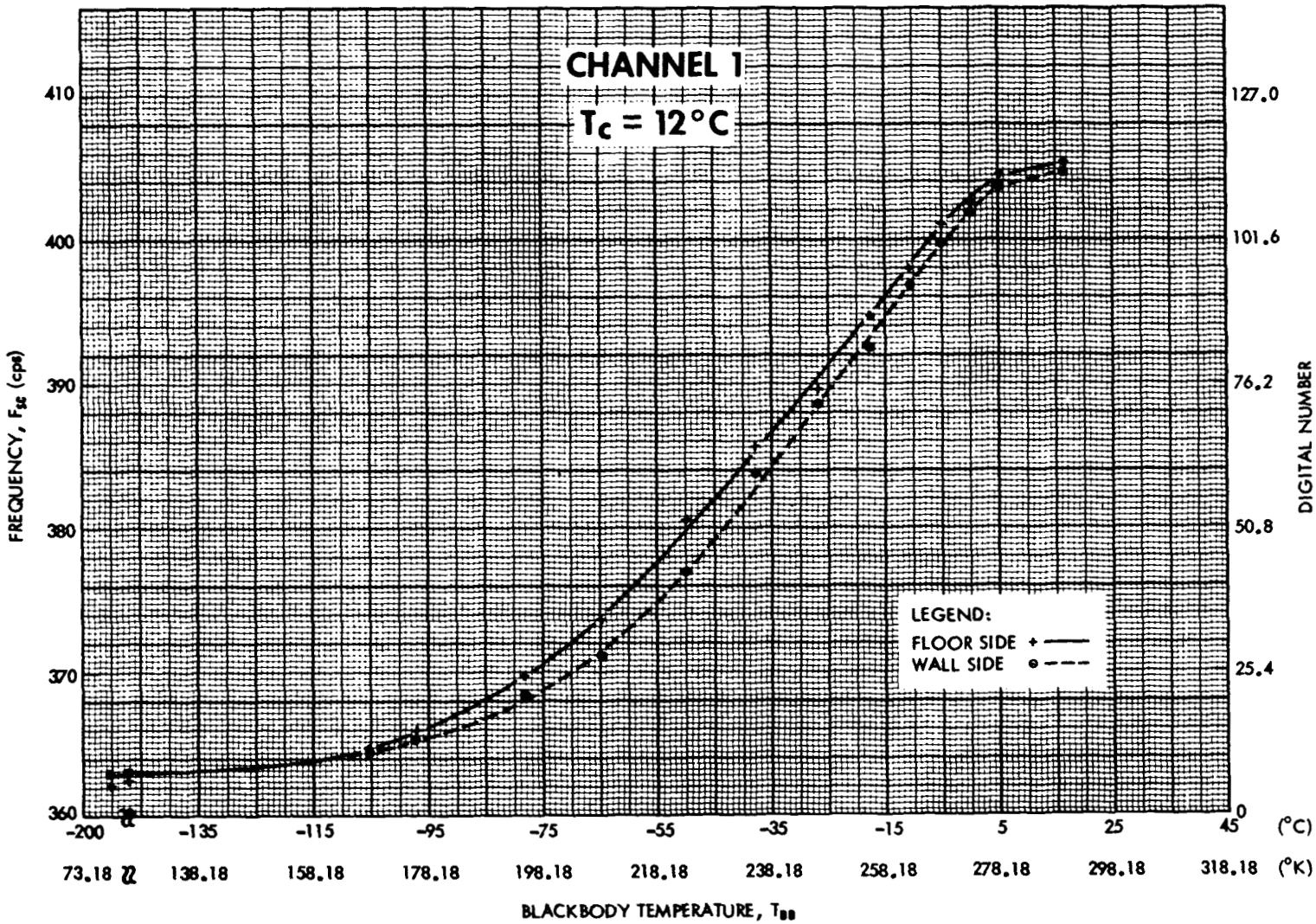

Figure 21—Subcarrier frequency and digital number versus equivalent blackbody temperature for floor and wall sides of channel 1. (T_c = 12°C)

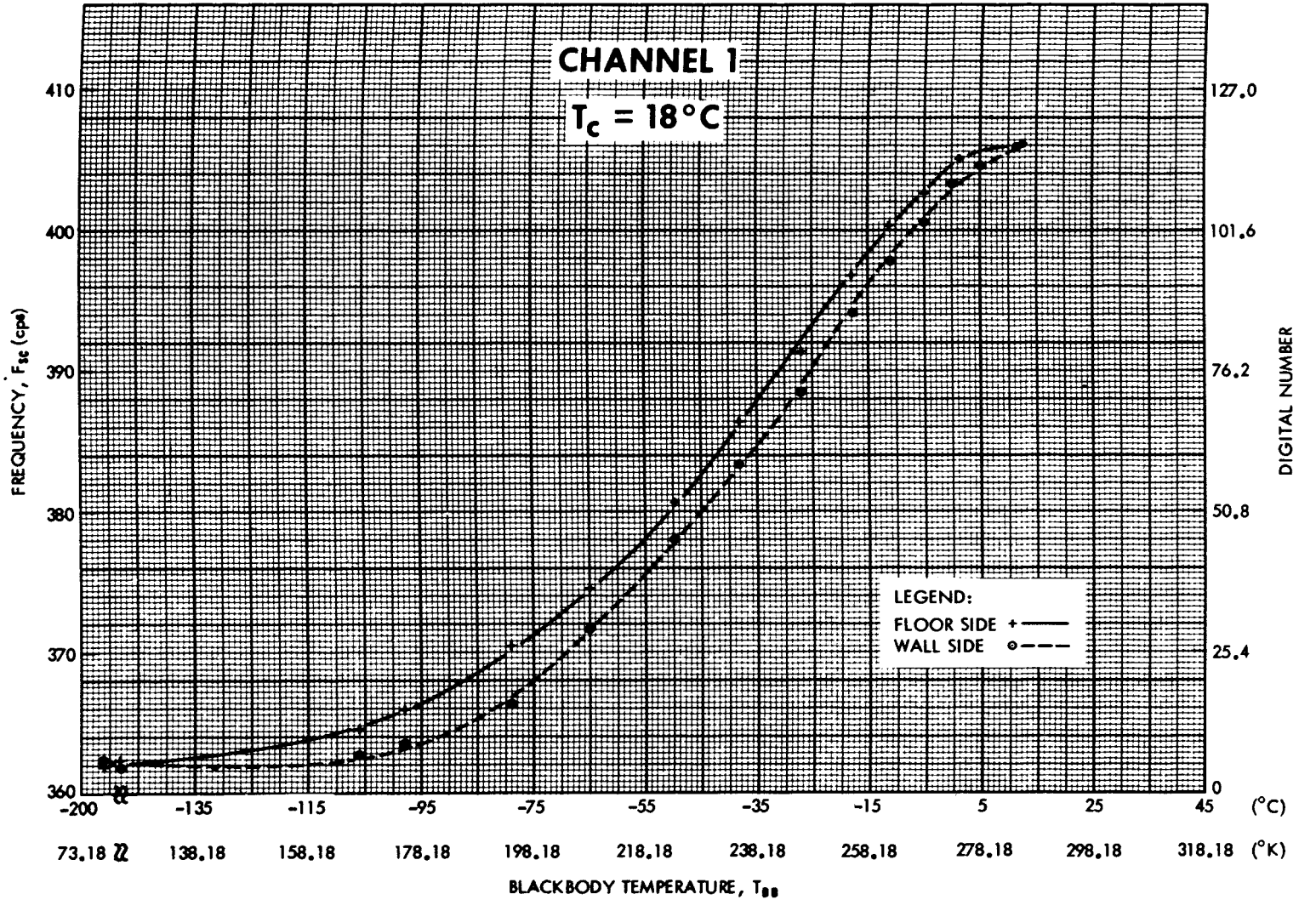

Figure 22—Subcarrier frequency and digital number versus equivalent blackbody temperature for floor and wall sides of channel 1. (T_c = 18°C)

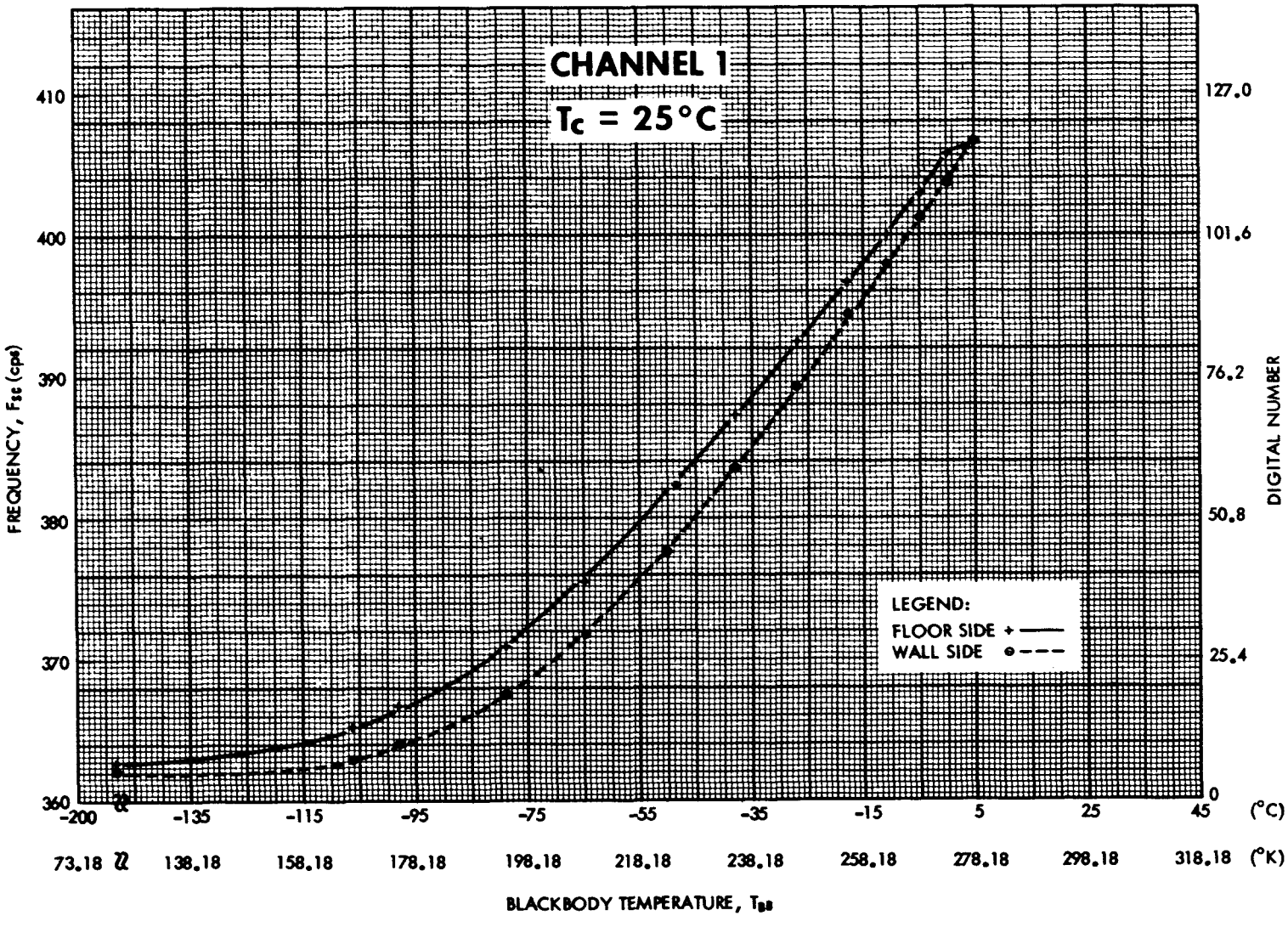

Figure 23—Subcarrier frequency and digital number versus equivalent blackbody temperature for floor and wall sides of channel 1. (T_c = 25°C)

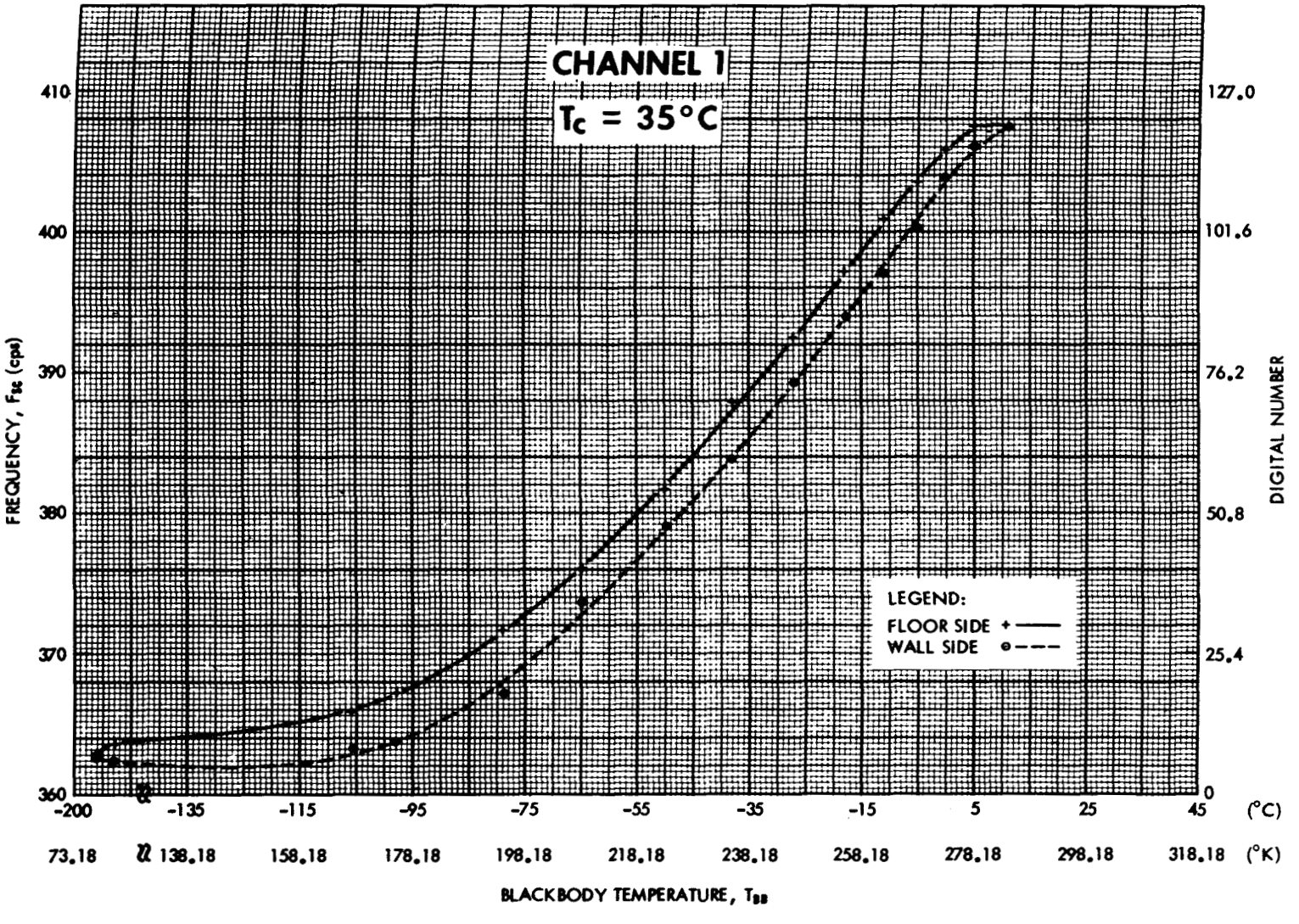

Figure 24—Subcarrier frequency and digital number versus equivalent blackbody temperature for floor and wall sides of channel 1. (T_C = 35°C)

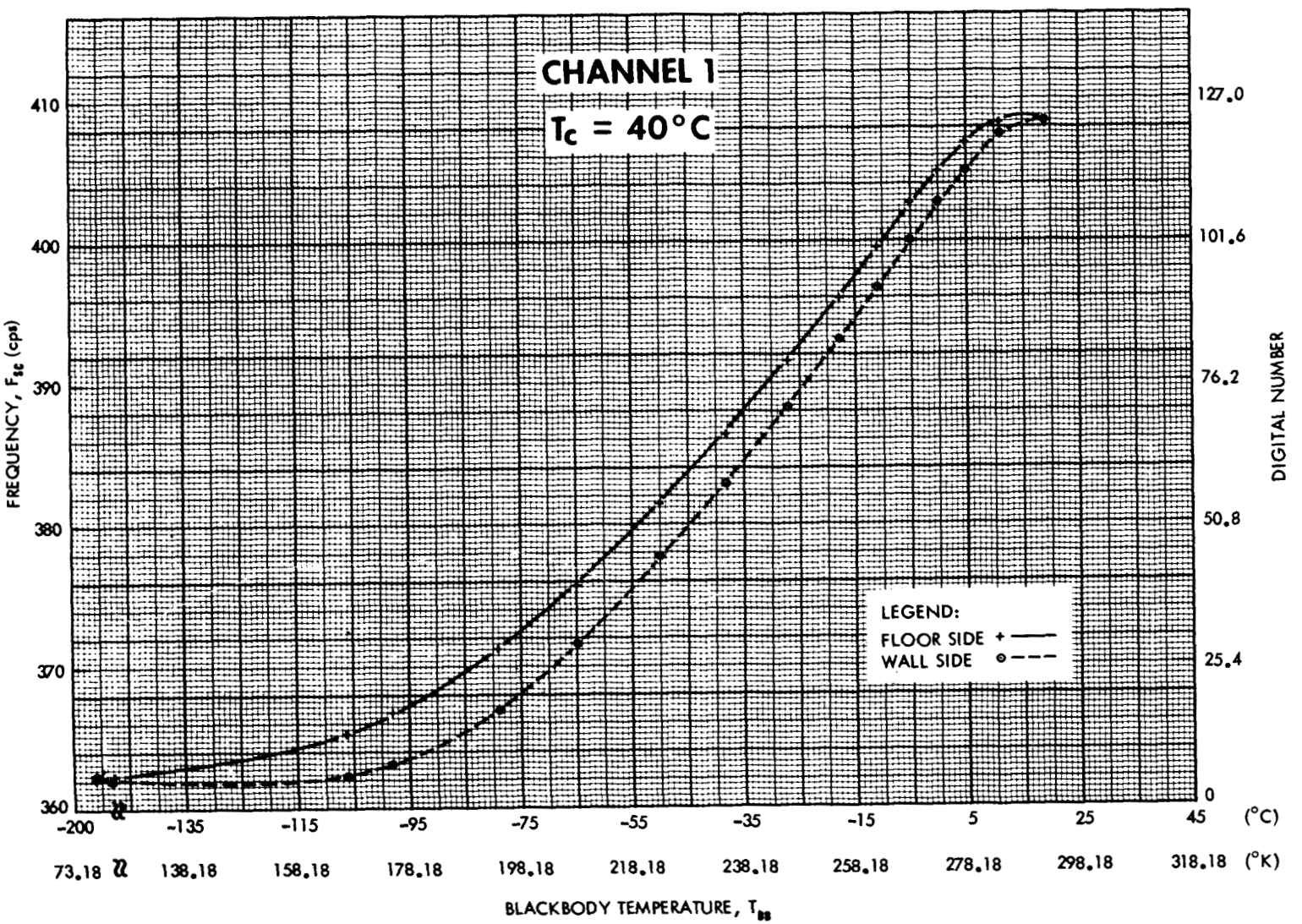

Figure 25—Subcarrier frequency and digital number versus equivalent blackbody temperature for floor and wall sides of channel 1. (T_c = 40°C)

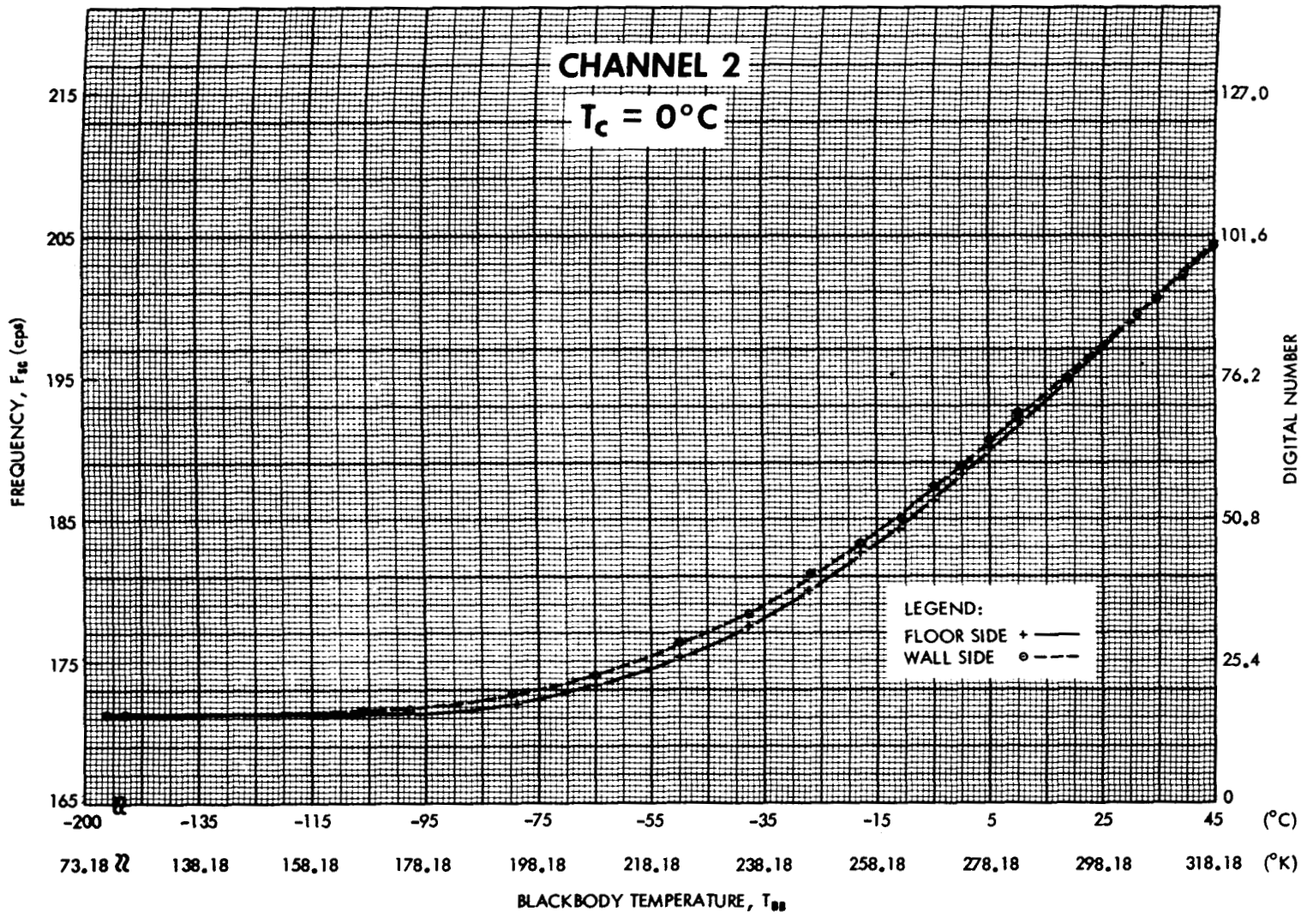

Figure 26—Subcarrier frequency and digital number versus equivalent blackbody temperature for floor and wall sides of channel 2. (T_c = 0°C)

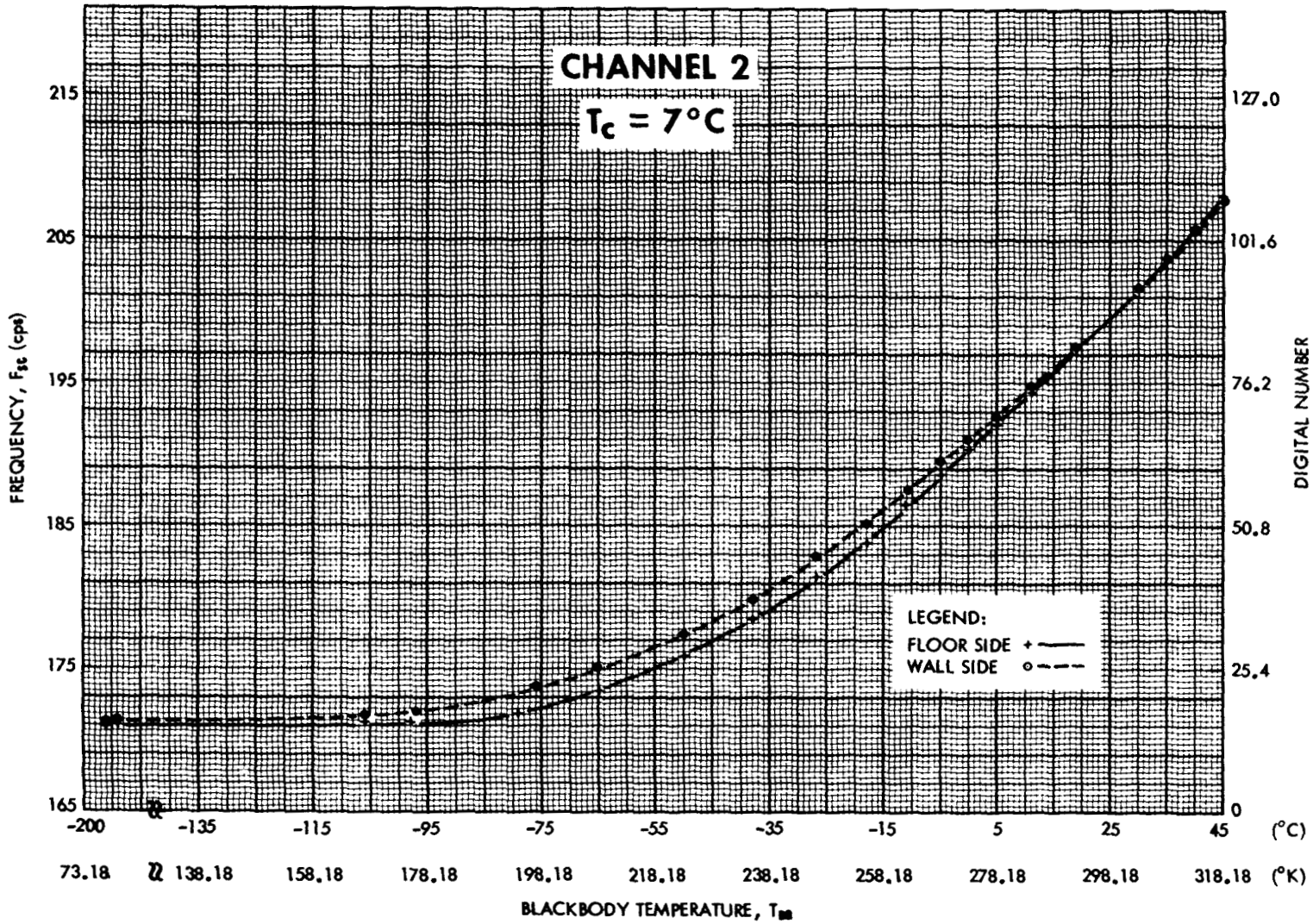

Figure 27—Subcarrier frequency and digital number versus equivalent blackbody temperature for floor and wall sides of channel 2. (T_c = 7°C)

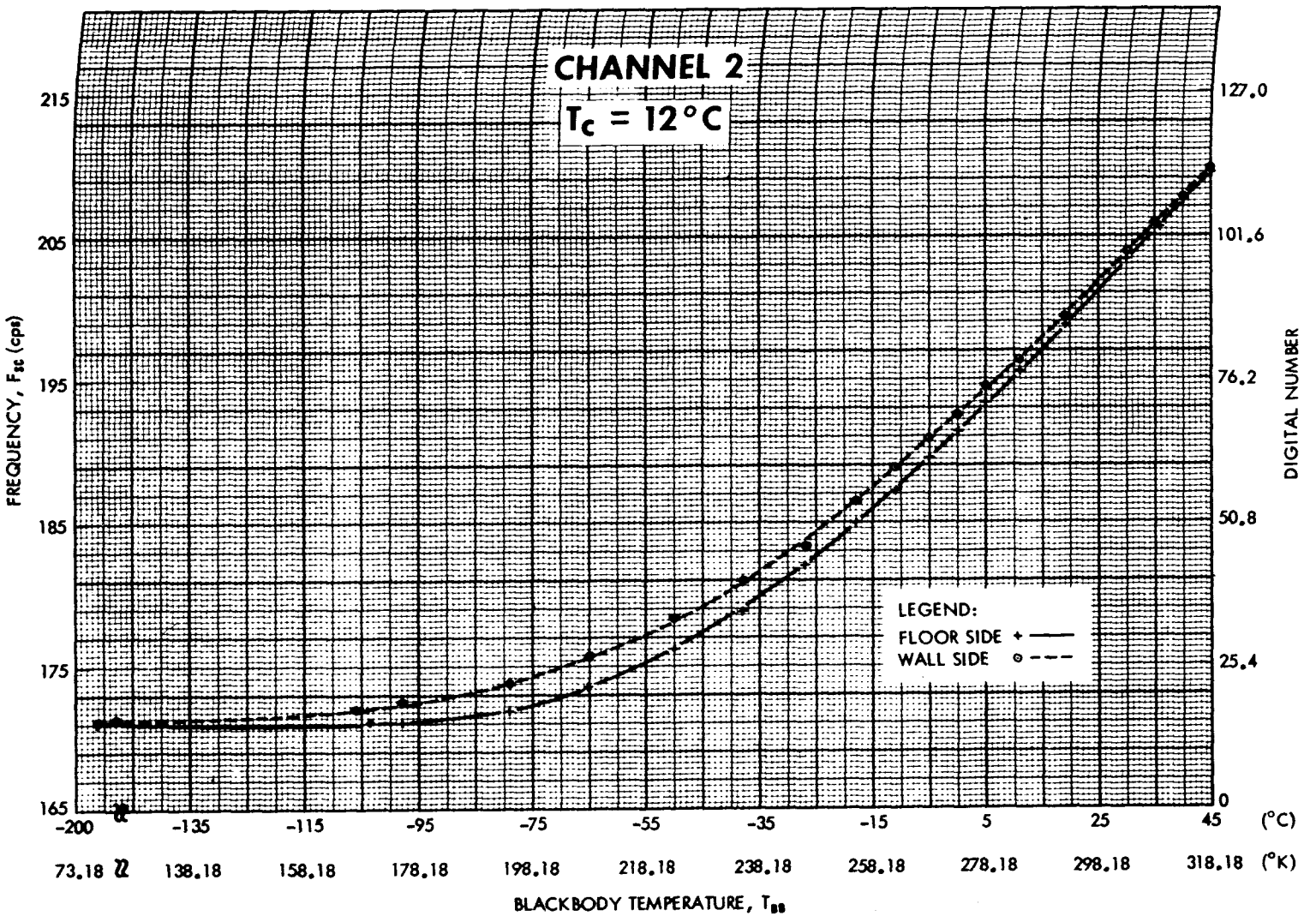

Figure 28—Subcarrier frequency and digital number versus equivalent blackbody temperature for floor and wall sides of channel 2. (T_c = 12°C)

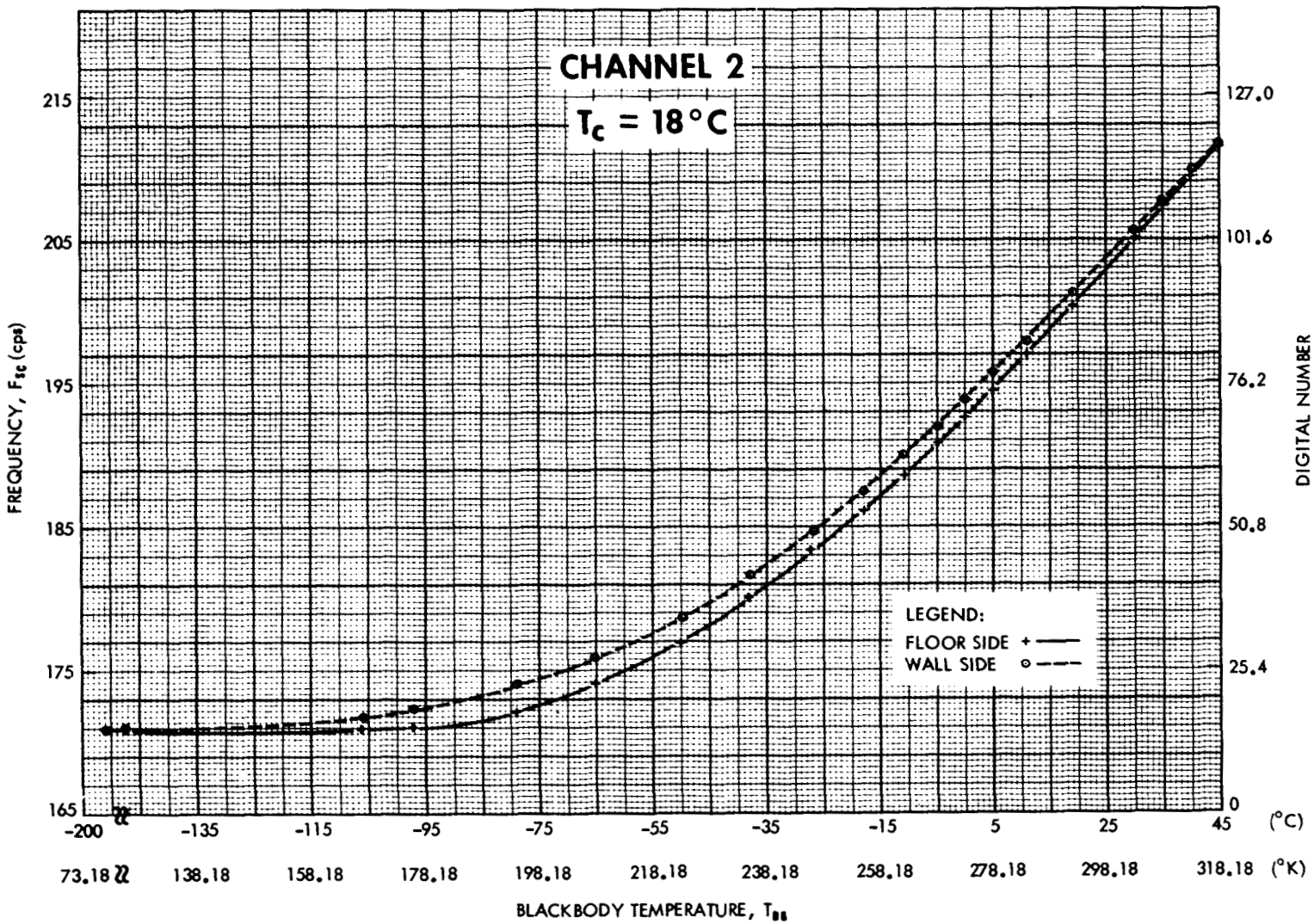

Figure 29—Subcarrier frequency and digital number versus equivalent blackbody temperature for floor and wall sides of channel 2. (T_c = 18°C)

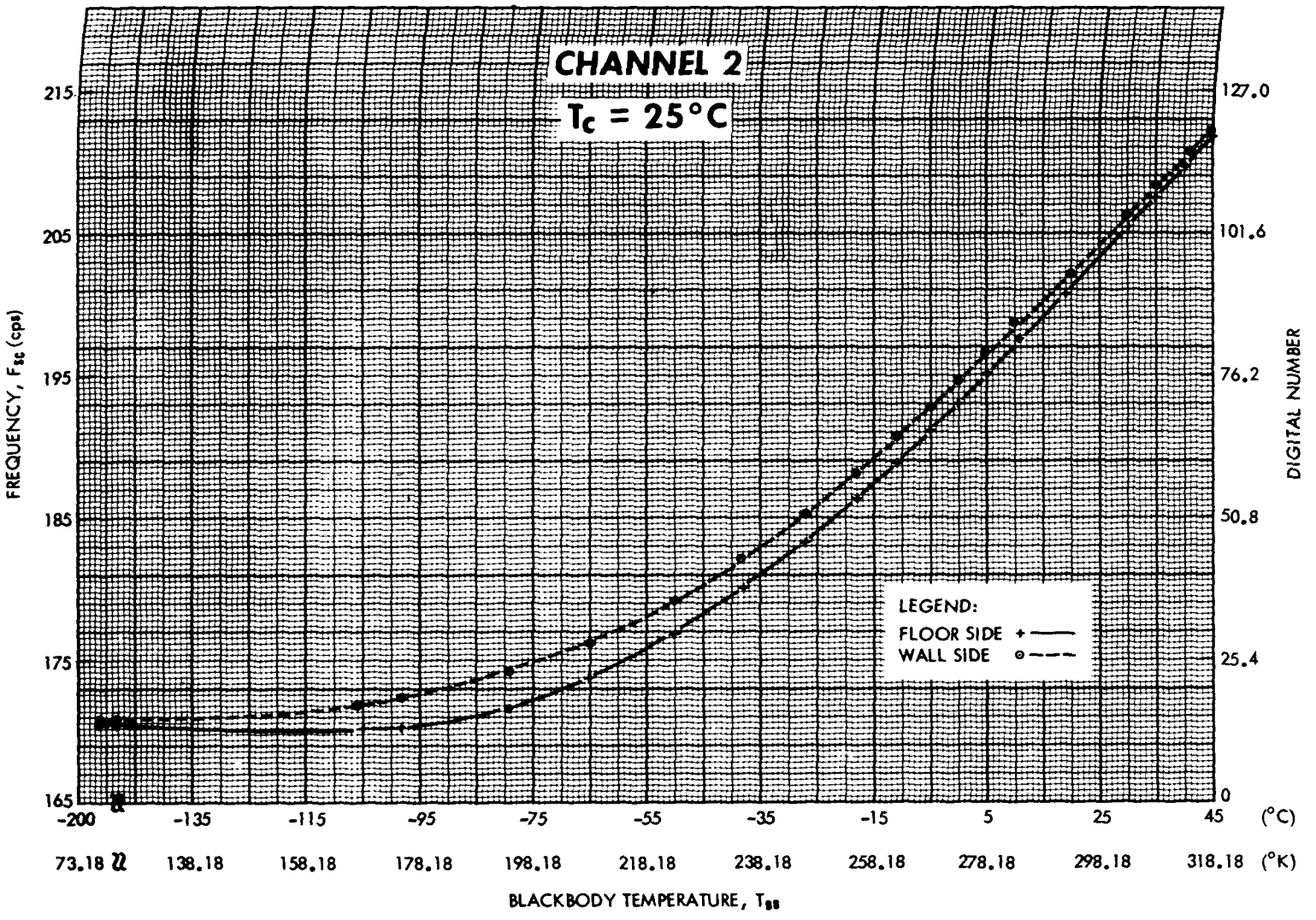

Figure 30—Subcarrier frequency and digital number versus equivalent blackbody temperature for floor and wall sides of channel 2. ($T_c \approx 25°C$)

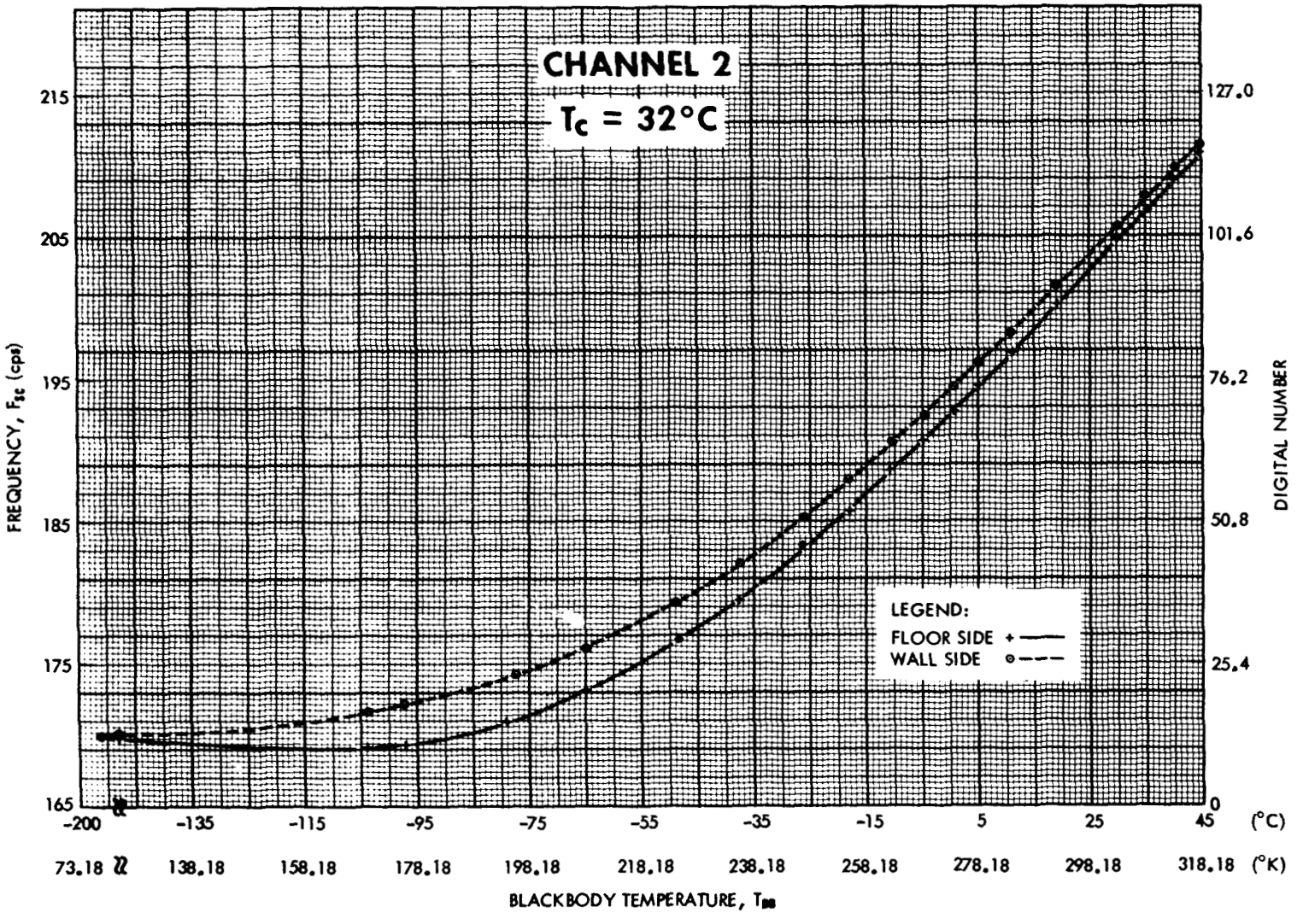

Figure 31—Subcarrier frequency and digital number versus equivalent blackbody temperature for floor and wall sides of channel 2. (T_c = 32°C)

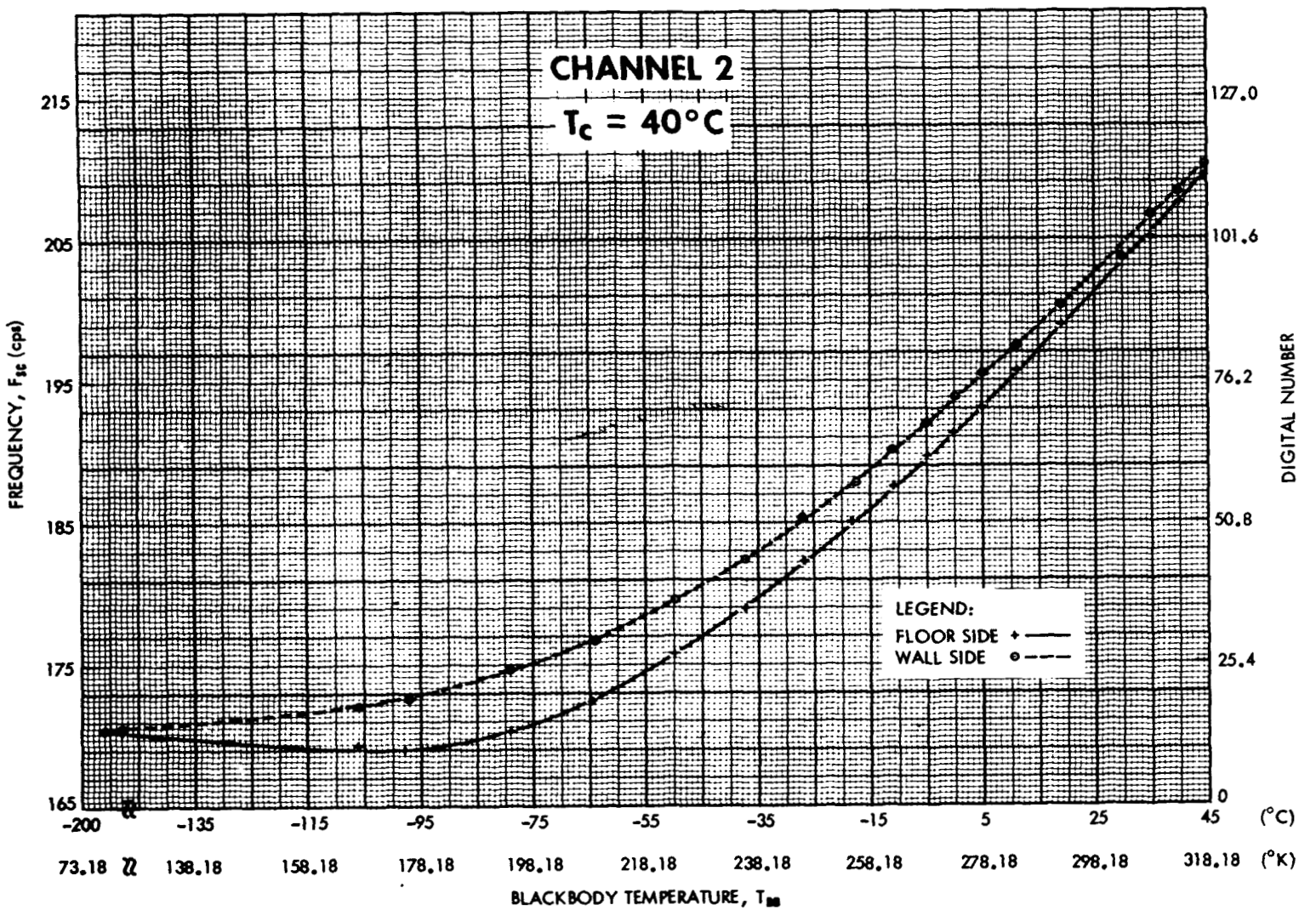

Figure 32—Subcarrier frequency and digital number versus equivalent blackbody temperature for floor and wall sides of channel 2. (T_c = 40°C)

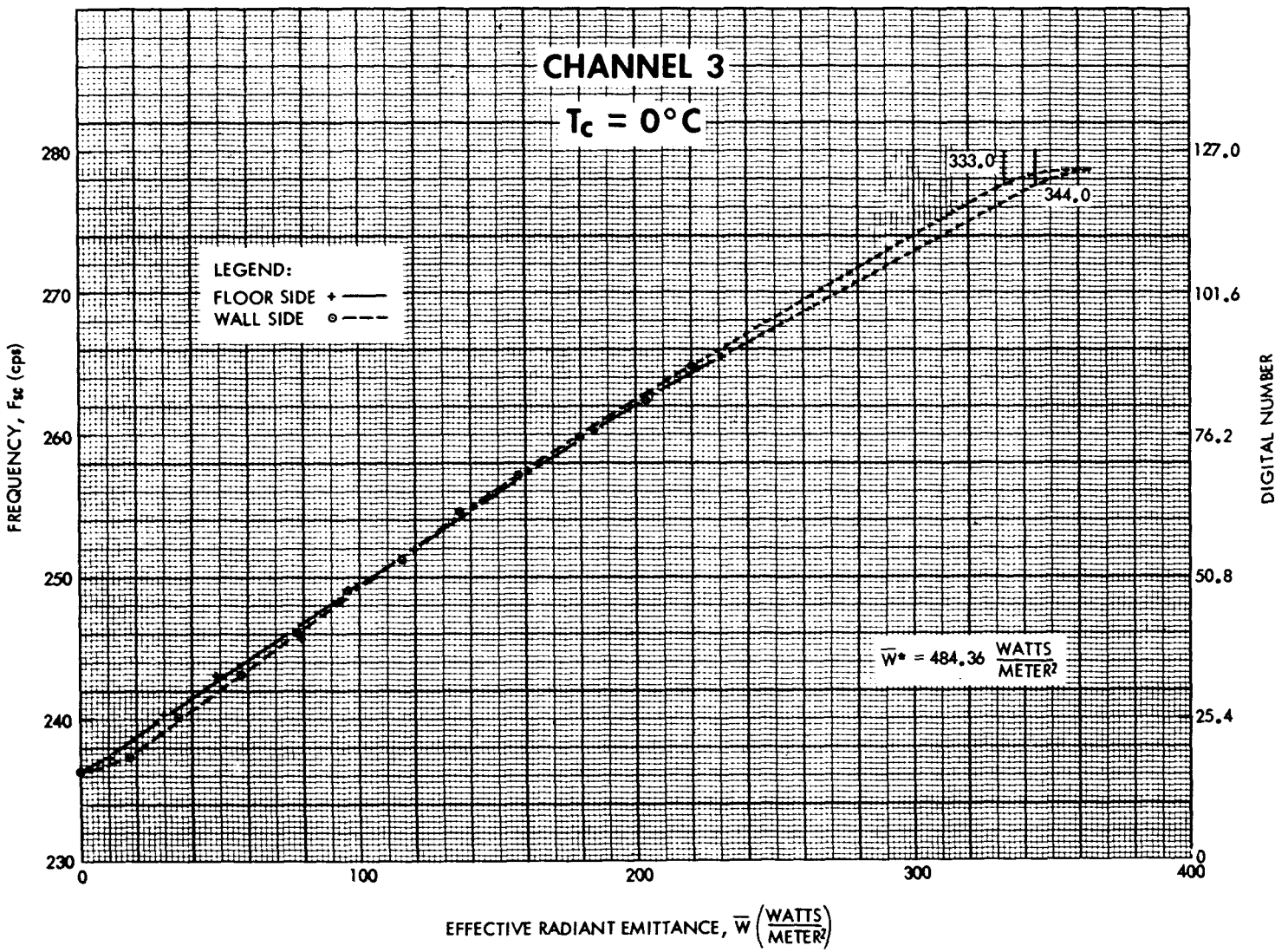

Figure 33—Subcarrier frequency and digital number versus effective radiant emittance for floor and wall sides of channel 3. (T_c = 0°C)

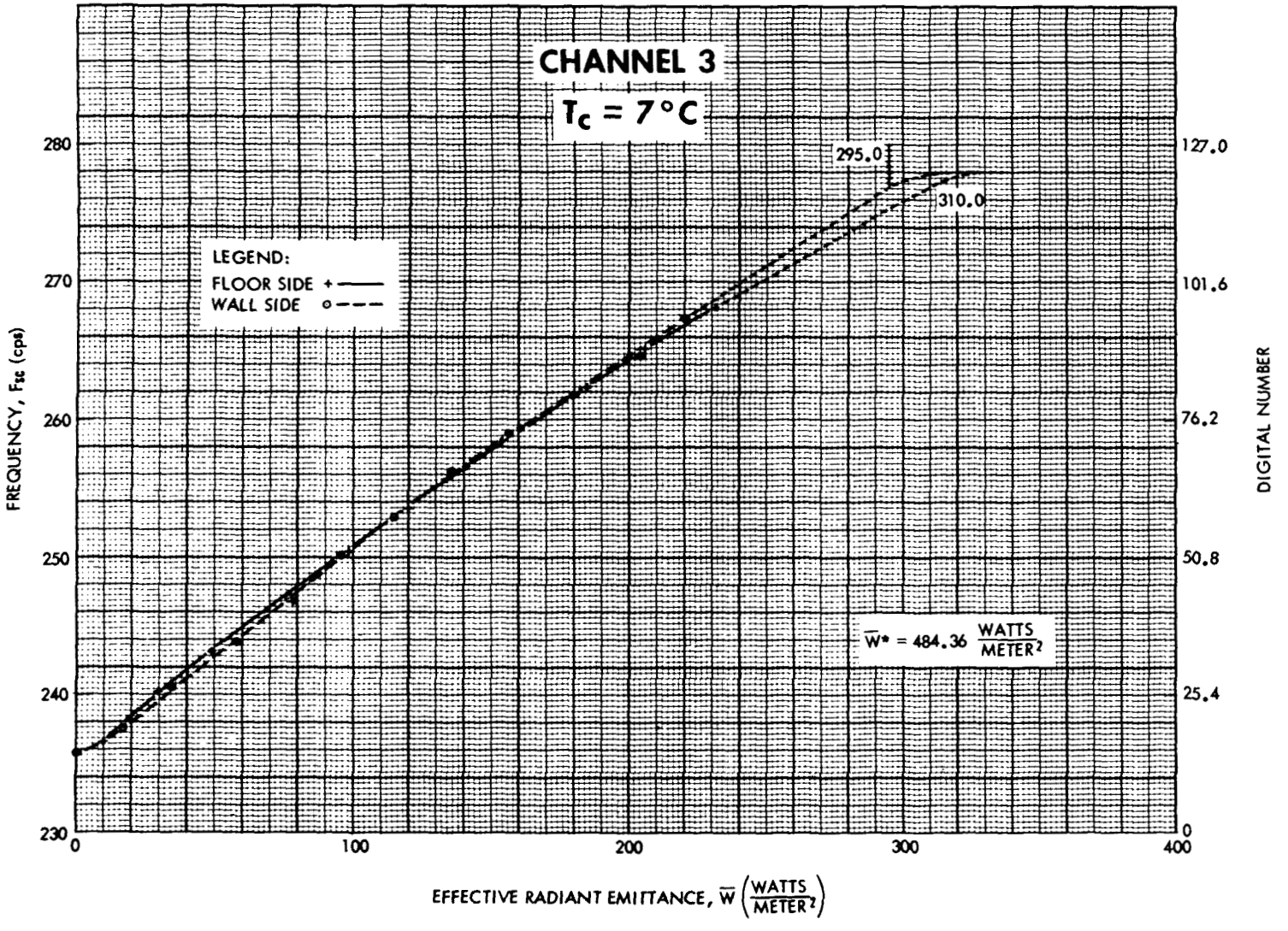

Figure 34—Subcarrier frequency and digital number versus effective radiant emittance for floor and wall sides of channel 3. (T_c = 7°C)

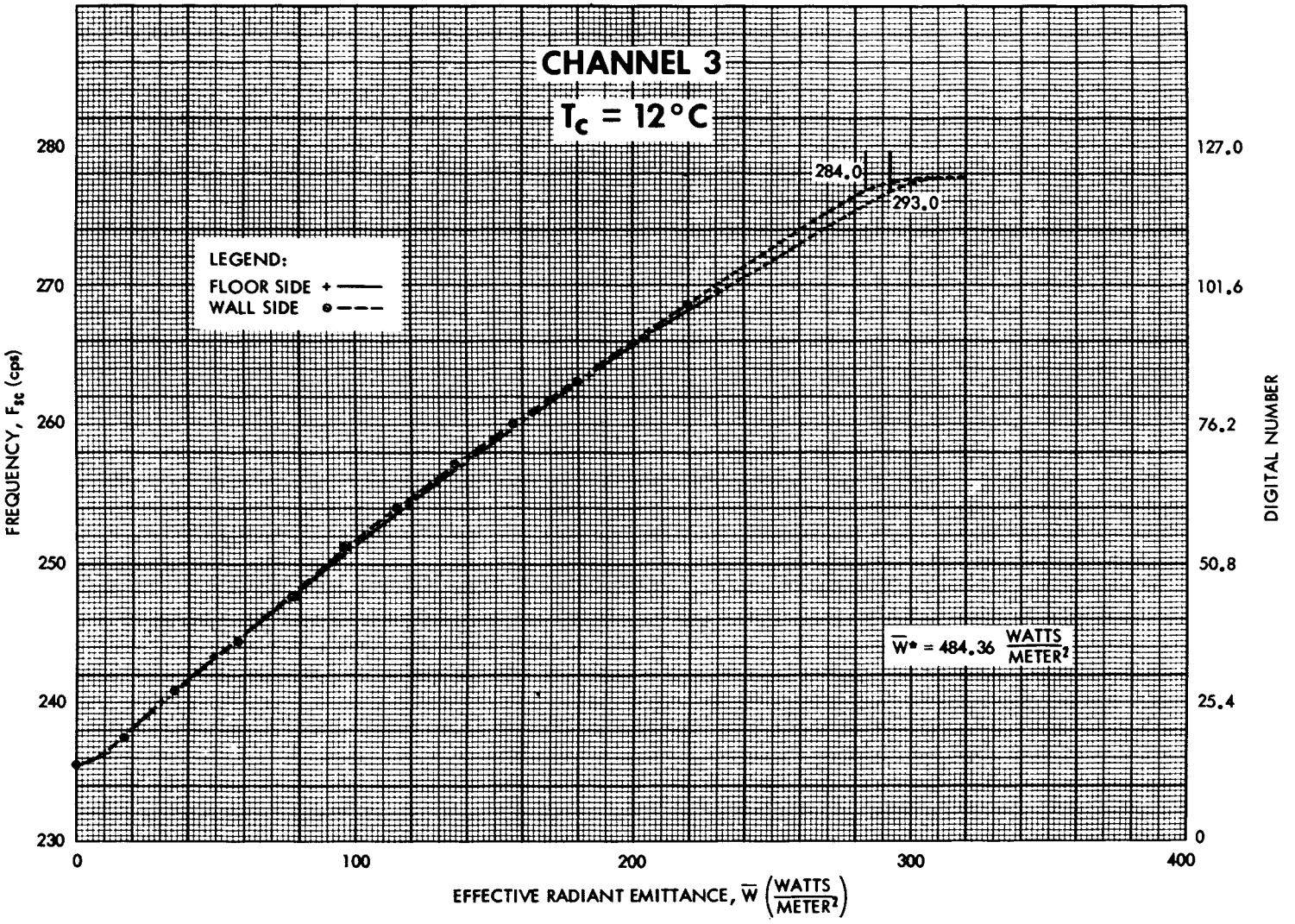

Figure 35—Subcarrier frequency and digital number versus effective radiant emittance for floor and wall sides of channel 3. (T_c = 12°C)

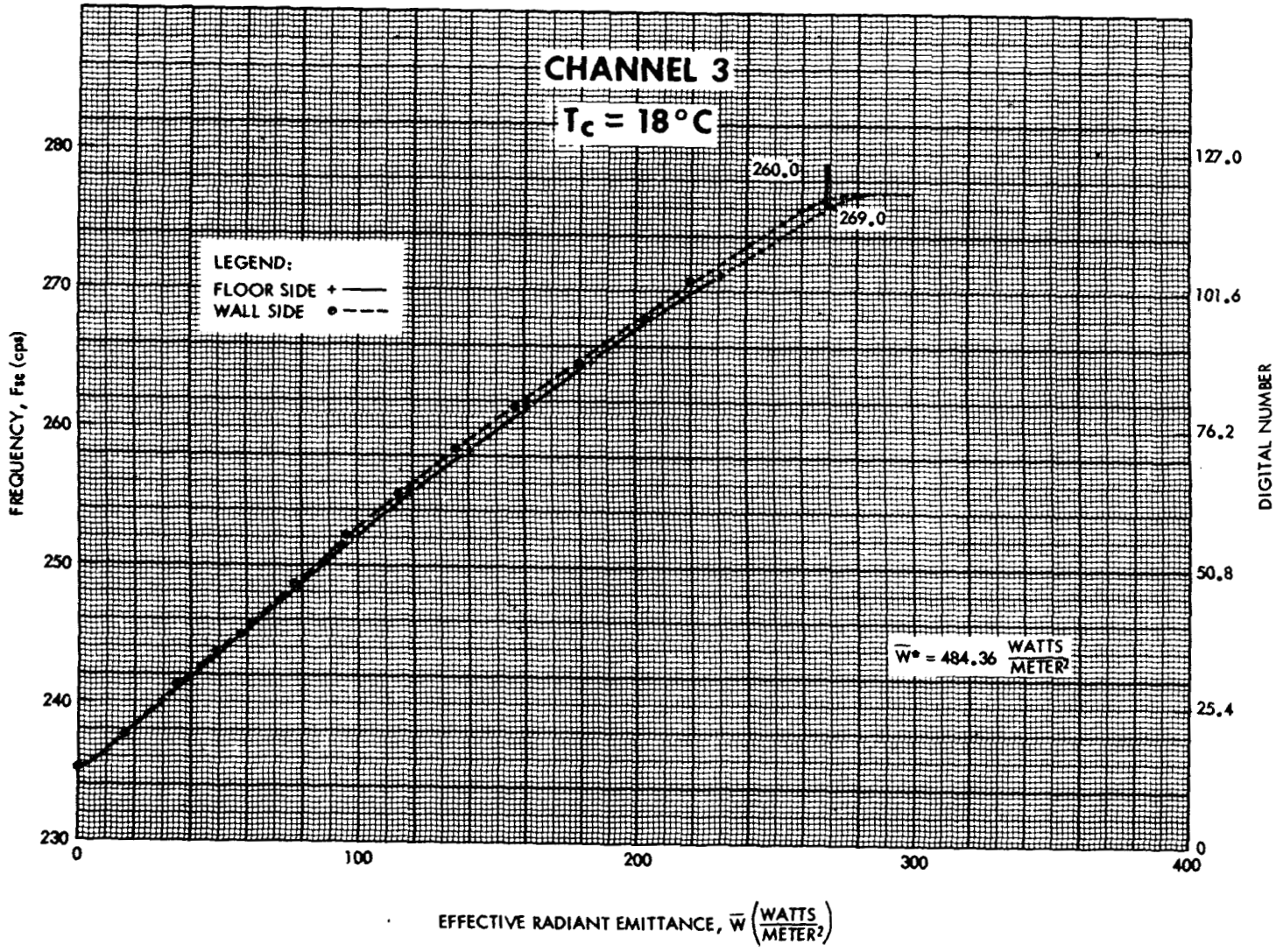

Figure 36—Subcarrier frequency and digital number versus effective radiant emittance for floor and wall sides of channel 3. (T_c = 18°C)

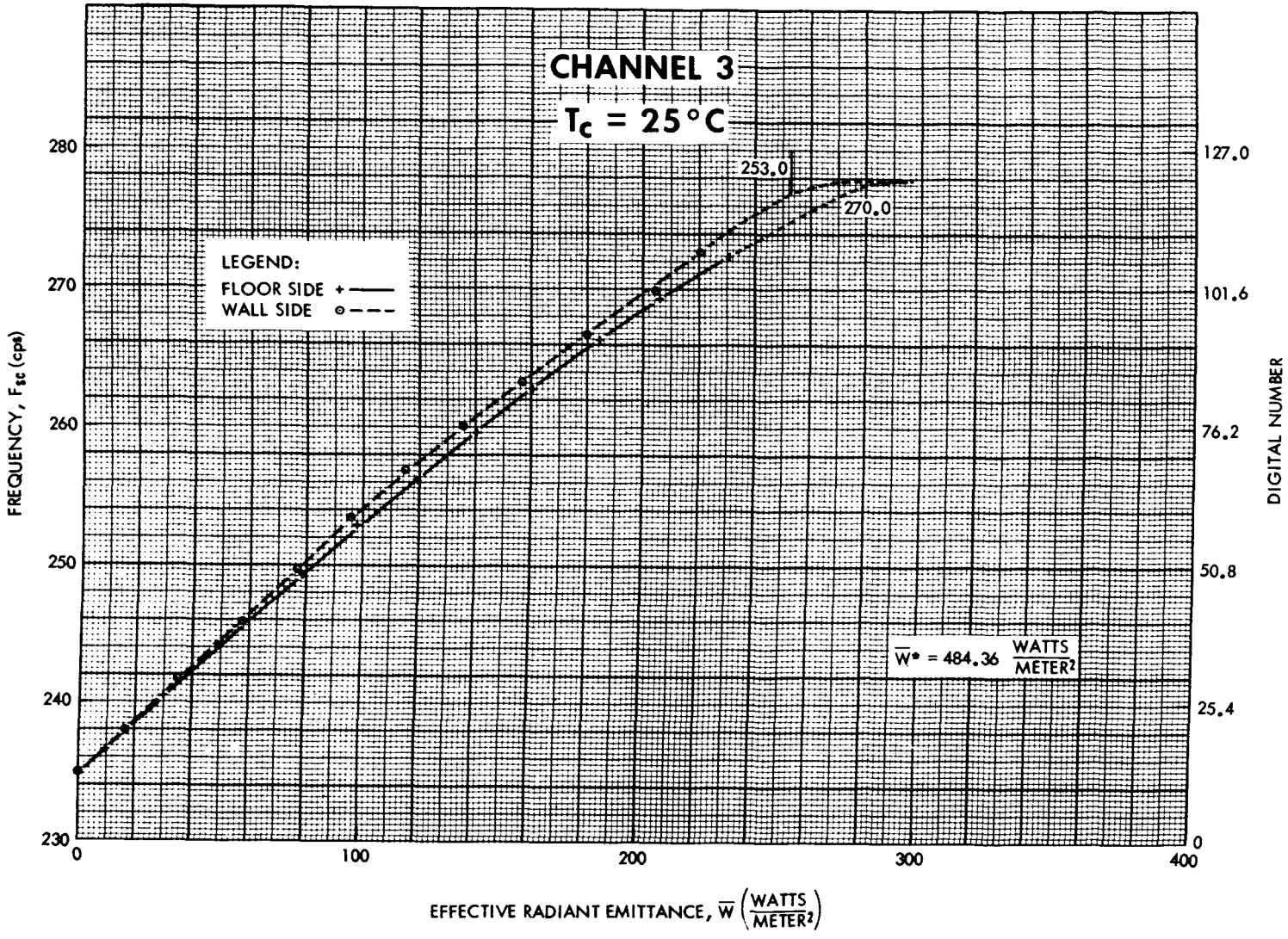

Figure 37—Subcarrier frequency and digital number versus effective radiant emittance for floor and wall sides of channel 3. (T_c = 25°C)

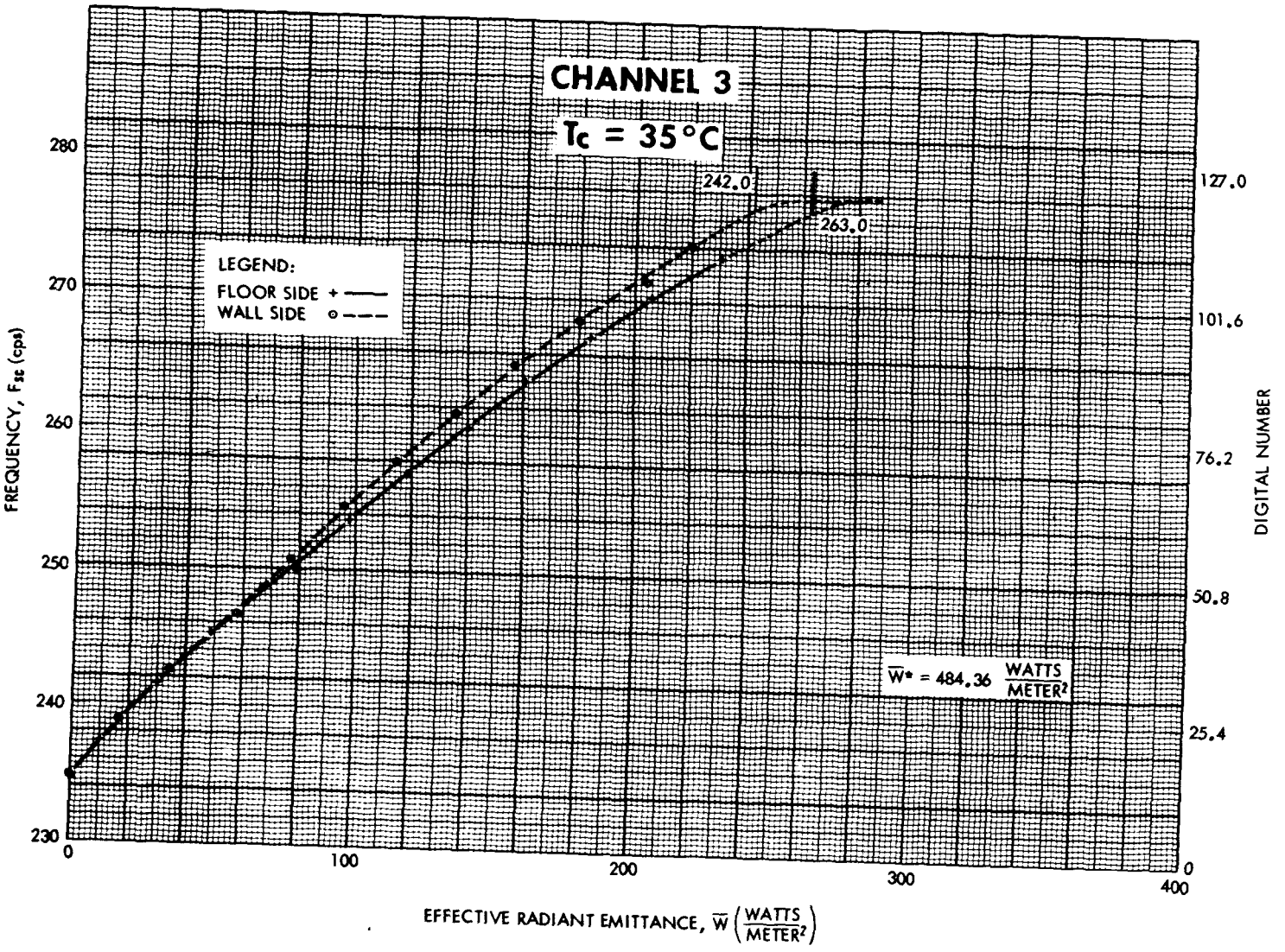

Figure 38—Subcarrier frequency and digital number versus effective radient emittance for floor and wall sides of channel 3. (T_c = 35°C)

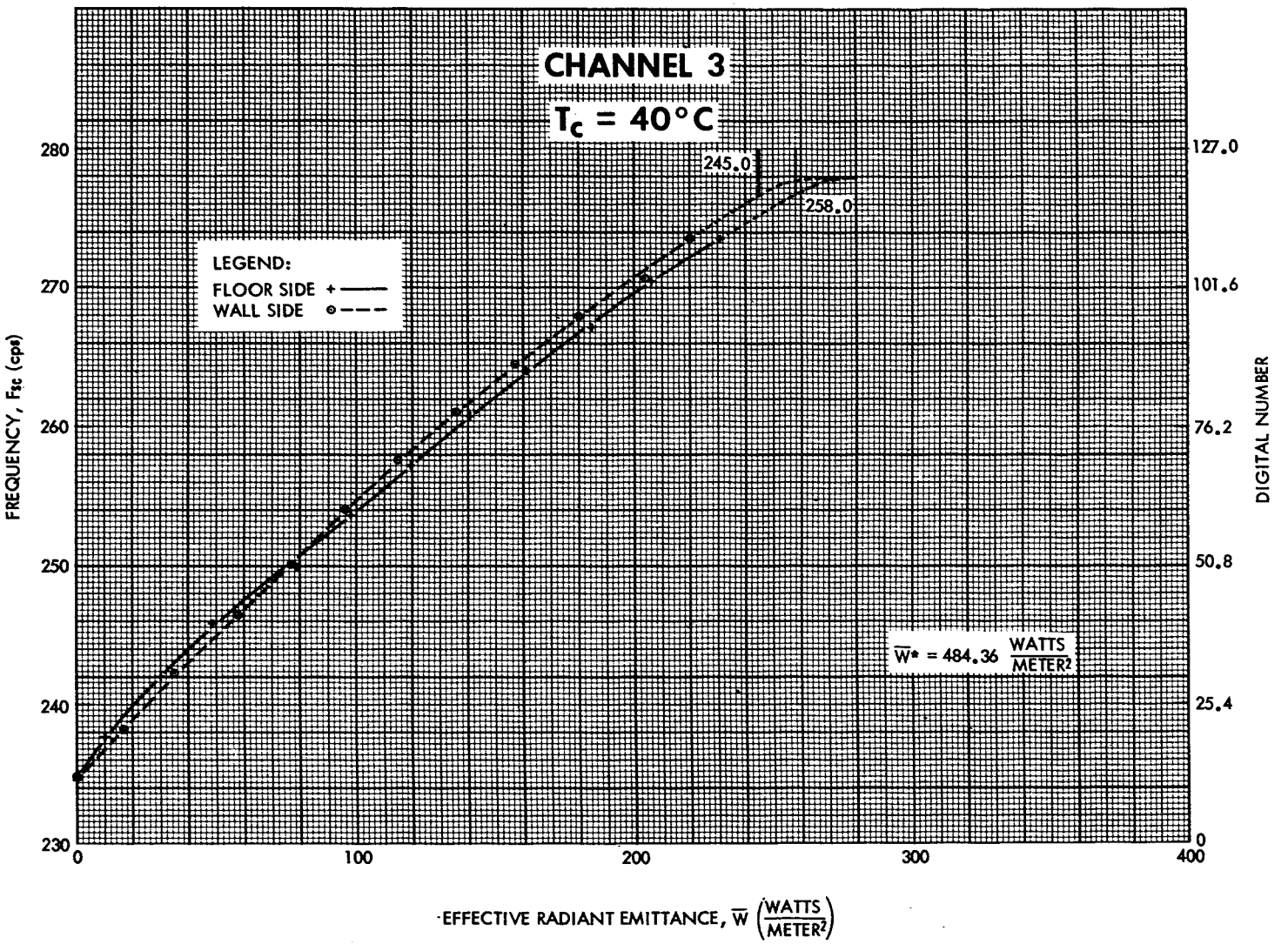

Figure 39—Subcarrier frequency and digital number versus effective radiant emittance for floor and wall sides of channel 3. (T_c = 40°C)

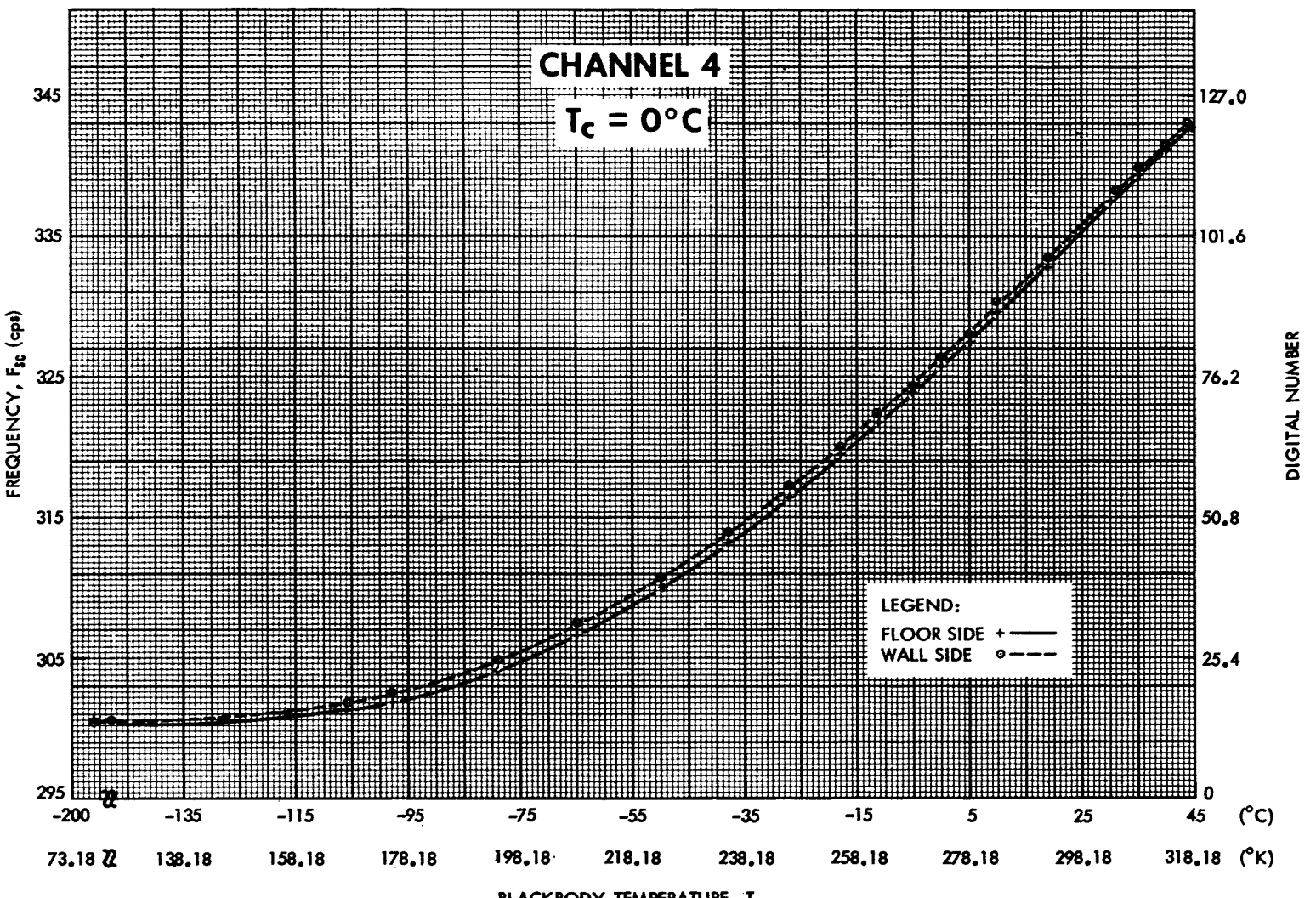

Figure 40—Subcarrier frequency and digital number versus equivalent blackbody temperature for floor and wall sides of channel 4. (T_c = 0°C)

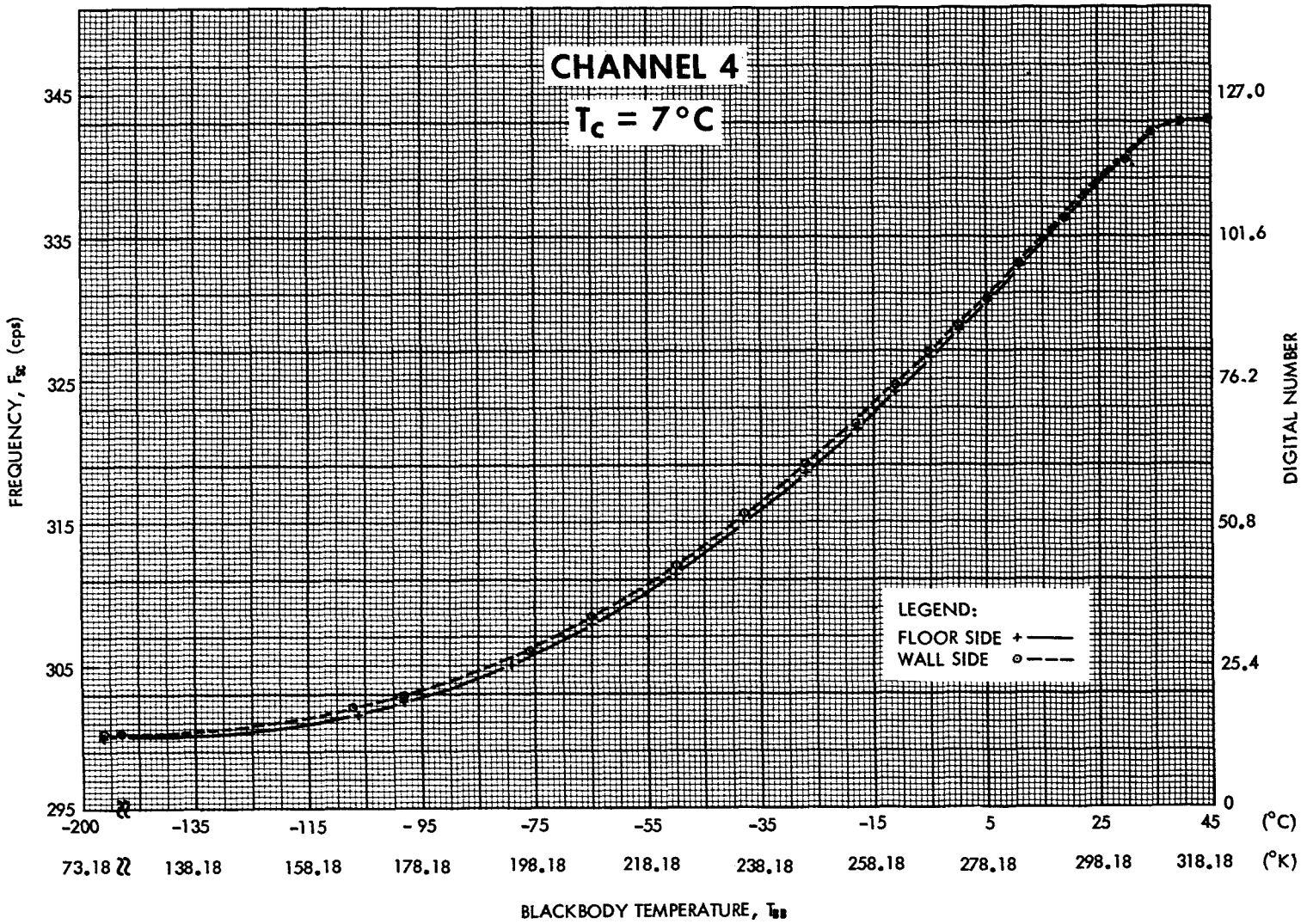

Figure 41—Subcarrier frequency and digital number versus equivalent blackbody temperature for floor and wall sides of channel 4. (T_c = 7°C)

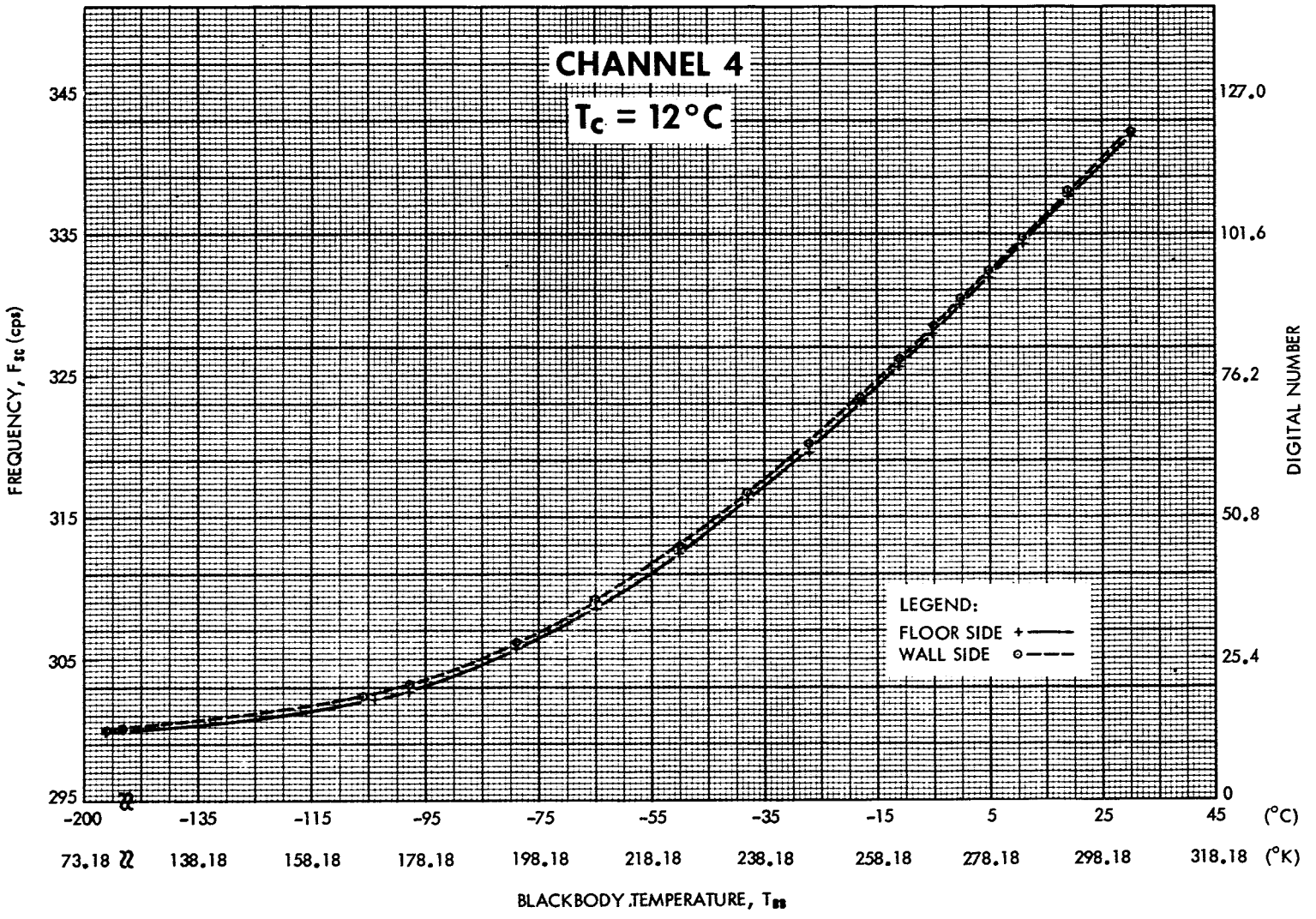

Figure 42—Subcarrier frequency and digital number versus equivalent blackbody temperature for floor and wall sides of channel 4. (T_c = 12°C)

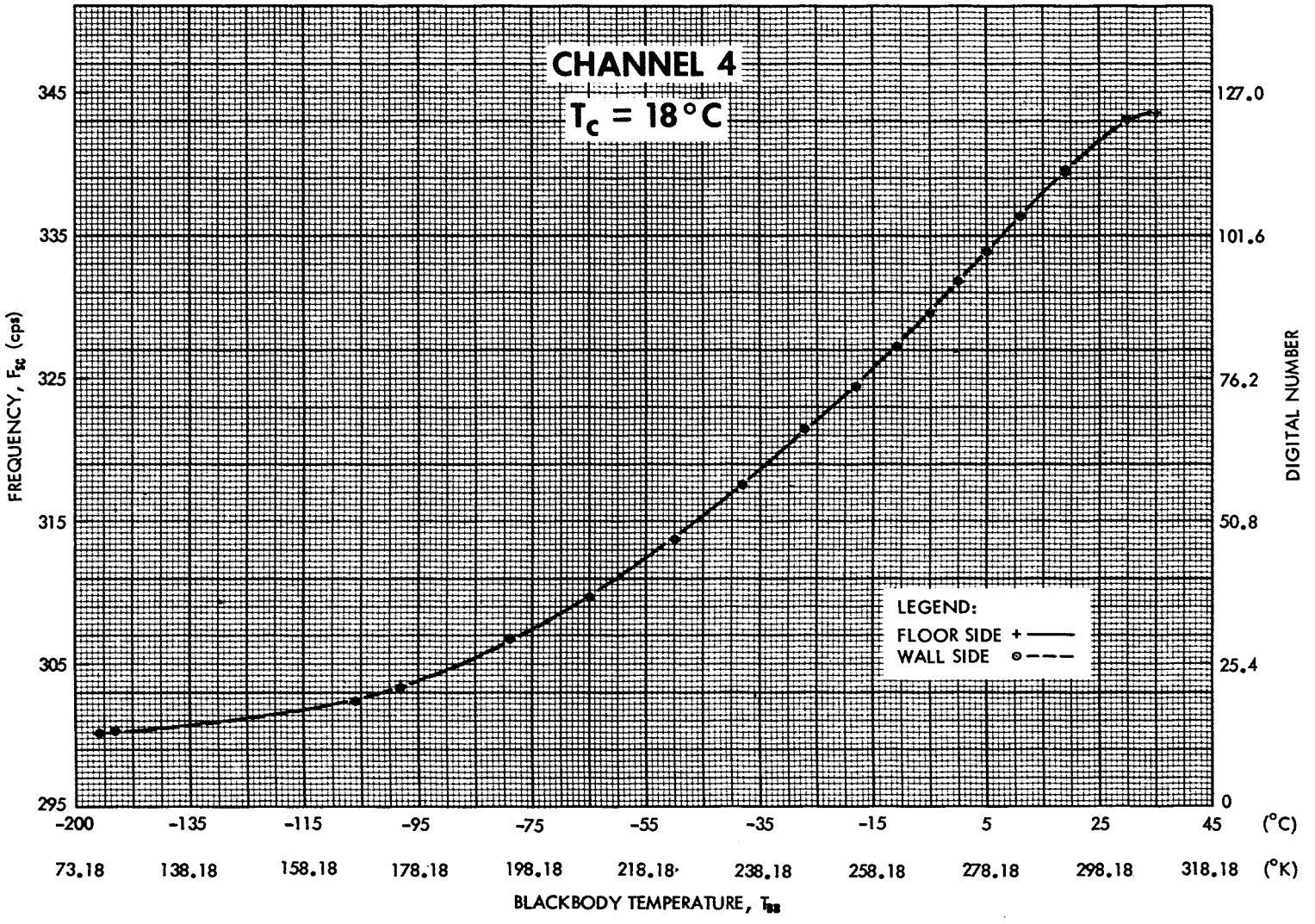

Figure 43—Subcarrier frequency and digital number versus equivalent blackbody temperature for floor and wall sides of channel 4. (T_c = 18°C)

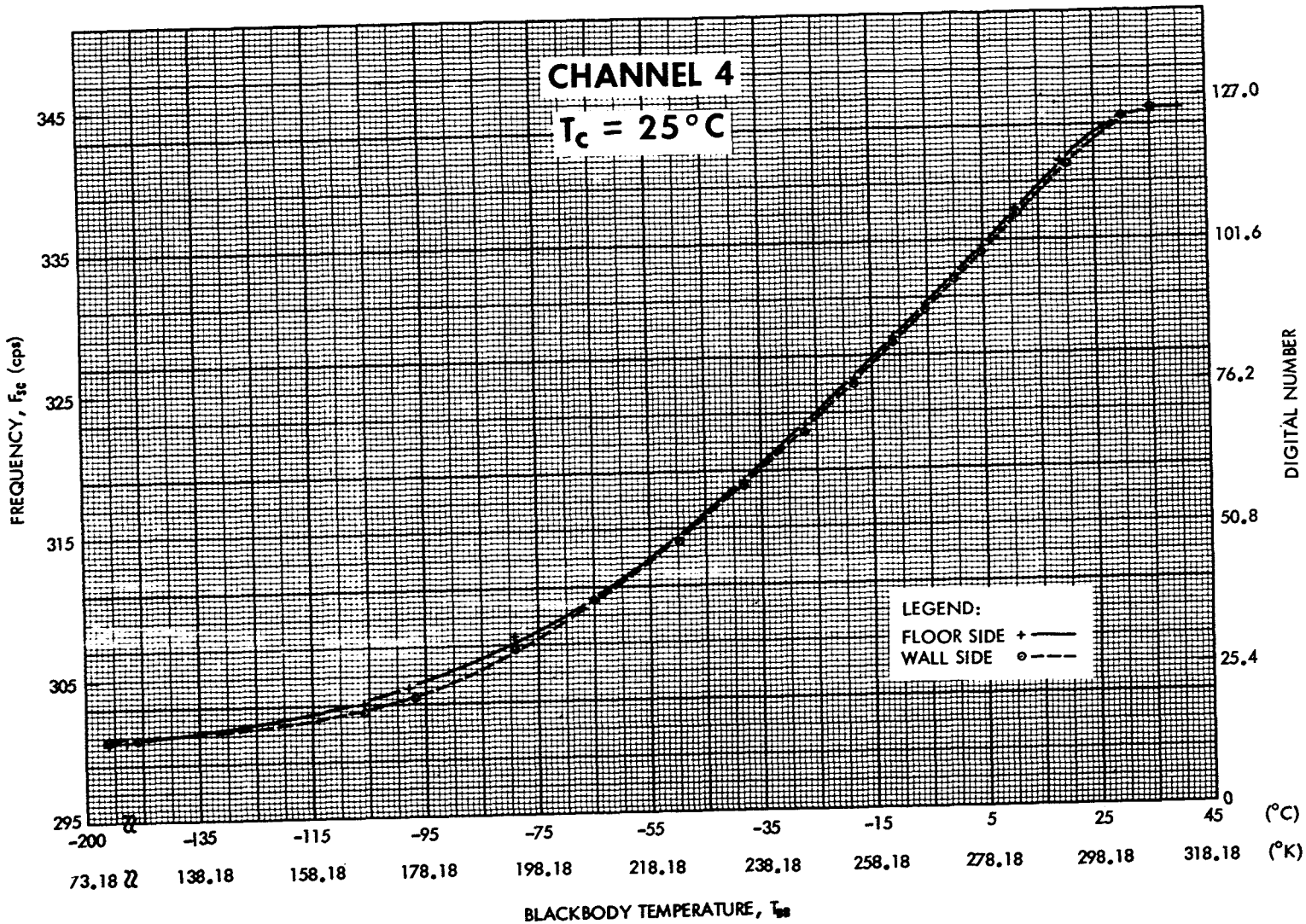

Figure 44—Subcarrier frequency and digital number versus equivalent blackbody temperature for floor and wall sides of channel 4. (T_c = 25°C)

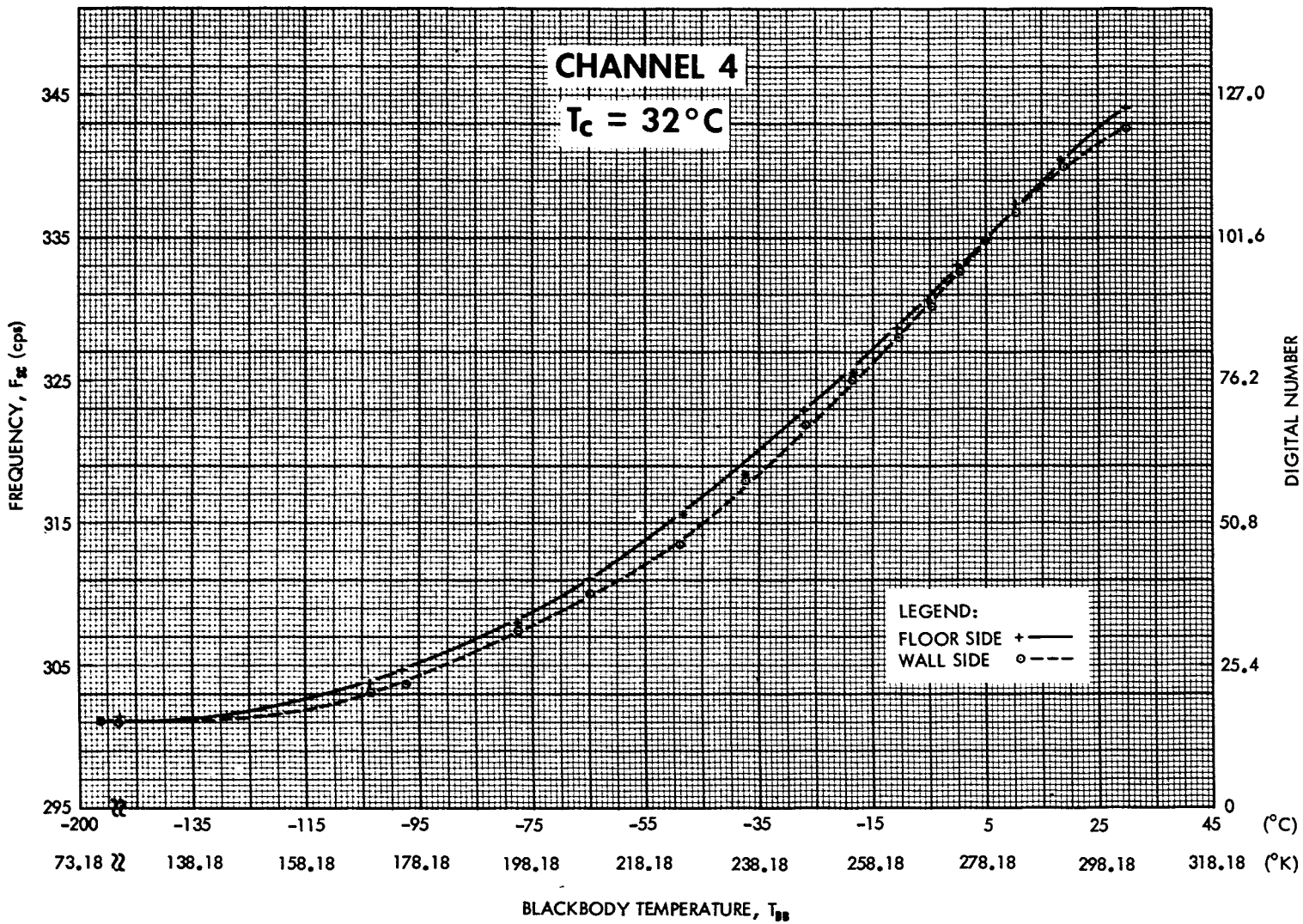

Figure 45—Subcarrier frequency and digital number versus equivalent blackbody temperature for floor and wall sides of channel 4. (T_c = 32°C)

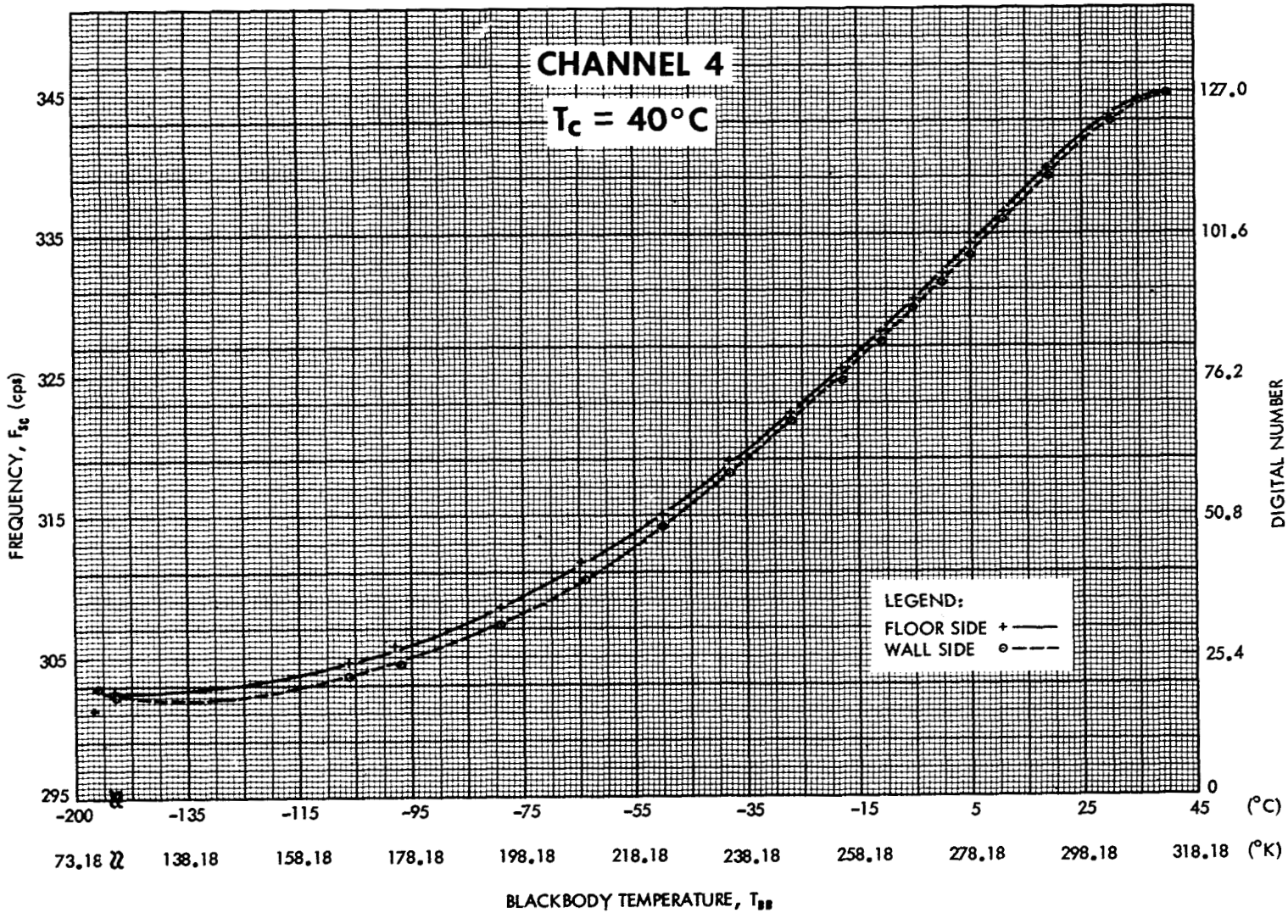

Figure 46—Subcarrier frequency and digital number versus equivalent blackbody temperature for floor and wall sides of channel 4. (T_c = 40°C)

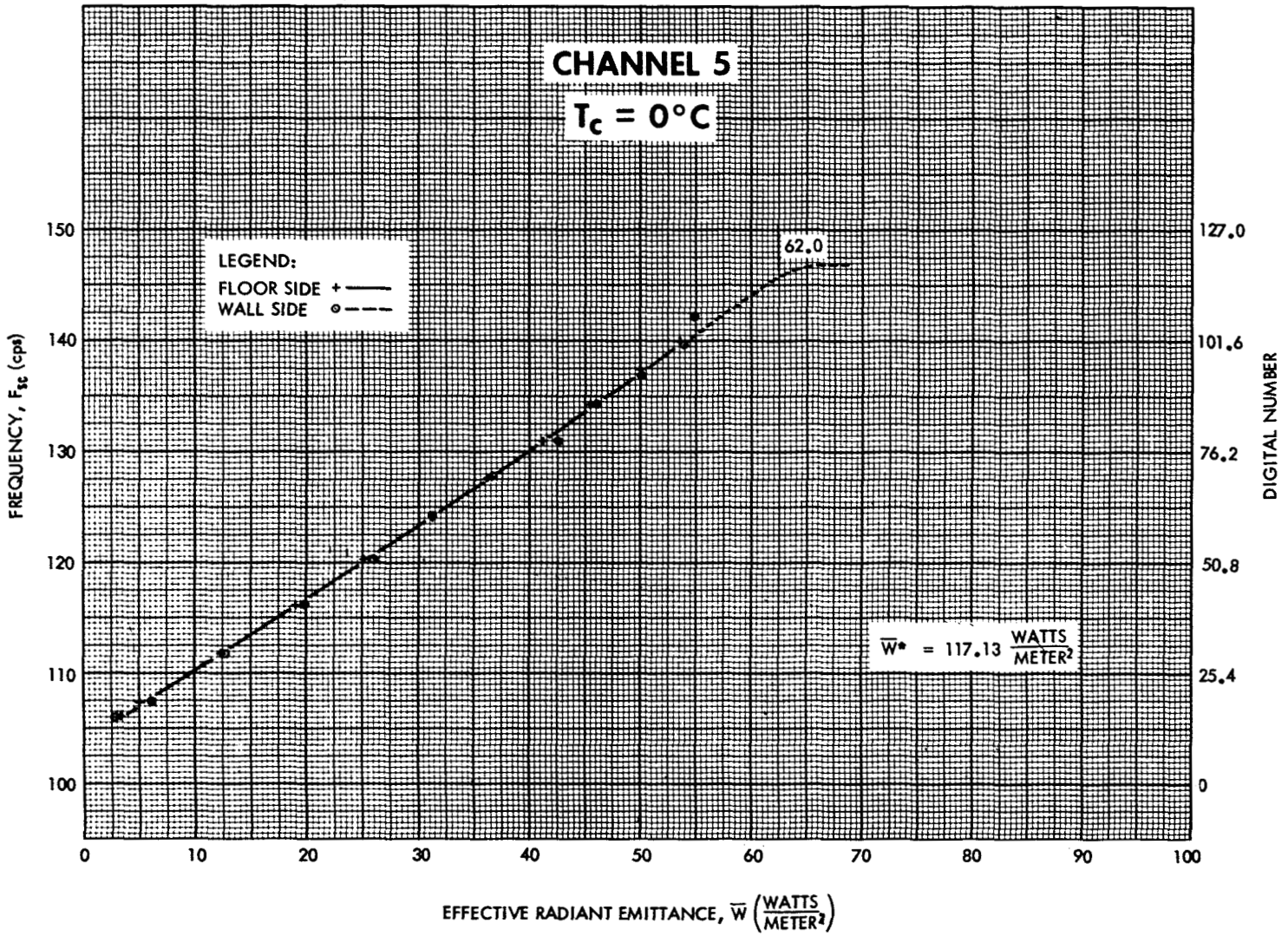

Figure 47—Subcarrier frequency and digital number versus effective radiant emittance for floor and wall sides of channel 5. (T_c = 0°C)

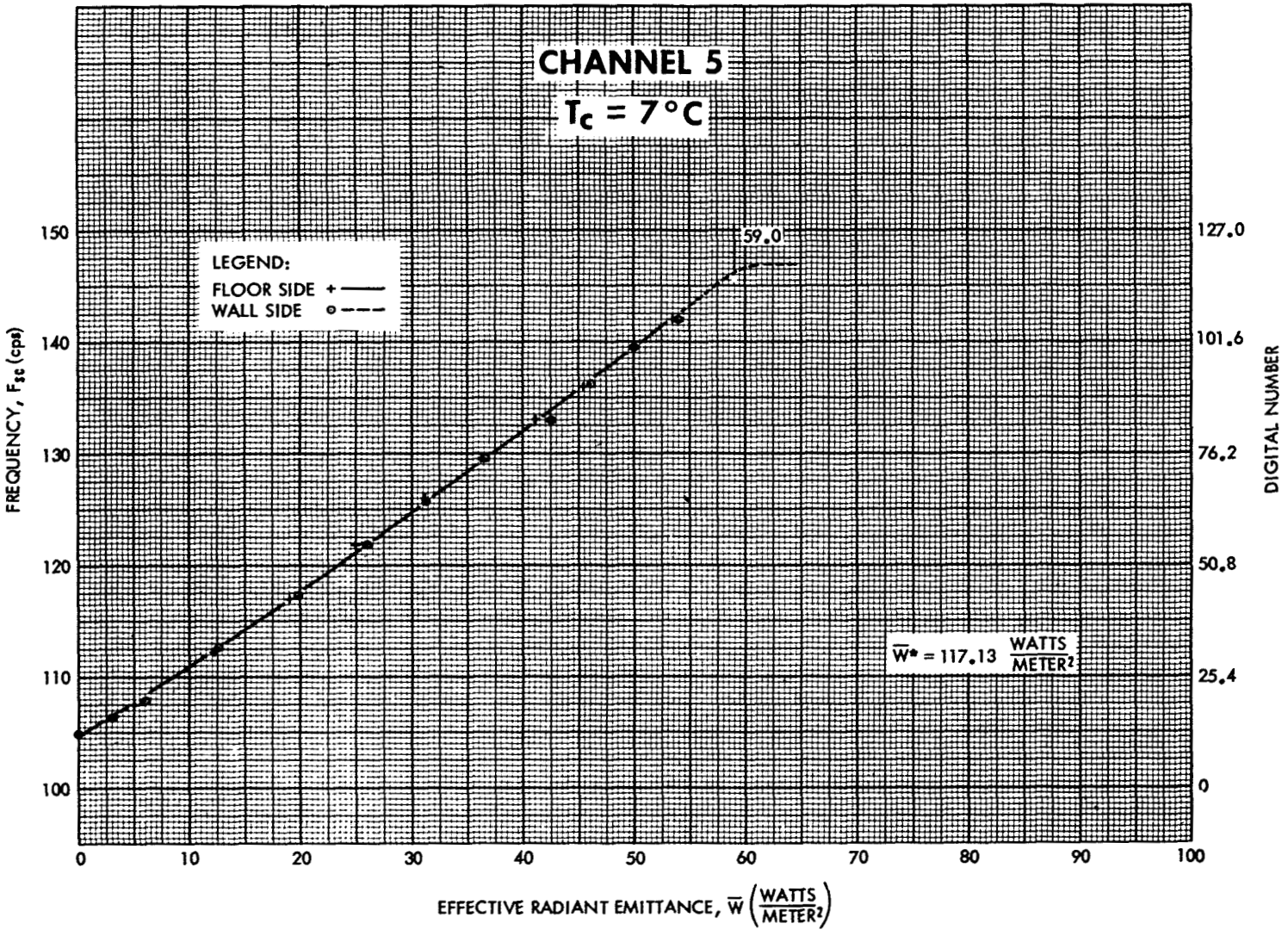

Figure 48—Subcarrier frequency and digital number versus effective radiant emittance for floor and wall sides of channel 5. (T_c = 7°C)

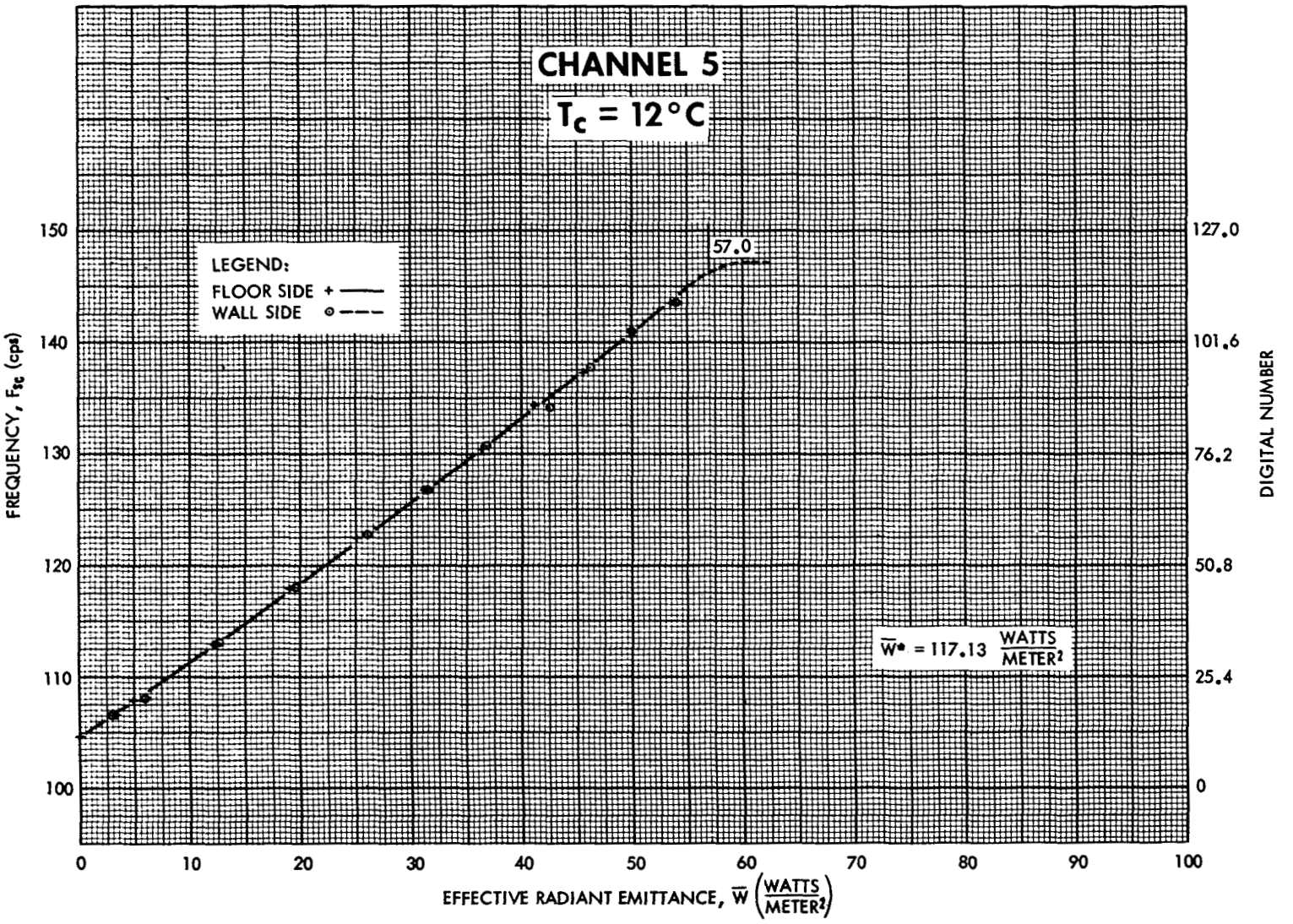

Figure 49—Subcarrier frequency and digital number versus effective radiant emittance for floor and wall sides of channel 5. (T_c = 12°C)

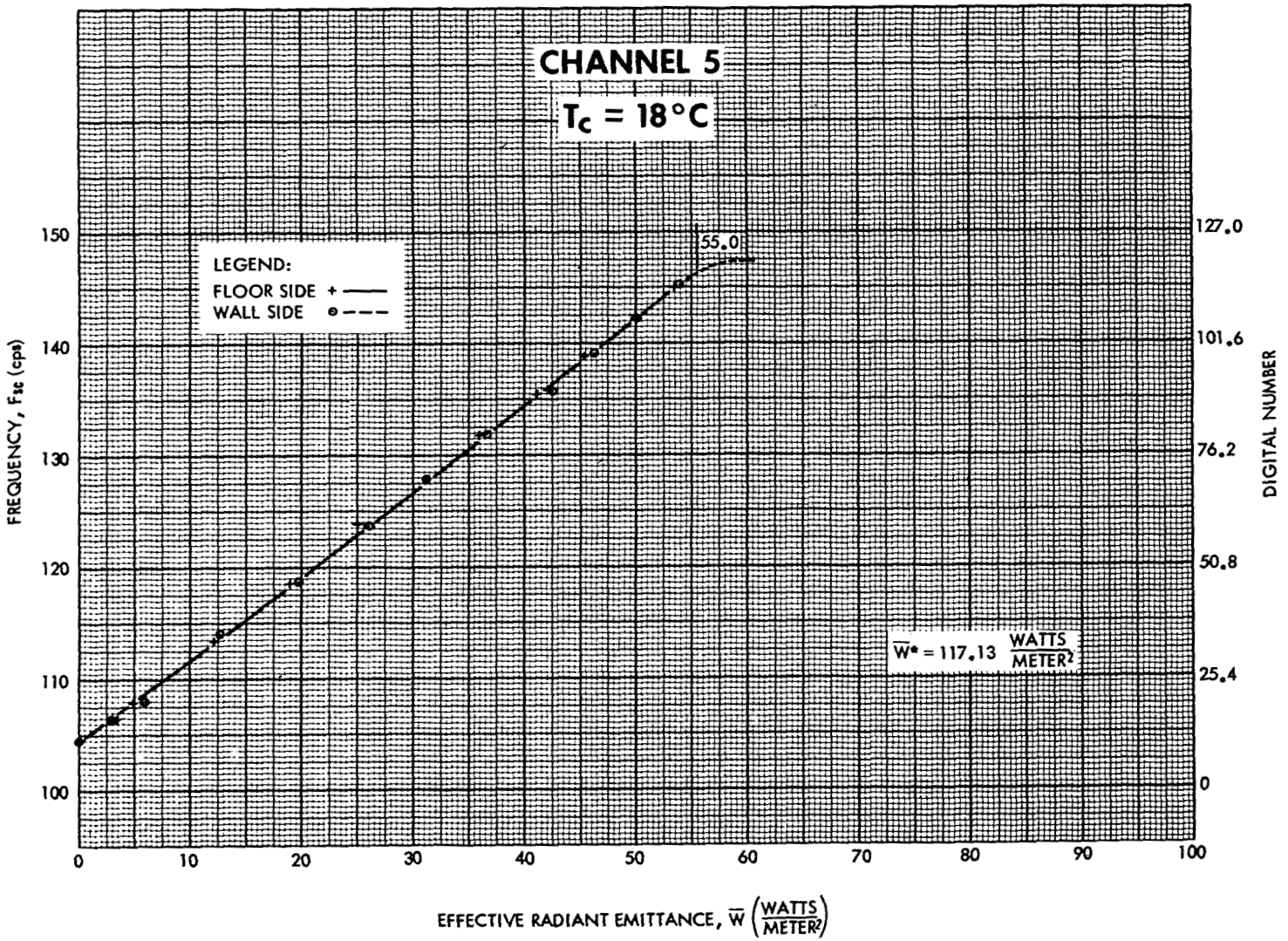

Figure 50—Subcarrier frequency and digital number versus effective radiant emittance for floor and wall sides of channel 5. (T_c = 18°C)

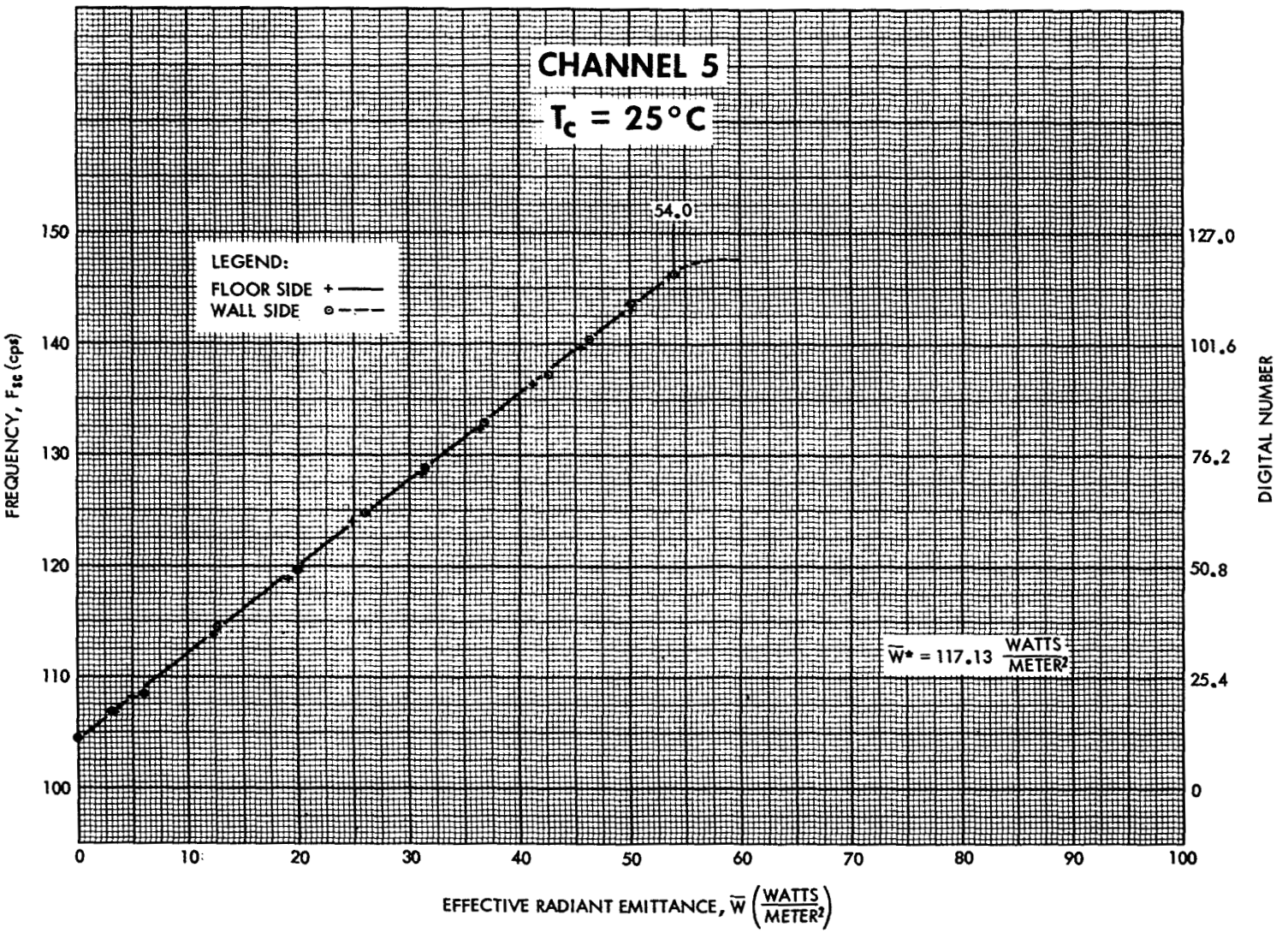

Figure 51—Subcarrier frequency and digital number versus effective radiant emittance for floor and wall sides of channel 5. (T_c = 25°C)

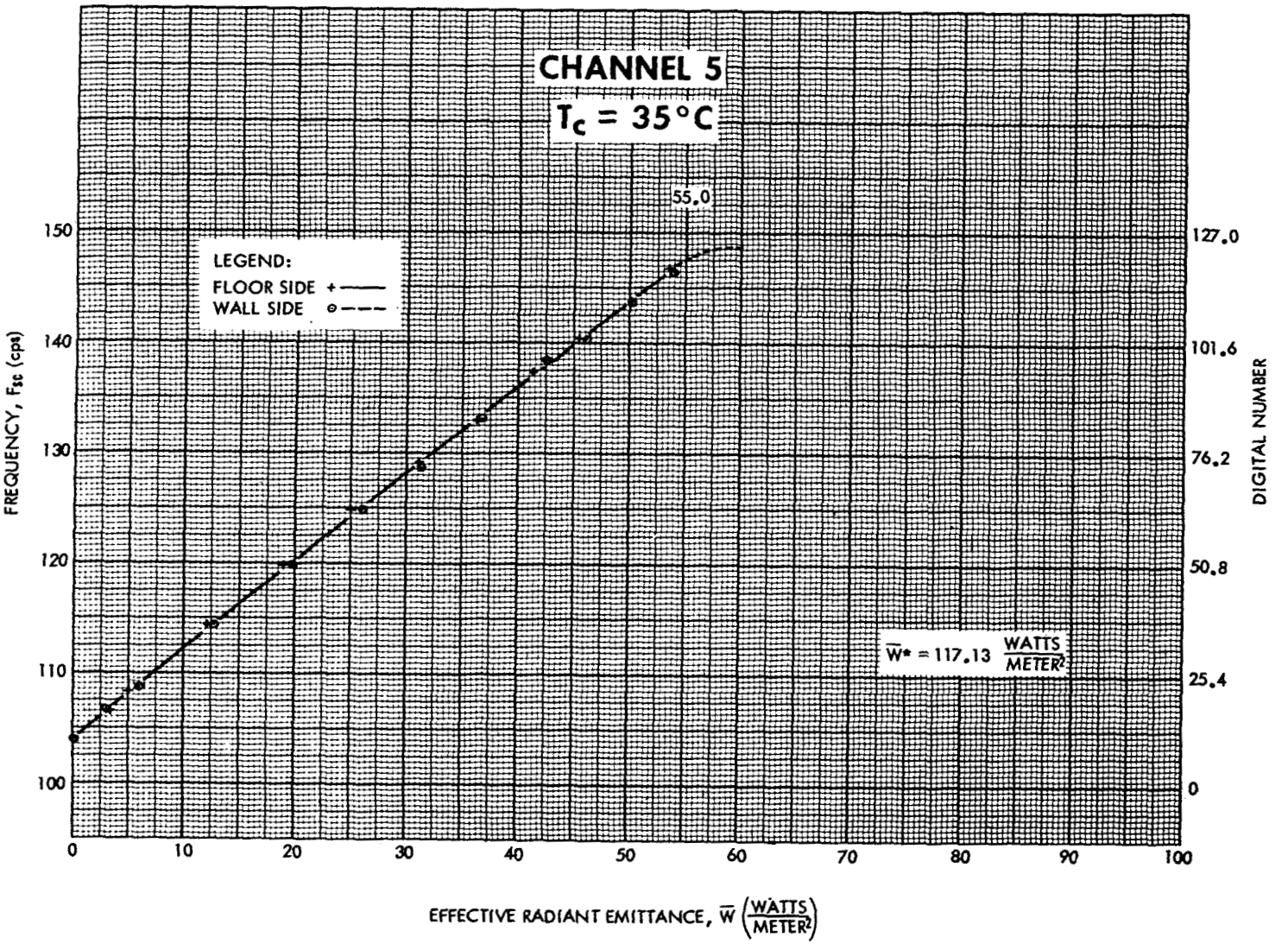

Figure 52—Subcarriers frequency and digital number versus effective radiant emittance for floor and wall sides of channel 5. (T_c = 35°C)

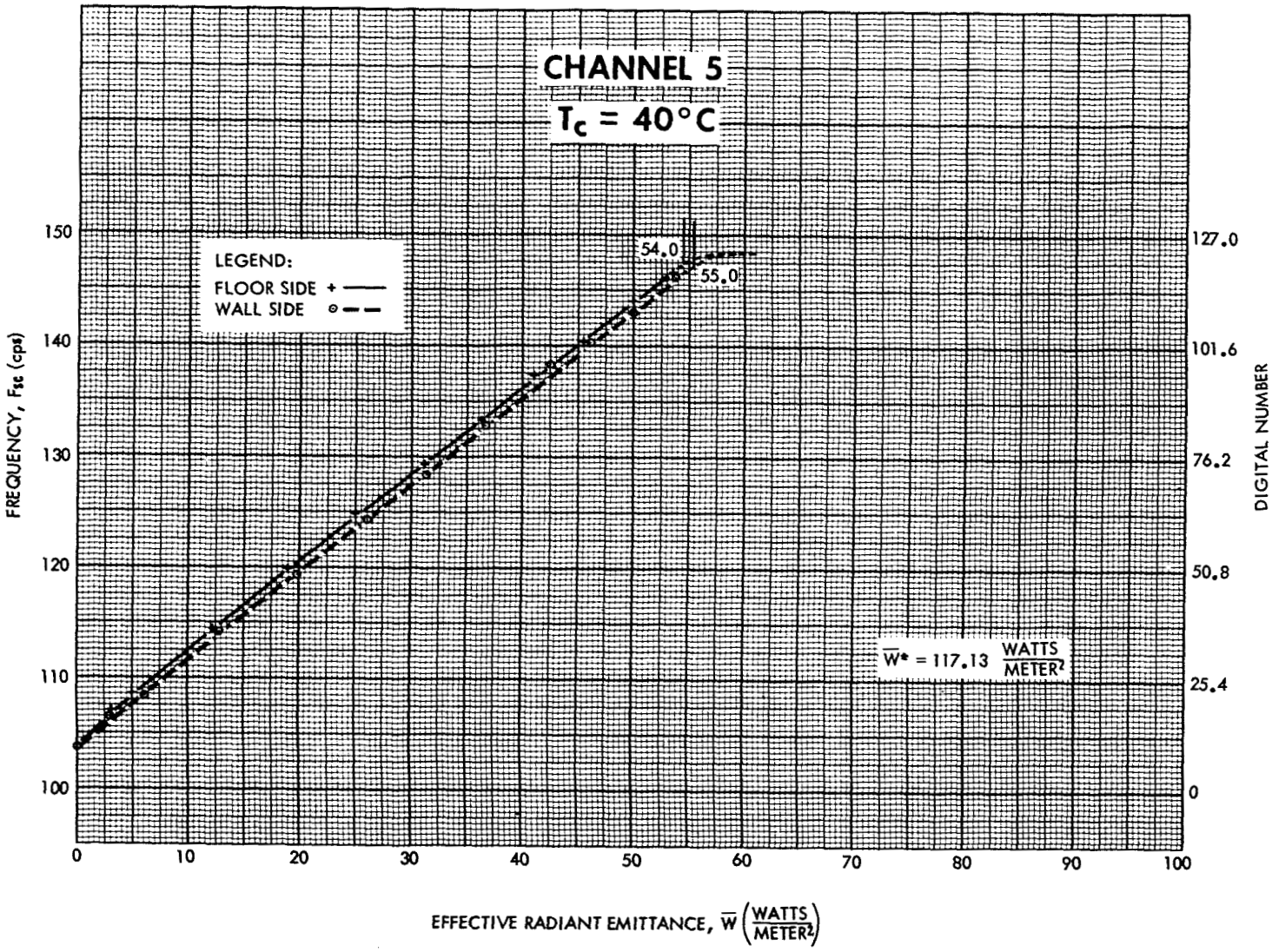

Figure 53—Subcarrier frequency and digital number versus effective radiant emittance for floor and wall sides of channel 5. (T_c = 40°C)

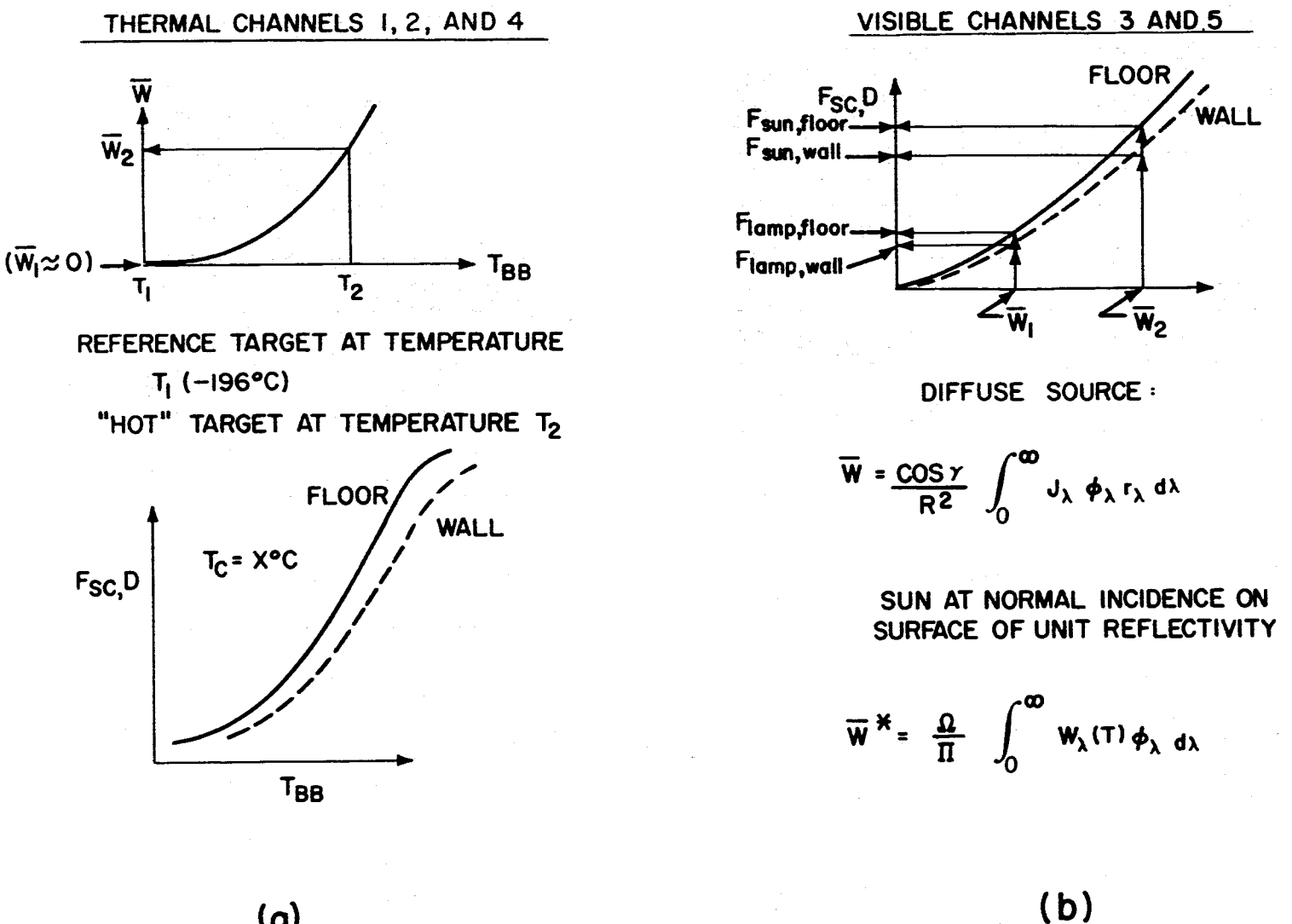

Figure 54—(a) Calibration of the emitted thermal radiation channels 1, 2, and 4.
(b) Calibration of the reflected solar radiation channels 3 and 5.

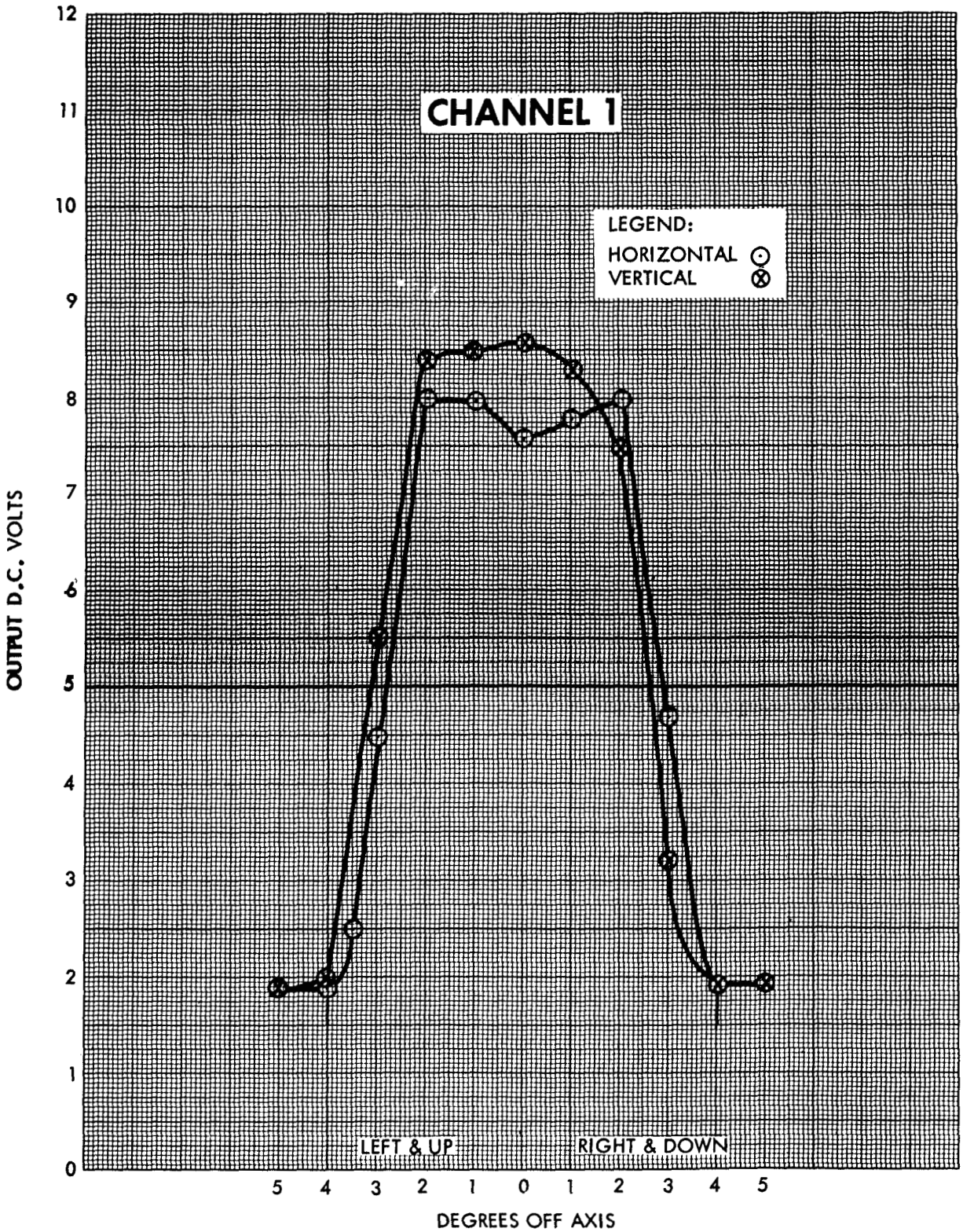

Figure 55—Field of view measurements for channel 1.

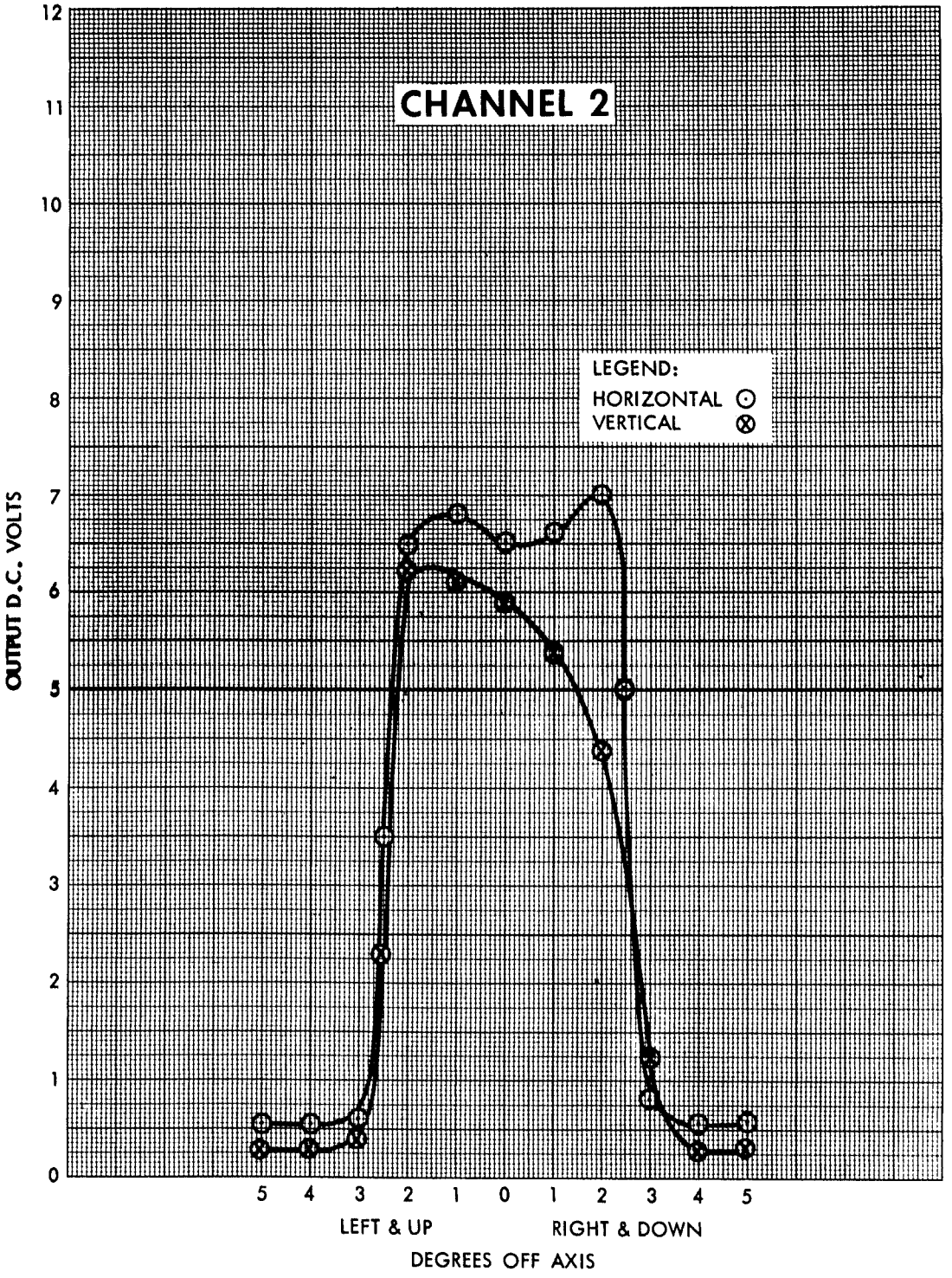

Figure 56—Field of view measurements for channel 2.

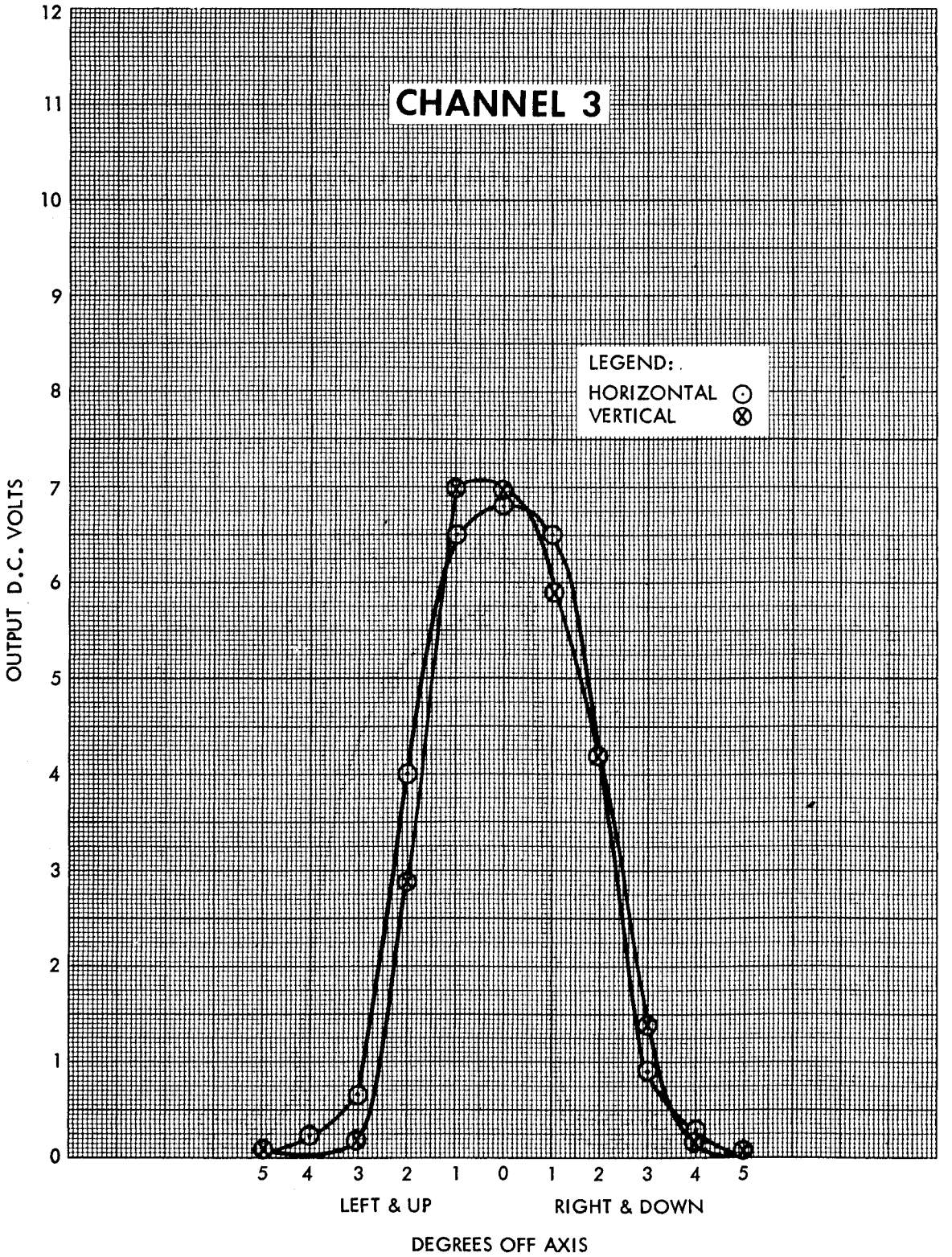

Figure 57—Field of view measurements for channel 3.

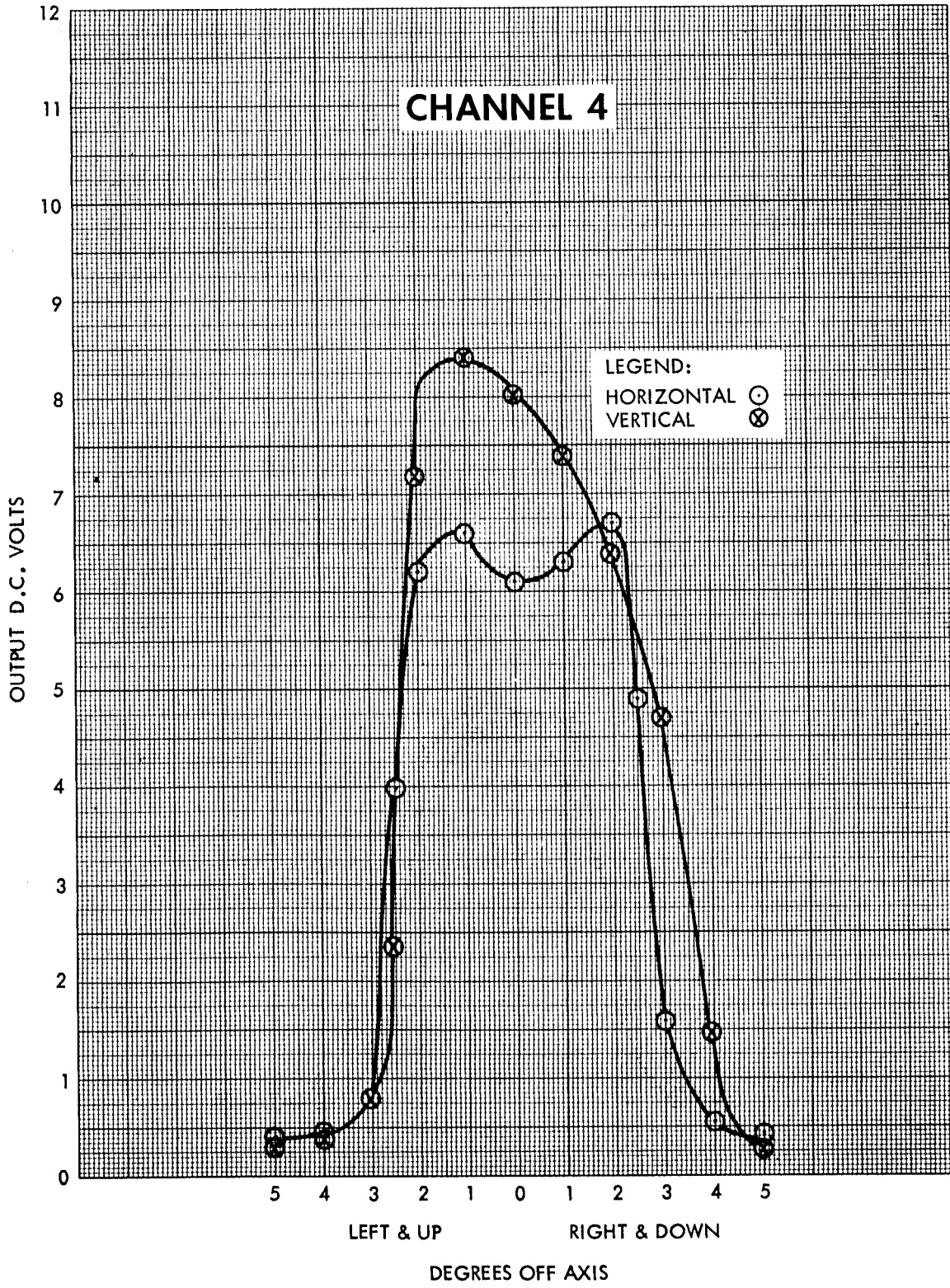

Figure 58—Field of view measurements for channel 4.

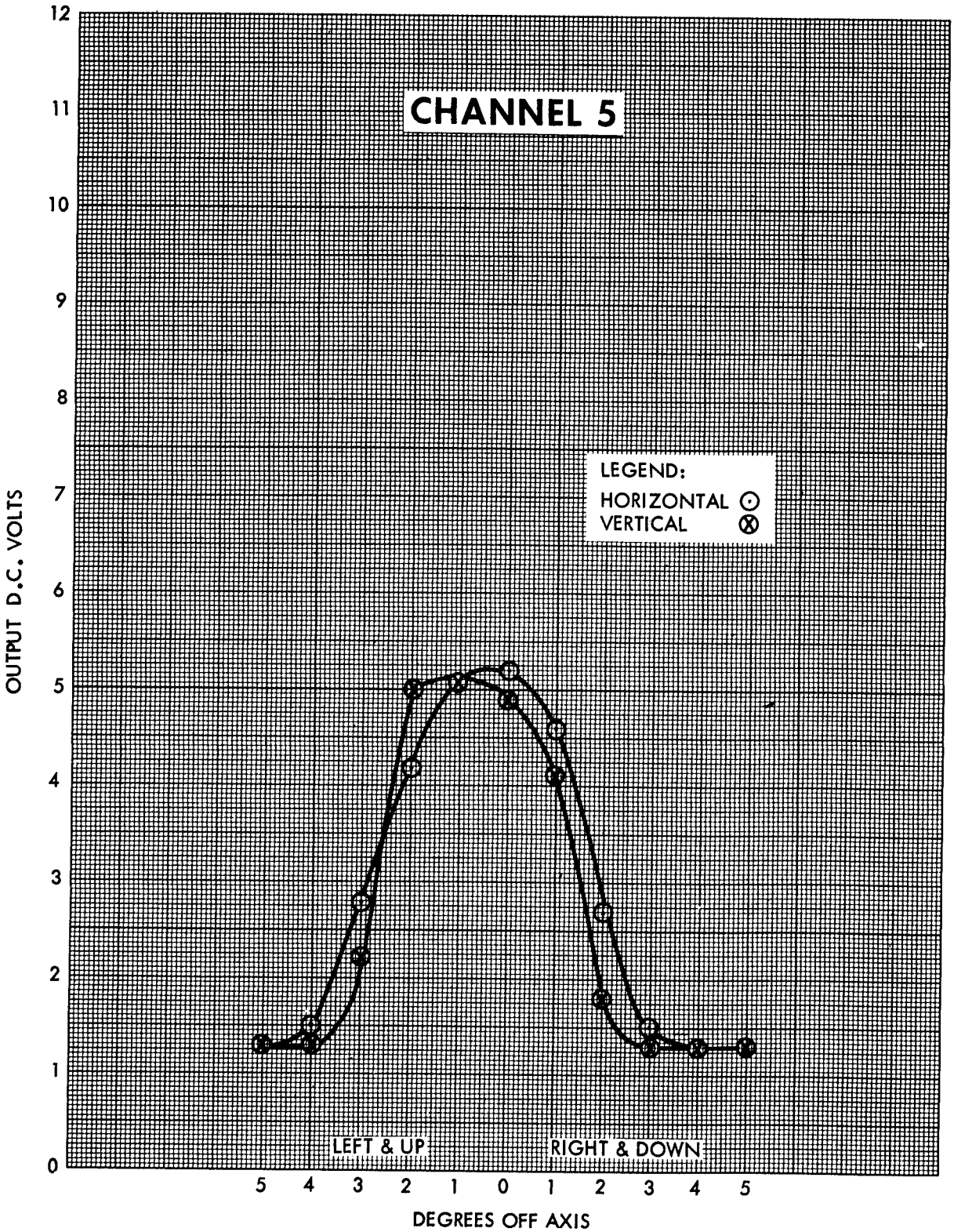

Figure 59—Field of view measurements for channel 5.

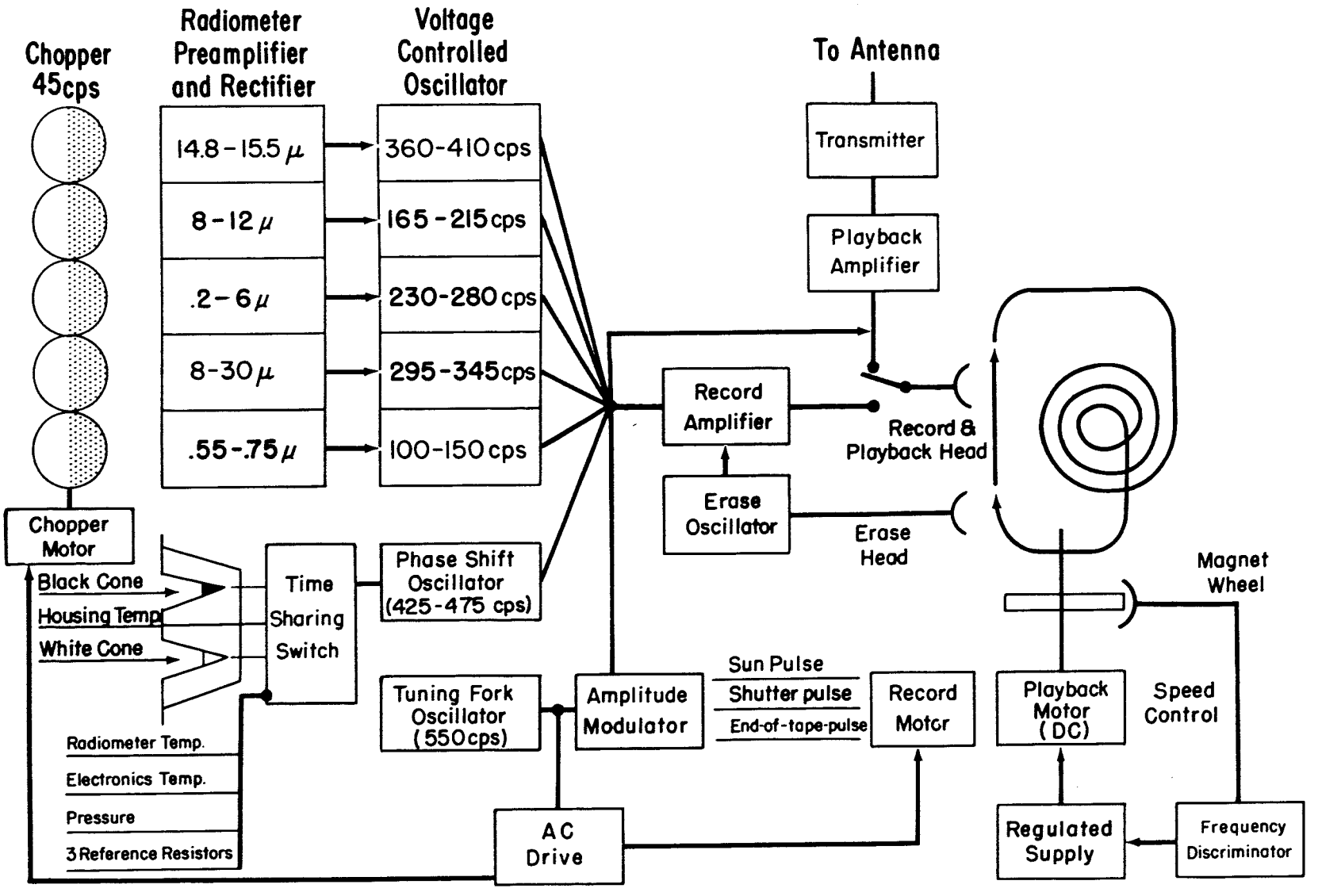

Figure 60—Block diagram of the radiation experiment in the satellite.

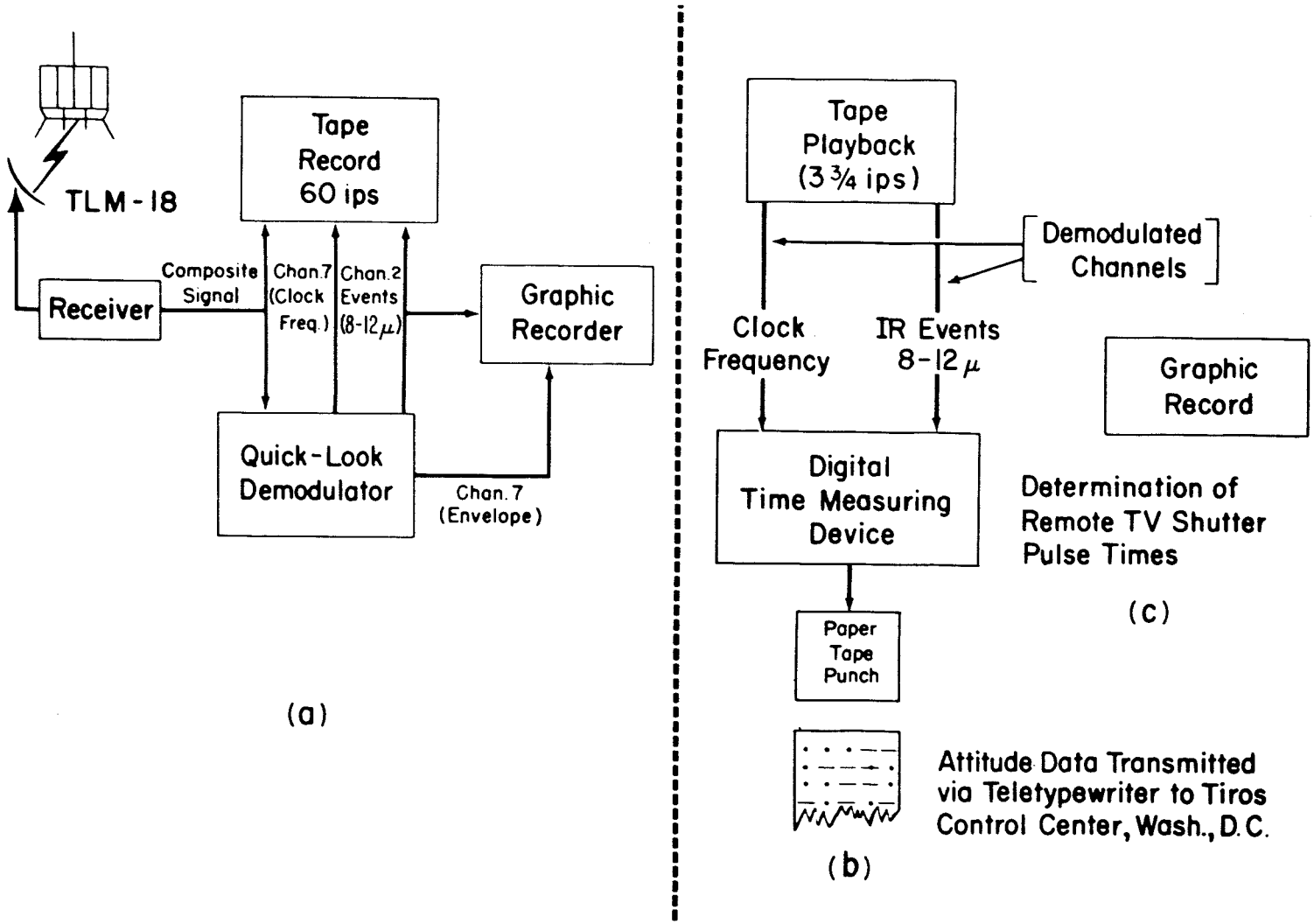

Figure 61—Block diagram of information flow at the Command and Data Acquisition Station including auxiliary uses of the radiation data.

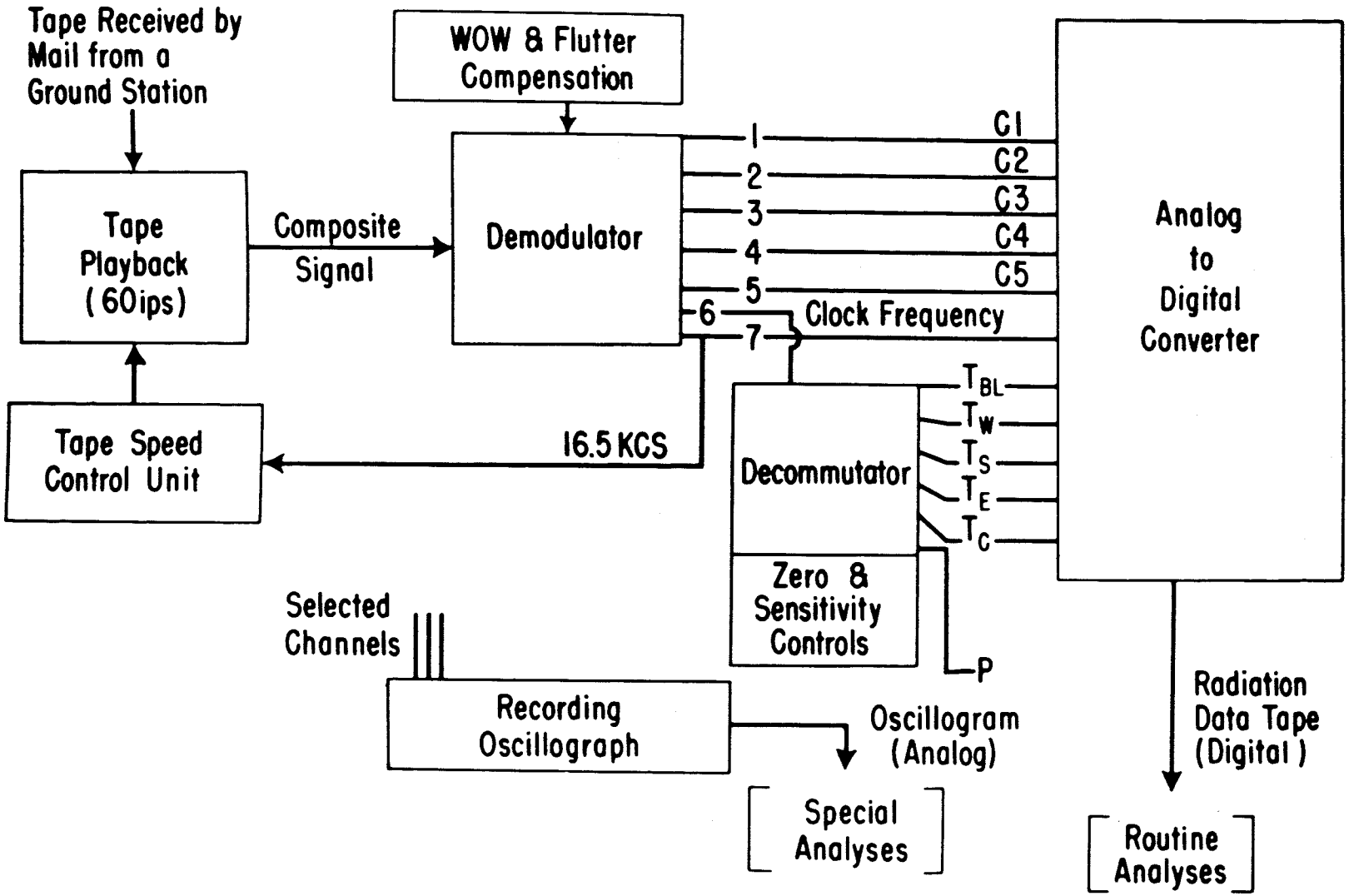

Figure 62—Block diagram of information flow at the Data Processing Center in producing a digital magnetic tape for computer input.

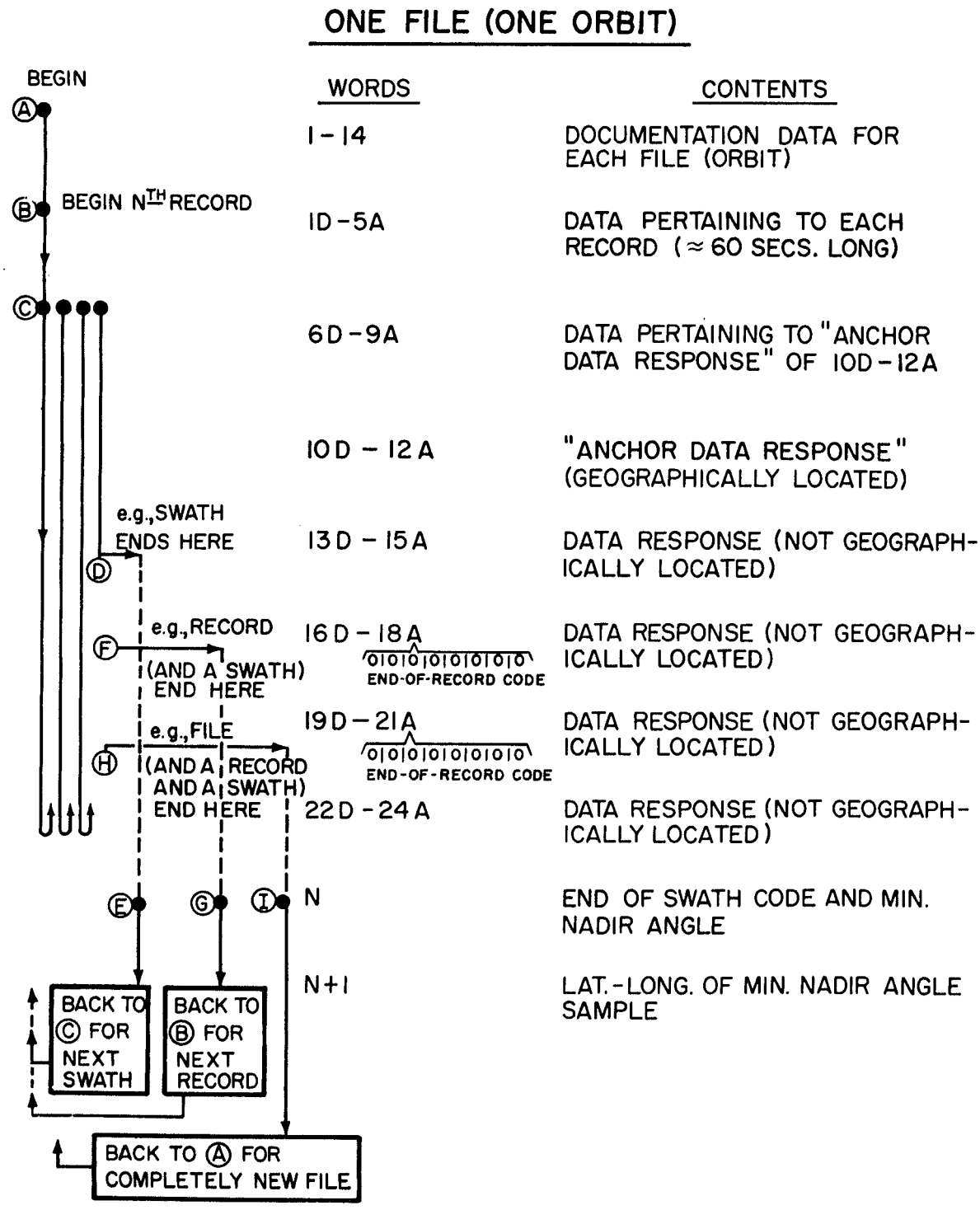

Figure 63—Diagram for interpretation of the FMR tape format.

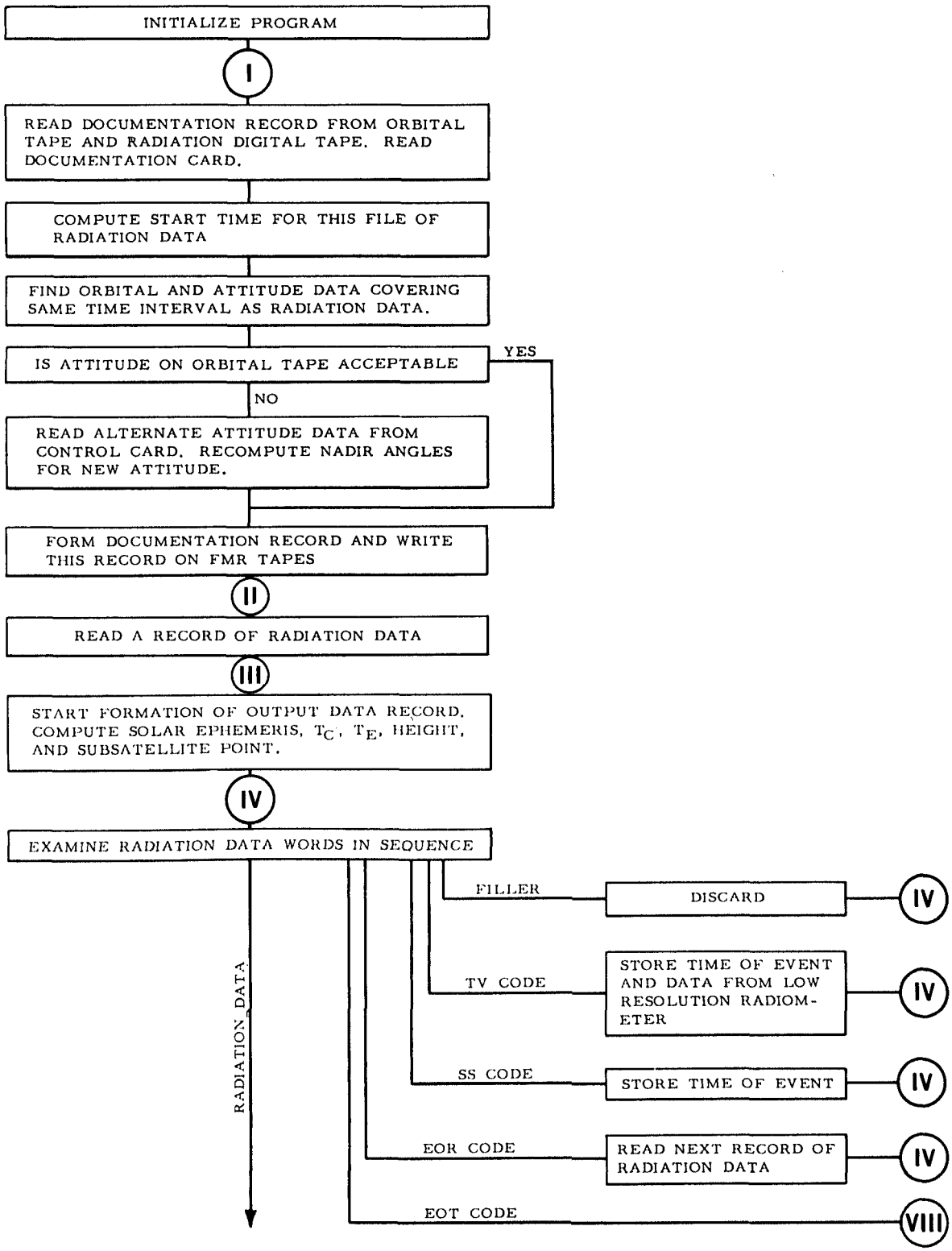

Figure 64—Flow diagram for the IBM 7094 computer program used in reducing the radiation data.

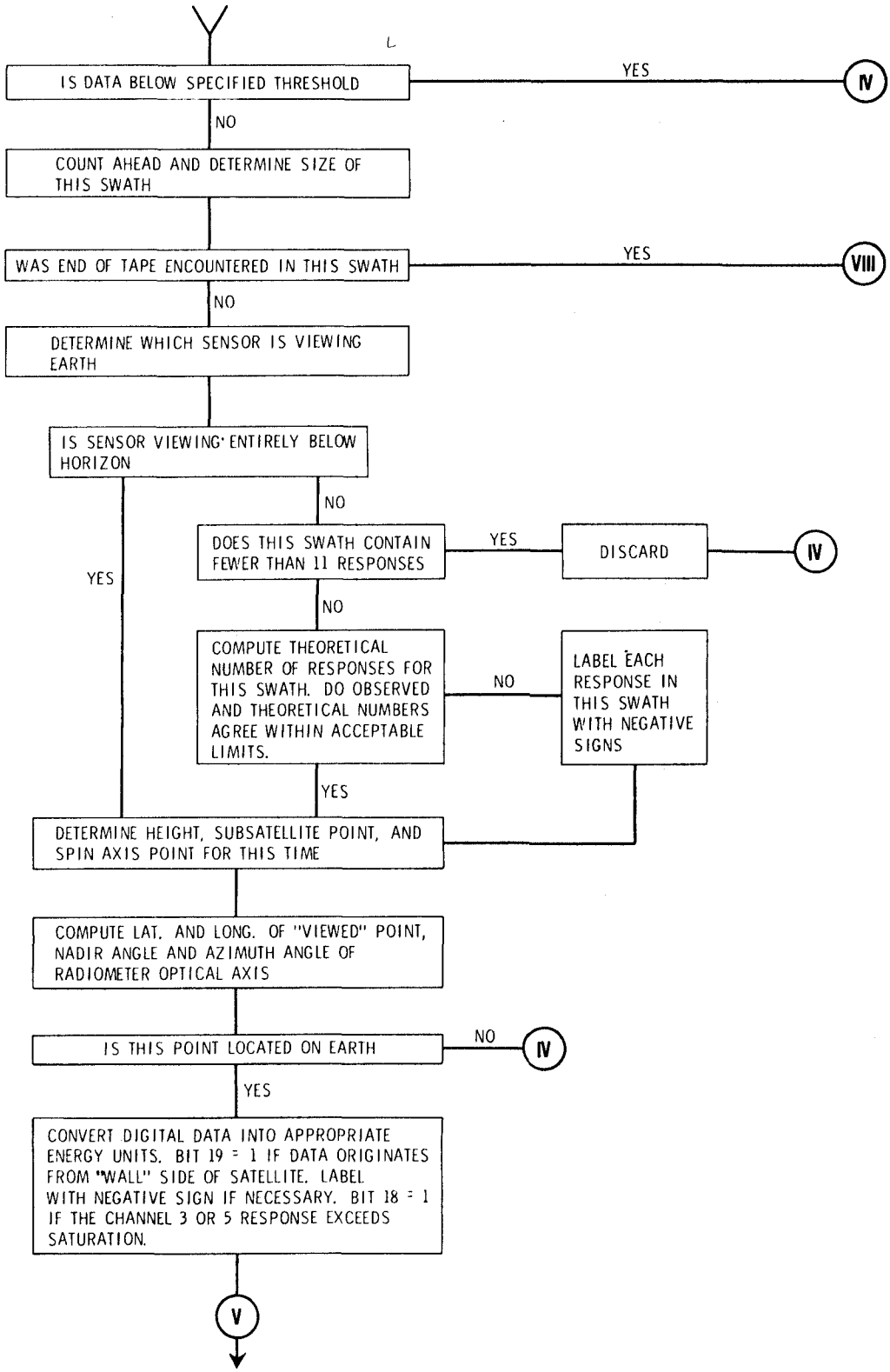
IS DATA BELOW SPECIFIED THRESHOLD
YES
IV
NO
COUNT AHEAD AND DETERMINE SIZE OF THIS SWATH
WAS END OF TAPE ENCOUNTERED IN THIS SWATH
YES
VIII
NO
DETERMINE WHICH SENSOR IS VIEWING EARTH
IS SENSOR VIEWING ENTIRELY BELOW HORIZON
NO
YES
DOES THIS SWATH CONTAIN FEWER THAN 11 RESPONSES
YES
DISCARD
IV
NO
COMPUTE THEORETICAL NUMBER OF RESPONSES FOR THIS SWATH. DO OBSERVED AND THEORETICAL NUMBERS AGREE WITHIN ACCEPTABLE LIMITS.
NO
LABEL EACH RESPONSE IN THIS SWATH WITH NEGATIVE SIGNS
YES
DETERMINE HEIGHT, SUBSATELLITE POINT, AND SPIN AXIS POINT FOR THIS TIME
COMPUTE LAT. AND LONG. OF "VIEWED" POINT, NADIR ANGLE AND AZIMUTH ANGLE OF RADIOMETER OPTICAL AXIS
IS THIS POINT LOCATED ON EARTH
NO
IV
YES
CONVERT DIGITAL DATA INTO APPROPRIATE ENERGY UNITS. BIT 19 = 1 IF DATA ORIGINATES FROM "WALL" SIDE OF SATELLITE. LABEL WITH NEGATIVE SIGN IF NECESSARY. BIT 18 = 1 IF THE CHANNEL 3 OR 5 RESPONSE EXCEEDS SATURATION.
V

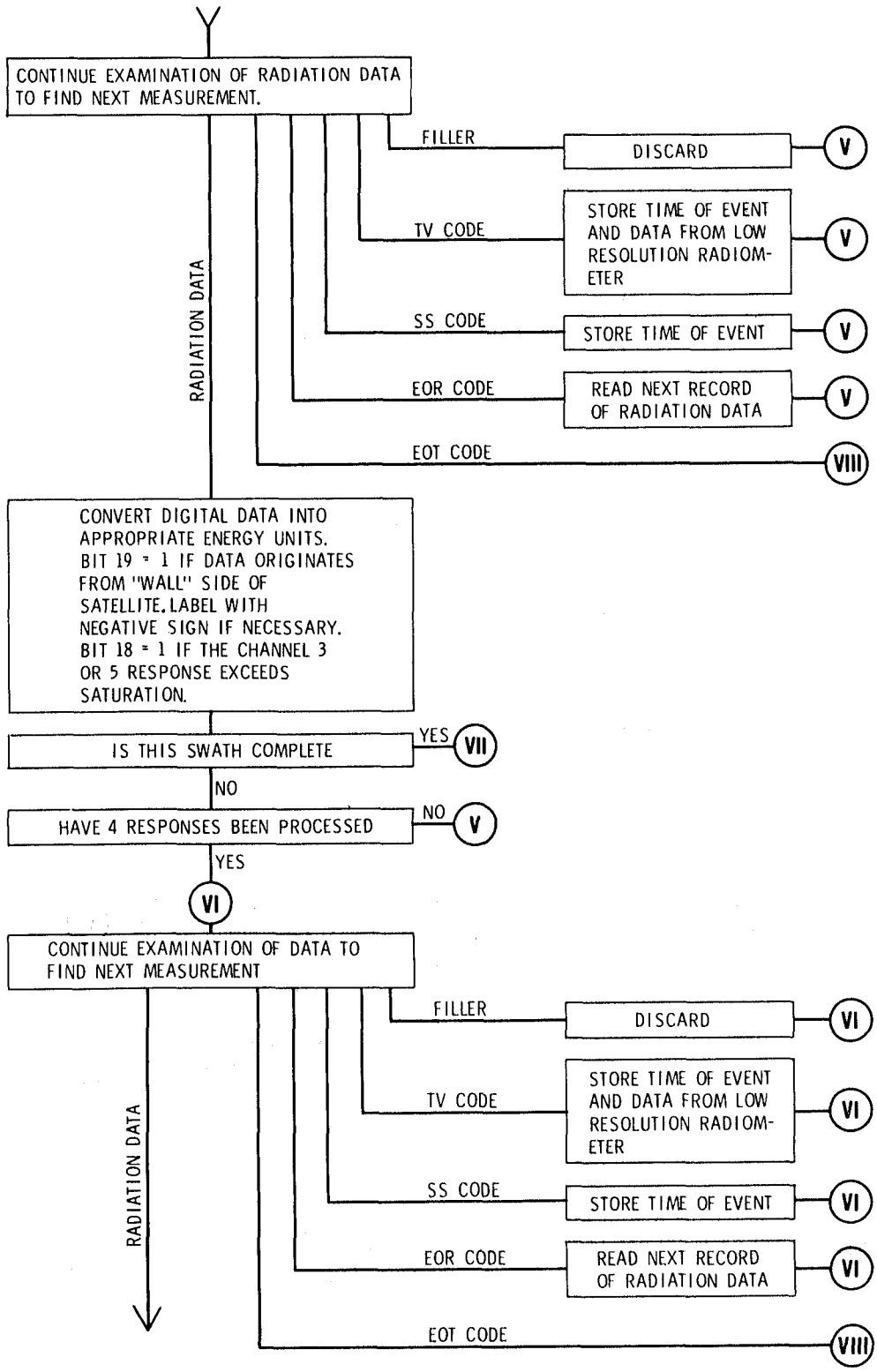
CONTINUE EXAMINATION OF RADIATION DATA TO FIND NEXT MEASUREMENT.
FILLER
DISCARD
V
TV CODE
STORE TIME OF EVENT AND DATA FROM LOW RESOLUTION RADIOMETER
V
SS CODE
STORE TIME OF EVENT
V
EOR CODE
READ NEXT RECORD OF RADIATION DATA
V
EOT CODE
VIII
RADIATION DATA
CONVERT DIGITAL DATA INTO APPROPRIATE ENERGY UNITS. BIT 19 = 1 IF DATA ORIGINATES FROM "WALL" SIDE OF SATELLITE. LABEL WITH NEGATIVE SIGN IF NECESSARY. BIT 18 = 1 IF THE CHANNEL 3 OR 5 RESPONSE EXCEEDS SATURATION.
IS THIS SWATH COMPLETE
YES
VII
NO
HAVE 4 RESPONSES BEEN PROCESSED
NO
V
YES
VI
CONTINUE EXAMINATION OF DATA TO FIND NEXT MEASUREMENT
FILLER
DISCARD
VI
TV CODE
STORE TIME OF EVENT AND DATA FROM LOW RESOLUTION RADIOMETER
VI
SS CODE
STORE TIME OF EVENT
VI
EOR CODE
READ NEXT RECORD OF RADIATION DATA
VI
EOT CODE
VIII
RADIATION DATA

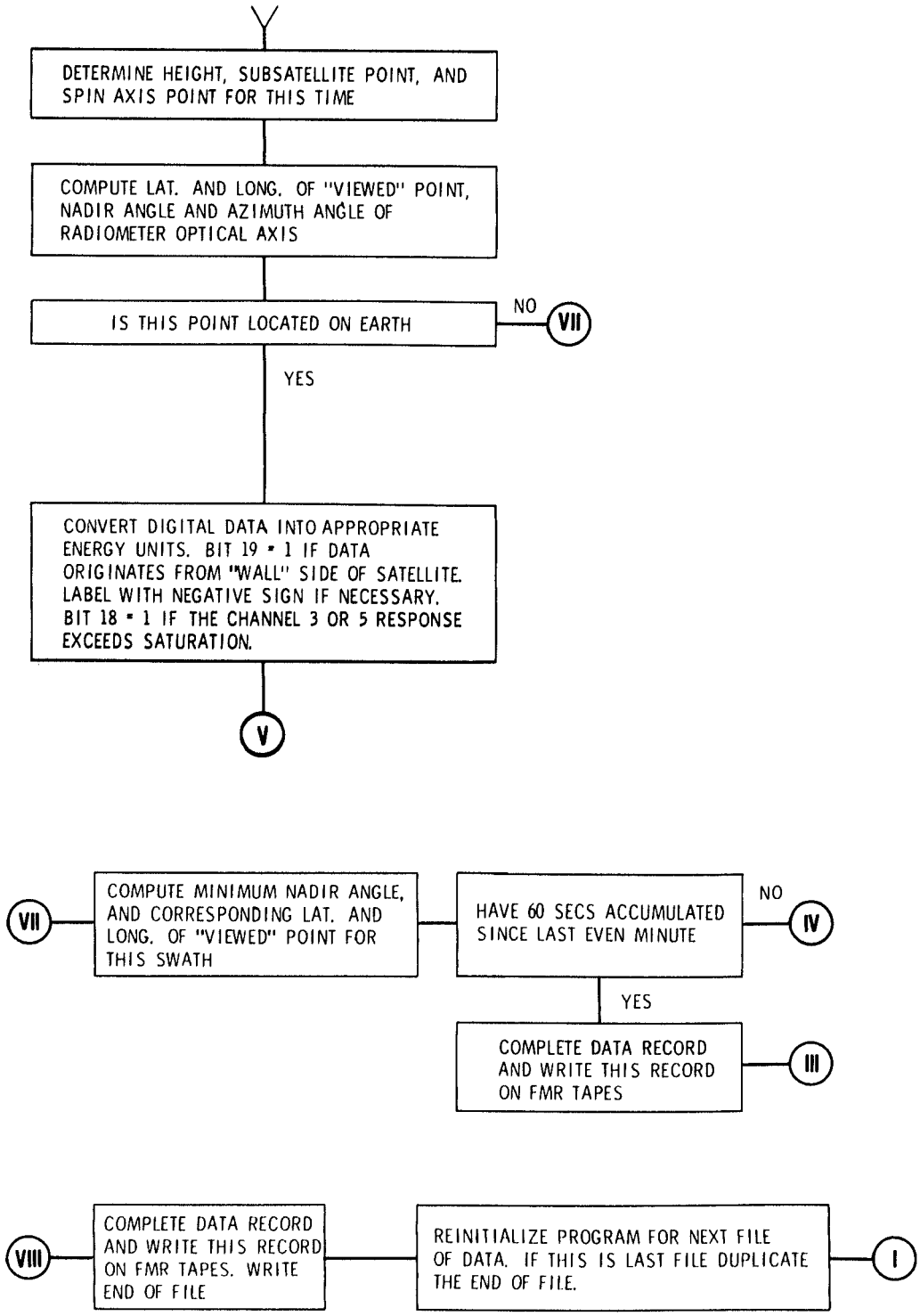
DETERMINE HEIGHT, SUBSATELLITE POINT, AND SPIN AXIS POINT FOR THIS TIME
COMPUTE LAT. AND LONG. OF "VIEWED" POINT, NADIR ANGLE AND AZIMUTH ANGLE OF RADIOMETER OPTICAL AXIS
IS THIS POINT LOCATED ON EARTH
NO
VII
YES
CONVERT DIGITAL DATA INTO APPROPRIATE ENERGY UNITS. BIT 19 = 1 IF DATA ORIGINATES FROM "WALL" SIDE OF SATELLITE. LABEL WITH NEGATIVE SIGN IF NECESSARY. BIT 18 = 1 IF THE CHANNEL 3 OR 5 RESPONSE EXCEEDS SATURATION.
V
VII
COMPUTE MINIMUM NADIR ANGLE, AND CORRESPONDING LAT. AND LONG. OF "VIEWED" POINT FOR THIS SWATH
HAVE 60 SECS ACCUMULATED SINCE LAST EVEN MINUTE
NO
IV
YES
COMPLETE DATA RECORD AND WRITE THIS RECORD ON FMR TAPES
III
VIII
COMPLETE DATA RECORD AND WRITE THIS RECORD ON FMR TAPES. WRITE END OF FILE
REINITIALIZE PROGRAM FOR NEXT FILE OF DATA. IF THIS IS LAST FILE DUPLICATE THE END OF FILE.
I

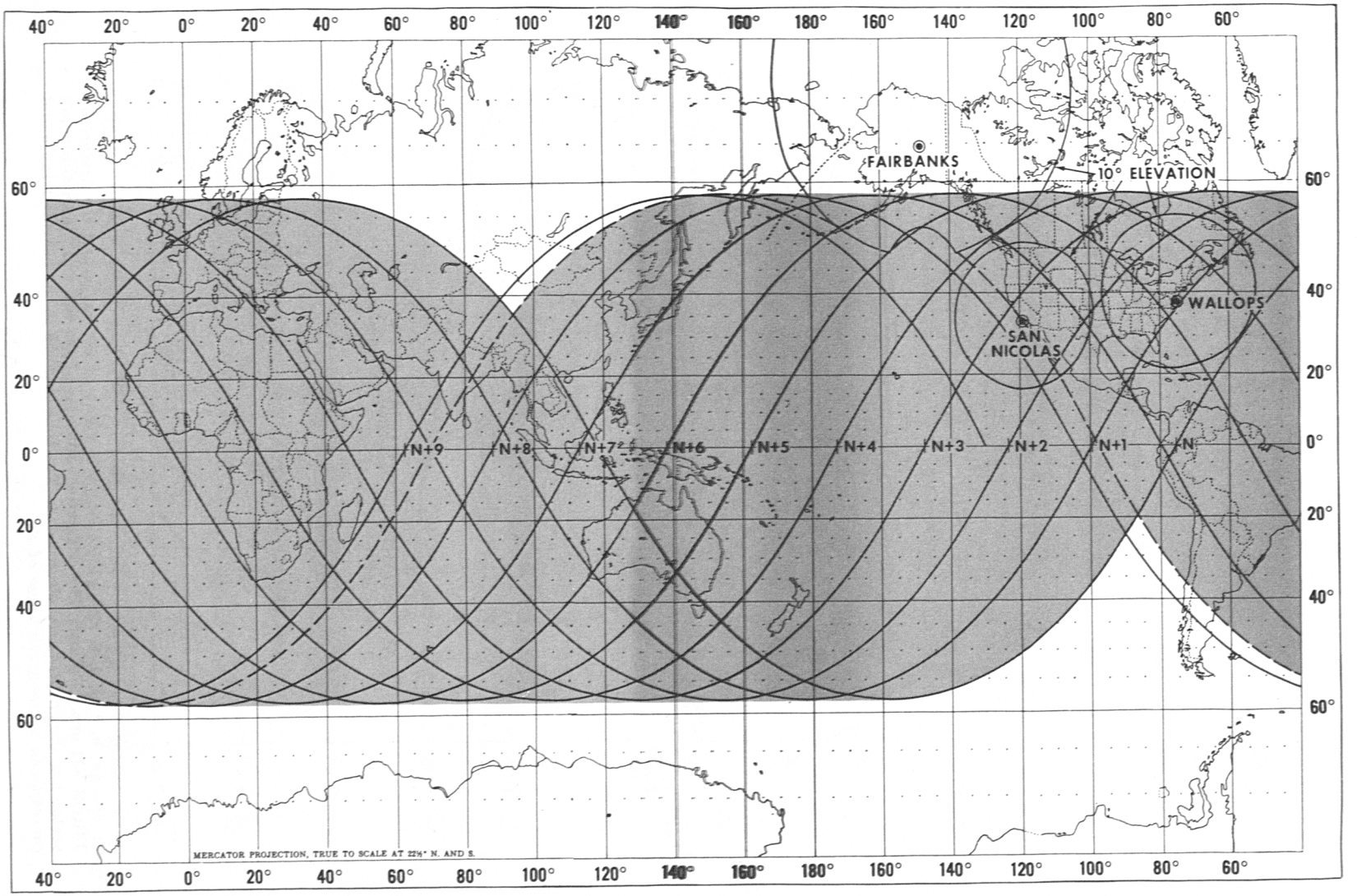

Figure 65—Nominal world-wide radiation data coverage. The shaded area shows the geographical areas from which nearly all radiation data are acquired. The data acquisition circles for a 10° antenna elevation angle at the CDA stations are also shown.

144 659

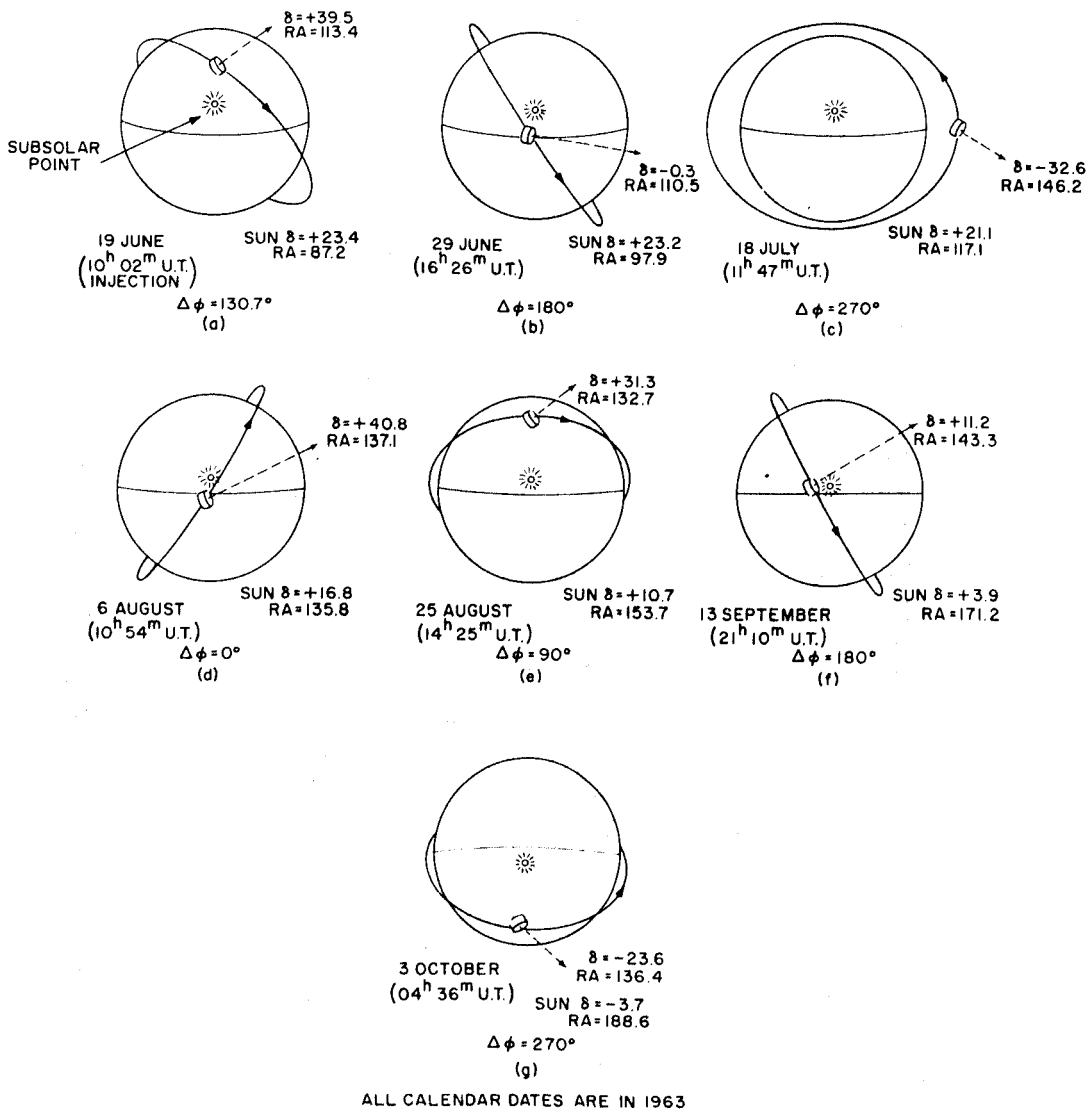

Figure 66—(a, b, c, d, e, f, and g) Heliocentric views of the earth and the precessing TIROS VII orbital plane. The celestial coordinates of the sun and the satellite spin vector are shown for each selected day. The time is given to the nearest minute and corresponds to the given value of $\Delta\phi$.

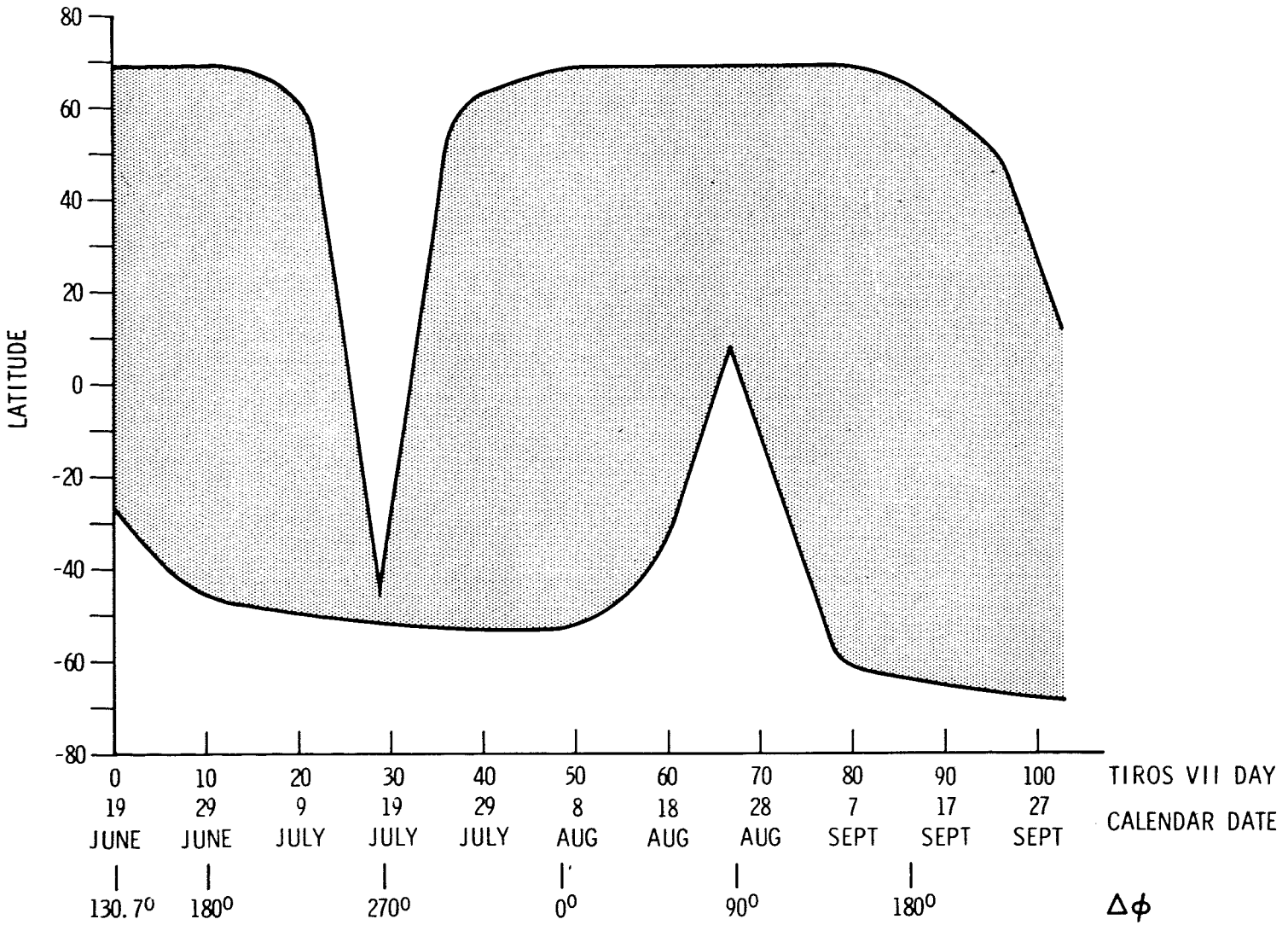

Figure 67—Solar illuminated latitudes for TIROS VII.

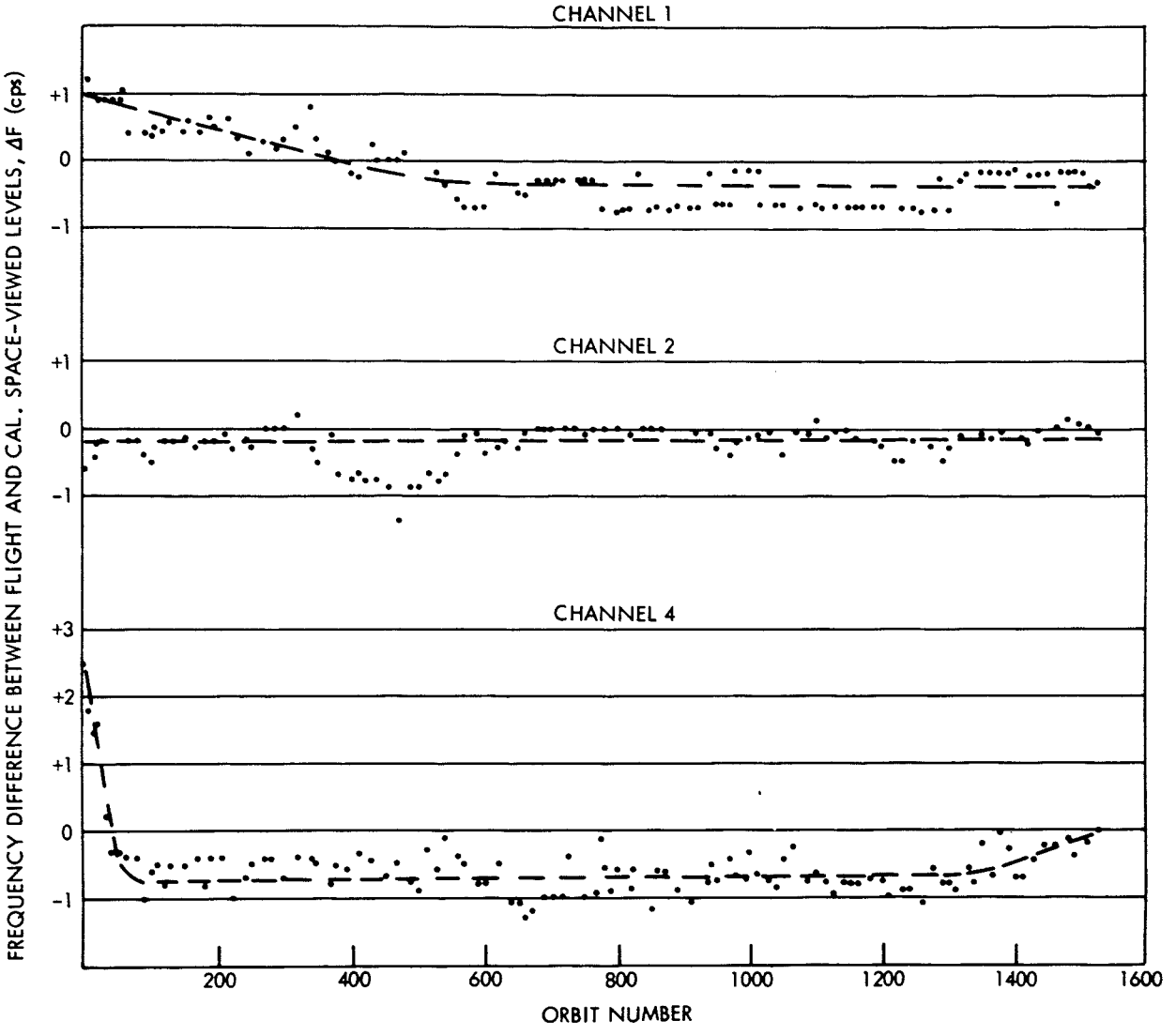

Figure 68a—Frequency difference between flight and calibrated space-viewed levels vs. orbit number for channels 1, 2, and 4.

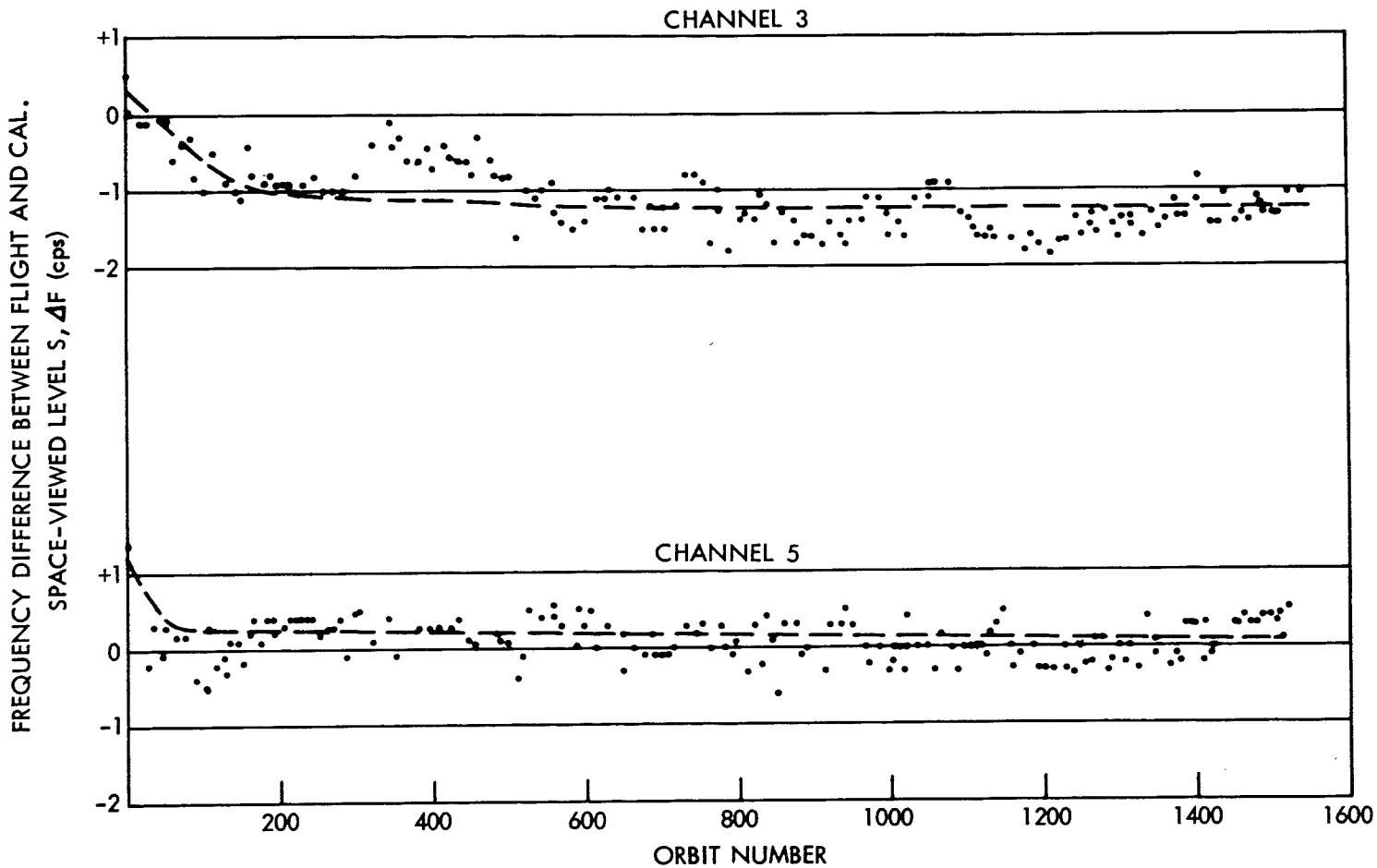

Figure 68b—Frequency difference between flight and calibrated space-viewed levels vs. orbit number for channels 3 and 5.

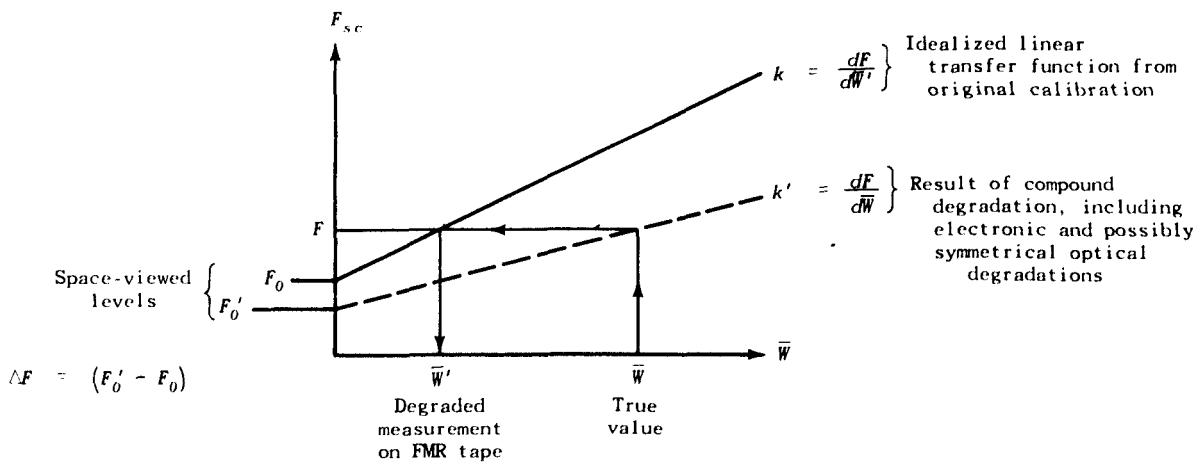

(a) $k\overline{W}' = (F - F_0)$

(b) $k'\overline{W} = (F - F_0') = (F - F_0) - (F_0' - F_0)$

(c) $\overline{W} = \left(\frac{k}{k'}\right)\left[\overline{W}' - \frac{\Delta F}{k}\right]$

At orbit i

(d) $\overline{W} = \kappa^i \left[\overline{W}' + \rho^i\right]$ where $\kappa^i = \left(\frac{k}{k'}\right)^i$ and $\rho^i = \left(\frac{-\Delta F}{k}\right)^i$

Figure 69—Schematic representation of the compound degradation model, including electronic and possibly symmetrical optical degradations. A true value, $\overline{W}$, is recorded as a measurement, $\overline{W}'$. Equation (d) converts the degraded measurement to its true value at orbit i.

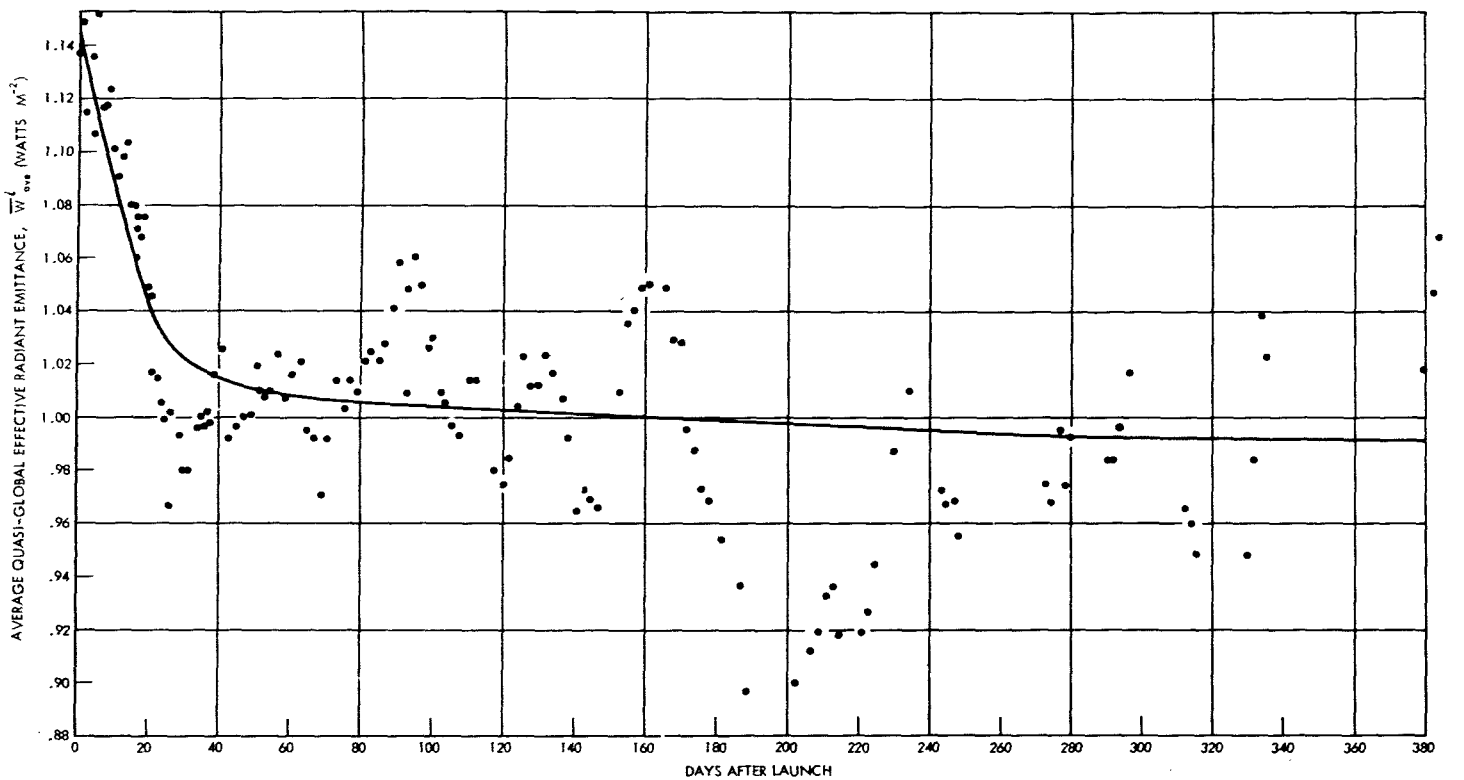

Figure 70—The average quasi-global effective radiant emittance, $\overline{W}^{1}_{ere}$, for channel 1 vs. days after launch.

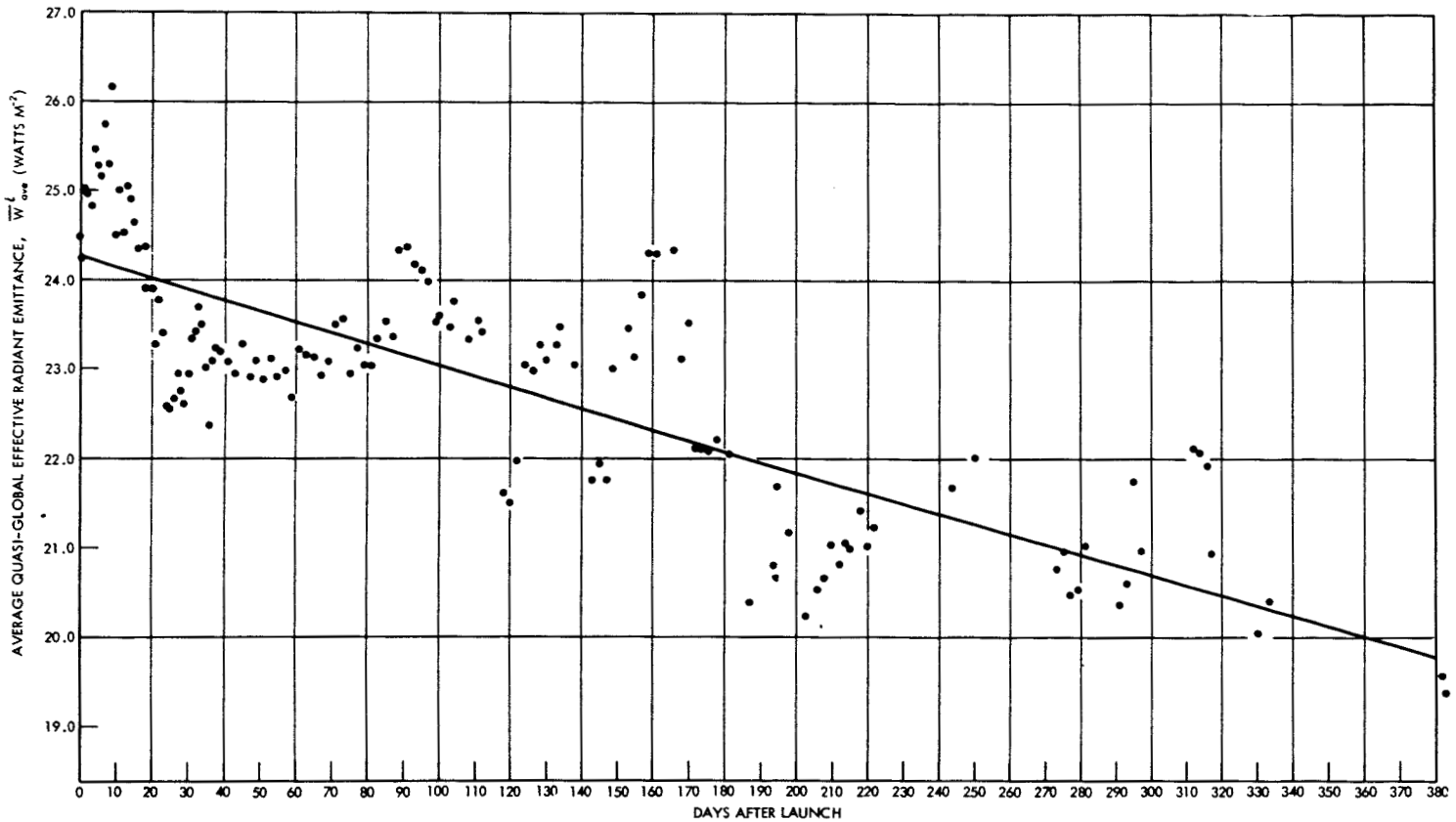

Figure 71—The average quasi-global effective radiant emittance, $\overline{W}^{i}_{ave}$, for channel 2 vs. days after launch.

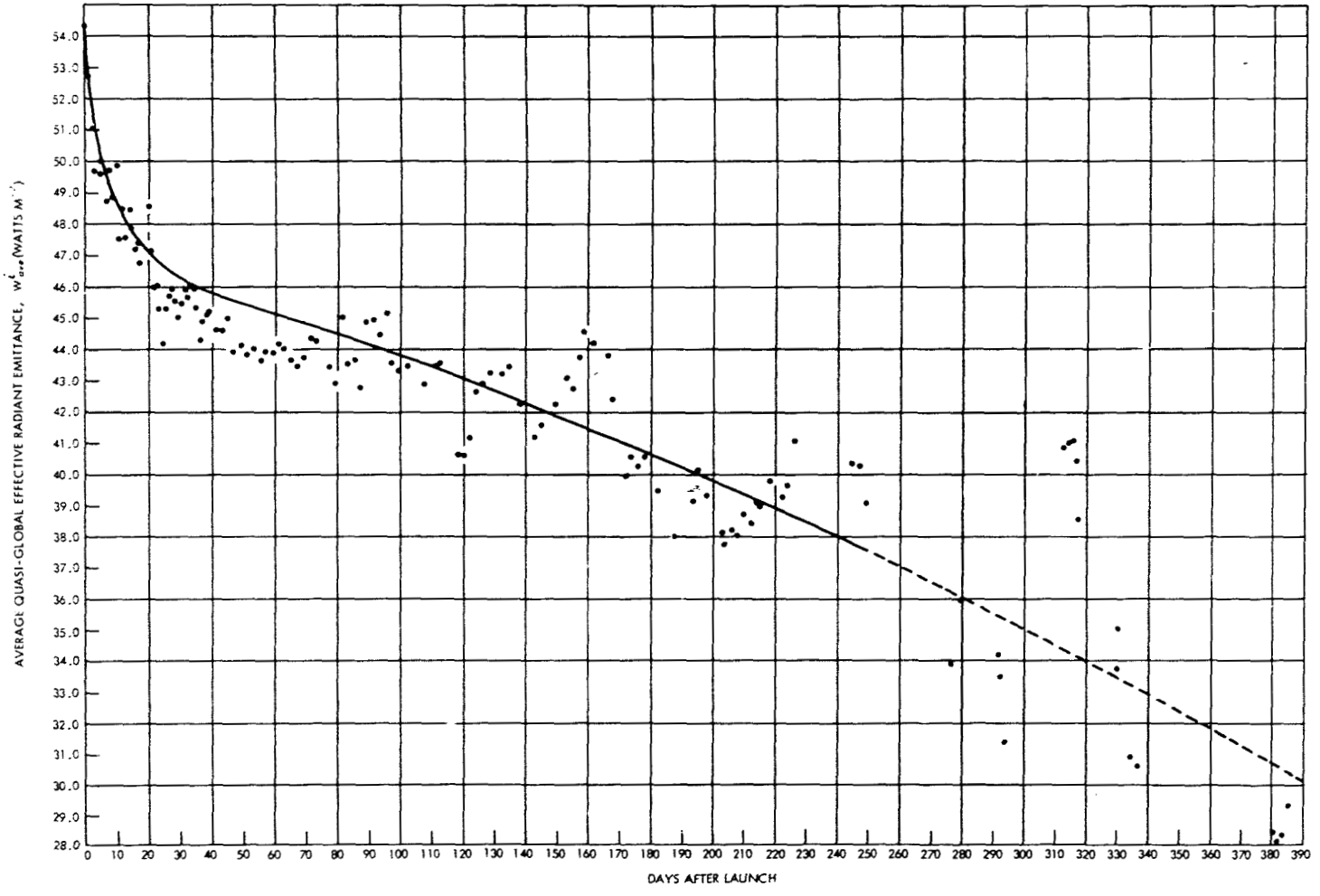

Figure 72—The average quasi-global effective radiant emittance, $\overline{W}'_{are}$, for channel 4 vs. days after launch. A dashed line follows day 249 when an erratic "stepped" characteristic was first noticed in the space-viewed portions of the analog presentations of the data.

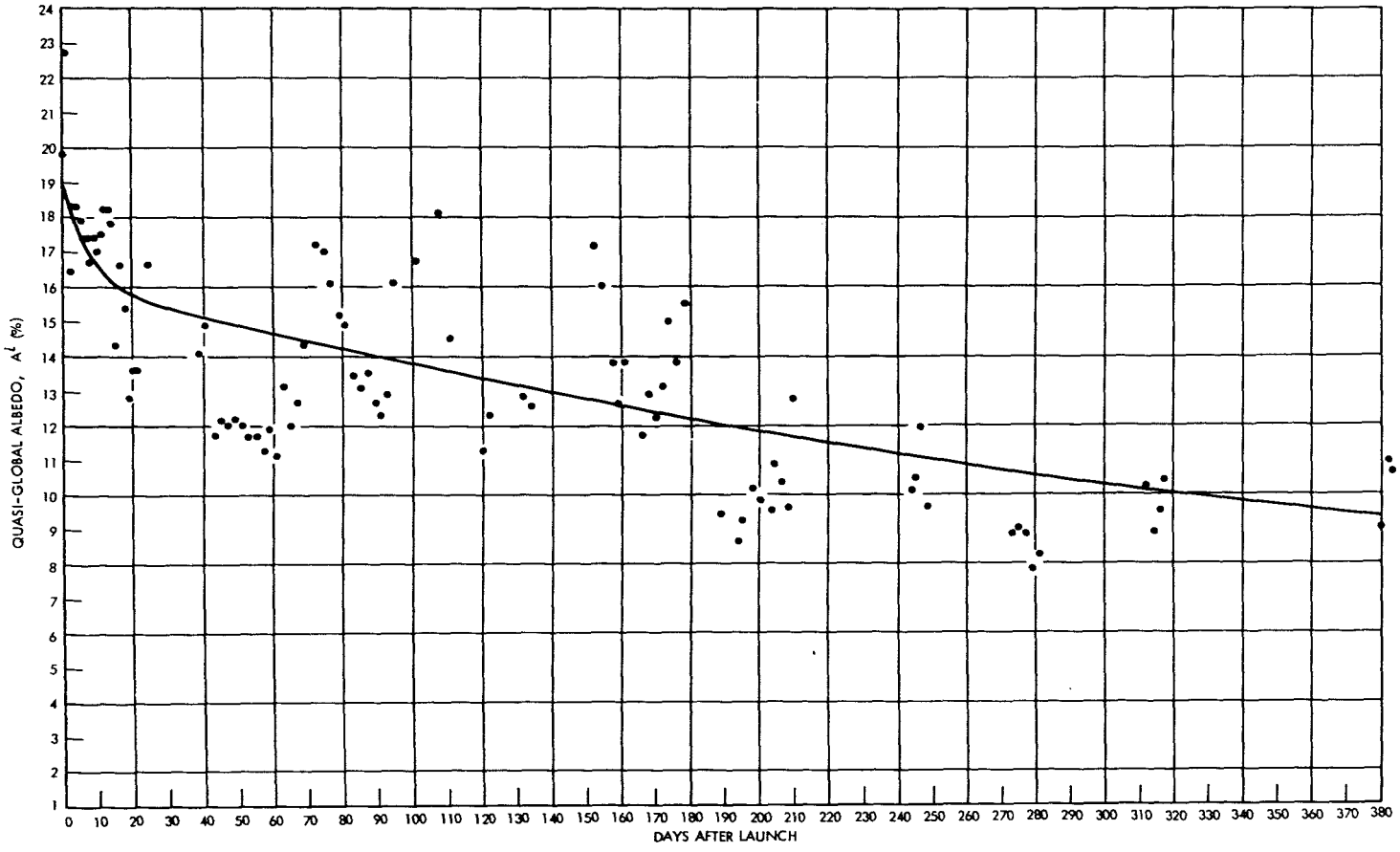

Figure 73—The quasi-global albedo, A^i, for channel 3 vs. days after launch.

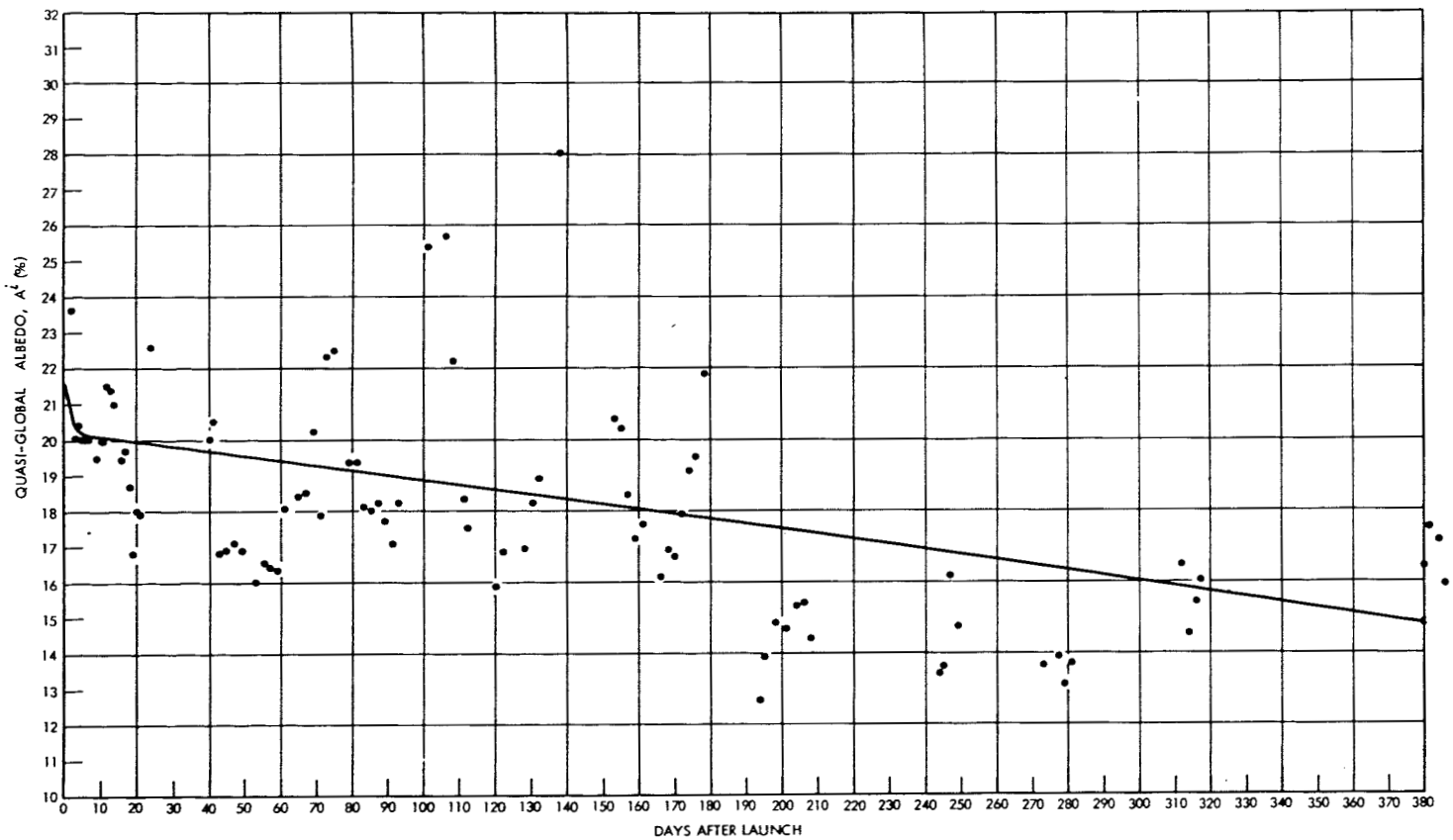

Figure 74—The quasi-global albedo, A', for channel 5 vs. days after launch.

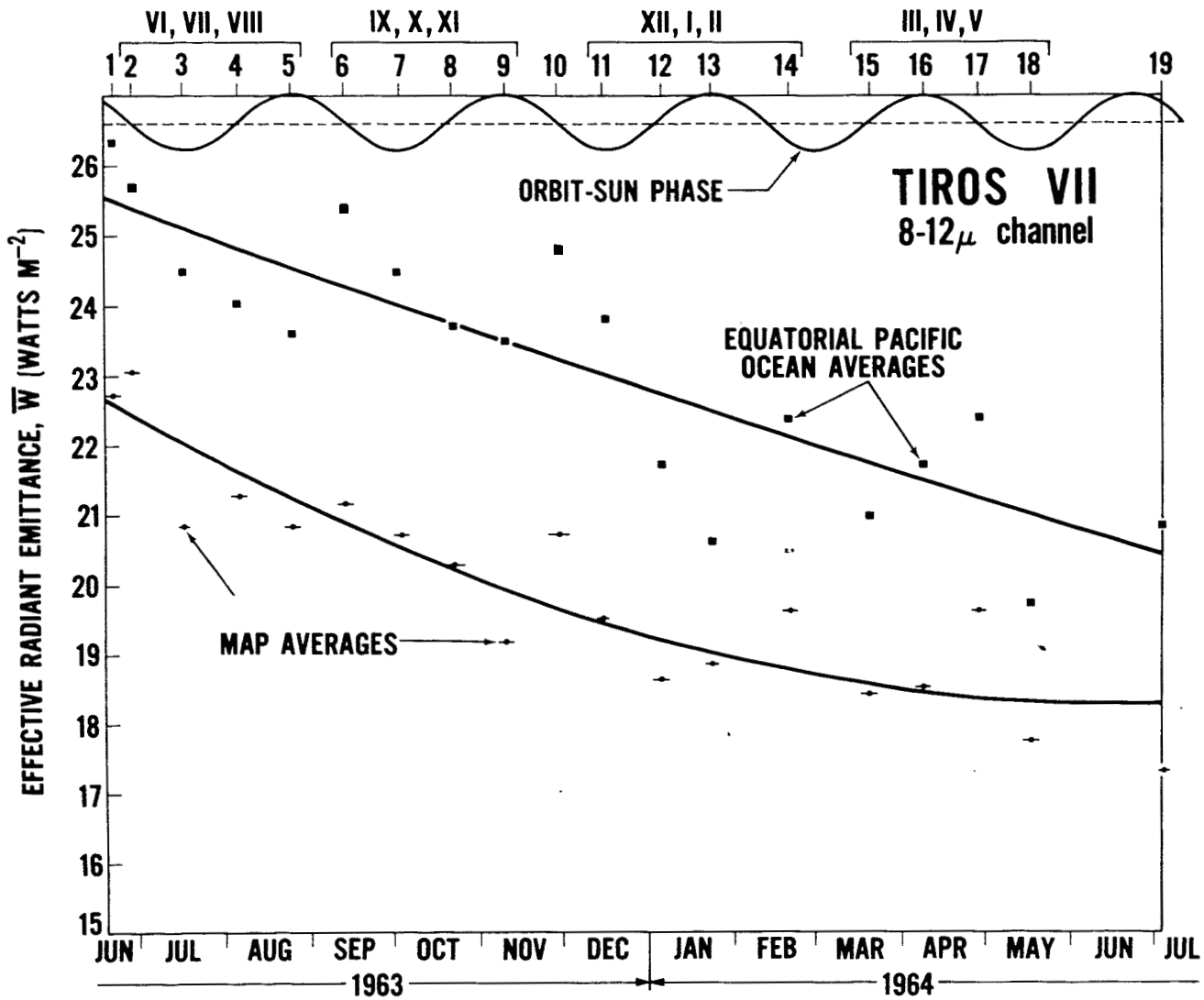

Figure 75—Effective radiant emittance, $\overline{W}$, vs. time from over-all map averages and equatorial Pacific Ocean averages over one year indicating a degradation of the instrumental response and a periodic variation with the orbit-sun phase geometry.

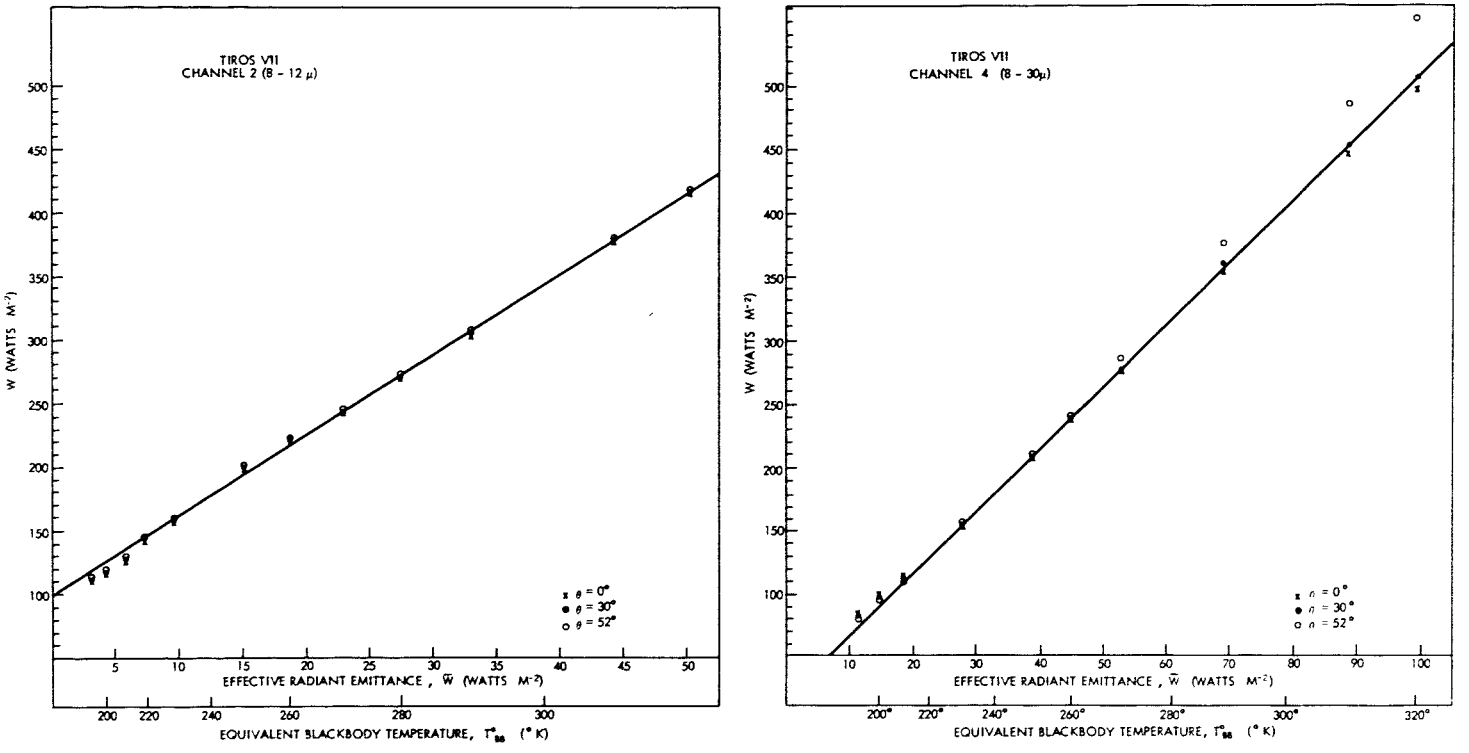

Figure 76—Total radiant emittance, $\overline{W}$, plotted as a function of effective radiant emittance to which an undegraded sensor responds, $\overline{W}$, for channel 2 (a) and channel 4 (b) at zenith angles of 0°, 30°, and 52°. The straight line approximations were adopted for further manipulation of the $\overline{W}$ values printed out by the computer.

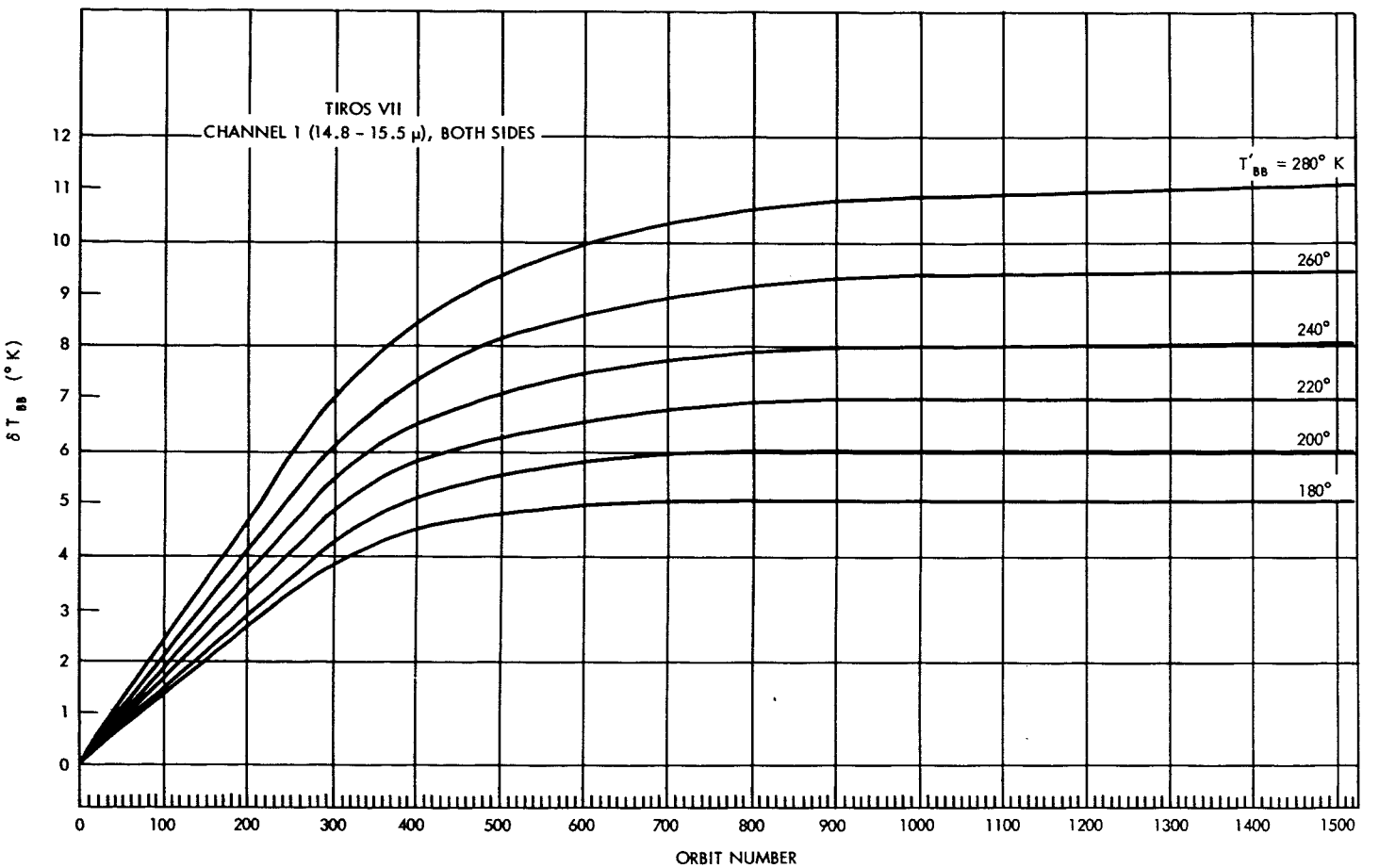

Figure 77—Temperature corrections, δT_{BB}, vs. orbit number, channel 1, both sides. An equivalent blackbody temperature measurement, T_{BB}', should be corrected by adding the δT_{BB} value corresponding to the appropriate orbit number. (There is some evidence that, *in addition to the nomogram corrections, approximately 2.5°K should be subtracted from measurements made through the floor and added to measurements made through the wall of channel 1*).

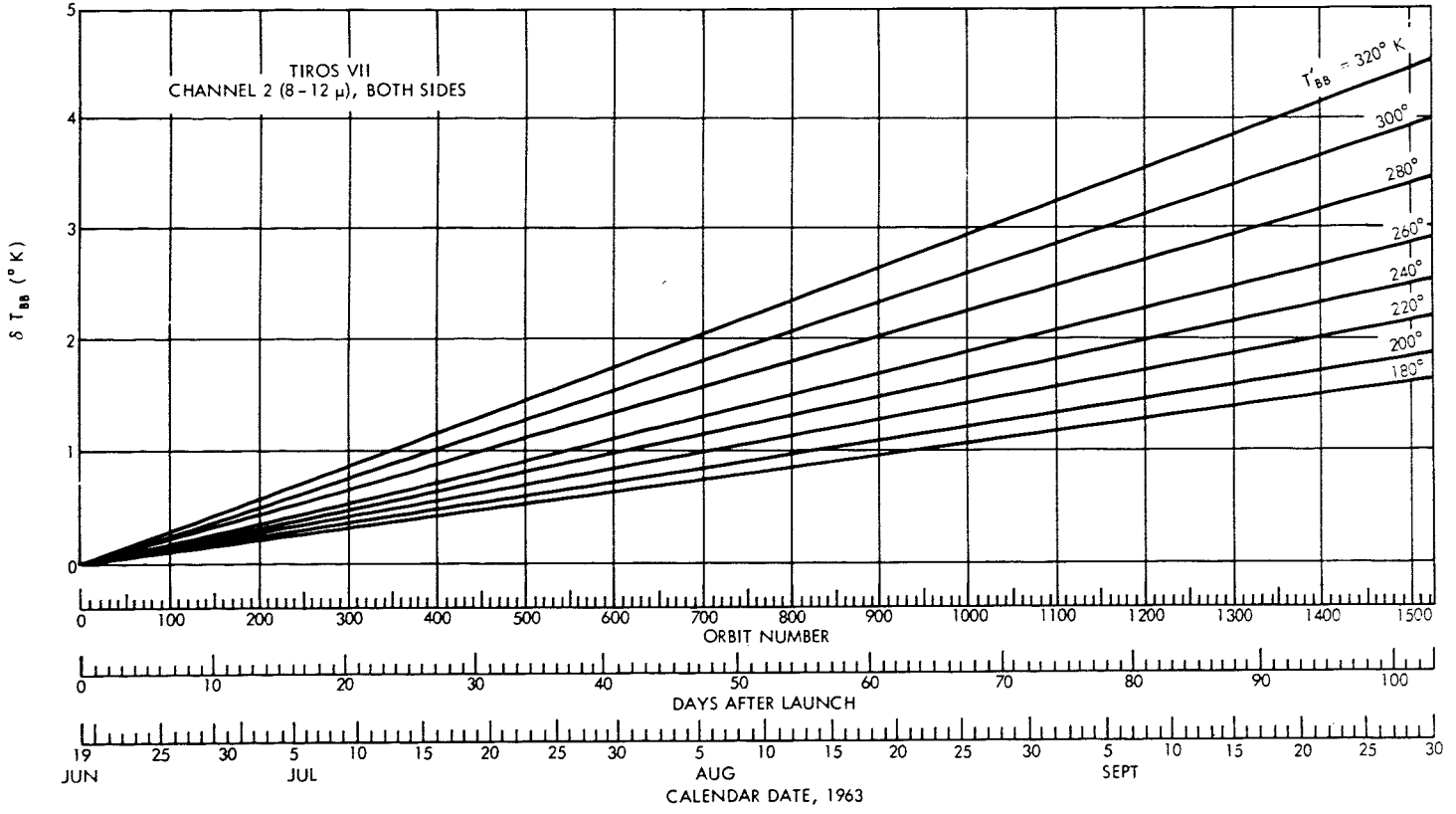

Figure 78—Temperature corrections, δT_{BB}, vs. orbit number channel 2, both sides. An equivalent blackbody temperature measurement, T_{BB}', should be corrected by adding the δT_{BB} value corresponding to the appropriate orbit number.

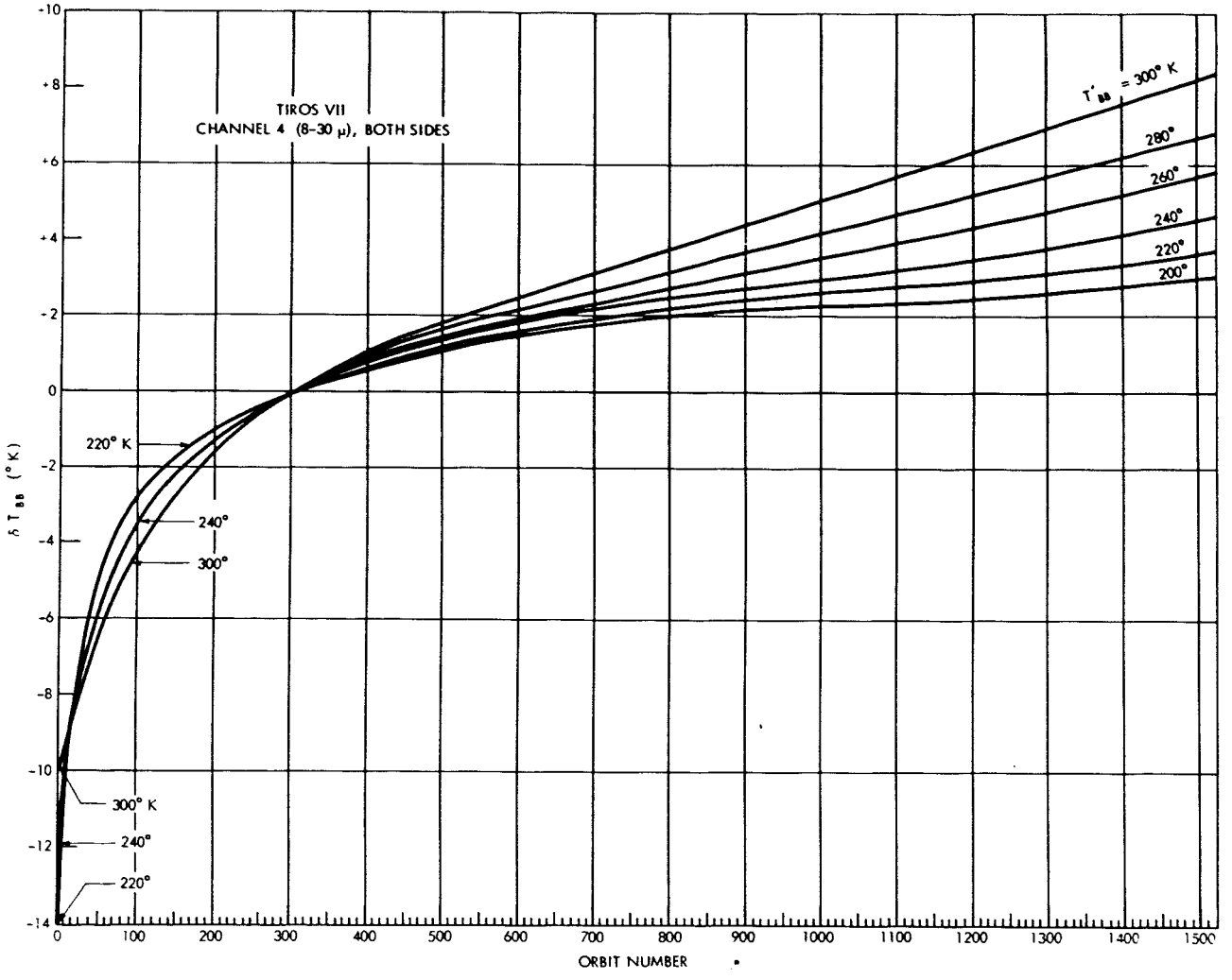

Figure 79—Temperature corrections, δT_{BB}, vs. orbit number, channel 4, both sides. An equivalent blackbody temperature measurement, T_{BB}', should be corrected by adding algebraically the δT_{BB} value corresponding to the appropriate orbit number.

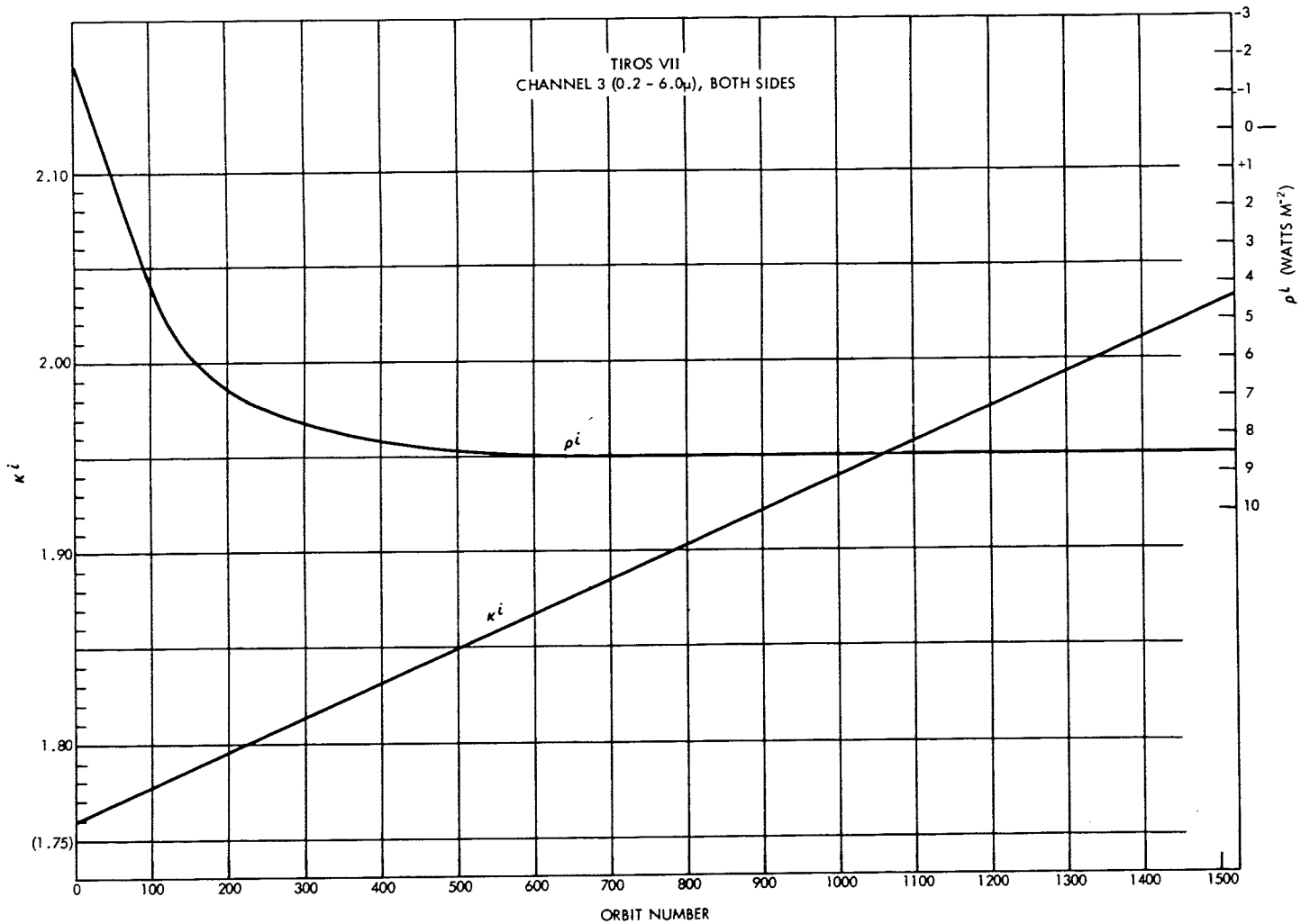

Figure 80—Normalizing parameters κ^i and ρ^i for channel 3. A measurement, $\overline{W}'$, should be corrected to yield $\overline{W}$ by means of the equation $\overline{W} = \kappa^i\,[\overline{W}' + \rho^i]$.

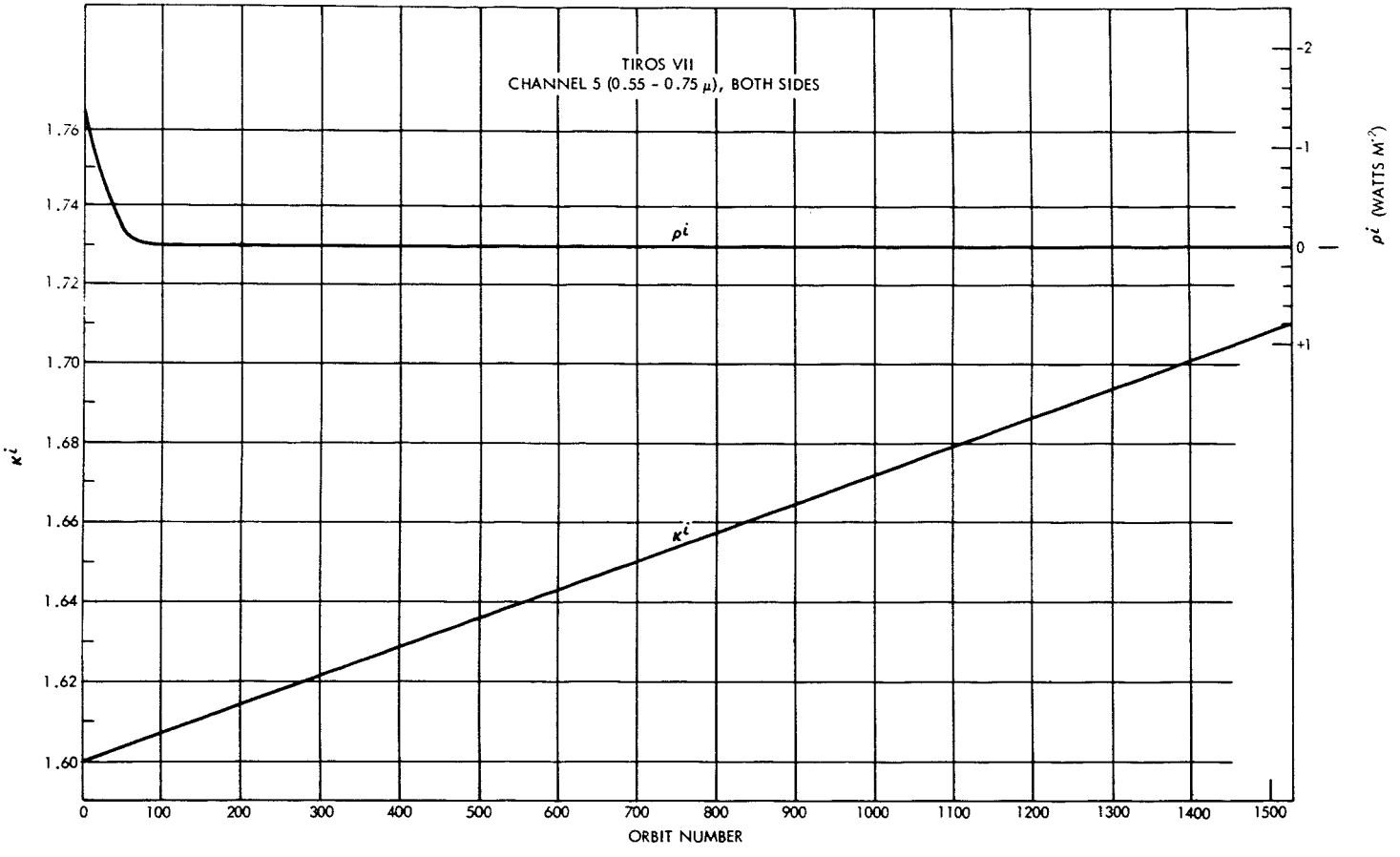

Figure 81—Normalizing parameters κ^i and ρ^i for channel 5. A measurement, W', should be corrected to yield W by means of the equation $W = \kappa^i [W' + \rho^i]$.

APPENDIX A

INDEX OF FINAL METEOROLOGICAL RADIATION TAPES

105 FMR tapes, containing data from 576 individual orbits of TIROS VII from launch, June 19, 1963, to September 30, 1963, are tabulated on the following pages. The FMR tapes for this period are numbered from 333 through 437. TIROS II, TIROS III, and TIROS IV radiation data are contained on the first 332 numbered tapes.

The Index is designed to be used in conjunction with the Mercator Projection World Maps in Appendix B and the master subpoint track overlay in the pocket at the rear of this volume. The subpoint track is divided into one minute intervals referred to ascending node time, with the "minus" and "plus" indicators corresponding to "before" and "after" ascending node time, respectively.

The Index is divided into two basic sections. One section contains information concerning the attitude of the satellite and the location of the subpoint track as a function of time for each orbit listed on the FMR tape. The second section of the Index contains information that gives the time for which radiation data are available on the FMR tape for each orbit listed. The nomenclature used in the Index is defined below.

INDEX NOMENCLATURE

Heading	Explanation
Orbit No.	The orbit number increases by one at each ascending node, orbit zero being from launch to the first ascending node. The orbit number given in the Index is the "readout" orbit number, i.e., the number of the orbit at the time of "readout" over the acquisition station. The "readout" orbit number applies to all of the data read out at one time, although some were acquired on the previous numbered orbit.
CDA Station	Command and Data Acquisition Station at which the satellite was interrogated. "1" is the Wallops Island, Virginia station, "2" is the San Nicolas Island, California station, and "3" is the Fairbanks, Alaska station.
Satellite Equator Crossing at Orbital Ascending Node (ANO)	
Earth longitude	The longitude on the earth at which the sub-satellite track crossed the equatorial plane going from south to north, measured in degrees from 0° to 180° west (designated by a "minus" sign) and from 180° to 0° east (designated by no sign).
Hours; minutes; seconds; (GMT)	Greenwich Mean Time of the occurrence of ANO in hours, minutes, and seconds.
Calendar date	Date on which the ascending node of the given orbit occurred.
TIROS Day	TIROS Day refers to TIROS VII Day which advances one for each succeeding calendar day after June 19, 1963, the day of launch. Launch day is TIROS VII Day "0."
Spin Vector Attitude	
Declination Right Ascension	Celestial coordinates of declination and right ascension of the satellite spin vector. The tabulated values for each orbit are for the time of ascending node. As these change only slightly throughout one or-

Heading	Explanation
	bit, the value at the time of ANO is adequate, for most purposes, for the entire orbit. Positive or negative values of declination refer to north or south, respectively.
Minimum Nadir (η_0)	Satellite attitude in a system which has the orbital coordinates chosen as a reference system. η_0 is the minimum satellite nadir angle during an orbital period and TOT is the time of occurrence of η_0. Positive or negative values of η_0 indicate that the spin axis (in the direction of the TV cameras) is pointed north or south of the subpoint track, respectively, while TOT is given in minutes after ANO.
TOT	
Spin Rate	Rate of rotation of the satellite about its spin axis.
Time Interval of File on FMR Tape	
Begin	The beginning time of the radiation data available on an FMR tape in minutes with respect to (W/R/T) the time of the occurrence of the ANO. Negative or positive values indicate the beginning of the file was before or after ANO, respectively.
End	The ending time of the radiation data available on the FMR tape. This value is given in absolute time (GMT) and in minutes with respect to (W/R/T) ANO. The ending time, for all orbits, occurs after the ANO.
Dropouts	The time of the dropouts (where no radiation data are available due to system noise, etc.) is listed in minutes with respect to (W/R/T) the ANO, either minus or plus.
FMR Tape Reel No.	Number of the magnetic tape reel on which the radiation data for an orbit are located.

To illustrate the use of the tabulated material, the entries in the row for orbit No. 277 indicate that when TIROS VII passed within range of the Wallops Island, Virginia, Command and Data Acquisition Station (indicated by a "1") radiation data were telemetered from the satellite. The ascending node (ANO) of orbit 277 was earth longitude 91.36°W (west indicated by the minus sign) when TIROS VII crossed the equatorial plane going from south to north at 03:28:26 GMT on July 8, 1963 which being the nineteenth day after launch day, is "TIROS VII Day 19." The declination and right ascension of the spin vector were 2.4° south of the celestial equator and 103.7° east of the Vernal Equinox. The minimum satellite nadir angle of the orbit was −29.8° and occurred 55.2 minutes after the ANO (or 04:23:38 GMT). The minus sign indicates that the intersection of the spin (camera) axis with the earth (the terrestrial scan-axis primary point) lay south of the subpoint track. The spin rate of the satellite was 48.256 degrees per second. The Index also shows that the FMR tape data began 94.2 minutes before the ascending node (01:54:14 GMT) and ended 10.6 minutes after ascending node, or 03:39:02 GMT. Further, it is seen that a dropout occurs on the tape between −54.4 and −53.4 minutes before

ascending node; i.e., between 02:34:02 and 02:35:02 GMT. Finally, it is seen that these data are recorded on FMR Tape Reel No. 352.

The spin vector celestial coordinates and the satellite spin rate are also presented in graphical form in Figures A1 and A2. Both figures are based on the data presented in the Index.

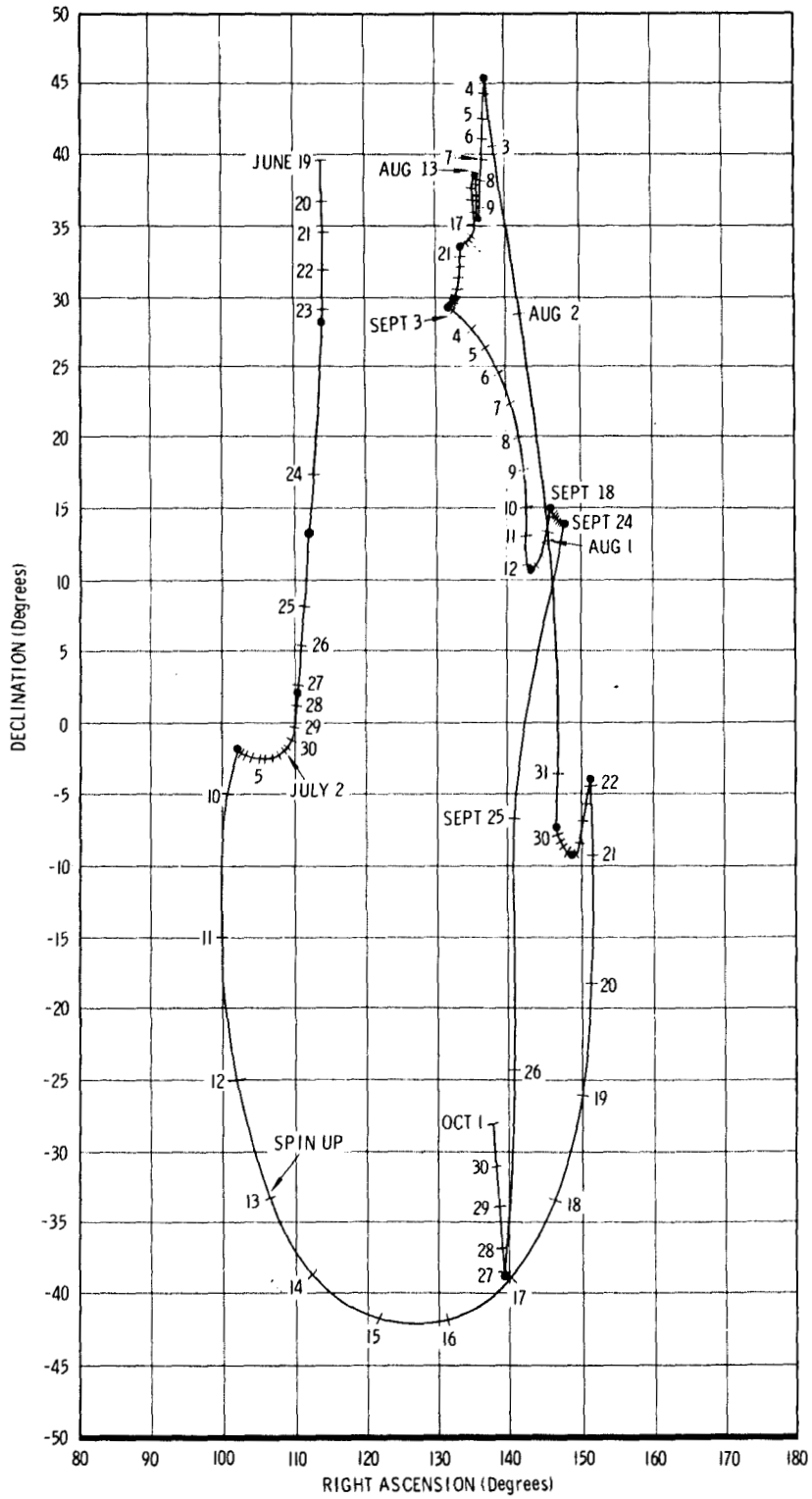

Figure A1—Observed motion of the TIROS VII spin vector on the celestial sphere. Each subdivision represents one day. Positions at 12 GMT each day are indicated.

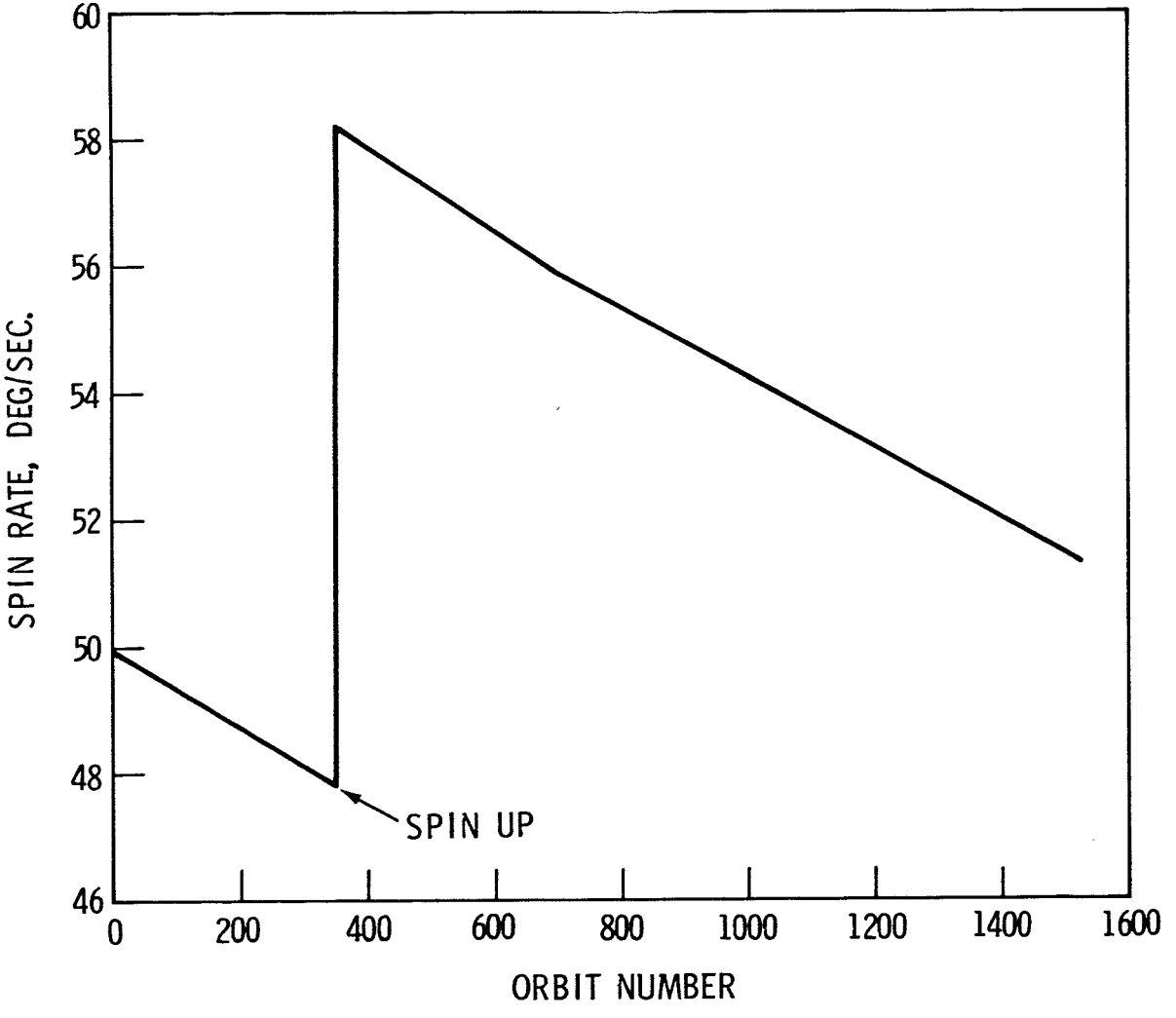

Figure A2—Time history of the TIROS VII spin rate.

READOUT						ORBIT					TIME INTERVAL OF FILE ON FMR TAPE					
		SATELLITE ORBITAL	EQUATOR ASCENDING	CROSSING NODE (ANO)		SPIN	VECTOR	ATTITUDE			BEGIN	END		DROPOUTS, MINUTES W/R/T ANO		
ORBIT NO.	CDA STA	EARTH LONGI -TUDE (DEG)	HOURS MINUTES SECONDS (GMT)	CALENDAR DATE	TIROS DAY	DECLI -NA -TION (DEG)	RIGHT ASCEN -SION (DEG)	MINI -MUM NADIR (DEG)	TOT (MIN. AFTER ANO)	SPIN RATE (DEG /SEC)	MINU -TES W/R/T ANO	HOURS MINUTES SECONDS (GMT)	MINU -TES W/R/T ANO	FROM-	TO-	FMR TAPE REEL NO.
1	1	-121.5[illegible]	11*23*15	6/19/63	0	39.6	114.0	-5.0	36.6	49.946	-65.7	11*32* 3	8.8			333
2	2	-146.18	13* 0*39	6/19/63	0	39.5	114.0	-5.1	36.6	49.937	-74.6	13*11* 3	10.4			333
4	1	164.46	16*15*29	6/19/63	0	39.2	114.0	-5.2	36.7	49.918	-25.6	16*45*33	30.1			333
5	1	139.79	17*52*53	6/19/63	0	39.1	114.0	-5.3	36.8	49.909	-56.6	18*28* 3	35.2			333
6	2	115.12	19*30*18	6/19/63	0	39.0	114.0	-5.4	36.8	49.900	-31.6	20* 3* 3	32.8			333
7	2	90.44	21* 7*42	6/19/63	0	38.8	114.1	-5.5	36.9	49.891	-59.2	21*42*33	34.9			333
14	1	-82.26	8*29*35	6/20/63	1	37.4	114.4	-6.1	37.5	49.831	-96.6	8*38* 3	8.5			334
19	1	154.36	16*36*38	6/20/63	1	36.7	114.2	-6.3	37.8	49.790	-63.6	17* 8* 3	31.4			334
20	1	129.69	18*14* 2	6/20/63	1	36.6	114.2	-6.4	37.9	49.782	13.2	18*51* 3	37.0			334
29	1	-92.36	8*50*44	6/21/63	2	34.8	114.5	-7.1	38.6	49.715	-95.2	9* 0*33	9.8			335
30	1	-117.[illegible]3	10*28* 9	6/21/63	2	34.7	114.4	-7.2	38.7	49.708	2.0	10*43*33	15.4			335
33	1	168.94	15*20*22	6/21/63	2	34.2	114.2	-7.3	38.8	49.687	-22.5	15*50* 3	29.7			335
34	1	144.27	16*57*47	6/21/63	2	34.1	114.2	-7.4	38.8	49.681	-62.0	17*34*24	36.6			335
35	1	119.59	18*35*12	6/21/63	2	34.0	114.2	-7.5	38.9	49.674	-55.2	19*11*53	36.7			335
43	1	-77.79	7*34*29	6/22/63	3	32.4	114.4	-8.2	39.5	49.622	-96.7	7*42*33	8.1			336
48	1	158.84	15*41*32	6/22/63	3	31.6	114.0	-8.5	39.9	49.591	-72.3	16*11*33	30.0			336
49	1	134.17	17*18*56	6/22/63	3	31.5	114.0	-8.5	39.9	49.585	-60.9	17*53* 3	34.1			336
50	2	109.49	18*56*21	6/22/63	3	31.3	114.0	-8.6	40.0	49.579	-52.8	19*28* 3	31.7			336
51	2	84.82	20*33*45	6/22/63	3	31.2	114.1	-8.7	40.0	49.573	-59.9	21* 9* 3	35.3			336
58	1	-87.89	7*55*38	6/23/63	4	29.8	114.1	-9.4	40.6	49.533	-96.6	8* 4* 3	8.4			337
59	1	-112.56	9*33* 2	6/23/63	4	29.6	114.0	-9.5	40.7	49.527	-49.2	9*46* 3	13.0			337
61	2	-161.9[illegible]	12*47*52	6/23/63	4	29.3	113.9	-9.6	40.7	49.516	-82.9	12*59*33	11.7			337
62	1	173.41	14*25*16	6/23/63	4	29.2	113.8	-9.6	40.8	49.510	-76.2	14*54* 3	28.8			337
63	1	148.74	16* 2*41	6/23/63	4	29.1	113.8	-9.7	40.9	49.505	-63.1	16*35*33	32.9			337
65	2	99.39	19*17*30	6/23/63	4	27.5	114.0	-9.8	41.1	49.494	-69.8	19*53* 3	35.6			337
73	1	-97.99	8*16*47	6/24/63	5	17.6	113.9	-6.6	43.7	49.451	-93.9	8*28* 3	11.3			338

READOUT						ORBIT					TIME INTERVAL OF FILE ON FMR TAPE				
		SATELLITE EQUATOR CROSSING AT ORBITAL ASCENDING NODE (AND)				SPIN VECTOR ATTITUDE					BEGIN	END		DROPOUTS, MINUTES W/R/T AND		
ORBIT NO.	CDA STA	EARTH LONGI -TUDE (DEG)	HOURS MINUTES SECONDS (GMT)	CALENDAR DATE	TIROS DAY	DECLI -NA -TION (DEG)	RIGHT ASCEN -SION (DEG)	MINI -MUM NADIR (DEG)	TOT (MIN. AFTER AND)	SPIN RATE (DEG /SEC)	MINU -TES W/R/T AND	HOURS MINUTES SECONDS (GMT)	MINU -TES W/R/T AND	FROM-	TO-	FMR TAPE REEL NO.
74	1	-122.67	9*54*11	6/24/63	5	16.5	113.5	-6.0	44.0	49.446	-80.7	10* 8* 3	13.9			338
75	2	-147.34	11*31*36	6/24/63	5	15.5	113.1	-5.3	44.2	49.443	-77.7	11*41* 3	9.5			338
77	1	163.35	14*46*25	6/24/63	5	13.7	112.3	-4.0	44.6	49.426	-74.6	15*17* 3	30.6			338
78	1	138.63	16*23*50	6/24/63	5	12.9	112.0	-3.5	44.8	49.418	-7.0	16*59* 3	35.2			338
87	1	-83.42	7* 0*31	6/25/63	6	8.6	111.9	-2.4	45.2	49.348	-95.9	7* 9* 3	8.5			339
88	1	-108.09	8*37*56	6/25/63	6	8.4	111.8	-2.5	45.3	49.341	-81.0	8*48* 3	10.1			339
89	2	-132.77	10*15*21	6/25/63	6	8.3	111.7	-2.6	45.4	49.333	-81.8	10*22* 3	6.7			339
90	2	-157.44	11*52*45	6/25/63	6	8.1	111.7	-2.6	45.4	49.326	-85.2	12* 3* 3	10.3			339
92	1	153.20	15* 7*34	6/25/63	6	7.8	111.5	-2.8	45.5	49.311	-74.3	15*38* 3	30.5			339
93	1	128.53	16*44*59	6/25/63	6	7.6	111.5	-2.9	45.6	49.304	-40.6	17*20* 3	35.1			339
94	2	103.86	18*22*24	6/25/63	6	7.4	111.5	-3.0	45.6	49.297	-56.3	18*58* 3	35.7			339
95	2	79.18	19*59*48	6/25/63	6	7.2	111.5	-3.1	45.7	49.290	-56.3	20*36* 3	36.3			339
102	1	-93.52	7*21*40	6/26/63	7	5.7	111.5	-3.8	47.3	49.257	-95.8	7*31* 3	9.4			340
103	1	-118.19	8*59* 5	6/26/63	7	5.6	111.4	-3.9	47.4	49.250	-82.0	9*13* 3	14.0			340
104	2	-142.87	10*36*30	6/26/63	7	5.4	111.3	-3.9	47.5	49.246	-78.0	10*47* 3	10.6			340
106	1	167.78	13*51*19	6/26/63	7	5.1	111.2	-4.1	47.6	49.235	-71.4	14*21* 3	29.7			340
107	1	143.10	15*28*44	6/26/63	7	4.9	111.1	-4.1	47.7	49.227	25.3	16* 2* 3	33.3			340
108	2	118.43	17* 6* 8	6/26/63	7	4.8	111.1	-4.2	47.8	49.222	-59.2	17*38* 3	31.9			340
109	2	93.76	18*43*33	6/26/63	7	4.6	111.1	-4.3	47.8	49.217	-60.3	19*21*33	38.0			340
117	1	-103.62	7*42*50	6/27/63	8	2.9	111.0	-5.2	48.5	49.170	-94.1	7*54* 3	11.2			341
119	2	-152.97	10*57*39	6/27/63	8	2.6	110.8	-5.3	48.6	49.158	-93.5	11* 8* 3	10.4			341
121	1	157.68	14*12*28	6/27/63	8	2.3	110.7	-5.4	48.7	49.145	-73.8	14*43*43	31.3			341
122	1	133.00	15*49*53	6/27/63	8	2.1	110.6	-5.5	48.8	49.140	-60.5	16*26*24	36.5			341
123	2	108.33	17*27*17	6/27/63	8	2.0	110.6	-5.6	48.8	49.135	-55.5	18* 2*33	35.3			341
124	2	83.66	19* 4*42	6/27/63	8	1.9	110.6	-5.7	48.9	49.130	-55.8	19*41* 3	36.4			341
131	1	-89.05	6*26*34	6/28/63	9	1.2	110.6	-6.9	49.3	49.087	-94.9	6*36* 3	9.5			342

READOUT						ORBIT					TIME INTERVAL OF FILE ON FMR TAPE					
		SATELLITE EQUATOR CROSSING AT ORBITAL ASCENDING NODE (ANO)				SPIN VECTOR ATTITUDE					BEGIN	END		DROPOUTS, MINUTES W/R/T ANO		
ORBIT NO.	CDA STA	EARTH LONGI-TUDE (DEG)	HOURS MINUTES SECONDS (GMT)	CALENDAR DATE	TIROS DAY	DECLI-NA-TION (DEG)	RIGHT ASCEN-SION (DEG)	MINI-MUM NADIR (DEG)	TOT (MIN. AFTER ANO)	SPIN RATE (DEG /SEC)	MINU-TES W/R/T ANO	HOURS MINUTES SECONDS (GMT)	MINU-TES W/R/T ANO	FROM-	TO-	FMR TAPE REEL NO.
132	1	-113.72	8* 3*59	6/29/63	9	1.1	110.5	-7.0	49.4	49.083	-82.0	8*16*33	12.6	-29.0	-27.0	342
134	2	-163.07	11*18*48	6/28/63	9	1.0	110.4	-7.3	49.5	49.070	-90.8	11*32*33	13.8			342
135	1	172.25	12*56*13	6/28/63	9	0.9	110.4	-7.4	49.5	49.065	-74.9	13*25*33	29.3			342
136	1	147.58	14*33*37	6/28/63	9	0.9	110.3	-7.6	49.6	49.060	22.3	15* 6*24	32.8			342
146	1	-99.15	6*47*43	6/29/63	10	-0.	110.2	-9.2	50.1	49.000	-69.0	6*59* 3	11.3			343
148	2	-148.49	10* 2*32	6/29/63	10	-0.1	110.2	-9.5	50.3	48.987	-93.6	10*13*33	11.0			343
150	1	162.15	13*17*22	6/29/63	10	-0.3	110.1	-9.7	50.3	48.977	28.2	13*49*33	32.2			343
151	1	137.48	14*54*46	6/29/63	10	-0.3	110.0	-9.9	50.3	48.970	-59.9	15*29* 3	34.3			343
152	2	112.80	16*32*11	6/29/63	10	-0.4	110.0	-10.0	50.4	48.965	-57.8	17* 5* 3	32.9			343
153	2	88.13	18* 9*35	6/29/63	10	-0.5	110.0	-10.2	50.4	48.959	-59.5	18*47* 3	37.5			343
161	1	-109.25	7* 8*52	6/30/63	11	-1.2	109.9	-11.5	50.9	48.910	-93.1	7*20* 3	11.2			344
163	2	-158.60	10*23*41	6/30/63	11	-1.3	109.8	-11.8	51.0	48.906	-91.8	10*36*33	12.9			344
166	1	127.37	15*15*55	6/30/63	11	-1.4	109.7	-12.2	51.1	48.880	-58.5	15*51*33	35.6			344
167	2	102.70	16*53*20	6/30/63	11	-1.5	109.6	-12.3	51.2	48.873	-55.6	17*26*33	33.2			344
168	2	78.03	18*30*44	6/30/63	11	-1.6	109.6	-12.5	51.3	48.869	-56.4	19* 8*33	37.8			344
175	1	-94.68	5*52*37	7/ 1/63	12	-2.0	109.5	-13.6	51.6	48.827	-95.2	6* 2* 3	9.4			345
179	1	166.62	12*22*15	7/ 1/63	12	-2.0	109.2	-14.3	51.8	48.806	-73.8	12*53* 3	30.8			345
180	1	141.95	13*59*40	7/ 1/63	12	-2.0	109.2	-14.5	51.7	48.801	25.3	14*33* 3	33.4			345
181	2	117.27	15*37* 4	7/ 1/63	12	-2.0	109.2	-14.6	51.7	48.796	-59.0	16*10* 3	33.0			345
182	2	92.60	17*14*29	7/ 1/63	12	-2.0	109.1	-14.8	51.8	48.791	-59.2	17*49*33	35.1			345
190	1	-104.79	6*13*46	7/ 2/63	13	-2.2	108.8	-16.2	52.1	48.751	-93.2	6*25* 3	11.3			346
192	2	-154.13	9*28*35	7/ 2/63	13	-2.2	108.7	-16.5	52.2	48.740	-94.1	9*39*33	11.0			346
205	1	-114.88	6*34*55	7/ 3/63	14	-2.3	108.1	-18.7	52.7	48.673	-92.1	6*48* 3	13.1			347
207	2	-164.23	9*49*44	7/ 3/63	14	-2.3	108.0	-19.0	52.8	48.663	-91.2	10* 3*33	13.8			347
208	1	171.39	11*27* 8	7/ 3/63	14	-2.3	107.9	-19.1	52.8	48.657	-8.2	11*57*33	30.4			347

READOUT						ORBIT					TIME INTERVAL OF FILE ON FMR TAPE				
		SATELLITE EQUATOR CROSSING AT ORBITAL ASCENDING NODE (AND)				SPIN VECTOR ATTITUDE					BEGIN	E N D		DROPOUTS, MINUTES W/R/T AND	
ORBIT NO.	CDA STA	EARTH LONGI -TUDE (DEG)	HOURS MINUTES SECONDS (GMT)	CALENDAR DATE	TIROS DAY	DECLI -NA -TION (DEG)	RIGHT ASCEN -SION (DEG)	MINI -MUM NADIR (DEG)	TOT (MIN. AFTER AND)	SPIN RATE (DEG /SEC)	MINU -TES W/R/T AND	HOURS MINUTES SECONDS (GMT)	MINU -TES W/R/T AND	FROM-	TO-	FMR TAPE REEL NO.
209	1	146.41	13* 4*33	7/ 3/63	14	-2.3	107.9	-19.3	52.7	48.652	-61.5	13*39*43	35.2			347
211	2	97.06	16*19*22	7/ 3/63	14	-2.3	107.8	-19.6	52.8	48.641	2.1	16*56* 3	36.7			347
220	2	-124.99	6*56* 4	7/ 4/63	15	-2.4	107.3	-21.1	53.1	48.593	-97.8	7* 3*33	7.5			348
223	1	160.98	11*48*18	7/ 4/63	15	-2.4	107.1	-21.5	53.3	48.576	-74.3	12*19*33	31.3			348
224	1	136.31	13*25*42	7/ 4/63	15	-2.4	107.1	-21.7	53.3	48.570	-60.7	14* 1*33	35.9			348
225	2	111.64	15* 3* 7	7/ 4/63	15	-2.4	107.0	-21.8	53.3	48.565	-56.4	15*36*33	33.4			348
233	1	-85.74	4* 2*24	7/ 5/63	16	-2.5	106.6	-23.1	53.6	48.519	-30.3	4*12* 3	9.7			349
234	1	-110.41	5*39*48	7/ 5/63	16	-2.5	106.5	-23.3	53.7	48.513	-82.3	5*51* 3	11.3			349
235	2	-135.08	7*17*13	7/ 5/63	16	-2.5	106.5	-23.4	53.7	48.507	-80.4	7*25* 3	7.8			349
236	2	-159.76	8*54*37	7/ 5/63	16	-2.5	106.4	-23.6	53.8	48.501	-84.2	9* 6*33	11.9			349
238	1	150.88	12* 9*26	7/ 5/63	16	-2.5	106.2	-23.9	53.8	48.489	-69.3	12*42*33	33.1			349
239	1	126.21	13*46*51	7/ 5/63	16	-2.4	106.2	-24.0	53.8	48.483	-58.8	14*23*33	36.7			349
240	2	101.54	15*24*16	7/ 5/63	16	-2.4	106.1	-24.2	53.8	48.477	-55.5	15*59* 3	34.8			349
241	2	76.87	17* 1*40	7/ 5/63	16	-2.5	106.1	-24.3	53.9	48.470	-56.0	17*40* 3	38.4			349
248	1	-95.84	4*23*32	7/ 6/63	17	-2.5	105.7	-25.4	54.2	48.427	-94.9	4*34* 3	10.5			350
249	1	-120.51	6* 0*57	7/ 6/63	17	-2.5	105.6	-25.6	54.1	48.420	-81.6	6*14*33	13.6			350
253	1	140.79	12*30*35	7/ 6/63	17	-2.4	105.3	-26.2	54.3	48.394	14.7	13* 4*33	34.0			350
254	2	116.11	14* 8* 0	7/ 6/63	17	-2.4	105.2	-26.3	54.3	48.388	-58.1	14*40*33	32.6			350
255	2	91.44	15*45*25	7/ 6/63	17	-2.4	105.2	-26.5	54.4	48.381	-58.8	16*21* 3	35.6			350
263	1	-105.94	4*44*41	7/ 7/63	18	-2.4	104.7	-27.7	54.6	48.345	-93.1	4*56* 3	11.4			351
264	2	-130.61	6*22* 6	7/ 7/63	18	-2.4	104.6	-27.9	54.7	48.339	-80.2	6*29*33	7.5			351
265	2	-155.28	7*59*31	7/ 7/63	18	-2.4	104.6	-28.0	54.7	48.332	-84.5	8*11*33	12.0			351
267	1	155.36	11*14*20	7/ 7/63	18	-2.4	104.4	-28.3	54.8	48.320	-72.0	11*47*33	33.2			351
268	1	130.69	12*51*44	7/ 7/63	18	-2.4	104.3	-28.5	54.9	48.313	-58.5	13*27* 3	35.3			351
269	2	106.01	14*29* 9	7/ 7/63	18	-2.4	104.2	-28.6	54.9	48.307	-56.4	15* 4*24	35.3			351

READOUT						ORBIT					TIME INTERVAL OF FILE ON FMR TAPE					
		SATELLITE EQUATOR CROSSING AT ORBITAL ASCENDING NODE (AND)				SPIN VECTOR ATTITUDE					BEGIN	E N D		DROPOUTS, MINUTES W/R/T AND		
ORBIT NO.	CDA STA	EARTH LONGI -TUDE (DEG)	HOURS MINUTES SECONDS (GMT)	CALENDAR DATE	TIROS DAY	DECLI -NA -TION (DEG)	RIGHT ASCEN -SION (DEG)	MINI -MUM NADIR (DEG)	TOT (MIN. AFTER AND)	SPIN RATE (DEG /SEC)	MINU -TES W/R/T AND	HOURS MINUTES SECONDS (GMT)	MINU -TES W/R/T AND	FROM-	TO-	FMR TAPE REEL NO.
270	2	81.34	16* 6*34	7/ 7/63	18	-2.4	104.2	-28.8	54.8	48.301	-57.6	16*43*24	36.8			351
277	1	-91.36	3*28*26	7/ 8/63	19	-2.4	103.7	-29.8	55.2	48.256	-94.2	3*39* 3	10.6	-54.4	-53.4	352
278	1	-116.04	5* 5*50	7/ 8/63	19	-2.4	103.7	-29.9	55.2	48.249	-81.5	5*20*33	14.7			352
279	2	-140.71	6*43*15	7/ 8/63	19	-2.3	103.6	-30.1	55.3	48.243	-77.2	6*53*33	10.3			352
281	1	169.93	9*58* 4	7/ 8/63	19	-2.3	103.4	-30.4	55.2	48.229	13.0	10*29*33	31.5			352
282	1	145.26	11*35*29	7/ 8/63	19	-2.3	103.3	-30.5	55.3	48.223	-17.4	12* 9* 3	33.6			352
284	2	95.91	14*50*18	7/ 8/63	19	-2.3	103.2	-30.8	55.4	48.210	-40.5	15*25* 3	34.8			352
293	2	-126.15	5*26*59	7/ 9/63	20	-2.2	102.7	-32.2	55.7	48.151	-89.5	5*42*33	15.6			353
294	2	-150.83	7* 4*24	7/ 9/63	20	-2.1	102.7	-32.4	55.8	48.145	-76.8	7*15*33	11.2			353
296	1	159.81	10*19*13	7/ 9/63	20	-2.1	102.7	-32.8	55.8	48.132	-73.1	10*51*33	32.3	-26.2	-25.2	353
297	1	135.14	11*56*38	7/ 9/63	20	-2.1	102.6	-33.0	55.9	48.125	-59.6	12*33* 3	36.4	-23.6	-21.6	353
298	2	110.47	13*34* 2	7/ 9/63	20	-2.0	102.6	-33.2	56.0	48.119	-55.8	14* 7*33	33.5			353
299	2	85.80	15*11*27	7/ 9/63	20	-2.0	102.6	-33.4	56.0	48.112	-58.5	15*48* 3	36.6			353
306	1	-86.91	2*33*19	7/10/63	21	-1.1	102.5	-35.2	56.1	48.067	-97.7	2*41* 3	7.7			354
307	1	-111.58	4*10*44	7/10/63	21	-1.9	102.1	-35.4	56.2	48.061	-84.6	4*23*33	12.8			354
309	2	-160.93	7*25*33	7/10/63	21	-3.0	101.3	-34.4	56.5	48.048	-92.1	7*38*33	13.0			354
311	1	149.72	10*40*22	7/10/63	21	-4.2	100.6	-33.4	56.6	48.036	-71.9	11*13*33	33.2	-22.4	-21.4	354
312	1	125.04	12*17*47	7/10/63	21	-5.0	100.4	-32.9	56.7	48.029	-59.6	12*54*33	36.8			354
313	2	100.37	13*55*11	7/10/63	21	-5.9	100.4	-32.4	56.9	48.023	-55.7	14*30* 3	34.9			354
314	2	75.69	15*32*36	7/10/63	21	-6.8	100.5	-32.0	57.2	48.017	-57.4	16*11* 3	38.5			354
321	1	-97.01	2*54*28	7/11/63	22	-12.1	101.1	-29.8	59.0	47.974	-95.0	3* 5* 3	10.6			355
322	1	-121.68	4*31*53	7/11/63	22	-12.7	100.9	-29.4	59.2	47.968	-36.8	4*46*33	14.7			355
323	2	-146.36	6* 9*17	7/11/63	22	-13.2	100.7	-29.0	59.3	47.962	-77.8	6*20*33	11.3			355
325	1	164.29	9*24* 6	7/11/63	22	-14.3	100.1	-28.2	59.6	47.950	-72.9	9*56*33	32.5			355
326	1	139.62	11* 1*31	7/11/63	22	-15.0	99.9	-27.8	59.7	47.944	-59.6	11*37*33	36.0			355

READOUT						ORBIT					TIME INTERVAL OF FILE ON FMR TAPE					
		SATELLITE ORBITAL EQUATOR CROSSING AT ASCENDING NODE (ANO)				SPIN VECTOR ATTITUDE					BEGIN	END		DROPOUTS, MINUTES W/R/T ANO		
ORBIT NO.	CDA STA	EARTH LONGI -TUDE (DEG)	HOURS MINUTES SECONDS (GMT)	CALENDAR DATE	TIROS DAY	DECLI -NA -TION (DEG)	RIGHT ASCEN -SION (DEG)	MINI -MUM NADIR (DEG)	TOT (MIN. AFTER ANO)	SPIN RATE (DEG /SEC)	MINU -TES W/R/T ANO	HOURS MINUTES SECONDS (GMT)	MINU -TES W/R/T ANO	FROM-	TO-	FMR TAPE REEL NO.
328	2	90.27	14*16*20	7/11/63	22	-16.6	100.1	-26.9	60.1	47.932	-69.8	14*51* 3	34.7			355
337	2	-131.78	4*53* 2	7/12/63	23	-22.8	102.2	-24.5	62.3	47.882	-96.8	5* 1* 3	8.0			356
338	2	-156.45	6*30*26	7/12/63	23	-23.2	102.1	-24.2	62.5	47.876	-84.5	6*42*33	12.1			356
340	1	154.19	9*45*15	7/12/63	23	-24.3	101.8	-23.6	62.6	47.866	-14.8	10*17*33	32.3			356
341	1	129.52	11*22*40	7/12/63	23	-24.9	101.8	-23.2	62.7	47.860	-60.1	11*58*33	35.9			356
342	2	104.84	13* 0* 5	7/12/63	23	-25.7	102.0	-22.8	62.9	47.855	-56.4	13*34* 3	34.0			356
343	2	80.17	14*37*29	7/12/63	23	-26.5	102.5	-22.4	63.2	47.850	-58.5	15*15* 3	37.6			356
350	1	-92.53	1*59*22	7/13/63	24	-30.7	105.9	-20.9	65.0	47.815	-95.8	2* 9* 3	9.7			357
351	1	-117.21	3*36*46	7/13/63	24	-31.1	106.1	-20.8	65.2	47.810	-82.9	3*50*33	13.8			357
354	1	168.76	8*29* 0	7/13/63	24	-32.4	106.2	-20.1	65.6	47.795	-74.7	8*59*33	30.6			357
356	1	119.42	11*43*49	7/13/63	24	-33.4	106.4	-19.5	65.9	58.200	-60.7	12*20* 3	36.2			357
357	2	94.74	13*21*14	7/13/63	24	-34.0	106.8	-19.2	66.1	58.195	-55.7	14* 0* 3	38.8			357
365	1	-102.63	2*20*31	7/14/63	25	-37.1	111.4	-18.2	67.9	58.150	-92.0	2*34* 3	13.5			358
366	2	-127.31	3*57*55	7/14/63	25	-37.3	111.7	-18.1	68.0	58.145	-78.2	4* 5*33	7.6			358
367	2	-151.98	5*35*20	7/14/63	25	-37.5	111.8	-18.1	68.2	58.138	-84.5	5*47*33	12.2			358
369	1	158.66	8*50* 9	7/14/63	25	-38.0	112.1	-17.8	68.3	58.129	-72.7	9*23* 3	32.9			358
370	1	133.99	10*27*34	7/14/63	25	-38.4	112.3	-17.7	68.4	58.126	-57.8	11* 4*33	37.0			358
371	2	109.32	12* 4*58	7/14/63	25	-38.8	112.7	-17.4	68.6	58.119	-55.1	12*39* 3	34.1			358
372	2	84.64	13*42*23	7/14/63	25	-39.3	113.4	-17.1	68.8	58.112	-58.1	14*20* 3	37.7			358
379	1	-88.06	1* 4*15	7/15/63	26	-40.8	118.8	-16.6	70.4	58.065	-93.9	1*15*33	11.3			359
380	1	-112.73	2*41*40	7/15/63	26	-40.9	119.2	-16.7	70.6	58.059	-80.8	2*54*33	12.9			359
382	2	-162.08	5*56*29	7/15/63	26	-41.0	119.8	-16.7	70.9	58.045	-82.0	6* 9*33	13.1			359
383	1	173.24	7*33*54	7/15/63	26	-41.1	120.1	-16.7	71.0	58.039	-75.6	8* 3*33	29.7			359
384	1	148.56	9*11*18	7/15/63	26	-41.3	120.3	-16.6	71.1	58.032	-62.7	9*43*33	32.3			359
385	1	123.89	10*48*43	7/15/63	26	-41.6	120.8	-16.5	71.3	58.025	-60.2	11*25*33	36.8			359

READOUT						ORBIT					TIME INTERVAL OF FILE ON FMR TAPE					
		SATELLITE EQUATOR CROSSING AT ORBITAL ASCENDING NODE (AND)				SPIN VECTOR ATTITUDE					BEGIN	END		DROPOUTS, MINUTES W/R/T AND		
ORBIT NO.	CDA STA	EARTH LONGI -TUDE (DEG)	HOURS MINUTES SECONDS (GMT)	CALENDAR DATE	TIROS DAY	DECLI -NA -TION (DEG)	RIGHT ASCEN -SION (DEG)	MINI -MUM NADIR (DEG)	TOT (MIN. AFTER AND)	SPIN RATE (DEG /SEC)	MINU -TES W/R/T AND	HOURS MINUTES SECONDS (GMT)	MINU -TES W/R/T AND	FROM-	TO-	FMR TAPE REEL NO.
386	2	99.22	12*26* 8	7/15/63	26	-41.9	121.5	-16.3	71.4	58.018	-55.7	13* 0*33	34.4			359
387	2	74.54	14* 3*32	7/15/63	26	-42.1	122.4	-16.1	71.6	58.012	-57.8	14*41*33	38.0			359
394	1	-98.17	1*25*25	7/16/63	27	-42.0	128.2	-16.0	73.3	57.964	-95.0	1*35*33	10.1			360
395	1	-122.85	3* 2*49	7/16/63	27	-41.9	128.7	-16.2	73.5	57.958	-82.5	3*17*33	14.7			360
396	2	-147.52	4*40*14	7/16/63	27	-41.8	129.0	-16.3	73.6	57.951	-77.7	4*50*33	10.3			360
398	1	163.12	7*55* 3	7/16/63	27	-41.7	129.5	-16.4	73.8	57.937	-74.0	8*26*33	31.5			360
399	1	138.45	9*32*28	7/16/63	27	-41.8	129.9	-16.4	73.9	57.930	-57.5	10* 7*33	35.1			360
400	2	113.78	11* 9*52	7/16/63	27	-41.9	130.5	-16.3	74.0	57.924	-57.3	11*42*33	32.7			360
401	2	89.10	12*47*17	7/16/63	27	-41.9	131.3	-16.1	74.2	57.917	-59.8	13*24*33	37.3			360
410	2	-132.95	3*23*58	7/17/63	28	-39.8	137.8	-16.8	76.3	57.856	-80.6	3*30*33	6.6			361
411	2	-157.62	5* 1*23	7/17/63	28	-39.5	138.0	-17.0	76.4	57.849	-85.6	5*13*33	12.2			361
413	1	153.02	8*16*12	7/17/63	28	-39.2	138.4	-17.2	76.7	57.835	-73.1	8*48*33	32.4			361
414	1	128.35	9*53*37	7/17/63	28	-39.1	138.8	-17.2	76.8	57.828	-60.1	10*29*33	35.9			361
415	2	103.68	11*31* 2	7/17/63	28	-39.1	139.4	-17.2	76.9	57.821	-56.7	12* 5*33	34.5			361
416	2	79.01	13* 8*26	7/17/63	28	-38.9	140.2	-17.1	77.1	57.815	-58.2	13*46*33	38.1			361
423	1	-93.70	0*30*19	7/18/63	29	-35.9	144.7	-17.8	78.8	57.767	-96.1	0*39*33	9.2			362
424	1	-118.37	2* 7*43	7/18/63	29	-35.4	144.9	-18.1	79.0	57.760	-81.0	2*22*43	15.0			362
427	1	167.60	6*59*57	7/18/63	29	-34.3	145.1	-18.9	79.3	57.739	-74.9	7*30*33	30.6			362
428	1	142.93	8*37*22	7/18/63	29	-34.1	145.3	-19.0	79.4	57.732	-18.1	9*11*54	34.5			362
429	2	118.25	10*14*46	7/18/63	29	-33.9	145.6	-19.1	79.5	57.725	-58.1	10*46*33	31.8			362
430	2	93.58	11*52*11	7/18/63	29	-33.6	146.2	-19.1	79.7	57.718	30.9	12*26* 3	33.9			362
437	1	-79.12	23*14* 3	7/18/63	29	-29.8	149.6	-20.0	81.3	57.670	-95.6	23*23*46	9.7			363
438	1	-103.80	0*51*28	7/19/63	30	-29.1	149.7	-20.3	81.6	57.663	-37.9	1* 1*19	9.9			363
439	2	-128.47	2*28*53	7/19/63	30	-28.6	149.7	-20.7	81.7	57.656	-82.1	2*36*33	7.7			363
440	2	-153.14	4* 6*17	7/19/63	30	-28.1	149.6	-21.0	81.9	57.650	-84.7	4*17*33	11.3			363

READOUT						ORBIT					TIME INTERVAL OF FILE ON FMR TAPE					
		SATELLITE EQUATOR CROSSING AT ORBITAL ASCENDING NODE (AND)				SPIN VECTOR ATTITUDE					BEGIN	END		DROPOUTS, MINUTES W/R/T AND		
ORBIT NO.	CDA STA	EARTH LONGI -TUDE (DEG)	HOURS MINUTES SECONDS (GMT)	CALENDAR DATE	TIROS DAY	DECLI -NA -TION (DEG)	RIGHT ASCEN -SION (DEG)	MINI -MUM NADIR (DEG)	TOT (MIN. AFTER AND)	SPIN RATE (DEG /SEC)	MINU -TES W/R/T AND	HOURS MINUTES SECONDS (GMT)	MINU -TES W/R/T AND	FROM-	TO-	FMR TAPE REEL NO.
442	1	157.50	7*21* 7	7/19/63	30	-27.4	149.5	-21.6	82.1	57.636	-72.9	7*53*33	32.4			363
443	1	132.83	8*58*31	7/19/63	30	-27.1	149.6	-21.8	82.2	57.629	-60.0	9*34*33	36.0			363
444	2	108.15	10*35*56	7/19/63	30	-26.7	149.9	-21.9	82.4	57.622	-56.3	11* 9*33	33.6			363
445	2	83.48	12*13*21	7/19/63	30	-26.3	150.3	-21.9	82.5	57.615	-58.6	12*50*33	37.2			363
452	1	-89.22	23*35*13	7/19/63	30	-21.7	152.3	-23.3	84.2	57.567	-95.5	23*44*33	9.3			364
453	1	-113.89	1*12*38	7/20/63	31	-21.0	152.2	-23.7	84.4	57.560	-81.6	1*25*33	12.9			364
454	2	-138.57	2*50* 2	7/20/63	31	-20.4	152.0	-24.2	84.5	57.553	-79.4	2*58*33	8.5			364
455	2	-163.24	4*27*27	7/20/63	31	-19.9	151.8	-24.6	84.7	57.546	-75.9	4*40*33	13.1			364
456	1	172.07	6* 4*51	7/20/63	31	-19.5	151.6	-24.9	84.7	57.539	-75.8	6*34*33	29.7			364
457	1	147.40	7*42*16	7/20/63	31	-19.1	151.5	-25.2	84.8	57.532	-61.7	8*16*33	34.3			364
458	1	122.73	9*19*41	7/20/63	31	-18.7	151.5	-25.5	84.9	57.525	-57.9	9*56*33	36.9			364
459	2	98.05	10*57* 5	7/20/63	31	-18.3	151.7	-25.6	85.0	57.518	-54.9	11*32*33	35.5			364
468	2	-123.99	1*33*47	7/21/63	32	-12.0	152.5	-28.0	87.0	57.456	-98.7	1*40*33	6.8			365
469	2	-148.67	3*11*12	7/21/63	32	-11.4	152.2	-28.4	87.2	57.449	-85.6	3*22*33	11.4			365
473	2	112.63	9*40*50	7/21/63	32	-9.6	151.4	-29.8	87.6	57.421	-56.5	10*13*33	32.7			365
474	2	87.95	11*18*15	7/21/63	32	-9.1	151.5	-30.0	87.7	57.414	-59.4	11*55*33	37.3			365
481	1	-84.75	22*40* 7	7/21/63	32	-3.9	151.6	-31.9	89.4	57.365	-39.5	22*47* 3	6.9			366
482	1	-109.42	0*17*32	7/22/63	33	-4.0	151.6	-32.4	89.6	57.358	-32.1	0*29*33	12.0			366
483	2	-134.09	1*54*57	7/22/63	33	-4.1	151.5	-32.2	89.6	57.351	-80.5	2* 3*33	8.6			366
484	2	-158.77	3*32*22	7/22/63	33	-4.2	151.5	-31.9	89.5	57.344	-83.7	3*44*33	12.2			366
486	1	151.88	6*47*11	7/22/63	33	-4.4	151.5	-31.4	89.6	57.331	-72.1	7*20*33	33.4			366
487	1	127.20	8*24*36	7/22/63	33	-4.4	151.4	-31.2	89.7	57.324	-59.0	9* 0*33	36.0			366
488	2	102.53	10* 2* 0	7/22/63	33	-4.5	151.4	-31.0	89.7	57.317	-56.5	10*36*33	34.6			366
489	2	77.86	11*39*25	7/22/63	33	-4.6	151.3	-30.8	89.7	57.310	-57.7	12*16*33	37.1			366
498	2	-144.25	2*16* 7	7/23/63	34	-5.5	151.0	-28.8	89.9	57.247	-78.4	2*24*33	8.4			367

READOUT						ORBIT					TIME INTERVAL OF FILE ON FMR TAPE					
		SATELLITE EQUATOR CROSSING AT ORBITAL ASCENDING NODE (ANO)				SPIN VECTOR ATTITUDE					BEGIN	E N D		DROPOUTS, MINUTES W/R/T ANO		
ORBIT NO.	CDA STA	EARTH LONGI -TUDE (DEG)	HOURS MINUTES SECONDS (GMT)	CALENDAR DATE	TIROS DAY	DECLI -NA -TION (DEG)	RIGHT ASCEN -SION (DEG)	MINI -MUM NADIR (DEG)	TOT (MIN. AFTER ANO)	SPIN RATE (DEG /SEC)	MINU -TES W/R/T ANO	HOURS MINUTES SECONDS (GMT)	MINU -TES W/R/T ANO	FROM-	TO-	FMR TAPE REEL NO.
500	1	166.39	5*30*56	7/23/63	34	-5.6	151.0	-28.3	90.0	57.233	-74.7	6* 1*33	30.6			367
501	1	141.72	7* 8*21	7/23/63	34	-5.7	150.9	-28.1	90.0	57.226	-57.5	7*40*33	32.2			367
502	2	117.04	8*45*45	7/23/63	34	-5.8	150.9	-27.9	90.0	57.219	-53.3	9*17*33	31.8			367
503	2	92.37	10*23*10	7/23/63	34	-5.9	150.8	-27.7	90.0	57.212	-60.4	10*57* 3	33.9			367
510	1	-80.34	21*45* 2	7/23/63	34	-6.5	150.5	-26.1	90.2	57.164	-48.6	21*53*33	8.5			368
511	1	-105.01	23*22*27	7/23/63	34	-6.6	150.5	-25.9	90.2	57.157	-83.8	23*33*33	11.1			368
512	1	-129.68	0*59*52	7/24/63	35	-6.7	150.5	-25.7	90.2	57.150	-81.3	1*15*33	15.7			368
513	2	-154.35	2*37*16	7/24/63	35	-6.8	150.4	-25.5	90.2	57.143	-76.7	2*48*33	11.3			368
515	1	156.29	5*52* 5	7/24/63	35	-6.9	150.4	-25.0	90.3	57.129	-72.9	6*24*33	32.5			368
516	1	131.62	7*29*30	7/24/63	35	-7.0	150.3	-24.8	90.3	57.122	-59.7	8* 5*33	36.1			368
517	2	106.94	9* 6*55	7/24/63	35	-7.1	150.3	-24.6	90.4	57.115	-56.0	9*40*33	33.6			368
526	1	-115.11	23*43*36	7/24/63	35	-7.9	149.9	-22.6	90.5	57.053	-92.2	23*56*33	13.0			369
528	2	-164.46	2*58*26	7/25/63	36	-8.1	149.8	-22.2	90.6	57.039	-85.6	3*11*33	13.1	-86.4	-85.4	369
529	1	170.85	4*35*50	7/25/63	36	-8.1	149.8	-22.0	90.6	57.033	-75.6	5* 5*33	29.7	-26.8	-25.8	369
530	1	146.18	6*13*15	7/25/63	36	-8.2	149.8	-21.7	90.6	57.026	-62.1	6*47*33	34.3	-23.2	-22.2	369
531	1	121.51	7*50*39	7/25/63	36	-8.3	149.8	-21.5	90.6	57.019	-57.5	8*27*33	36.9			369
532	2	96.84	9*28* 4	7/25/63	36	-8.3	149.7	-21.3	90.6	57.012	-55.0	10* 3*33	35.5			369
533	2	72.16	11* 5*29	7/25/63	36	-8.4	149.7	-21.1	90.7	57.005	-56.8	11*44*33	39.1			369
540	1	-100.54	22*27*21	7/25/63	36	-9.1	149.4	-19.6	90.7	56.957	-40.1	22*38* 3	10.7			370
541	2	-125.22	0* 4*46	7/26/63	37	-9.2	149.3	-19.3	90.8	56.950	-81.4	0*13*26	8.7			370
542	2	-149.89	1*42*10	7/26/63	37	-9.2	149.3	-19.1	90.8	56.943	-83.5	1*52* 3	9.9			370
544	1	160.75	4*57* 9	7/26/63	37	-9.4	149.3	-18.6	90.9	56.929	-73.8	5*28* 3	31.1			370
545	1	136.08	6*34*24	7/26/63	37	-9.4	149.3	-18.4	90.9	56.923	-61.4	7* 9*33	35.2			370
546	2	111.40	8*11*49	7/26/63	37	-9.4	149.2	-18.2	90.9	56.916	-57.4	8*45*33	33.7			370
547	2	86.73	9*49*14	7/26/63	37	-9.4	149.2	-18.1	91.0	56.909	-58.6	10*26*33	37.3			370

READOUT						ORBIT					TIME INTERVAL OF FILE ON FMR TAPE					
		SATELLITE EQUATOR CROSSING AT ORBITAL ASCENDING NODE (ANO)				SPIN VECTOR ATTITUDE					BEGIN	END		DROPOUTS, MINUTES W/R/T ANO		
ORBIT NO.	CDA STA	EARTH LONGI -TUDE (DEG)	HOURS MINUTES SECONDS (GMT)	CALENDAR DATE	TIROS DAY	DECLI -NA -TION (DEG)	RIGHT ASCEN -SION (DEG)	MINI -MUM NADIR (DEG)	TOT (MIN. AFTER ANO)	SPIN RATE (DEG /SEC)	MINU -TES W/R/T ANO	HOURS MINUTES SECONDS (GMT)	MINU -TES W/R/T ANO	FROM-	TO-	FMR TAPE REEL NO.
554	1	-85.97	21*11* 6	7/26/63	37	-9.3	148.9	-16.9	91.3	56.861	-95.4	21*21* 3	10.0			371
555	1	-110.65	22*48*31	7/26/63	37	-9.3	148.9	-16.8	91.3	56.854	-82.2	23* 0*33	12.0			371
556	2	-135.32	0*25*55	7/27/63	38	-9.2	148.8	-16.6	91.4	56.847	-80.2	0*36* 3	10.1			371
557	2	-160.00	2* 3*20	7/27/63	38	-9.2	148.8	-16.5	91.4	56.841	-82.0	2*16*27	13.1			371
559	1	150.65	5*18* 9	7/27/63	38	-9.2	148.7	-16.2	91.4	56.827	-72.0	5*51*33	33.4			371
560	1	125.98	6*55*34	7/27/63	38	-9.2	148.6	-16.0	91.4	56.820	-58.7	7*32*33	37.0			371
561	2	101.30	8*32*58	7/27/63	38	-9.2	148.6	-15.8	91.5	56.813	-54.9	9* 7* 3	34.1			371
562	2	76.63	10*10*23	7/27/63	38	-9.2	148.6	-15.7	91.5	56.807	-58.0	10*48*33	38.2			371
569	1	-96.08	21*32*15	7/27/63	38	-9.0	148.4	-14.5	91.8	56.759	-94.6	21*43* 3	10.8			372
570	1	-120.75	23* 9*40	7/27/63	38	-9.0	148.3	-14.4	91.9	56.752	-80.8	23*23*33	13.9			372
571	2	-145.43	0*47* 5	7/28/63	39	-9.0	148.3	-14.2	91.9	56.745	-78.3	0*59* 3	12.0	-26.1	-25.1	372
573	1	165.22	4* 1*54	7/28/63	39	-9.0	148.2	-13.9	92.0	56.732	-63.9	4*32*33	30.7			372
574	1	140.54	5*39*19	7/28/63	39	-8.9	148.1	-13.7	92.1	56.725	-54.7	6*13*33	34.2			372
575	2	115.87	7*16*43	7/28/63	39	-8.9	148.1	-13.6	92.1	56.718	-51.5	7*50* 3	33.3			372
576	2	91.20	8*54* 8	7/28/63	39	-8.9	148.1	-13.4	92.2	56.712	-51.6	9*30*33	36.4			372
584	1	-106.19	21*53*25	7/28/63	39	-8.7	147.8	-12.1	92.5	56.658	-74.1	22* 6* 3	12.6			373
586	2	-155.53	1* 8*14	7/29/63	40	-8.7	147.8	-11.7	92.6	56.645	-80.8	1*21* 3	12.8			373
588	1	155.11	4*23* 3	7/29/63	40	-8.6	147.7	-11.4	92.6	56.631	-59.2	4*55*33	32.5			373
589	1	130.44	6* 0*28	7/29/63	40	-8.6	147.6	-11.3	92.6	56.624	-52.7	6*36*33	36.1	-25.5	-24.5	373
591	2	81.09	9*15*17	7/29/63	40	-8.6	147.6	-10.9	92.7	56.611	-40.0	9*52*33	37.3			373
599	1	-116.29	22*14*34	7/29/63	40	-8.3	147.4	-9.5	93.0	56.558	-79.3	22*27*33	13.0			374
603	1	145.01	4*44*13	7/30/63	41	-8.2	147.2	-8.9	93.2	56.531	-56.9	5*18*33	34.3	-24.2	-23.2	374
605	2	95.66	7*59* 2	7/30/63	41	-8.2	147.2	-8.6	93.3	56.518	-53.5	8*34* 3	35.0			374
613	1	-101.72	20*58*19	7/30/63	41	-7.9	147.0	-7.2	93.6	56.466	-74.0	21* 9*33	11.2			375
615	2	-151.06	0*13* 8	7/31/63	42	-7.8	146.9	-6.9	93.8	56.453	-75.1	0*24* 3	10.9			375

READOUT						ORBIT					TIME INTERVAL OF FILE ON FMR TAPE				
		SATELLITE EQUATOR CROSSING AT ORBITAL ASCENDING NODE (ANO)				SPIN VECTOR ATTITUDE					BEGIN	END		DROPOUTS, MINUTES W/R/T ANO		
ORBIT NO.	CDA STA	EARTH LONGI -TUDE (DEG)	HOURS MINUTES SECONDS (GMT)	CALENDAR DATE	TIROS DAY	DECLI -NA -TION (DEG)	RIGHT ASCEN -SION (DEG)	MINI -MUM NADIR (DEG)	TOT (MIN. AFTER ANO)	SPIN RATE (DEG /SEC)	MINU -TES W/R/T ANO	HOURS MINUTES SECONDS (GMT)	MINU -TES W/R/T ANO	FROM-	TO-	FMR TAPE REEL NO.
617	1	159.58	3*27*57	7/31/63	42	-7.7	146.9	-6.5	93.8	56.440	-58.3	3*58*33	30.6			375
619	2	110.23	6*42*46	7/31/63	42	-6.5	146.8	-6.4	93.9	56.426	-46.1	7*15*33	32.8			375
620	2	85.56	8*20*11	7/31/63	42	-5.5	146.9	-6.7	94.2	56.420	-51.8	8*57*33	37.4			375
627	1	-87.15	19*42* 3	7/31/63	42	2.4	146.8	-9.2	96.2	56.375	-83.8	19*51* 3	9.0			376
628	1	-111.82	21*19*28	7/31/63	42	3.4	146.5	-9.7	96.5	56.368	-75.0	21*32* 3	12.6			376
630	2	-161.17	0*34*17	8/ 1/63	43	5.1	145.8	-10.9	95.9	56.355	-81.8	0*46*33	12.3			376
632	1	149.48	3*49* 7	8/ 1/63	43	6.6	145.0	-11.9	97.3	56.342	-59.8	4*21*33	32.4			376
634	2	100.13	7* 3*56	8/ 1/63	43	8.3	144.6	-13.0	0.2	56.330	-53.4	7*38*33	34.6			376
642	1	-97.25	20* 3*13	8/ 1/63	43	17.1	144.1	-15.9	2.5	56.279	-86.9	20*13* 3	9.8	-28.2	-27.2	377
644	2	-146.59	23*18* 2	8/ 1/63	43	18.9	143.4	-17.0	3.0	56.266	-62.2	23*28* 3	10.0	-19.0	-17.0	377
647	1	139.38	4*10*16	8/ 2/63	44	21.2	142.1	-18.5	3.5	56.247	-51.3	4*43*33	33.3			377
649	2	90.03	7*25* 5	8/ 2/63	44	23.0	141.7	-19.4	3.9	56.234	-37.3	8* 1*33	36.5			377
658	2	-132.02	22* 1*47	8/ 2/63	44	32.6	140.4	-22.7	6.5	56.178	-68.5	22* 9*33	7.8			378
659	2	-156.69	23*39*11	8/ 2/63	44	33.4	139.9	-23.1	6.8	56.172	-76.6	23*51* 3	11.9			378
661	1	153.95	2*54* 1	8/ 3/63	45	34.9	139.0	-24.1	7.2	56.159	-60.2	3*26*33	32.5			378
662	1	129.27	4*31*25	8/ 3/63	45	35.6	138.5	-24.5	7.4	56.153	-51.7	5* 6*33	35.1			378
672	1	-117.45	20*45*31	8/ 3/63	45	45.3	137.2	-27.8	10.3	56.092	-78.9	20*58*33	13.0			379
673	2	-142.12	22*22*56	8/ 3/63	45	45.2	137.3	-27.4	10.4	56.085	-70.4	22*33* 3	10.1			379
678	2	94.50	6*29*59	8/ 4/63	46	44.7	137.3	-26.4	10.3	56.055	-37.7	7* 5*33	35.6			379
686	1	-102.88	19*29*16	8/ 4/63	46	43.7	137.1	-24.8	10.1	56.007	-77.6	19*40* 3	10.8			380
687	2	-127.55	21* 6*41	8/ 4/63	46	43.6	137.1	-24.6	10.1	56.001	-72.4	21*14* 3	7.4			380
688	2	-152.22	22*44* 5	8/ 4/63	46	43.5	137.1	-24.4	10.1	55.995	-75.7	22*55* 3	11.0			380
690	1	158.42	1*58*55	8/ 5/63	47	43.3	137.1	-24.0	10.1	55.983	-60.6	2*29*33	30.6			380
691	1	133.75	3*36*19	8/ 5/63	47	43.2	137.1	-23.8	10.1	55.977	-53.5	4*11*33	35.2			380
692	2	109.07	5*13*44	8/ 5/63	47	43.1	137.1	-23.5	10.2	55.971	-47.4	5*47* 3	33.3			380

READOUT						ORBIT					TIME INTERVAL OF FILE ON FMR TAPE					
		SATELLITE EQUATOR CROSSING AT ORBITAL ASCENDING NODE (ANO)				SPIN VECTOR ATTITUDE					BEGIN	END		DROPOUTS, MINUTES W/R/T ANO		
ORBIT NO.	CDA STA	EARTH LONGI -TUDE (DEG)	HOURS MINUTES SECONDS (GMT)	CALENDAR DATE	TIROS DAY	DECLI -NA -TION (DEG)	RIGHT ASCEN -SION (DEG)	MINI -MUM NADIR (DEG)	TOT (MIN. AFTER ANO)	SPIN RATE (DEG /SEC)	MINU -TES W/R/T ANO	HOURS MINUTES SECONDS (GMT)	MINU -TES W/R/T ANO	FROM-	TO-	FMR TAPE REEL NO.
702	2	-137.65	21*27*50	8/ 5/63	47	41.9	136.9	-21.5	10.0	55.912	-68.5	21*37* 3	9.2		-	381
705	1	148.29	2*20* 4	8/ 6/63	48	41.6	136.9	-20.8	9.9	55.895	-57.8	2*53*33	33.5			381
706	1	123.62	3*57*28	8/ 6/63	48	41.5	136.9	-20.6	10.0	55.889	-50.8	4*33*33	36.1			381
715	1	-98.43	18*34*10	8/ 6/63	48	40.5	136.7	-18.8	9.9	55.838	-87.8	18*45* 3	10.9			382
717	2	-147.78	21*48*59	8/ 6/63	48	40.3	136.7	-18.4	9.9	55.826	-73.5	21*59*33	10.6			382
719	1	162.86	1* 3*48	8/ 7/63	49	40.1	136.7	-17.9	9.9	55.815	-60.5	1*34*33	30.8			382
720	1	138.19	2*41*13	8/ 7/63	49	40.0	136.7	-17.7	9.9	55.809	-53.0	3*15*33	34.3			382
722	2	88.84	5*56* 2	8/ 7/63	49	39.8	136.6	-17.3	9.9	55.798	-55.6	6*32*33	36.5			382
729	1	-83.86	17*17*54	8/ 7/63	49	39.0	136.4	-15.9	9.9	55.759	-86.8	17*29* 3	11.2			383
730	1	-108.53	18*55*19	8/ 7/63	49	38.9	136.4	-15.6	9.9	55.754	-72.7	19* 7*33	12.2			383
731	2	-133.21	20*32*44	8/ 7/63	49	38.9	136.4	-15.4	9.9	55.748	-69.5	20*40* 3	7.3			383
735	1	128.09	3* 2*22	8/ 8/63	50	38.5	136.4	-14.6	9.9	55.706	-51.1	3*38*33	36.2			383
736	2	103.42	4*39*47	8/ 8/63	50	38.4	136.4	-14.4	9.9	55.700	-47.3	5*14* 3	34.3			383
737	2	78.74	6*17*11	8/ 8/63	50	38.3	136.4	-14.2	9.9	55.694	-50.0	6*55*33	38.4			383
744	1	-93.96	17*39* 4	8/ 8/63	50	37.6	136.2	-12.7	9.9	55.654	-84.4	17*50* 3	11.0			384
745	1	-118.64	19*16*28	8/ 8/63	50	37.5	136.2	-12.5	9.9	55.648	-73.5	19*30* 3	13.6			384
748	1	167.34	0* 8*42	8/ 9/63	51	37.3	136.2	-11.9	9.9	55.631	-61.4	0*39* 3	30.4			384
749	1	142.66	1*46* 7	8/ 9/63	51	37.2	136.2	-11.7	10.0	55.625	-33.4	2*18*33	32.4			384
751	2	93.32	5* 0*56	8/ 9/63	51	37.0	136.1	-11.3	10.0	55.614	-39.8	5*36* 3	35.1			384
761	2	-153.41	21*15* 2	8/ 9/63	51	36.3	135.8	-9.3	10.1	55.558	-80.2	21*27* 3	12.0			385
764	1	132.56	2* 7*16	8/10/63	52	36.4	135.8	-8.9	10.1	55.541	-51.8	2*42*33	35.3	-18.3	-17.3	385
765	2	107.89	3*44*40	8/10/63	52	36.4	135.7	-8.7	10.2	55.536	-48.5	4*18*33	33.9			385
766	2	83.21	5*22* 5	8/10/63	52	36.5	135.7	-8.6	10.2	55.530	-50.8	5*59* 3	37.0			385
774	1	-114.17	18*21*22	8/10/63	52	36.7	135.7	-7.4	10.5	55.487	-58.5	18*34* 3	12.7			386
775	2	-138.84	19*58*47	8/10/63	52	36.8	135.7	-7.3	10.5	55.481	-74.6	20*10* 3	11.3			386

READOUT						ORBIT					TIME INTERVAL OF FILE ON FMR TAPE					
		SATELLITE EQUATOR CROSSING AT ORBITAL ASCENDING NODE (ANO)				SPIN VECTOR ATTITUDE					BEGIN	END		DROPOUTS, MINUTES W/R/T ANO		
ORBIT NO.	COA STA	EARTH LONGI-TUDE (DEG)	HOURS MINUTES SECONDS (GMT)	CALENDAR DATE	TIROS DAY	DECLI-NA-TION (DEG)	RIGHT ASCEN-SION (DEG)	MINI-MUM NADIR (DEG)	TOT (MIN. AFTER ANO)	SPIN RATE (DEG /SEC)	MINU-TES W/R/T ANO	HOURS MINUTES SECONDS (GMT)	MINU-TES W/R/T ANO	FROM-	TO-	FMR TAPE REEL NO.
776	2	-163.51	21*36*11	8/10/63	52	36.8	135.7	-7.1	10.6	55.476	-75.1	21*49*33	13.4			386
779	1	122.46	2*28*25	8/11/63	53	36.9	135.6	-6.7	10.7	55.460	-53.7	3* 5* 3	36.6			386
780	2	97.78	4* 5*50	8/11/63	53	36.9	135.6	-6.6	10.8	55.454	-49.0	4*41* 3	35.2			386
788	1	-99.59	17* 5* 7	8/11/63	53	37.2	135.6	-5.4	11.1	55.411	-64.4	17*15* 3	9.9			387
789	1	-124.27	18*42*31	8/11/63	53	37.3	135.6	-5.3	11.1	55.406	-67.8	18*58* 3	15.5			387
790	2	-148.94	20*19*56	8/11/63	53	37.3	135.6	-5.1	11.2	55.401	-71.6	20*30*33	10.6			387
792	1	161.70	23*34*45	8/11/63	53	37.3	135.5	-4.9	11.2	55.390	-64.3	0* 6* 3	31.3			387
793	1	137.03	1*12*10	8/12/63	54	37.4	135.5	-4.7	11.2	55.385	-56.0	1*46* 3	33.9			387
794	2	112.36	2*49*34	8/12/63	54	37.4	135.5	-4.6	11.3	55.380	-53.2	3*23* 3	33.5			387
795	2	87.68	4*26*59	8/12/63	54	37.4	135.5	-4.5	11.3	55.374	-52.9	5* 3*33	36.6			387
802	1	-85.02	15*48*51	8/12/63	54	37.7	135.6	-3.5	11.6	55.337	-85.8	15*57*33	8.7			388
803	1	-109.69	17*26*15	8/12/63	54	37.8	135.6	-3.4	11.6	55.332	-77.2	17*38* 3	11.8			388
805	2	-159.04	20*41* 5	8/12/63	54	37.8	135.6	-3.1	11.7	55.322	-79.9	20*54* 3	13.0			388
807	1	151.60	23*55*54	8/12/63	54	37.9	135.5	-2.8	11.8	55.311	-61.6	0*28* 3	32.2			388
808	1	126.92	1*33*19	8/13/63	55	37.9	135.5	-2.7	11.9	55.306	-54.8	2* 9* 3	35.7			388
809	2	102.24	3*10*43	8/13/63	55	38.0	135.5	-2.6	11.9	55.301	-51.5	3*45* 3	34.3			388
810	2	77.57	4*48* 8	8/13/63	55	38.0	135.6	-2.4	12.0	55.295	-52.1	5*26*33	38.4			388
818	1	-119.81	17*47*25	8/13/63	55	38.2	135.8	-1.3	12.3	55.254	-78.9	18* 2*33	15.1			389
821	1	166.17	22*39*38	8/13/63	55	38.0	135.8	-0.7	12.4	55.238	-66.9	23*10* 3	30.4			389
831	1	-80.56	14*53*44	8/14/63	56	37.3	135.7	1.3	12.6	55.186	-95.4	15* 3* 3	9.3			390
832	1	-105.23	16*31* 9	8/14/63	56	37.2	135.7	1.4	12.6	55.181	-78.5	16*43*33	12.4			390
836	1	156.06	23* 0*47	8/14/63	56	37.0	135.8	2.2	12.7	55.160	-8.4	23*33* 3	32.3			390
837	1	131.39	0*38*12	8/15/63	57	36.9	135.8	2.4	12.8	55.155	-54.7	1*14* 3	35.9			390
838	2	106.72	2*15*37	8/15/63	57	36.9	135.8	2.6	12.8	55.150	-51.3	2*50* 3	34.4			390
839	2	82.04	3*53* 1	8/15/63	57	36.8	135.8	2.8	12.8	55.145	-51.8	4*30* 3	37.0			390

READOUT						ORBIT					TIME INTERVAL OF FILE ON FMR TAPE					
		SATELLITE EQUATOR CROSSING AT ORBITAL ASCENDING NODE (ANO)				SPIN VECTOR ATTITUDE					BEGIN	END		DROPOUTS, MINUTES W/R/T ANO		
ORBIT NO.	CDA STA	EARTH LONGI -TUDE (DEG)	HOURS MINUTES SECONDS (GMT)	CALENDAR DATE	TIROS DAY	DECLI -NA -TION (DEG)	RIGHT ASCEN -SION (DEG)	MINI -MUM NADIR (DEG)	TOT (MIN. AFTER ANO)	SPIN RATE (DEG /SEC)	MINU -TES W/R/T ANO	HOURS MINUTES SECONDS (GMT)	MINU -TES W/R/T ANO	FROM-	TO-	FMR TAPE REEL NO.
846	1	-96.66	15*14*54	8/15/63	57	36.3	135.7	4.1	13.0	55.109	-85.5	15*25* 3	10.2			391
847	1	-115.33	16*52*13	8/15/63	57	36.3	135.7	4.3	13.0	55.103	-75.3	17* 6* 3	13.8			391
851	1	145.96	23*21*57	8/15/63	57	36.1	135.8	5.0	13.2	55.083	-57.6	23*56*25	34.5			391
853	2	96.62	2*36*46	8/16/63	58	36.0	135.8	5.4	13.2	55.072	-31.3	3*11*33	34.8			391
861	1	-100.76	15*36* 3	8/16/63	58	35.5	135.7	6.9	13.5	55.031	-76.4	15*47* 3	11.0			392
865	1	160.54	22* 5*41	8/16/63	58	35.3	135.8	7.6	13.6	55.010	-59.9	22*37*27	31.8			392
866	1	135.86	23*43* 6	8/16/63	58	35.3	135.9	7.8	13.6	55.004	-53.2	0*19*11	36.1			392
868	2	86.52	2*57*55	8/17/63	59	35.2	135.9	8.2	13.7	54.994	-57.0	3*35* 3	37.1			392
875	1	-86.19	14*19*47	8/17/63	59	34.8	135.8	9.4	13.9	54.957	-84.8	14*29*27	9.7			393
881	1	125.76	0* 4*15	8/18/63	60	34.6	136.0	10.4	14.1	54.925	-53.7	0*41* 3	36.8			393
882	2	101.09	1*41*39	8/18/63	60	34.5	135.9	10.6	14.2	54.920	-49.5	2*16* 3	34.4			393
890	1	-96.29	14*40*56	8/18/63	60	34.1	135.3	11.7	14.4	54.877	-75.9	14*51* 3	10.1			394
892	2	-145.64	17*55*46	8/18/63	60	34.1	135.3	11.9	14.4	54.867	-64.2	18* 7* 3	11.3			394
894	1	165.11	21*10*35	8/18/63	60	34.1	135.3	12.2	14.5	54.856	-63.8	21*41* 3	30.5			394
895	1	140.33	22*47*59	8/18/63	60	34.1	135.3	12.3	14.6	54.850	-56.6	23*24* 3	36.1			394
896	2	115.66	0*25*24	8/19/63	61	34.1	135.3	12.5	14.7	54.845	-50.9	0*57*33	32.2			394
904	1	-81.72	13*24*41	8/19/63	61	33.7	134.7	13.5	14.8	54.801	-79.3	13*34* 3	9.4			395
906	2	-131.16	16*39*30	8/19/63	61	33.7	134.7	13.7	14.9	54.790	-66.0	16*48* 3	8.6			395
909	1	154.90	21*31*44	8/19/63	61	33.7	134.8	14.1	15.1	54.774	-64.1	22* 4* 3	32.3			395
910	1	130.23	23* 9* 8	8/19/63	61	33.7	134.8	14.2	15.2	54.768	-55.2	23*45* 3	35.9			395
911	2	105.55	0*46*33	8/20/63	62	33.7	134.8	14.3	15.2	54.763	-51.7	1*21* 3	34.5			395
912	2	80.87	2*23*57	8/20/63	62	33.7	134.7	14.4	15.2	54.757	-52.5	3* 1*33	37.6			395
919	1	-91.83	13*45*50	8/20/63	62	33.4	134.3	15.3	15.5	54.712	-79.3	13*55* 3	9.2			396
921	2	-141.18	17* 0*39	8/20/63	62	33.4	134.4	15.5	15.6	54.705	-63.3	17*10* 3	9.4			396
925	1	120.12	23*30*17	8/20/63	62	33.5	134.5	16.0	15.8	54.686	-57.5	0* 8*33	38.3			396

READOUT						ORBIT					TIME INTERVAL OF FILE ON FMR TAPE					
		SATELLITE EQUATOR CROSSING AT ORBITAL ASCENDING NODE (AND)				SPIN VECTOR ATTITUDE					BEGIN	END		DROPOUTS, MINUTES W/R/T AND		
ORBIT NO.	CDA STA	EARTH LONGI -TUDE (DEG)	HOURS MINUTES SECONDS (GMT)	CALENDAR DATE	TIROS DAY	DECLI -NA -TION (DEG)	RIGHT ASCEN -SION (DEG)	MINI -MUM NADIR (DEG)	TOT (MIN. AFTER AND)	SPIN RATE (DEG /SEC)	MINU -TES W/R/T AND	HOURS MINUTES SECONDS (GMT)	MINU -TES W/R/T AND	FROM-	TO-	FMR TAPE REEL NO.
926	2	95.45	1* 7*42	8/21/63	63	33.4	134.4	16.1	15.9	54.680	-23.4	1*41*33	33.9			396
934	1	-101.93	14* 6*58	8/21/63	63	32.9	133.8	17.2	16.0	54.640	-31.0	14*19* 3	12.1			397
936	2	-151.29	17*21*48	8/21/63	63	32.8	134.0	17.5	16.1	54.630	-79.0	17*32*33	10.8			397
938	1	159.37	20*36*37	8/21/63	63	32.8	134.1	17.9	16.3	54.620	-63.5	21* 8*33	31.9			397
939	1	134.69	22*14* 1	8/21/63	63	32.7	134.1	18.0	16.4	54.615	-55.2	22*50* 3	36.0			397
940	2	110.02	23*51*26	8/21/63	63	32.7	134.1	18.1	16.4	54.610	-51.6	0*26* 3	34.6			397
941	2	85.35	1*28*51	8/22/63	64	32.6	134.0	18.3	16.5	54.605	-52.5	2* 6*33	37.7			397
948	1	-87.36	12*50*43	8/22/63	64	32.1	133.5	19.3	16.6	54.568	-85.2	13* 0* 3	9.3			398
949	1	-112.03	14*28* 7	8/22/63	64	32.0	133.6	19.4	16.7	54.563	-77.2	14*41* 3	12.9			398
950	2	-136.70	16* 5*32	8/22/63	64	32.0	133.7	19.6	16.8	54.557	-67.7	16*14* 3	8.5			398
951	2	-161.38	17*42*57	8/22/63	64	32.0	133.8	19.7	16.8	54.552	-78.3	17*56* 3	13.1			398
953	1	149.27	20*57*46	8/22/63	64	31.9	134.0	20.1	16.9	54.542	-61.9	21*31* 3	33.3			398
954	1	124.59	22*35*10	8/22/63	64	31.8	134.0	20.3	17.0	54.537	-54.0	23*12* 3	36.9			398
955	2	99.92	0*12*35	8/23/63	65	31.8	134.0	20.4	17.0	54.532	-50.6	0*48* 3	35.5			398
956	2	75.25	1*50* 0	8/23/63	65	31.7	133.9	20.6	17.1	54.527	-51.2	2*28*33	38.6			398
963	1	-97.46	13*11*52	8/23/63	65	31.3	133.6	21.5	17.3	54.490	-85.5	13*23* 3	11.2			399
964	1	-122.13	14*49*16	8/23/63	65	31.2	133.6	21.6	17.4	54.485	-76.1	15* 4* 3	14.8			399
967	1	163.84	19*41*30	8/23/63	65	31.1	133.7	22.0	17.6	54.470	-68.0	20*13* 3	31.6			399
968	1	139.17	21*18*55	8/23/63	65	31.0	133.7	22.2	17.6	54.465	-55.1	21*56* 3	37.1			399
969	2	114.49	22*56*19	8/23/63	65	31.0	133.7	22.3	17.7	54.460	-50.3	23*29* 3	32.7			399
970	2	89.82	0*33*44	8/24/63	66	30.9	133.7	22.5	17.8	54.455	-54.0	1*12* 3	38.3			399
977	1	-92.69	11*55*36	8/24/63	66	30.5	133.3	23.4	18.0	54.416	-86.1	12* 4* 3	8.5			400
978	1	-107.56	13*33* 1	8/24/63	66	30.5	133.3	23.5	18.1	54.412	-79.1	13*45*33	12.5			400
980	2	-156.90	16*47*50	8/24/63	66	30.4	133.3	23.7	18.2	54.404	-83.5	16*58*33	10.7			400
982	1	153.74	20* 2*39	8/24/63	66	30.4	133.4	23.9	18.3	54.396	-64.3	20*35* 3	32.4			400

READOUT						ORBIT					TIME INTERVAL OF FILE ON FMR TAPE					
		SATELLITE EQUATOR CROSSING AT ORBITAL ASCENDING NODE (AND)				SPIN VECTOR ATTITUDE					BEGIN	END		DROPOUTS, MINUTES W/R/T AND		
ORBIT NO.	CDA STA	EARTH LONGI-TUDE (DEG)	HOURS MINUTES SECONDS (GMT)	CALENDAR DATE	TIROS DAY	DECLI-NA-TION (DEG)	RIGHT ASCEN-SION (DEG)	MINI-MUM NADIR (DEG)	TOT (MIN. AFTER AND)	SPIN RATE (DEG /SEC)	MINU-TES W/R/T AND	HOURS MINUTES SECONDS (GMT)	MINU-TES W/R/T AND	FROM-	TO-	FMR TAPE REEL NO.
983	1	129.[illegible]7	21*4[illegible]* 4	8/24/63	66	30.3	133.4	24.0	18.3	54.391	-55.0	22*16* 3	36.0			400
984	2	104.39	23*17*28	8/24/63	66	30.3	133.4	24.2	18.4	54.387	-51.7	23*52*24	34.9			400
985	2	79.72	[illegible]*54*53	8/25/63	67	30.2	133.4	24.3	18.5	54.382	-52.4	1*33* 3	38.2			400
992	1	-92.98	12*16*45	8/25/63	67	29.9	133.0	25.0	18.7	54.345	-84.8	12*27* 3	10.3			401
993	1	-117.66	13*54*1[illegible]	8/25/63	67	29.9	133.0	25.1	18.8	54.340	-76.0	14* 8*27	14.3			401
994	2	-142.33	15*31*34	8/25/63	67	29.9	133.0	25.2	18.9	54.334	-7.5	15*39*33	8.0			401
996	1	168.32	18*46*23	8/25/63	67	29.9	133.1	25.4	19.0	54.322	-67.2	19*16*33	30.2			401
997	1	143.64	20*23*48	8/25/63	67	29.9	133.1	25.5	19.1	54.316	18.6	20*56* 3	32.3			401
999	2	94.29	23*38*37	8/25/63	67	29.7	133.1	25.7	19.3	54.304	-22.3	0*14* 3	35.4			401
1006	1	-78.41	11* 0*29	8/26/63	68	29.5	132.8	26.4	19.6	54.262	-88.8	11* 9* 3	8.6	-15.5	-14.5	402
1008	1	-127.76	14*15*18	8/26/63	68	29.5	132.8	26.5	19.7	54.249	-80.9	14*31* 3	15.8			402
1009	2	-152.43	15*52*43	8/26/63	68	29.5	132.8	26.5	19.8	54.243	-71.0	16* 3* 3	10.3			402
1011	1	158.21	19* 7*32	8/26/63	68	29.5	132.9	26.7	19.9	54.231	-62.9	19*40* 3	32.5			402
1012	1	133.54	2[illegible]*44*57	8/26/63	68	29.5	132.9	26.7	20.0	54.225	-54.7	21*20* 3	35.1			402
1013	2	1[illegible]8.87	22*22*21	8/26/63	68	29.5	132.9	26.8	20.0	54.219	-51.2	22*56* 3	33.7			402
1014	2	84.19	23*59*46	8/26/63	68	29.4	132.9	26.9	20.1	54.214	-53.2	0*36* 3	36.3			402
1021	1	-88.54	11*21*38	8/27/63	69	29.4	132.6	27.4	20.5	54.175	-87.4	11*30* 3	8.4			403
1026	1	148.[illegible]9	19*29*41	8/27/63	69	29.4	132.8	27.6	20.8	54.151	-66.0	20* 2* 3	33.4			403
1027	1	123.41	21* 6* 6	8/27/63	69	29.4	132.8	27.6	20.9	54.147	0.9	21*43* 3	37.0			403
1028	2	98.74	22*43*30	8/27/63	69	29.3	132.8	27.7	21.0	54.143	-50.2	23*19*27	36.0			403
1036	1	-98.64	11*42*47	8/28/63	70	29.3	132.4	28.1	21.4	54.105	-88.9	11*52*33	9.8			404
1040	1	162.66	18*12*25	8/28/63	70	29.4	132.6	28.1	21.7	54.083	-68.1	18*43* 3	30.6			404
1041	1	137.98	19*49*50	8/28/63	70	29.4	132.6	28.2	21.8	54.078	-56.5	20*25* 3	35.2			404
1042	2	113.31	21*27*14	8/28/63	70	29.4	132.6	28.2	21.9	54.072	-52.3	22* 0* 3	32.8			404
1043	2	88.64	23* 4*39	8/28/63	70	29.3	132.6	28.3	21.9	54.066	-53.5	23*42* 3	37.4			404

READOUT						ORBIT					TIME INTERVAL OF FILE ON FMR TAPE					
		SATELLITE EQUATOR CROSSING AT ORBITAL ASCENDING NODE (AND)				SPIN VECTOR ATTITUDE					BEGIN	END		DROPOUTS, MINUTES W/R/T AND		
ORBIT NO.	CDA STA	EARTH LONGI -TUDE (DEG)	HOURS MINUTES SECONDS (GMT)	CALENDAR DATE	TIROS DAY	DECLI -NA -TION (DEG)	RIGHT ASCEN -SION (DEG)	MINI -MUM NADIR (DEG)	TOT (MIN. AFTER AND)	SPIN RATE (DEG /SEC)	MINU -TES W/R/T AND	HOURS MINUTES SECONDS (GMT)	MINU -TES W/R/T AND	FROM-	TO-	FMR TAPE REEL NO.
1050	1	-84.07	10*26*31	8/29/63	71	29.2	132.3	28.6	22.3	54.028	-85.8	10*36* 3	9.5			405
1051	1	-108.74	12* 3*56	8/29/63	71	29.2	132.4	28.6	22.4	54.022	-77.2	12*16* 3	12.1			405
1052	1	-133.41	13*41*20	8/29/63	71	29.2	132.4	28.7	22.5	54.017	-75.3	13*49* 3	7.7			405
1053	2	-158.09	15*18*45	8/29/63	71	29.2	132.5	28.7	22.5	54.012	-79.6	15*31* 3	12.3			405
1055	1	152.55	18*33*34	8/29/63	71	29.1	132.6	28.8	22.7	54.001	-62.3	19* 6*33	33.0			405
1058	2	78.53	23*25*48	8/29/63	71	29.0	132.6	29.0	22.9	53.984	-52.7	0* 3*33	37.8			405
1065	1	-94.17	10*47*40	8/30/63	72	28.9	132.3	29.2	23.3	53.946	-28.0	10*58* 3	10.4			406
1066	1	-118.84	12*25* 4	8/30/63	72	28.9	132.4	29.2	23.4	53.941	-74.8	12*39* 3	14.0			406
1067	2	-143.51	14* 2*29	8/30/63	72	28.9	132.4	29.2	23.5	53.935	-73.3	14*11* 3	8.6			406
1072	2	93.11	22* 9*32	8/30/63	72	28.8	132.6	29.4	23.9	53.908	-38.9	22*44* 3	34.5			406
1080	1	-104.27	11* 8*49	8/31/63	73	28.8	132.4	29.5	24.4	53.865	-81.1	11*19*33	10.7			407
1081	2	-128.94	12*46*13	8/31/63	73	28.8	132.4	29.5	24.5	53.859	-75.5	12*54* 3	7.8			407
1082	2	-153.62	14*23*38	8/31/63	73	28.8	132.5	29.4	24.6	53.854	-79.5	14*35* 3	11.4			407
1084	1	157.03	17*38*27	8/31/63	73	28.8	132.6	29.4	24.6	53.843	-60.9	18*10* 3	31.6			407
1087	2	83.01	22*30*41	8/31/63	73	28.6	132.6	29.5	24.9	53.827	-55.7	23* 8*33	37.9			407
1094	1	-89.70	9*52*33	9/ 1/63	74	28.7	132.3	29.4	25.3	53.789	-84.6	10* 2* 3	9.5			408
1095	1	-114.37	11*29*57	9/ 1/63	74	28.7	132.4	29.4	25.4	53.784	-76.1	11*43* 3	13.1			408
1096	2	-139.04	13* 7*22	9/ 1/63	74	28.7	132.4	29.3	25.4	53.779	-72.1	13*17* 3	9.7			408
1099	1	146.92	17*59*36	9/ 1/63	74	28.7	132.6	29.3	25.7	53.763	-16.5	18*33* 3	33.5			408
1101	2	97.58	21*14*25	9/ 1/63	74	28.7	132.6	29.3	25.9	53.752	-51.1	21*52* 3	37.6			408
1109	1	-99.80	10*13*42	9/ 2/63	75	28.8	132.3	29.0	26.3	53.709	-71.7	10*24* 3	10.4			409
1110	2	-124.47	11*51* 6	9/ 2/63	75	28.8	132.3	29.0	26.4	53.704	-74.7	11*58* 3	7.0			409
1111	2	-149.15	13*28*31	9/ 2/63	75	28.8	132.4	28.9	26.5	53.698	-80.0	13*39* 3	10.5			409
1113	1	161.50	16*43*20	9/ 2/63	75	28.8	132.5	28.8	26.7	53.688	-62.9	17*15* 3	31.7			409
1116	2	87.48	21*35*34	9/ 2/63	75	28.8	132.7	28.7	26.9	53.672	-53.3	22*14*33	39.0			409

READOUT						ORBIT					TIME INTERVAL OF FILE ON FMR TAPE					
		SATELLITE ORBITAL ASCENDING NODE (ANO)				SPIN VECTOR ATTITUDE					BEGIN	END		DROPOUTS, MINUTES W/R/T ANO		
ORBIT NO.	CDA STA	EARTH LONGI -TUDE (DEG)	HOURS MINUTES SECONDS (GMT)	CALENDAR DATE	TIROS DAY	DECLI -NA -TION (DEG)	RIGHT ASCEN -SION (DEG)	MINI -MUM NADIR (DEG)	TOT (MIN. AFTER ANO)	SPIN RATE (DEG /SEC)	MINU -TES W/R/T ANO	HOURS MINUTES SECONDS (GMT)	MINU -TES W/R/T ANO	FROM-	TO-	FMR TAPE REEL NO.
1123	1	-85.22	8*57*26	9/ 3/63	76	28.5	133.5	28.5	27.6	53.634	-83.8	9* 7* 3	9.6			410
1124	1	-109.89	10*34*50	9/ 3/63	76	28.4	133.6	28.5	27.7	53.629	-75.9	10*47* 3	12.2			410
1125	2	-134.57	12*12*15	9/ 3/63	76	28.4	133.7	28.5	27.8	53.624	-57.4	12*21* 3	8.8			410
1126	2	-159.24	13*49*40	9/ 3/63	76	28.4	133.8	28.5	27.9	53.618	-78.0	14* 2* 3	12.4			410
1128	1	151.42	17* 4*29	9/ 3/63	76	28.3	133.9	28.4	28.1	53.608	-61.5	17*37*27	33.0			410
1130	2	102.06	20*19*18	9/ 3/63	76	28.2	134.1	28.3	28.2	53.597	-41.2	20*56*33	37.3			410
1138	1	-95.32	9*18*34	9/ 4/63	77	27.8	135.0	28.0	29.0	53.554	-74.0	9*29* 3	10.5			411
1139	1	-119.99	10*55*59	9/ 4/63	77	27.7	135.1	28.0	29.1	53.549	-11.0	11*10* 3	14.1			411
1140	2	-144.67	12*33*24	9/ 4/63	77	27.7	135.1	28.0	29.2	53.544	-73.2	12*42*33	9.2			411
1142	1	165.98	15*48*13	9/ 4/63	77	27.6	135.3	27.9	29.4	53.533	-65.2	16*18*33	30.3			411
1143	1	141.31	17*25*37	9/ 4/63	77	27.5	135.4	27.8	29.5	53.528	-13.6	17*58*33	32.9			411
1145	2	91.96	20*40*27	9/ 4/63	77	27.5	135.6	27.7	29.7	53.517	-41.5	21*17*33	37.1			411
1152	1	-80.74	8* 2*19	9/ 5/63	78	26.7	136.6	27.5	30.5	53.480	-86.5	8*12* 3	9.7			412
1153	1	-105.42	9*39*43	9/ 5/63	78	26.6	136.7	27.5	30.6	53.474	-23.4	9*50*33	10.8			412
1154	2	-130.09	11*17* 8	9/ 5/63	78	26.4	136.8	27.5	30.7	53.469	-37.6	11*25* 3	7.9			412
1155	2	-154.76	12*54*32	9/ 5/63	78	26.3	136.9	27.5	30.8	53.464	-78.7	13* 6* 3	11.5			412
1157	1	155.88	16* 9*22	9/ 5/63	78	26.1	137.0	27.4	30.9	53.453	-61.7	16*41*33	32.2			412
1159	2	106.53	19*24*11	9/ 5/63	78	26.0	137.3	27.3	31.1	53.442	-40.3	19*59* 3	34.9			412
1160	2	81.86	21* 1*35	9/ 5/63	78	25.9	137.4	27.3	31.2	53.437	-49.0	21*41*58	40.4			412
1167	1	-90.84	8*23*27	9/ 6/63	79	24.8	138.5	27.0	32.1	53.399	-82.4	8*33* 3	9.6			413
1169	2	-140.19	11*38*16	9/ 6/63	79	24.5	138.7	27.0	32.3	53.389	-74.0	11*46*33	8.3			413
1172	1	145.78	16*30*30	9/ 6/63	79	24.2	138.8	26.9	32.5	53.373	-59.6	17* 4* 3	33.6			413
1174	2	96.43	19*45*19	9/ 6/63	79	24.0	139.1	26.8	32.8	53.362	-39.4	20*22* 3	36.7			413
1182	2	-100.94	8*44*36	9/ 7/63	80	22.6	140.2	26.4	33.8	53.319	-73.6	8*55* 3	10.5			414
1183	2	-125.62	10*22* 1	9/ 7/63	80	22.5	140.2	26.4	33.9	53.313	-74.7	10*29* 3	7.0			414

READOUT						ORBIT					TIME INTERVAL OF FILE ON FMR TAPE					
		SATELLITE ORBITAL EQUATOR CROSSING AT ASCENDING NODE (ANO)				SPIN VECTOR ATTITUDE					BEGIN	END		DROPOUTS, MINUTES W/R/T ANO		
ORBIT NO.	CDA STA	EARTH LONGI -TUDE (DEG)	HOURS MINUTES SECONDS (GMT)	CALENDAR DATE	TIROS DAY	DECLI -NA -TION (DEG)	RIGHT ASCEN -SION (DEG)	MINI -MUM NADIR (DEG)	TOT (MIN. AFTER ANO)	SPIN RATE (DEG /SEC)	MINU -TES W/R/T ANO	HOURS MINUTES SECONDS (GMT)	MINU -TES W/R/T ANO	FROM-	TO-	FMR TAPE REEL NO.
1184	2	-150.29	11*59*25	9/ 7/63	80	22.3	140.2	26.4	34.0	53.308	-61.9	12*10*33	11.1			414
1186	2	160.36	15*14*14	9/ 7/63	80	22.0	140.3	26.4	34.2	53.297	-63.0	15*45*55	31.7			414
1188	2	111.01	18*29* 4	9/ 7/63	80	21.8	140.5	26.3	34.3	53.286	-43.2	19* 3* 3	34.0			414
1189	2	86.33	20* 6*28	9/ 7/63	80	21.7	140.6	26.2	34.4	53.281	-51.3	20*44* 3	37.6			414
1196	2	-86.37	7*28*20	9/ 8/63	81	20.3	141.5	25.8	35.3	53.243	-85.7	7*38* 3	9.7			415
1197	2	-111.04	9* 5*45	9/ 8/63	81	20.1	141.5	25.8	35.4	53.238	-76.6	9*18* 3	12.3			415
1198	2	-135.72	10*43* 9	9/ 8/63	81	19.9	141.5	25.8	35.4	53.232	-74.1	10*52*27	9.3			415
1199	2	-160.39	12*20*34	9/ 8/63	81	19.7	141.5	25.8	35.5	53.227	-77.0	12*33*33	13.0			415
1201	2	150.25	15*35*23	9/ 8/63	81	19.5	141.6	25.7	35.7	53.216	-61.3	16* 8*33	33.2			415
1203	2	100.91	18*50*12	9/ 8/63	81	19.2	141.7	25.6	35.9	53.205	-41.7	19*25* 3	34.9			415
1211	1	-96.47	7*49*29	9/ 9/63	82	17.7	142.3	25.1	36.8	53.162	-76.6	8* 0* 3	10.6			416
1212	1	-121.14	9*26*53	9/ 9/63	82	17.5	142.3	25.0	36.9	53.156	-75.1	9*41* 3	14.2			416
1213	2	-145.82	11* 4*18	9/ 9/63	82	17.4	142.3	25.0	37.0	53.151	-72.4	11*14*33	10.3			416
1215	1	164.83	14*19* 7	9/ 9/63	82	17.1	142.3	24.9	37.2	53.140	-63.5	14*49*33	30.4			416
1216	1	140.16	15*56*32	9/ 9/63	82	17.0	142.3	24.8	37.2	53.134	-54.6	16*31* 3	34.5			416
1218	2	90.81	19*11*21	9/ 9/63	82	16.8	142.3	24.7	37.3	53.123	-57.3	19*47*28	36.1			416
1225	1	-81.92	6*33*13	9/10/63	83	15.7	142.5	24.2	38.0	53.085	-88.8	6*42*33	9.3			417
1226	1	-106.59	8*10*38	9/10/63	83	15.5	142.5	24.1	38.1	53.079	-75.2	8*21* 3	10.4			417
1230	3	154.71	14*40*16	9/10/63	83	15.0	142.5	23.9	38.4	53.057	-24.2	14*59*33	19.3			417
1231	1	130.03	16*17*40	9/10/63	83	14.9	142.4	23.8	38.5	53.052	-67.8	16*53* 3	35.4			417
1233	2	80.69	19*32*30	9/10/63	83	14.6	142.5	23.6	38.6	53.041	-66.6	20*10* 3	37.6			417
1241	1	-116.69	8*31*46	9/11/63	84	13.3	142.6	23.0	39.3	52.996	-70.9	8*45* 3	13.3			418
1242	2	-141.36	10* 9*11	9/11/63	84	13.1	142.6	23.0	39.4	52.991	-71.9	10*17*33	8.4			418
1244	1	169.28	13*24* 0	9/11/63	84	12.8	142.5	22.9	39.6	52.980	-63.7	13*54* 3	30.1			418
1245	3	144.61	15* 1*25	9/11/63	84	12.7	142.5	22.8	39.7	52.974	-57.0	15*22* 3	20.6			418

READOUT						ORBIT					TIME INTERVAL OF FILE ON FMR TAPE					
		SATELLITE EQUATOR CROSSING AT ORBITAL ASCENDING NODE (AND)				SPIN VECTOR ATTITUDE					BEGIN	END		DROPOUTS, MINUTES W/R/T AND		
ORBIT NO.	CDA STA	EARTH LONGI -TUDE (DEG)	HOURS MINUTES SECONDS (GMT)	CALENDAR DATE	TIROS DAY	DECLI -NA -TION (DEG)	RIGHT ASCEN -SION (DEG)	MINI -MUM NADIR (DEG)	TOT (MIN. AFTER AND)	SPIN RATE (DEG /SEC)	MINU -TES W/R/T AND	HOURS MINUTES SECONDS (GMT)	MINU -TES W/R/T AND	FROM-	TO-	FMR TAPE REEL NO.
1246	3	119.94	16*38*49	9/11/63	84	12.6	142.4	22.7	39.7	52.968	-64.9	17* 2* 3	23.2			418
1255	1	-102.11	7*15*30	9/12/63	85	11.2	142.7	21.8	40.5	52.918	-76.2	7*25*58	10.5			419
1256	1	-126.79	8*52*55	9/12/63	85	11.0	142.8	21.7	40.6	52.912	-74.6	9* 8*28	15.6			419
1259	3	159.19	13*45* 9	9/12/63	85	10.6	142.8	21.4	40.9	52.895	-50.1	14* 4* 3	18.9			419
1262	2	85.17	18*37*22	9/12/63	85	10.5	142.9	21.0	41.0	52.878	-50.3	19*16* 3	38.7			419
1269	1	-87.54	5*59*14	9/13/63	86	10.7	143.2	19.3	41.4	52.838	-84.5	6* 9* 3	9.8			420
1270	1	-112.21	7*36*39	9/13/63	86	10.7	143.2	19.0	41.4	52.833	-75.9	7*49* 3	12.4			420
1272	2	-161.56	10*51*28	9/13/63	86	10.8	143.4	18.5	41.5	52.821	-82.6	11* 4*28	13.0			420
1276	2	99.74	17*21* 6	9/13/63	86	10.9	143.6	17.5	41.7	52.798	-62.5	17*56* 3	35.0			420
1284	1	-97.64	6*20*23	9/14/63	87	11.2	143.8	15.5	42.0	52.752	-76.6	6*31* 3	10.7			421
1285	1	-122.31	7*57*47	9/14/63	87	11.2	143.9	15.3	42.1	52.746	-75.7	8*12* 3	14.3			421
1286	2	-146.98	9*35*12	9/14/63	87	11.3	143.9	15.0	42.1	52.740	-73.2	9*45*28	10.3			421
1289	3	138.99	14*27*26	9/14/63	87	11.3	144.1	14.2	42.3	52.723	-54.2	14*49*28	22.0			421
1291	2	89.64	17*42*15	9/14/63	87	11.4	144.2	13.7	42.3	52.714	-52.8	18*18*28	36.2			421
1298	1	-83.06	5* 4* 7	9/15/63	88	11.8	144.3	12.0	42.6	52.673	-88.3	5*13*28	9.4			422
1299	1	-107.73	6*41*31	9/15/63	88	11.8	144.4	11.7	42.6	52.668	-76.6	6*53* 3	11.5			422
1300	2	-132.41	8*18*56	9/15/63	88	11.8	144.4	11.5	42.7	52.662	-76.3	8*27* 3	8.1			422
1301	2	-157.08	9*56*21	9/15/63	88	11.9	144.5	11.2	42.7	52.656	-74.2	10* 8*28	12.1			422
1303	3	153.56	13*11*10	9/15/63	88	11.9	144.6	10.7	42.7	52.644	-63.9	13*31* 3	19.9			422
1304	3	128.89	14*48*34	9/15/63	88	12.0	144.6	10.4	42.8	52.639	-66.8	15*11* 3	22.5			422
1306	2	79.54	18* 3*23	9/15/63	88	12.1	144.7	9.9	42.9	52.627	-56.2	18*41* 3	37.7			422
1313	1	-93.16	5*25*15	9/16/63	89	12.5	144.8	8.2	43.1	52.586	-84.8	5*35* 3	9.8			423
1314	1	-117.83	7* 2*40	9/16/63	89	12.5	144.8	7.9	43.1	52.580	-75.6	7*16* 3	13.4			423
1315	2	-142.51	8*40* 5	9/16/63	89	12.6	144.9	7.6	43.1	52.574	-71.1	8*49* 3	9.0			423
1318	3	143.46	13*32*18	9/16/63	89	12.7	145.0	6.8	43.3	52.557	-60.2	13*53* 3	20.8			423

READOUT						ORBIT					TIME INTERVAL OF FILE ON FMR TAPE					
		SATELLITE EQUATOR CROSSING AT ORBITAL ASCENDING NODE (AND)				SPIN VECTOR ATTITUDE					BEGIN	END		DROPOUTS, MINUTES W/R/T AND		
ORBIT NO.	CDA STA	EARTH LONGI -TUDE (DEG)	HOURS MINUTES SECONDS (GMT)	CALENDAR DATE	TIROS DAY	DECLI -NA -TION (DEG)	RIGHT ASCEN -SION (DEG)	MINI -MUM NADIR (DEG)	TOT (MIN. AFTER AND)	SPIN RATE (DEG /SEC)	MINU -TES W/R/T AND	HOURS MINUTES SECONDS (GMT)	MINU -TES W/R/T AND	FROM-	TO-	FMR TAPE REEL NO.
1328	1	-103.28	5*46*24	9/17/63	90	13.4	145.2	4.3	43.5	52.498	-78.9	5*56*33	10.2			424
1329	2	-127.96	7*23*49	9/17/63	90	13.4	145.2	4.0	43.6	52.492	-73.8	7*31* 3	7.2			424
1330	2	-152.63	9* 1*13	9/17/63	90	13.5	145.3	3.8	43.6	52.486	-79.3	9*12* 3	10.8			424
1332	3	158.01	12*16* 2	9/17/63	90	13.6	145.3	3.2	43.7	52.475	-64.9	12*35* 3	19.0			424
1333	3	133.34	13*53*27	9/17/63	90	13.6	145.4	3.0	43.7	52.469	-68.5	14*15* 3	21.6			424
1335	2	83.99	17* 8*16	9/17/63	90	13.8	145.4	2.5	43.7	52.457	-57.2	17*45* 3	36.8			424
1343	1	-113.39	6* 7*32	9/18/63	91	14.4	145.5	0.4	44.0	52.410	-76.8	6*20* 3	12.5			425
1344	2	-138.06	7*44*57	9/18/63	91	14.5	145.5	-0.1	43.9	52.404	-73.7	7*55* 0	10.1			425
1345	2	-162.73	9*22*22	9/18/63	91	14.5	145.6	-0.2	43.9	52.398	-77.6	9*35* 3	12.7			425
1348	3	123.24	14*14*35	9/18/63	91	14.7	145.7	-1.0	44.0	52.380	-70.7	14*38* 3	23.5			425
1357	1	-98.81	4*51*16	9/19/63	92	14.4	145.8	-2.8	44.4	52.327	-76.3	5* 1* 3	9.8			426
1358	1	-123.48	6*28*41	9/19/63	92	14.4	145.8	-3.1	44.5	52.321	-75.4	6*43* 3	14.4			426
1359	2	-148.16	8* 6* 5	9/19/63	92	14.4	145.8	-3.3	44.5	52.315	-72.5	8*16* 3	10.0			426
1362	3	137.81	12*58*19	9/19/63	92	14.3	145.8	-3.9	44.7	52.297	-59.4	13*20* 3	21.7			426
1363	2	113.14	14*35*44	9/19/63	92	14.3	145.9	-4.1	44.7	52.291	-64.8	15*11* 3	35.3			426
1364	2	88.46	16*13* 8	9/19/63	92	14.3	145.9	-4.3	44.8	52.285	-52.0	16*48*33	35.4			426
1371	1	-84.24	3*35* 0	9/20/63	93	14.1	145.9	-5.7	45.0	52.244	-87.5	3*44* 3	9.1			427
1372	1	-108.91	5*12*25	9/20/63	93	14.1	145.9	-5.9	45.1	52.238	-76.5	5*24* 3	11.6			427
1373	2	-133.58	6*49*49	9/20/63	93	14.1	145.9	-6.1	45.1	52.232	-76.0	6*58* 3	8.2			427
1374	2	-158.26	8*27*14	9/20/63	93	14.1	145.9	-6.3	45.2	52.226	-77.7	8*39* 3	11.8			427
1376	3	152.38	11*42* 3	9/20/63	93	14.0	145.9	-6.7	45.2	52.214	-36.6	12* 2* 3	20.0			427
1377	3	127.71	13*19*28	9/20/63	93	14.0	145.9	-6.9	45.2	52.208	4.3	13*42* 3	22.6			427
1379	2	78.37	16*34*17	9/20/63	93	14.0	145.9	-7.4	45.3	52.196	-56.7	17*12* 3	37.8			427
1387	1	-119.01	5*33*33	9/21/63	94	13.9	145.9	-8.9	45.6	52.149	-76.2	5*47* 3	13.5			428
1388	2	-143.69	7*10*58	9/21/63	94	13.8	145.8	-9.1	45.6	52.143	-72.3	7*20* 3	9.1			428

READOUT						ORBIT					TIME INTERVAL OF FILE ON FMR TAPE					
		SATELLITE EQUATOR CROSSING AT ORBITAL ASCENDING NODE (ANO)				SPIN VECTOR ATTITUDE					BEGIN	END		DROPOUTS, MINUTES W/R/T ANO		
ORBIT NO.	CDA STA	EARTH LONGI -TUDE (DEG)	HOURS MINUTES SECONDS (GMT)	CALENDAR DATE	TIROS DAY	DECLI -NA -TION (DEG)	RIGHT ASCEN -SION (DEG)	MINI -MUM NADIR (DEG)	TOT (MIN. AFTER ANO)	SPIN RATE (DEG /SEC)	MINU -TES W/R/T ANO	HOURS MINUTES SECONDS (GMT)	MINU -TES W/R/T ANO	FROM-	TO-	FMR TAPE REEL NO.
1390	3	166.96	10*25*47	9/21/63	94	13.8	145.8	-9.5	45.7	52.131	-63.5	10*44*28	18.7			428
1391	3	142.29	12* 3*11	9/21/63	94	13.8	145.8	-9.7	45.7	52.125	-66.9	12*24* 3	20.9			428
1393	2	92.94	15*18* 0	9/21/63	94	13.8	145.8	-10.1	45.8	52.113	-55.3	15*53* 3	35.1			428
1401	1	-104.44	4*17*17	9/22/63	95	13.7	145.8	-11.7	45.1	52.066	-80.9	4*28* 3	10.8			429
1402	2	-129.11	5*54*41	9/22/63	95	13.7	145.8	-12.0	45.2	52.060	-75.1	6* 4* 3	9.4			429
1403	2	-153.78	7*32* 6	9/22/63	95	13.7	145.8	-12.2	45.2	52.054	-77.3	7*43* 3	11.0			429
1408	2	82.84	15*39* 9	9/22/63	95	13.7	146.0	-13.4	45.3	52.024	-56.4	16*16* 3	36.9			429
1415	1	-89.86	3* 1* 1	9/23/63	96	13.7	146.1	-15.0	45.7	51.982	-85.9	3*10* 3	9.0			430
1416	1	-114.54	4*38*25	9/23/63	96	13.7	146.1	-15.2	46.7	51.977	-75.3	4*51* 3	12.6			430
1417	2	-139.21	6*15*50	9/23/63	96	13.7	146.1	-15.4	45.8	51.971	-63.5	6*24* 3	8.2			430
1418	2	-163.88	7*53*14	9/23/63	96	13.7	146.0	-15.6	45.8	51.965	-77.8	8* 6*33	13.3			430
1422	2	97.41	14*22*52	9/23/63	96	13.8	146.1	-16.6	45.8	51.941	-53.9	14*58* 3	35.2			430
1430	1	-99.96	3*22* 9	9/24/63	97	14.1	146.0	-18.4	47.0	51.894	-75.9	3*31* 3	8.9			431
1431	1	-124.63	4*59*33	9/24/63	97	13.2	145.6	-18.6	47.1	51.888	-77.2	5*15* 3	15.5			431
1432	2	-149.31	6*36*58	9/24/63	97	12.3	145.1	-18.0	47.3	51.882	-70.2	6*47* 3	10.1			431
1434	3	161.33	9*51*47	9/24/63	97	10.5	144.1	-16.7	47.7	51.870	-62.0	10*10* 3	18.3			431
1435	3	136.66	11*29*11	9/24/63	97	9.6	143.7	-16.1	47.8	51.864	10.9	11*51* 3	21.9			431
1436	2	111.99	13* 6*36	9/24/63	97	8.6	143.5	-15.5	48.1	51.858	-60.9	13*40* 3	33.5			431
1437	2	87.32	14*44* 1	9/24/63	97	7.4	143.5	-15.0	48.3	51.852	-53.0	15*21* 3	37.0			431
1444	1	-85.38	2* 5*52	9/25/63	98	-1.1	143.0	-11.8	50.5	51.811	-85.4	2*15* 3	9.2			432
1445	1	-110.06	3*43*17	9/25/63	98	-2.1	142.6	-11.2	50.8	51.805	-76.2	3*55* 3	11.8			432
1447	2	-159.41	6*58* 6	9/25/63	98	-4.0	141.8	-9.9	51.2	51.793	-3.1	7*10* 3	12.0			432
1450	3	126.57	11*50*20	9/25/63	98	-6.7	140.6	-8.0	51.8	51.776	-4.2	12*13* 3	22.7			432
1461	2	-144.83	5*41*50	9/26/63	99	-19.4	140.2	-2.8	55.0	51.711	0.2	5*51* 3	9.2			433
1466	2	91.80	13*48*52	9/26/63	99	-24.4	138.9	-0.2	56.0	51.682	-55.3	14*26* 3	37.2			433

READOUT						ORBIT					TIME INTERVAL OF FILE ON FMR TAPE				
		SATELLITE EQUATOR CROSSING AT ORBITAL ASCENDING NODE (AND)				SPIN VECTOR ATTITUDE					BEGIN	END		DROPOUTS, MINUTES W/R/T AND	
ORBIT NO.	CDA STA	EARTH LONGI -TUDE (DEG)	HOURS MINUTES SECONDS (GMT)	CALENDAR DATE	TIROS DAY	DECLI -NA -TION (DEG)	RIGHT ASCEN -SION (DEG)	MINI -MUM NADIR (DEG)	TOT (MIN. AFTER AND)	SPIN RATE (DEG /SEC)	MINU -TES W/R/T AND	HOURS MINUTES SECONDS (GMT)	MINU -TES W/R/T AND	FROM-	TO-	FMR TAPE REEL NO.
1473	1	-80.91	1*10*44	9/27/63	100	-32.9	140.3	3.0	58.3	51.641	-87.1	1*19*33	8.8			434
1474	1	-105.58	2*48* 9	9/27/63	100	-34.0	140.3	3.4	58.5	51.636	-79.1	2*59* 3	10.9			434
1475	2	-130.25	4*25*33	9/27/63	100	-34.9	140.1	3.8	58.8	51.630	-76.7	4*35* 3	9.5			434
1476	2	-154.92	6* 2*58	9/27/63	100	-35.9	140.0	4.3	59.1	51.624	-76.7	6*14* 3	11.1			434
1478	1	155.72	9*17*47	9/27/63	100	-37.6	139.5	5.3	59.5	51.612	-61.9	9*50* 3	32.3			434
1480	2	106.37	12*32*36	9/27/63	100	-39.1	139.3	6.4	59.9	51.601	-54.9	13* 7* 3	34.5			434
1481	2	81.70	14*10* 1	9/27/63	100	-39.1	139.2	6.5	60.1	51.595	-51.7	14*48* 3	38.0			434
1489	1	-115.68	3* 9*18	9/28/63	101	-38.8	139.0	5.2	60.2	51.549	-76.9	3*23* 3	13.8			435
1490	2	-140.35	4*46*40	9/28/63	101	-37.3	138.7	4.4	59.9	51.543	-70.8	4*55* 3	8.4			435
1493	1	145.62	9*38*54	9/28/63	101	-36.9	138.7	3.7	59.9	51.526	-50.8	10*12* 3	33.2			435
1503	1	-101.10	1*52*59	9/29/63	102	-35.0	138.1	1.3	59.8	51.469	-72.2	2* 3* 3	10.1			436
1504	1	-125.77	3*30*24	9/29/63	102	-34.9	138.1	1.0	59.8	51.463	-74.4	3*46* 3	15.7			436
1505	2	-150.44	5* 7*48	9/29/63	102	-34.7	138.1	0.7	59.8	51.457	-71.0	5*18* 3	10.3			436
1507	1	160.20	8*22*38	9/29/63	102	-34.4	138.2	0.3	59.8	51.446	-62.9	8*54* 3	31.4			436
1508	1	135.53	10* 0* 2	9/29/63	102	-34.3	138.2	0.1	59.9	51.440	-54.9	10*35* 3	35.0			436
1510	2	86.18	13*14*51	9/29/63	102	-33.9	138.1	-0.5	59.8	51.429	-30.1	13*52* 3	37.2			436
1517	1	-86.53	0*36*43	9/30/63	103	-32.5	137.6	-2.3	59.7	51.389	-78.0	0*46* 3	9.3			437
1518	1	-111.20	2*14* 8	9/30/63	103	-32.3	137.6	-2.5	59.7	51.384	-58.8	2*26* 3	11.9			437
1519	2	-135.87	3*51*32	9/30/63	103	-32.2	137.6	-2.8	59.8	51.378	-19.7	4* 0* 3	8.5			437
1520	2	-160.54	5*28*57	9/30/63	103	-32.0	137.6	-3.1	59.8	51.372	-78.2	5*42* 3	13.1			437
1522	1	150.10	8*43*46	9/30/63	103	-31.7	137.7	-3.6	59.7	51.361	-60.2	9*16* 3	32.3			437
1523	1	125.43	10*21*10	9/30/63	103	-31.5	137.7	-3.9	59.7	51.356	-54.0	10*58* 3	36.9			437
1524	2	100.75	11*58*35	9/30/63	103	-31.3	137.6	-4.2	59.7	51.350	-50.6	12*34* 3	35.5			437
1525	2	76.08	13*36* 0	9/30/63	103	-31.1	137.6	-4.5	59.7	51.344	-51.3	14*15* 3	39.1			437

APPENDIX B

SUBPOINT TRACK SUMMARY OF AVAILABLE RADIATION DATA

In this section, the time interval for which radiation data are available on the FMR tapes for TIROS VII from launch, June 19, 1963, to September 30, 1963 is summarized diagrammatically by means of subpoint tracks for each interrogation day. As discussed previously, an interrogation day may be contained within the calendar day, or it may consist of parts of two calendar days. This method of presentation enables the data user to quickly appraise the orbits containing data in an area of interest.

Before discussing the subpoint track summaries, however, the various scanning modes of the TIROS radiometer and the relationship between the satellite nadir angle (the angle between the local vertical and the spin axis in the direction of the television cameras) and the optical axis of the medium resolution radiometer will be illustrated.

The three possible earth scanning patterns, or modes, of the TIROS radiometer may be characterized as follows (Figure B1):

(a) Closed Mode—All scan spots throughout a number of spin cycles of the satellite are earth viewed, either through the wall sensor or the floor sensor.

(b) Single Open Mode—Some scan spots of a spin cycle are space viewed and the remainder are earth viewed through the wall sensor only or through the floor sensor only.

(c) Alternating Open Mode—The scan spots of a spin cycle are a combination of space and earth viewed, alternately through the wall sensor and the floor sensor.

In Figure B2, on an earth cross-section, are shown nominal satellite nadir angle values bounding the various radiometer scanning modes. These values are for a height above the earth of about 635 km. It has been assumed that the spin vector coordinates remain constant throughout one orbit and that the minimum nadir angle is zero. Generally, the minimum nadir angle encountered throughout an orbit is not zero, hence diminishing the time period of the closed mode. In a number of orbits, the minimum nadir angle is greater than 20.5°, and hence there is no closed mode.

On the subpoint track summaries, each interrogation day is denoted by its calendar date or dates as the case may be. Dropouts are indicated by a symbol | — | where each dash represents one minute for which data are not available. Dropouts which occur at the beginning of tape have been left off the subpoint summaries. Each orbit is identified by orbit number and the time of occurrence of the ANO, to the hour and nearest minute in GMT. The symbol "⊙" indicates the point with respect to the orbital subpoint track where the minimum satellite nadir (η_o) angle for the interrogation day occurs and its location is the point at which the spin axis intersects the earth's surface. The orbit to which η_o applies is indicated by a straight line drawn normal to that orbit and the value of η_o to the nearest degree is also indicated. In cases where any ambiguity might arise as to the orbit to which η_o applies, an arrow parallel to the applicable subpoint track is used (e.g. on page 180, $\eta_o = -19°$ applies to Readout Orbit 427). The spin vector changes only slightly in declination and right ascension during one interrogation day; and, thus, the minimum nadir angle is essentially constant and remains at approximately the same relative position to each orbit during one interrogation day.

To illustrate the use of the subpoint summaries, we use the same example as was used in Appendix A. If the master subpoint track overlay from the back cover of the Catalog-Manual is placed over the subpoint track for orbit 277 (page 170) with the ascending node at longitude 91.36° West, then the subpoint track shown is applicable to the available data acquired during this interrogation. For a limiting scan nadir angle of 58°, the radiometer can acquire data from an area along the subpoint track which is within 11° of great circle arc on either side of the track. It can be seen that the data began 94.2 minutes before and ended 10.6 minutes after the ascending node time which

was approximately 03:28 GMT. Also, a one minute dropout occurs between −54.4 and −53.4 minutes with respect to the ascending node time. The minimum satellite nadir angle to the nearest whole degree, and sufficiently accurate to apply to the entire interrogation day, was −30° on orbit 279. The intersection of the spin (camera) axis with the earth, indicated by an "⊙", lay south of the subpoint track as indicated by the negative value of the minimum satellite nadir angle.

The bounding orbits of .periods where there exists direct solar radiation interference in the reduced channel 3 and 5 data (as described in Section VI) are given in the lower right hand corner of the Subpoint Track Summaries for the period in which they apply. For example, direct solar radiation interference in channels 3 and 5 on all orbits from 0321 to 0343 inclusive is indicated on the Subpoint Track Summaries for the days July 11 and 12, 1963.

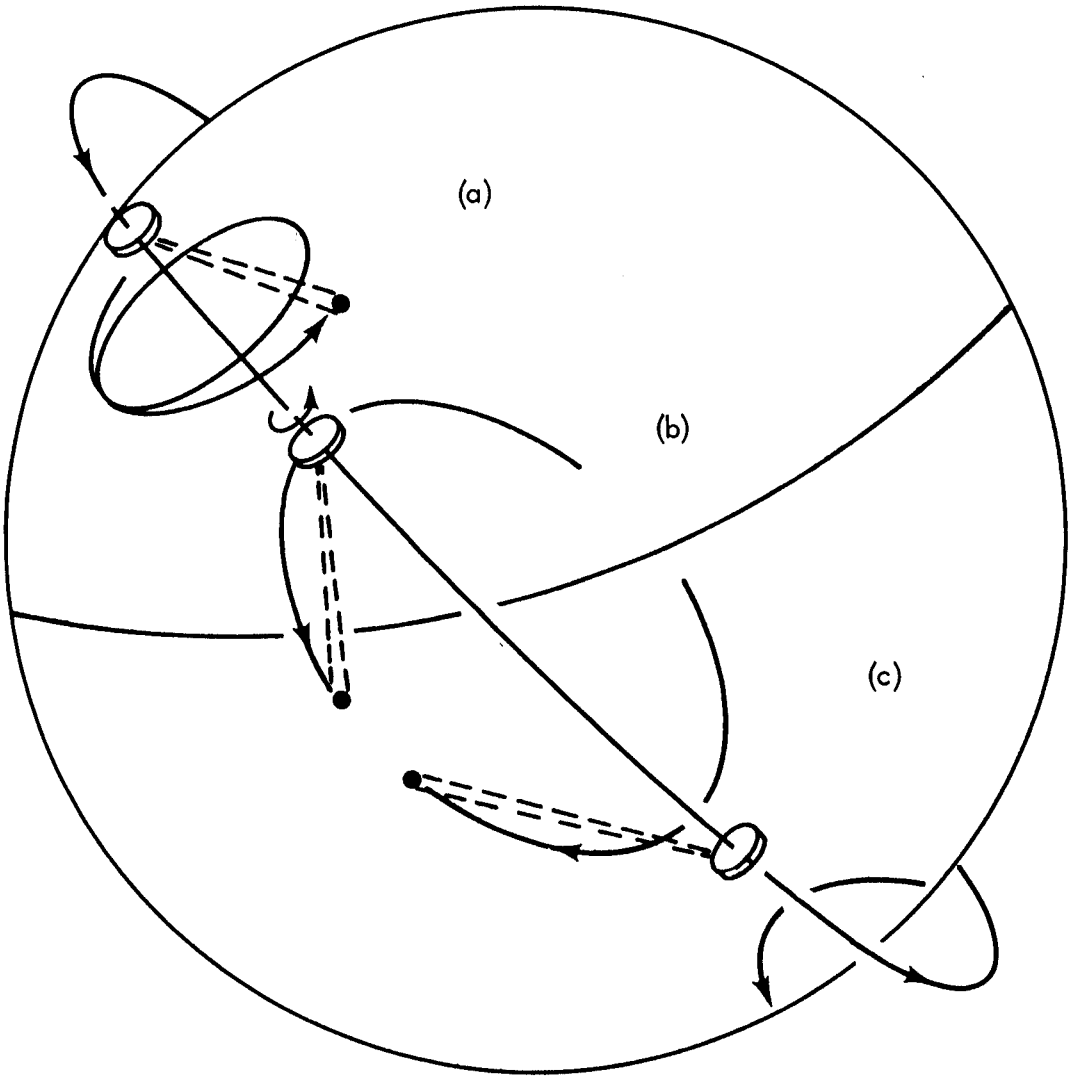

Figure B1—Scanning modes of the TIROS radiometer: (a) closed mode, (b) single open mode, and (c) alternating open mode.

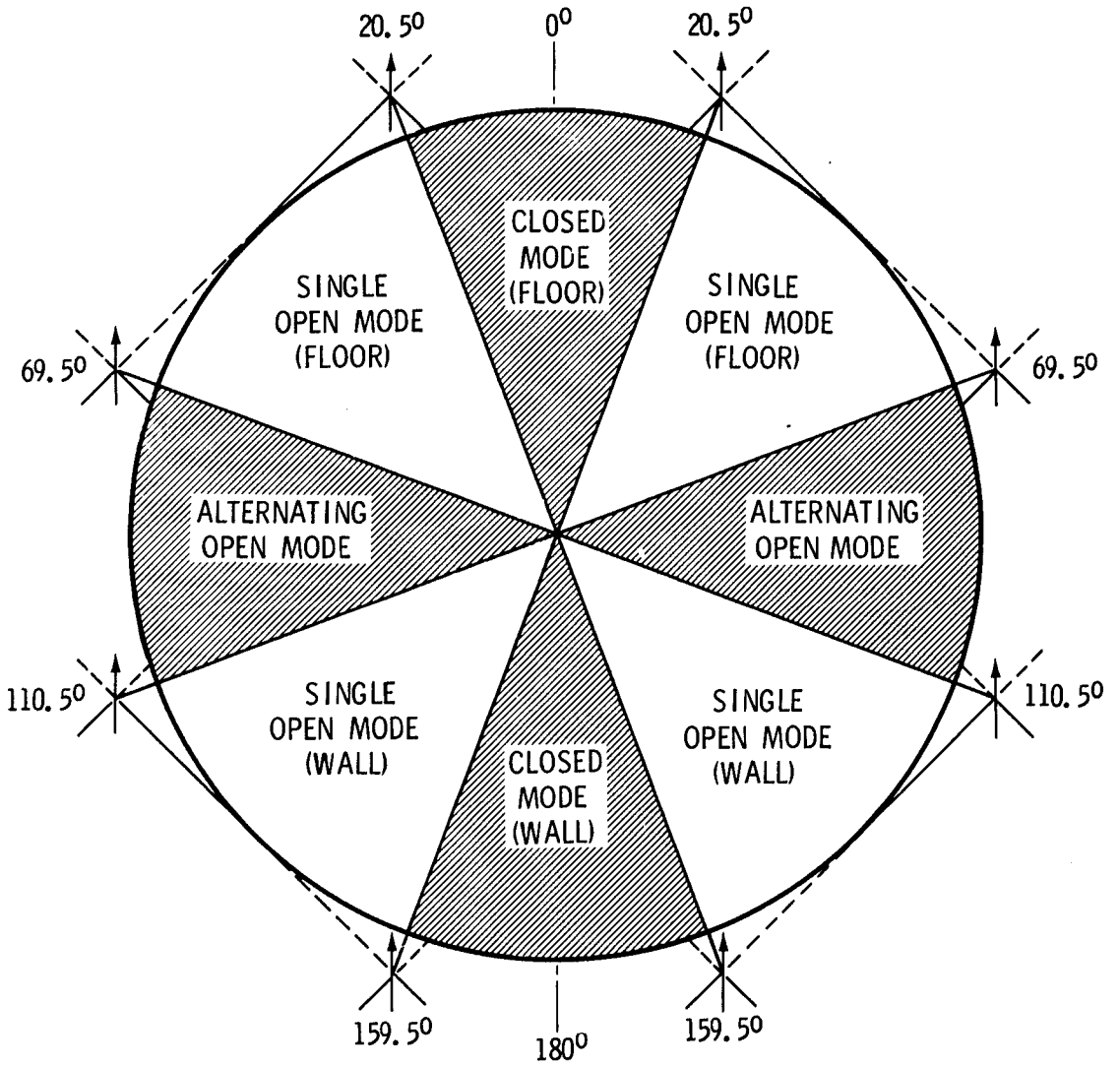

Figure B2—Nominal boundary satellite nadir angles for the various scanning modes at a height of about 635 km. Arrows indicate the spin vector through the top of the satellite, and the nadir angles refer to the opposite direction, viz., the spin (camera) axis. Solid lines at 45° to the arrows indicate the floor and dashed lines the wall scans of the radiometer.

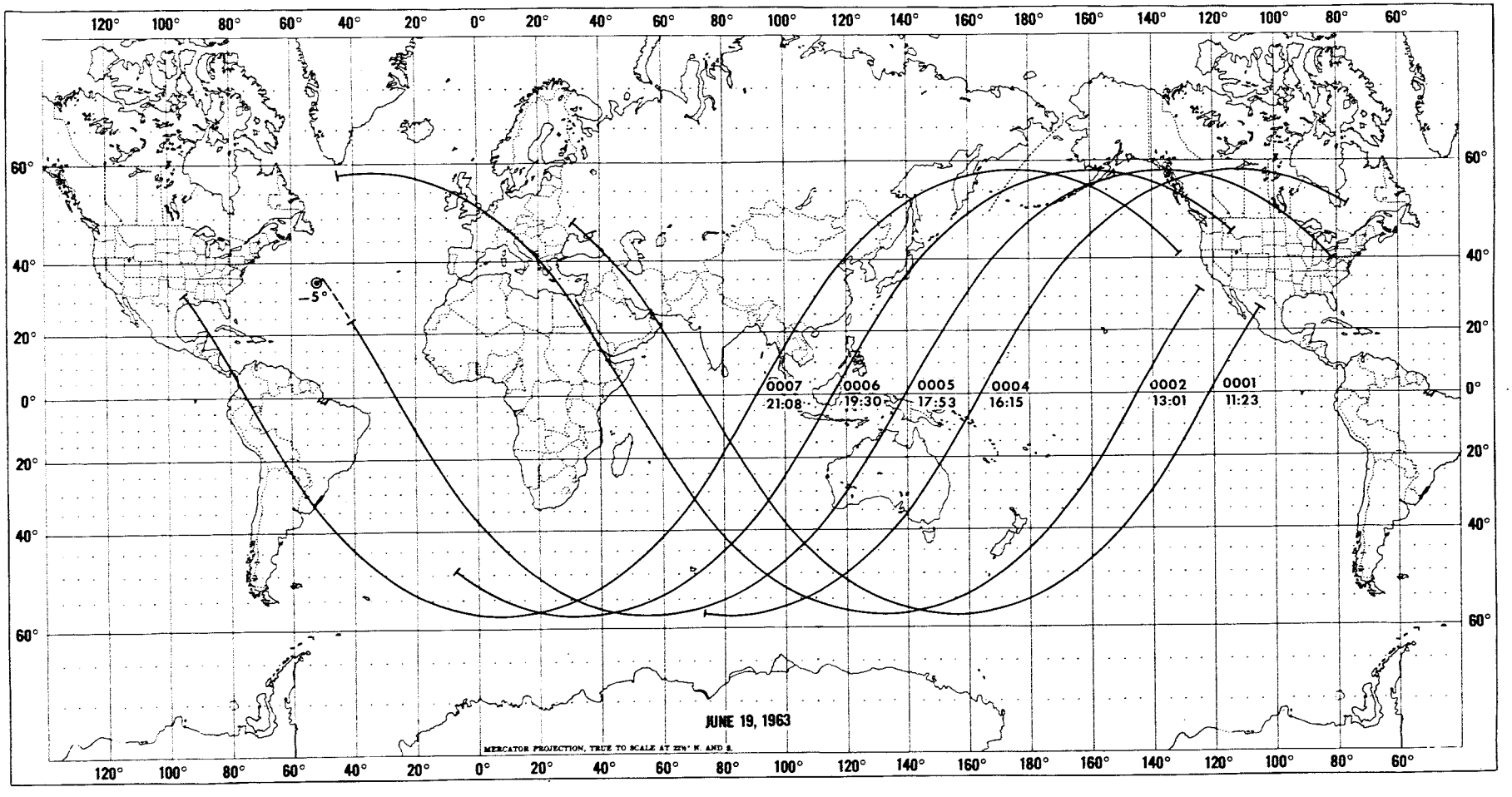
0007
21:08
0006
19:30
0005
17:53
0004
16:15
0002
13:01
0001
11:23
-5°
JUNE 19, 1963
MERCATOR PROJECTION, TRUE TO SCALE AT 22½° N. AND S.

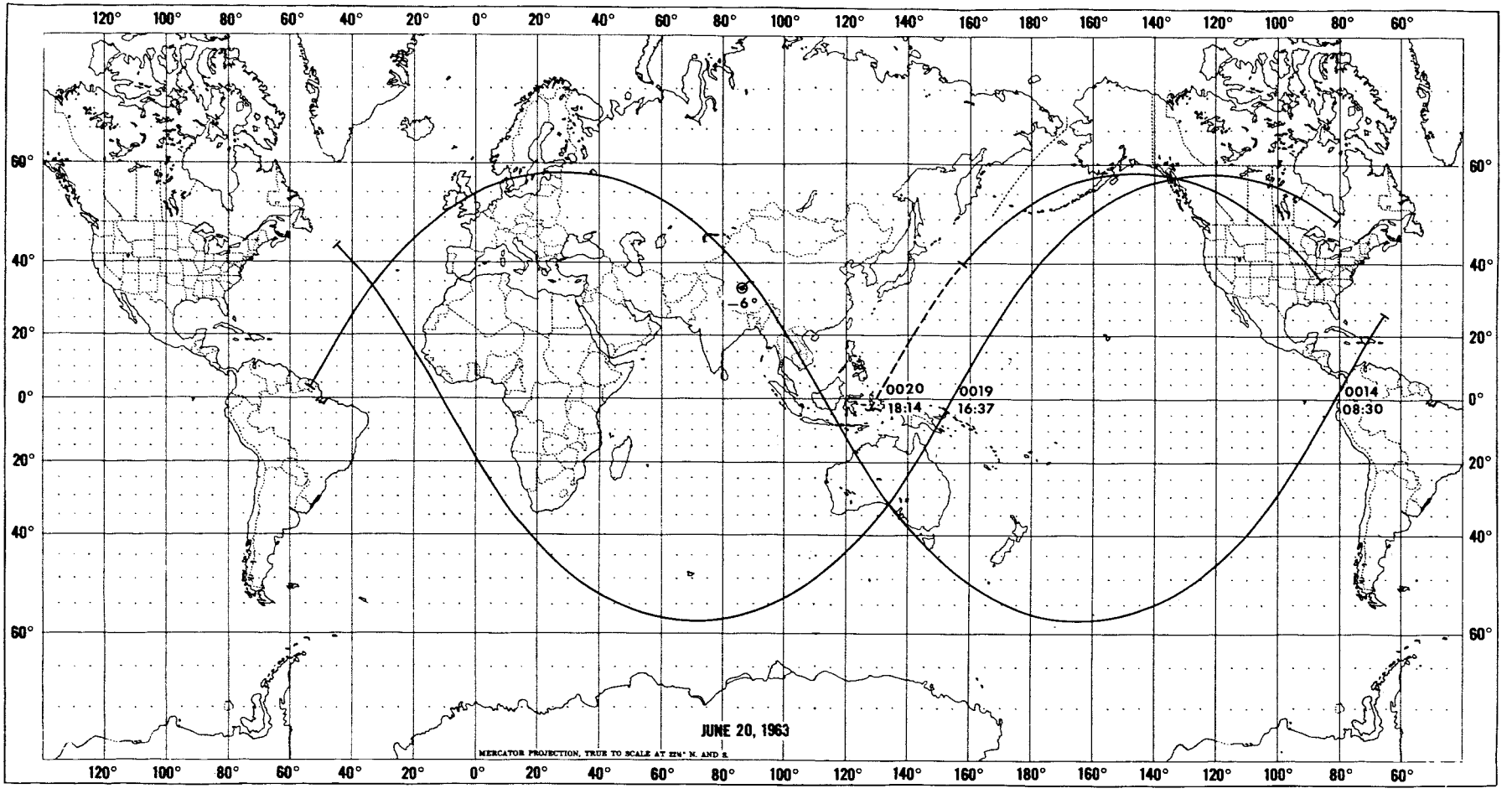
120° 100° 80° 60° 40° 20° 0° 20° 40° 60° 80° 100° 120° 140° 160° 180° 160° 140° 120° 100° 80° 60°
60° 40° 20° 0° 20° 40° 60°
-6°
0020
18:14
0019
16:37
0014
08:30
JUNE 20, 1963
MERCATOR PROJECTION, TRUE TO SCALE AT 22½° N. AND S.

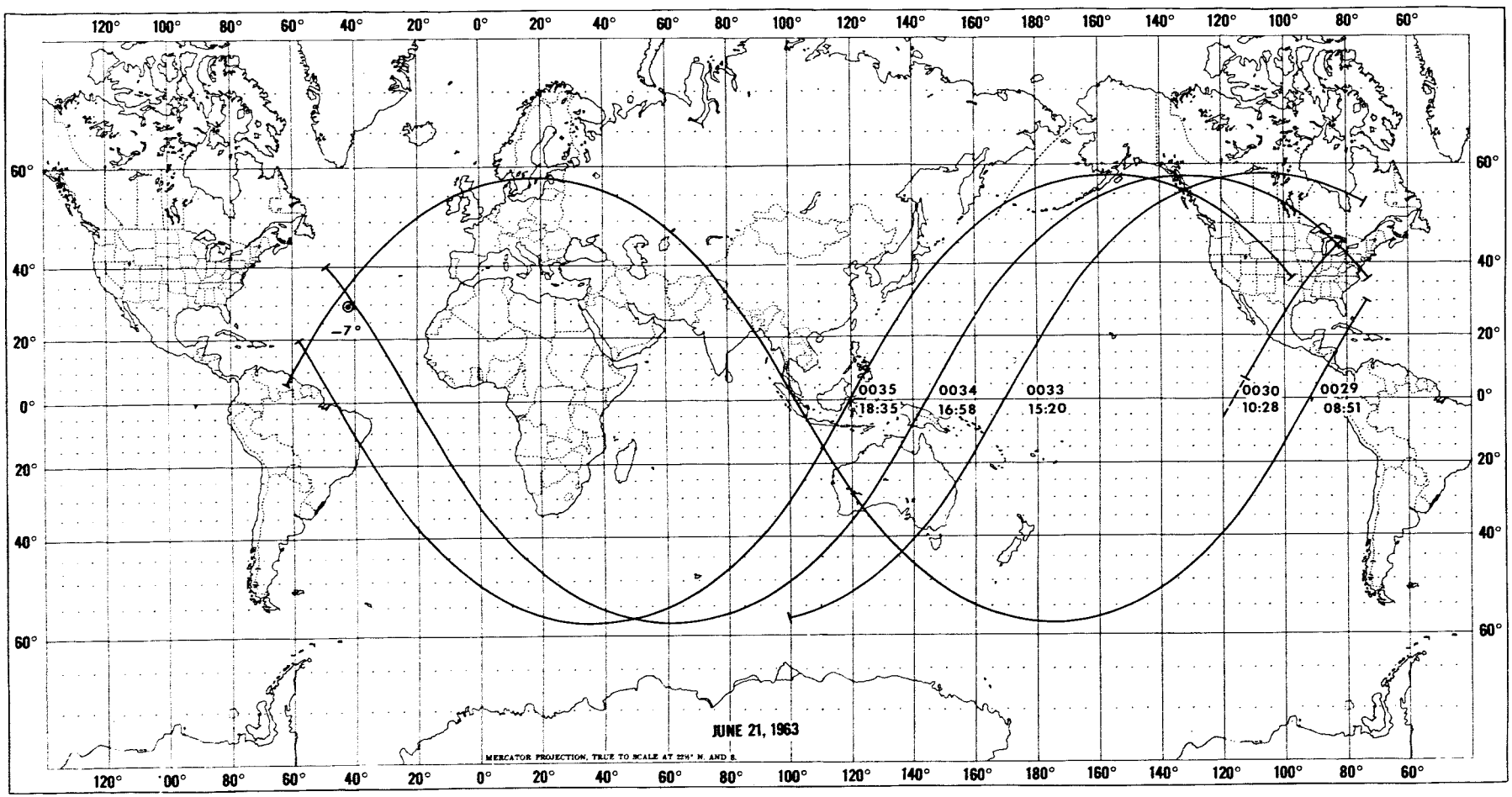
120° 100° 80° 60° 40° 20° 0° 20° 40° 60° 80° 100° 120° 140° 160° 180° 160° 140° 120° 100° 80° 60°
60° 40° 20° 0° 20° 40° 60°
-7°
0035
18:35
0034
16:58
0033
15:20
0030
10:28
0029
08:51
JUNE 21, 1963
MERCATOR PROJECTION, TRUE TO SCALE AT 22½° N. AND S.

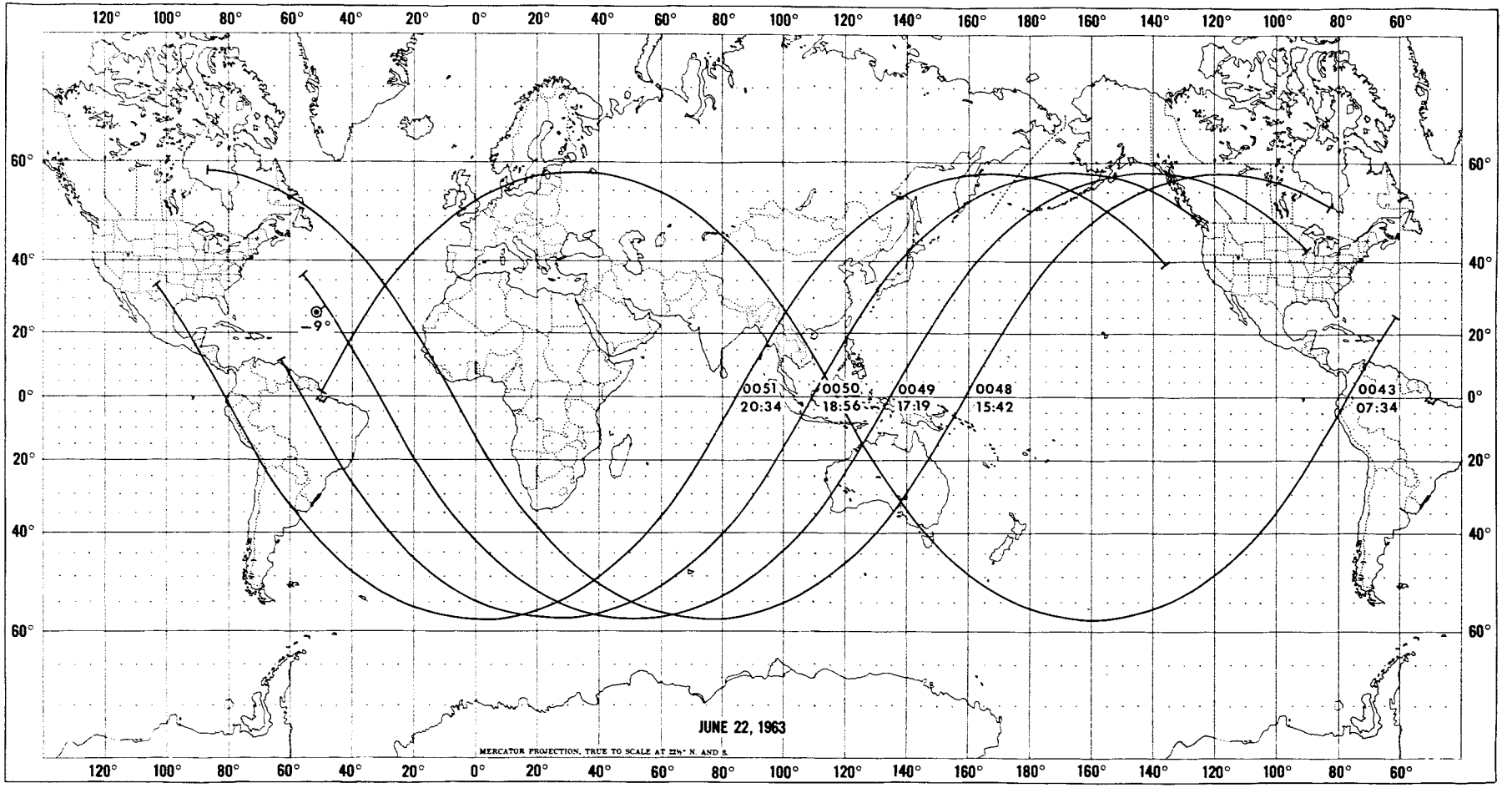
0051
20:34
0050
18:56
0049
17:19
0048
15:42
0043
07:34
-9°
JUNE 22, 1963
MERCATOR PROJECTION, TRUE TO SCALE AT 22½° N. AND S.

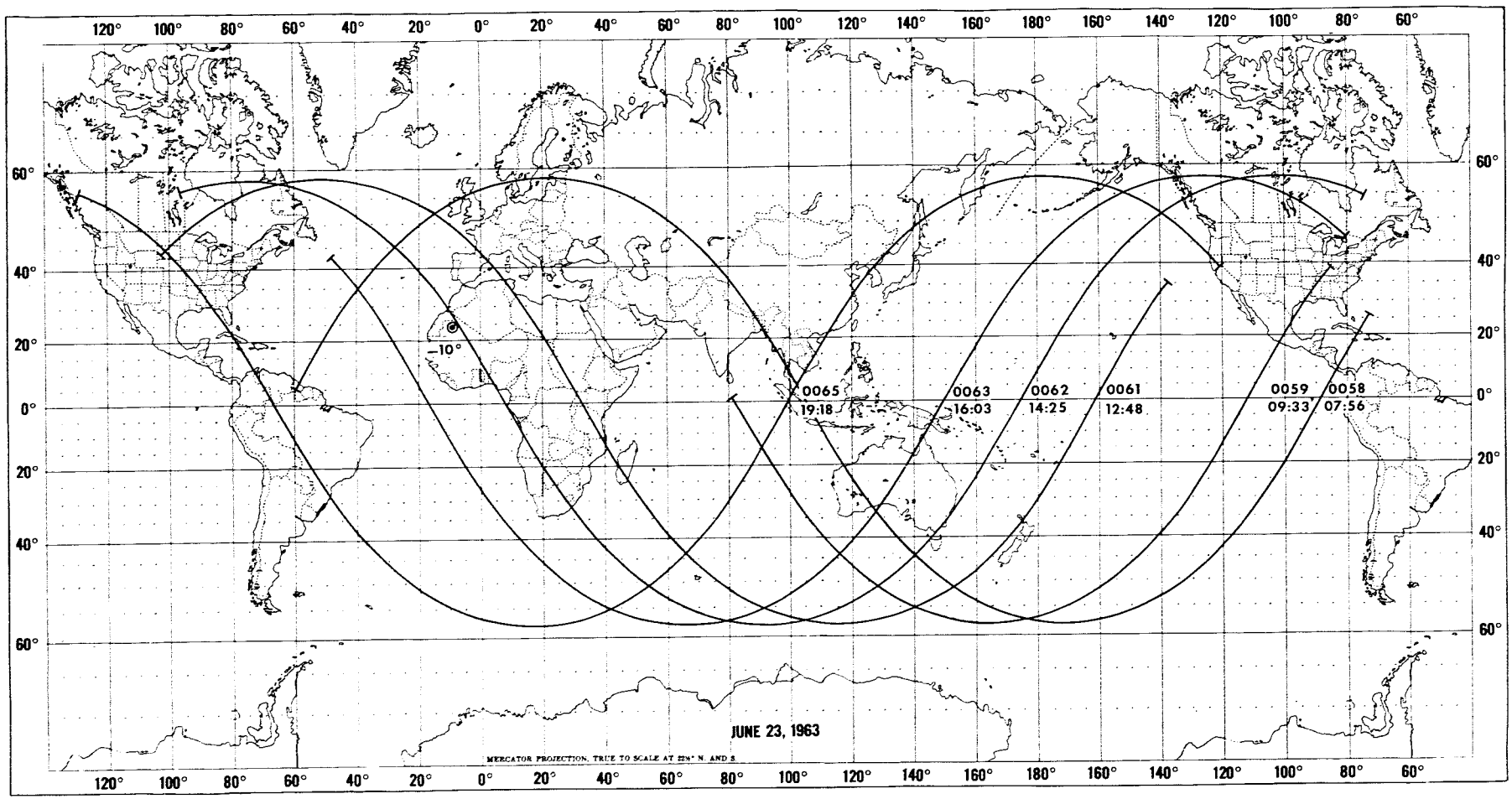
120° 100° 80° 60° 40° 20° 0° 20° 40° 60° 80° 100° 120° 140° 160° 180° 160° 140° 120° 100° 80° 60°
60° 40° 20° 0° 20° 40° 60°
-10°
0065
19:18
0063
16:03
0062
14:25
0061
12:48
0059
09:33
0058
07:56
JUNE 23, 1963
MERCATOR PROJECTION, TRUE TO SCALE AT 22½° N. AND S.

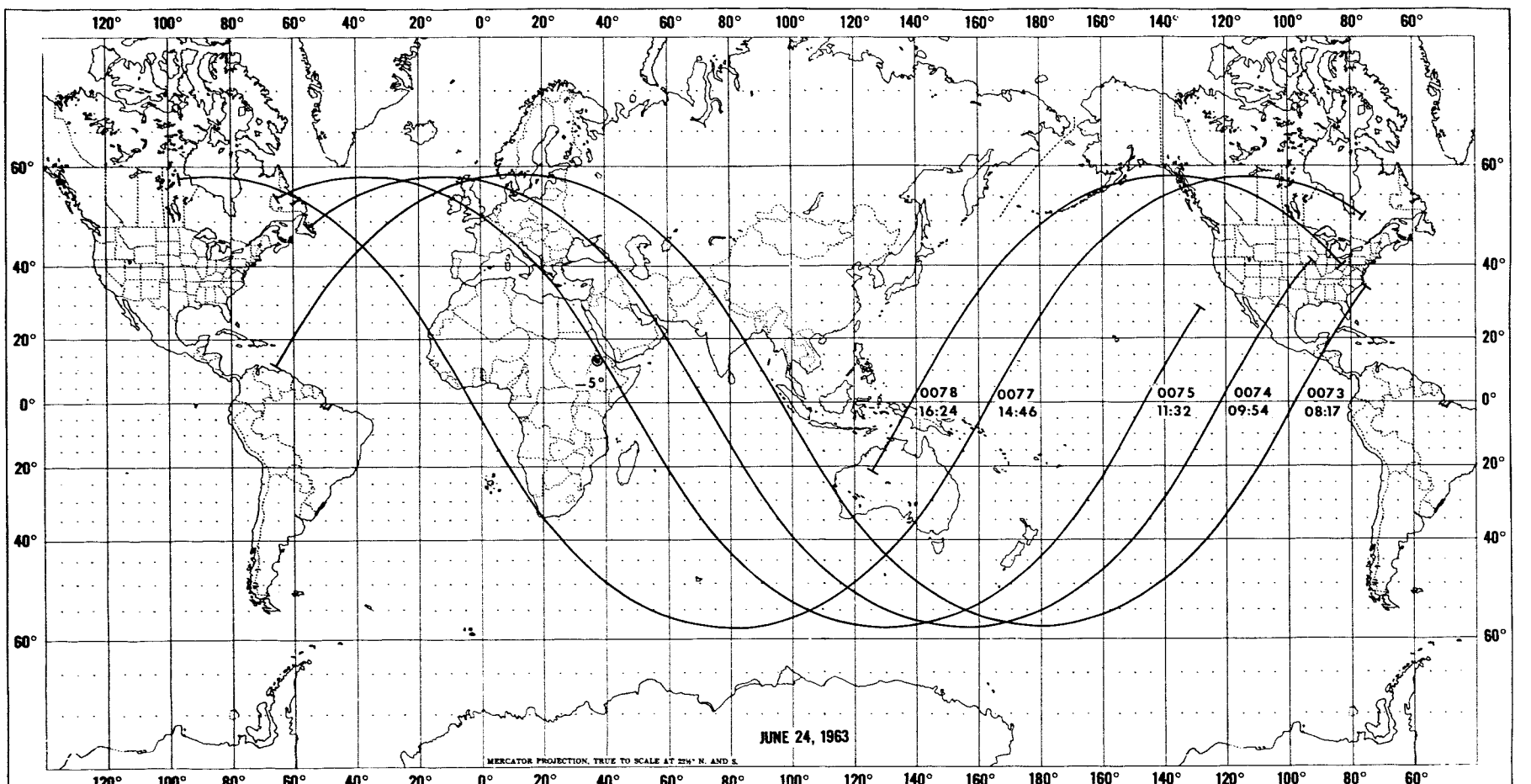
120° 100° 80° 60° 40° 20° 0° 20° 40° 60° 80° 100° 120° 140° 160° 180° 160° 140° 120° 100° 80° 60°
60° 40° 20° 0° 20° 40° 60°
0078
16:24
0077
14:46
0075
11:32
0074
09:54
0073
08:17
-5°
JUNE 24, 1963
MERCATOR PROJECTION, TRUE TO SCALE AT 22½° N. AND S.

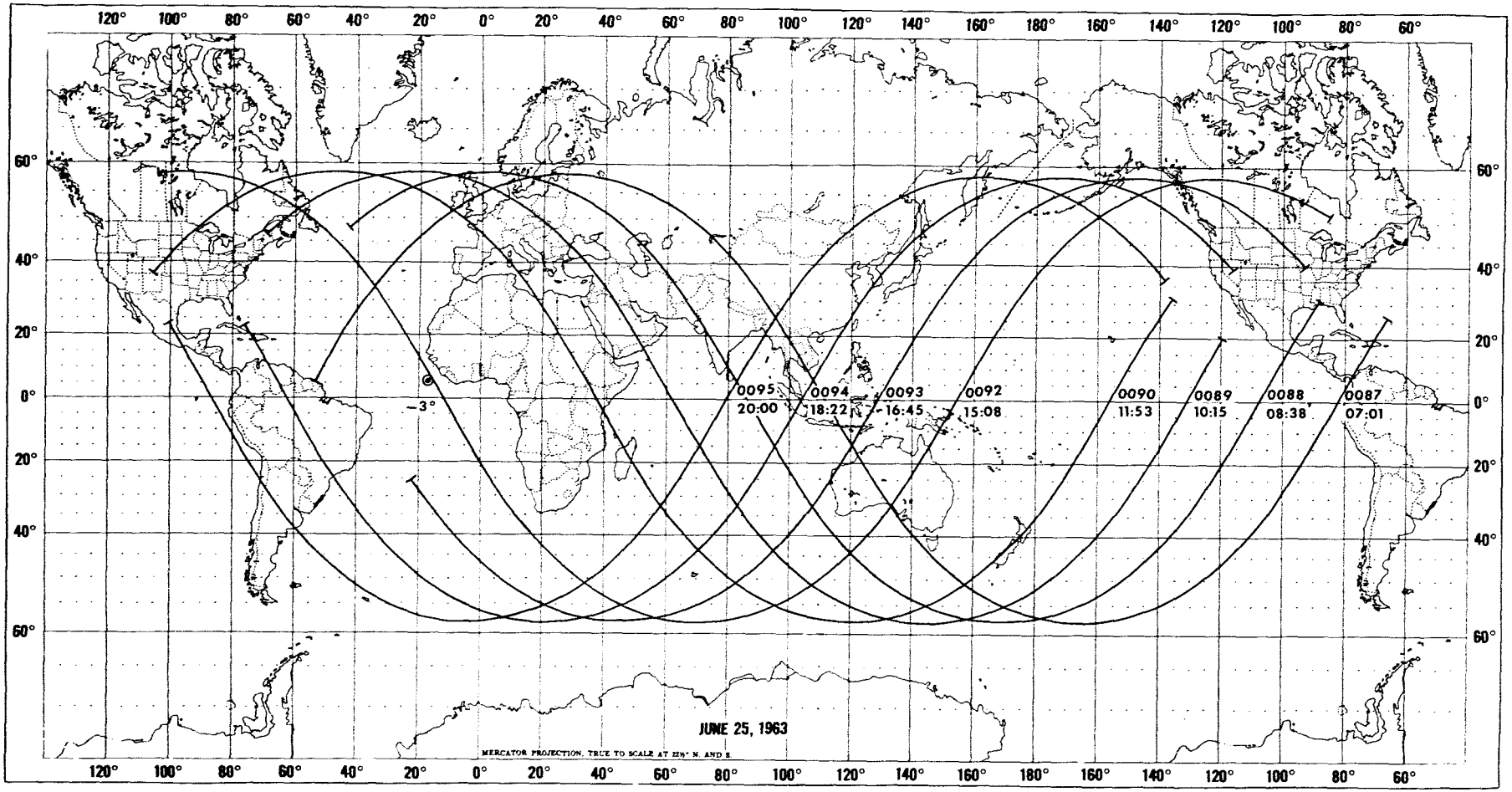
120° 100° 80° 60° 40° 20° 0° 20° 40° 60° 80° 100° 120° 140° 160° 180° 160° 140° 120° 100° 80° 60°
60° 40° 20° 0° 20° 40° 60°
0095 20:00
0094 18:22
0093 16:45
0092 15:08
0090 11:53
0089 10:15
0088 08:38
0087 07:01
-3°
JUNE 25, 1963
MERCATOR PROJECTION, TRUE TO SCALE AT 22½° N. AND S.

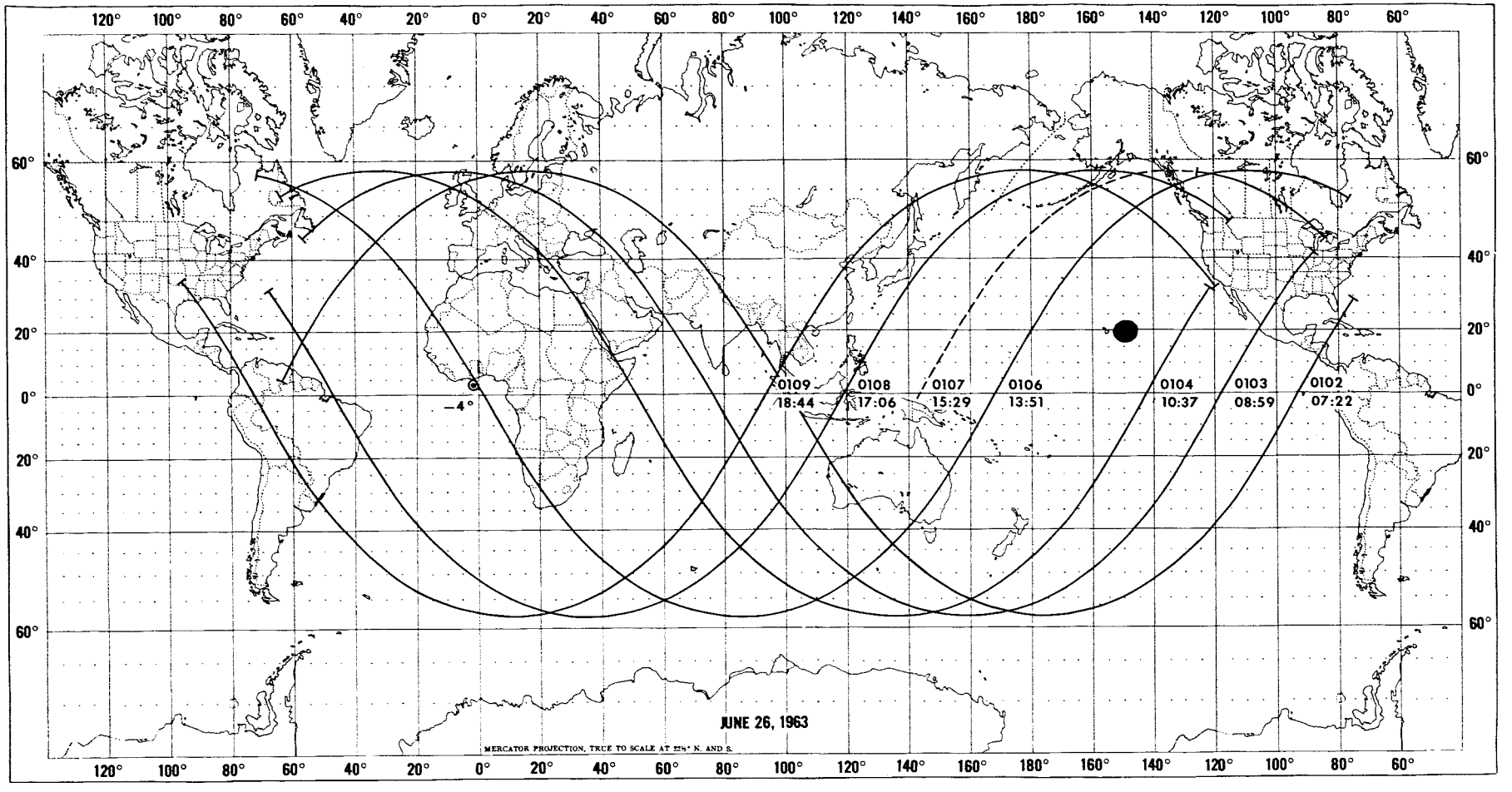
120° 100° 80° 60° 40° 20° 0° 20° 40° 60° 80° 100° 120° 140° 160° 180° 160° 140° 120° 100° 80° 60°
60° 40° 20° 0° 20° 40° 60°
0109 18:44
0108 17:06
0107 15:29
0106 13:51
0104 10:37
0103 08:59
0102 07:22
−4°
JUNE 26, 1963
MERCATOR PROJECTION, TRUE TO SCALE AT 22½° N. AND S.

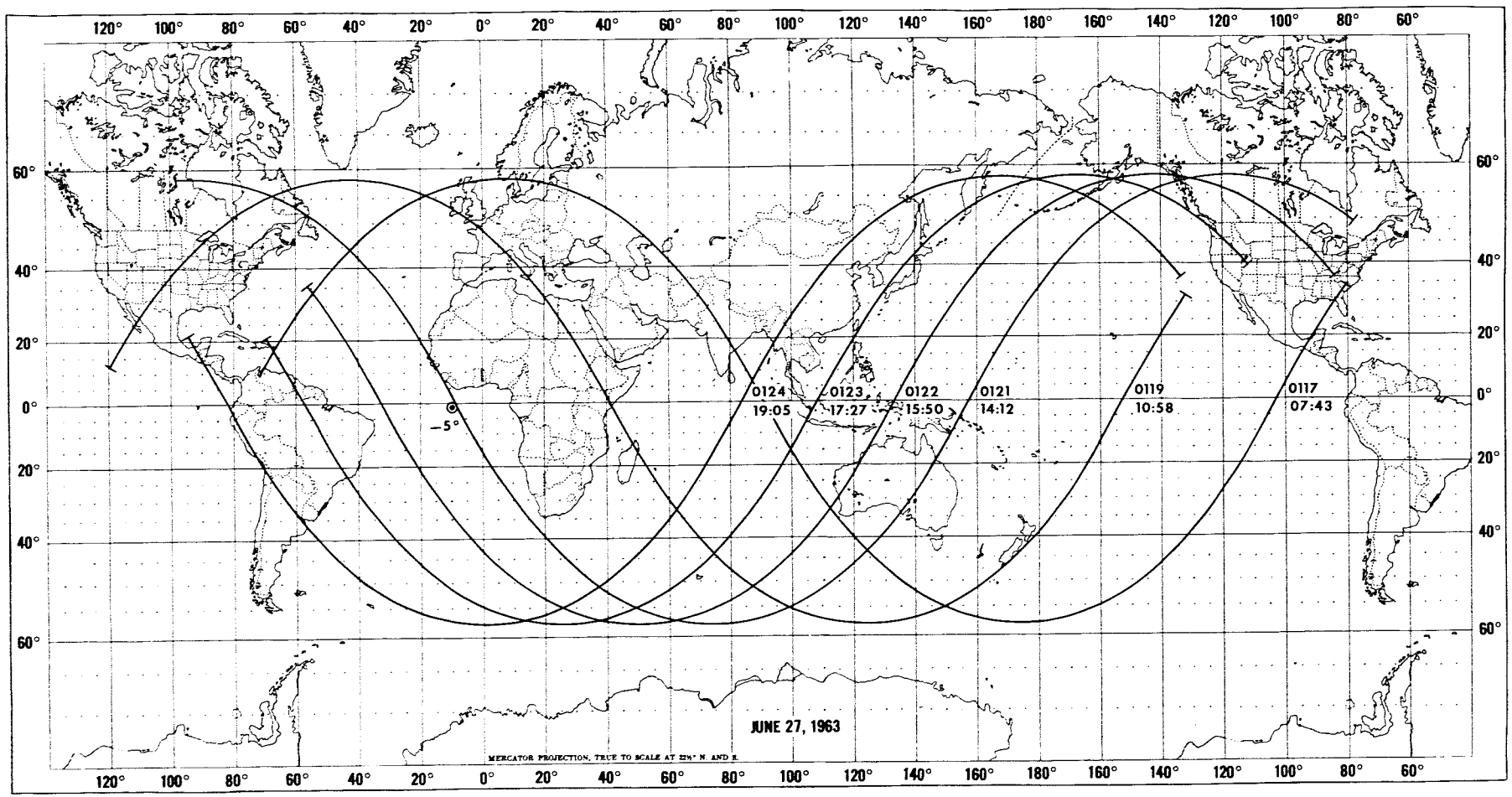
120° 100° 80° 60° 40° 20° 0° 20° 40° 60° 80° 100° 120° 140° 160° 180° 160° 140° 120° 100° 80° 60°
60° 40° 20° 0° 20° 40° 60°
0124
19:05
0123
17:27
0122
15:50
0121
14:12
0119
10:58
0117
07:43
−5°
JUNE 27, 1963
MERCATOR PROJECTION, TRUE TO SCALE AT 22½° N. AND S.

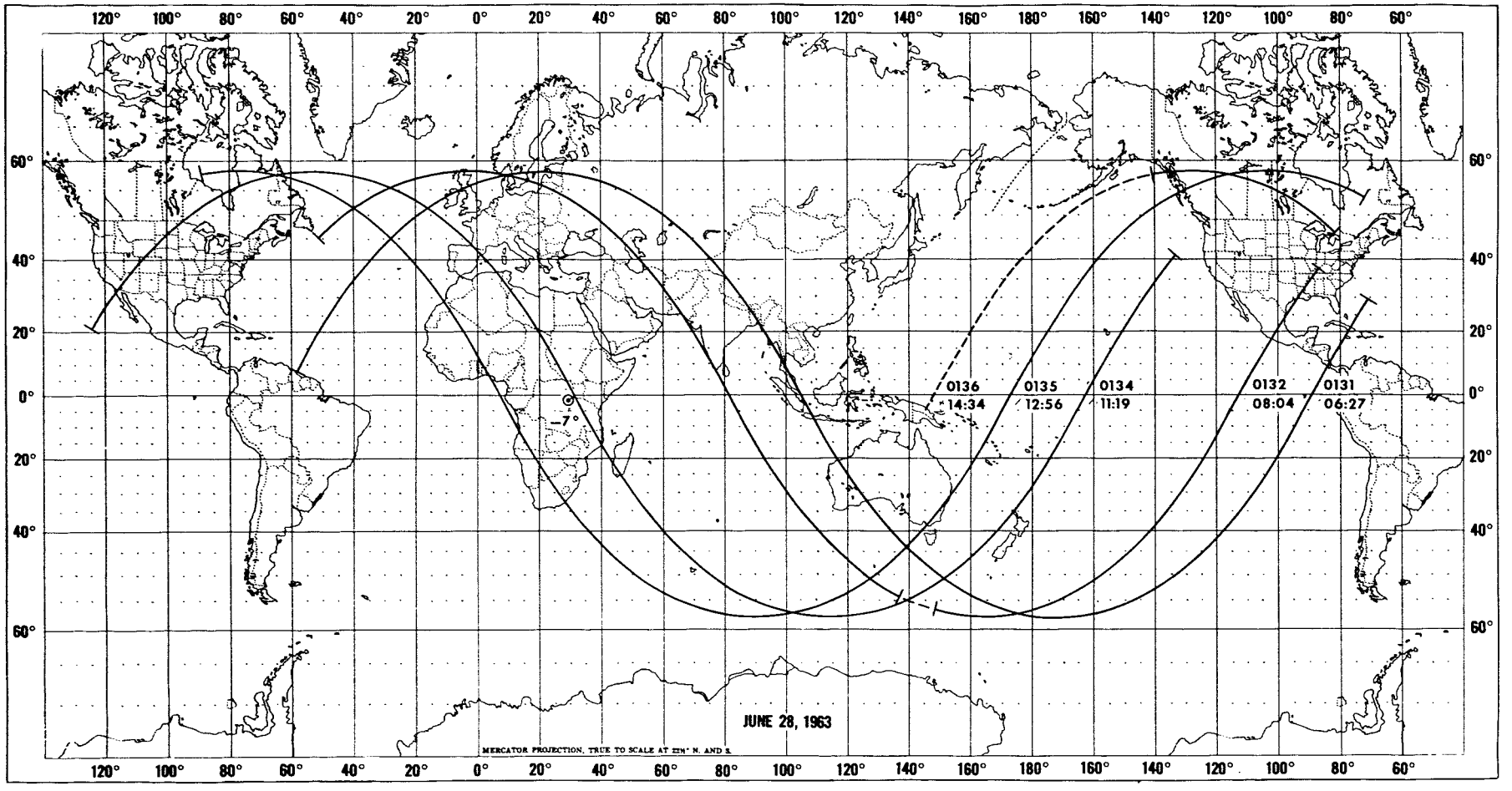
120° 100° 80° 60° 40° 20° 0° 20° 40° 60° 80° 100° 120° 140° 160° 180° 160° 140° 120° 100° 80° 60°
60° 40° 20° 0° 20° 40° 60°
0136
14:34
0135
12:56
0134
11:19
0132
08:04
0131
06:27
-7°
JUNE 28, 1963
MERCATOR PROJECTION, TRUE TO SCALE AT 22½° N. AND S.

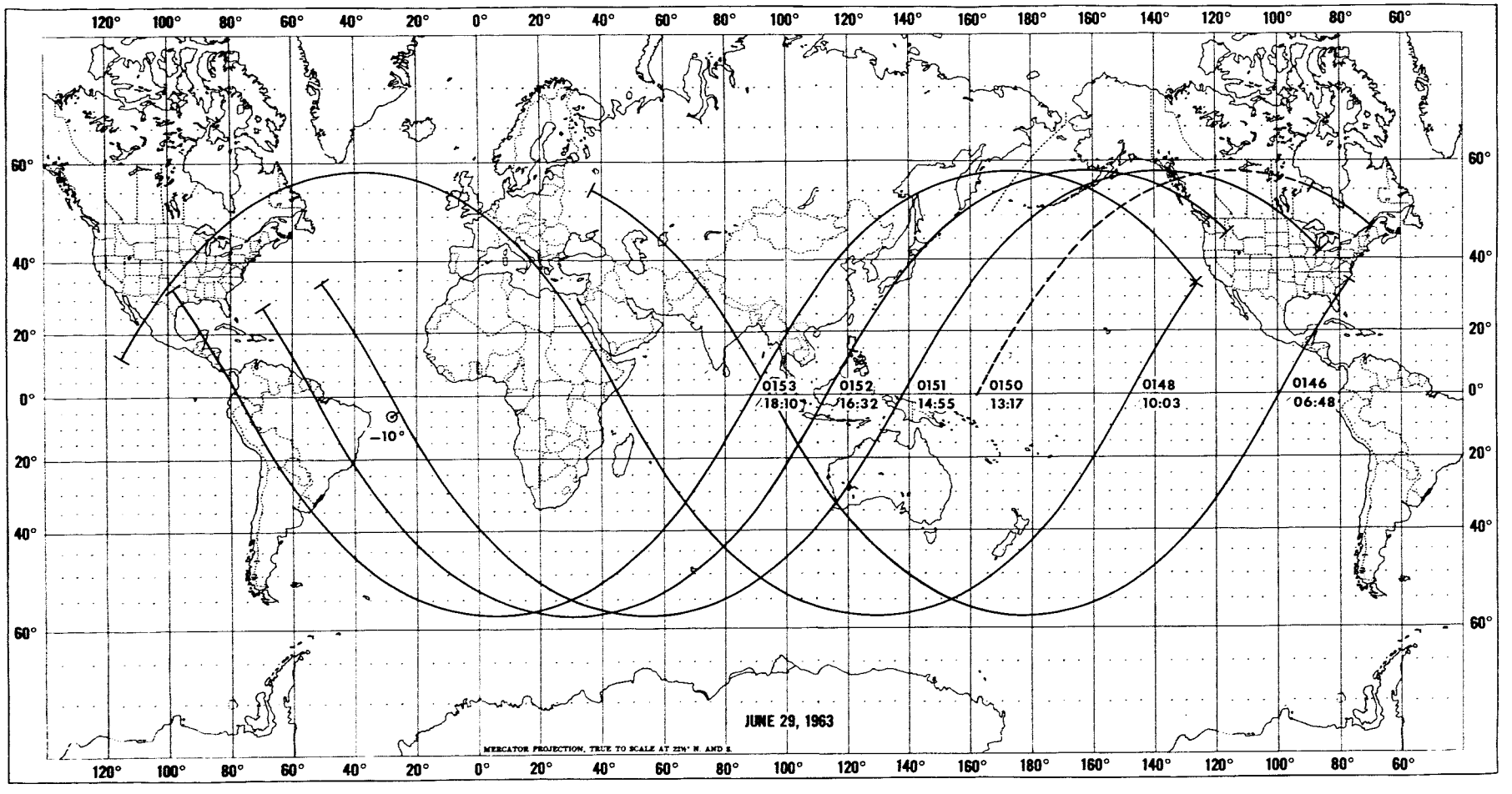
120° 100° 80° 60° 40° 20° 0° 20° 40° 60° 80° 100° 120° 140° 160° 180° 160° 140° 120° 100° 80° 60°
60° 40° 20° 0° 20° 40° 60°
0153
18:10
0152
16:32
0151
14:55
0150
13:17
0148
10:03
0146
06:48
−10°
JUNE 29, 1963
MERCATOR PROJECTION, TRUE TO SCALE AT 22½° N. AND S.

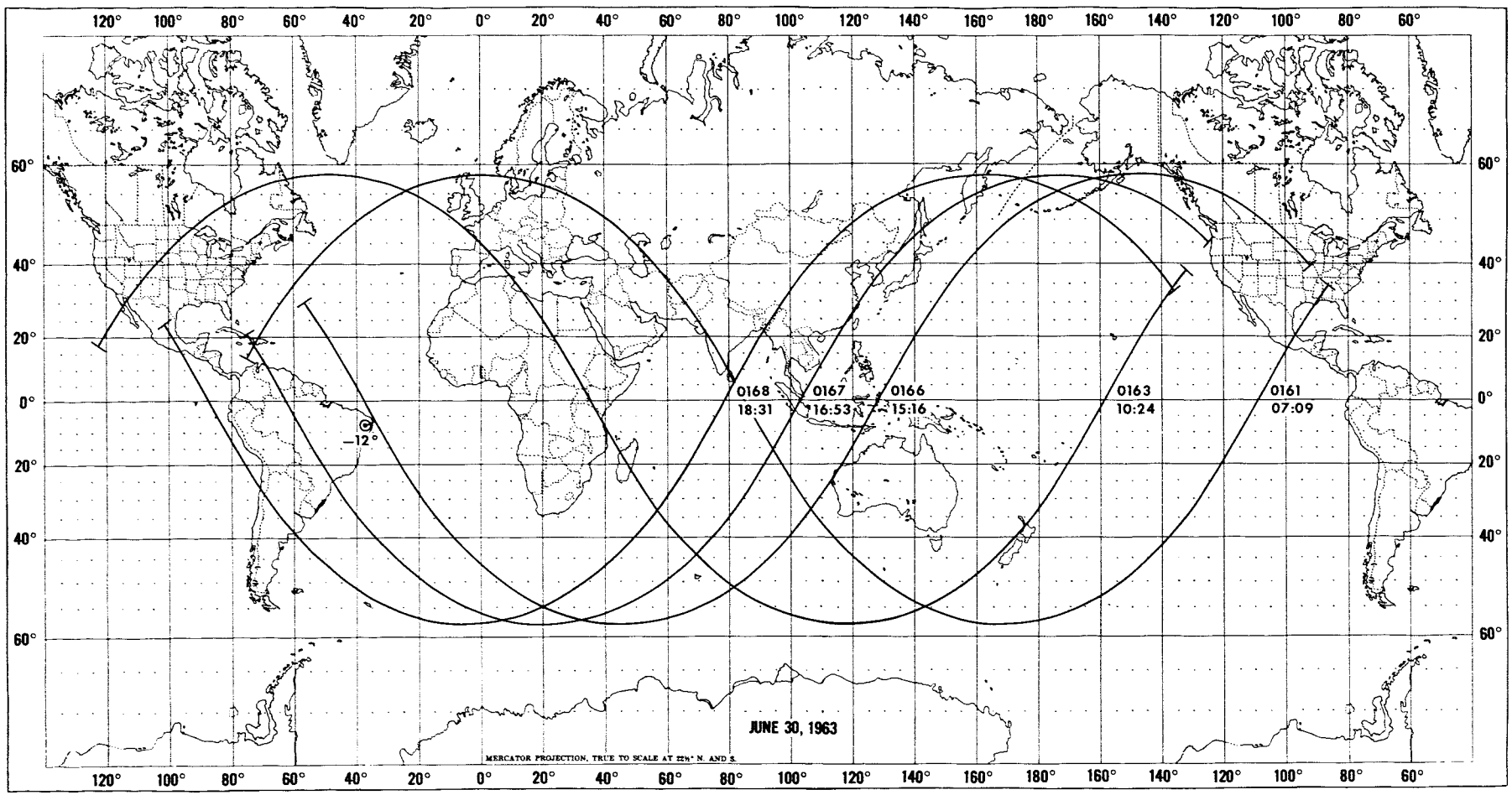
0168
18:31
0167
16:53
0166
15:16
0163
10:24
0161
07:09
−12°
JUNE 30, 1963
MERCATOR PROJECTION, TRUE TO SCALE AT 22½° N. AND S.

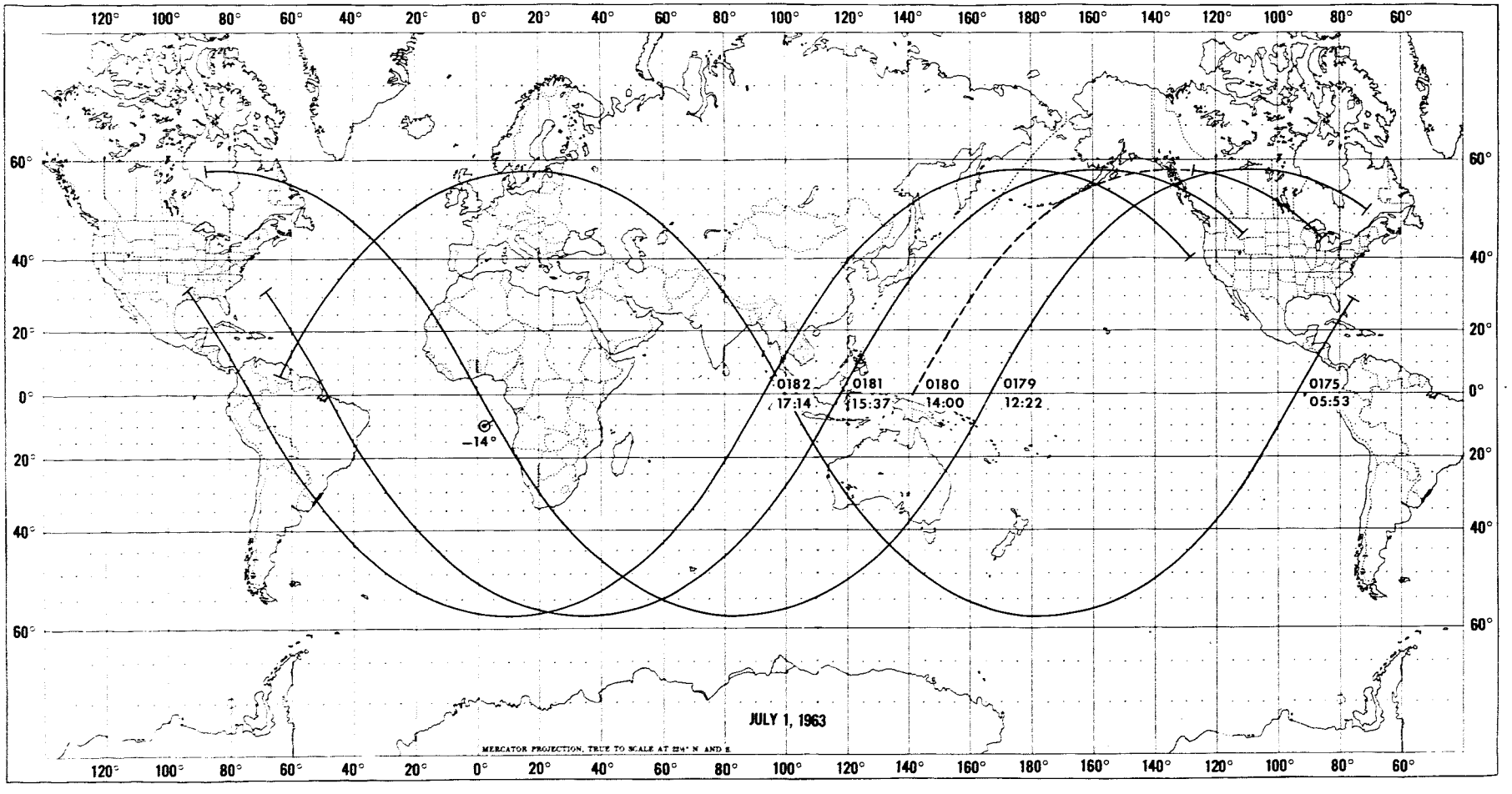
120° 100° 80° 60° 40° 20° 0° 20° 40° 60° 80° 100° 120° 140° 160° 180° 160° 140° 120° 100° 80° 60°
60° 40° 20° 0° 20° 40° 60°
0182
17:14
0181
15:37
0180
14:00
0179
12:22
0175
05:53
−14°
JULY 1, 1963
MERCATOR PROJECTION, TRUE TO SCALE AT 22½° N AND S

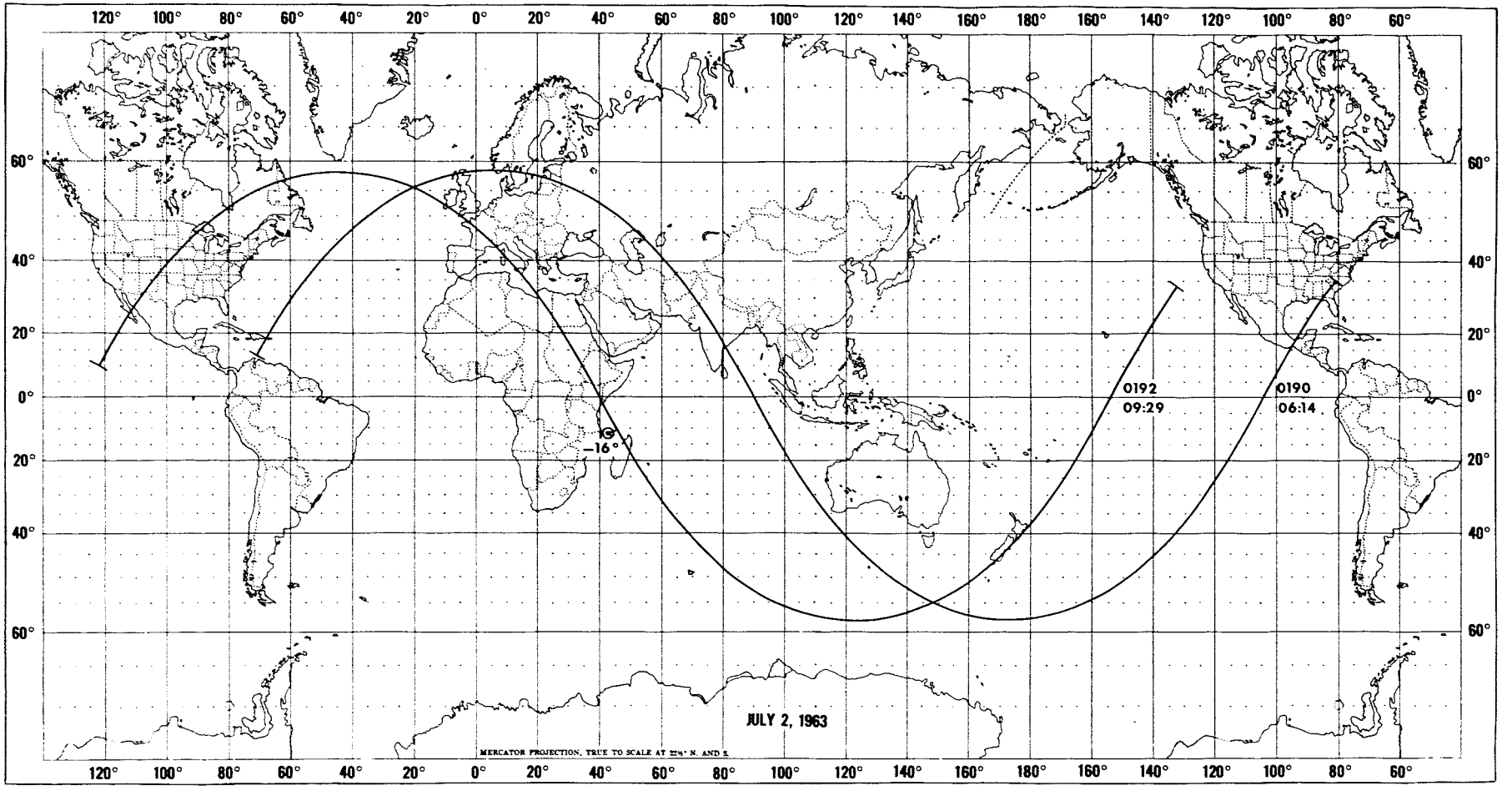
120° 100° 80° 60° 40° 20° 0° 20° 40° 60° 80° 100° 120° 140° 160° 180° 160° 140° 120° 100° 80° 60°
60° 40° 20° 0° 20° 40° 60°
0192
09:29
0190
06:14
−16°
JULY 2, 1963
MERCATOR PROJECTION, TRUE TO SCALE AT 22½° N. AND S.

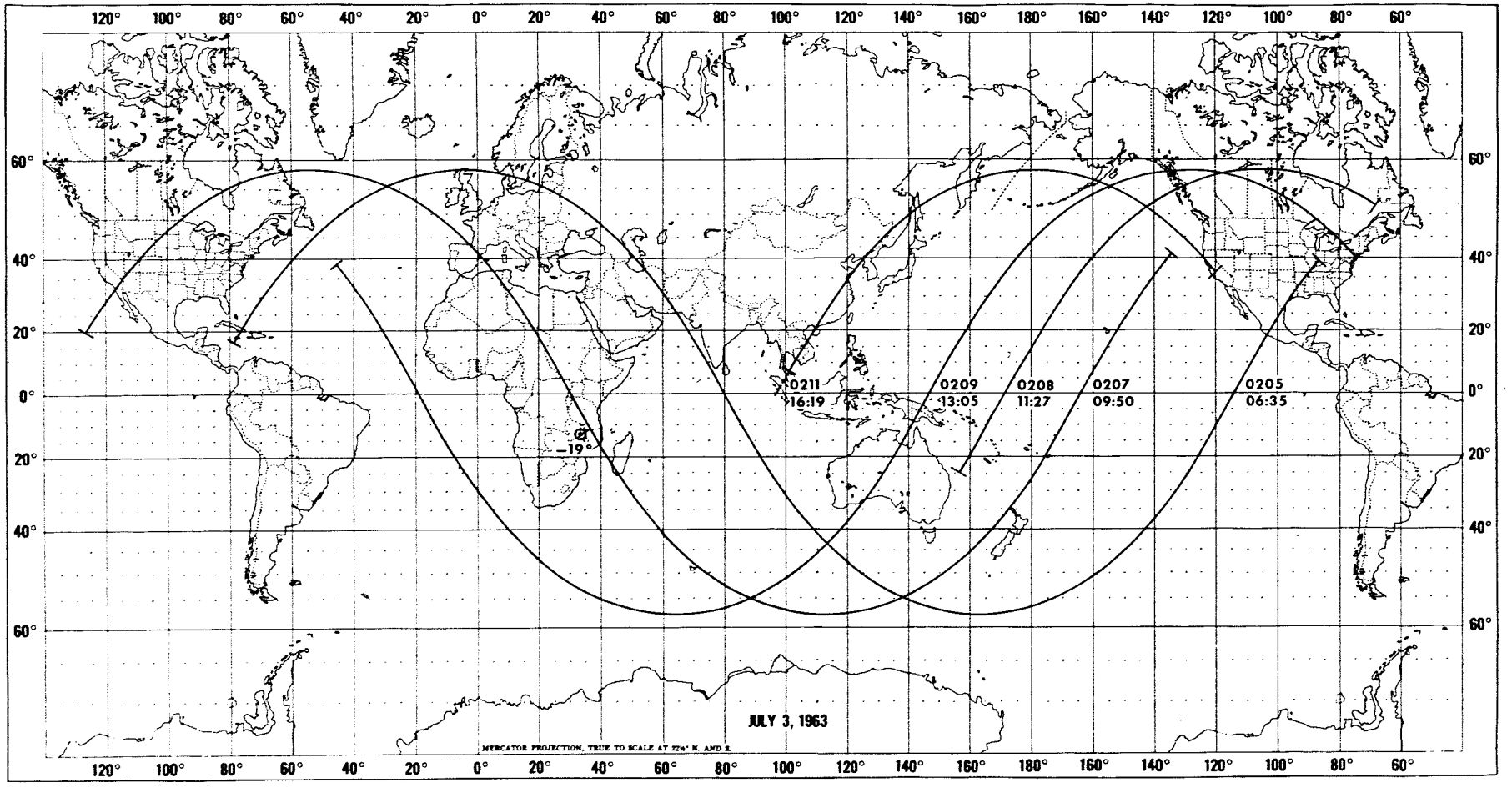
120° 100° 80° 60° 40° 20° 0° 20° 40° 60° 80° 100° 120° 140° 160° 180° 160° 140° 120° 100° 80° 60°
60° 40° 20° 0° 20° 40° 60°
0211
16:19
0209
13:05
0208
11:27
0207
09:50
0205
06:35
-19°
JULY 3, 1963
MERCATOR PROJECTION, TRUE TO SCALE AT 22½° N. AND S.

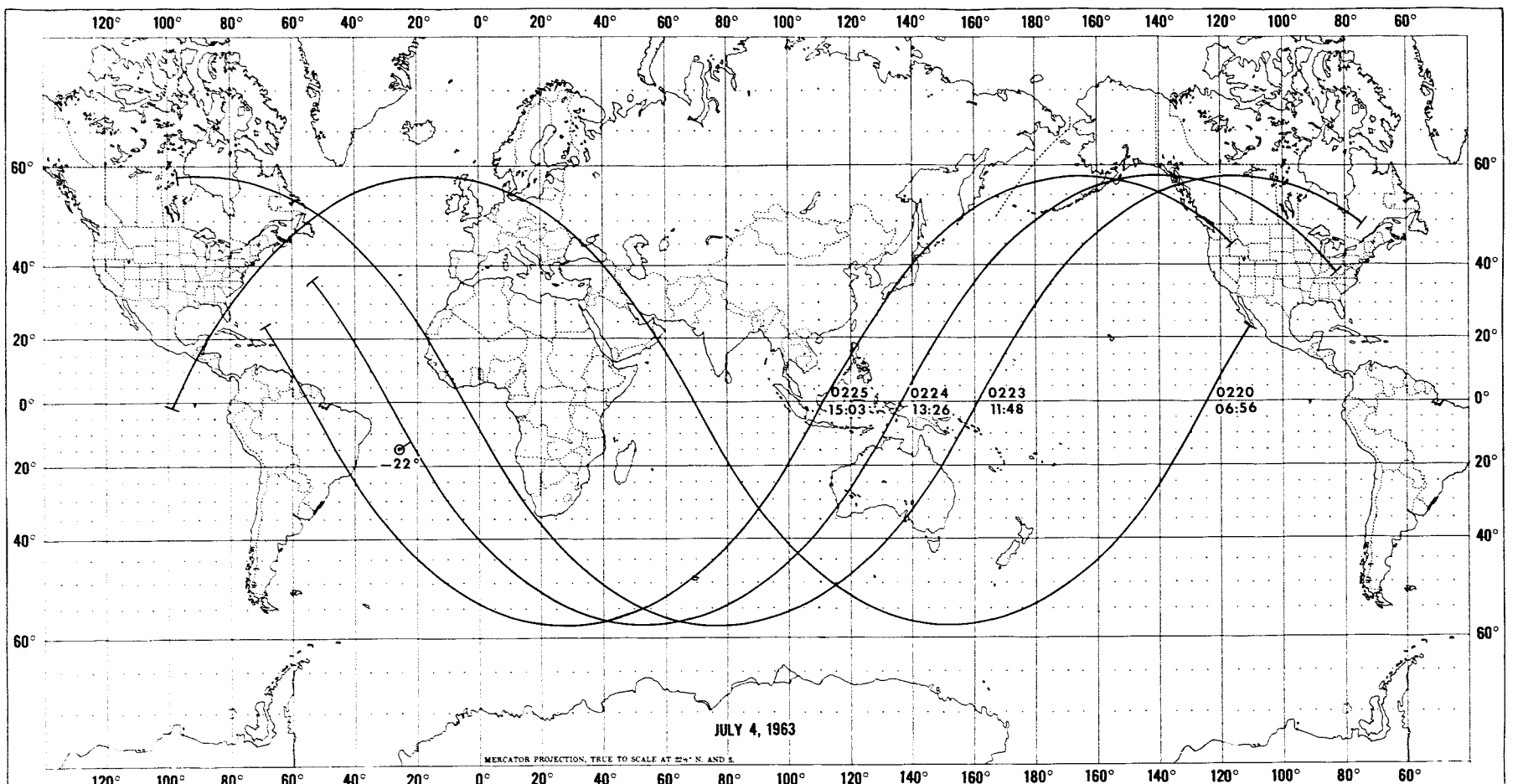
120° 100° 80° 60° 40° 20° 0° 20° 40° 60° 80° 100° 120° 140° 160° 180° 160° 140° 120° 100° 80° 60°
60°
40°
20°
0°
20°
40°
60°
0225
15:03
0224
13:26
0223
11:48
0220
06:56
22°
JULY 4, 1963
MERCATOR PROJECTION, TRUE TO SCALE AT 22° N. AND S.

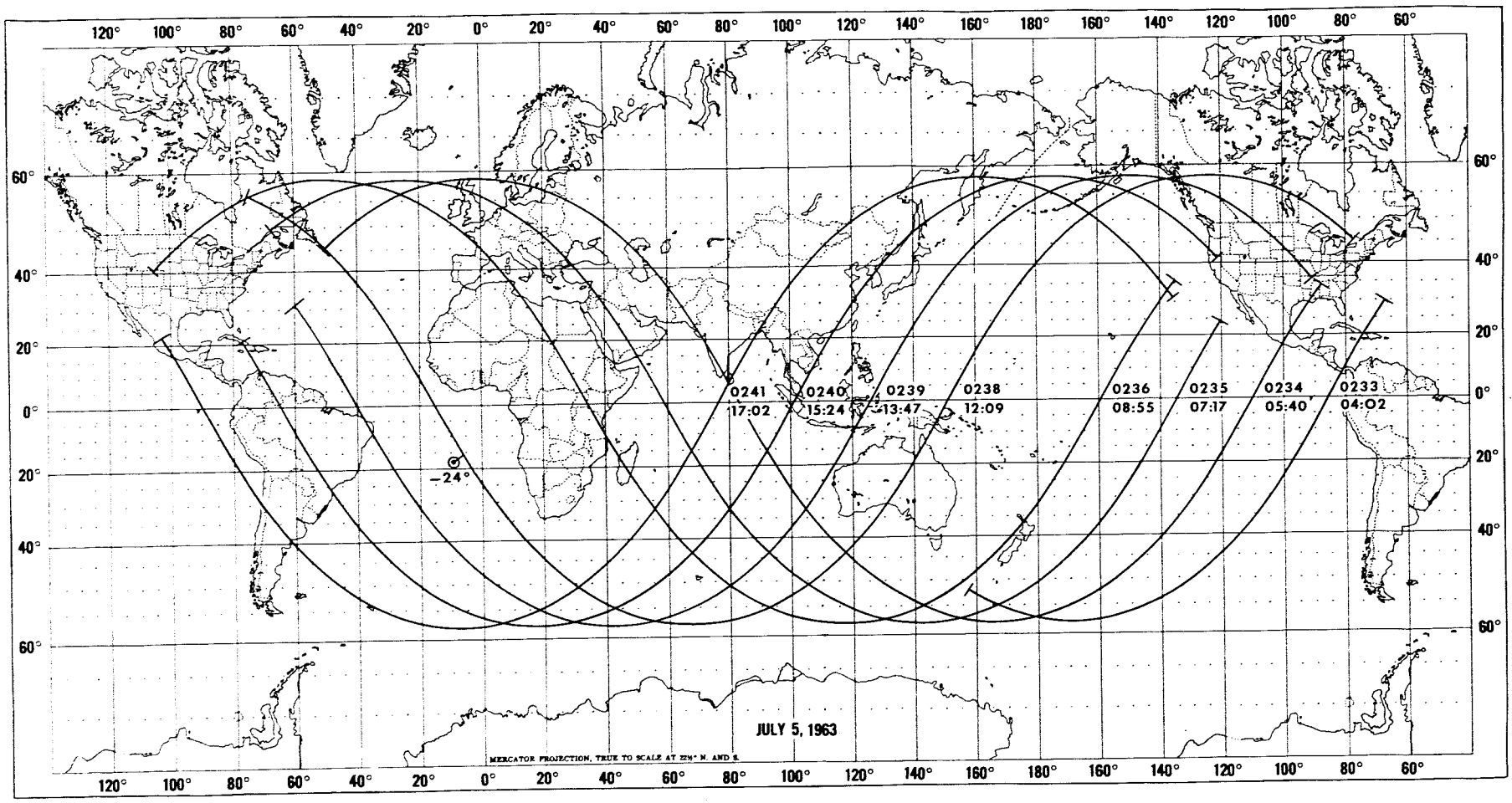
0241
17:02
0240
15:24
0239
13:47
0238
12:09
0236
08:55
0235
07:17
0234
05:40
0233
04:02
-24°
JULY 5, 1963
MERCATOR PROJECTION, TRUE TO SCALE AT 22½° N. AND S.

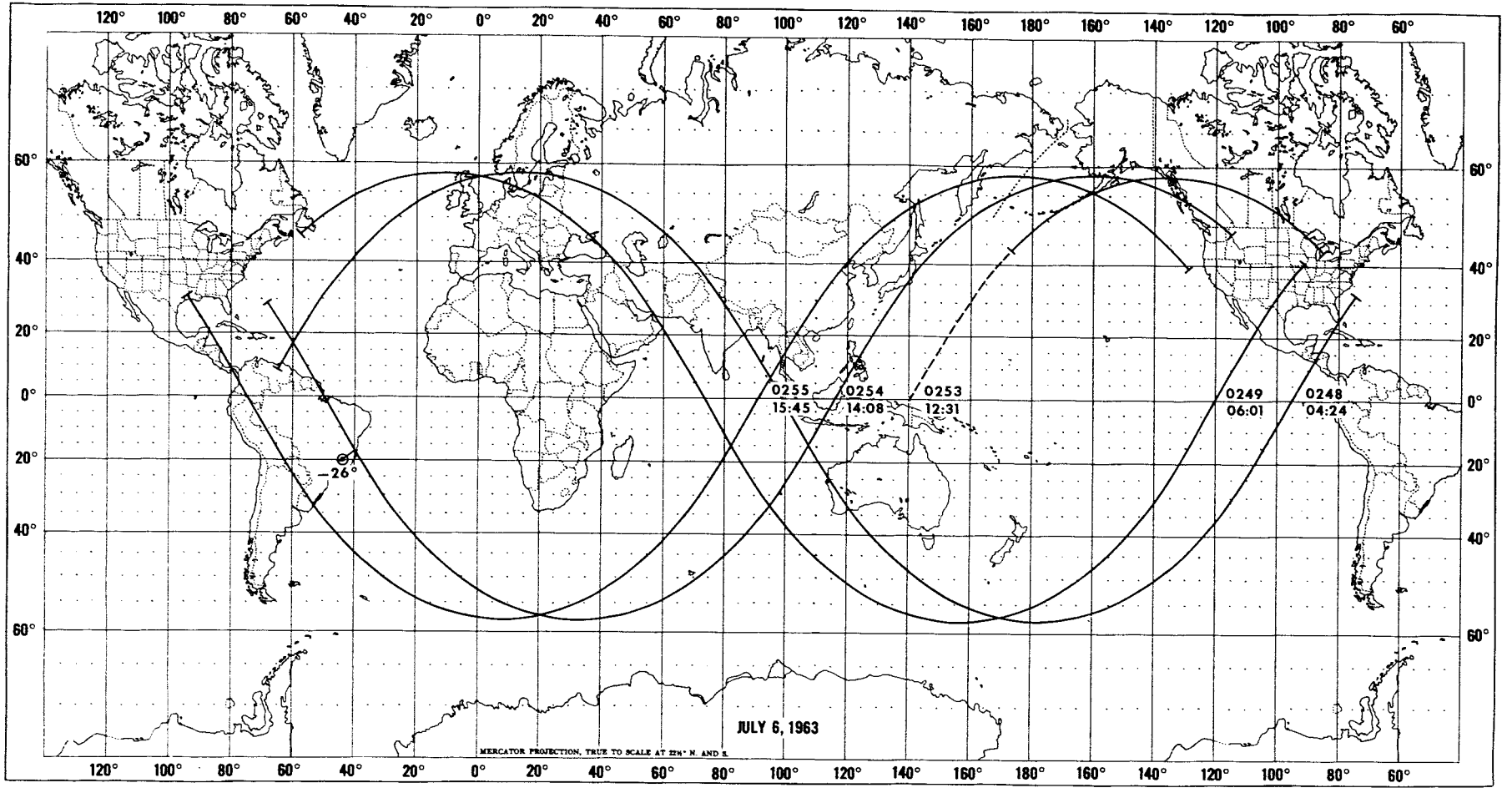
120° 100° 80° 60° 40° 20° 0° 20° 40° 60° 80° 100° 120° 140° 160° 180° 160° 140° 120° 100° 80° 60°
60° 40° 20° 0° 20° 40° 60°
0255
15:45
0254
14:08
0253
12:31
0249
06:01
0248
04:24
-26°
JULY 6, 1963
MERCATOR PROJECTION, TRUE TO SCALE AT 22½° N. AND S.

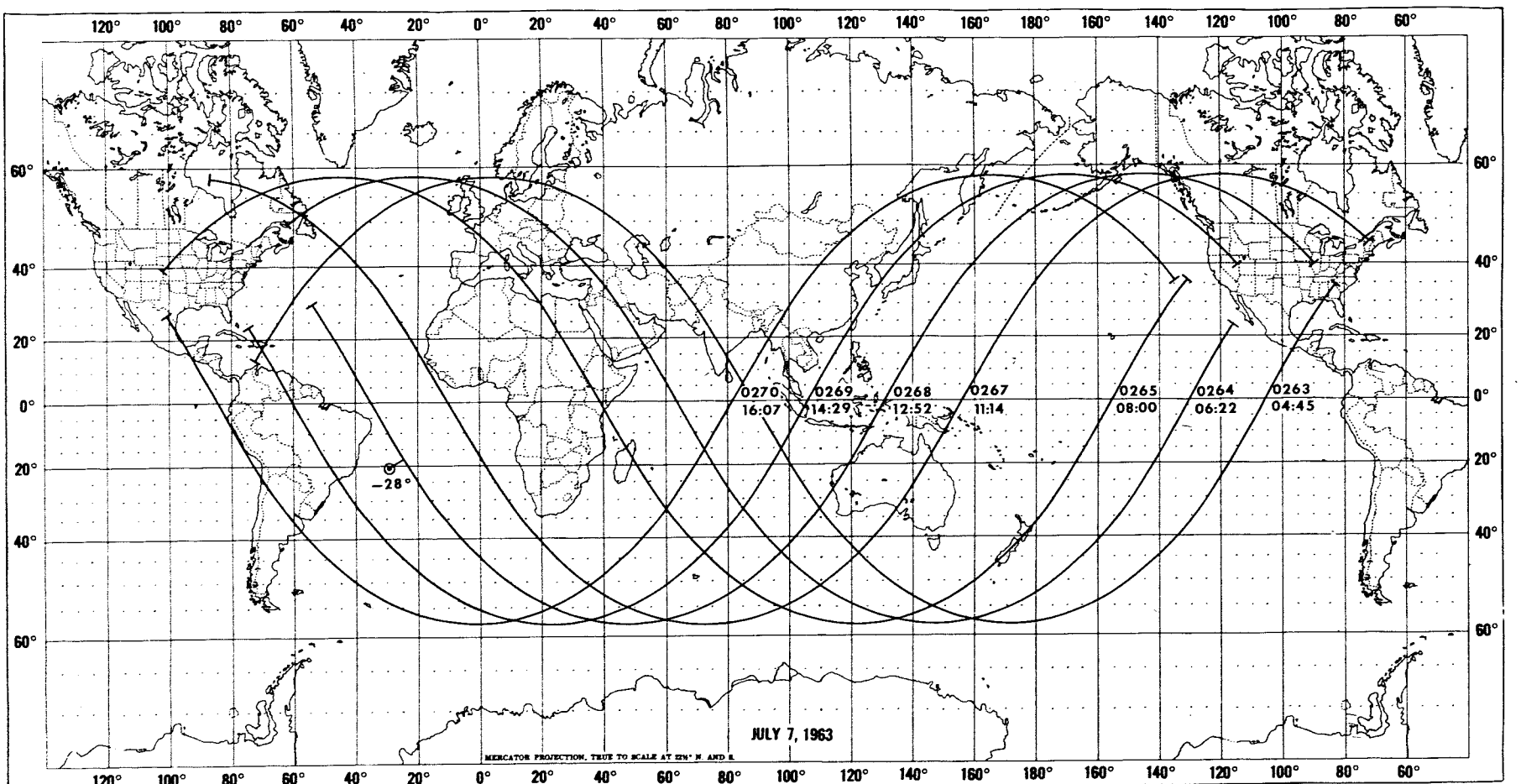
0270
16:07
0269
14:29
0268
12:52
0267
11:14
0265
08:00
0264
06:22
0263
04:45
-28°
JULY 7, 1963
MERCATOR PROJECTION, TRUE TO SCALE AT 22½° N AND S

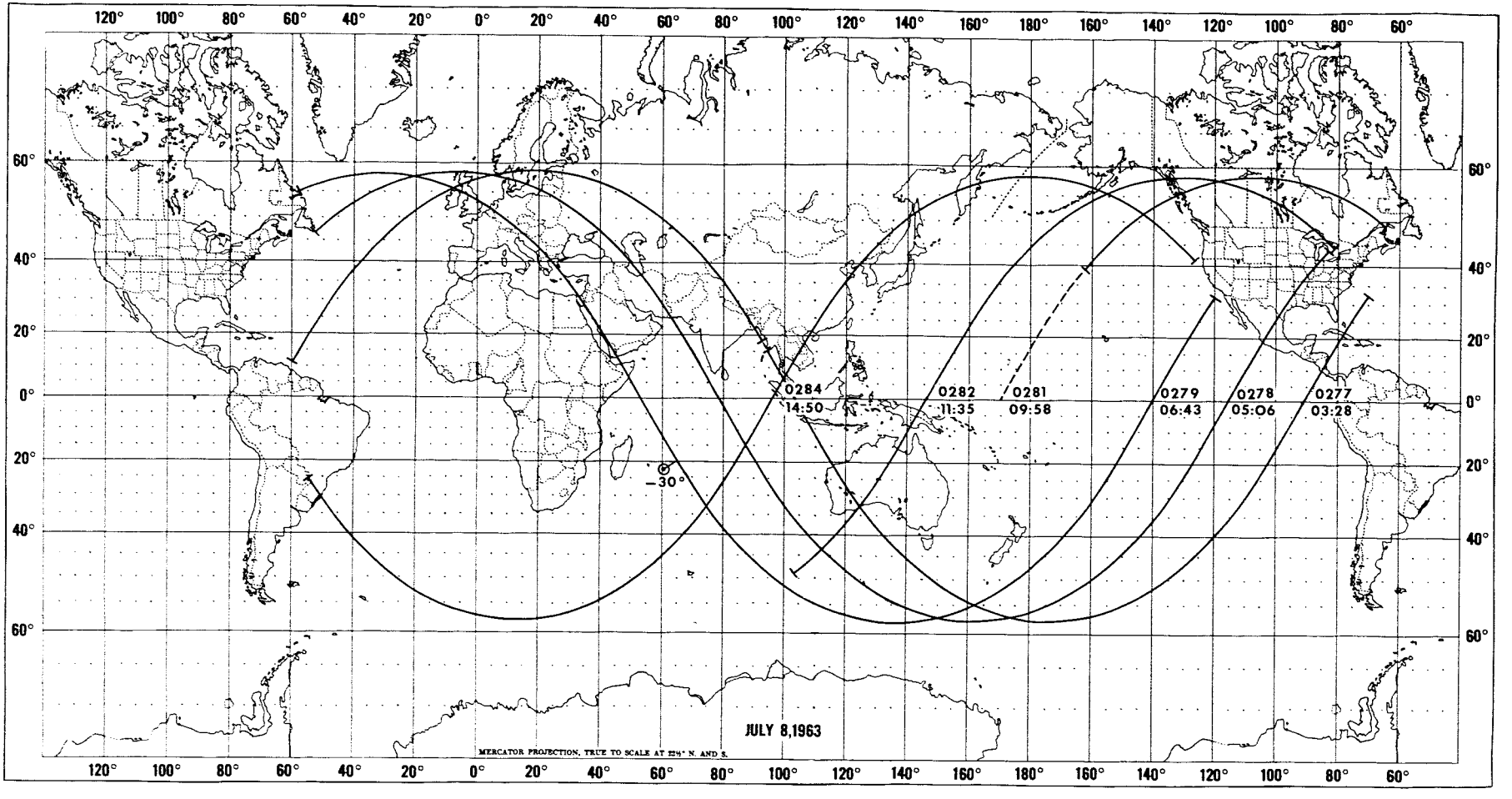
0284
14:50
0282
11:35
0281
09:58
0279
06:43
0278
05:06
0277
03:28
−30°
JULY 8,1963
MERCATOR PROJECTION, TRUE TO SCALE AT 22½° N. AND S.

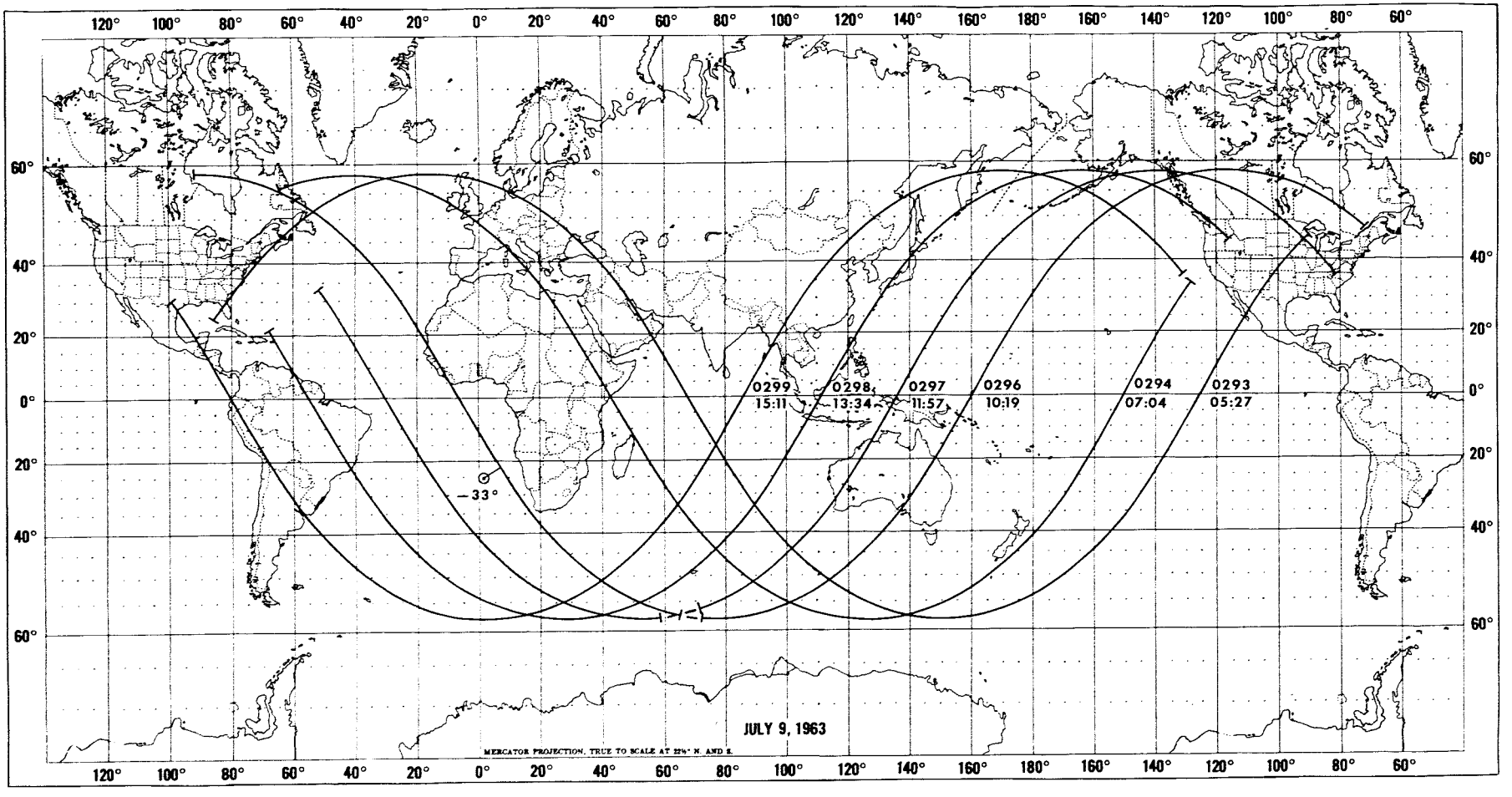
0299
15:11
0298
13:34
0297
11:57
0296
10:19
0294
07:04
0293
05:27
−33°
JULY 9, 1963
MERCATOR PROJECTION, TRUE TO SCALE AT 22½° N. AND S.

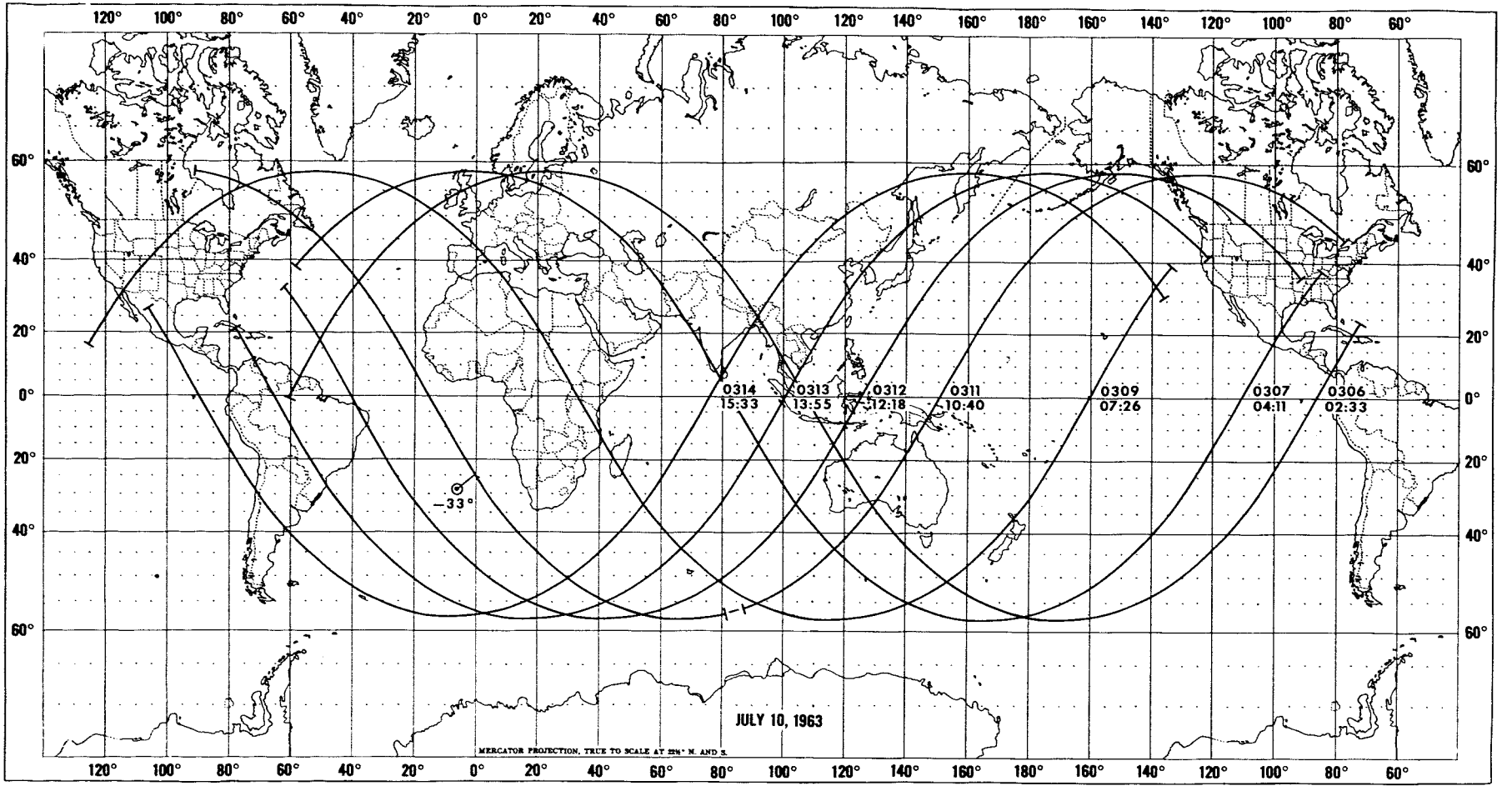
120° 100° 80° 60° 40° 20° 0° 20° 40° 60° 80° 100° 120° 140° 160° 180° 160° 140° 120° 100° 80° 60°
60° 40° 20° 0° 20° 40° 60°
0314 15:33
0313 13:55
0312 12:18
0311 10:40
0309 07:26
0307 04:11
0306 02:33
-33°
JULY 10, 1963
MERCATOR PROJECTION, TRUE TO SCALE AT 22½° N. AND S.

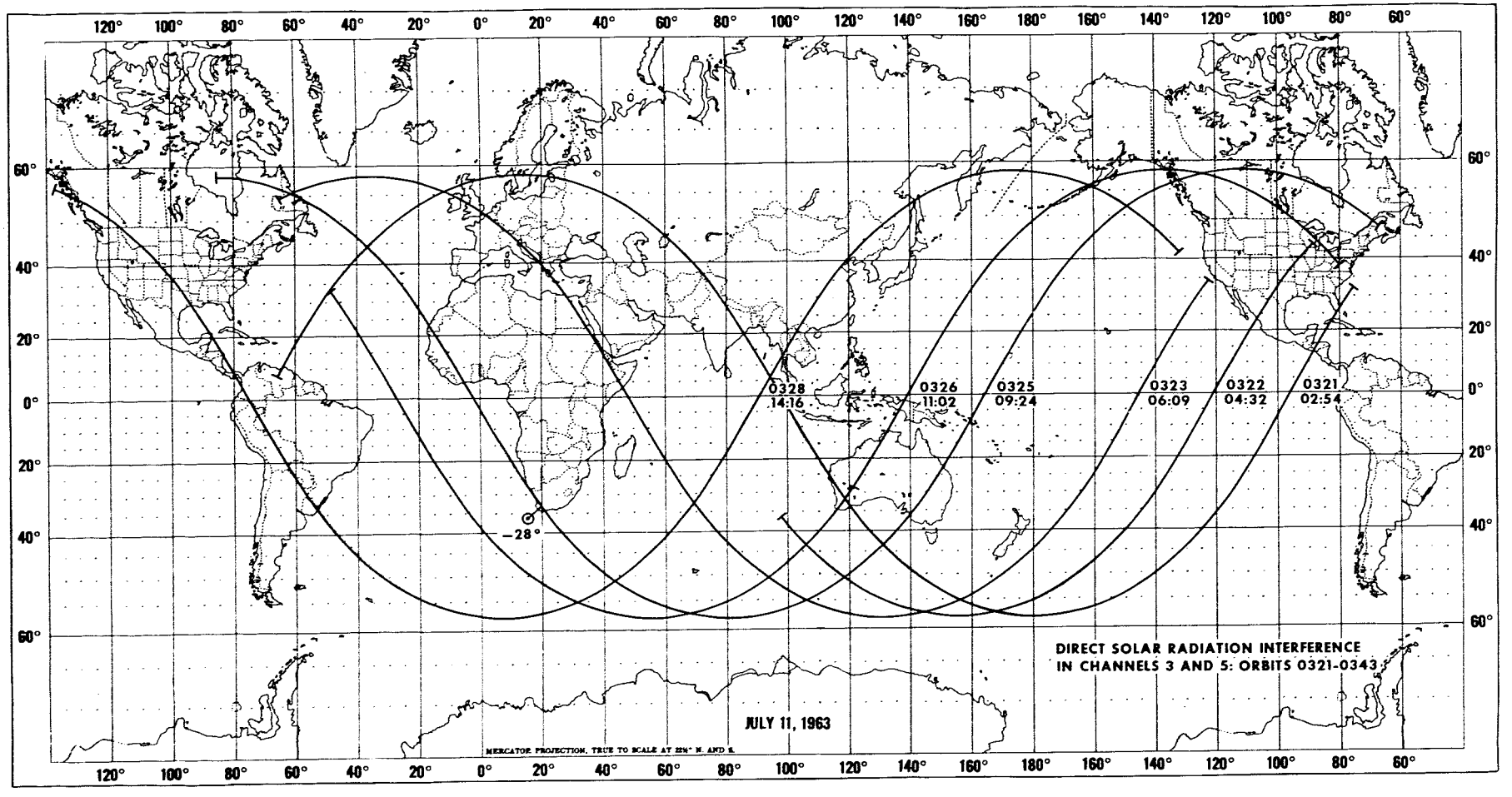
0328
14:16
0326
11:02
0325
09:24
0323
06:09
0322
04:32
0321
02:54
−28°
DIRECT SOLAR RADIATION INTERFERENCE
IN CHANNELS 3 AND 5: ORBITS 0321-0343
JULY 11, 1963
MERCATOR PROJECTION, TRUE TO SCALE AT 22½° N. AND S.

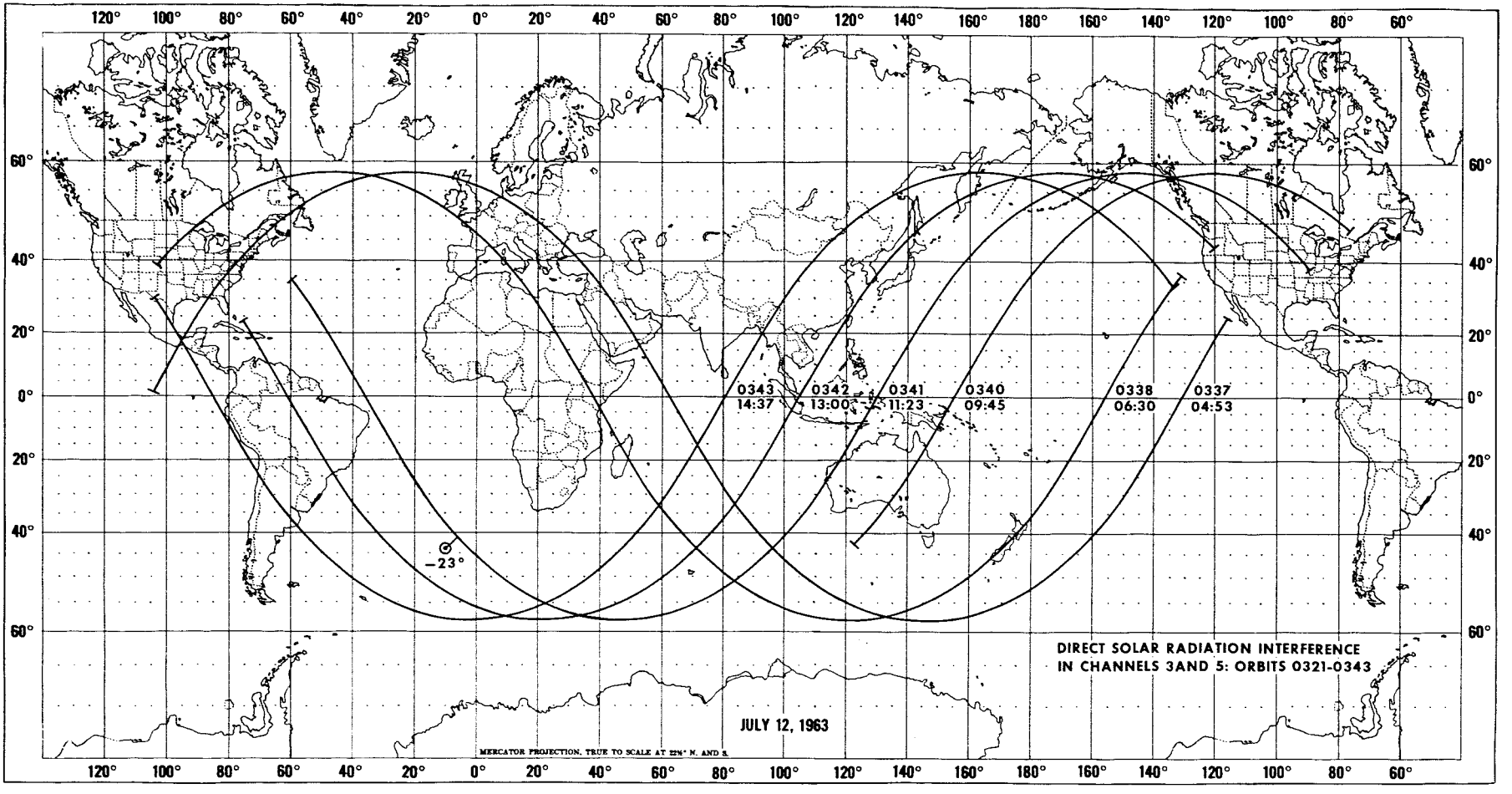
0343
14:37
0342
13:00
0341
11:23
0340
09:45
0338
06:30
0337
04:53
−23°
DIRECT SOLAR RADIATION INTERFERENCE
IN CHANNELS 3AND 5: ORBITS 0321-0343
JULY 12, 1963
MERCATOR PROJECTION, TRUE TO SCALE AT 22½° N. AND S.

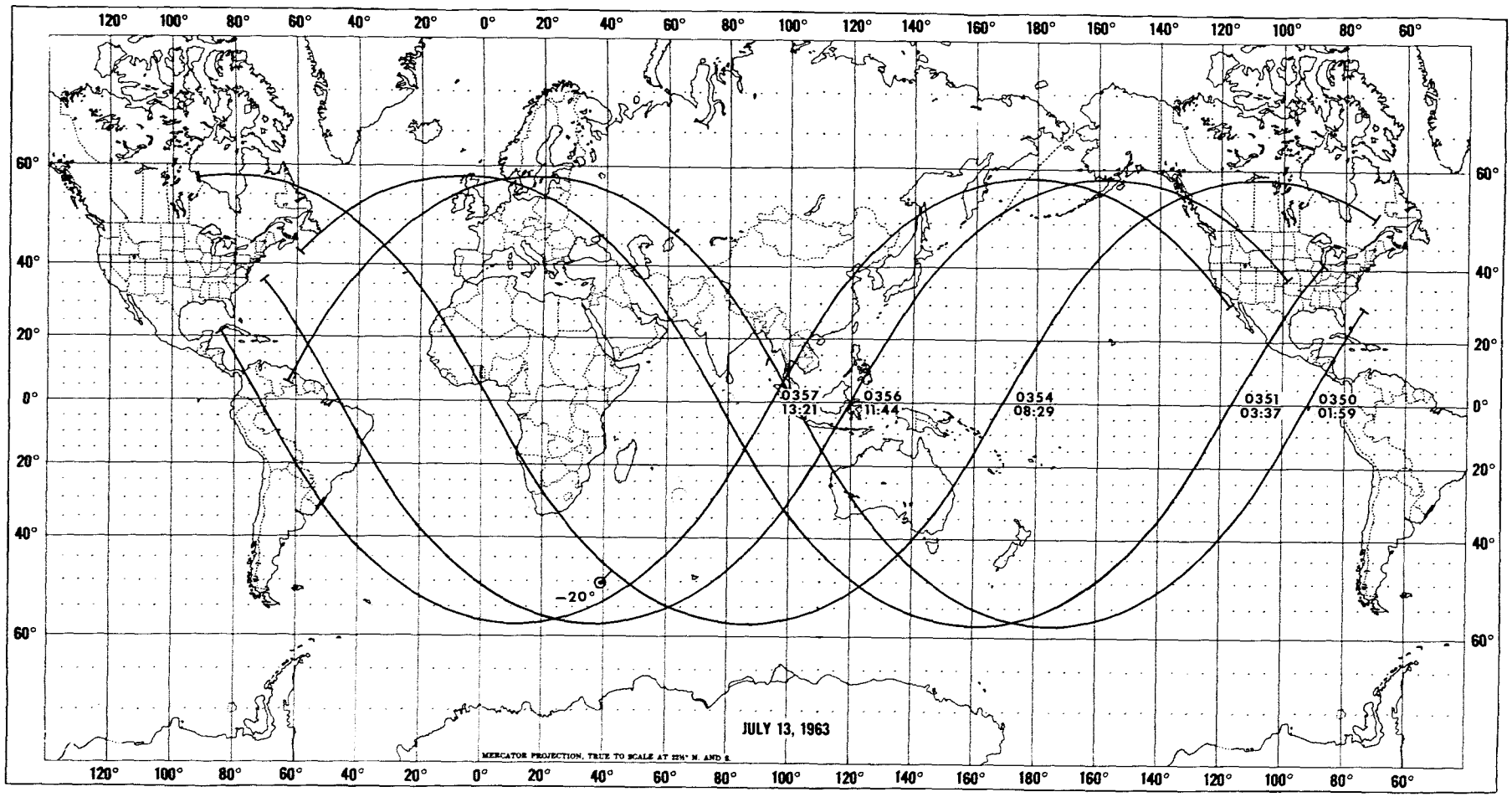
0357
13:21
0356
11:44
0354
08:29
0351
03:37
0350
01:59
-20°
JULY 13, 1963
MERCATOR PROJECTION, TRUE TO SCALE AT 22½° N. AND S.

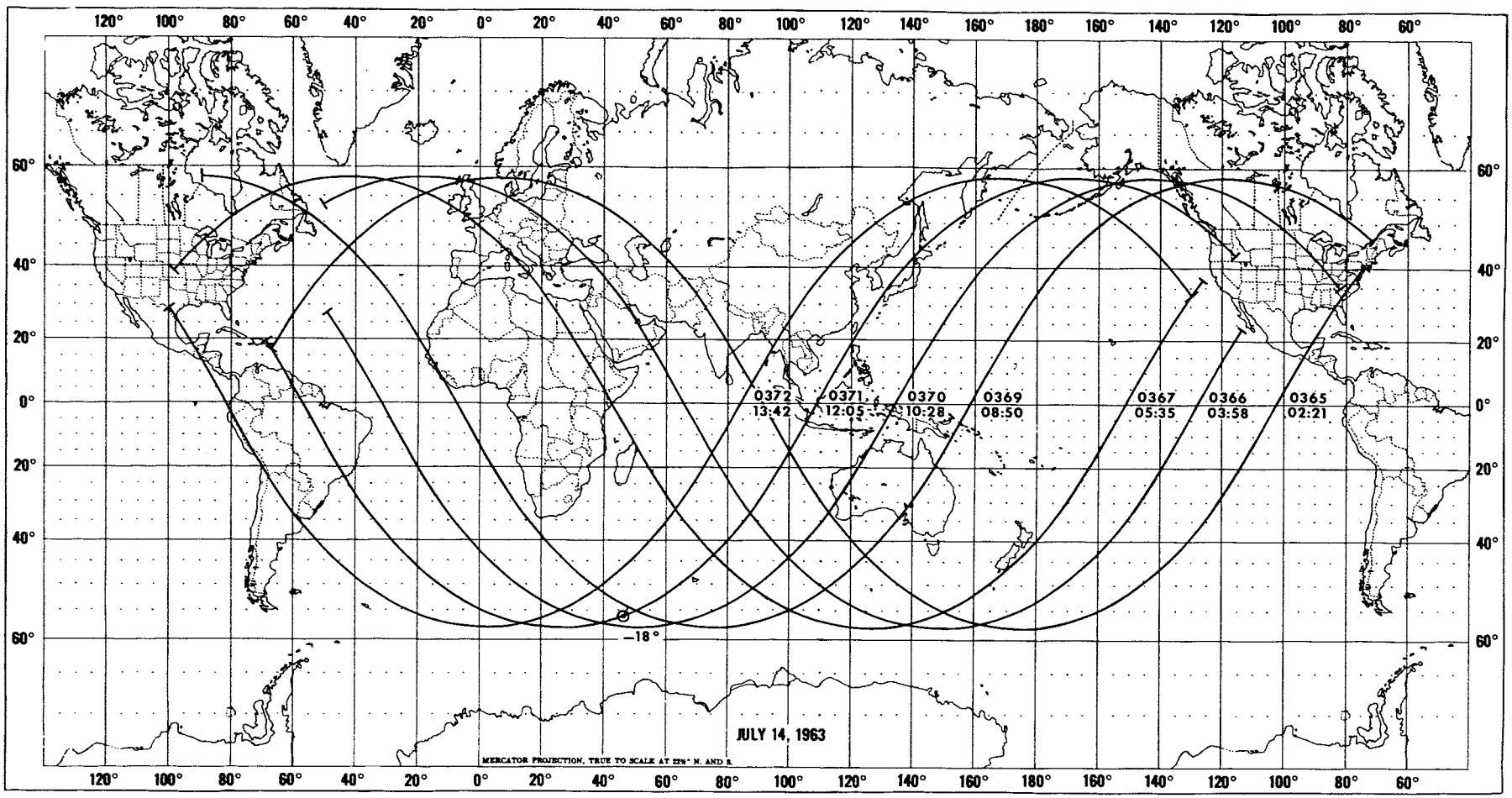
0372
13:42
0371
12:05
0370
10:28
0369
08:50
0367
05:35
0366
03:58
0365
02:21
−18°
JULY 14, 1963
MERCATOR PROJECTION, TRUE TO SCALE AT 22½° N. AND S.

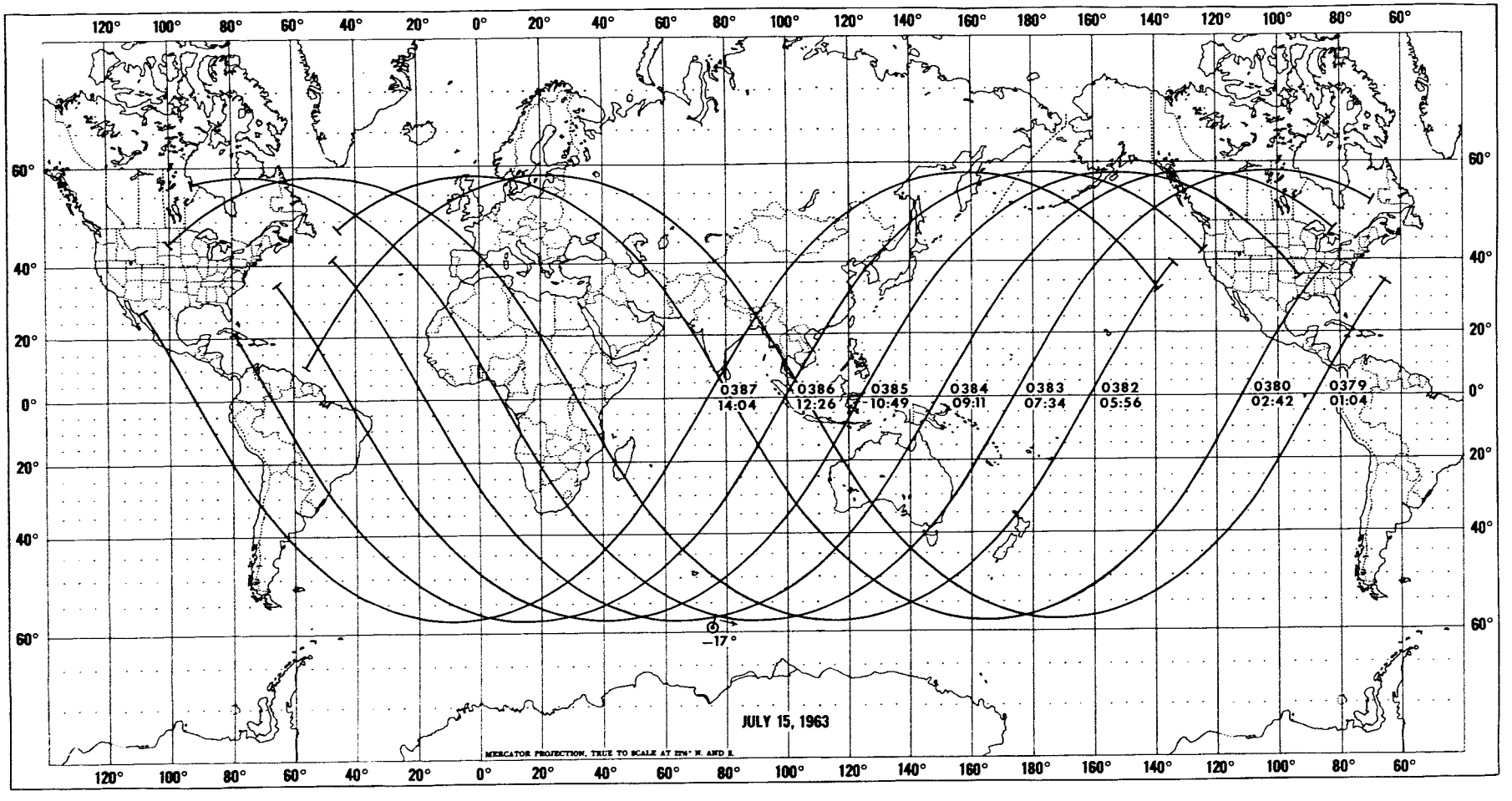
0387
14:04
0386
12:26
0385
10:49
0384
09:11
0383
07:34
0382
05:56
0380
02:42
0379
01:04
−17°
JULY 15, 1963
MERCATOR PROJECTION, TRUE TO SCALE AT 23½° N. AND S.

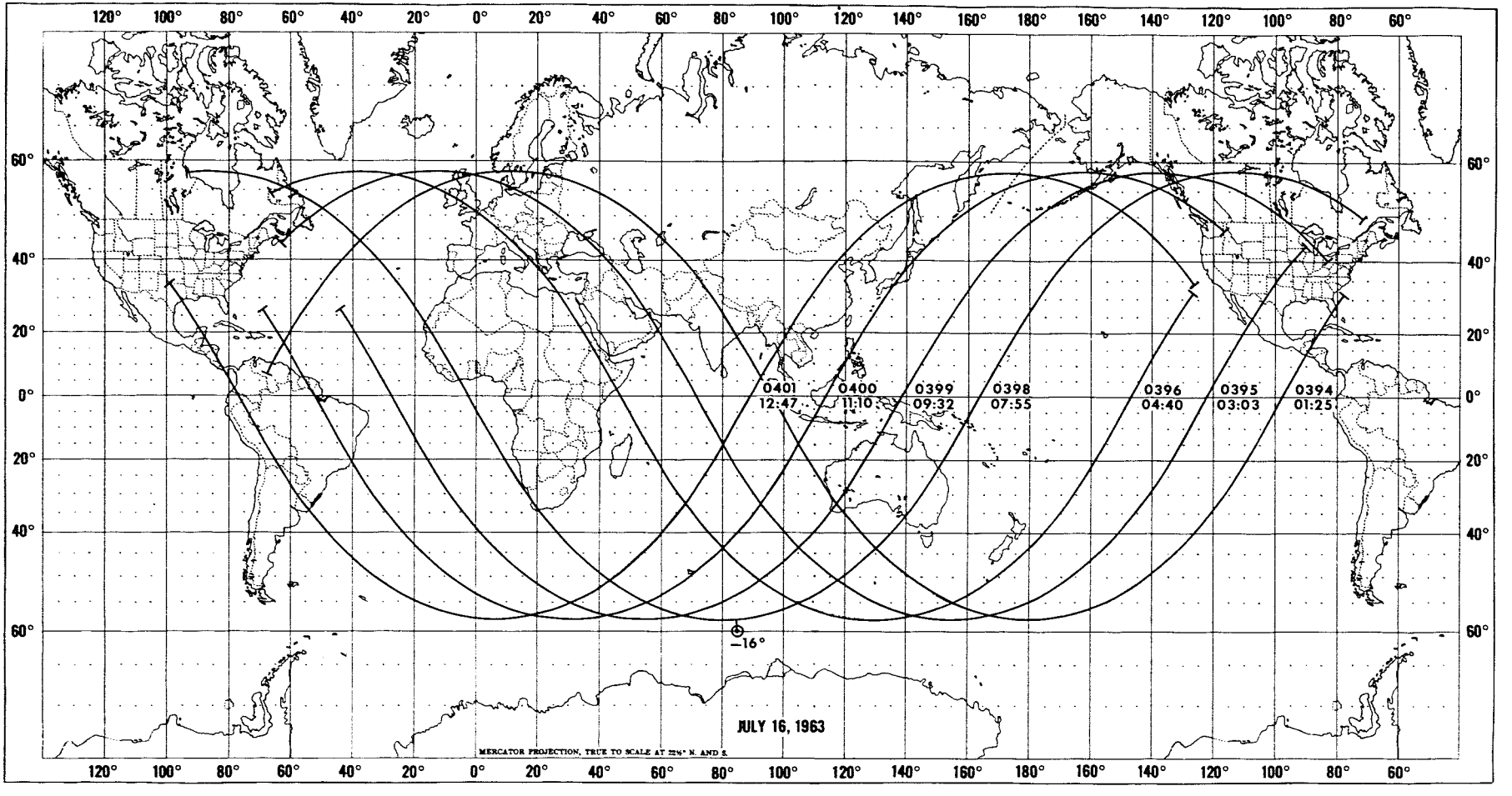
120° 100° 80° 60° 40° 20° 0° 20° 40° 60° 80° 100° 120° 140° 160° 180° 160° 140° 120° 100° 80° 60°
60° 40° 20° 0° 20° 40° 60°
0401 12:47
0400 11:10
0399 09:32
0398 07:55
0396 04:40
0395 03:03
0394 01:25
−16°
JULY 16, 1963
MERCATOR PROJECTION, TRUE TO SCALE AT 22½° N. AND S.

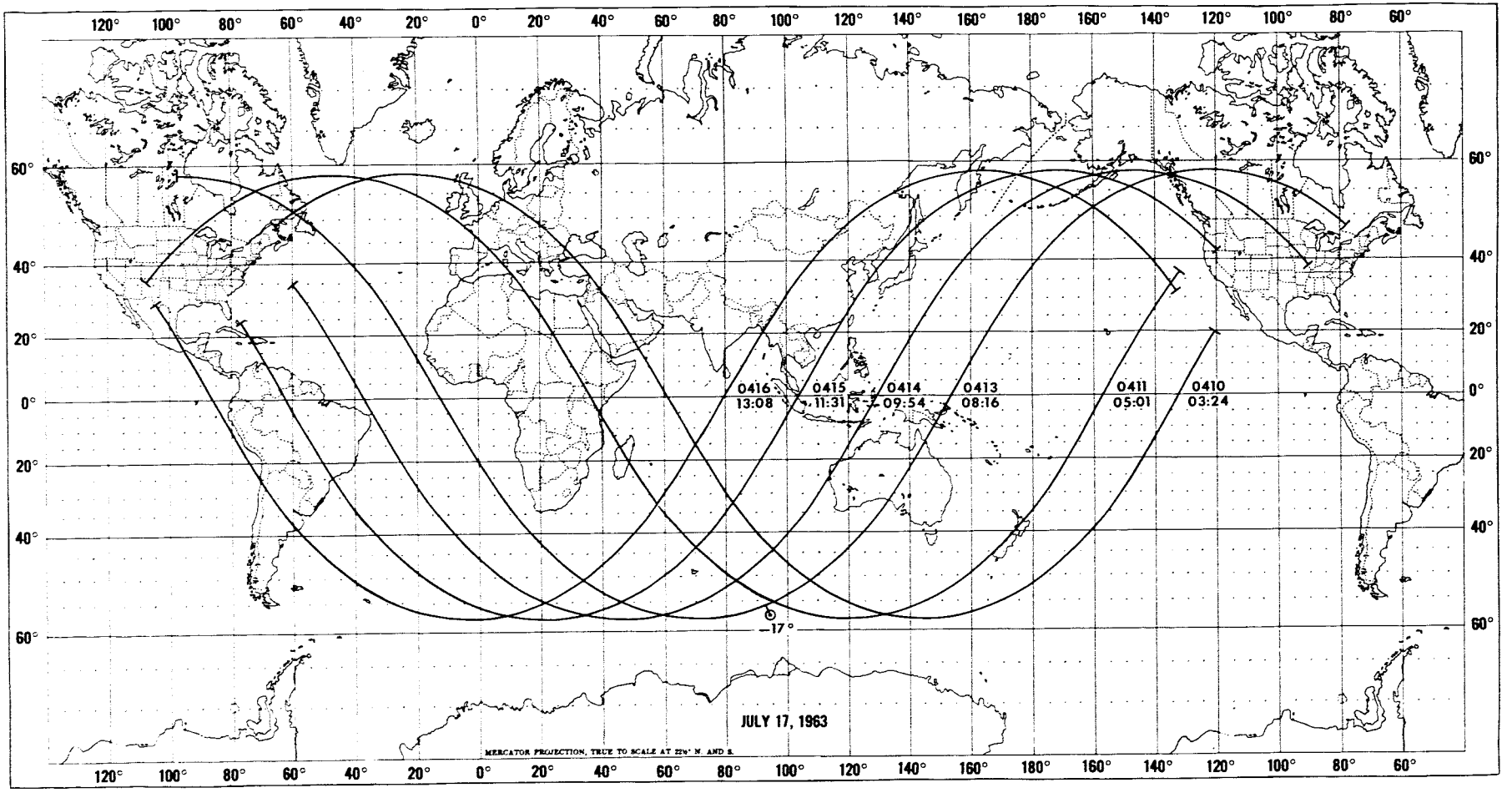
120° 100° 80° 60° 40° 20° 0° 20° 40° 60° 80° 100° 120° 140° 160° 180° 160° 140° 120° 100° 80° 60°
60°
40°
20°
0°
20°
40°
60°
0416
13:08
0415
11:31
0414
09:54
0413
08:16
0411
05:01
0410
03:24
-17°
JULY 17, 1963
MERCATOR PROJECTION, TRUE TO SCALE AT 22½° N. AND S.

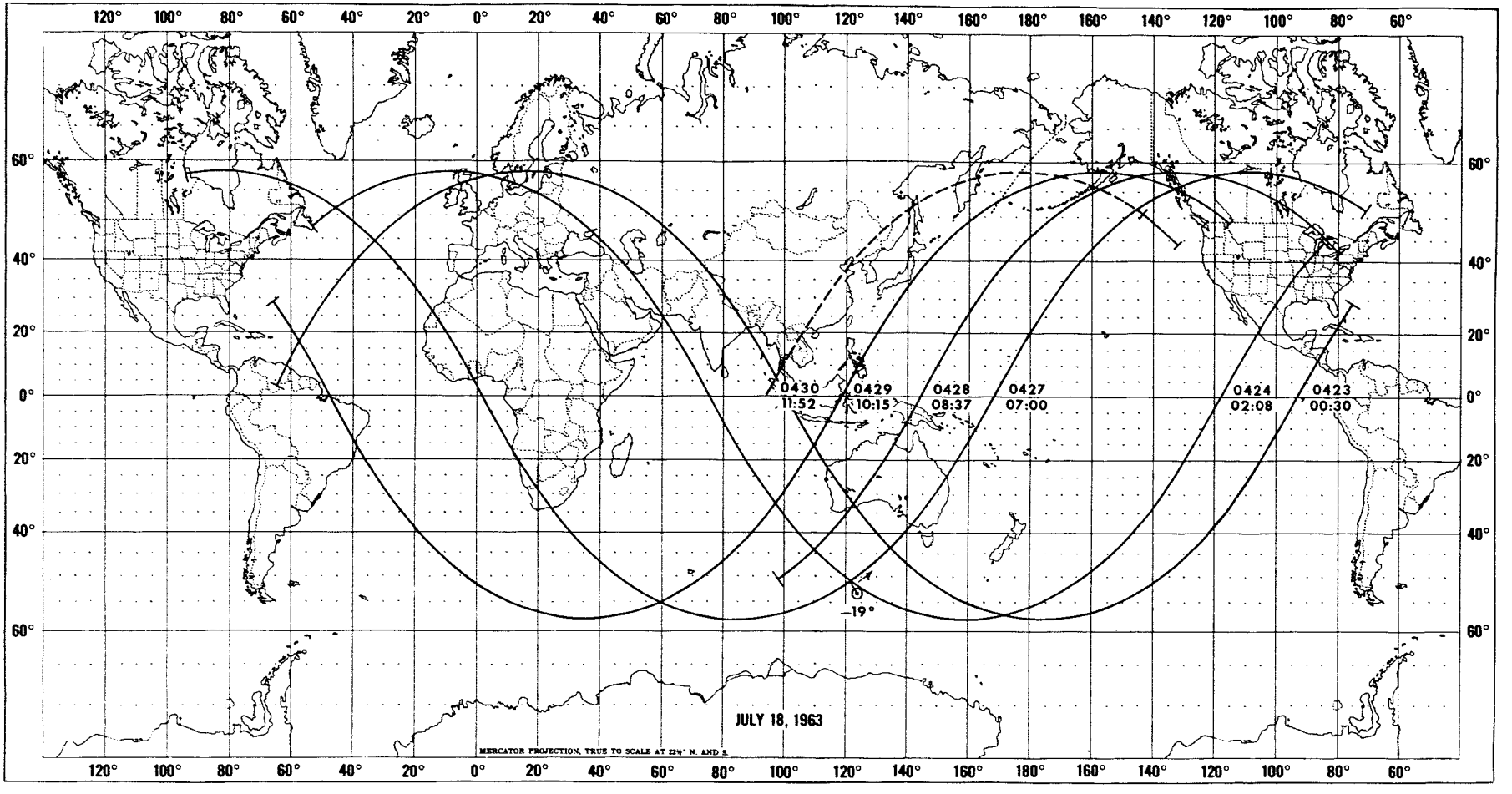
0430
11:52
0429
10:15
0428
08:37
0427
07:00
0424
02:08
0423
00:30
−19°
JULY 18, 1963
MERCATOR PROJECTION, TRUE TO SCALE AT 22½° N. AND S.

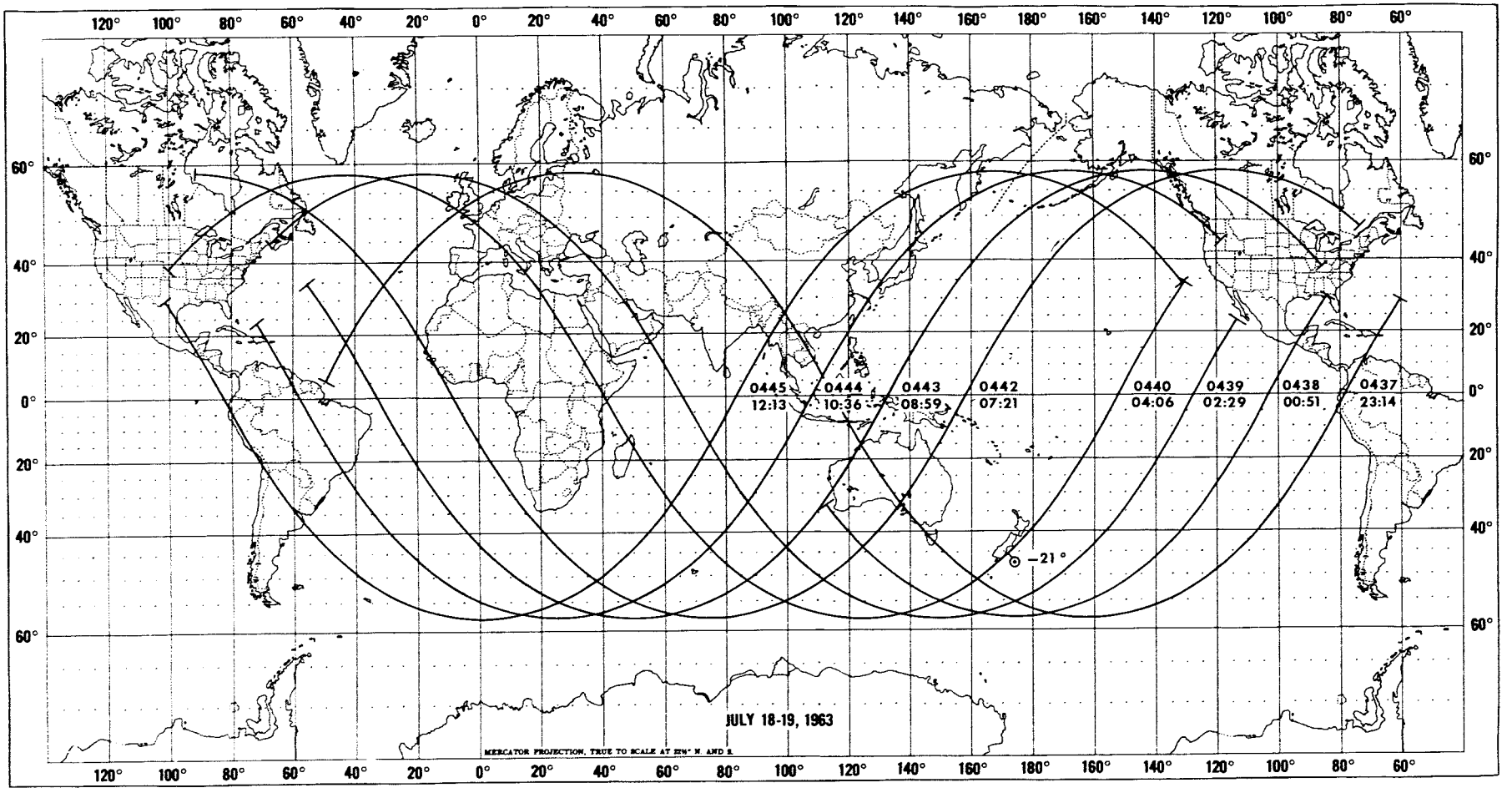
0445
12:13
0444
10:36
0443
08:59
0442
07:21
0440
04:06
0439
02:29
0438
00:51
0437
23:14
−21°
JULY 18-19, 1963
MERCATOR PROJECTION, TRUE TO SCALE AT 25N° N AND S

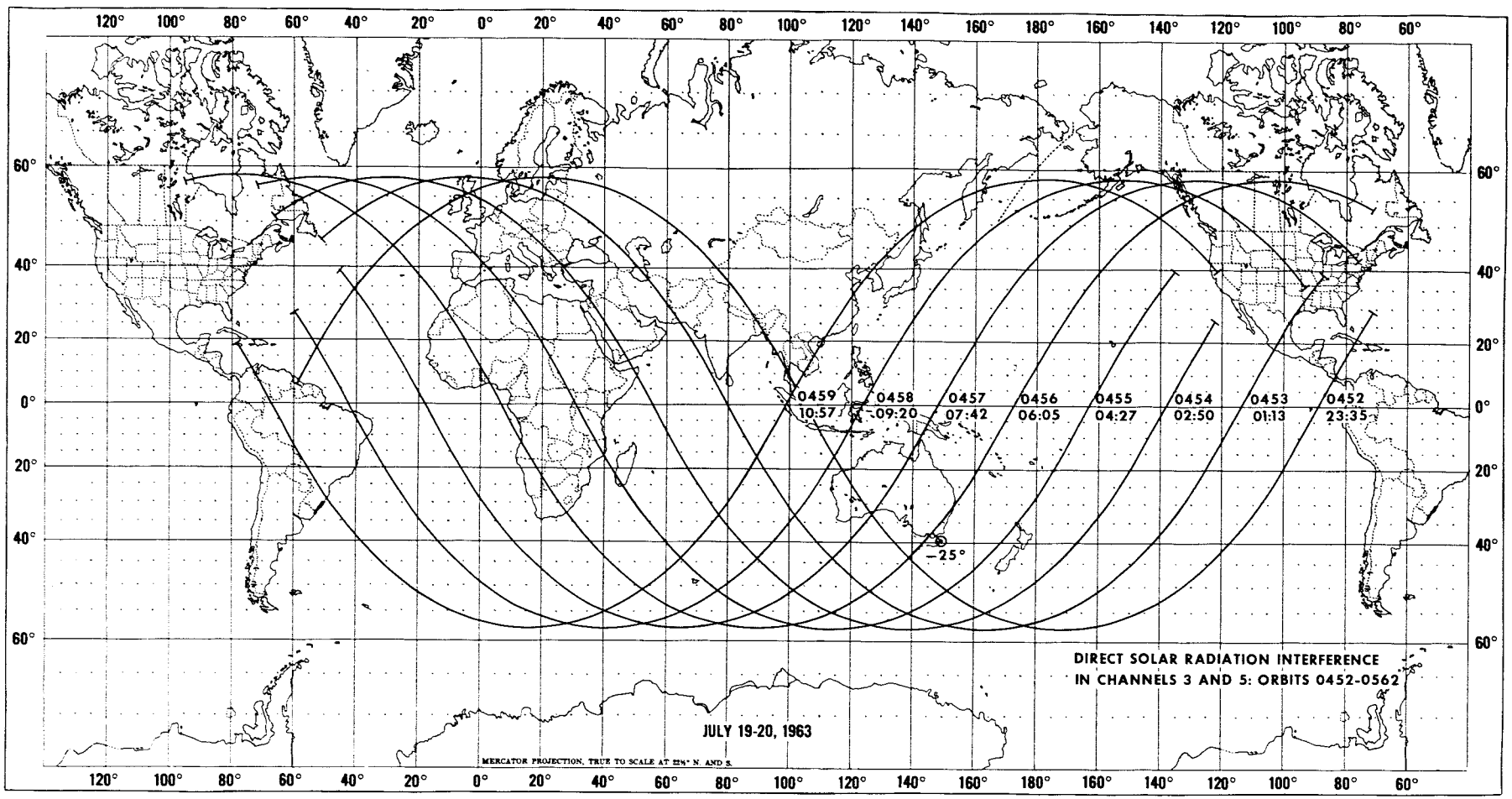
0459
10:57
0458
09:20
0457
07:42
0456
06:05
0455
04:27
0454
02:50
0453
01:13
0452
23:35
−25°
DIRECT SOLAR RADIATION INTERFERENCE
IN CHANNELS 3 AND 5: ORBITS 0452-0562
JULY 19-20, 1963
MERCATOR PROJECTION, TRUE TO SCALE AT 22½° N. AND S.

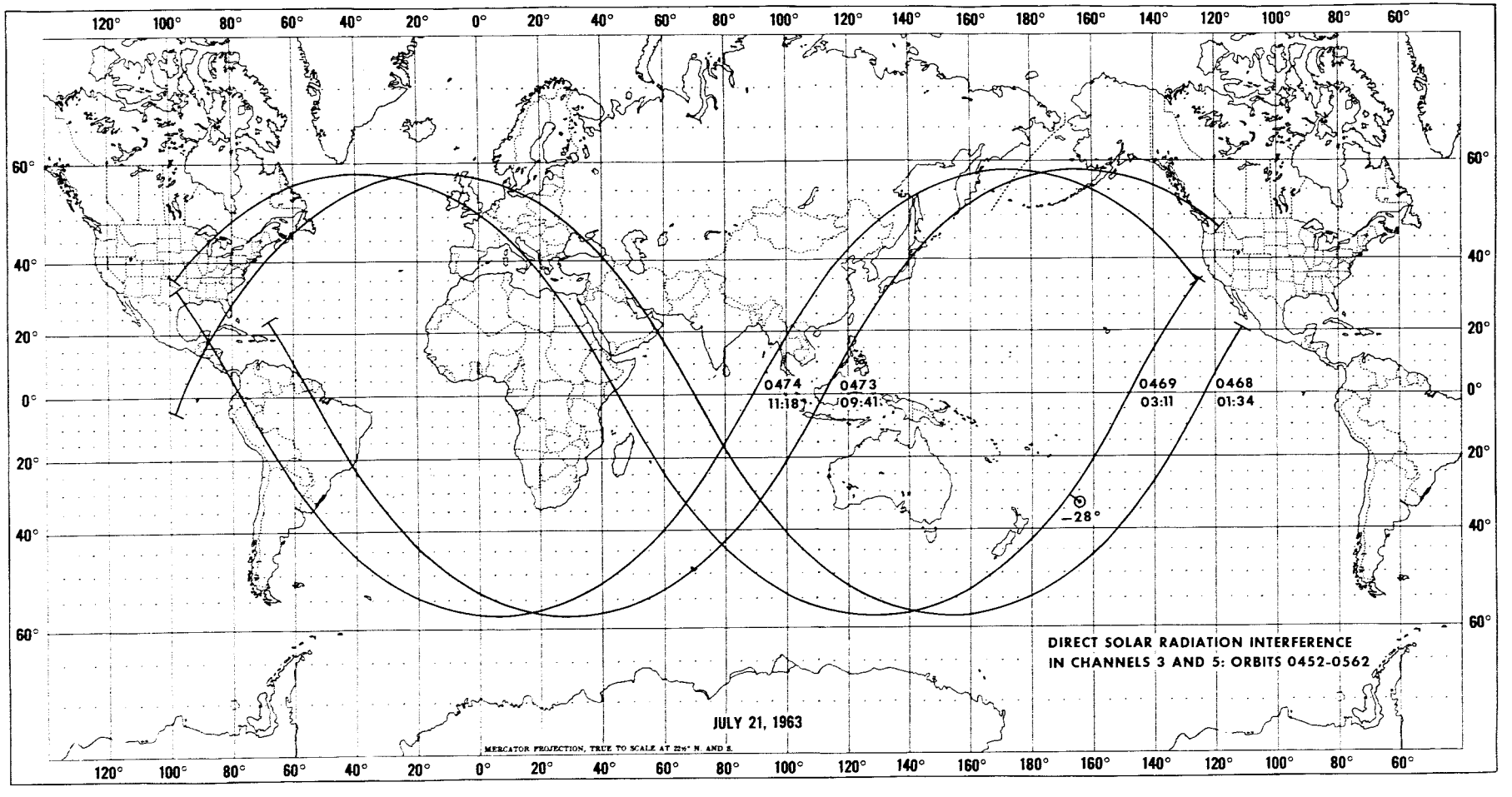
0474
11:18
0473
09:41
0469
03:11
0468
01:34
−28°
DIRECT SOLAR RADIATION INTERFERENCE
IN CHANNELS 3 AND 5: ORBITS 0452-0562
JULY 21, 1963
MERCATOR PROJECTION, TRUE TO SCALE AT 22½° N. AND S.

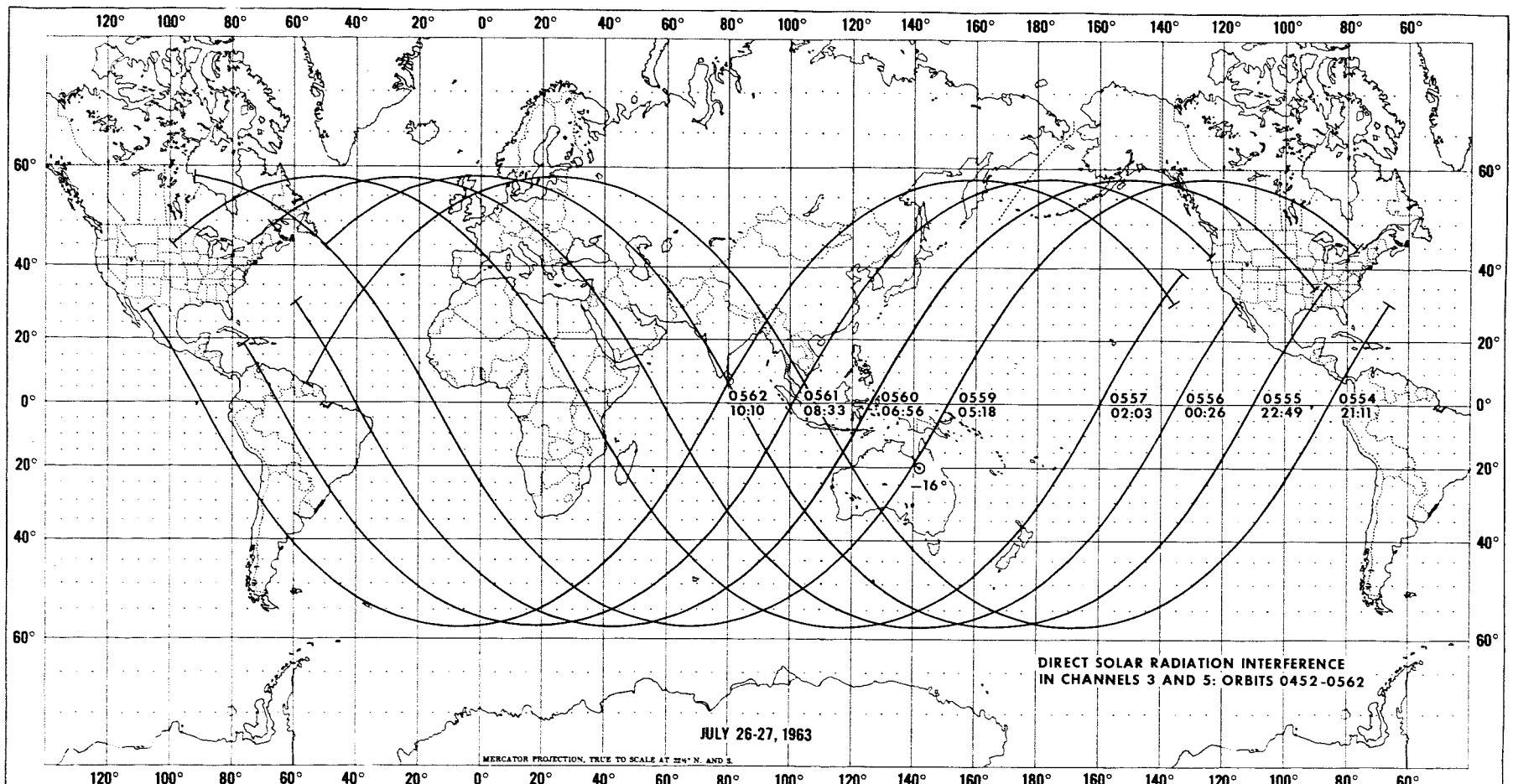
0562
10:10
0561
08:33
0560
06:56
0559
05:18
0557
02:03
0556
00:26
0555
22:49
0554
21:11
-16°
DIRECT SOLAR RADIATION INTERFERENCE
IN CHANNELS 3 AND 5: ORBITS 0452-0562
JULY 26-27, 1963
MERCATOR PROJECTION, TRUE TO SCALE AT 22½° N. AND S.

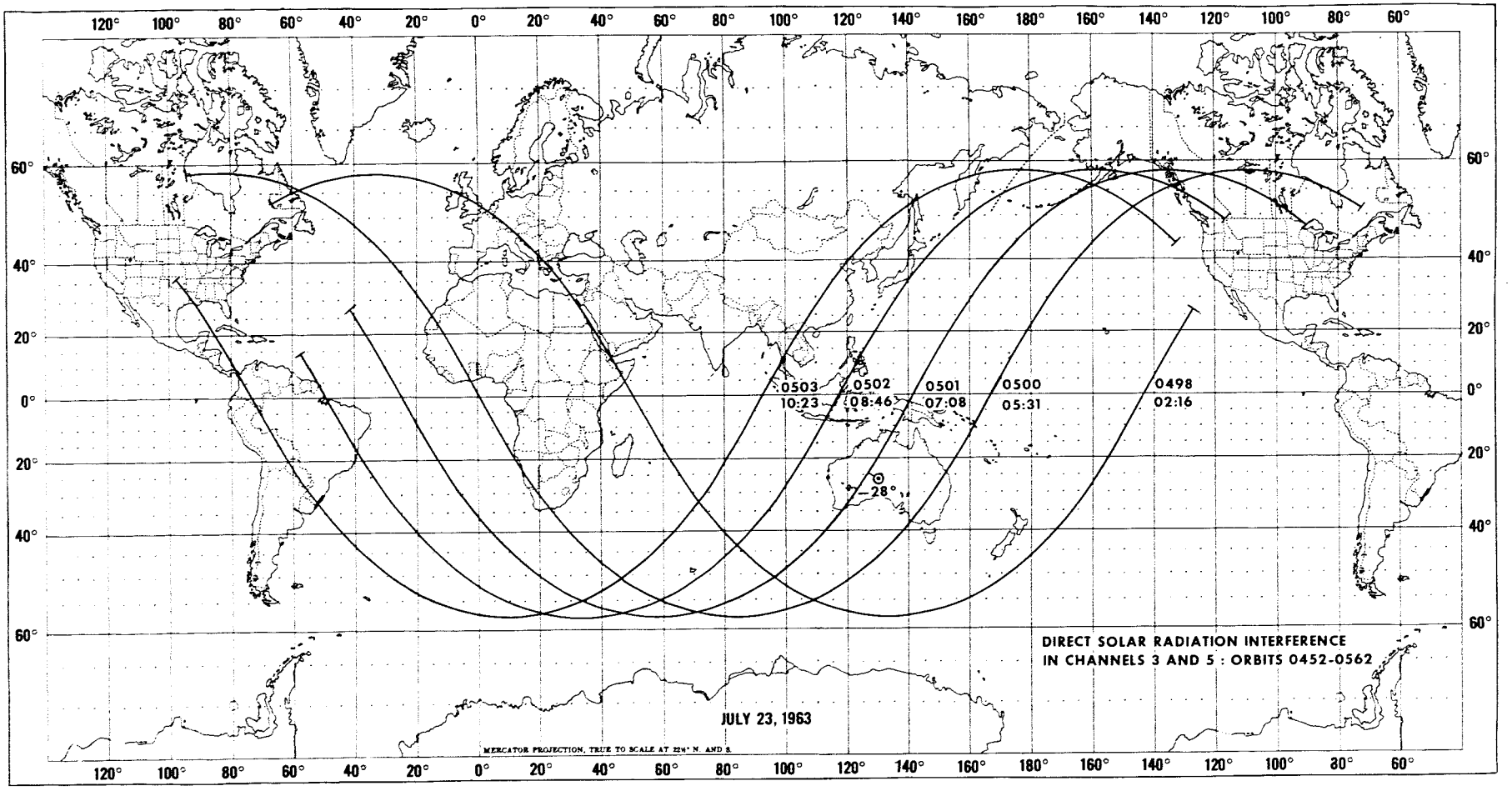
0503
10:23
0502
08:46
0501
07:08
0500
05:31
0498
02:16
28°
DIRECT SOLAR RADIATION INTERFERENCE
IN CHANNELS 3 AND 5 : ORBITS 0452-0562
JULY 23, 1963
MERCATOR PROJECTION, TRUE TO SCALE AT 22½° N. AND S.

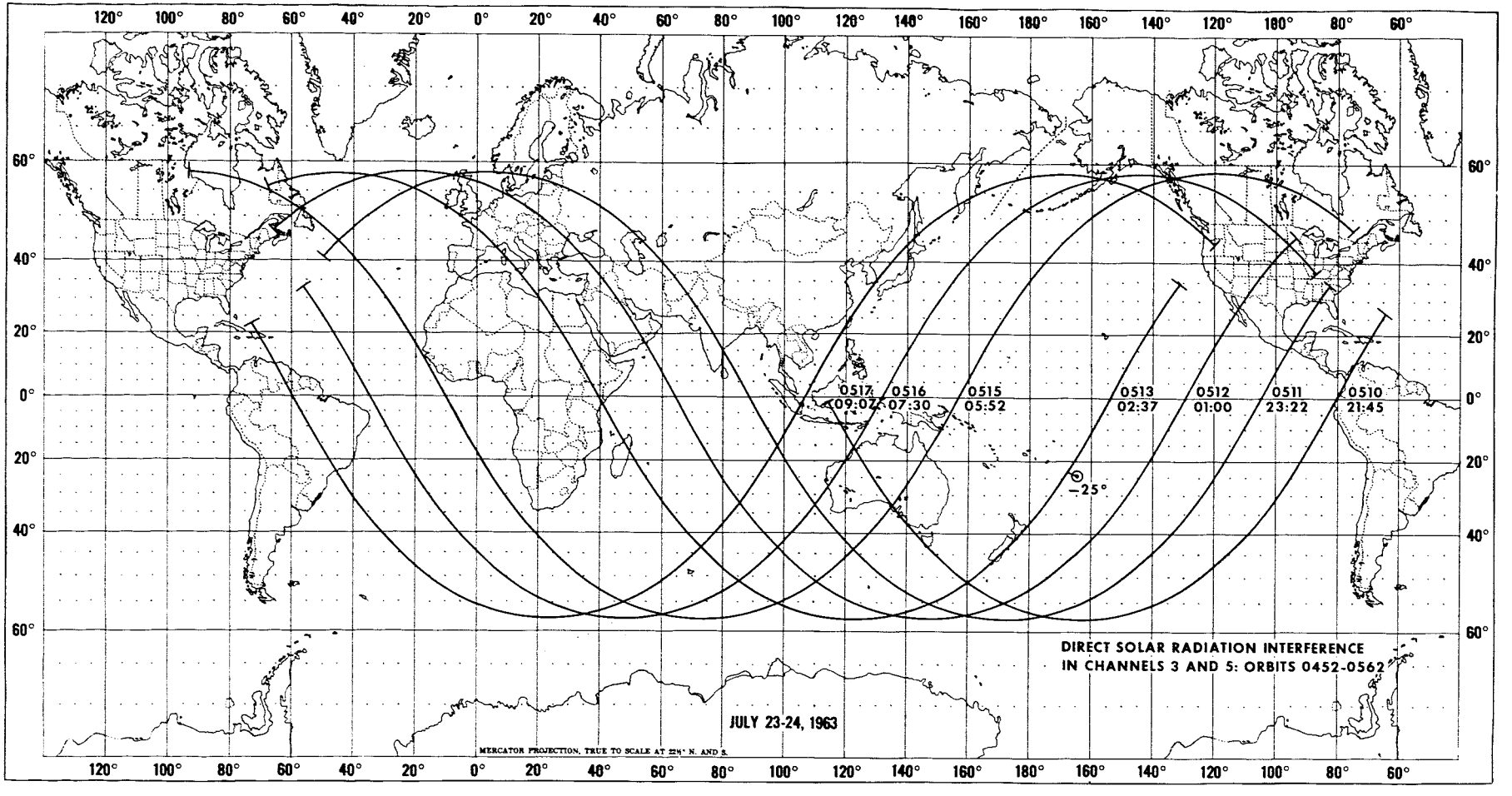
0517
09:02
0516
07:30
0515
05:52
0513
02:37
0512
01:00
0511
23:22
0510
21:45
-25°
DIRECT SOLAR RADIATION INTERFERENCE
IN CHANNELS 3 AND 5: ORBITS 0452-0562
JULY 23-24, 1963
MERCATOR PROJECTION, TRUE TO SCALE AT 22½° N. AND S.

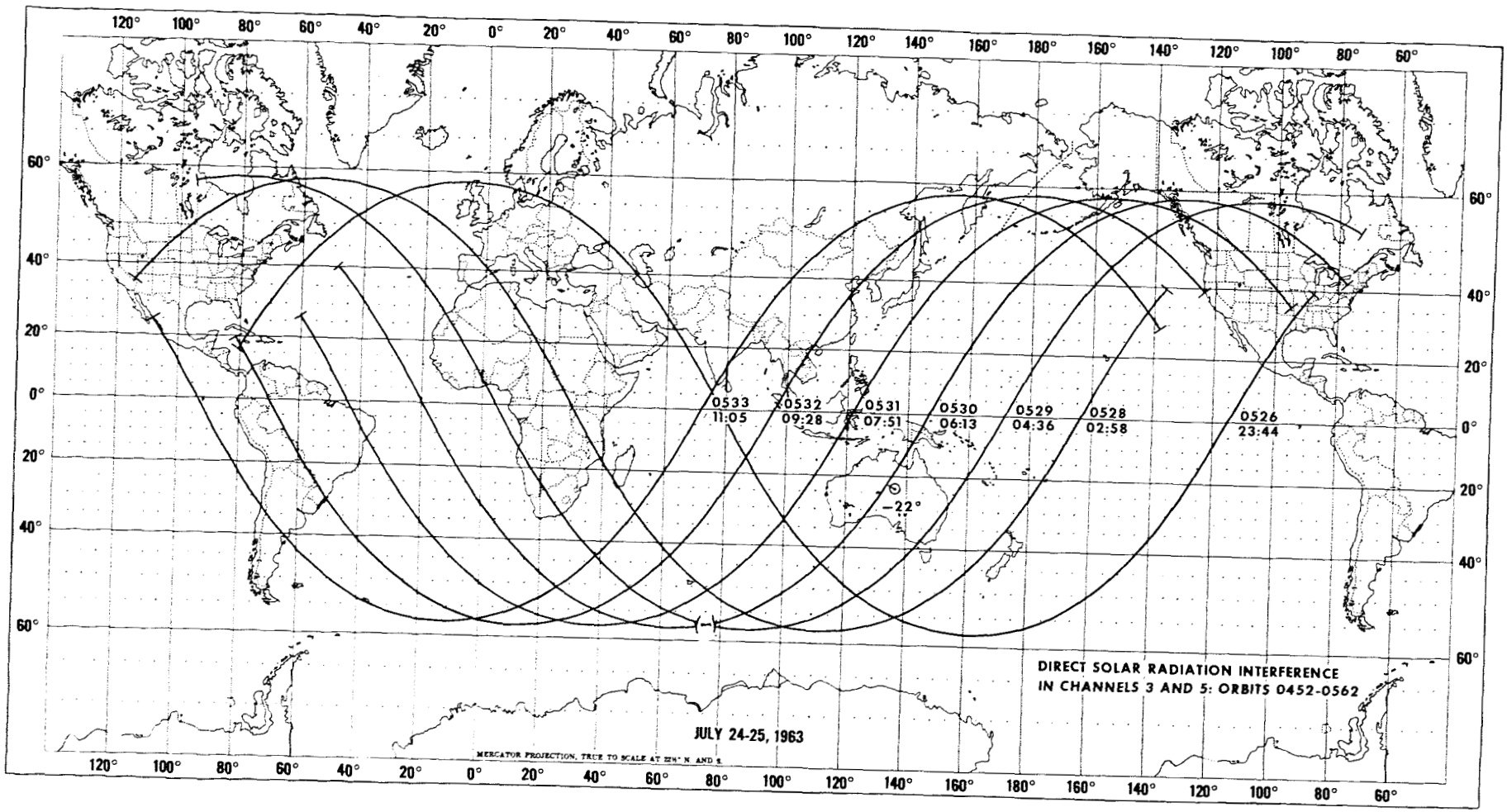
0533
11:05
0532
09:28
0531
07:51
0530
06:13
0529
04:36
0528
02:58
0526
23:44
−22°
DIRECT SOLAR RADIATION INTERFERENCE
IN CHANNELS 3 AND 5: ORBITS 0452-0562
JULY 24-25, 1963
MERCATOR PROJECTION, TRUE TO SCALE AT 22½° N AND S

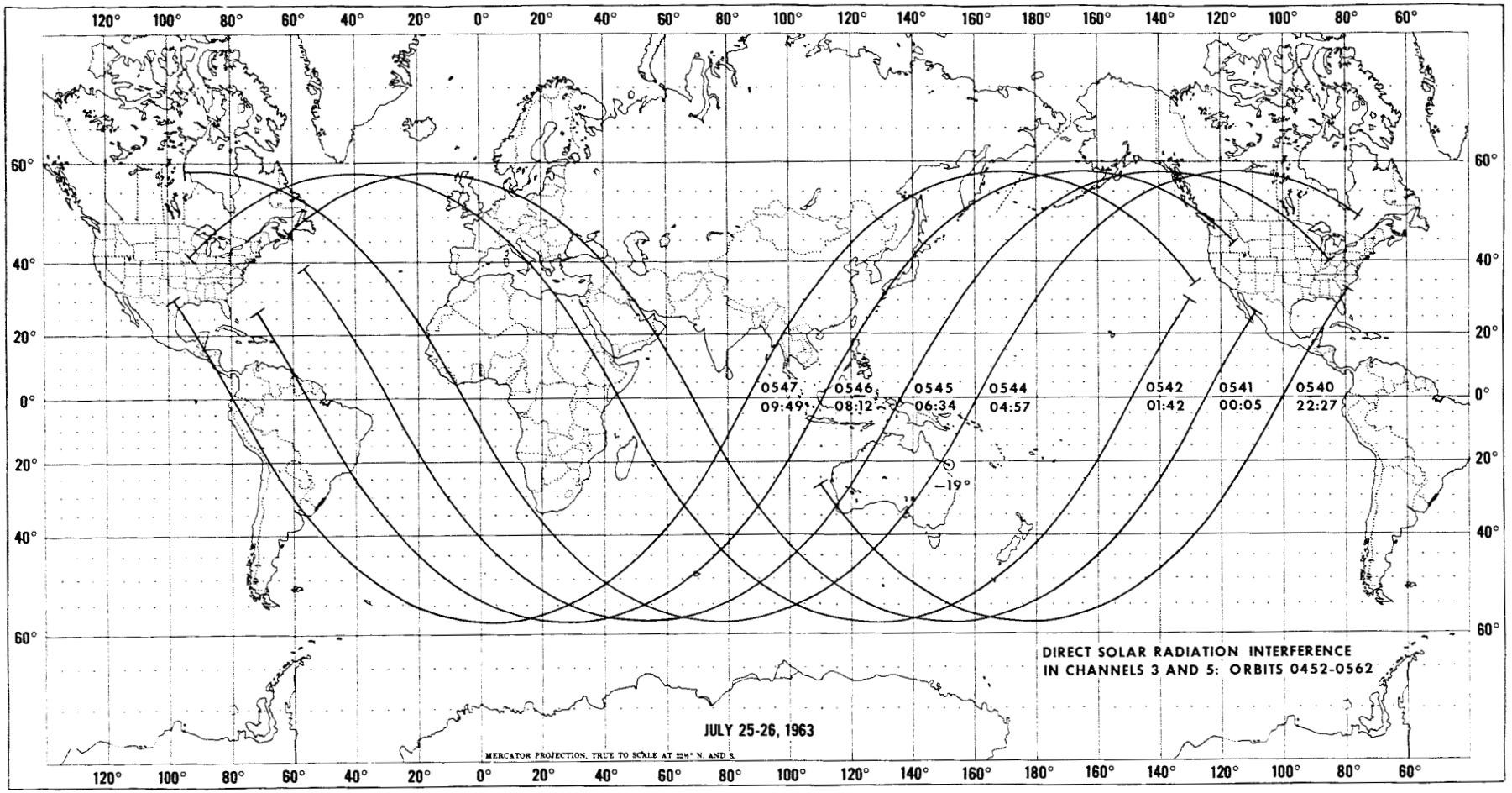
0547
09:49
0546
08:12
0545
06:34
0544
04:57
0542
01:42
0541
00:05
0540
22:27
−19°
DIRECT SOLAR RADIATION INTERFERENCE
IN CHANNELS 3 AND 5: ORBITS 0452-0562
JULY 25-26, 1963
MERCATOR PROJECTION, TRUE TO SCALE AT 22½° N. AND S.

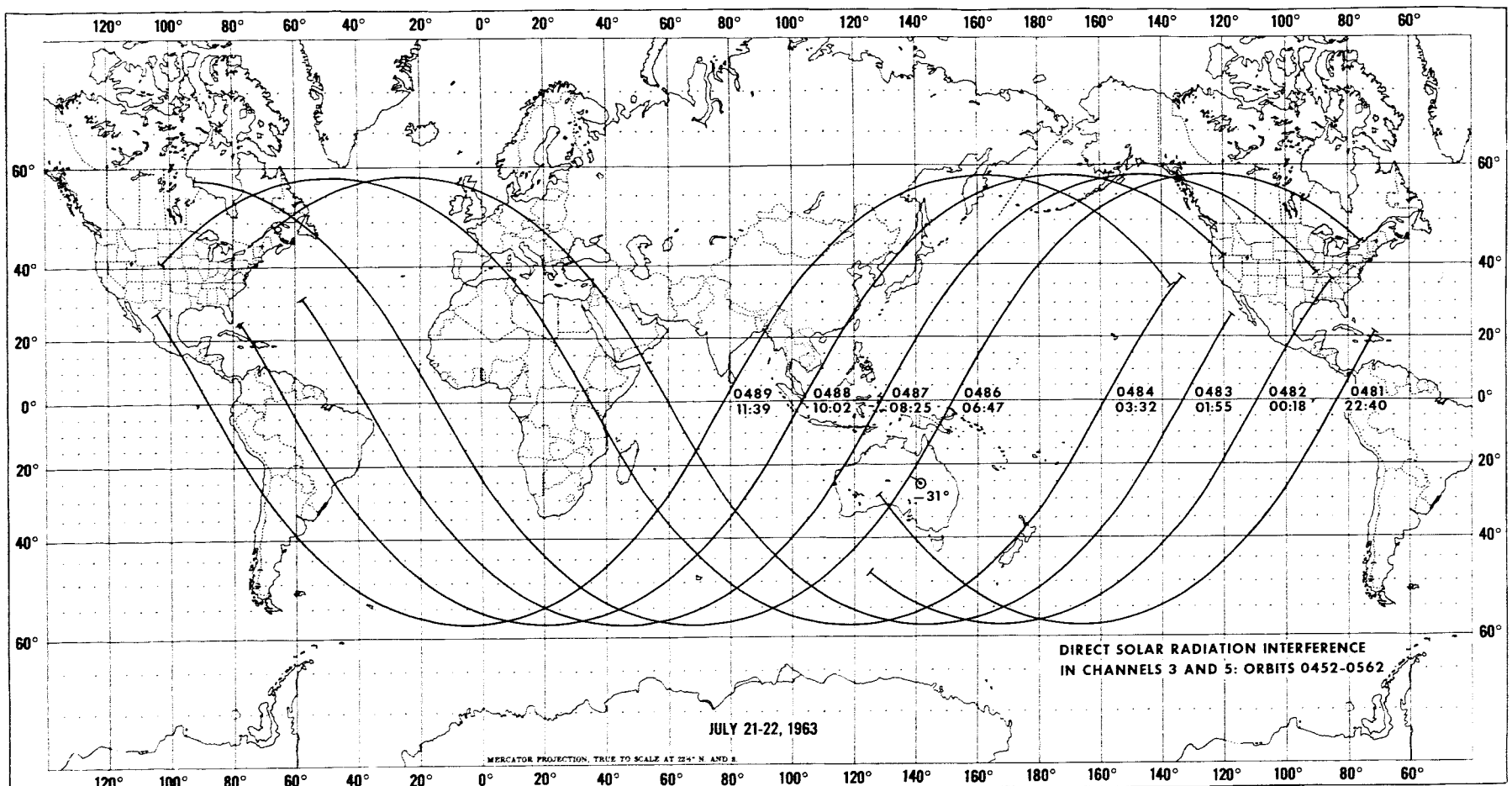
0489
11:39
0488
10:02
0487
08:25
0486
06:47
0484
03:32
0483
01:55
0482
00:18
0481
22:40
−31°
DIRECT SOLAR RADIATION INTERFERENCE
IN CHANNELS 3 AND 5: ORBITS 0452-0562
JULY 21-22, 1963
MERCATOR PROJECTION, TRUE TO SCALE AT 22.4° N. AND S.

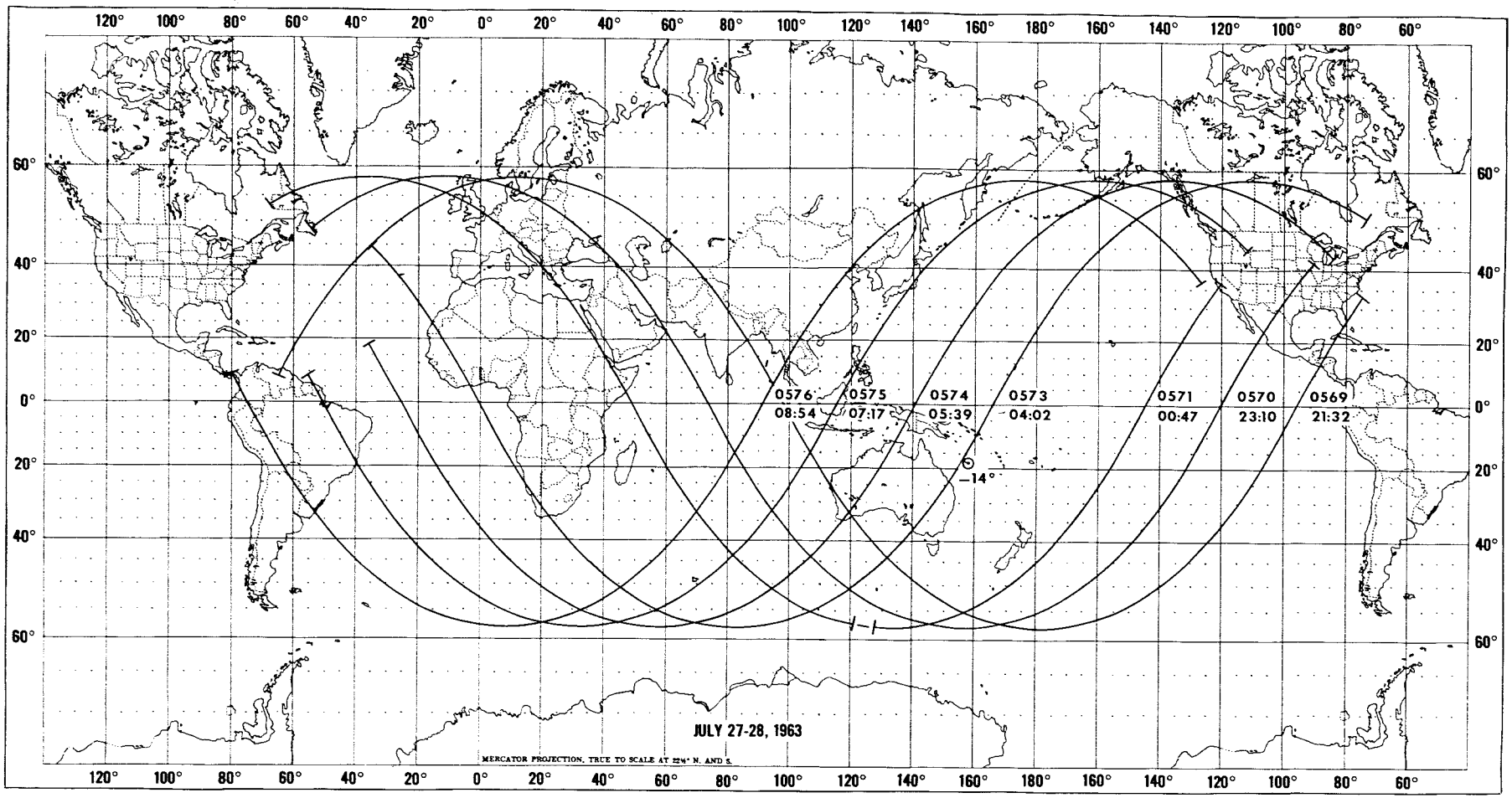
0576
08:54
0575
07:17
0574
05:39
0573
04:02
0571
00:47
0570
23:10
0569
21:32
−14°
JULY 27-28, 1963
MERCATOR PROJECTION, TRUE TO SCALE AT 22½° N. AND S.

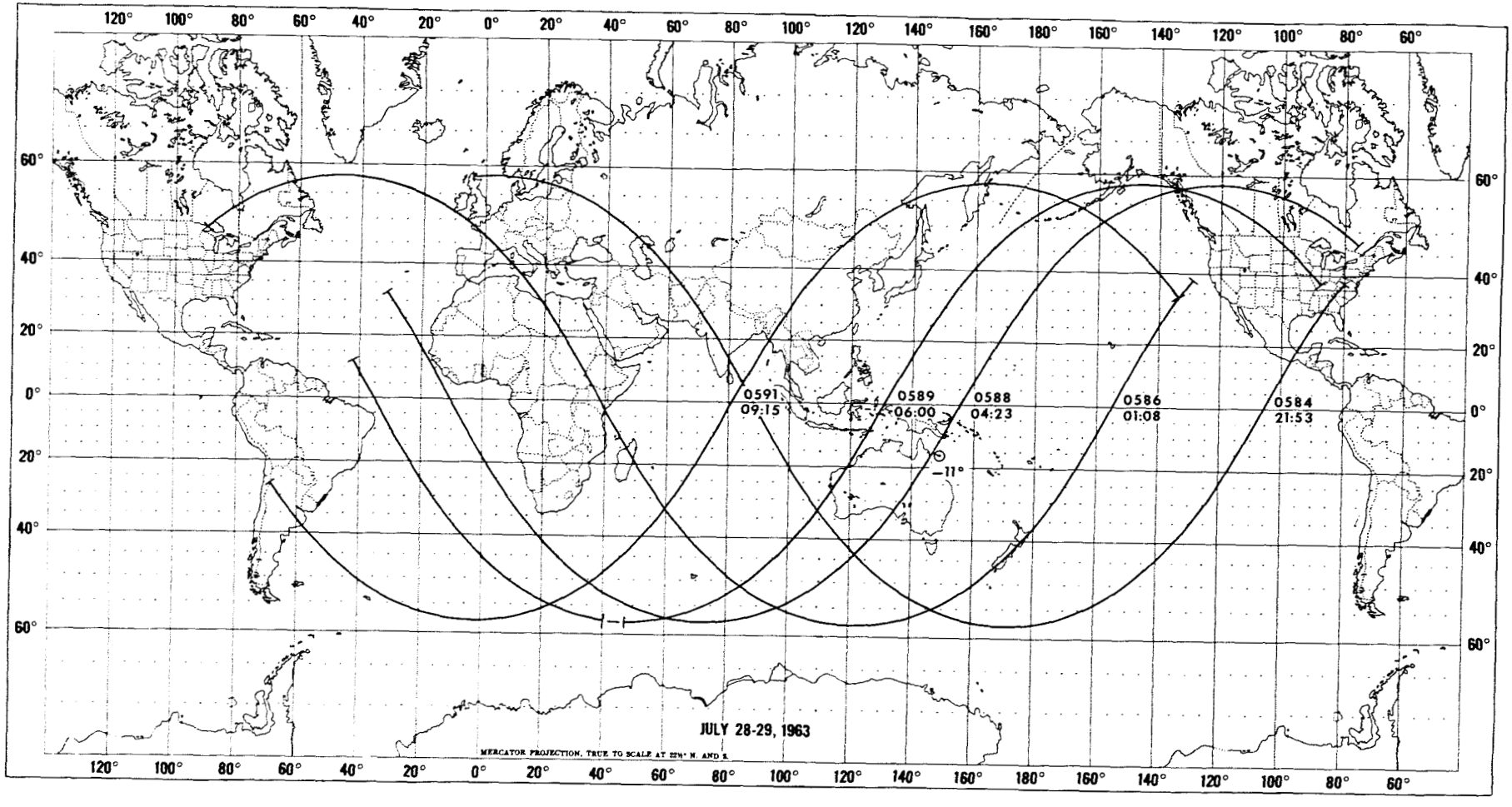
0591
09:15
0589
06:00
0588
04:23
0586
01:08
0584
21:53
-11°
JULY 28-29, 1963
MERCATOR PROJECTION, TRUE TO SCALE AT 22½° N. AND S.

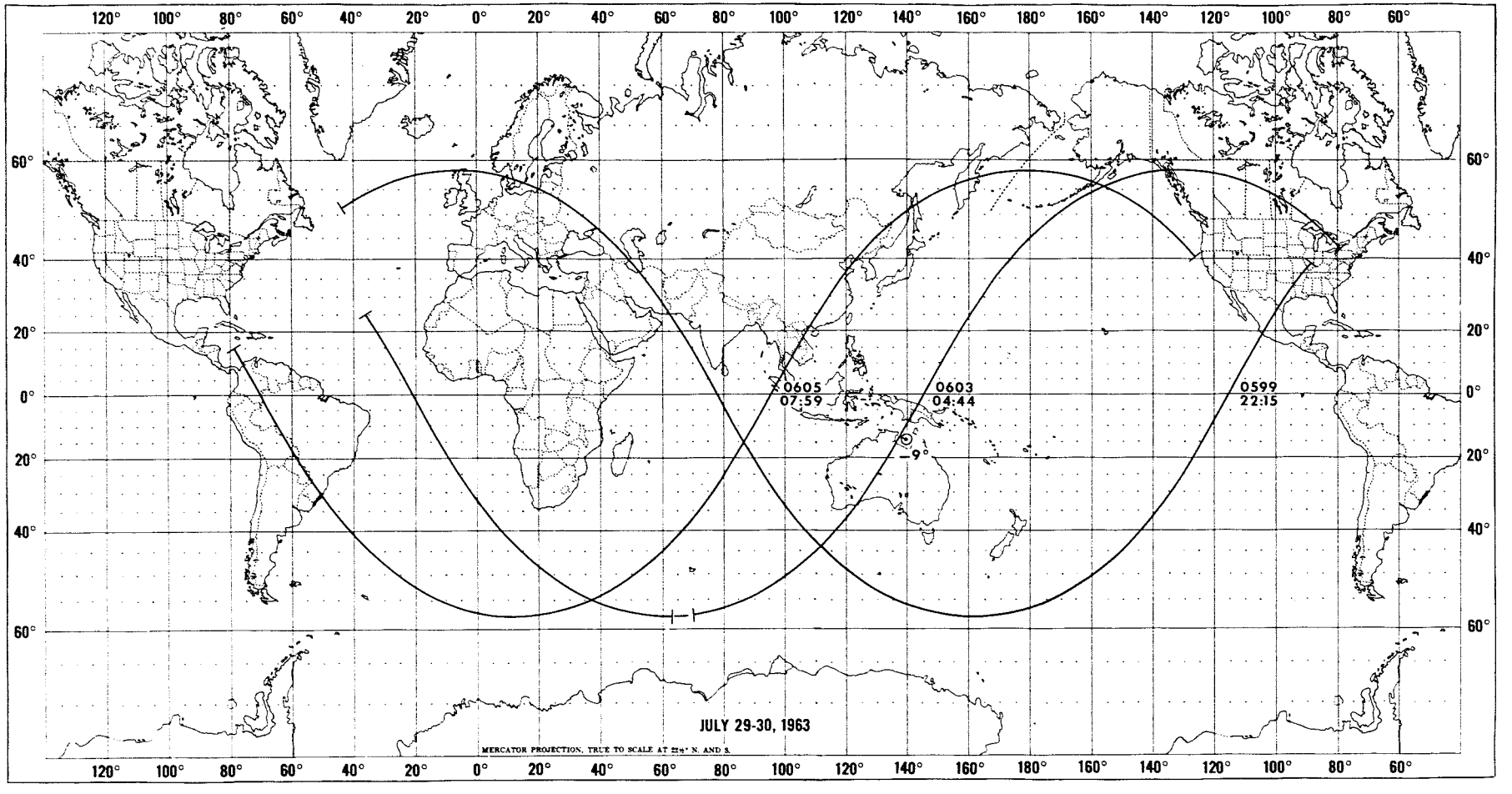
0605
07:59
0603
04:44
0599
22:15
-9°
JULY 29-30, 1963
MERCATOR PROJECTION, TRUE TO SCALE AT 22½° N. AND S.

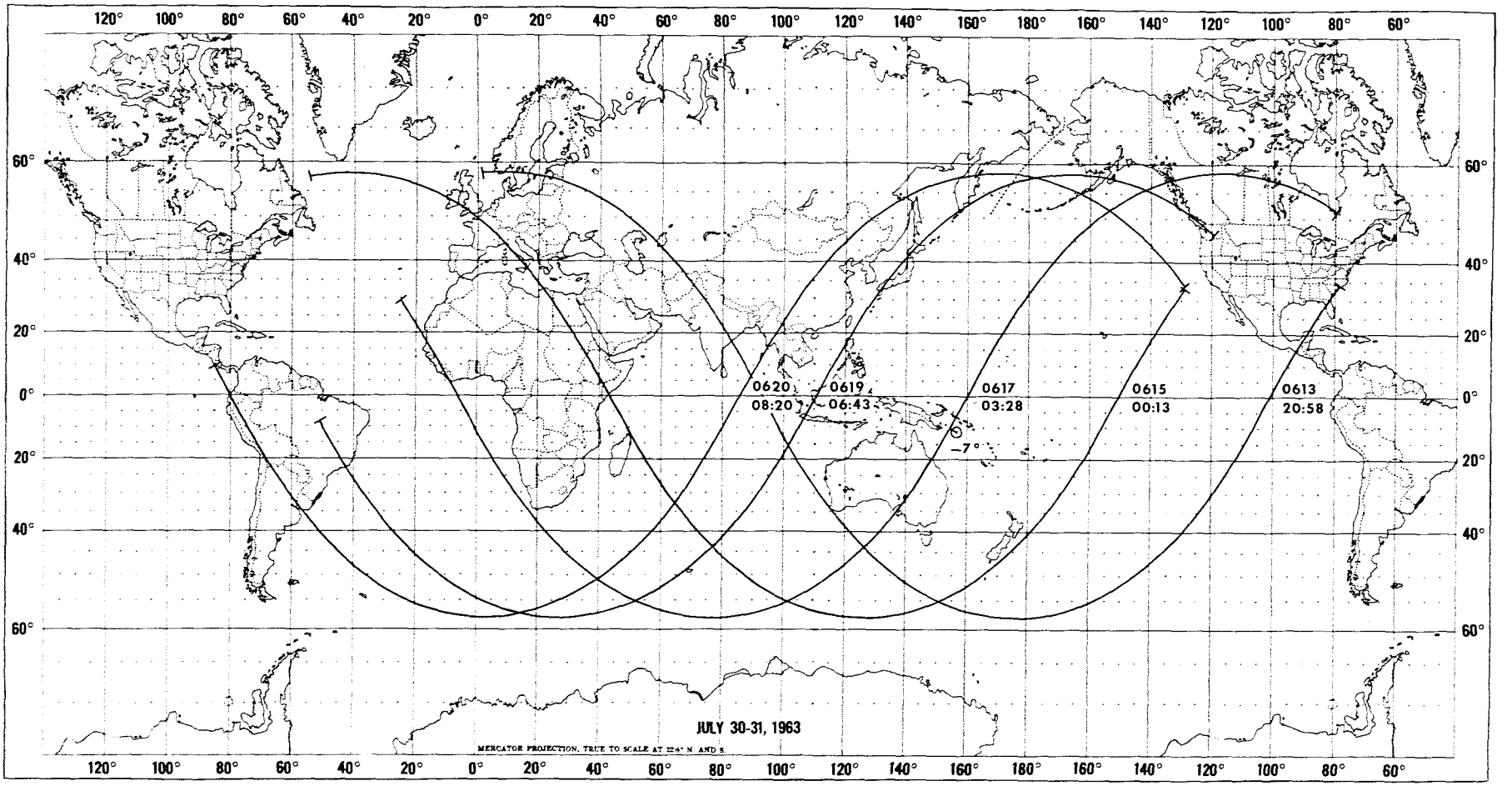
0620
08:20
0619
06:43
0617
03:28
0615
00:13
0613
20:58
−7°
JULY 30-31, 1963
MERCATOR PROJECTION, TRUE TO SCALE AT 22.4° N. AND S.

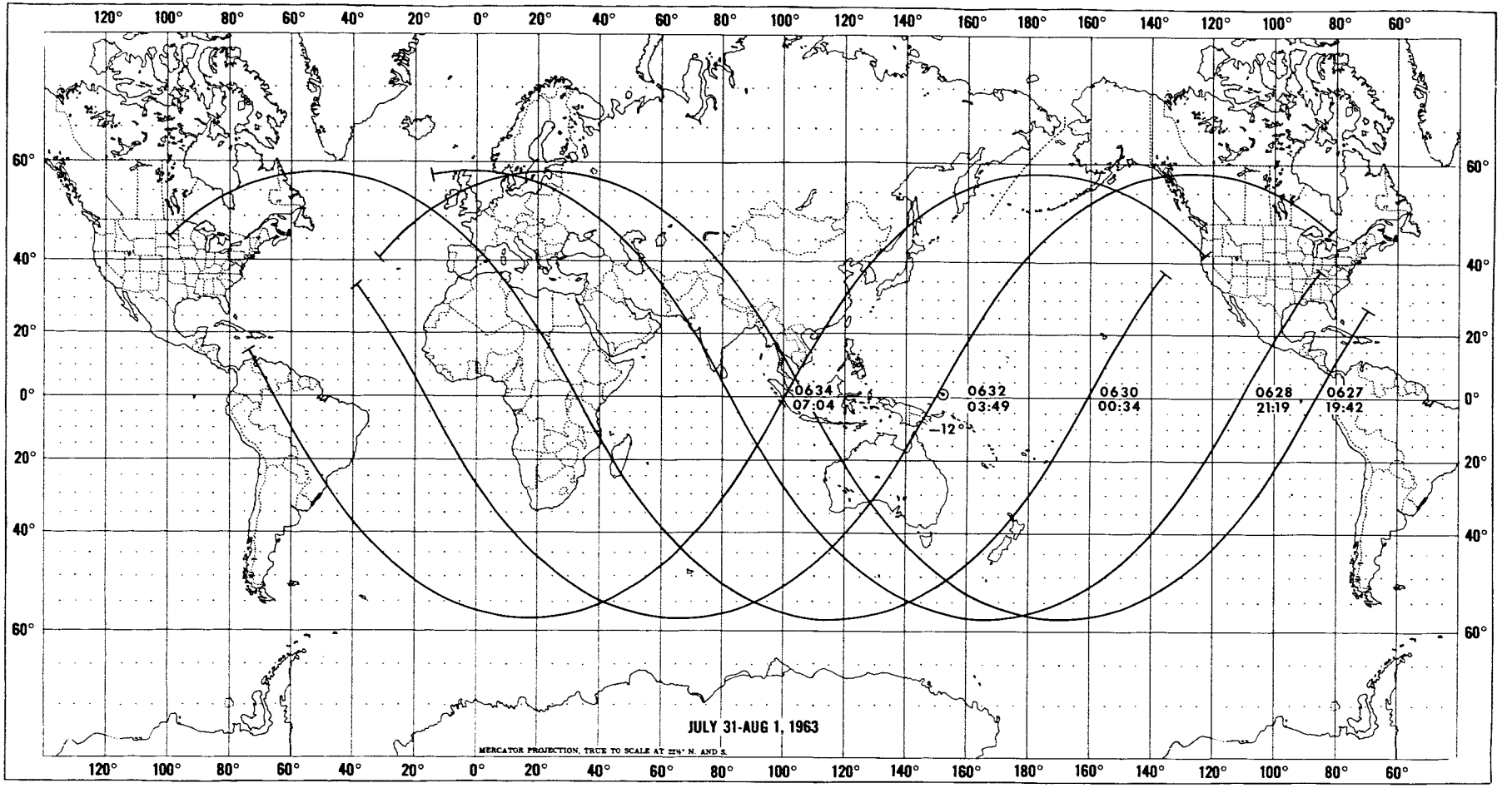
0634
07:04
0632
03:49
0630
00:34
0628
21:19
0627
19:42
−12°
JULY 31-AUG 1, 1963
MERCATOR PROJECTION, TRUE TO SCALE AT 22½° N. AND S.

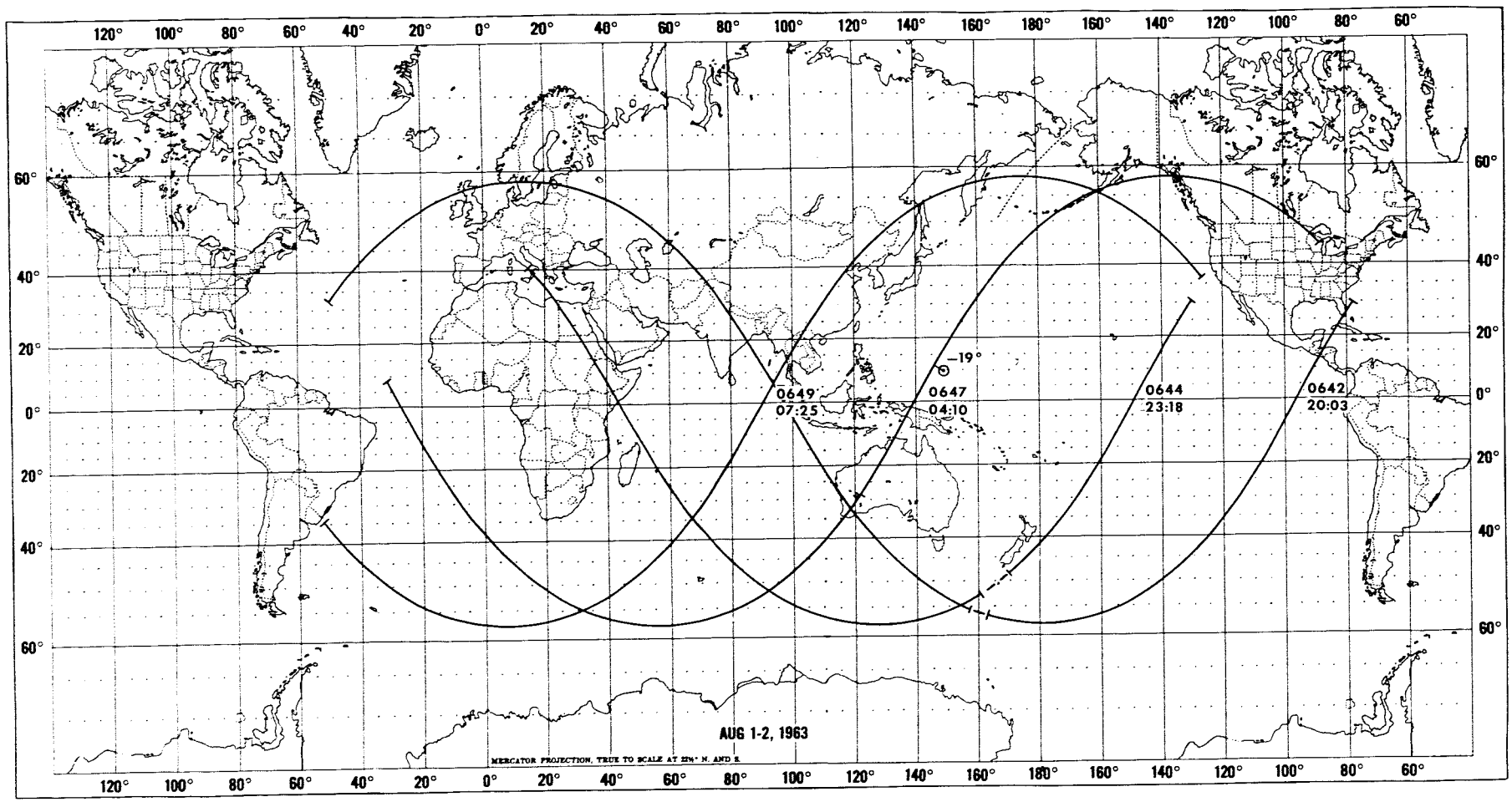
120° 100° 80° 60° 40° 20° 0° 20° 40° 60° 80° 100° 120° 140° 160° 180° 160° 140° 120° 100° 80° 60°
60° 40° 20° 0° 20° 40° 60°
0649
07:25
0647
04:10
−19°
0644
23:18
0642
20:03
AUG 1-2, 1963
MERCATOR PROJECTION, TRUE TO SCALE AT 25½° N. AND S.

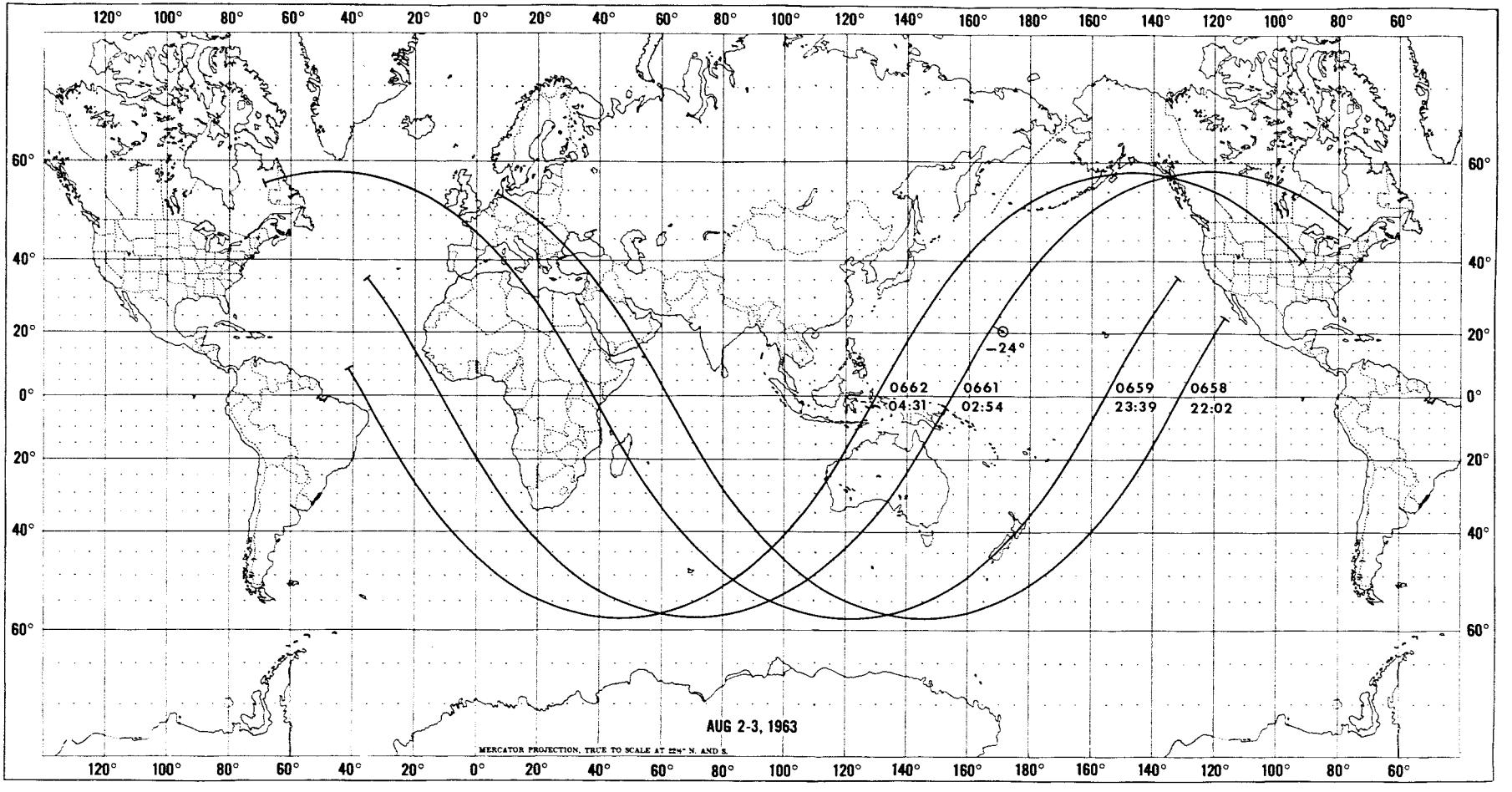
120° 100° 80° 60° 40° 20° 0° 20° 40° 60° 80° 100° 120° 140° 160° 180° 160° 140° 120° 100° 80° 60°
60° 40° 20° 0° 20° 40° 60°
−24°
0662
04:31
0661
02:54
0659
23:39
0658
22:02
AUG 2-3, 1963
MERCATOR PROJECTION, TRUE TO SCALE AT 22½° N. AND S.

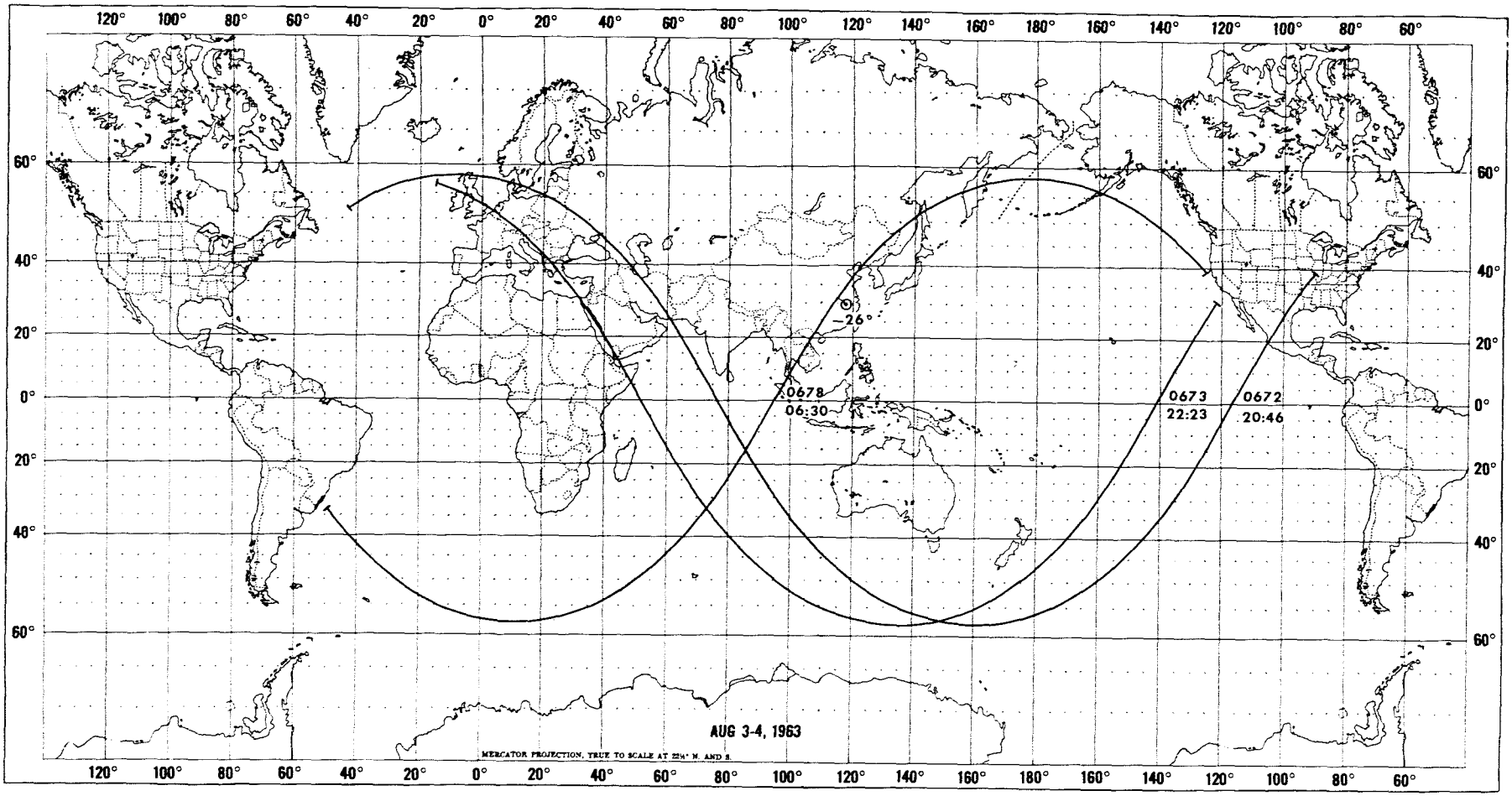
120° 100° 80° 60° 40° 20° 0° 20° 40° 60° 80° 100° 120° 140° 160° 180° 160° 140° 120° 100° 80° 60°
60° 40° 20° 0° 20° 40° 60°
-26°
0678
06:30
0673
22:23
0672
20:46
AUG 3-4, 1963
MERCATOR PROJECTION, TRUE TO SCALE AT 22½° N. AND S.

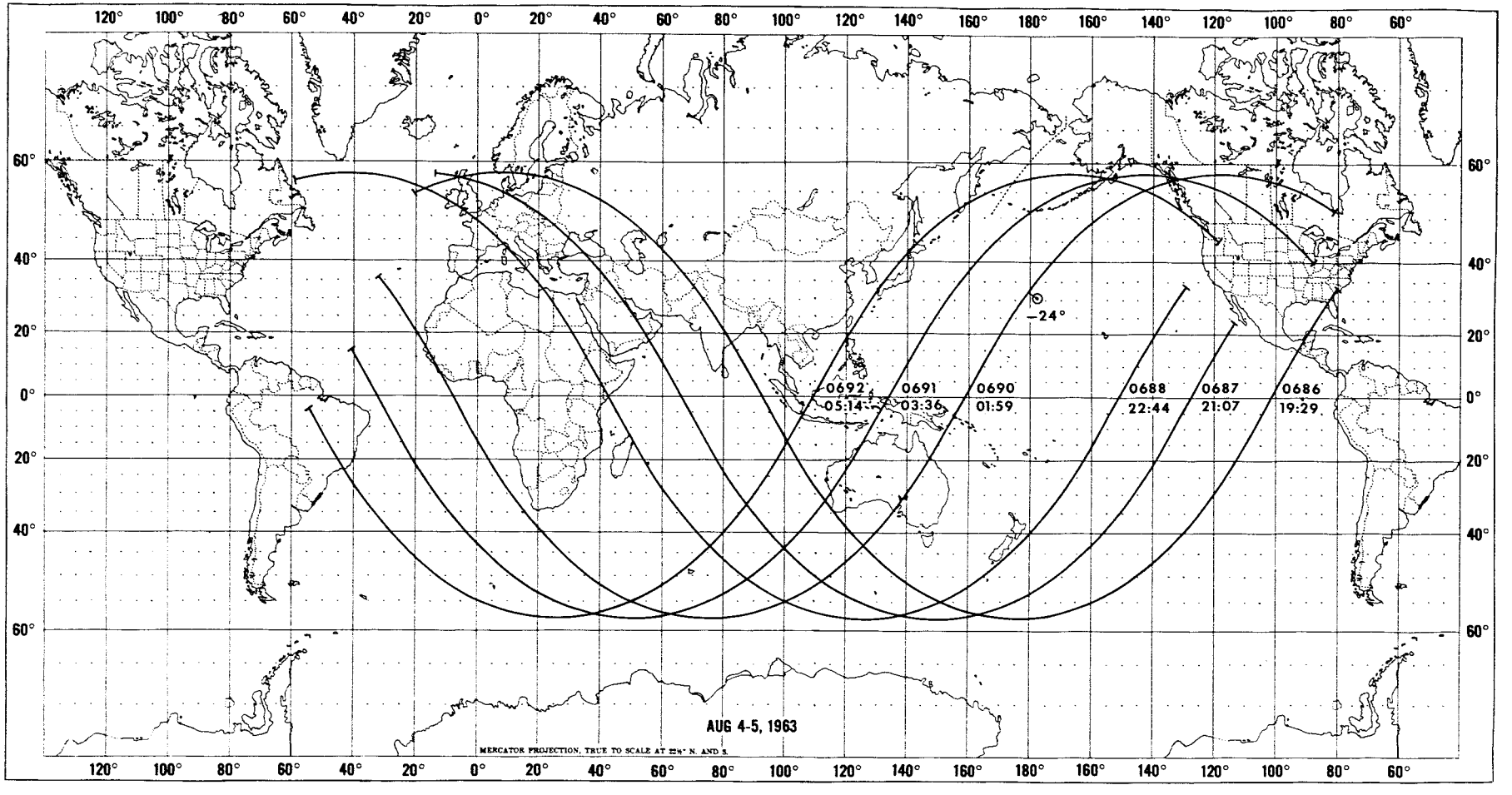
120° 100° 80° 60° 40° 20° 0° 20° 40° 60° 80° 100° 120° 140° 160° 180° 160° 140° 120° 100° 80° 60°
60° 40° 20° 0° 20° 40° 60°
0692 05:14
0691 03:36
0690 01:59
0688 22:44
0687 21:07
0686 19:29
−24°
AUG 4-5, 1963
MERCATOR PROJECTION, TRUE TO SCALE AT 22½° N. AND S.

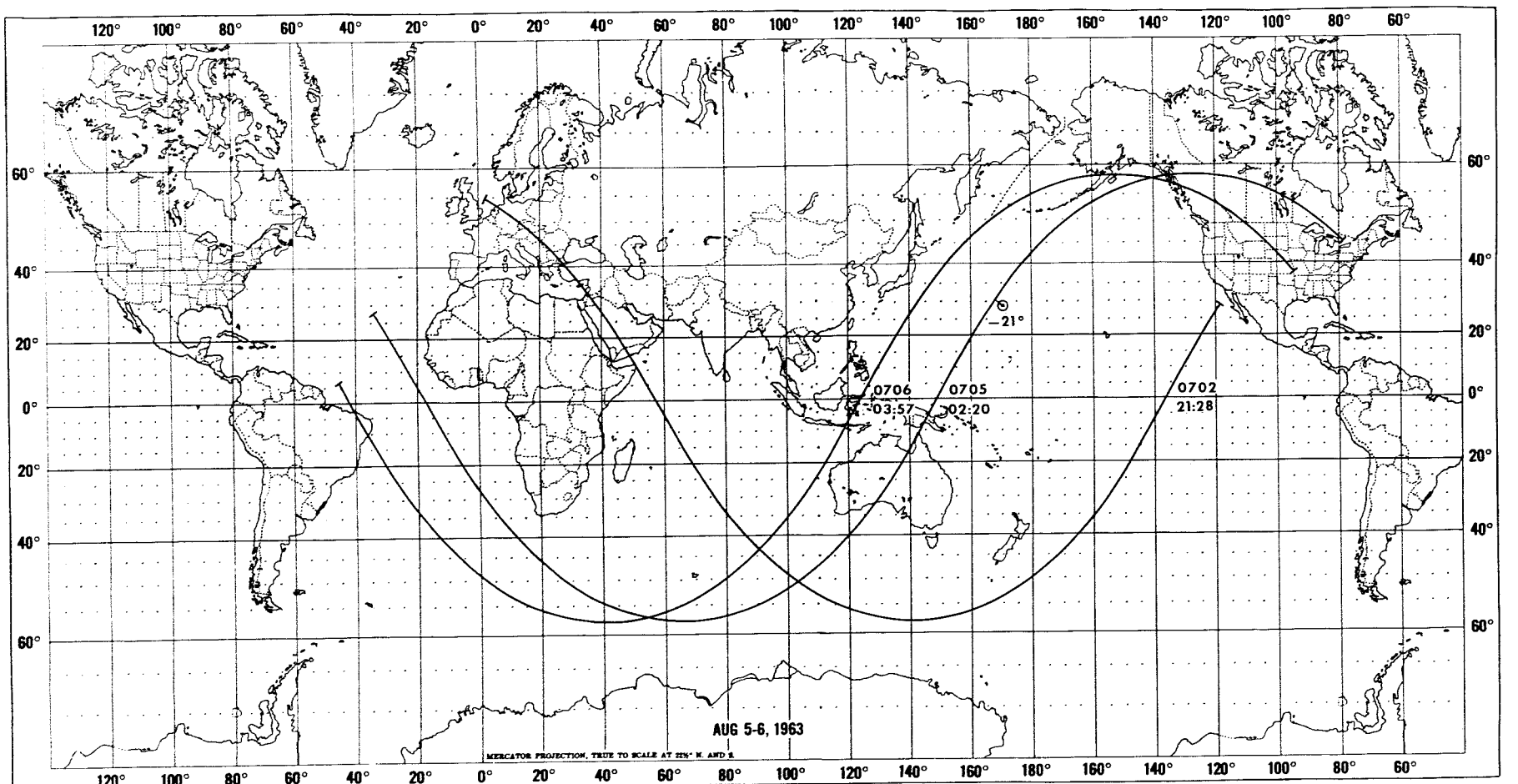
120° 100° 80° 60° 40° 20° 0° 20° 40° 60° 80° 100° 120° 140° 160° 180° 160° 140° 120° 100° 80° 60°
60° 40° 20° 0° 20° 40° 60°
−21°
0706
03:57
0705
02:20
0702
21:28
AUG 5-6, 1963
MERCATOR PROJECTION, TRUE TO SCALE AT 22½° N. AND S.

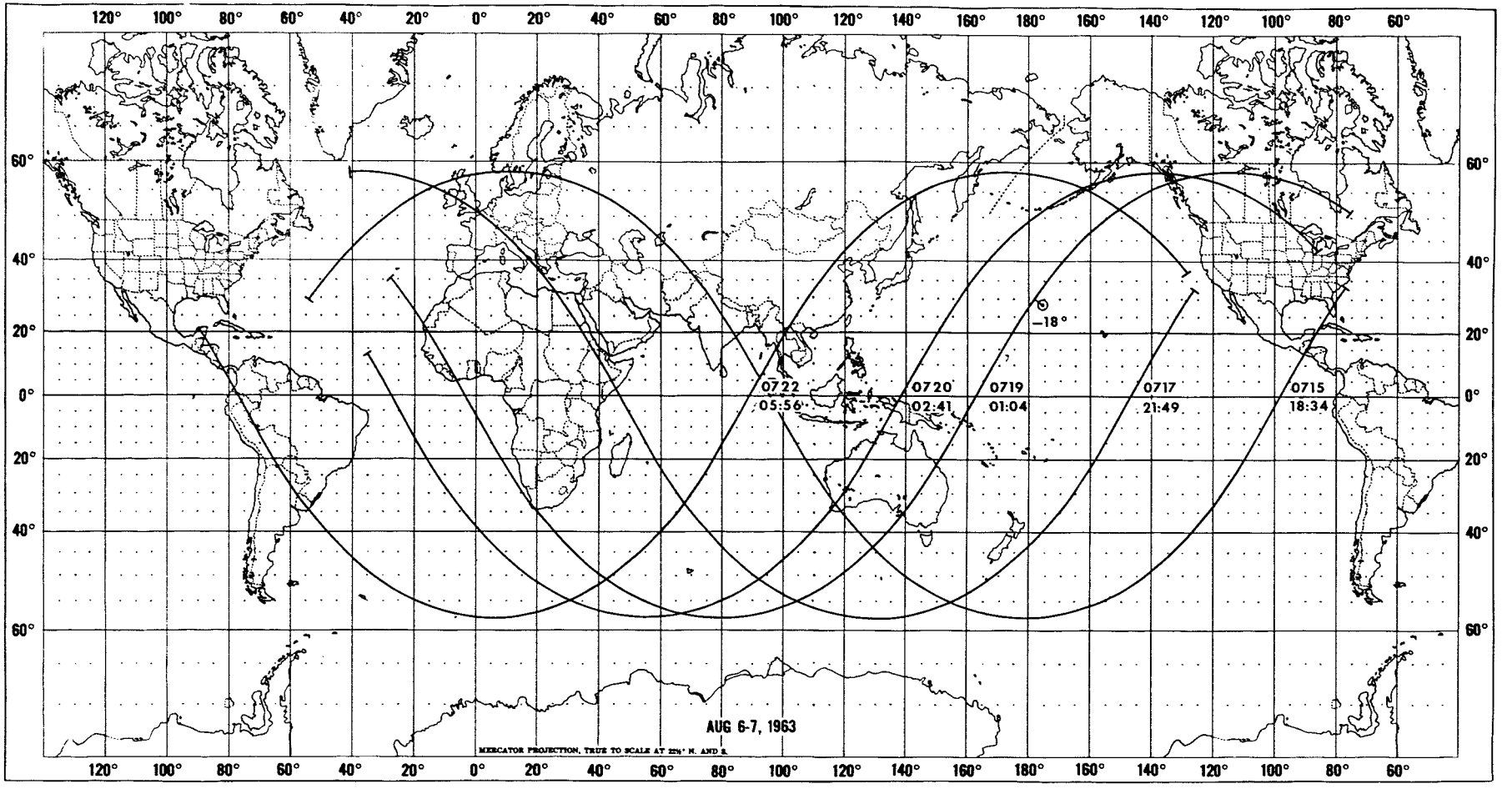
0722
05:56
0720
02:41
0719
01:04
0717
21:49
0715
18:34
−18°
AUG 6-7, 1963
MERCATOR PROJECTION, TRUE TO SCALE AT 22½° N. AND S.

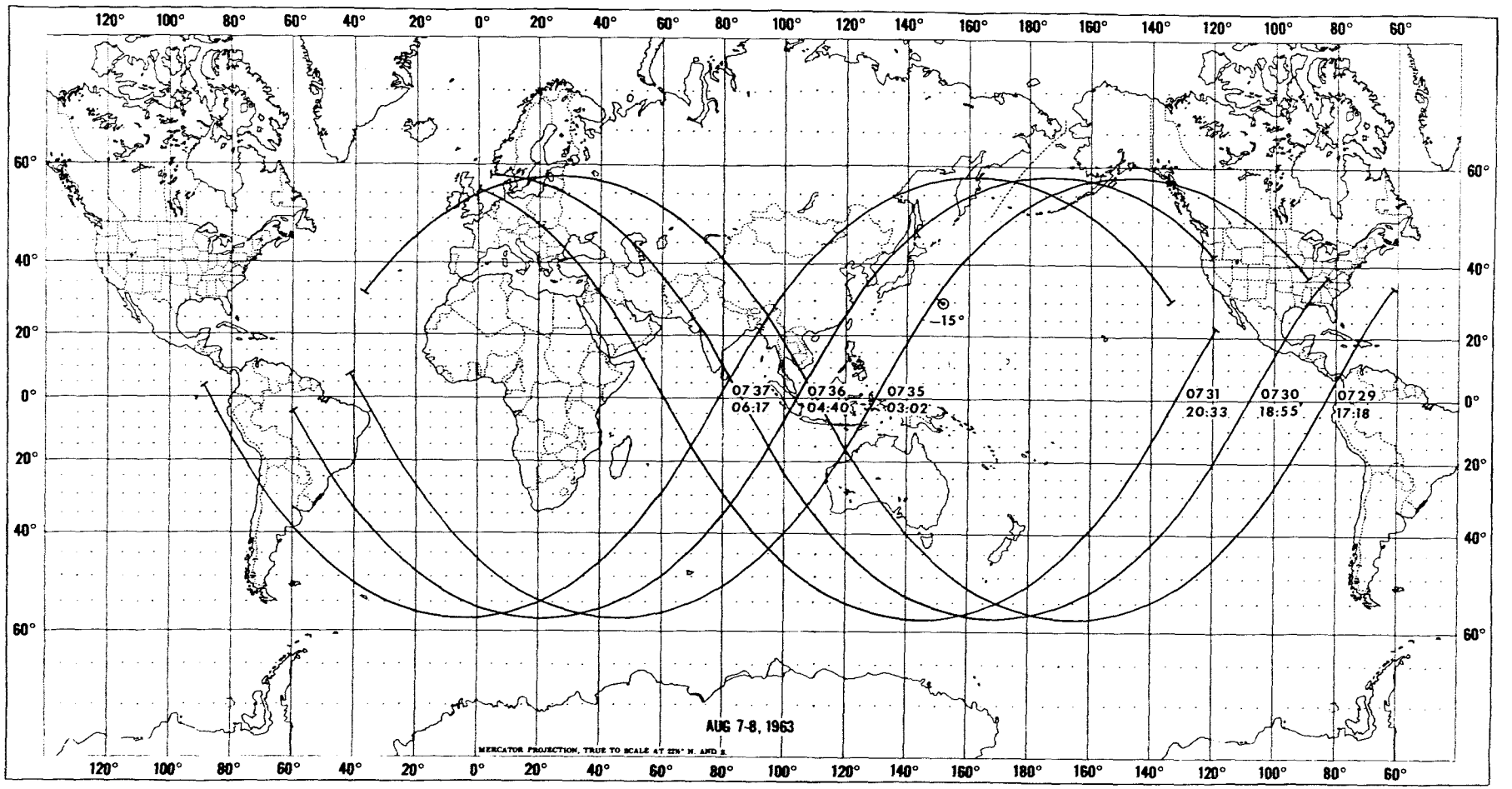
120° 100° 80° 60° 40° 20° 0° 20° 40° 60° 80° 100° 120° 140° 160° 180° 160° 140° 120° 100° 80° 60°
60° 40° 20° 0° 20° 40° 60°
-15°
0737
06:17
0736
04:40
0735
03:02
0731
20:33
0730
18:55
0729
17:18
AUG 7-8, 1963
MERCATOR PROJECTION, TRUE TO SCALE AT 22½° N. AND S.

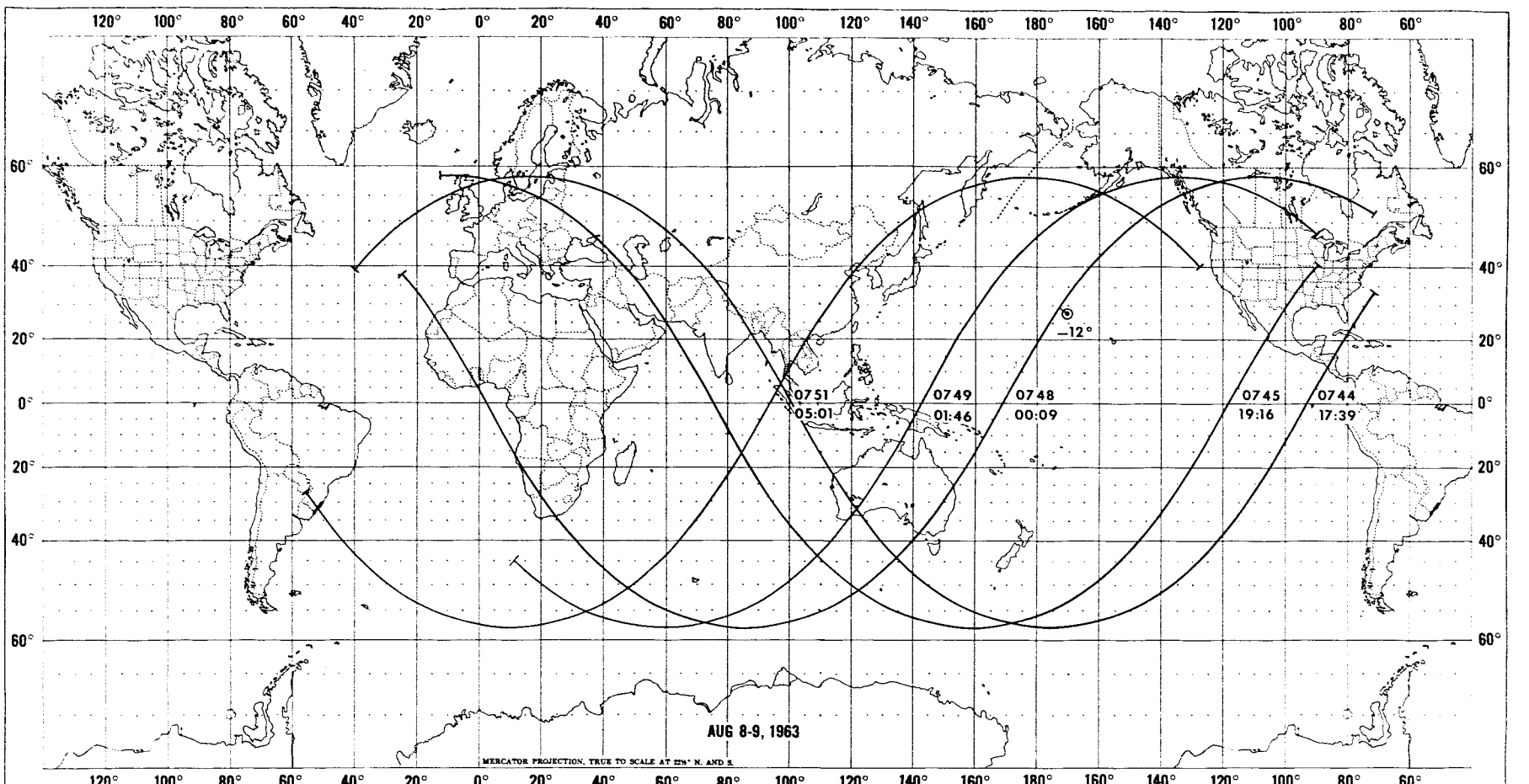
120° 100° 80° 60° 40° 20° 0° 20° 40° 60° 80° 100° 120° 140° 160° 180° 160° 140° 120° 100° 80° 60°
60° 40° 20° 0° 20° 40° 60°
0751
05:01
0749
01:46
0748
00:09
0745
19:16
0744
17:39
−12°
AUG 8-9, 1963
MERCATOR PROJECTION, TRUE TO SCALE AT 22½° N. AND S.

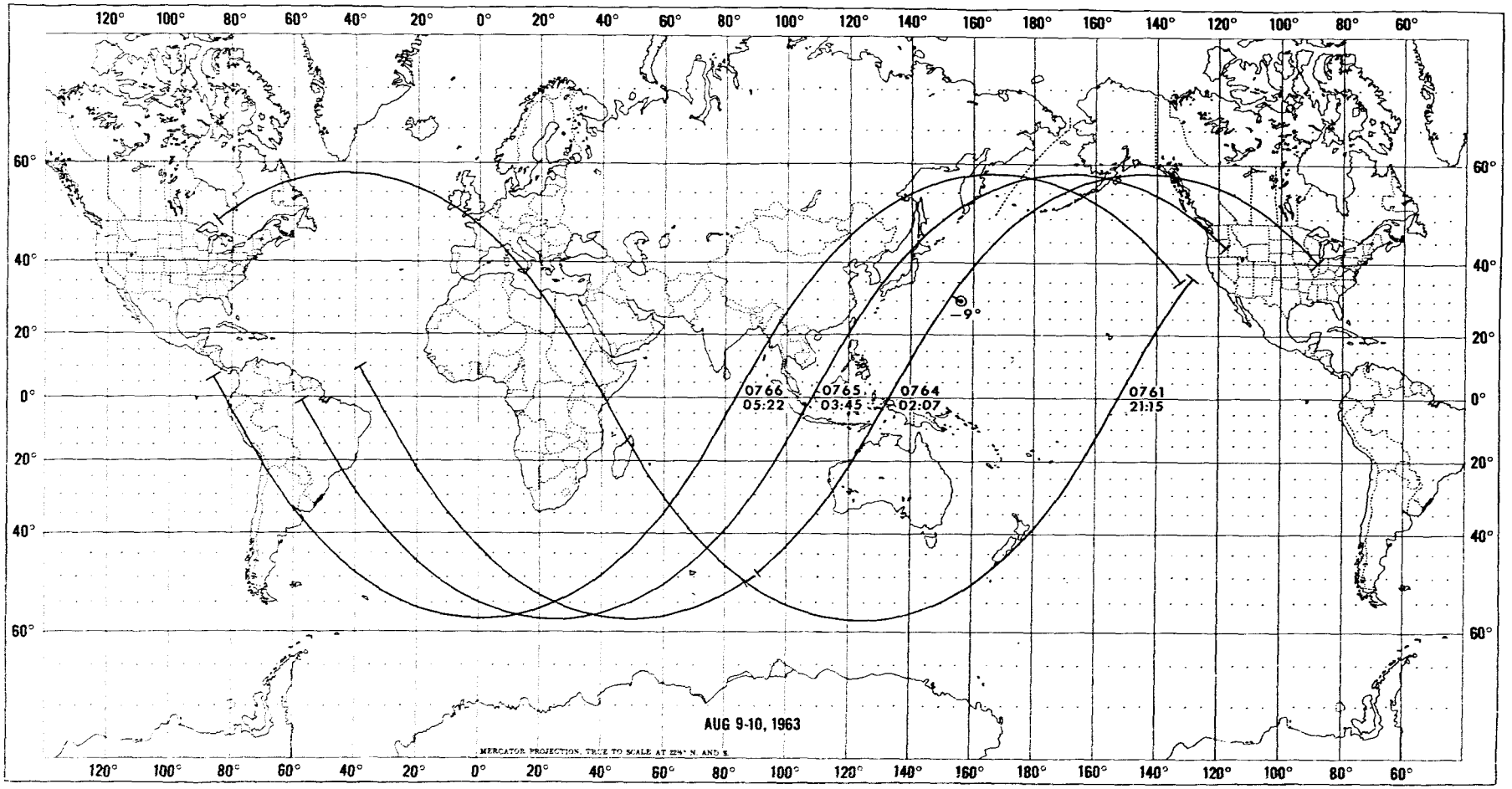
120° 100° 80° 60° 40° 20° 0° 20° 40° 60° 80° 100° 120° 140° 160° 180° 160° 140° 120° 100° 80° 60°
60° 40° 20° 0° 20° 40° 60°
0766
05:22
0765
03:45
0764
02:07
0761
21:15
-9°
AUG 9-10, 1963
MERCATOR PROJECTION, TRUE TO SCALE AT 22½° N. AND S.

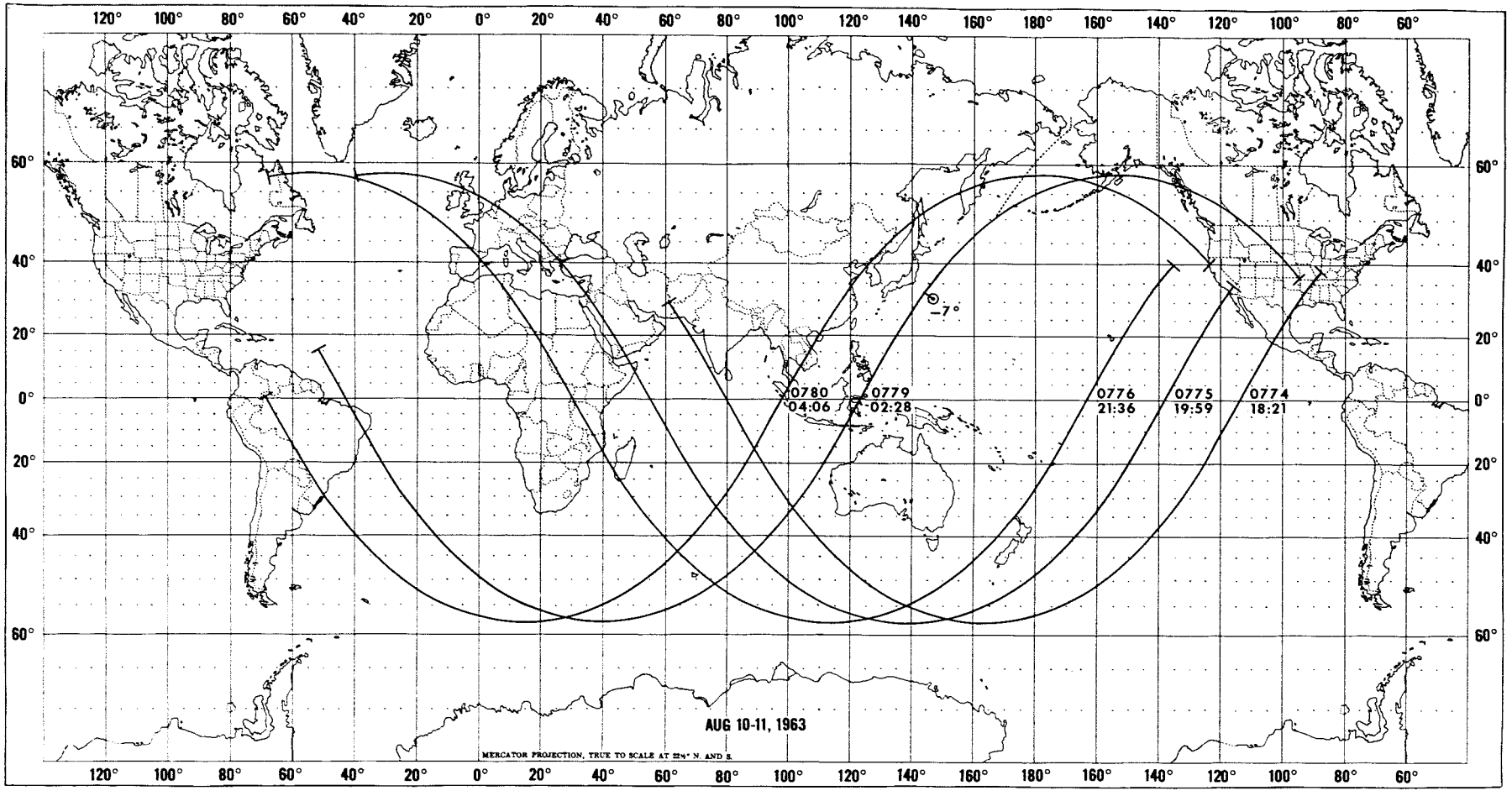
120° 100° 80° 60° 40° 20° 0° 20° 40° 60° 80° 100° 120° 140° 160° 180° 160° 140° 120° 100° 80° 60°
60° 40° 20° 0° 20° 40° 60°
0780
04:06
0779
02:28
0776
21:36
0775
19:59
0774
18:21
−7°
AUG 10-11, 1963
MERCATOR PROJECTION, TRUE TO SCALE AT 22½° N. AND S.

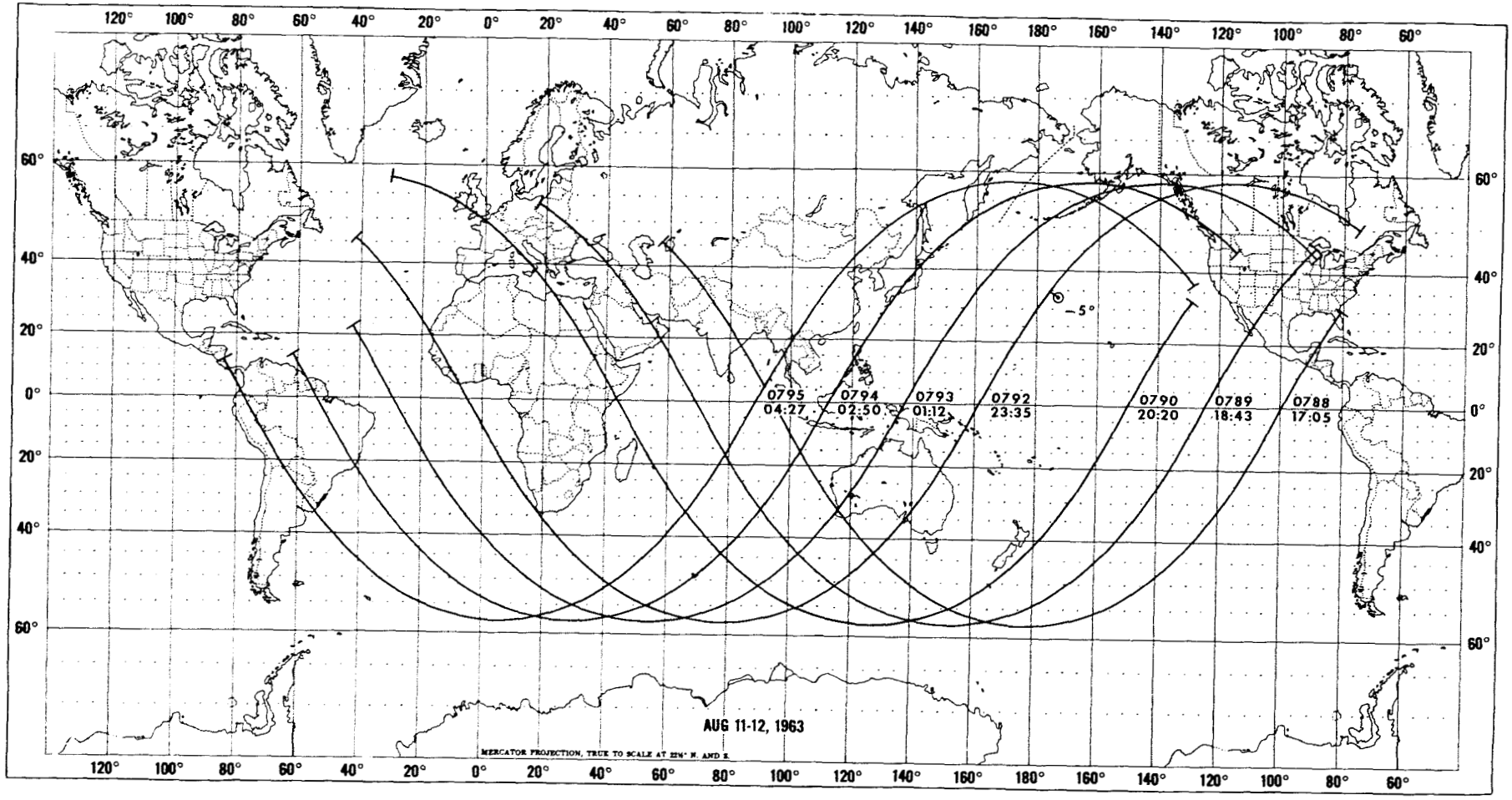
0795
04:27
0794
02:50
0793
01:12
0792
23:35
0790
20:20
0789
18:43
0788
17:05
-5°
AUG 11-12, 1963
MERCATOR PROJECTION, TRUE TO SCALE AT 22½° N. AND S.

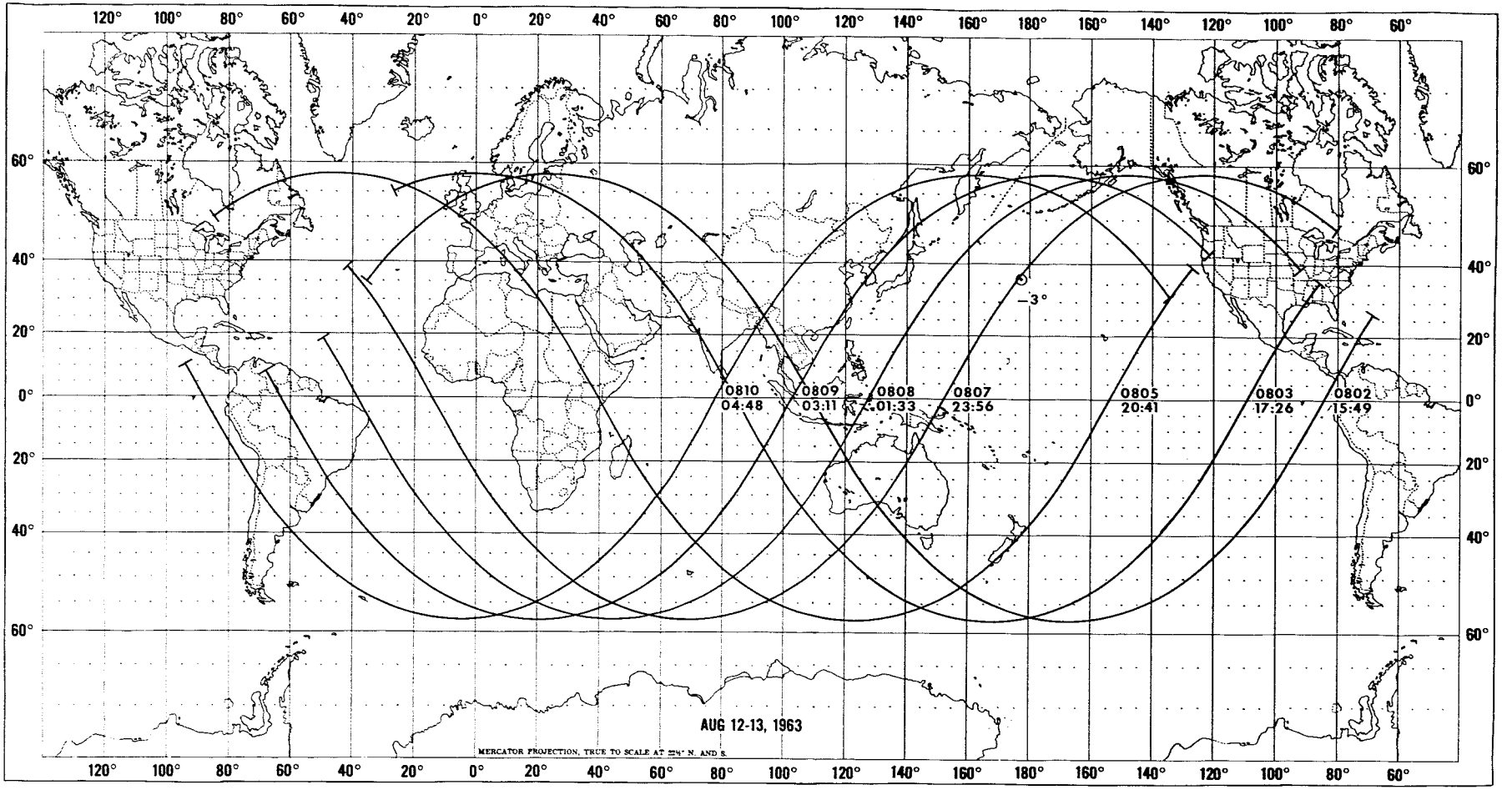
120° 100° 80° 60° 40° 20° 0° 20° 40° 60° 80° 100° 120° 140° 160° 180° 160° 140° 120° 100° 80° 60°
60° 40° 20° 0° 20° 40° 60°
0810
04:48
0809
03:11
0808
01:33
0807
23:56
0805
20:41
0803
17:26
0802
15:49
-3°
AUG 12-13, 1963
MERCATOR PROJECTION, TRUE TO SCALE AT 22½° N. AND S.

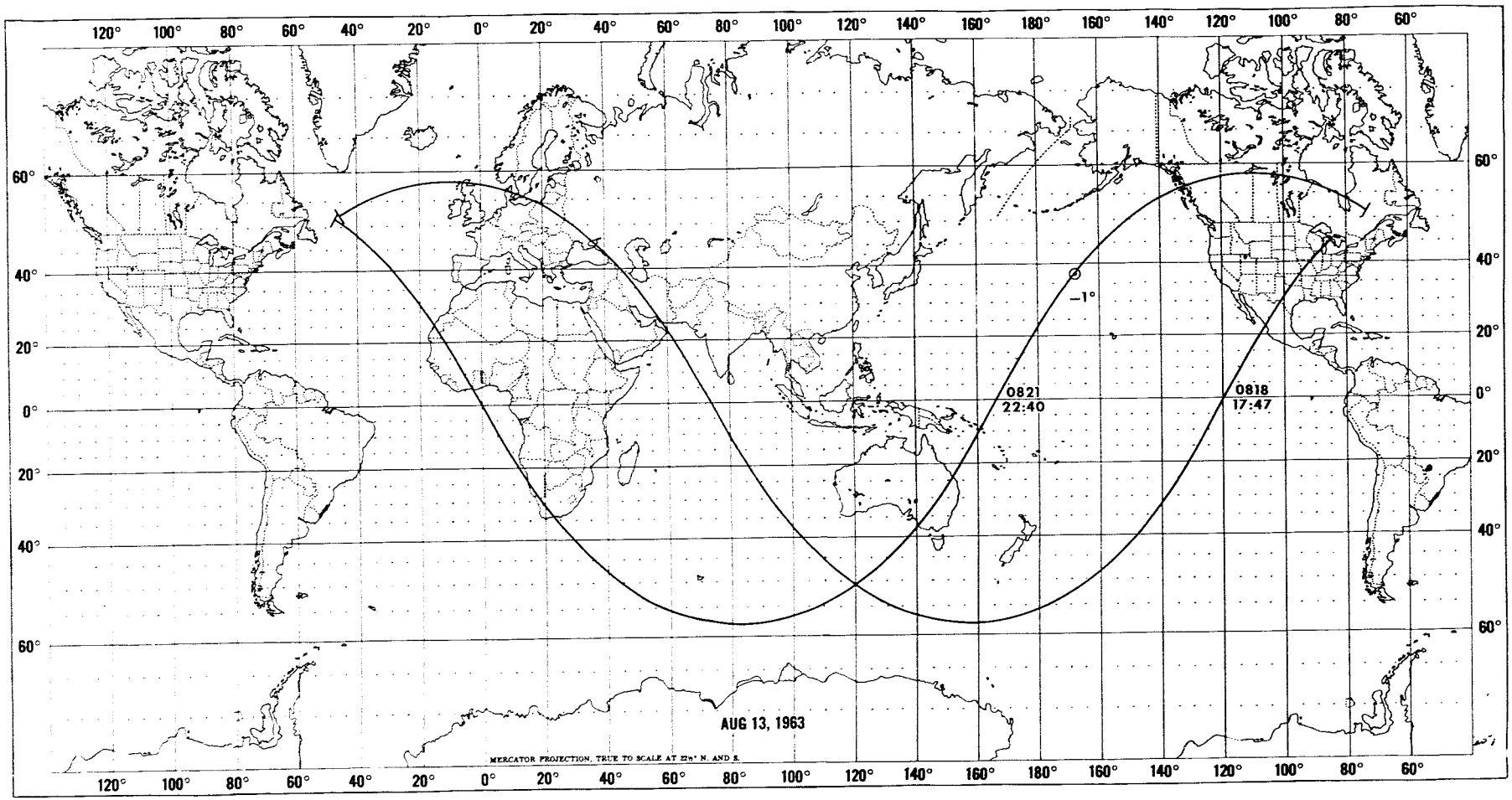
120° 100° 80° 60° 40° 20° 0° 20° 40° 60° 80° 100° 120° 140° 160° 180° 160° 140° 120° 100° 80° 60°
60°
40°
20°
0°
20°
40°
60°
−1°
0821
22:40
0818
17:47
AUG 13, 1963
MERCATOR PROJECTION, TRUE TO SCALE AT 22½° N. AND S.

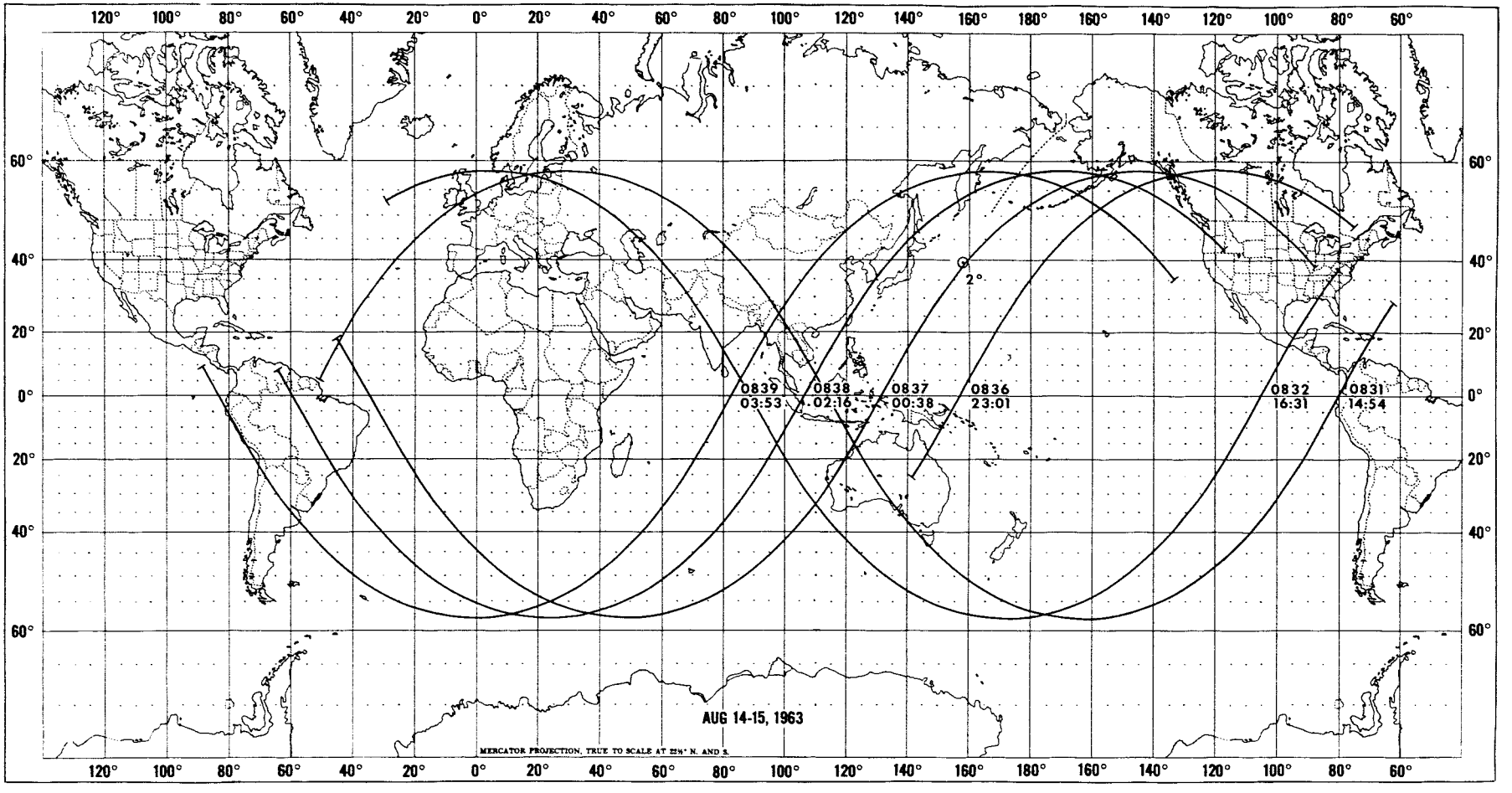
120° 100° 80° 60° 40° 20° 0° 20° 40° 60° 80° 100° 120° 140° 160° 180° 160° 140° 120° 100° 80° 60°
60° 40° 20° 0° 20° 40° 60°
0839
03:53
0838
02:16
0837
00:38
0836
23:01
0832
16:31
0831
14:54
2°
AUG 14-15, 1963
MERCATOR PROJECTION, TRUE TO SCALE AT 22½° N. AND S.

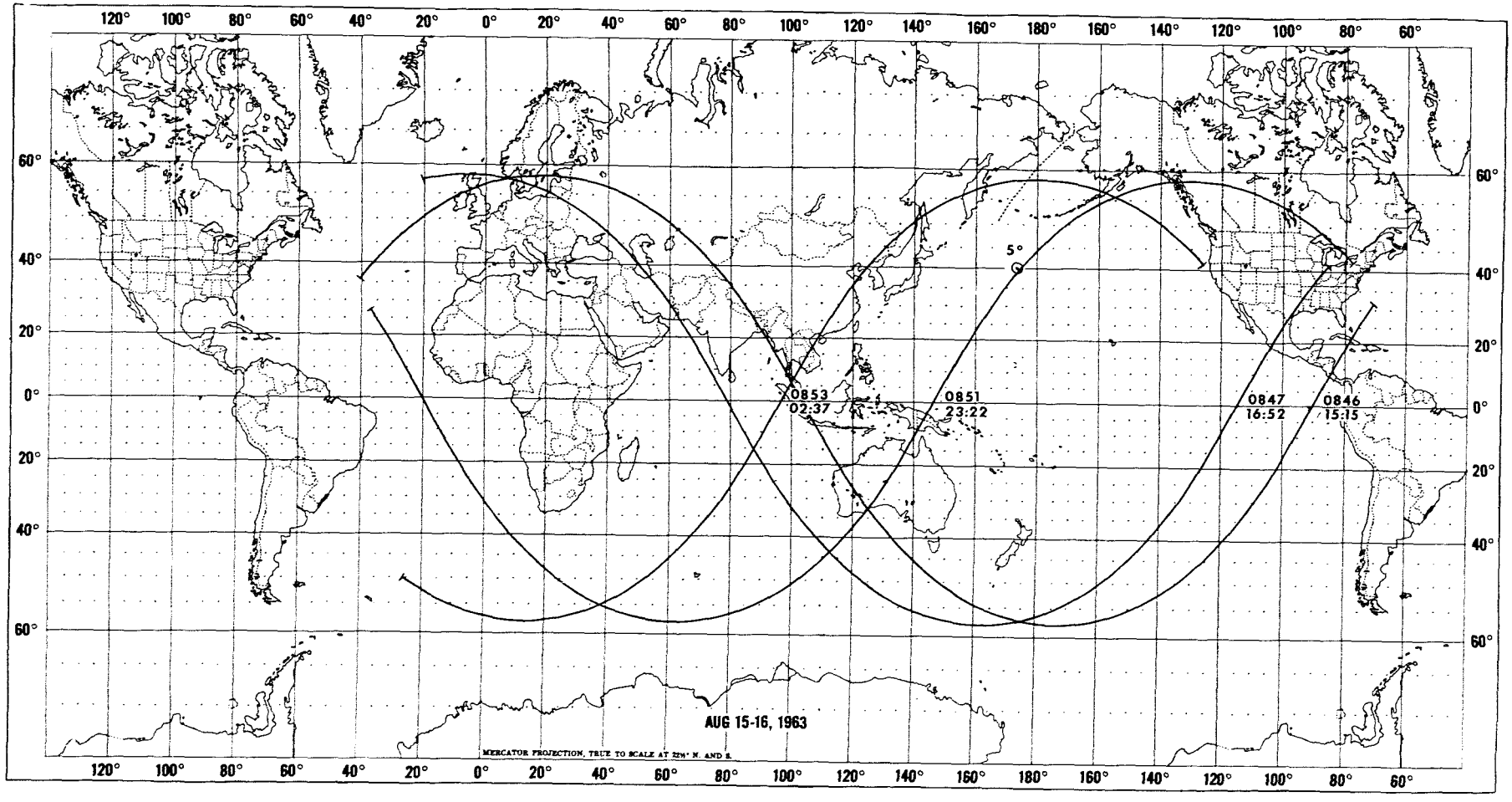
120° 100° 80° 60° 40° 20° 0° 20° 40° 60° 80° 100° 120° 140° 160° 180° 160° 140° 120° 100° 80° 60°
60° 40° 20° 0° 20° 40° 60°
5°
0853
02:37
0851
23:22
0847
16:52
0846
15:15
AUG 15-16, 1963
MERCATOR PROJECTION, TRUE TO SCALE AT 22½° N. AND S.

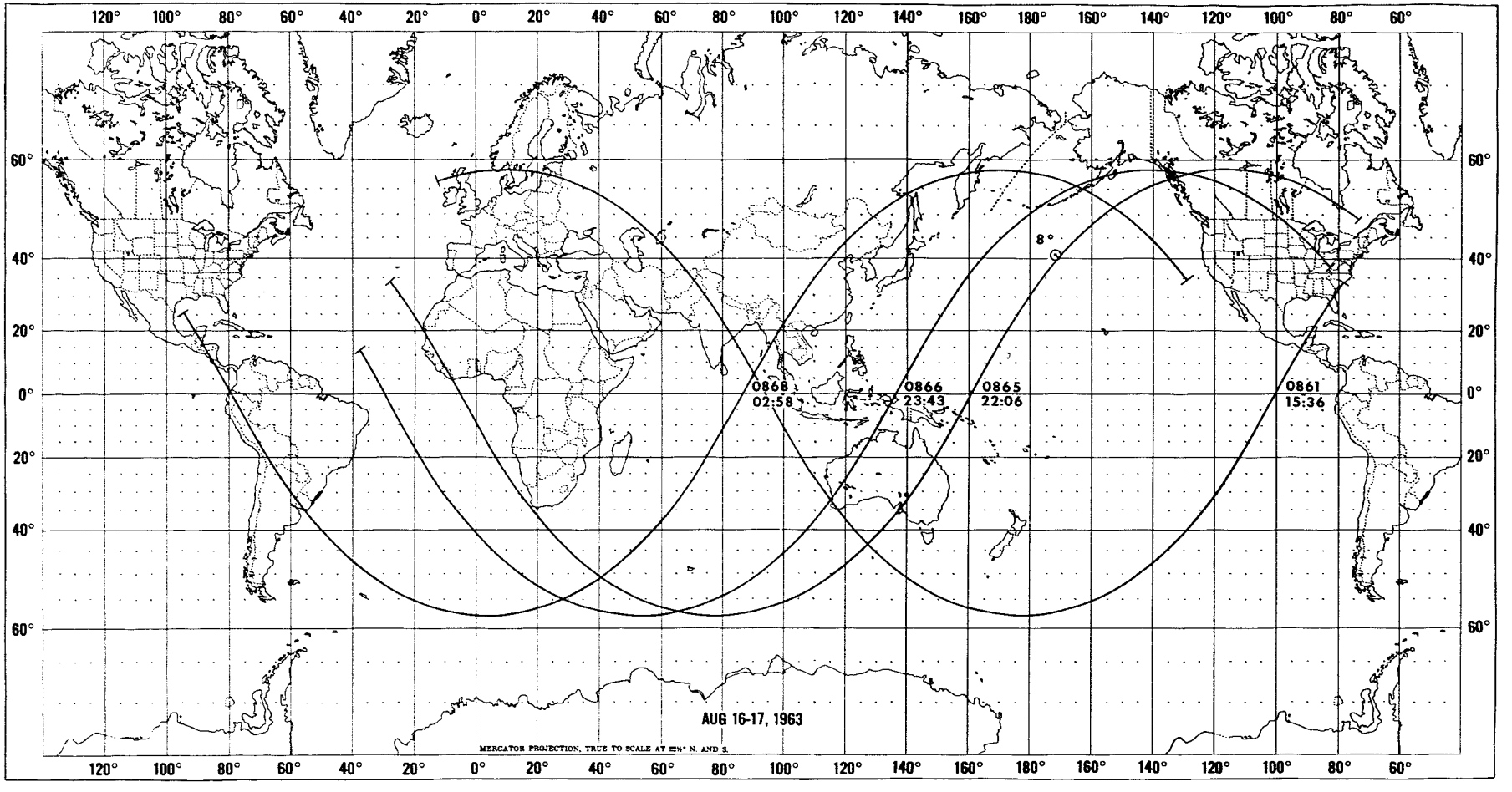
120° 100° 80° 60° 40° 20° 0° 20° 40° 60° 80° 100° 120° 140° 160° 180° 160° 140° 120° 100° 80° 60°
60° 40° 20° 0° 20° 40° 60°
0868
02:58
0866
23:43
0865
22:06
0861
15:36
8°
AUG 16-17, 1963
MERCATOR PROJECTION, TRUE TO SCALE AT 55° N. AND S.

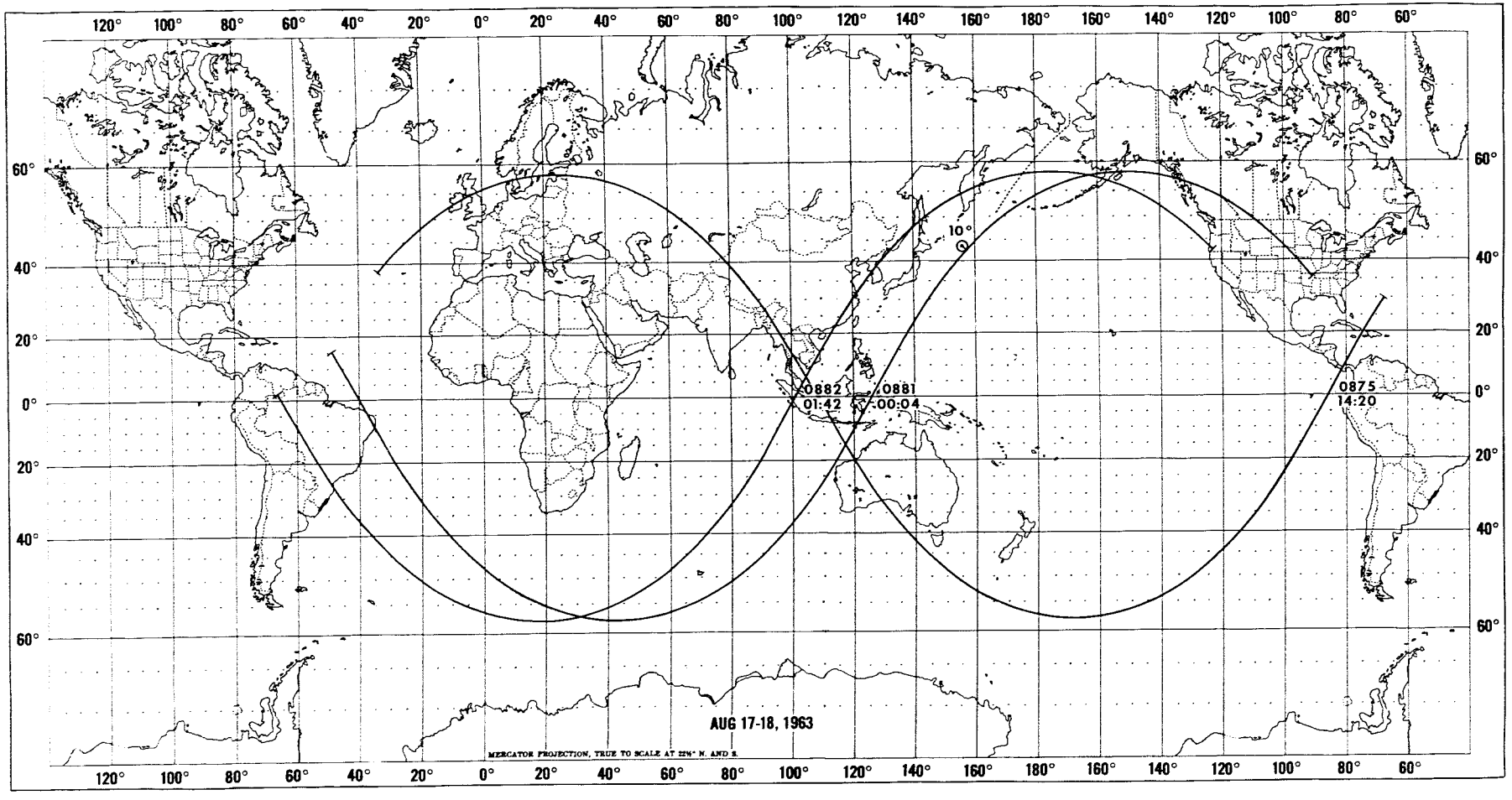
120° 100° 80° 60° 40° 20° 0° 20° 40° 60° 80° 100° 120° 140° 160° 180° 160° 140° 120° 100° 80° 60°
60° 40° 20° 0° 20° 40° 60°
10°
0882
01:42
0881
00:04
0875
14:20
AUG 17-18, 1963
MERCATOR PROJECTION, TRUE TO SCALE AT 22½° N. AND S.

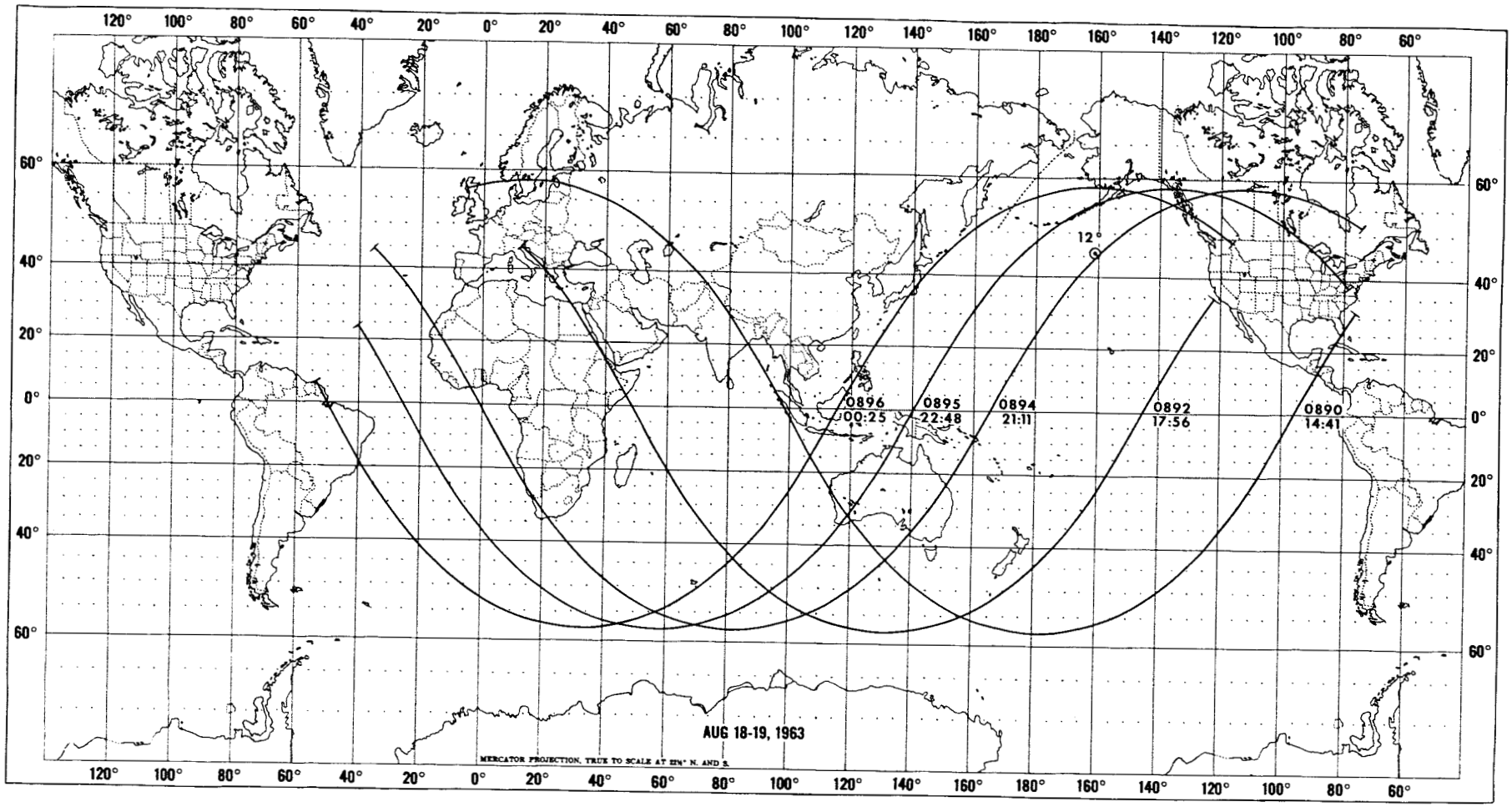
0896
00:25
0895
22:48
0894
21:11
0892
17:56
0890
14:41
12°
AUG 18-19, 1963
MERCATOR PROJECTION, TRUE TO SCALE AT 22½° N. AND S.

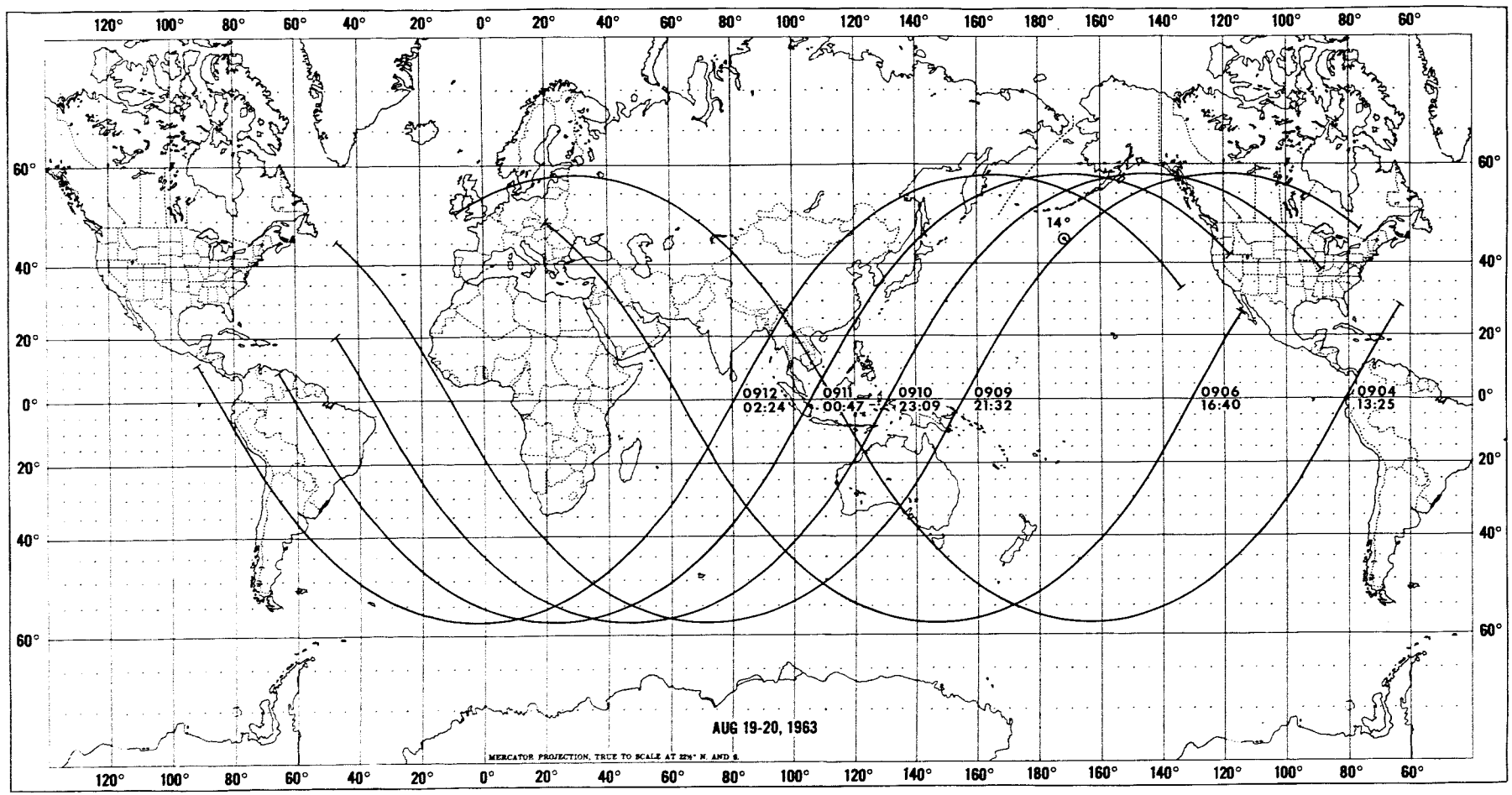
120° 100° 80° 60° 40° 20° 0° 20° 40° 60° 80° 100° 120° 140° 160° 180° 160° 140° 120° 100° 80° 60°
60° 40° 20° 0° 20° 40° 60°
14°
0912
02:24
0911
00:47
0910
23:09
0909
21:32
0906
16:40
0904
13:25
AUG 19-20, 1963
MERCATOR PROJECTION, TRUE TO SCALE AT 22½° N. AND S.

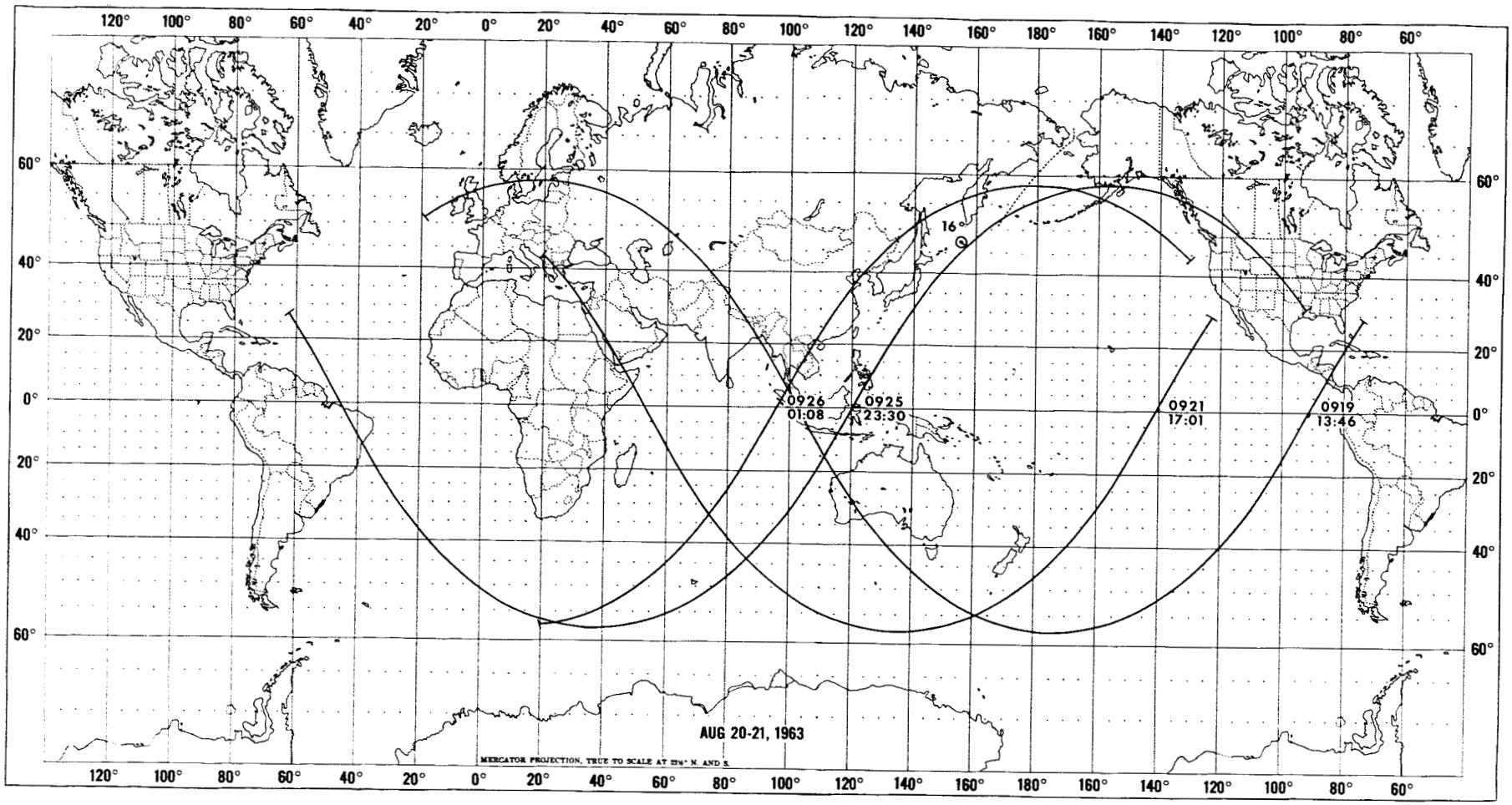
120° 100° 80° 60° 40° 20° 0° 20° 40° 60° 80° 100° 120° 140° 160° 180° 160° 140° 120° 100° 80° 60°
60° 40° 20° 0° 20° 40° 60°
16
0926
01:08
0925
23:30
0921
17:01
0919
13:46
AUG 20-21, 1963
MERCATOR PROJECTION, TRUE TO SCALE AT 22½° N. AND S.

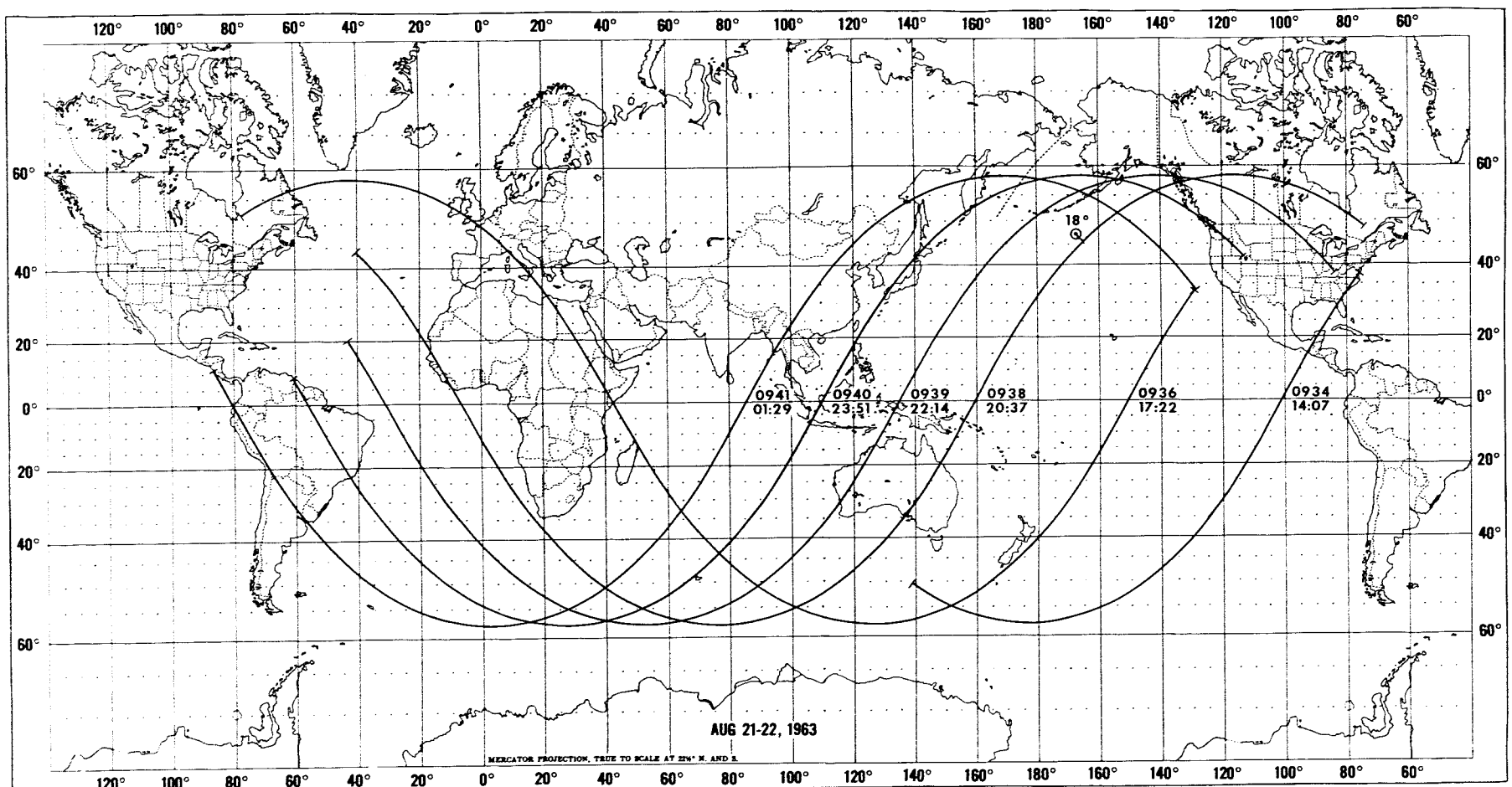
120° 100° 80° 60° 40° 20° 0° 20° 40° 60° 80° 100° 120° 140° 160° 180° 160° 140° 120° 100° 80° 60°
60° 40° 20° 0° 20° 40° 60°
18°
0941
01:29
0940
23:51
0939
22:14
0938
20:37
0936
17:22
0934
14:07
AUG 21-22, 1963
MERCATOR PROJECTION, TRUE TO SCALE AT 22½° N. AND S.

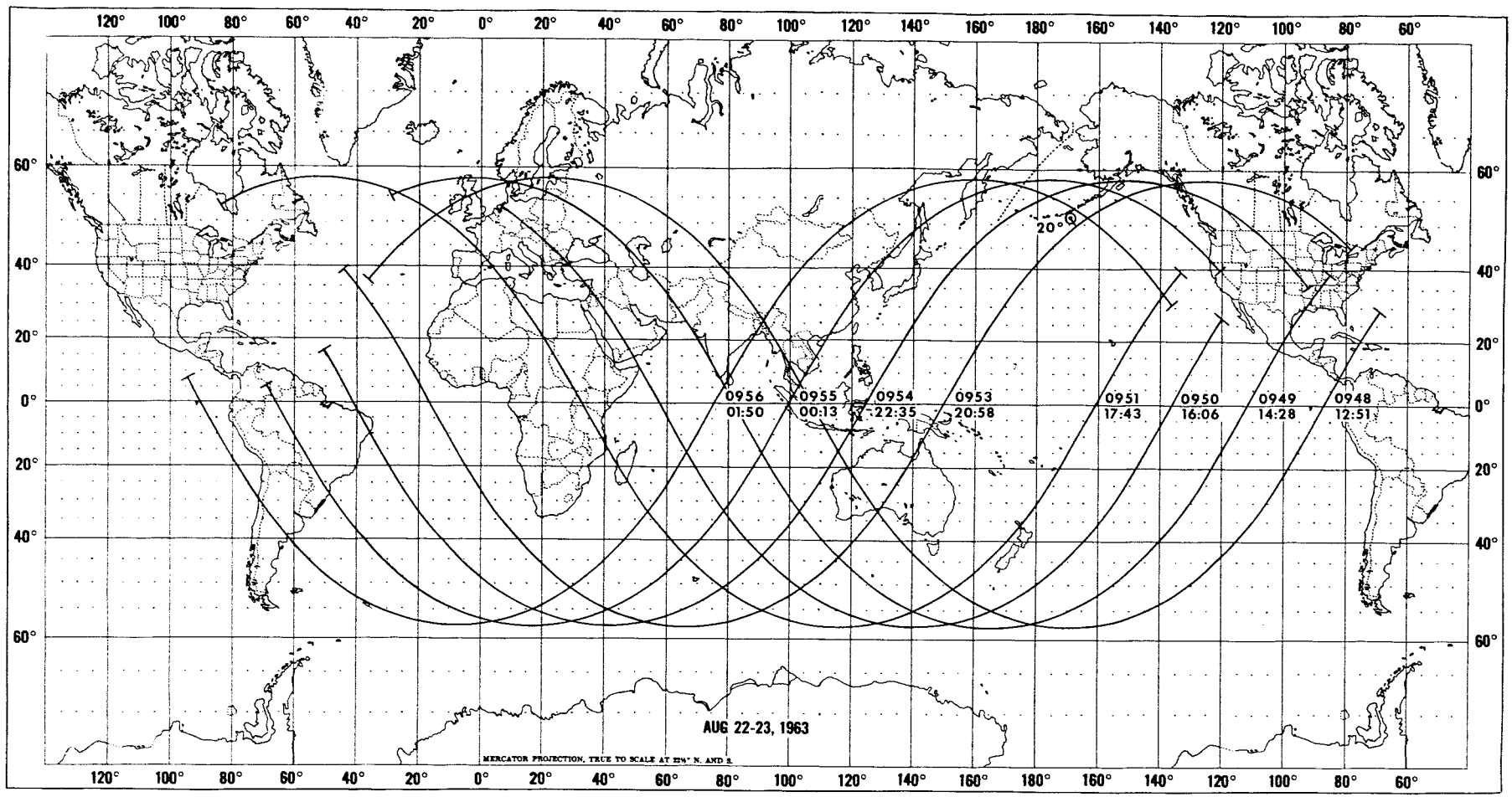
120° 100° 80° 60° 40° 20° 0° 20° 40° 60° 80° 100° 120° 140° 160° 180° 160° 140° 120° 100° 80° 60°
60° 40° 20° 0° 20° 40° 60°
0956
01:50
0955
00:13
0954
22:35
0953
20:58
0951
17:43
0950
16:06
0949
14:28
0948
12:51
20°
AUG 22-23, 1963
MERCATOR PROJECTION, TRUE TO SCALE AT 22½° N. AND S.

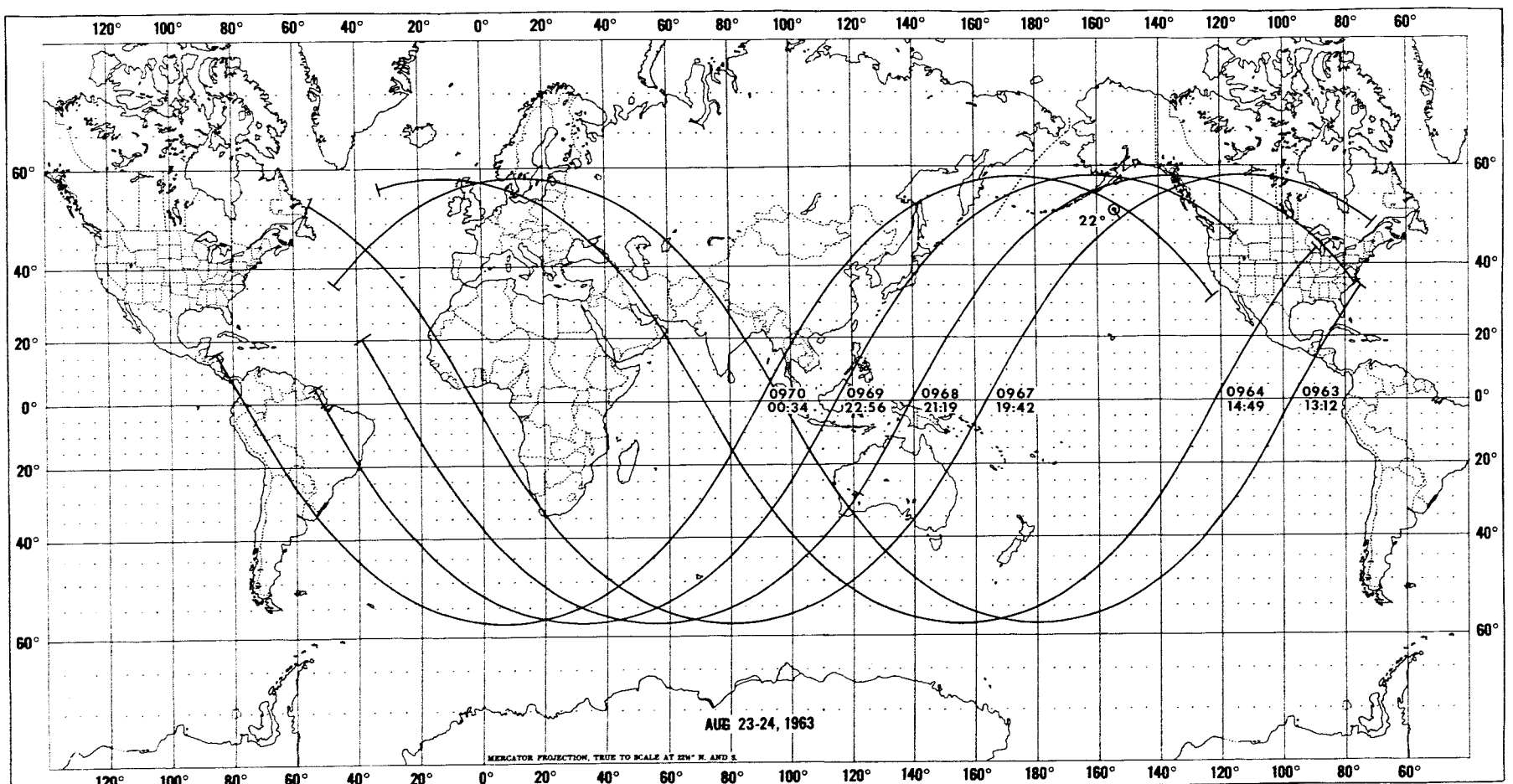
120° 100° 80° 60° 40° 20° 0° 20° 40° 60° 80° 100° 120° 140° 160° 180° 160° 140° 120° 100° 80° 60°
60° 40° 20° 0° 20° 40° 60°
22°
0970 00:34
0969 22:56
0968 21:19
0967 19:42
0964 14:49
0963 13:12
AUG 23-24, 1963
MERCATOR PROJECTION, TRUE TO SCALE AT 22½° N. AND S.

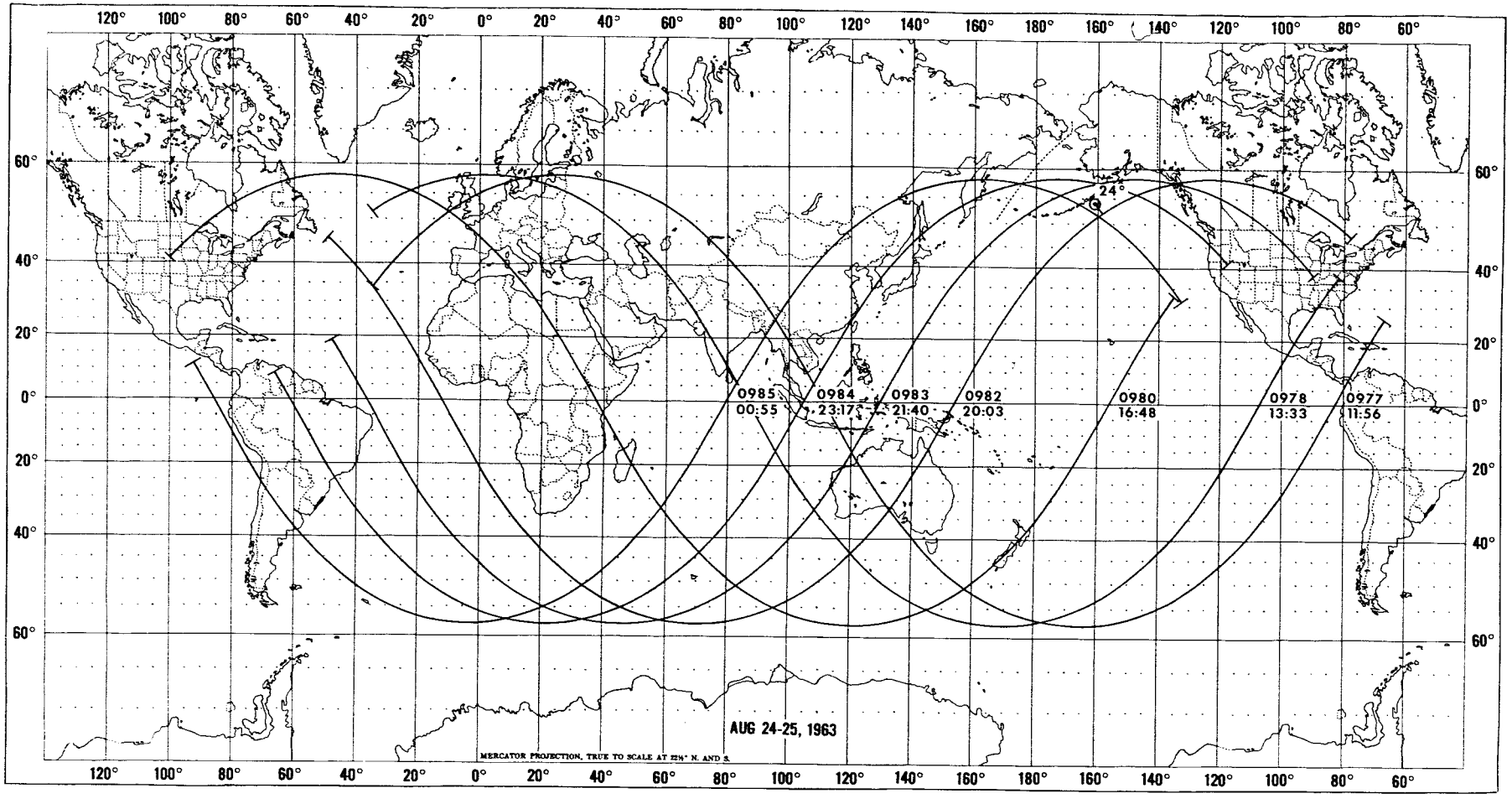
120° 100° 80° 60° 40° 20° 0° 20° 40° 60° 80° 100° 120° 140° 160° 180° 160° 140° 120° 100° 80° 60°
60° 40° 20° 0° 20° 40° 60°
0985
00:55
0984
23:17
0983
21:40
0982
20:03
0980
16:48
0978
13:33
0977
11:56
24°
AUG 24-25, 1963
MERCATOR PROJECTION, TRUE TO SCALE AT 22½° N. AND S.

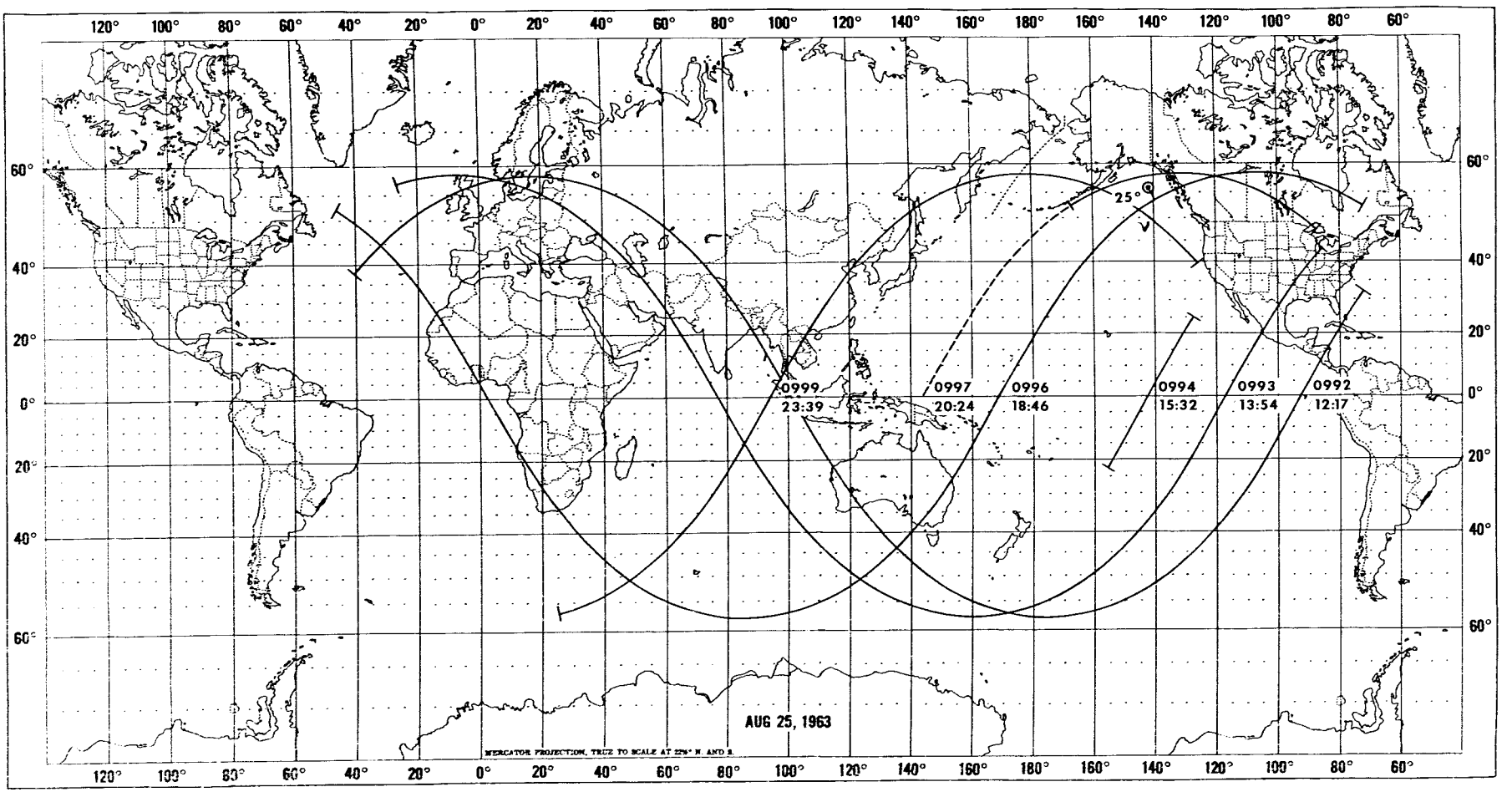
120° 100° 80° 60° 40° 20° 0° 20° 40° 60° 80° 100° 120° 140° 160° 180° 160° 140° 120° 100° 80° 60°
60° 40° 20° 0° 20° 40° 60°
0999
23:39
0997
20:24
0996
18:46
0994
15:32
0993
13:54
0992
12:17
25°
AUG 25, 1963
MERCATOR PROJECTION, TRUE TO SCALE AT 22½° N. AND S.

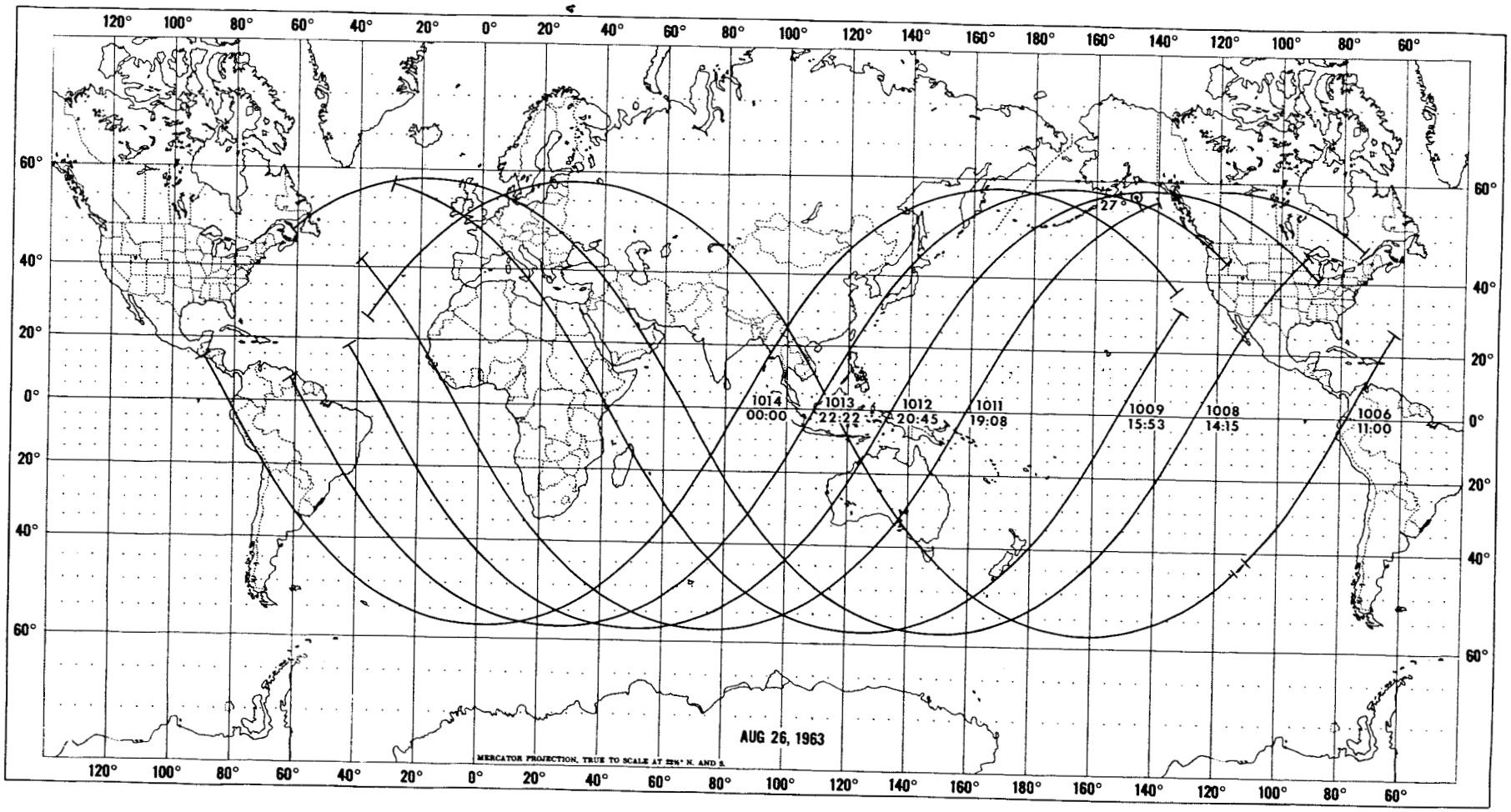
1014
00:00
1013
22:22
1012
20:45
1011
19:08
1009
15:53
1008
14:15
1006
11:00
27°
AUG 26, 1963
MERCATOR PROJECTION, TRUE TO SCALE AT 32½° N. AND S.

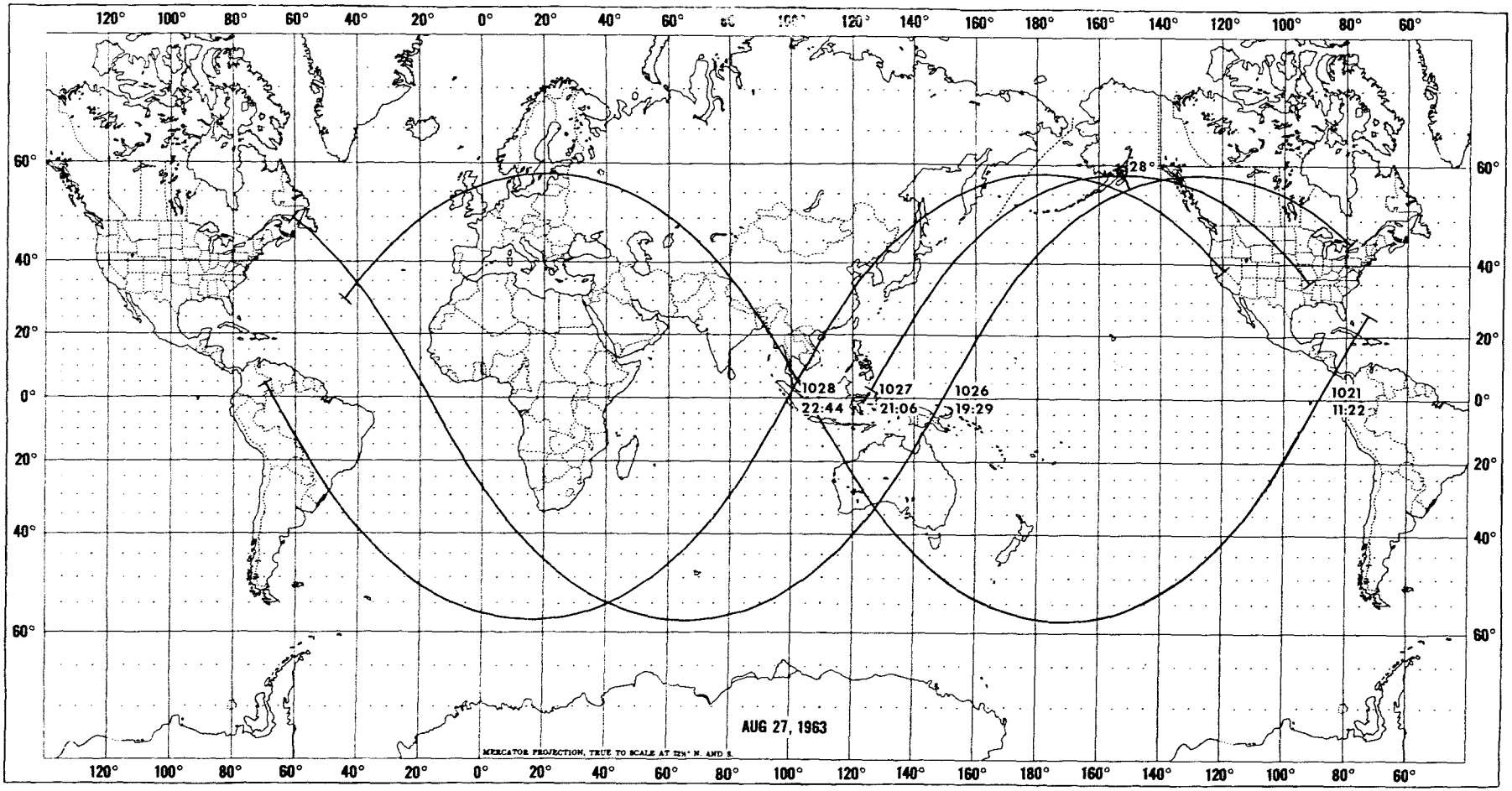
1028
22:44
1027
21:06
1026
19:29
1021
11:22
AUG 27, 1963
MERCATOR PROJECTION, TRUE TO SCALE AT 12½° N. AND S.

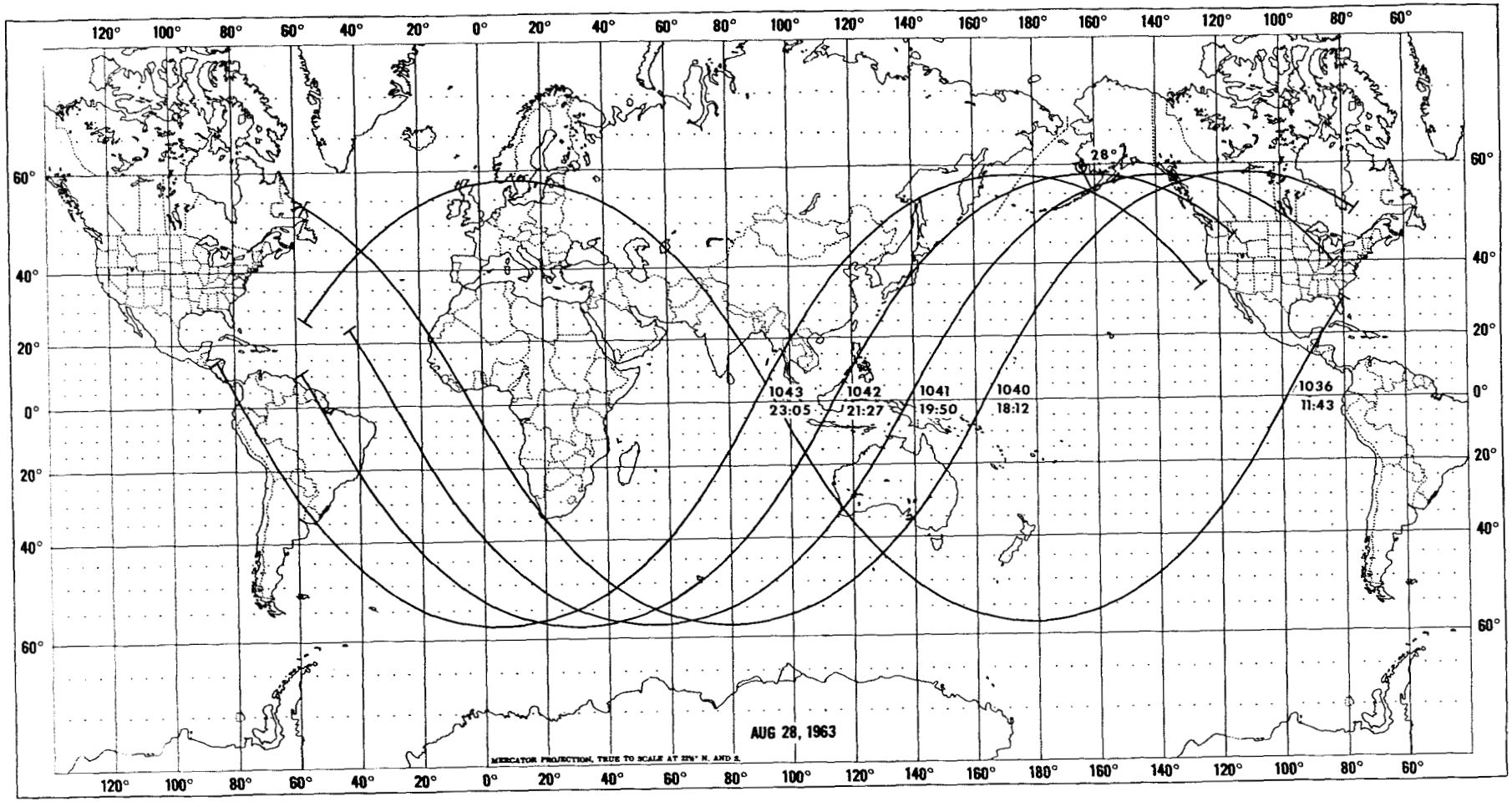
120° 100° 80° 60° 40° 20° 0° 20° 40° 60° 80° 100° 120° 140° 160° 180° 160° 140° 120° 100° 80° 60°
60° 40° 20° 0° 20° 40° 60°
28°
1043
23:05
1042
21:27
1041
19:50
1040
18:12
1036
11:43
AUG 28, 1963
MERCATOR PROJECTION, TRUE TO SCALE AT 22½° N. AND S.

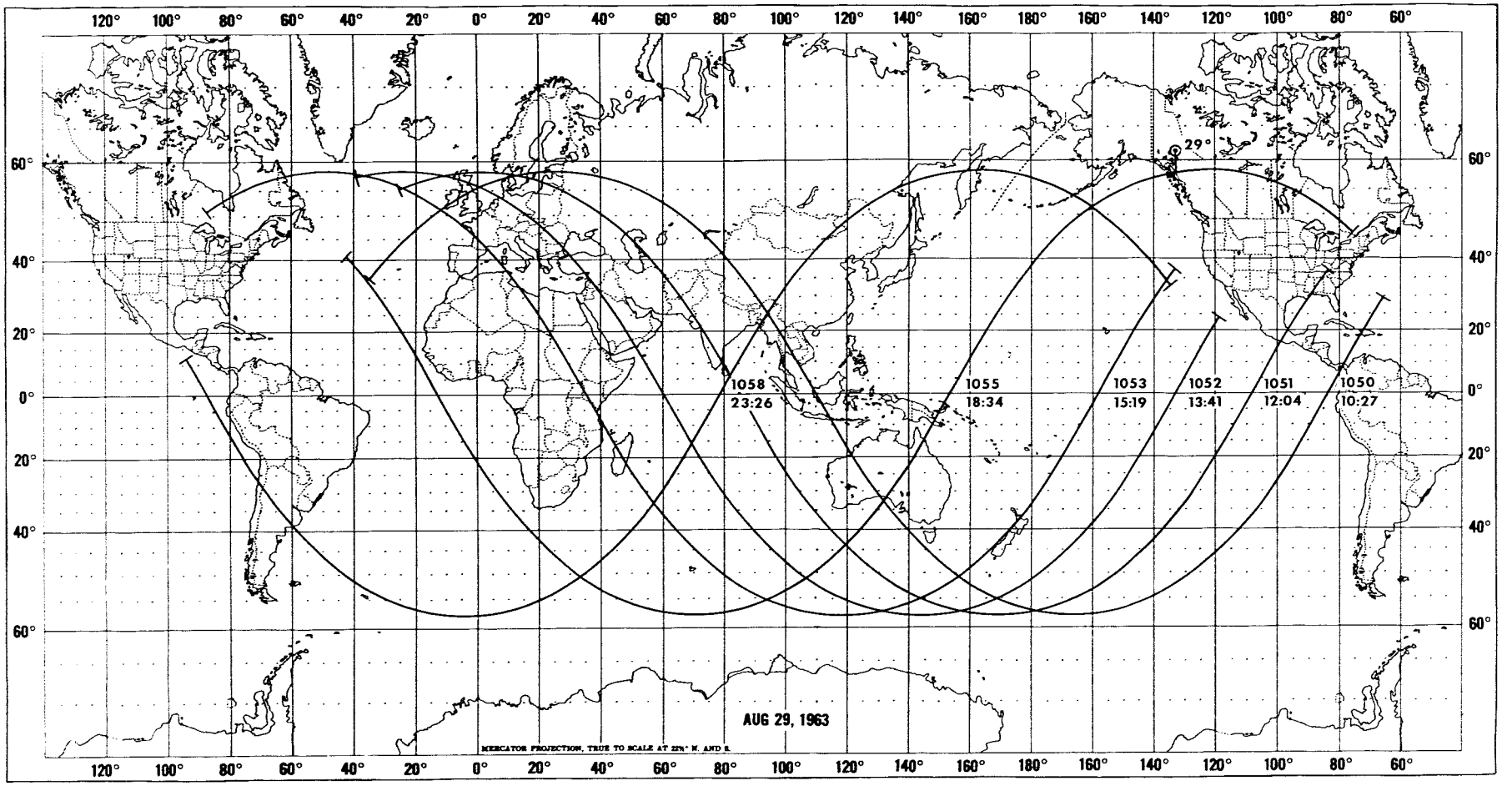
120° 100° 80° 60° 40° 20° 0° 20° 40° 60° 80° 100° 120° 140° 160° 180° 160° 140° 120° 100° 80° 60°
60° 40° 20° 0° 20° 40° 60°
29°
1058
23:26
1055
18:34
1053
15:19
1052
13:41
1051
12:04
1050
10:27
AUG 29, 1963
MERCATOR PROJECTION, TRUE TO SCALE AT 22½° N. AND S.

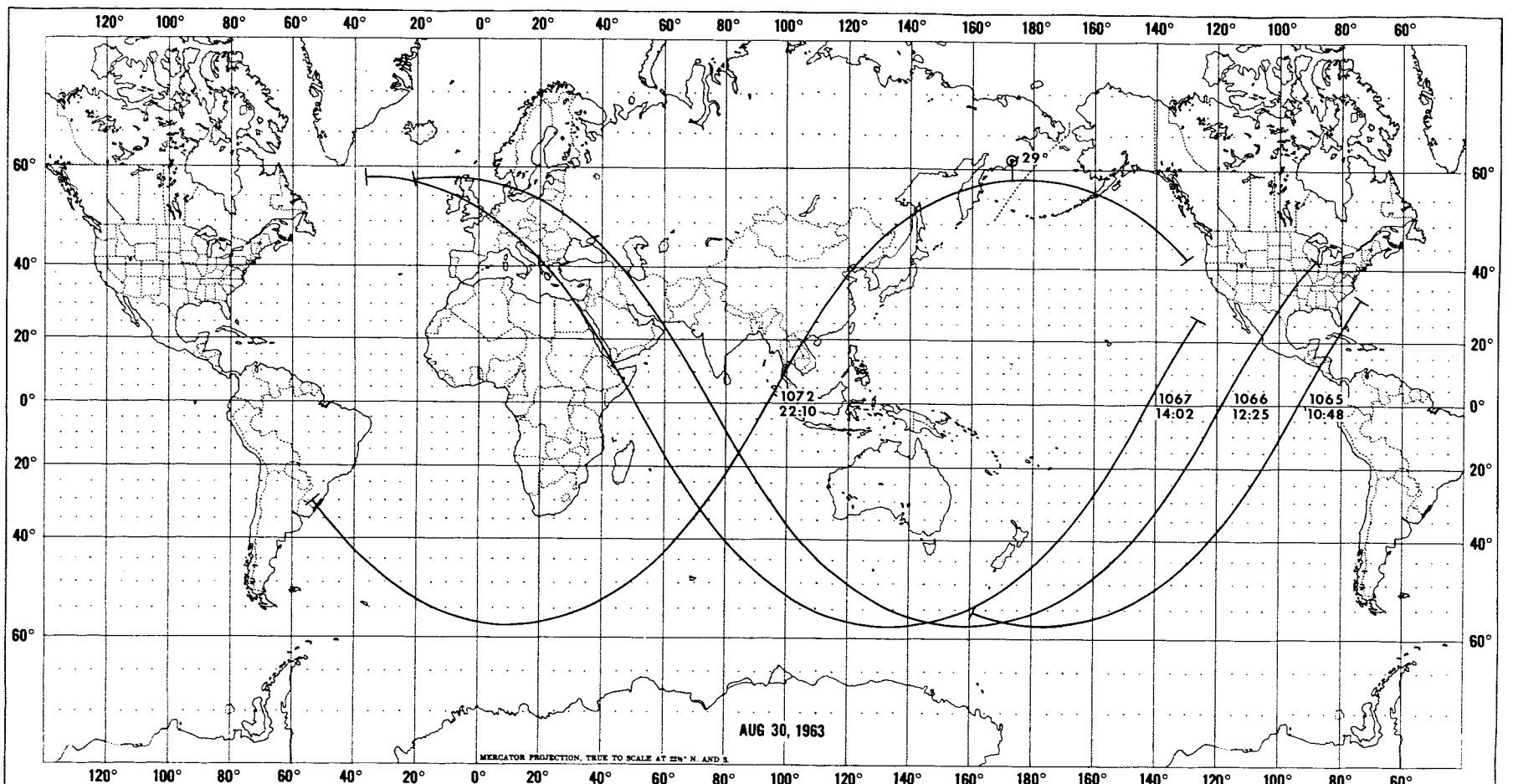
120° 100° 80° 60° 40° 20° 0° 20° 40° 60° 80° 100° 120° 140° 160° 180° 160° 140° 120° 100° 80° 60°
60° 40° 20° 0° 20° 40° 60°
29°
1072
22:10
1067
14:02
1066
12:25
1065
10:48
AUG 30, 1963
MERCATOR PROJECTION, TRUE TO SCALE AT 22½° N. AND S.

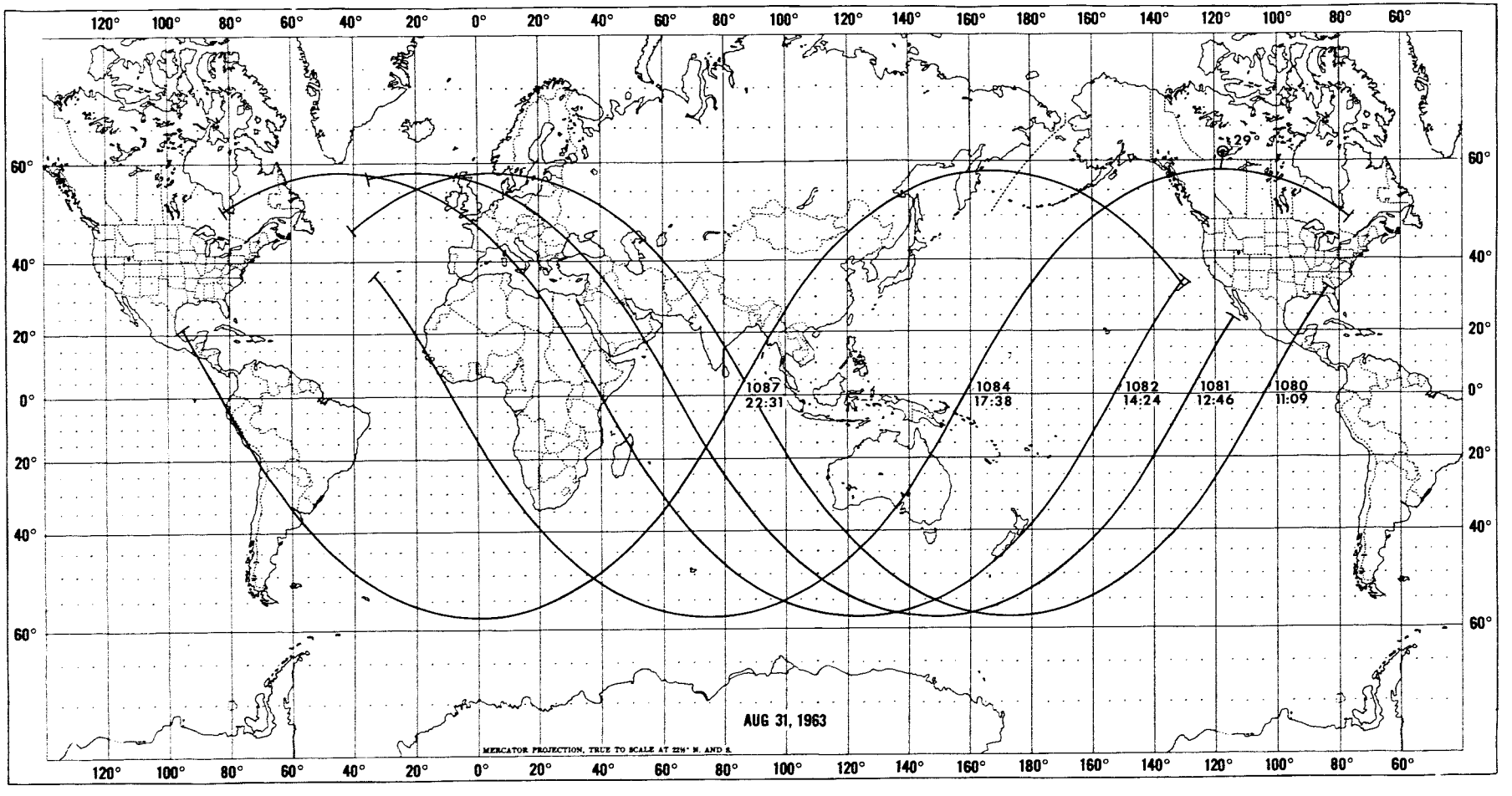
120° 100° 80° 60° 40° 20° 0° 20° 40° 60° 80° 100° 120° 140° 160° 180° 160° 140° 120° 100° 80° 60°
60° 40° 20° 0° 20° 40° 60°
29°
1087
22:31
1084
17:38
1082
14:24
1081
12:46
1080
11:09
AUG 31, 1963
MERCATOR PROJECTION, TRUE TO SCALE AT 22½° N. AND S.

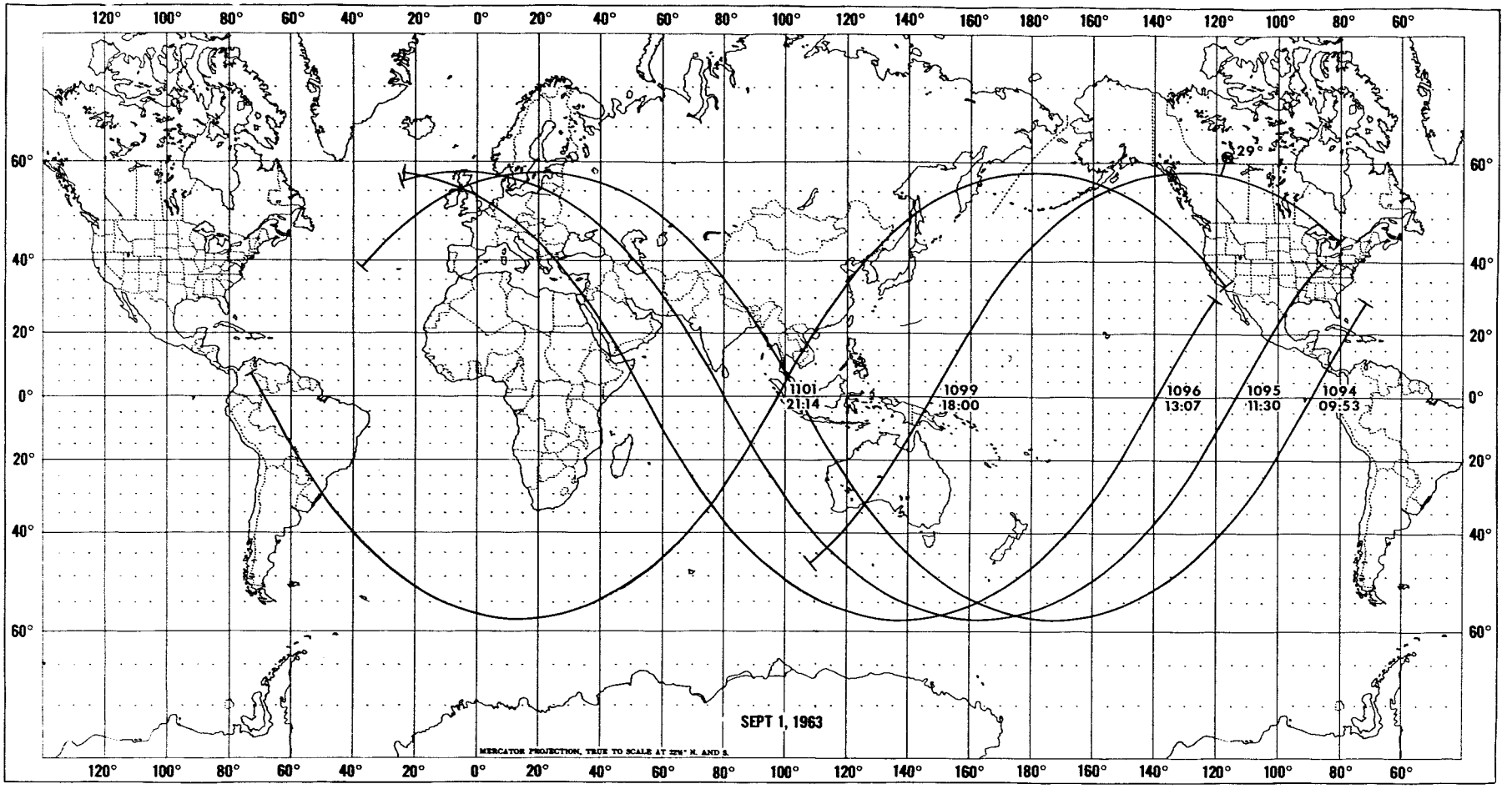
120° 100° 80° 60° 40° 20° 0° 20° 40° 60° 80° 100° 120° 140° 160° 180° 160° 140° 120° 100° 80° 60°
60° 40° 20° 0° 20° 40° 60°
29°
1101
21:14
1099
18:00
1096
13:07
1095
11:30
1094
09:53
SEPT 1, 1963
MERCATOR PROJECTION, TRUE TO SCALE AT 22½° N. AND S.

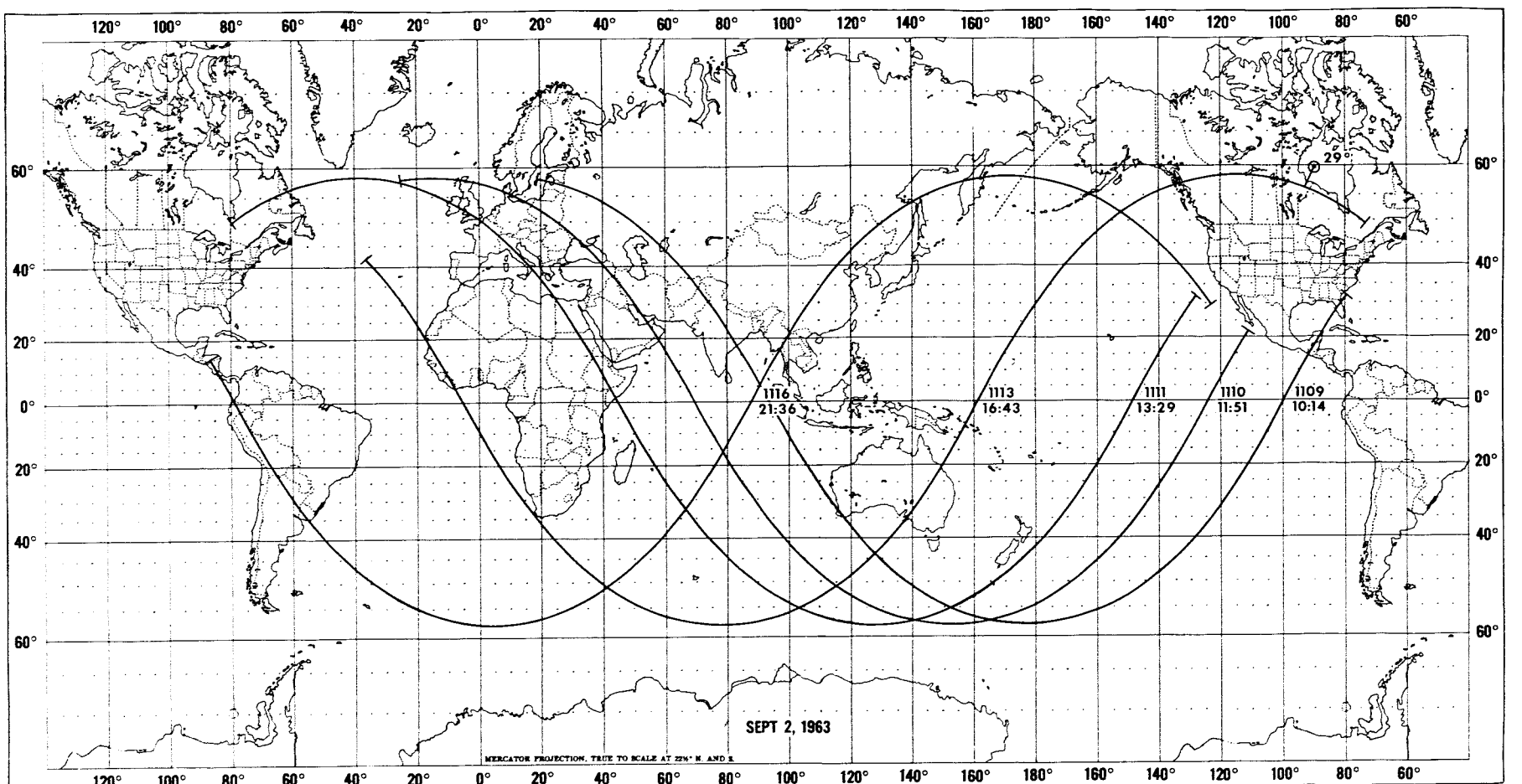
1116
21:36
1113
16:43
1111
13:29
1110
11:51
1109
10:14
29°
SEPT 2, 1963
MERCATOR PROJECTION, TRUE TO SCALE AT 22½° N. AND S.

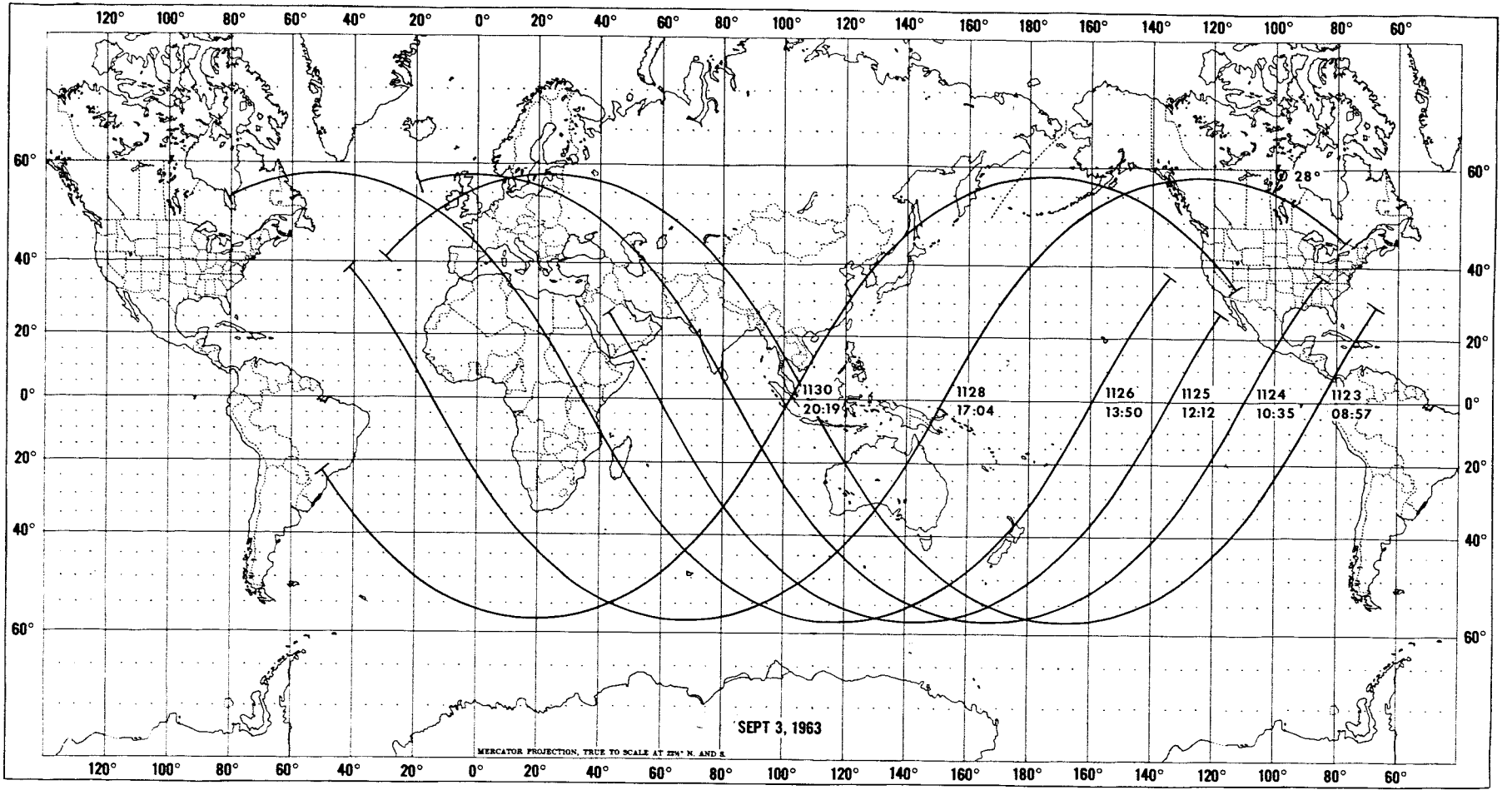
120° 100° 80° 60° 40° 20° 0° 20° 40° 60° 80° 100° 120° 140° 160° 180° 160° 140° 120° 100° 80° 60°
60° 40° 20° 0° 20° 40° 60°
28°
1130
20:19
1128
17:04
1126
13:50
1125
12:12
1124
10:35
1123
08:57
SEPT 3, 1963
MERCATOR PROJECTION, TRUE TO SCALE AT 22½° N. AND S.

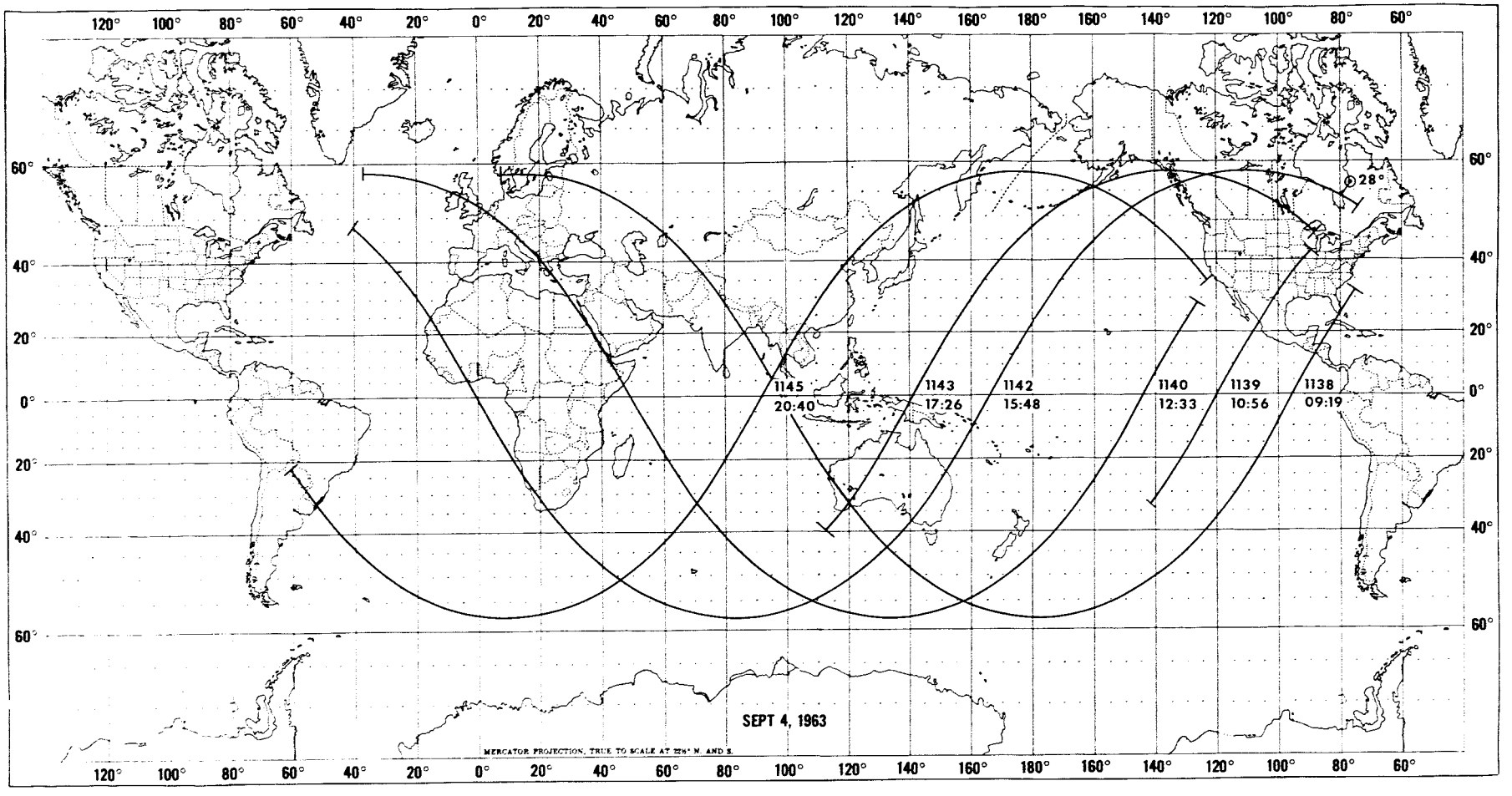
120° 100° 80° 60° 40° 20° 0° 20° 40° 60° 80° 100° 120° 140° 160° 180° 160° 140° 120° 100° 80° 60°
60° 40° 20° 0° 20° 40° 60°
28°
1145
20:40
1143
17:26
1142
15:48
1140
12:33
1139
10:56
1138
09:19
SEPT 4, 1963
MERCATOR PROJECTION, TRUE TO SCALE AT 22½° N. AND S.

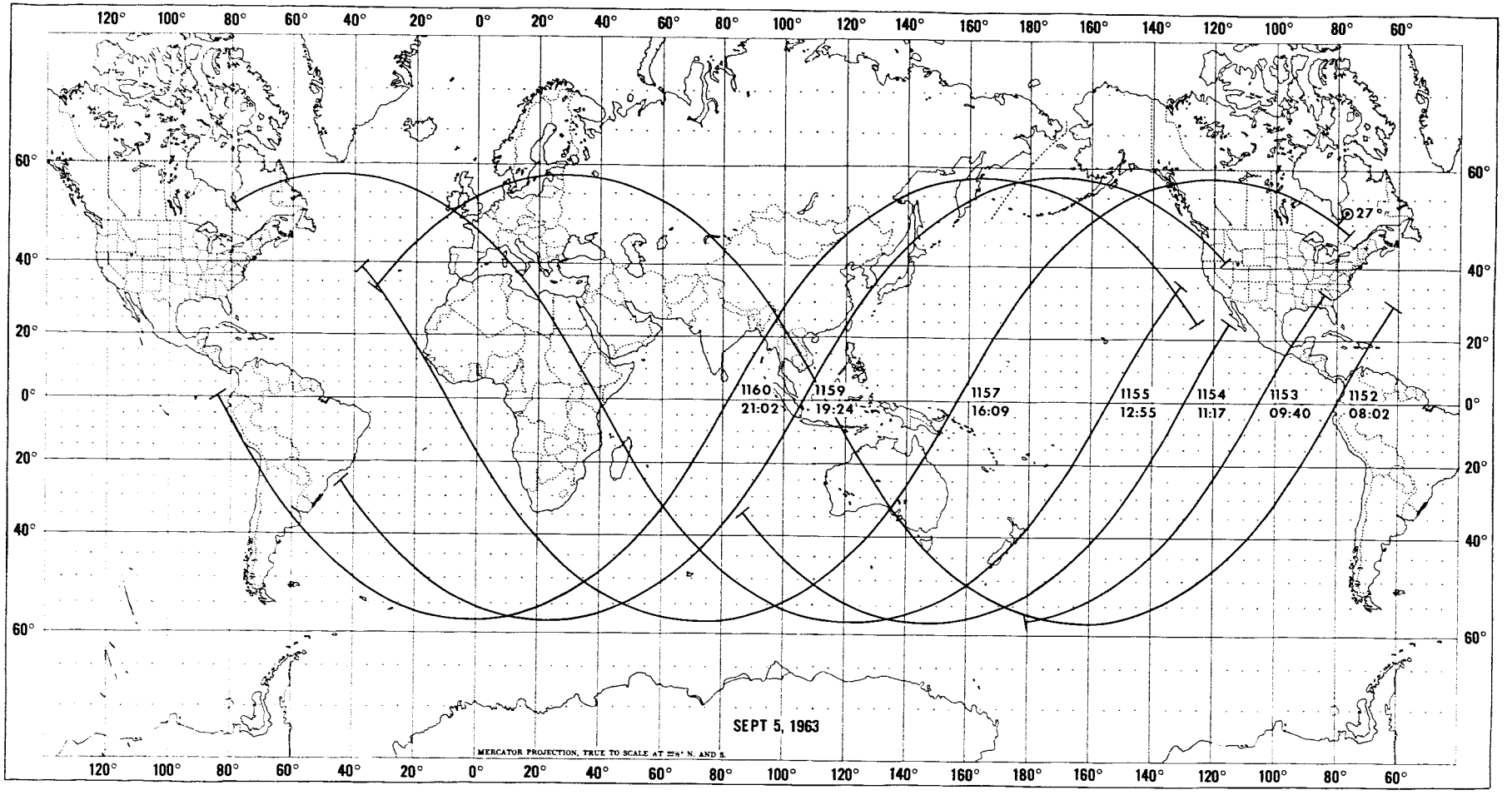
120° 100° 80° 60° 40° 20° 0° 20° 40° 60° 80° 100° 120° 140° 160° 180° 160° 140° 120° 100° 80° 60°
60° 40° 20° 0° 20° 40° 60°
1160
21:02
1159
19:24
1157
16:09
1155
12:55
1154
11:17
1153
09:40
1152
08:02
27°
SEPT 5, 1963
MERCATOR PROJECTION, TRUE TO SCALE AT 22½° N. AND S.

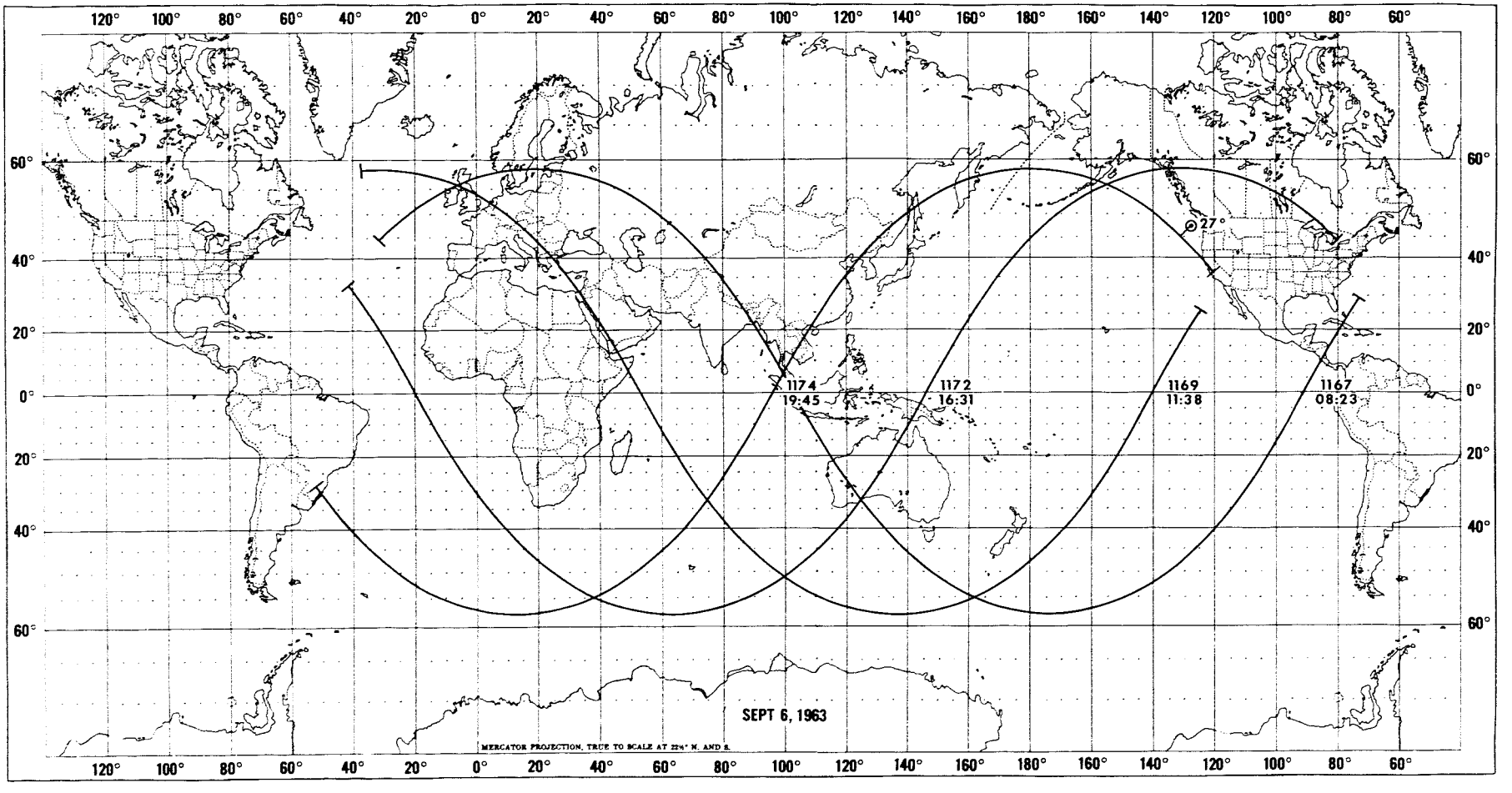
120° 100° 80° 60° 40° 20° 0° 20° 40° 60° 80° 100° 120° 140° 160° 180° 160° 140° 120° 100° 80° 60°
60° 40° 20° 0° 20° 40° 60°
27°
1174
19:45
1172
16:31
1169
11:38
1167
08:23
SEPT 6, 1963
MERCATOR PROJECTION, TRUE TO SCALE AT 22½° N. AND S.

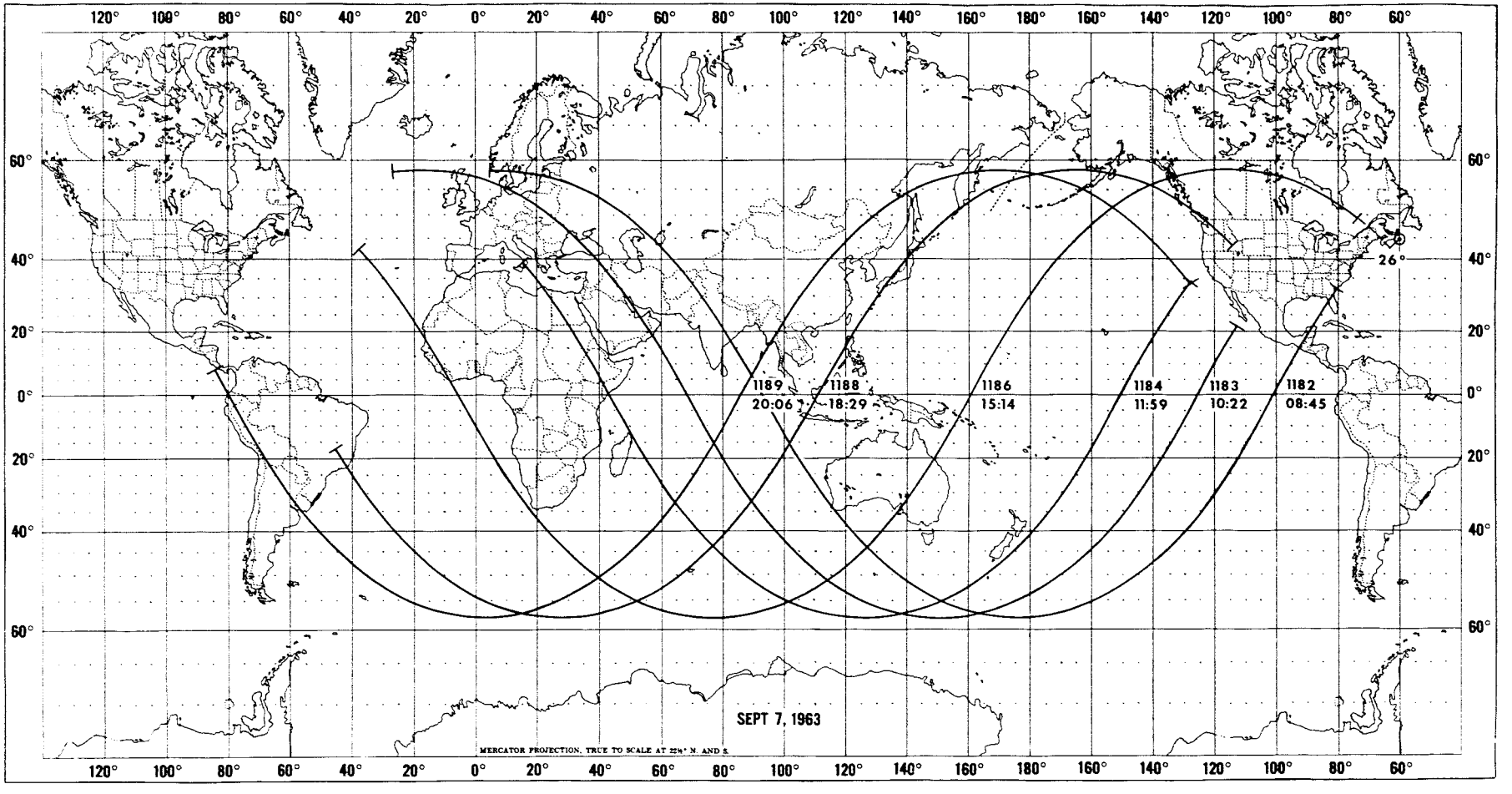
1189
20:06
1188
18:29
1186
15:14
1184
11:59
1183
10:22
1182
08:45
26°
SEPT 7, 1963
MERCATOR PROJECTION, TRUE TO SCALE AT 22½° N. AND S.

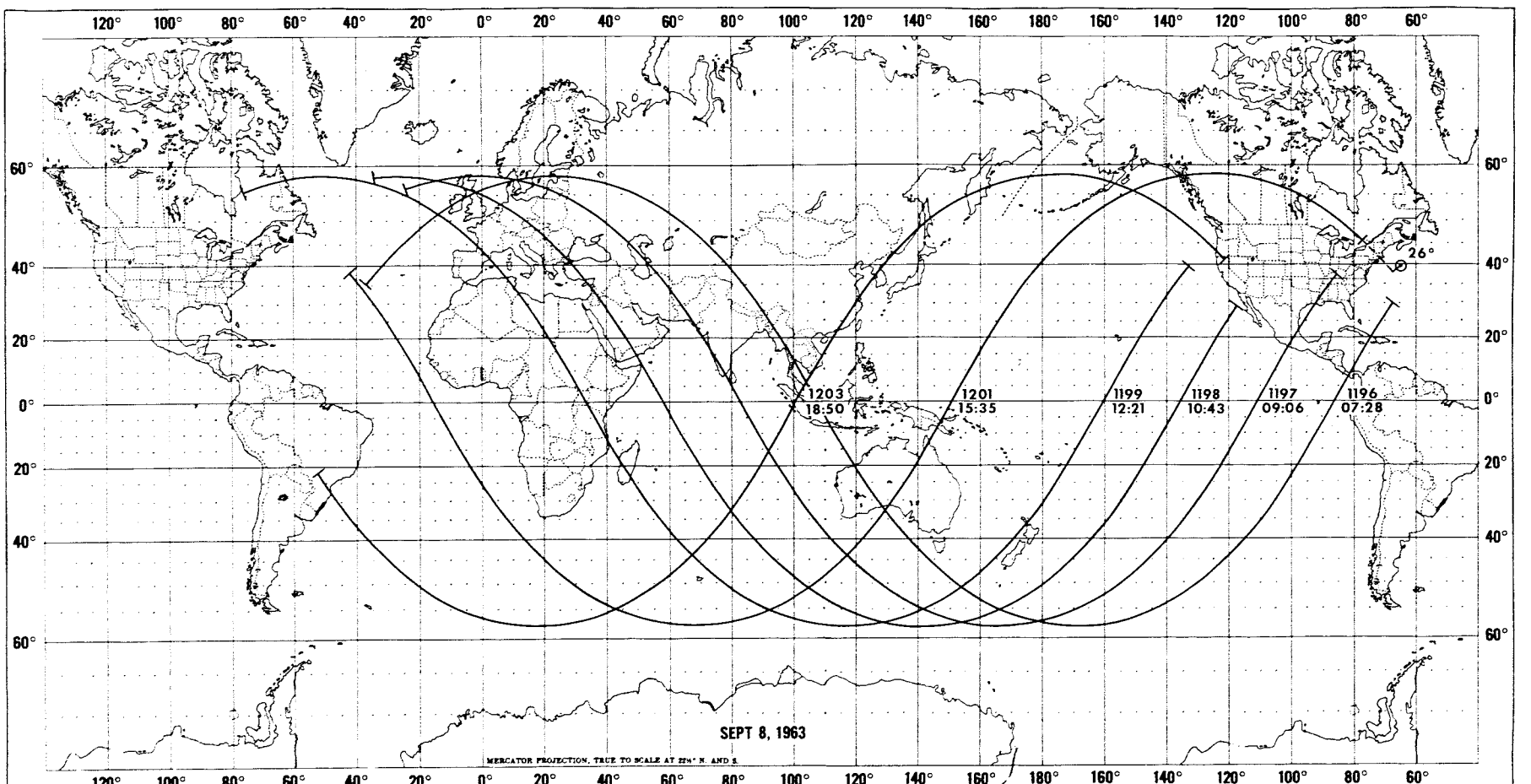
120° 100° 80° 60° 40° 20° 0° 20° 40° 60° 80° 100° 120° 140° 160° 180° 160° 140° 120° 100° 80° 60°
60° 40° 20° 0° 20° 40° 60°
26°
1203
18:50
1201
15:35
1199
12:21
1198
10:43
1197
09:06
1196
07:28
SEPT 8, 1963
MERCATOR PROJECTION, TRUE TO SCALE AT 22½° N. AND S.

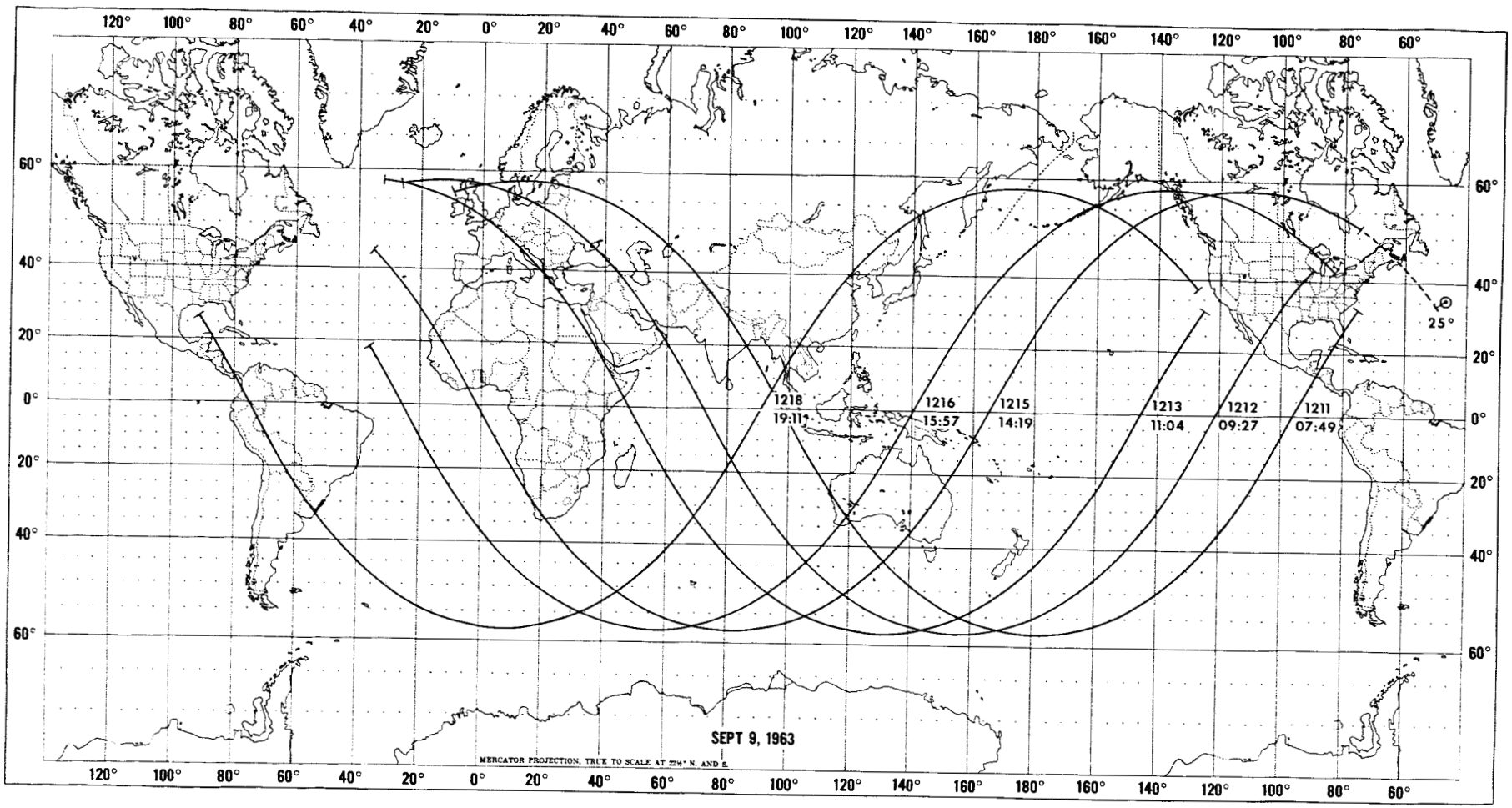
1218
19:11
1216
15:57
1215
14:19
1213
11:04
1212
09:27
1211
07:49
25°
SEPT 9, 1963
MERCATOR PROJECTION, TRUE TO SCALE AT 22½° N. AND S.

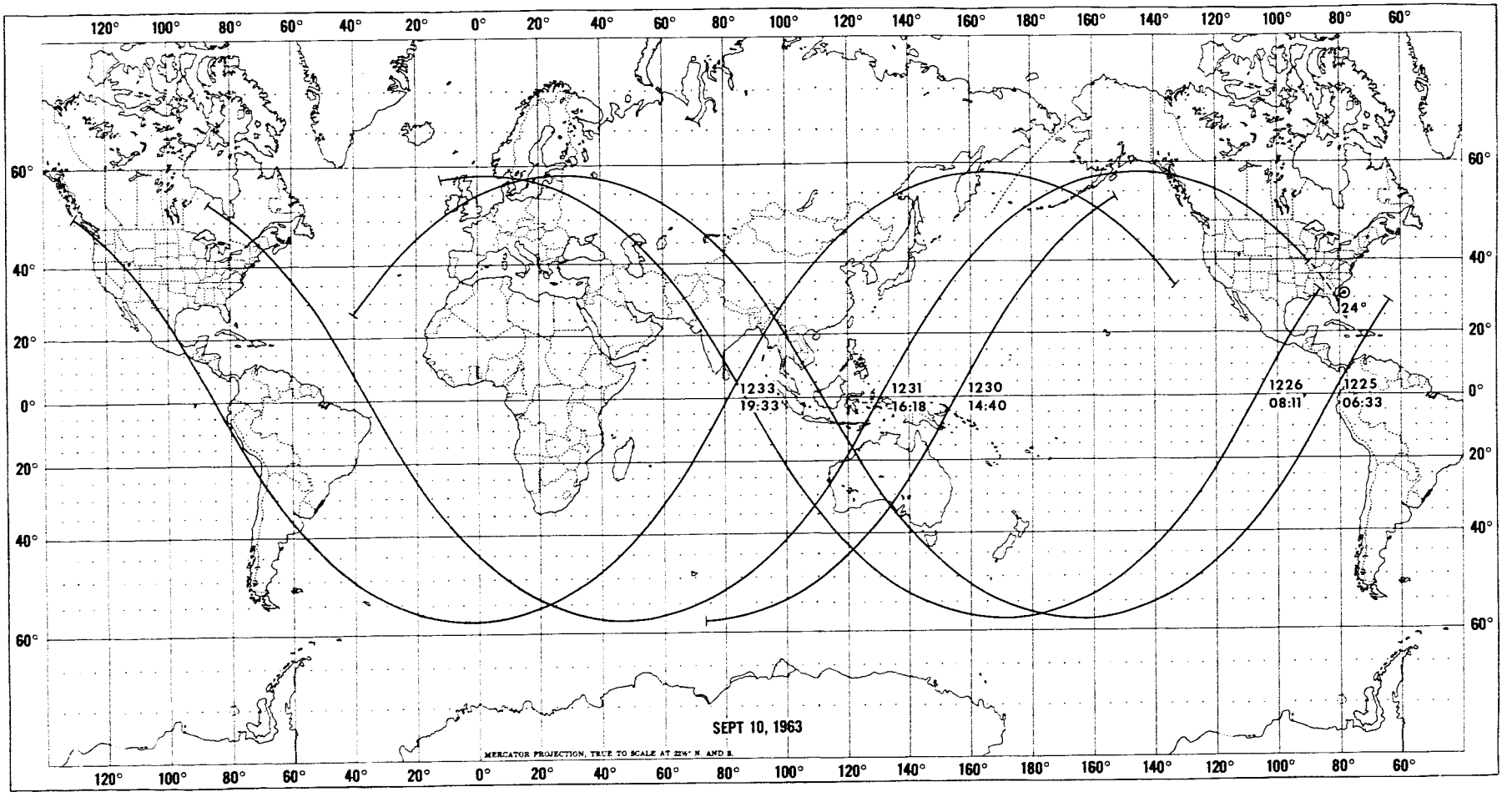
120° 100° 80° 60° 40° 20° 0° 20° 40° 60° 80° 100° 120° 140° 160° 180° 160° 140° 120° 100° 80° 60°
60° 40° 20° 0° 20° 40° 60°
1233
19:33
1231
16:18
1230
14:40
1226
08:11
1225
06:33
24°
SEPT 10, 1963
MERCATOR PROJECTION, TRUE TO SCALE AT 22½° N. AND S.

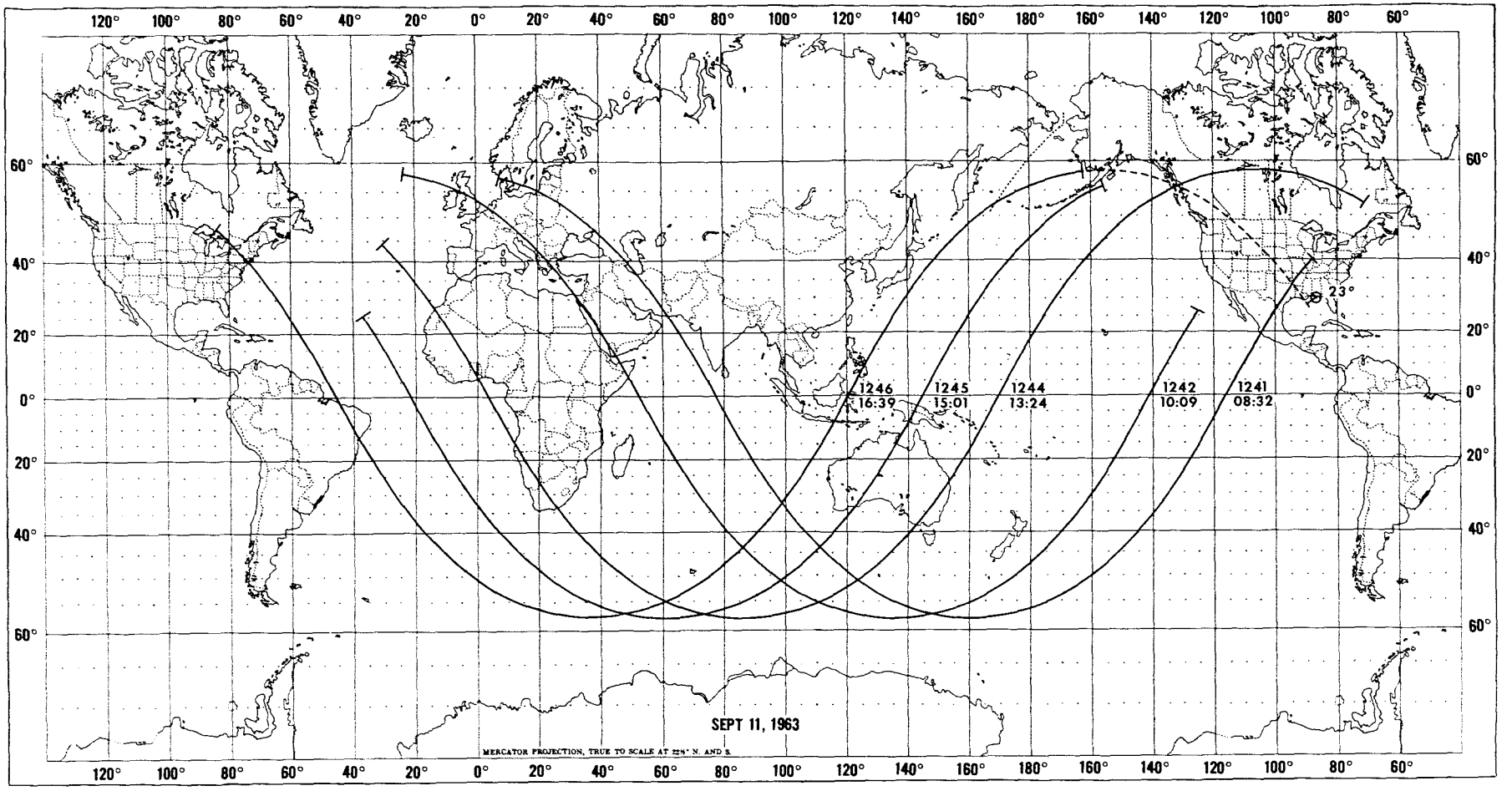
120° 100° 80° 60° 40° 20° 0° 20° 40° 60° 80° 100° 120° 140° 160° 180° 160° 140° 120° 100° 80° 60°
60°
40°
20°
0°
20°
40°
60°
1246
16:39
1245
15:01
1244
13:24
1242
10:09
1241
08:32
23°
SEPT 11, 1963
MERCATOR PROJECTION, TRUE TO SCALE AT 22½° N. AND S.

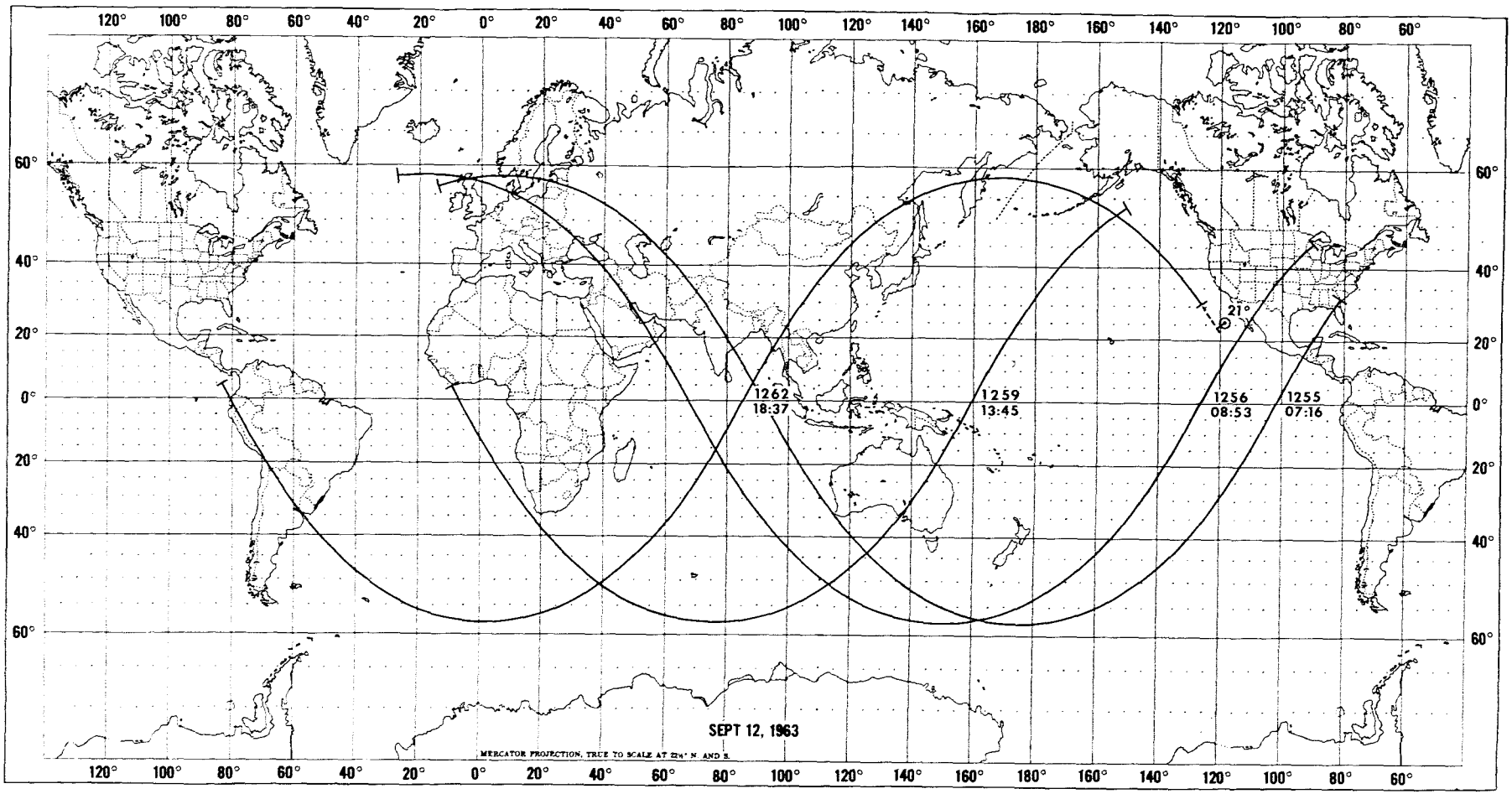
120° 100° 80° 60° 40° 20° 0° 20° 40° 60° 80° 100° 120° 140° 160° 180° 160° 140° 120° 100° 80° 60°
60° 40° 20° 0° 20° 40° 60°
1262
18:37
1259
13:45
1256
08:53
1255
07:16
21°
SEPT 12, 1963
MERCATOR PROJECTION, TRUE TO SCALE AT 22½° N AND S.

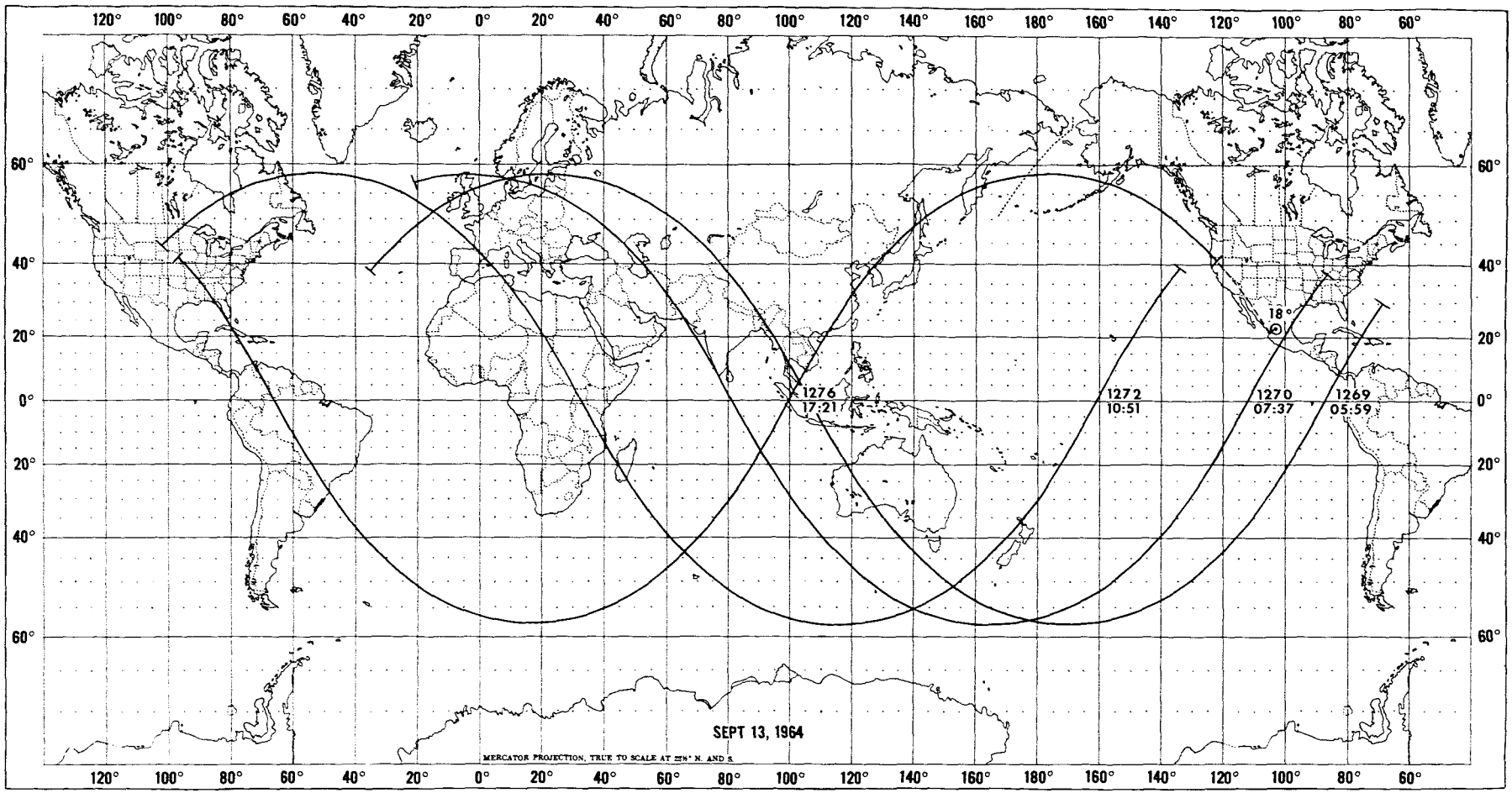
120° 100° 80° 60° 40° 20° 0° 20° 40° 60° 80° 100° 120° 140° 160° 180° 160° 140° 120° 100° 80° 60°
60° 40° 20° 0° 20° 40° 60°
1276
17:21
1272
10:51
1270
07:37
1269
05:59
18°
SEPT 13, 1964
MERCATOR PROJECTION, TRUE TO SCALE AT 28° N. AND S.

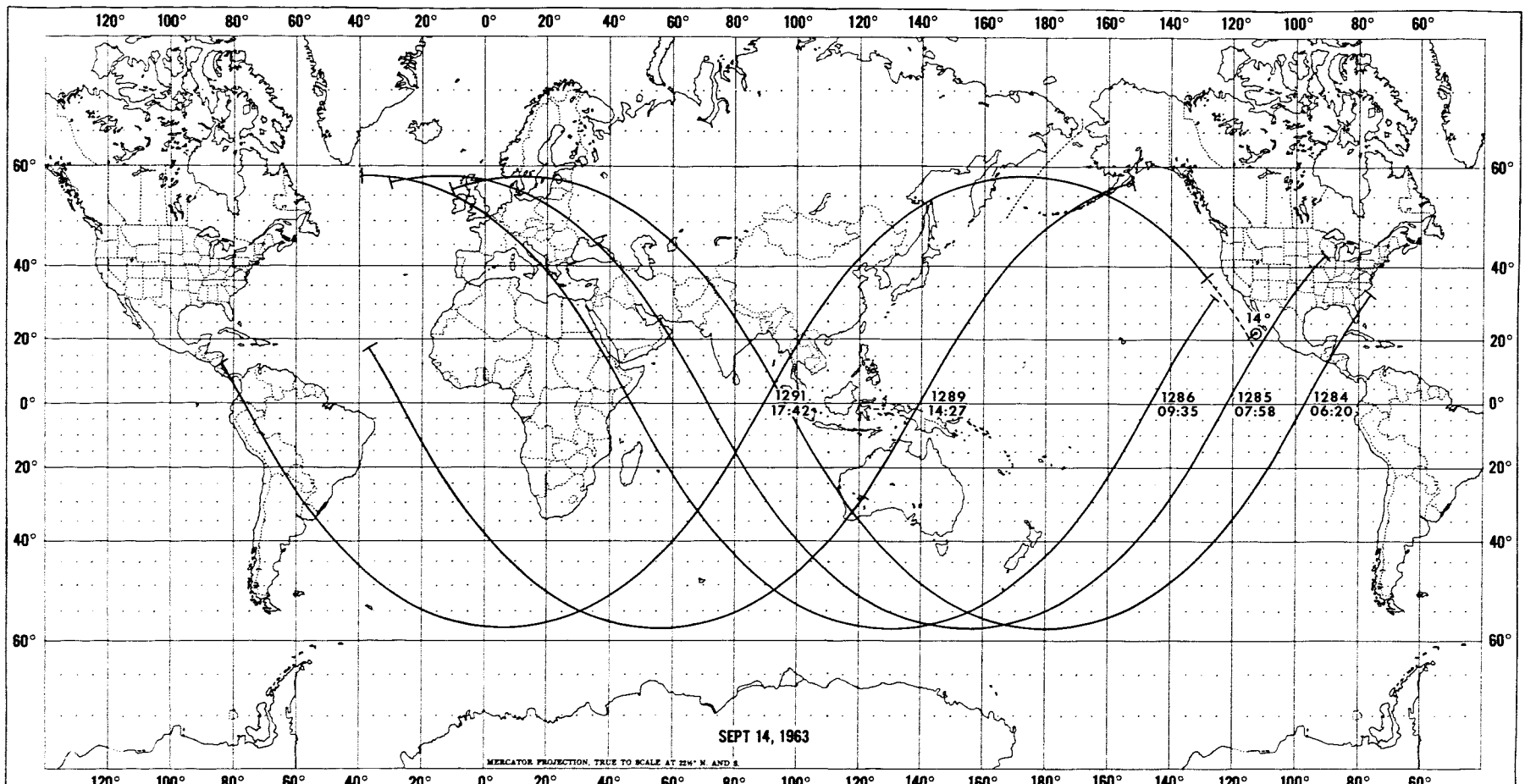
120° 100° 80° 60° 40° 20° 0° 20° 40° 60° 80° 100° 120° 140° 160° 180° 160° 140° 120° 100° 80° 60°
60° 40° 20° 0° 20° 40° 60°
1291
17:42
1289
14:27
1286
09:35
1285
07:58
1284
06:20
14°
SEPT 14, 1963
MERCATOR PROJECTION, TRUE TO SCALE AT 22½° N. AND S.

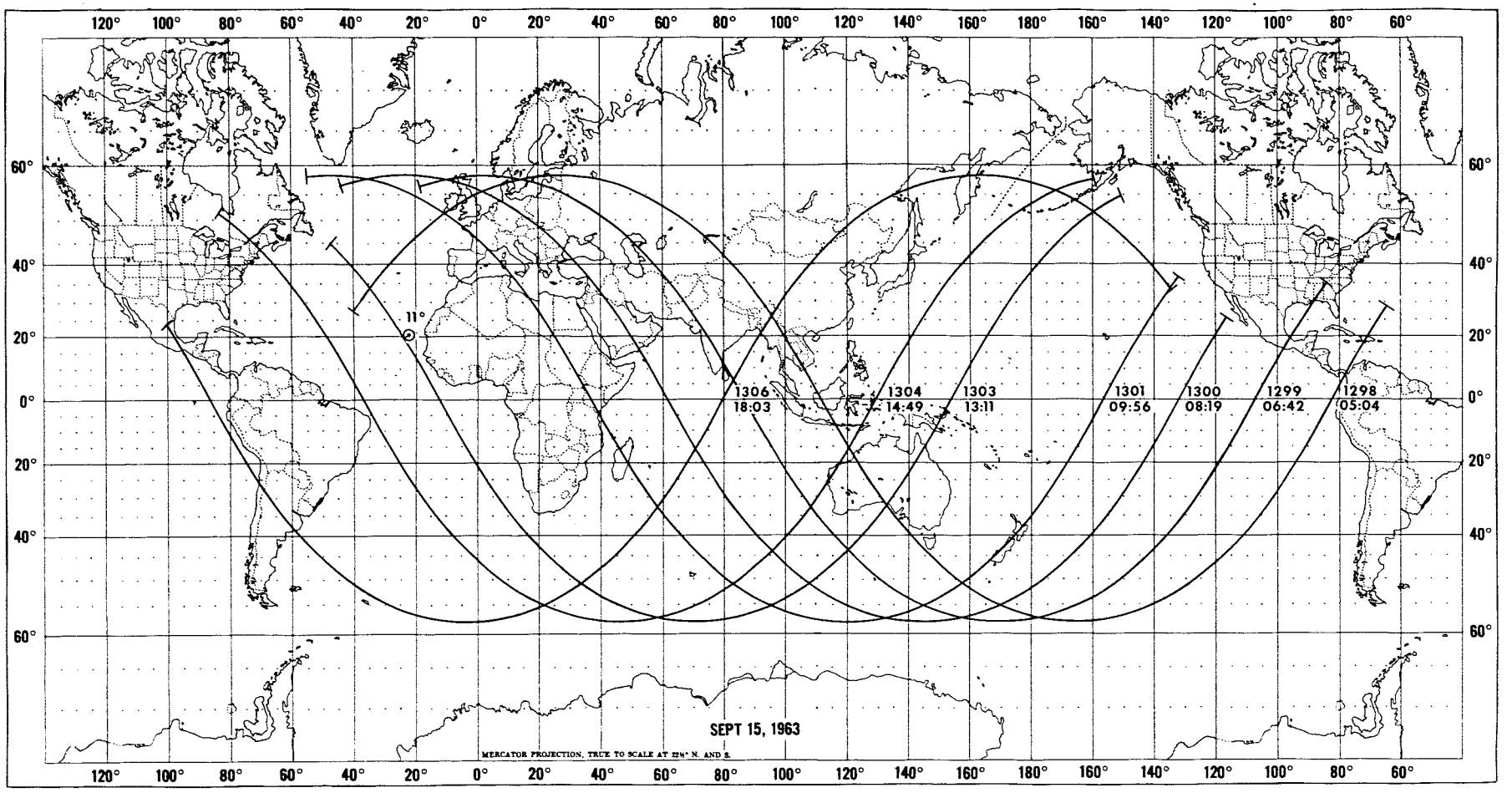
120° 100° 80° 60° 40° 20° 0° 20° 40° 60° 80° 100° 120° 140° 160° 180° 160° 140° 120° 100° 80° 60°
60° 40° 20° 0° 20° 40° 60°
11°
1306
18:03
1304
14:49
1303
13:11
1301
09:56
1300
08:19
1299
06:42
1298
05:04
SEPT 15, 1963
MERCATOR PROJECTION, TRUE TO SCALE AT 22½° N. AND S.

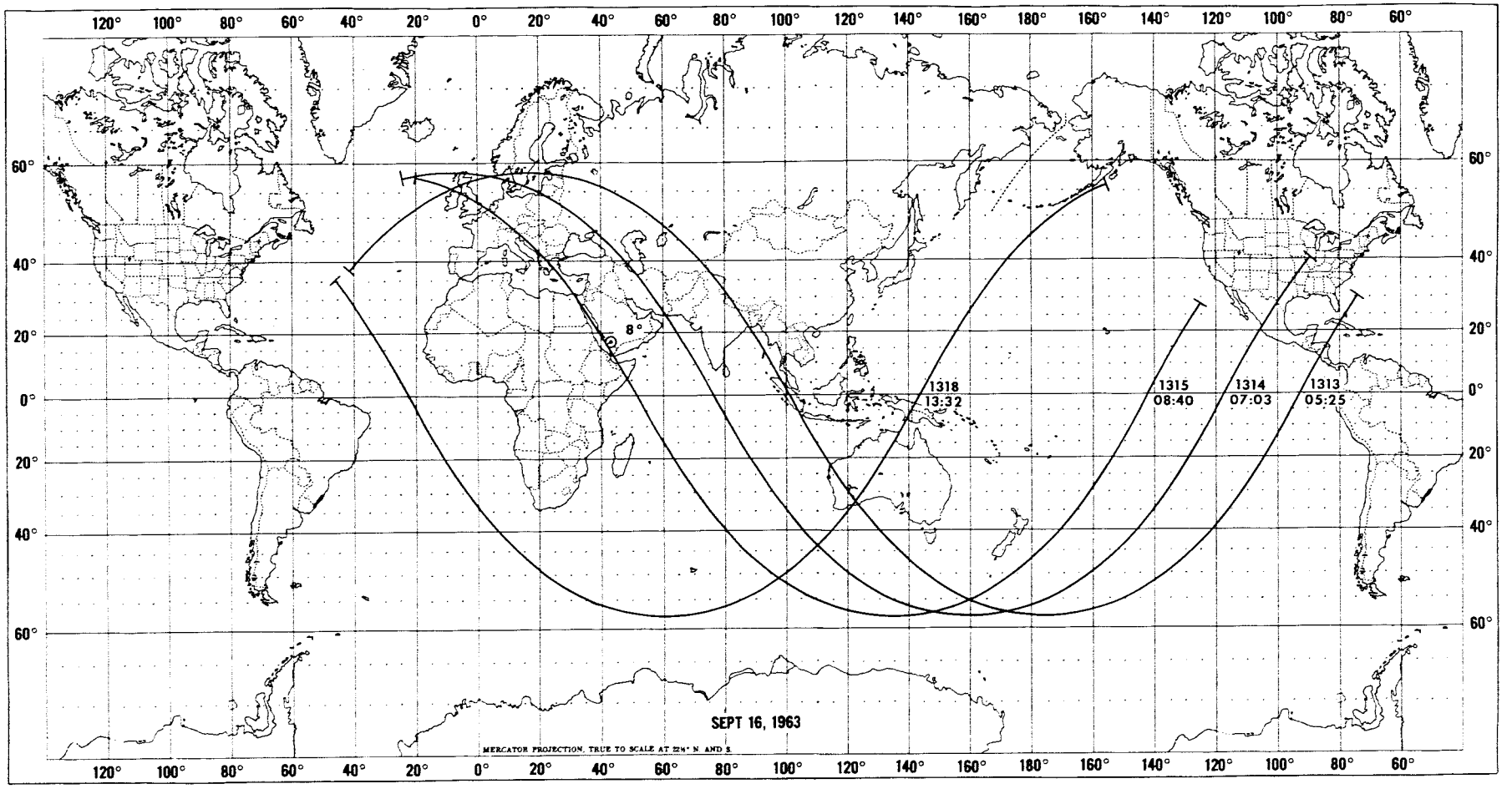
120° 100° 80° 60° 40° 20° 0° 20° 40° 60° 80° 100° 120° 140° 160° 180° 160° 140° 120° 100° 80° 60°
60°
40°
20°
0°
20°
40°
60°
8°
1318
13:32
1315
08:40
1314
07:03
1313
05:25
SEPT 16, 1963
MERCATOR PROJECTION, TRUE TO SCALE AT 22½° N AND S

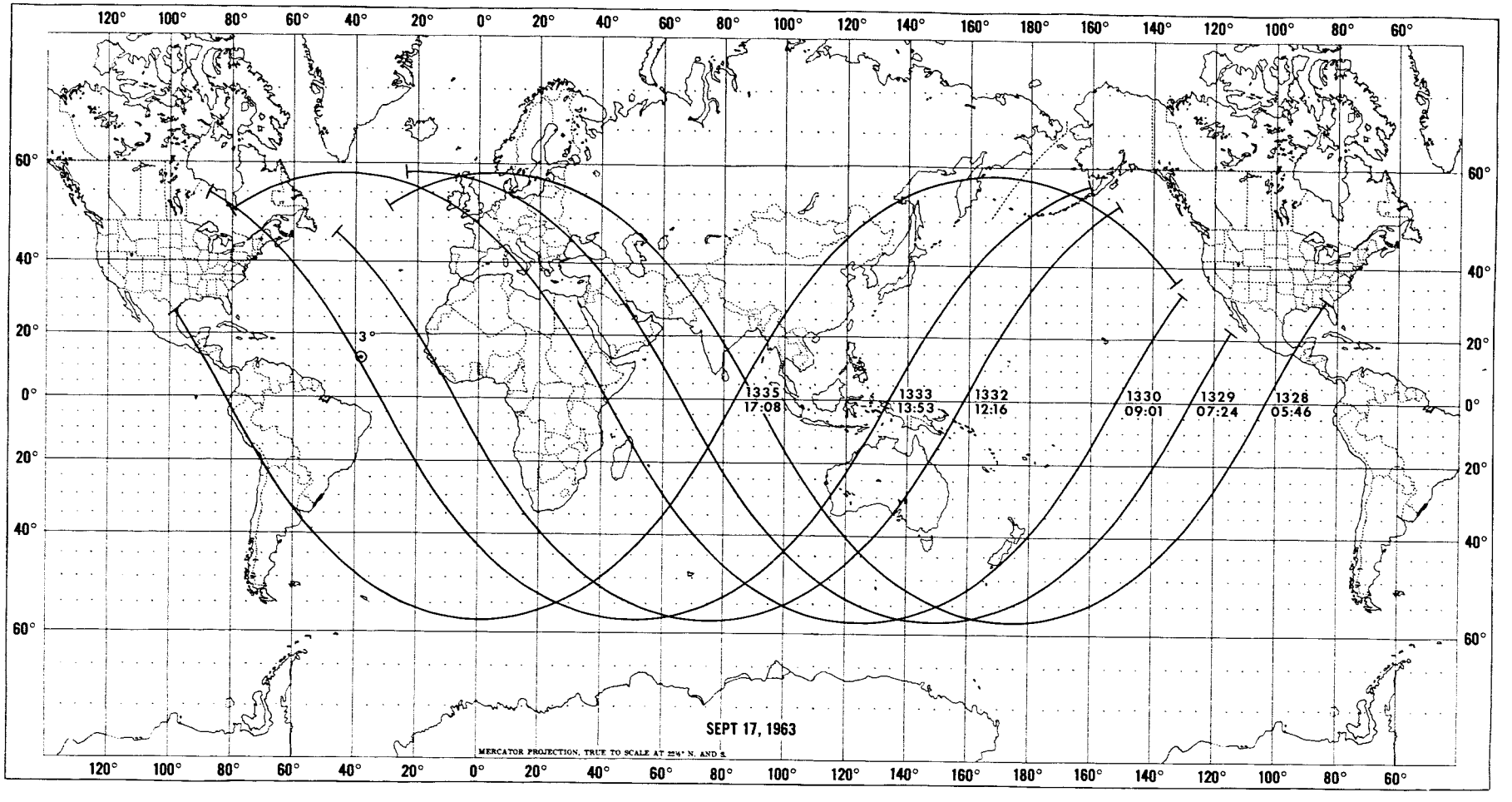
120° 100° 80° 60° 40° 20° 0° 20° 40° 60° 80° 100° 120° 140° 160° 180° 160° 140° 120° 100° 80° 60°
60° 40° 20° 0° 20° 40° 60°
3°
1335
17:08
1333
13:53
1332
12:16
1330
09:01
1329
07:24
1328
05:46
SEPT 17, 1963
MERCATOR PROJECTION, TRUE TO SCALE AT 22½° N. AND S.

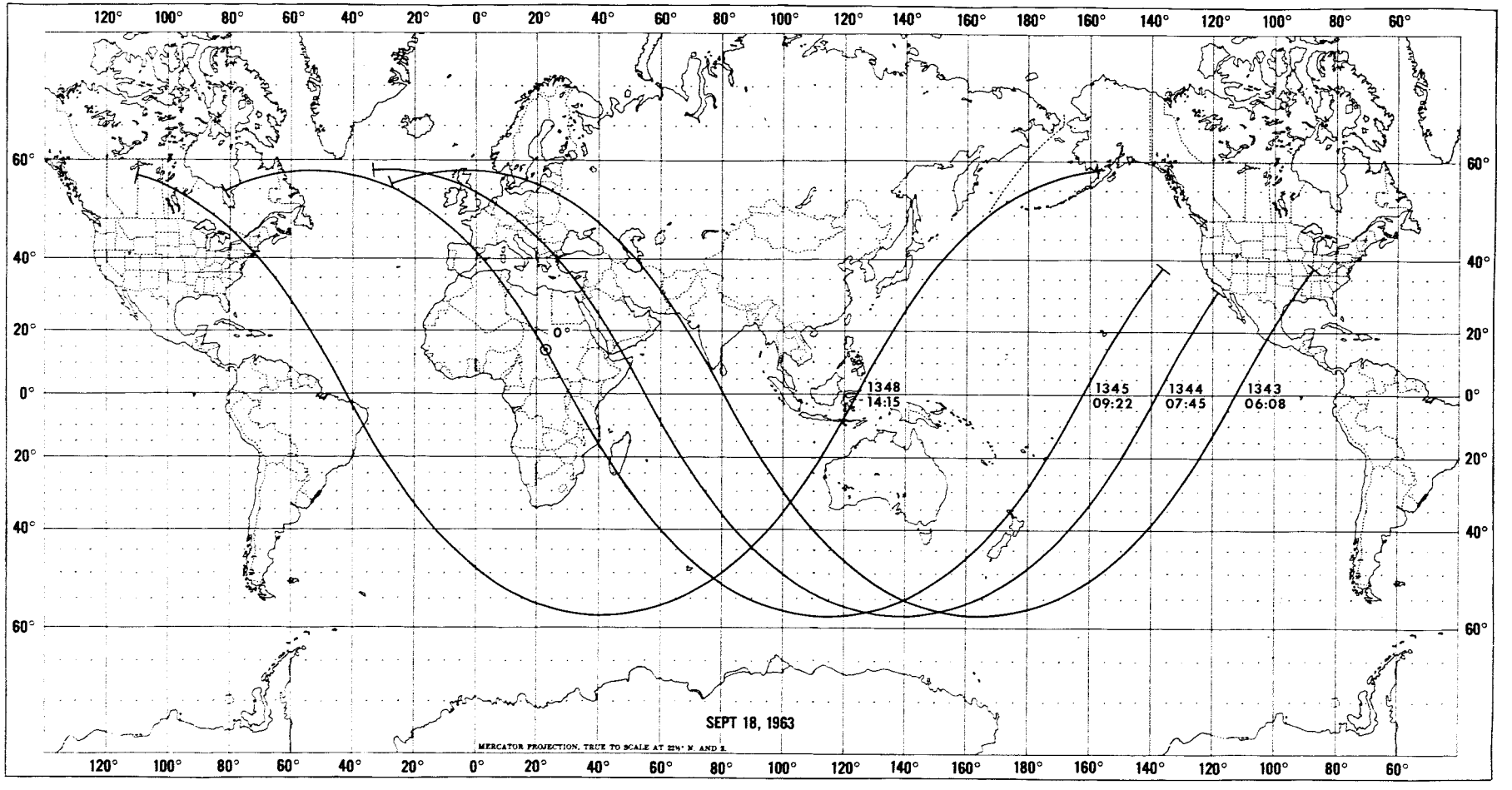
120° 100° 80° 60° 40° 20° 0° 20° 40° 60° 80° 100° 120° 140° 160° 180° 160° 140° 120° 100° 80° 60°
60° 40° 20° 0° 20° 40° 60°
0°
1348
14:15
1345
09:22
1344
07:45
1343
06:08
SEPT 18, 1963
MERCATOR PROJECTION, TRUE TO SCALE AT 22½° N. AND S.

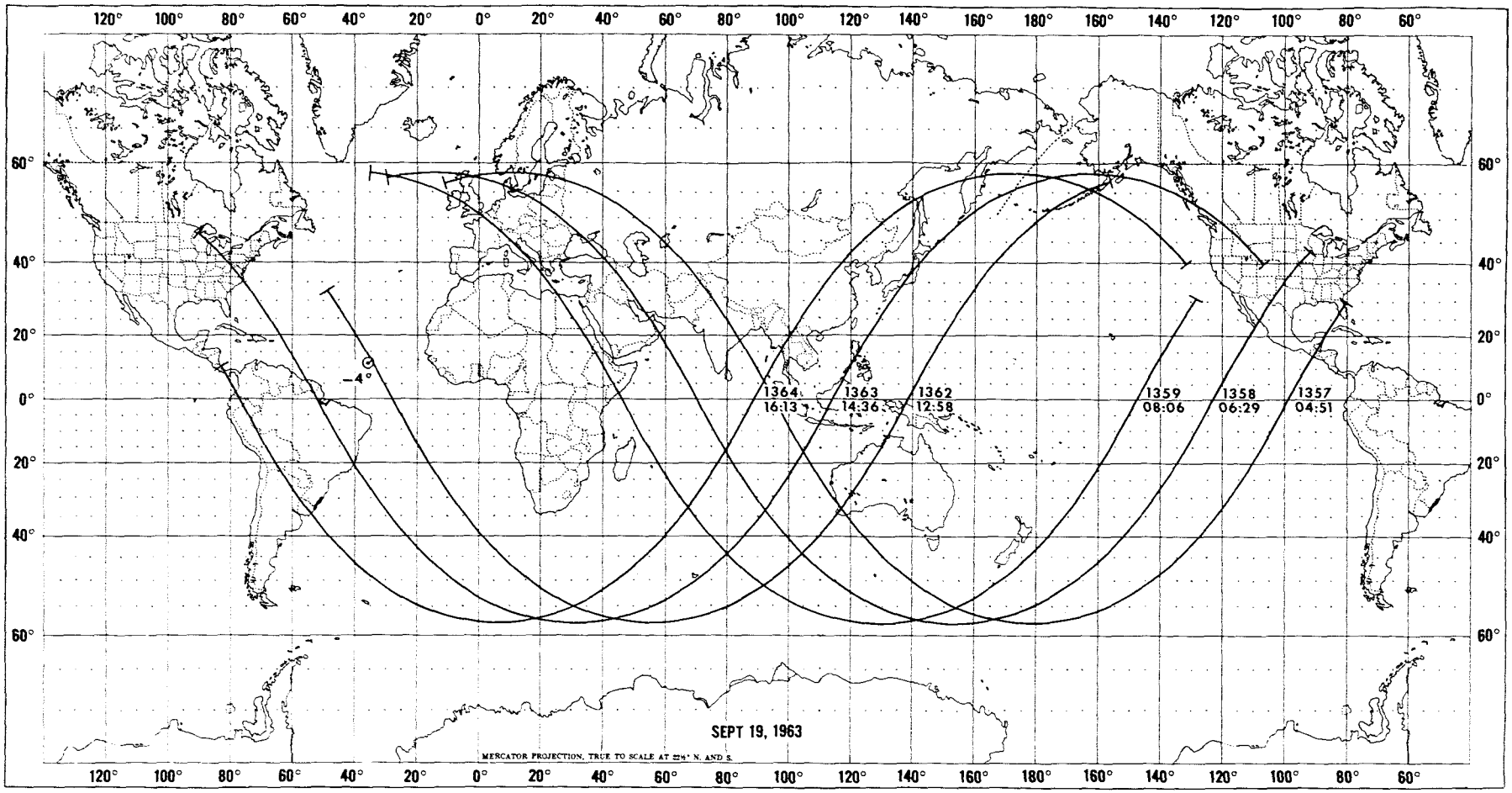
120° 100° 80° 60° 40° 20° 0° 20° 40° 60° 80° 100° 120° 140° 160° 180° 160° 140° 120° 100° 80° 60°
60° 40° 20° 0° 20° 40° 60°
-4°
1364
16:13
1363
14:36
1362
12:58
1359
08:06
1358
06:29
1357
04:51
SEPT 19, 1963
MERCATOR PROJECTION, TRUE TO SCALE AT 22½° N. AND S.

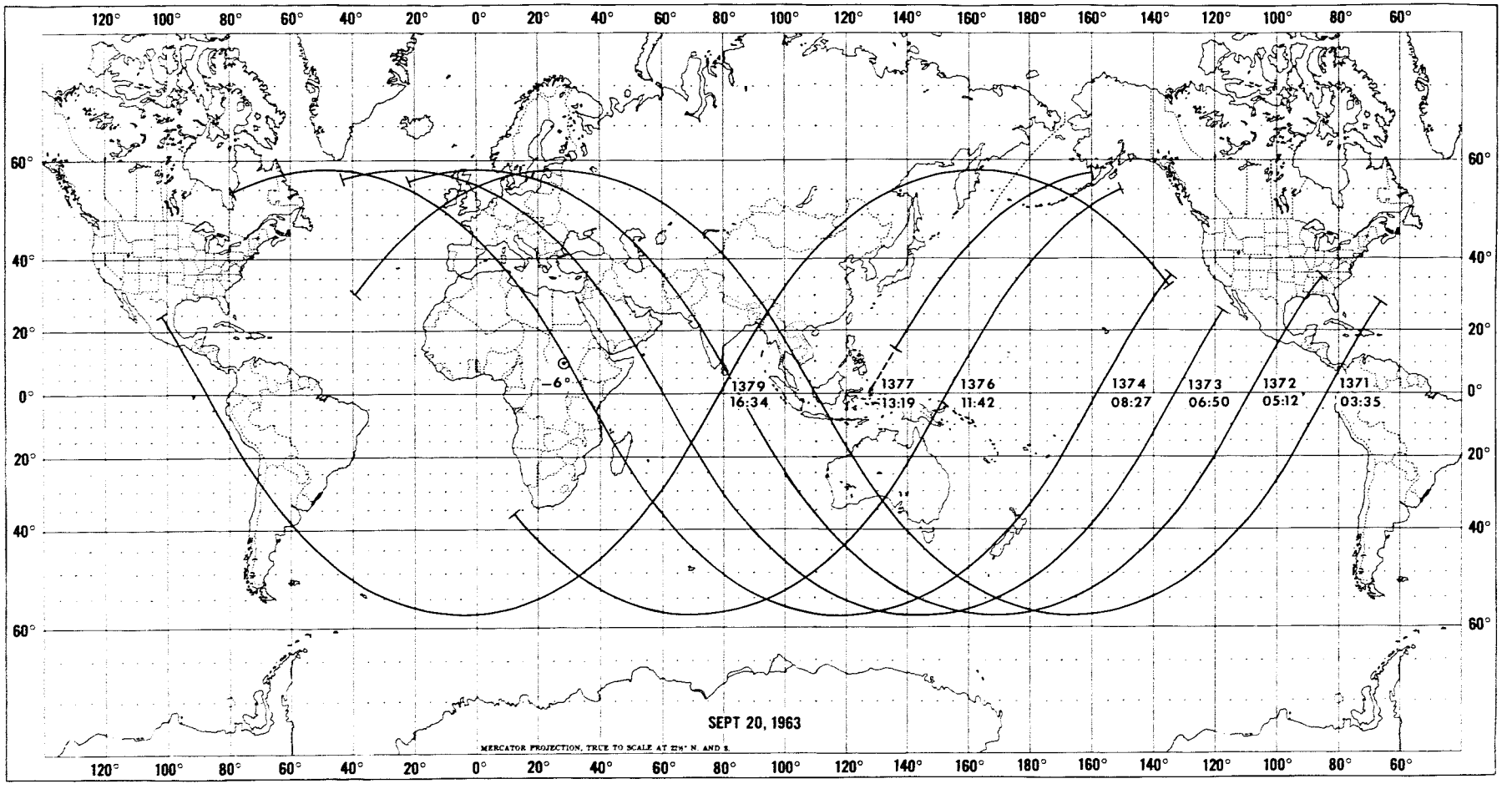
120° 100° 80° 60° 40° 20° 0° 20° 40° 60° 80° 100° 120° 140° 160° 180° 160° 140° 120° 100° 80° 60°
60° 40° 20° 0° 20° 40° 60°
-6°
1379
16:34
1377
13:19
1376
11:42
1374
08:27
1373
06:50
1372
05:12
1371
03:35
SEPT 20, 1963
MERCATOR PROJECTION, TRUE TO SCALE AT 22½° N. AND S.

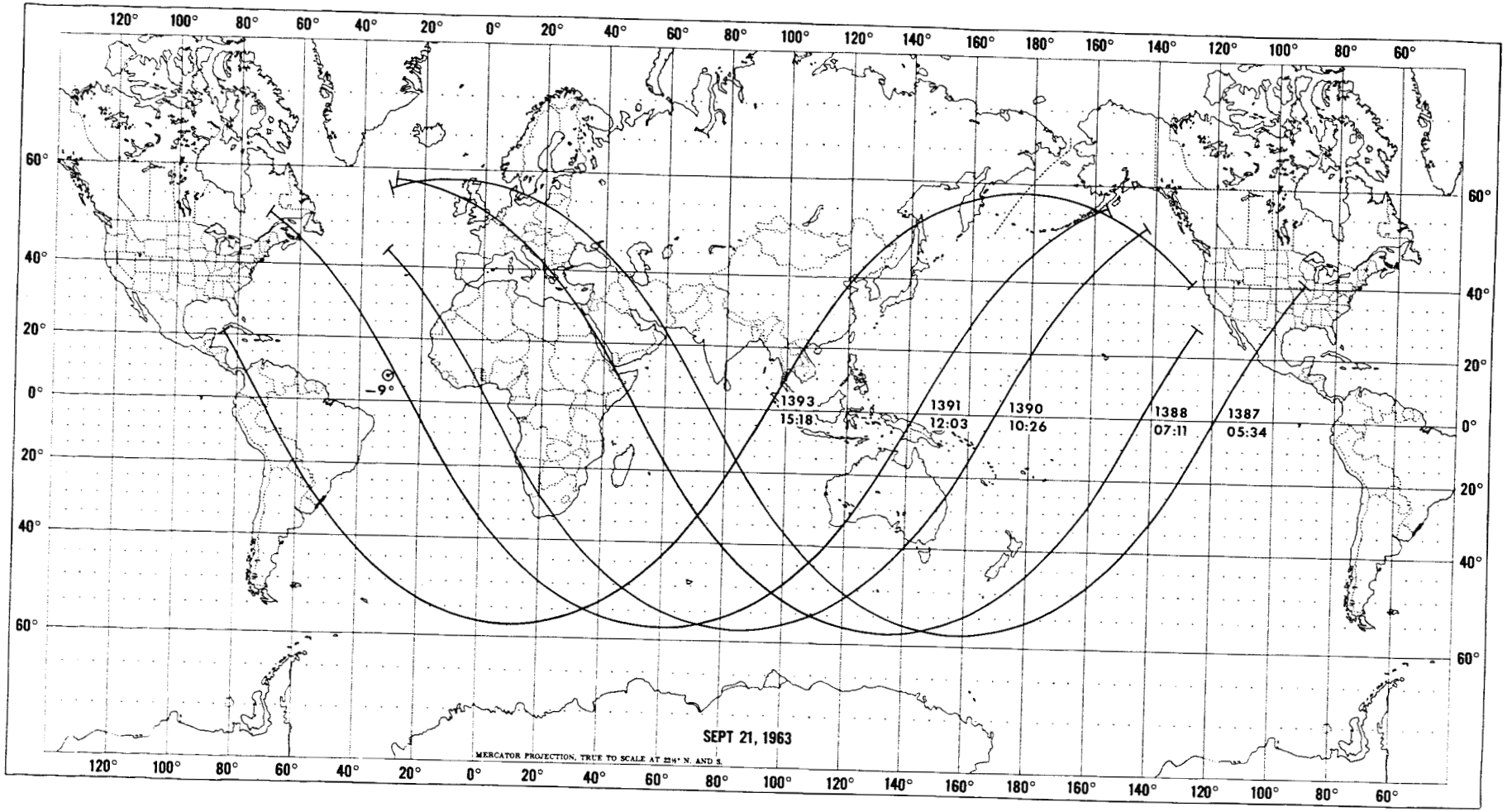
SEPT 21, 1963
MERCATOR PROJECTION, TRUE TO SCALE AT 22½° N. AND S.
1393
15:18
1391
12:03
1390
10:26
1388
07:11
1387
05:34
-9°

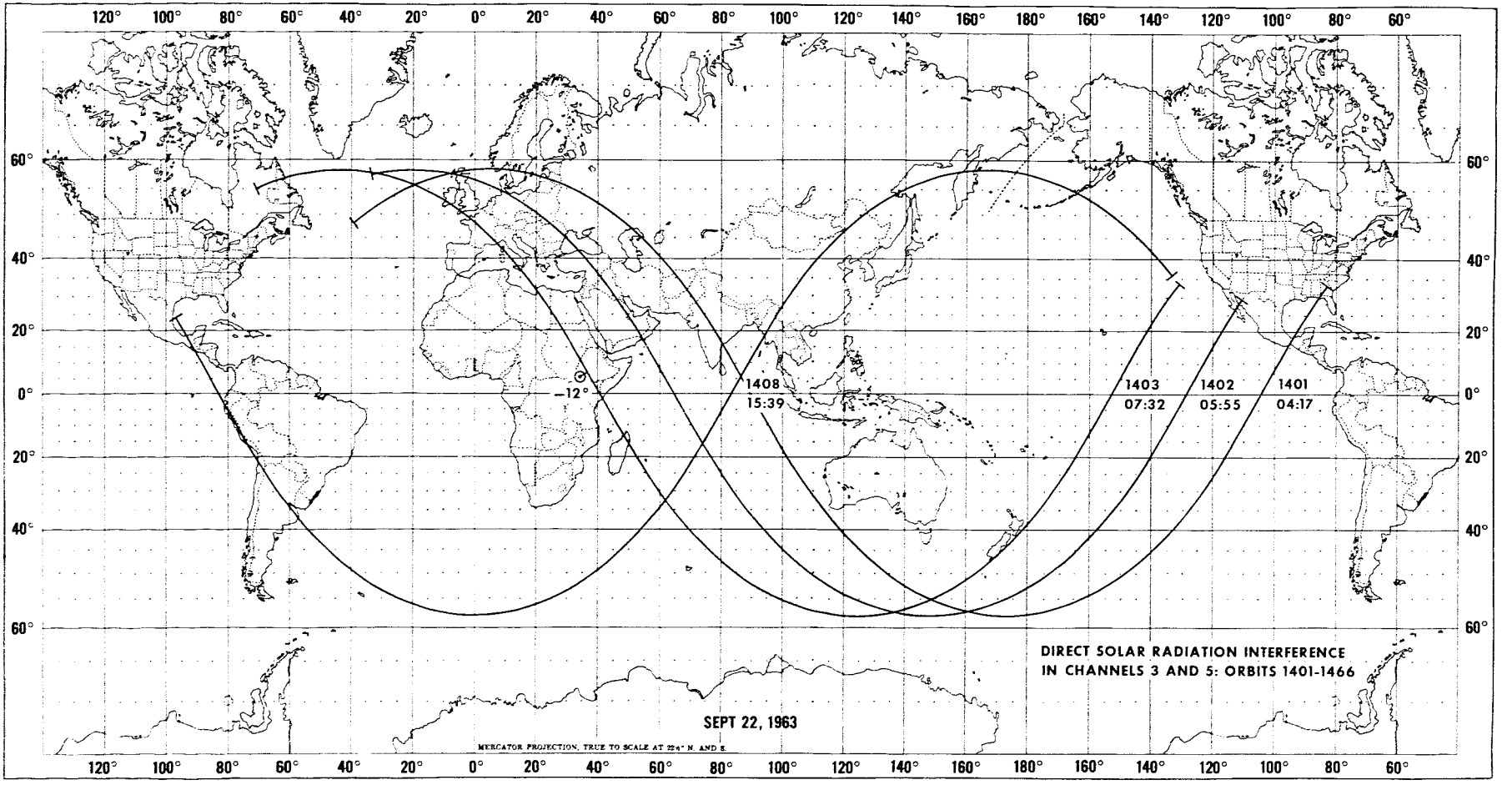
120° 100° 80° 60° 40° 20° 0° 20° 40° 60° 80° 100° 120° 140° 160° 180° 160° 140° 120° 100° 80° 60°
60° 40° 20° 0° 20° 40° 60°
1408
15:39
1403
07:32
1402
05:55
1401
04:17
-12°
DIRECT SOLAR RADIATION INTERFERENCE
IN CHANNELS 3 AND 5: ORBITS 1401-1466
SEPT 22, 1963
MERCATOR PROJECTION, TRUE TO SCALE AT 22½° N. AND S.

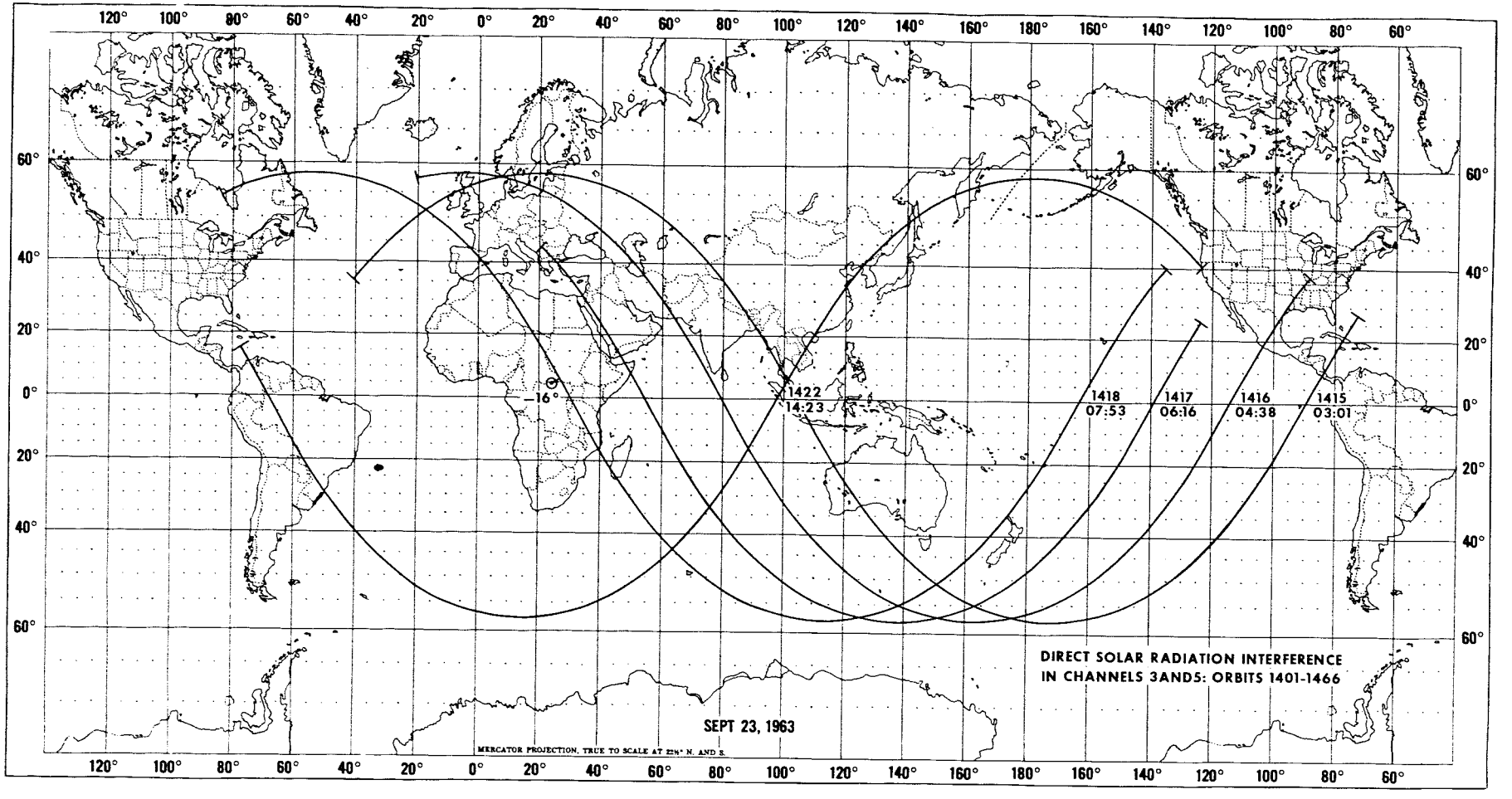
DIRECT SOLAR RADIATION INTERFERENCE
IN CHANNELS 3AND5: ORBITS 1401-1466
SEPT 23, 1963
MERCATOR PROJECTION, TRUE TO SCALE AT 22½° N. AND S.
1422
14:23
1418
07:53
1417
06:16
1416
04:38
1415
03:01
-16°

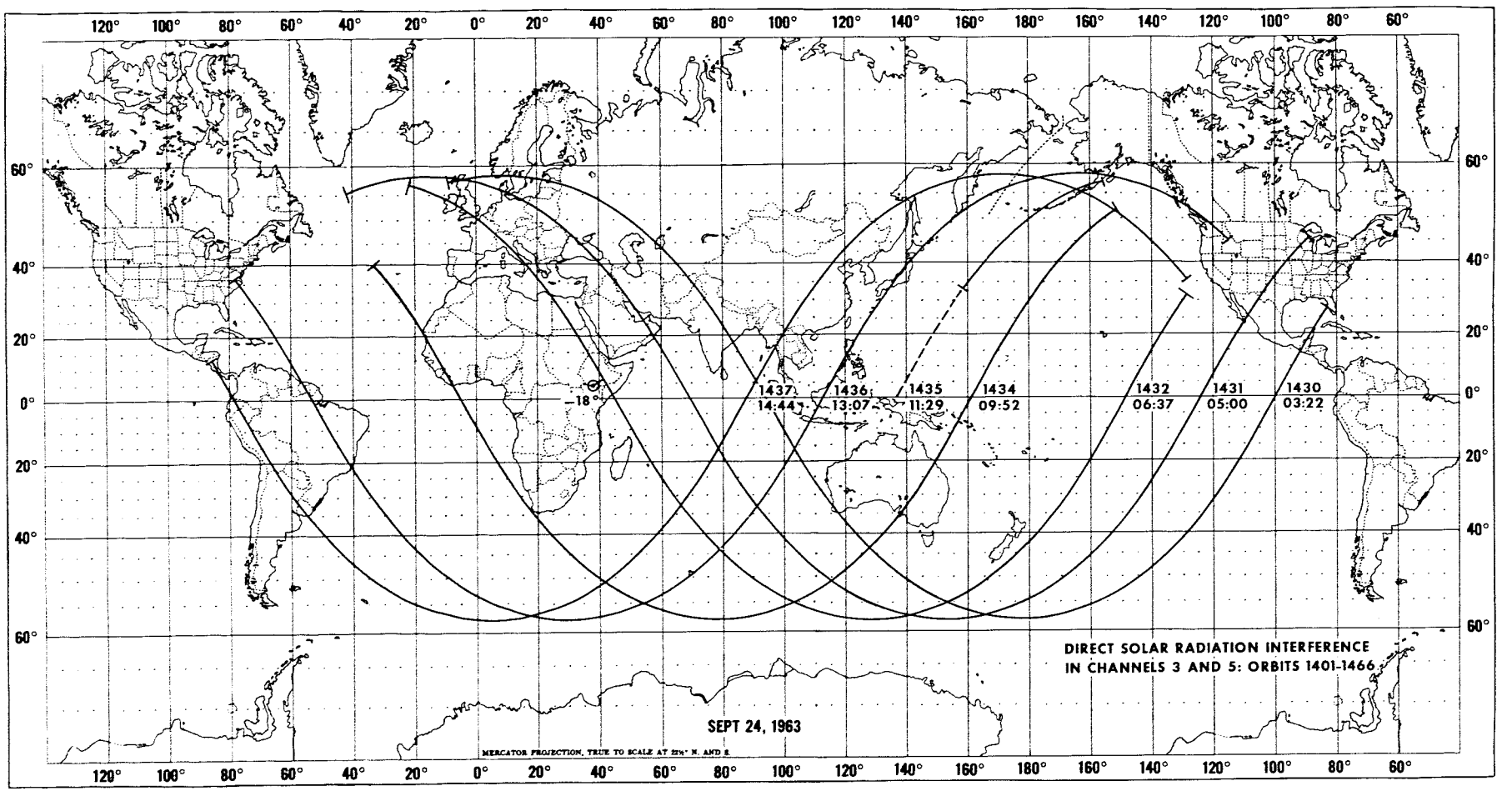
1437
14:44
1436
13:07
1435
11:29
1434
09:52
1432
06:37
1431
05:00
1430
03:22
-18°
DIRECT SOLAR RADIATION INTERFERENCE
IN CHANNELS 3 AND 5: ORBITS 1401-1466
SEPT 24, 1963
MERCATOR PROJECTION, TRUE TO SCALE AT 22½° N. AND S.

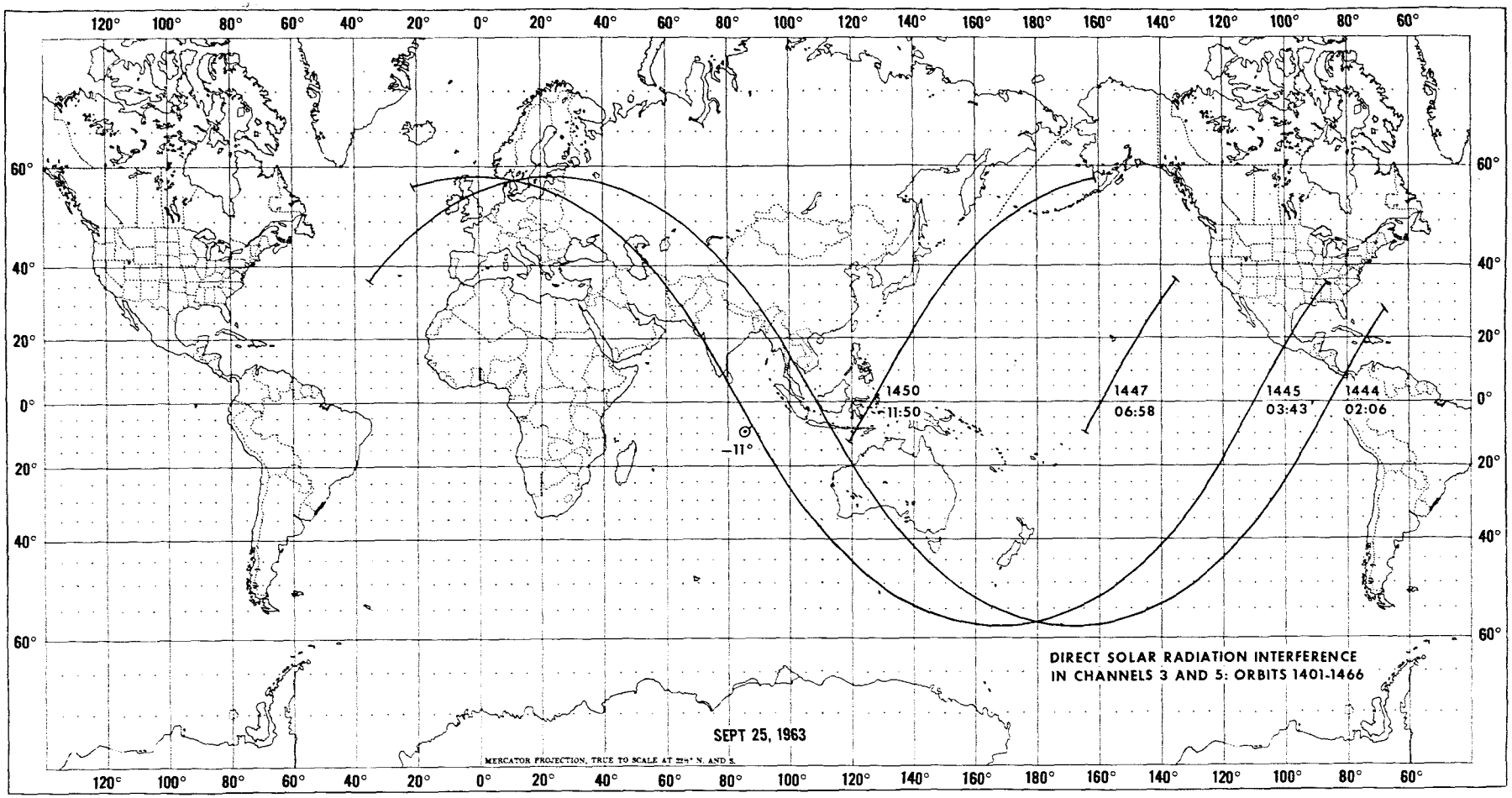
1450
11:50
1447
06:58
1445
03:43
1444
02:06
-11°
SEPT 25, 1963
DIRECT SOLAR RADIATION INTERFERENCE
IN CHANNELS 3 AND 5: ORBITS 1401-1466
MERCATOR PROJECTION, TRUE TO SCALE AT 23½° N. AND S.

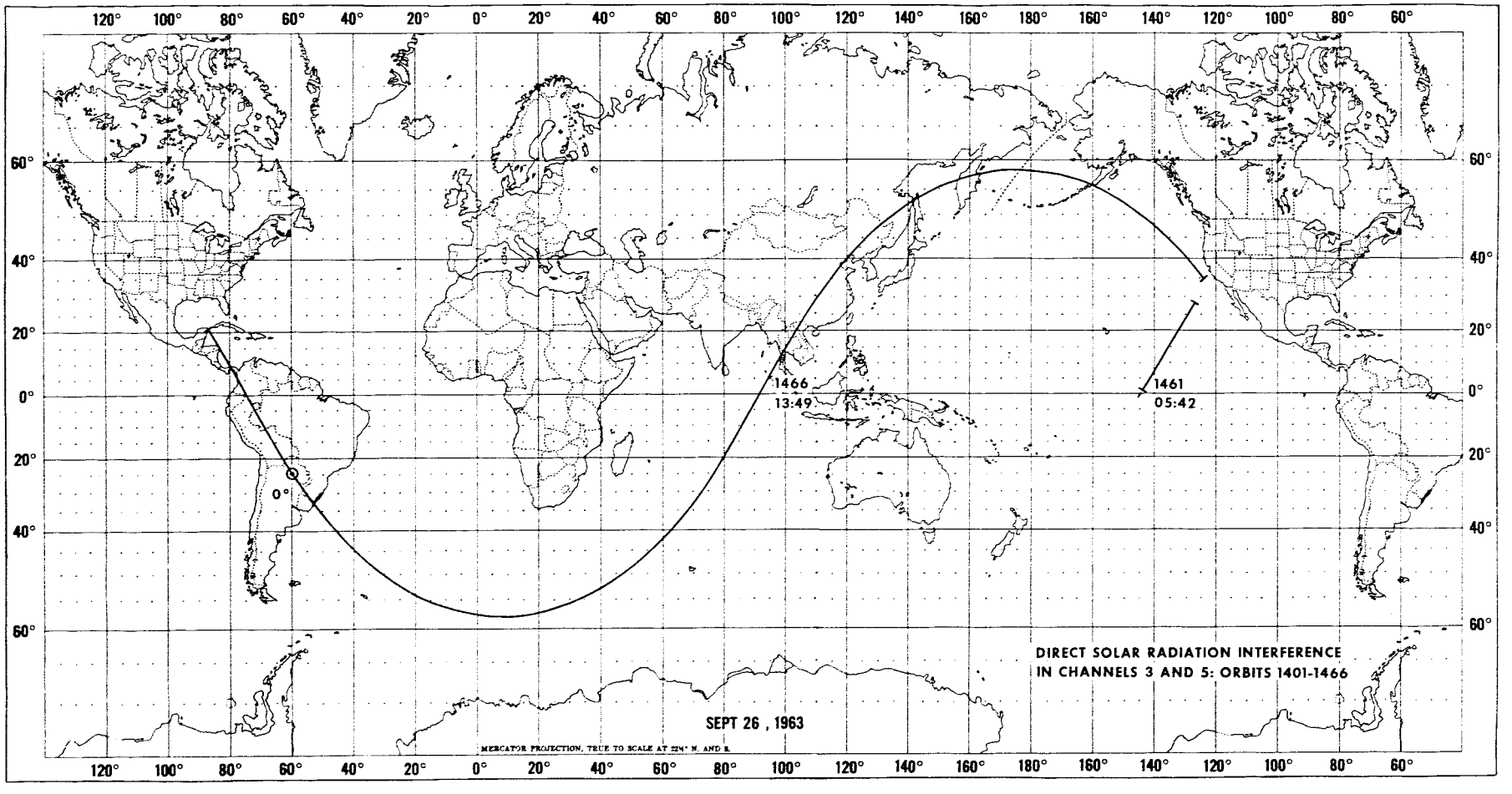
120° 100° 80° 60° 40° 20° 0° 20° 40° 60° 80° 100° 120° 140° 160° 180° 160° 140° 120° 100° 80° 60°
60° 40° 20° 0° 20° 40° 60°
1466
13:49
1461
05:42
0°
DIRECT SOLAR RADIATION INTERFERENCE
IN CHANNELS 3 AND 5: ORBITS 1401-1466
SEPT 26 , 1963
MERCATOR PROJECTION, TRUE TO SCALE AT 22½° N. AND S.

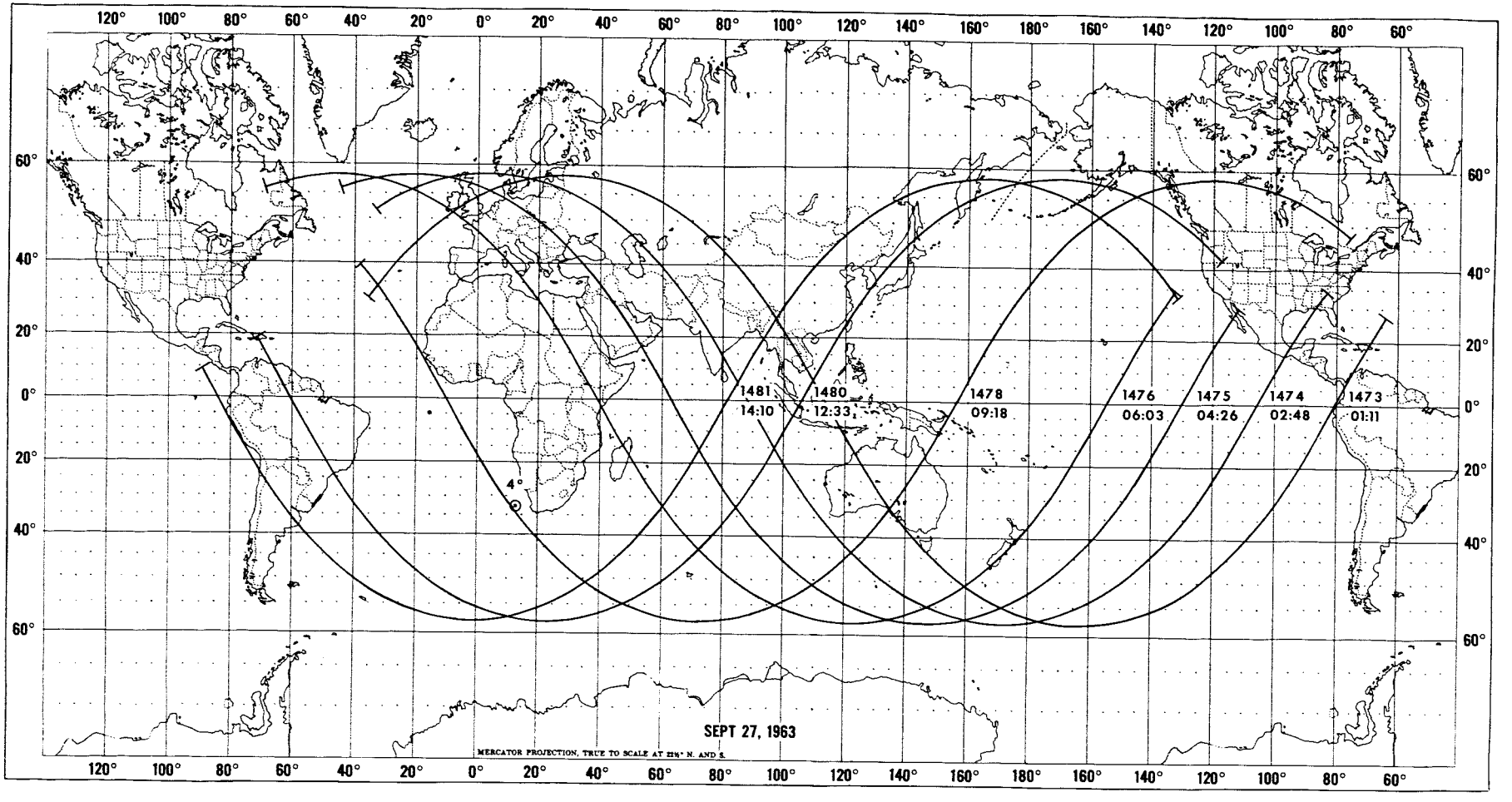
1481
14:10
1480
12:33
1478
09:18
1476
06:03
1475
04:26
1474
02:48
1473
01:11
4°
SEPT 27, 1963
MERCATOR PROJECTION, TRUE TO SCALE AT 22½° N. AND S.

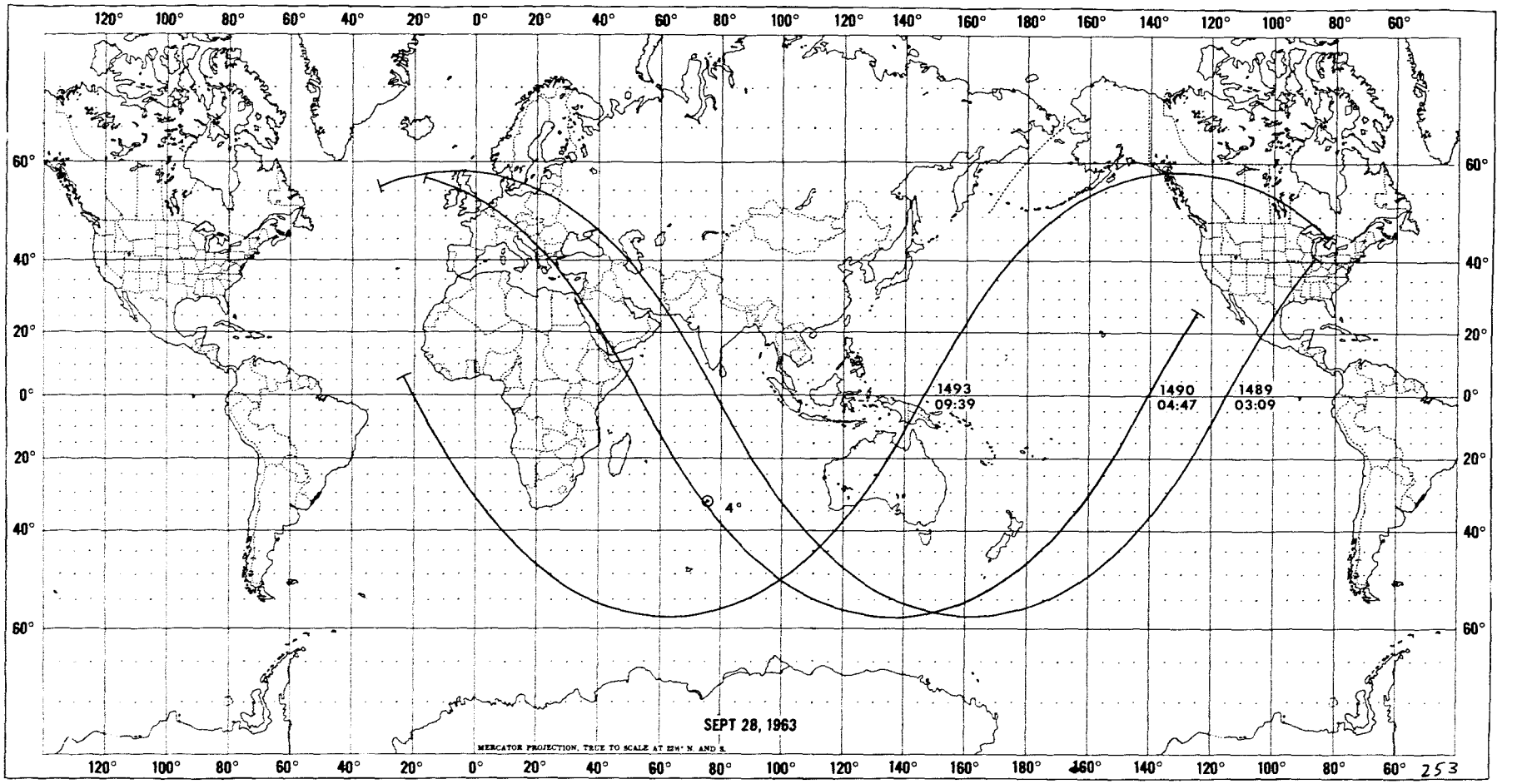
1493
09:39
1490
04:47
1489
03:09
4°
SEPT 28, 1963
MERCATOR PROJECTION, TRUE TO SCALE AT 22½° N. AND S.
253

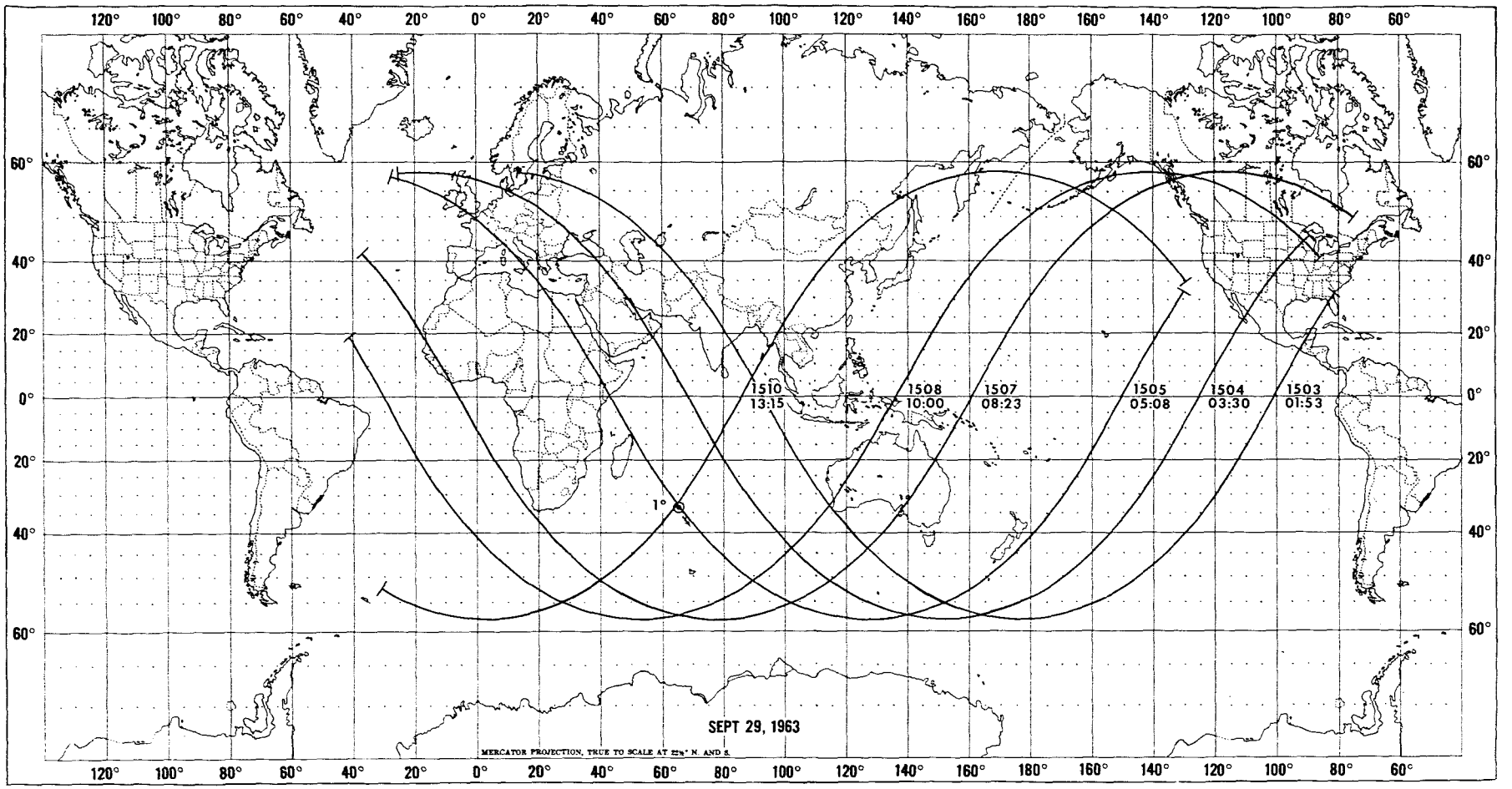
1510
13:15
1508
10:00
1507
08:23
1505
05:08
1504
03:30
1503
01:53
1°
SEPT 29, 1963
MERCATOR PROJECTION, TRUE TO SCALE AT 22½° N. AND S.

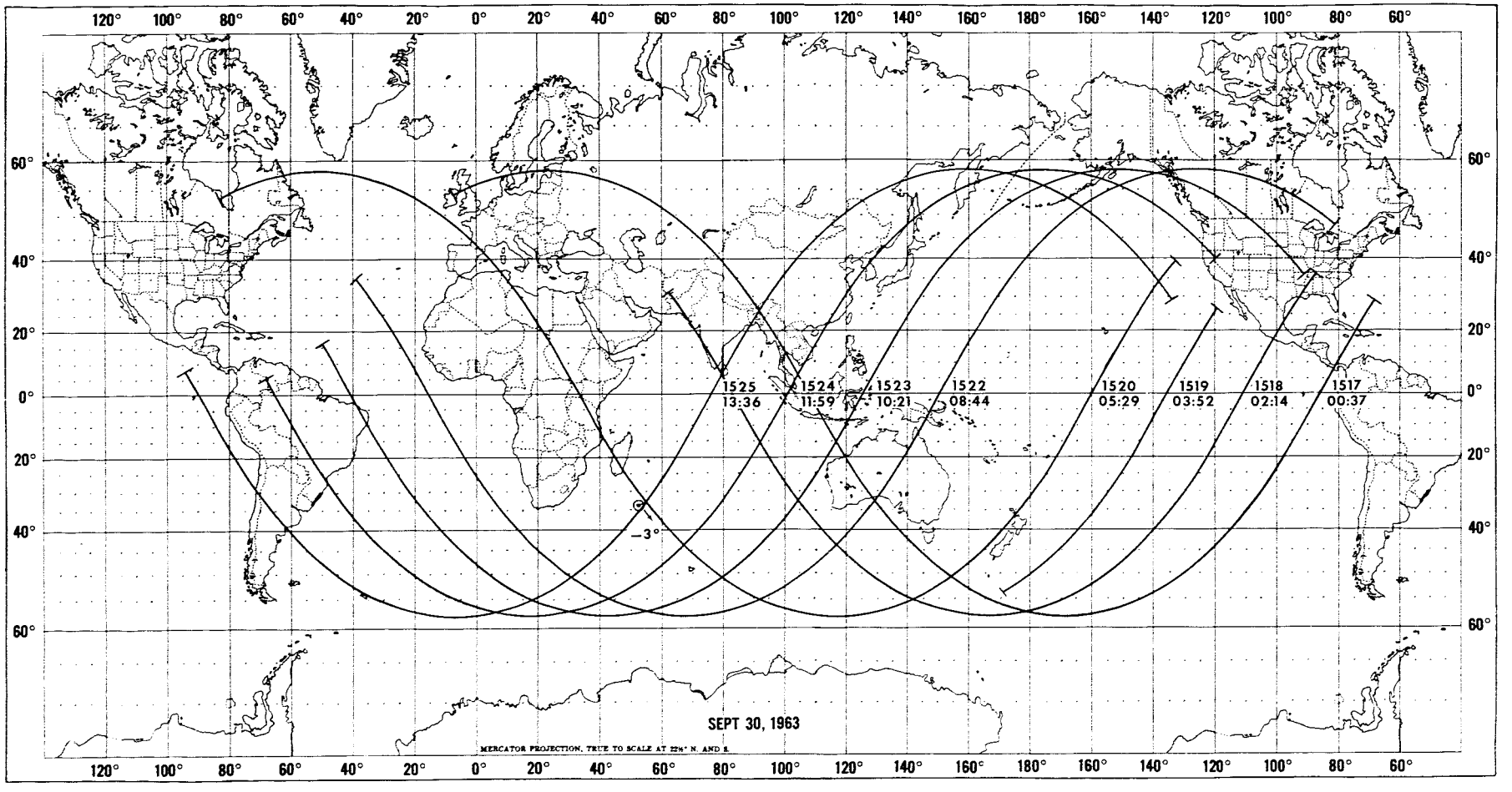
120° 100° 80° 60° 40° 20° 0° 20° 40° 60° 80° 100° 120° 140° 160° 180° 160° 140° 120° 100° 80° 60°
60° 40° 20° 0° 20° 40° 60°
1525 13:36
1524 11:59
1523 10:21
1522 08:44
1520 05:29
1519 03:52
1518 02:14
1517 00:37
−3°
SEPT 30, 1963
MERCATOR PROJECTION, TRUE TO SCALE AT 22½° N. AND S.

TIROS VII SUB-POINT TRACK

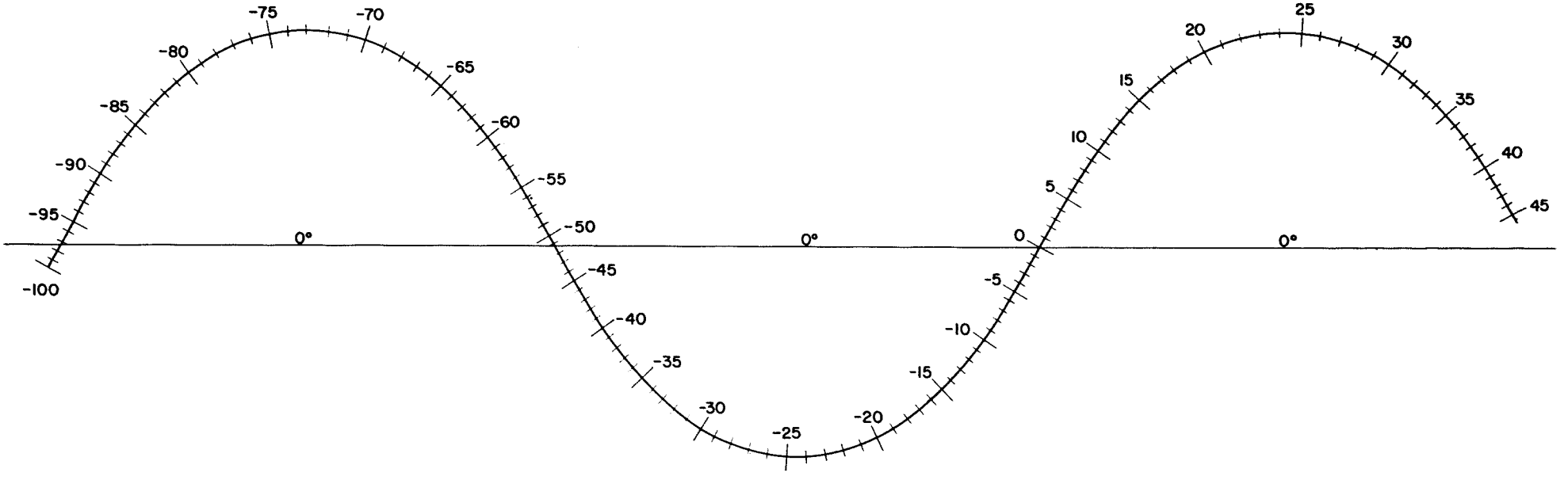

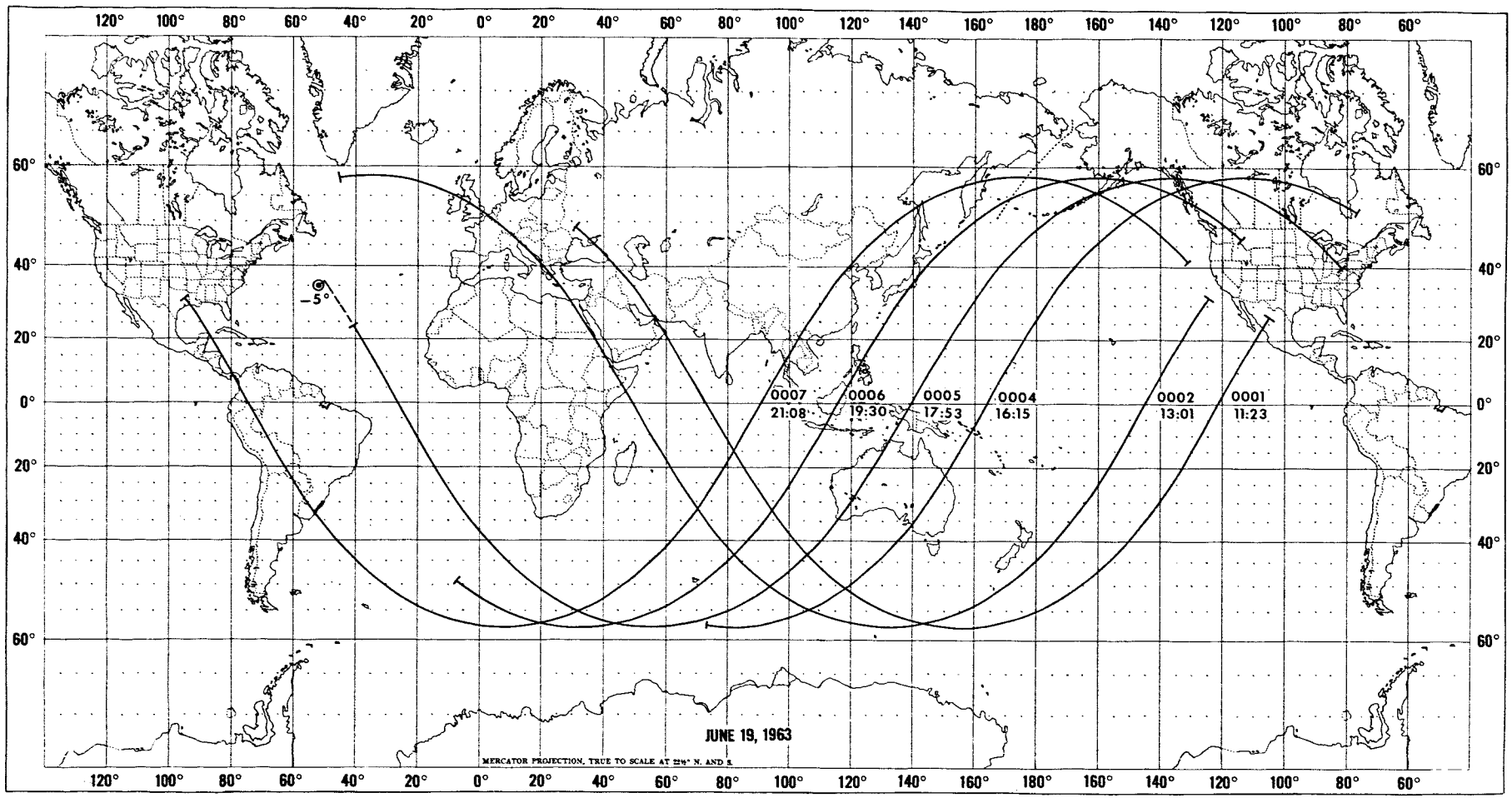
120° 100° 80° 60° 40° 20° 0° 20° 40° 60° 80° 100° 120° 140° 160° 180° 160° 140° 120° 100° 80° 60°
60° 40° 20° 0° 20° 40° 60°
-5°
0007
21:08
0006
19:30
0005
17:53
0004
16:15
0002
13:01
0001
11:23
JUNE 19, 1963
MERCATOR PROJECTION, TRUE TO SCALE AT 22½° N. AND S.